Electrochemical Society

Philadelphia Meeting Program Issue

WE URGE YOU

• • • to take full advantage of the facilities of our modern Research Department in developing custom-made anodes that will materially lower your cell-room operating costs.

PRODUCTS ELECTRODE GLC DIVISION YOU CAN TRUST

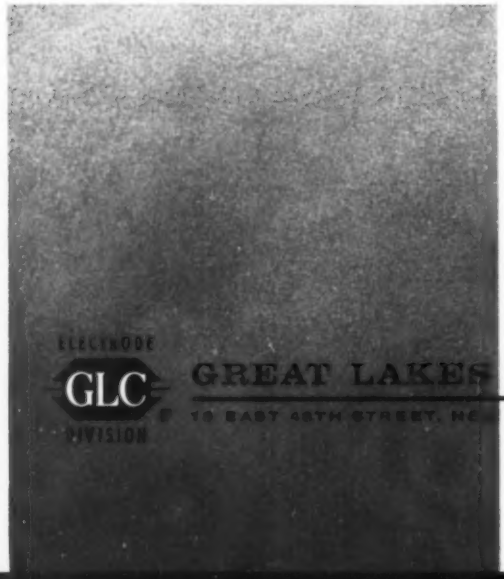

ELECTRODE GLC DIVISION

GREAT LAKES CARBON CORPORATION

10 EAST 40TH STREET, NEW YORK 17, N. Y. OFFICES IN PRINCIPAL CITIES

EDITORIAL STAFF

H. H. Uhlig, Chairman, Publication Committee

Cecil V. King, Editor

Norman Hackerman, Technical Editor

Ruth G. Sterns, Managing Editor

U. B. Thomas, News Editor

H. W. Salzberg, Book Review Editor

Natalie Michalski, Assistant Editor

DIVISIONAL EDITORS

W. C. Vosburgh, Battery

Milton Stern, Corrosion, I

R. T. Foley, Corrosion, II

T. D. Callinan, Electric Insulation

Abner Brenner, Electrodeposition

H. C. Froelich, Electronics

Ernest Paskell, Electronics—Semiconductors

Sherlock Swann, Jr., Electro-Organic, I

Stanley Wawzonek, Electro-Organic, II

John M. Blocher, Jr., Electrothermics and Metallurgy, I

A. U. Seybolt, Electrothermics and Metallurgy, II

N. J. Johnson, Industrial Electrolytic

C. W. Tobias, Theoretical Electrochemistry, I

A. J. deBethune, Theoretical Electrochemistry, II

REGIONAL EDITORS

Howard T. Francis, Chicago

Joseph Schulein, Pacific Northwest

J. C. Schumacher, Los Angeles

G. W. Heise, Cleveland

G. H. Fetterley, Niagara Falls

Oliver Osborn, Houston

Earl A. Gulbransen, Pittsburgh

A. C. Holm, Canada

J. W. Cuthbertson, Great Britain

T. L. Rama Char, India

ADVERTISING OFFICE

ECS
1860 Broadway, New York 23, N. Y.

ECS OFFICERS

Sherlock Swann, Jr., President
University of Illinois, Urbana, Ill.

W. C. Gardiner, Vice-President
Olin Mathieson Chemical Corp., Niagara Falls, N. Y.

R. A. Schaefer, Vice-President
Cleveland Graphite Bronze Div., Clevite Corp., Cleveland, Ohio

Henry B. Linford, Vice-President
Columbia University, New York, N. Y.

Lyle I. Gilbertson, Treasurer
Air Reduction Co., Murray Hill, N. J.

I. E. Campbell, Interim Secretary
National Steel Corp., Weirton, W. Va.

Robert K. Shannon, Executive Secretary
National Headquarters, The ECS, 1860 Broadway, New York 23, N. Y.

Journal of the

Electrochemical Society

MARCH 1959 **VOL. 106 • NO. 3**

CONTENTS

Editorial

Tuas Res Agitur 42C

Technical Papers

Ammonia Vapor Activated Batteries. *H. S. Gleason, J. M. Freund, L. J. Minnick, and W. F. Meyers* 157

General and Intergranular Corrosion of Austenitic Stainless Steels in Acids. Effect of Cations in the Acids and the Influence of Heat Treatment and Grain Size of the Steel. *M. A. Streicher* 161

The Diffusion of Oxygen in Alpha and Beta Zircaloy 2 and Zircaloy 3 at High Temperatures. *M. W. Mallett, W. M. Albrecht, and P. R. Wilson* 181

Reaction of Aluminum and Carbon Tetrachloride, I. *J. D. Minford, M. H. Brown, and R. H. Brown* 185

Reaction of Aluminum and Carbon Tetrachloride, II. *R. H. Brown, E. H. Cook, M. H. Brown, and J. D. Minford* 192

Copper-Activated Calcium Orthophosphate and Related Phosphors. *Y. Uehara, Y. Kobuke, and I. Masuda* 200

Crystal Growth of Electrodeposited Zinc. An Electron Diffraction and Electron Microscopic Study. *R. Sato* 206

Changes in Trapping Levels of Zinc Sulfide Phosphors Resulting from Positive Ion Bombardment. *W. T. Allen and C. H. Bachman* 211

Influence of Firing Conditions, Composition, and Screening Media on the Zeta Potentials of ZnS Phosphors as Related to Adherence to Glass Surfaces. *B. Levy* 218

Associated Donor-Acceptor Luminescent Centers in Zinc Sulfide Phosphors. *E. F. Apple and F. E. Williams* 224

Effect of Various Etches on Recombination Centers at Germanium Surfaces. *G. Wallis and S. Wang* 231

Principles and Applications of the Iodide Process. *A. C. Loonam* 238

Techniques and Results of Zone Refining Some Metals. *J. H. Wernick, D. Dorsi, and J. J. Byrnes* 245

Effects of Electrolytes and of Gelatin on the Half-Wave Potentials of Carbon Tetrachloride, Dibromoacetate, and p-Dinitrobenzene. *L. E. I. Hummelstedt and L. B. Rogers* 248

Kinetics of the Cathodic Reduction of Anions: Germanium Oxides. *M. Green and P. H. Robinson* 253

The Electrical Conductivity of Sweat, II. The Interionic Attraction Factor and the Conductivity of Undiluted Sweat in the Study of Cystic Fibrosis. *A. J. deBethune, T. S. Licht, M. Stern, and H. Shwachman* 261

The System LiF-LiCl, LiF-NaCl, LiF-KCl. *H. M. Haendler, P. S. Sennett, and C. M. Wheeler, Jr.* 264

Technical Notes

Study of Magnetic Oxides by Cathode Rays. *S. Yamaguchi* 268

The Mechanism of Blackening of Nickel Anodes. *T. C. Franklin and J. Goodwyn* 269

ZnS Phosphors with P, As, Sb Coactivators. *E. F. Apple* 271

Brief Communication

Titanium Coatings on Molybdenum Wire. *R. L. Bronnes* 272

Philadelphia Meeting Program **45C-76C**

Current Affairs **78C-87C**

Published monthly by The Electrochemical Society, Inc., from Manchester, N. H., **Executive Offices, Editorial Office** and **Circulation Dept.**, and **Advertising Office** at 1860 Broadway, New York 23, N. Y., combining the JOURNAL and TRANSACTIONS OF THE ELECTROCHEMICAL SOCIETY. Statements and opinions given in articles and papers in the JOURNAL OF THE ELECTROCHEMICAL SOCIETY are those of the contributors, and The Electrochemical Society assumes no responsibility for them. Nondeductible subscription to members $5.00; subscription to nonmembers $18.00. Single copies $1.25 to members, $1.75 to nonmembers.

Copyright 1959 by The Electrochemical Society, Inc.

Entered as second-class matter at the Post Office at Manchester, N. H., under the act of August 24, 1912.

KEITHLEY MODEL 502 MILLIOHMMETER

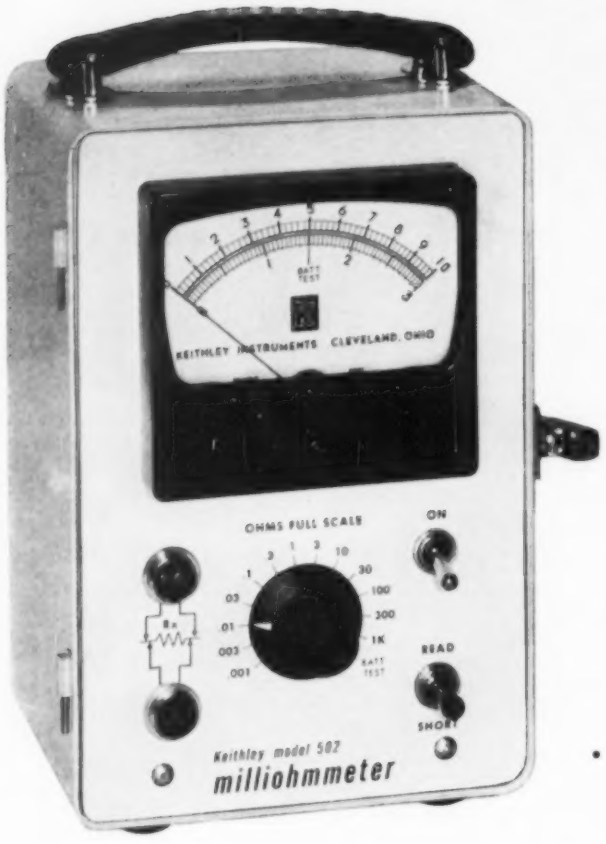

measures resistances down to 30 *micro-ohms with only two micro-watts through sample*

THE KEITHLEY MODEL 502 provides fast, accurate, easy measurement of low resistances. Its linear scales assure high resolution on 13 overlapping ranges from 0.001 ohm to 1000 ohms full scale, minimum detectable resistance is about 30 micro-ohms, and maximum dissipation through a sample is two micro-watts. Full scale accuracy is within 3%, except on the one-milliohm range where it is within 5%.

FEATURES include instantaneous indication of resistance without zero drift, calibration adjustments, or errors due to thermal EMF's; battery operation; ruggedized construction, light weight and a protective cover.

USES of the Model 502 include measurements of conductivity in semi-conductors and liquids, corrosion tests, and checking resistivity of relay contacts, printed circuits, fuses and grounding systems. Emphasis on safety makes it ideal for field tests of squibs, carbon bridges and similar explosive devices.

SEND TODAY for your copy of Keithley Engineering Notes, Vol. 6, No. 3, containing detailed data about the Model 502.

MODEL 502 measuring 0.008 ohm printed circuit path. Four terminal measuring system eliminates errors due to clip and lead resistance.

BRIEF SPECIFICATIONS

RANGES: linear scales with 13 overlapping ranges from 0.001 ohm to 1000 ohms full scale.

ACCURACY: within 3% of full scale on all ranges except the 0.001 range, where it is 5%.

MAXIMUM POWER DISSIPATION through a sample is normally two micro-watts; with a component failure, four micro-watts.

PRICE: $375.00

KEITHLEY INSTRUMENTS, INC.
12415 EUCLID AVENUE CLEVELAND 6, OHIO

GRACE Si

For

low boron

content . . .

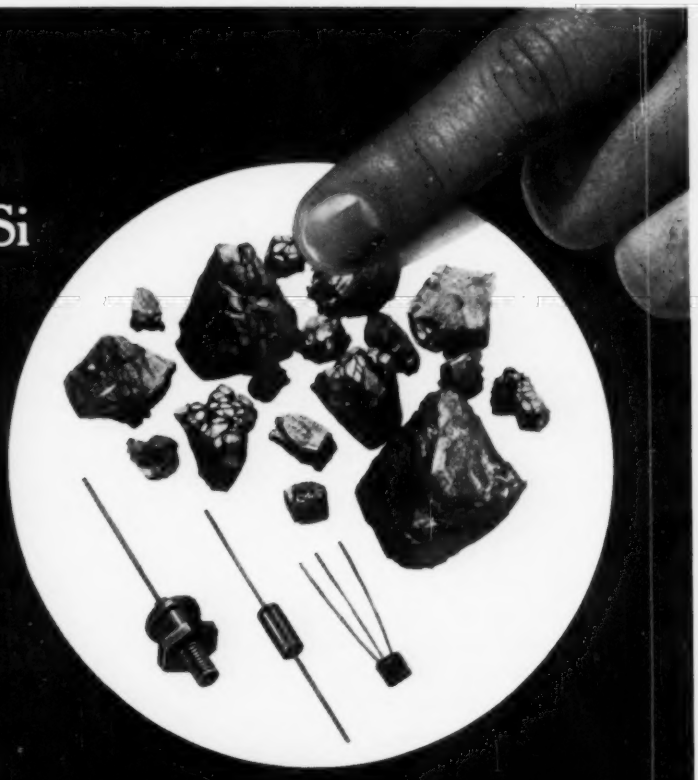

GRACE SILICON

(*ultra-high-purity*)

"For want of a nail the battle was lost" becomes painfully true when translated to lack of purity in the semi-conductor material you choose for your transistors, diodes or other silicon devices.

The Pechiney process, used in the manufacture of Grace Silicon, is noted for a product with low boron content as well as overall high purity.

May we suggest that whenever top quality silicon is desired—silicon combining both high purity and uniform quality—you get in touch with GRACE ELECTRONIC CHEMICALS, INC., at PLaza 2-7699, 101 N. Charles Street in Baltimore.

GRACE ELECTRONIC CHEMICALS, INC.

101 N. Charles St., Baltimore, Maryland

Subsidiary of W. R. GRACE & CO.

Editorial

Tuas Res Agitur

IN a fascinating editorial in the December 26, 1958 issue of *Science*, Graham DuShane brings us up to date on the fantastic story of the "battery additive" AD-X2 and the relations between its manufacturer and seller and the U. S. Government. This almost unbelievable, true story is a case of primary concern to every one of us, both as chemists and as private citizens.

You may recall that the product AD-X2 was tested by the National Bureau of Standards in 1952, at the request of the Post Office Dept. and the Federal Trade Commission. According to the Bureau's report, it was found to have no beneficial effect on battery performance. The resulting controversy led to the resignation (by request) of Allen V. Astin as director of the Bureau, in 1953, and his ultimate reinstatement to that position by the Secretary of Commerce. However, because of enthusiastic testimonials by users, all charges of false and misleading advertising by the manufacturer of AD-X2 were dismissed by the Federal Trade Commission, and the company was able to resume its former advertising and selling methods.

Obviously, the Federal Government had interfered with the operation of a private business, causing damage and financial loss to the company and its owner. In such circumstances, there are various ways of seeking redress. For example, if the owner of a mink (or skunk) farm suffers damage because of low-flying Army planes, it may be possible to make a direct appeal to Congress for damages. In the case at point, John J. Allen, Jr., Representative from California, introduced a bill "for the relief of Pioneers, Incorporated, and Jess M. Ritchie, individually." By resolution introduced by Representative Allen, the case was referred to the Court of Claims for investigation and recommendation. A petition to the Court by Pioneers, Inc., asks for compensation to the extent of more than $2,000,000. In the meantime, Allen is no longer a member of Congress but is quite likely to be Undersecretary of Commerce, by Presidential appointment.

Many preparations sold as battery additives have been investigated by the Bureau of Standards and elsewhere, and found to be worthless. They usually consist of a simple salt or mixture of salts, sold with glowing claims at many times their cost. Thanks to the Federal action in 1953, they are freely available in automobile supply stores and from mail-order houses. The principal ingredient also is sold widely as a promoter of bacterial action in septic tanks and cesspools.

It is, of course, not unusual to find simple, cheap materials sold at comparatively high prices, in containers which cost more than the contents. If such preparations serve a purpose, and the sellers do not make extravagant, unfounded claims, no one is the loser, because the convenience, the saving of time and bother, and the service rendered make the price insignificant. But, we have every right to expect that the honest findings of Government agencies which have been set up to protect the public will be respected and supported by other Government agencies, by the Congress, and by the Administration. Truly, some of the "shenanigans" of our lawmakers and administrators can put the pitiful imaginations of our science fiction writers to shame!

—CVK

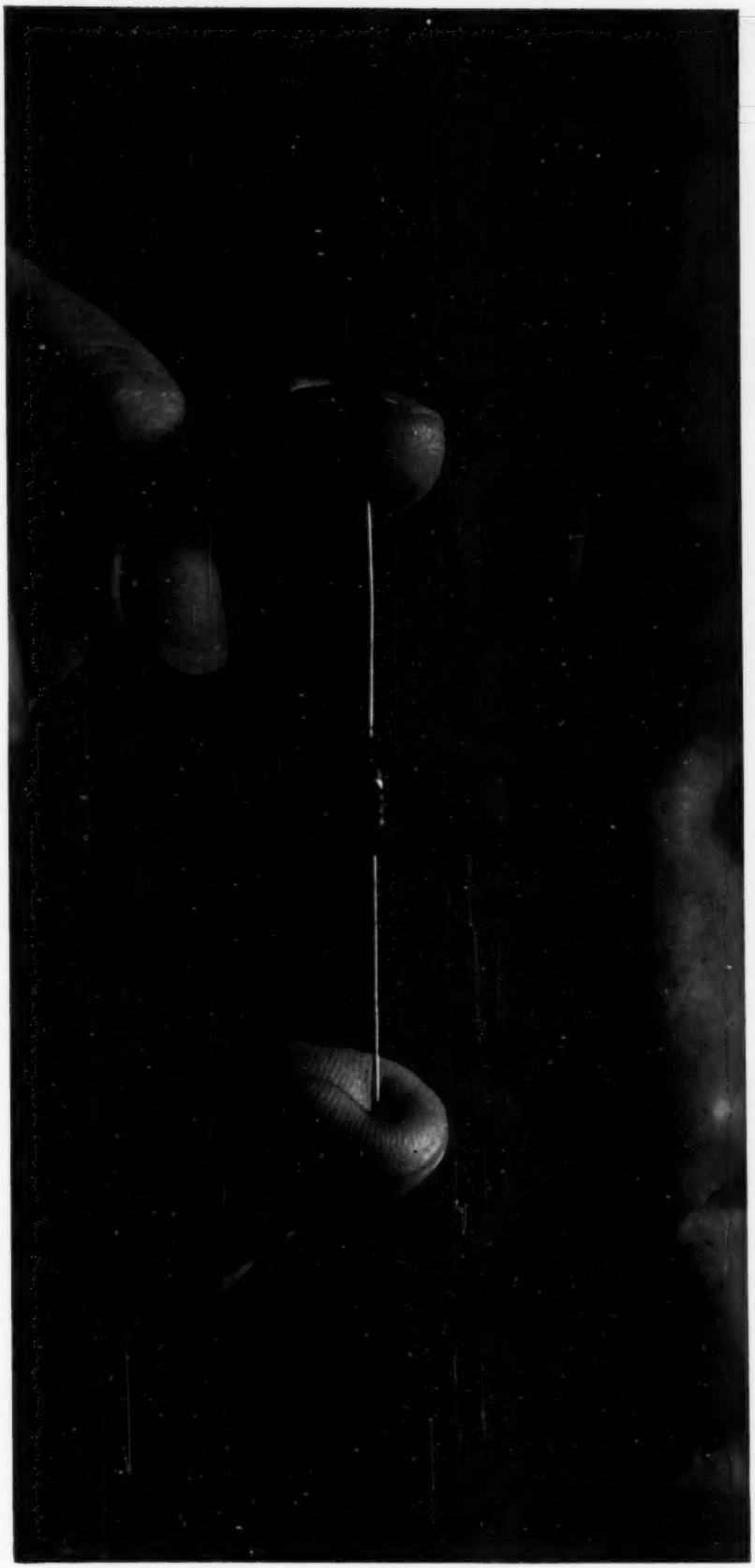

semiconductor research and development

Advanced research and development activity at Hughes Products, the commercial activity of Hughes, is opening new vistas in the semiconductor field. Representative programs underway include:

Basic research on semiconductor surfaces, alloying and diffusion techniques, and materials characterization studies to determine electrical effects of imperfections and impurities.

Development of new semiconductor devices such as parametric amplifiers, high frequency performance diodes, and improved types of silicon transistors.

New techniques for casting silicon into various configurations. These techniques may be extended to a broad field associated with infra-red applications.

Development of new intermetallic compounds for use in devices, resulting in superior device performance characteristics.

These are but a few of the many semiconductor research and development projects undertaken by Hughes Products. To delve further into these, and other semiconductor areas, an immediate need exists for Solid State Physicists, Physical Chemists, Physical Metallurgists, and Electronics Engineers, United States Citizenship is not a requirement. Investigate further by writing to Mr. Charles Blocher at the address below. All inquiries will be treated with strict confidence.

Creating a new world with electronics

HUGHES PRODUCTS

©1959, HUGHES AIRCRAFT COMPANY

International Airport Station
Los Angeles 17, California

THEY PROBE THE FUTURE OF DEEP-SEA TELEPHONY

"Dry Land Ocean," under construction at Bell Laboratories, simulates ocean floor conditions, is used to test changes in cable loss. Sample cables are housed in pipes which contain salt water under deep-sea pressure. The completed trough is roofed in and is filled with water which maintains the pipes at 37° F., the temperature of the ocean floor.

Deep in the ocean, a submarine telephone cable system is extremely hard to get at for adjustment or repair. This makes it vitally important to find out what can happen to such a system *before* it is installed.

Bell Laboratories engineers do this by means of tests which simulate ocean floor conditions on dry land. Among many factors they test for are the effects of immense pressures on amplifier housings and their water-resistant seals. They also test for agents which work very slowly, yet can cause serious destruction over the years—chemical action, marine borers and several species of bacteria which strangely thrive under great pressures.

Through this and other work, Bell Telephone Laboratories engineers are learning how to create better deep-sea telephone systems to connect America to the rest of the world.

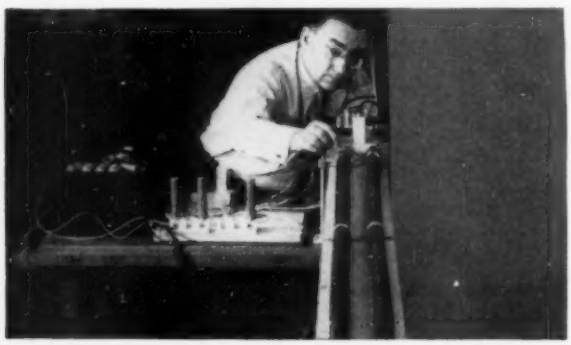

Highly precise instruments developed by Bell Laboratories engineers are used to detect infinitesimal changes in cable loss—to an accuracy of ten millionths of a decibel.

Seawater and sediment in bottle characterize ocean floor. Test sample of insulation on coiled wire is checked for bacterial attack by conductance and capacitance tests.

BELL TELEPHONE LABORATORIES

WORLD CENTER OF COMMUNICATIONS
RESEARCH AND DEVELOPMENT

Ammonia Vapor Activated Batteries

H. S. Gleason and J. M. Freund

Apparatus & Optical Division, Eastman Kodak Company, Rochester, New York

and L. J. Minnick and W. F. Meyers

G. and W. H. Corson, Inc., Plymouth Meeting, Pennsylvania

ABSTRACT

A new type of reserve battery is described. In storage, the solvent for the electrolyte, liquid ammonia, is kept separate from the dry, deliquescent solute. On activation, ammonia vapor is released to condense rapidly in the cells and energize the battery. A large number of practical cells can be built using this principle. Characteristics of several are presented. Some properties of electrolytes in liquid ammonia are also discussed.

For more than a century the solvent properties of liquid ammonia have intrigued chemists. A large body of literature has derived from the research of Franklin and of Kraus and their students. Franklin (1), Audrieth and Kleinberg (2), and Sneed, *et al.* (3) have surveyed liquid ammonia chemistry.

Many substances dissolve in liquid ammonia to form conducting solutions. Most investigators have been concerned with dilute solutions, particularly their behavior with respect to relationships such as those of Debye and Hückel, Onsager, and Walden. The solutions used in the batteries under discussion are highly concentrated, and, as in the case of concentrated aqueous solutions, adequate theoretical relationships between various properties and concentration have not been derived. The literature on concentrated solutions deals largely with the solubility of salts at various temperatures. This information is well summarized by both Audrieth and Kleinberg (2) and Sneed, *et al.* (3). Data are also given by Seidell (4).

Vapor pressure studies on the systems NH_4SCN-NH_4NO_3-NH_3 and NH_4SCN-NH_3-H_2O were made by Foote, Brinkley, and Hunter (5-7) and on solutions of NH_4Cl, NH_4Br, NH_4I, and NH_4NO_3 in NH_3 by Hunt and Larsen (8).

The conductance at −40°C of solutions of eighteen salts was measured by Pleskov (9), whose data extend only to regions of moderate concentration. Specific conductances at 0°C for the system NH_4SCN-NH_3 are given by Foote and Hunter (7).

Standard oxidation potentials in liquid ammonia are discussed by Jolly (10) whose table includes most of the previously published data. A series of papers on potentiometric titrations in liquid ammonia has been published by Watt and his students (11).

The development of ammonia vapor activated batteries derives from research into the recovery of calcium from lime deposits carried out by Minnick and Presgrave (12), who developed a process for electrowinning this metal from solutions of its salts in liquid ammonia at −50°C. The process was later enlarged to include other materials such as alkali metals. In the course of investigating these cells, a rechargeable current-producing cell system capable of delivering about 4.5 v was discovered. It was possible to operate lamps and other devices for a considerable period with the cell at −50°C. The physical chemistry of electrolyte solutions potentially desirable for use in batteries was extensively studied by Minnick, Presgrave, and Meyers, and the behavior of elementary cells incorporating various electrodes was investigated with the particular objective of high-rate, short-duration discharge. Many cells suitable for such applications were found to self-discharge rapidly and were deemed unsatisfactory for batteries in general.

An interesting discovery during these studies was that a cell could be built in which one constituent of the electrolyte was placed in a dry condition between the electrodes. Activation of the cell was accomplished merely by exposure to a vapor, in this case ammonia. Among the advantages of gas or vapor activation is the fact that there is no liquid to be moved as in the conventional types of reserve batteries. The geometry of the stack is therefore less critical and internal short circuits arising from electrolytic paths across edges are virtually eliminated.

Electrolytes

The ammonium salts, which are the acids in liquid ammonia chemistry, and salts with nitrogen-containing anions are useful as solutes for AVA (ammonia vapor activated) batteries. NH_4SCN solutions, for example, have been found particularly effective. On exposure of the dry salt to ammonia vapor, condensation occurs rapidly, forming a colorless solution. The vapor pressure of saturated solutions is less than 4% of that of pure ammonia at temperatures between −55° and +75°C and never exceeds 1 atm in this range. For some solutions formed in AVA batteries, pressures may be well above atmospheric under extreme environmental conditions.

The conductance of NH_4SCN solutions is high over a wide temperature range and has a smaller temperature coefficient than is characteristic of

aqueous solutions. Foote and Hunter (5) list specific conductances at 0°C ranging from 0.20 to 0.11 ohm^{-1} cm^{-1} for solutions ranging from 25 to 43 mole % NH_4SCN. This high conductivity is related in part to the low viscosity of the solvent.

Other solutes and mixtures of solutes have been used successfully in AVA cells, although in most instances the rate of condensation is appreciably slower than when NH_4SCN is used.

Electrodes

The principal metals used for anodes have been magnesium, zinc, and lead. The magnesium has usually been an alloy of the AZ31 series, but pure vapor-deposited magnesium has also been tried. Both rolled zinc, either pure or containing a small percentage of lead and cadmium, and electroplated zinc have been used. The lead anodes have generally been electrodeposits, but some tests were made using lead foil. In no case has there been any appreciable difference in performance between the "pure" coatings and the alloys. Experiments have also been performed using cadmium, lithium, lithium-aluminum alloys, calcium, and other anodes.

Much of the work has included the use of manganese dioxide and lead dioxide cathodes. The former has been electro ore mixed with carbon black for the most part, but some tests have also been run with MnO_2 electrodeposited on carbon rods. The lead dioxide has usually been electrodeposited on a stainless steel base. An extensive test program using silver chloride and silver oxide cathodes was fairly successful. However, the high solubility of silver compounds in ammonia limits their usefulness for many applications. Numerous other materials can be used as cathodes.

Structures

Most of the development studies on AVA cells have been carried out using cells of laminar construction. Thin electrodes were blanked from strip stock, between which one or more dry electrolyte pads were placed. The basic experimental cells have been annular in shape, with NH_3 admitted from the center. Electrolyte pads have comprised a porous vehicle, of which filter paper is a typical example, impregnated from an aqueous solution of the desired salt and dried. It has been found that for a given vehicle, the weight of salt impregnated per unit area from a solution of given concentration is reproducible within 10%, even with rudimentary controls, and that the uniformity of impregnation of the vehicle in sheet form is acceptable. Inclusion of more than one electrolyte pad in a cell permits the use of differing amounts of salt in the catholyte and the anolyte pads. Some 20 cellulose papers ranging in free volume from 35 to 82% and two glass fiber papers of 29 and 95% free volume have been used.

In the cells using MnO_2-C as the depolarizer mix, a somewhat similar construction has generally been employed. The basic cells have been sandwiches of circular disks, with NH_3 admitted from the outer perimeter. The anode has been the same type of material used in the annular cells. The pads, however, have been blanked and then impregnated by addition of a definite volume of solution from a buret. The MnO_2-C has been pelletized by compression, and a carbon cathode has been used. Corson has also done some work with cylindrical cells using variations of the typical Leclanché cell structure.

Cells are connected as required by the application and are placed in a suitable container, which to date has been either steel or aluminum, although magnesium is also practical. The ammonia source may be either external, in which case a suitable fitting is provided, or internal, using a releaser within the battery actuated by a mechanical or electrical impulse. Depending on the rapidity of activation required, a source of heat may be included in the releaser to achieve rapid evaporation of NH_3.

The container is hermetically sealed after evacuation to a "soft" vacuum of 1 mm Hg or slightly less, primarily to remove all but the last traces of water or NH_3 and to avoid back pressure in the cells. The battery is provided with an exhaust hole over which a cap is soldered under vacuum. The cap may be unsoldered in an ammonia atmosphere and the battery checked electrically. The NH_3 is then exhausted, the battery re-evacuated, and the cap resoldered returning the battery to an inert condition. This feature is unique among reserve batteries insofar as the authors are aware, and should enhance the reliability of the product.

Cell Characteristics

The program to evaluate design parameters has comprised thousands of cell discharges. Each particular construction of cell has been tested at room temperature by discharge at constant current immediately after activation from a source of NH_3 at about 10 atm to depletion of the cell by exhaustion of depolarizer or electrolyte. The evaluation has included tests at several current densities. Variations in construction have involved (*a*) the anode metal, (*b*) the amount of depolarizer on the cathode, and (*c*) the type of electrolyte vehicle and the effect of varying the salt content thereof. The more promising constructions are then evaluated at several temperatures and also by testing after various periods of activated stand.

The nature of the electrolyte solutions has dictated that even the most elementary tests be conducted in special test vessels; working in open vessels or in glass is impractical. For repeated use in test equipment, parts coming in contact with cell components are best made of Teflon or polyethylene, although nylon is adequate unless the stand time or discharge is prolonged. Insulation of wires requires also that Teflon, nylon, polyethylene, or similar materials be used.

As expected, there is no one combination of components that gives the best performance under all conditions. Figures 1, 2, and 3 present discharge voltages as a function of delivered capacity for the $Mg/NH_4SCN/PbO_2$, $Zn/NH_4SCN/PbO_2$, and $Pb/NH_4SCN/PbO_2$ systems, using for each the construction

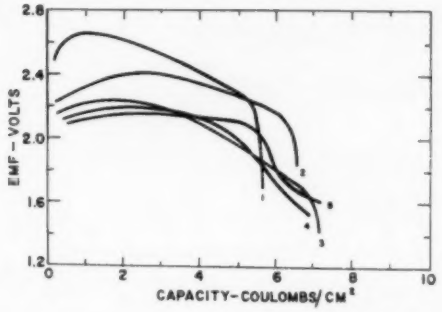

Fig. 1. Discharge characteristics of $Mg/NH_4SCN/PbO_2$ AVA cells at 25°C (77°F).
(Theoretical capacity, based on NH_4SCN, 10 coulombs/cm²)

Curve	Current density	
	ma/cm²	ma/in.²
1	7.7	50
2	15.5	100
3	23.7	153
4	35.3	228
5	47.3	305

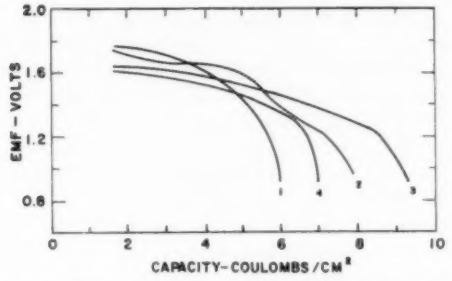

Fig. 2. Discharge characteristics of $Zn/NH_4SCN/PbO_2$ AVA cells at 25°C (77°F).
(Theoretical capacity, based on NH_4SCN, 12 coulombs/cm²)

Curve	Current density	
	ma/cm²	ma/in.²
1	23.7	153
2	35.3	228
3	59.2	382
4	70.8	457

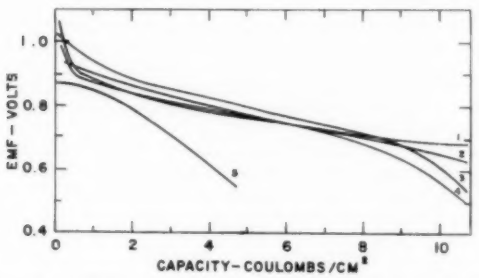

Fig. 3. Discharge characteristics of $Pb/NH_4SCN/PbO_2$ AVA cells at 25°C (77°F).
(Theoretical capacity, based on PbO_2, 11 coulombs/cm²)

Curve	Current Density	
	ma/cm²	ma/in.²
1	0.15	0.95
2	1.5	9.5
3	7.4	47.5
4	29.4	190
5	88	570

that has thus far given the most energy per unit volume of cell. The most efficient Mg and Zn cells, on this basis, are electrolyte limited. Their capacity depends on the amount of NH_4SCN initially in the cell and not on the total amount of PbO_2 present. On the other hand, Pb cells with the same amounts of NH_4SCN and PbO_2 are limited in capacity by the depletion of PbO_2. This results from the relatively rapid reaction of Mg and Zn with the acid solution, which removes NH_4^+ ion that would have been available for the cathode reaction. Lead, however, is cathodic to hydrogen in acid solutions in ammonia. This makes it possible to operate lead cells for long periods at very light loads or after extended activated stand, whereas Mg or Zn cells are subject to rapid self-discharge. Figures 4, 5, and 6 show capacity to depletion of Mg, Zn, and Pb cells, respectively, as a function of current density. Current densities are cited in terms of the equal apparent areas of the electrodes. The effect of self-discharge in the Mg and Zn cells may be perceived by comparing the ordinates with the theoretical capacities of 10 and 12 coulombs/cm², respectively. At current densities below 31 ma/cm² (200 ma/in.²), the Pb cells operate essentially at 100% cathode efficiency. If the proportion of NH_4SCN in Mg or Zn cells is made large with respect to the amount of PbO_2 on the cathode, the PbO_2 can be made limiting so that efficiency of Mg or Zn cells approaches 100% based on PbO_2. The energy density suffers considerably in doing this.

Figure 7 shows the effect of temperature on cell capacity for the $Zn/NH_4SCN/PbO_2$ system. The results are attributed to more rapid corrosion of the Zn as the temperature is increased.

Tests of the $Mg/NH_4SCN/MnO_2$-C cell have been concerned with modifications of the electrolyte to reduce or eliminate the self-discharge at the anode. Self-discharge in this system can be reduced significantly by using additives that buffer the electrolyte, neutral salts such as $Mg(SCN)_2$, or substances that limit the diffusion of NH_4^+ ion toward the anode to a rate less than that of transport toward the cathode.

The ability to evacuate AVA cells rapidly has been used to obtain information on chemical changes as a function of stand time and discharge. Such tests show qualitatively that on activation there is a reaction between MnO_2 and SCN^- ion, resulting in an appreciable decrease in the available oxygen of the depolarizer mix. However, a product of this reaction is presumably thiocyanogen, which is available as a depolarizer in the cell, but which is leached from the MnO_2 prior to analysis for available oxygen. The increase in Mg^{++} ion in the cell was found to be the sum of the amounts formed by self-discharge, as determined from stand tests without discharge and the amount electrochemically equivalent to the capacity delivered.

A unique apparatus for analyzing the characteristics of the components of operating cells has been developed by Meyers. It involves a Haring cell operated with breaker techniques. It is intended to describe this test method in a future paper. Tests

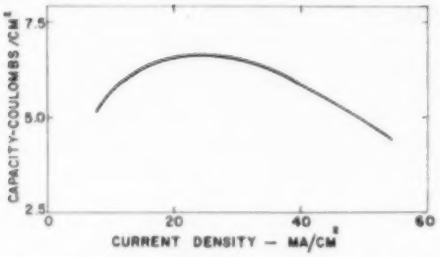

Fig. 4. Capacity to NH_4SCN depletion for Mg/NH_4SCN/PbO_2 AVA cells at 25°C (77°F). Theoretical capacity = 10. coulombs/cm².

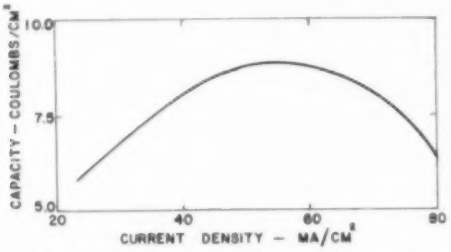

Fig. 5. Capacity to NH_4SCN depletion for Zn/NH_4SCN/PbO_2 AVA cells at 25°C (77°F). Theoretical capacity — 12 coulombs/cm².

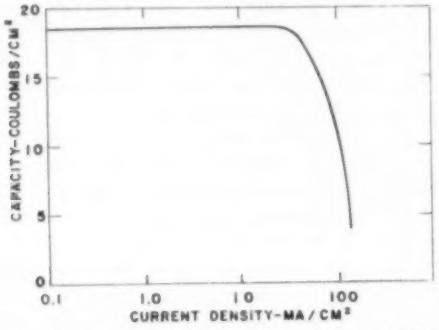

Fig. 6. Capacity to PbO_2 depletion for Pb/NH_4SCN/PbO_2 AVA cells at 25°C (77°F). Theoretical capacity — 18.6 coulombs/cm².

of the Mg/NH_4SCN/MnO_2-C cell showed that anode polarization increases at a small constant rate during discharge. The anode, electrolyte, and over-all cell resistances also increase linearly during discharge. The resistivity of the cells was initially 55 ohm-cm and increased to 100 ohm-cm during complete discharge (to 0 v), the major part of the increase being in the anode film. Similar evaluation of cells with PbO_2 cathodes is now in process. Surge discharges of Pb/PbO_2 cells of 0.3 amp/cm² (2.0 amp/in.²) for 10 msec result in over 80% instantaneous recovery of voltage on removal of the load, and complete recovery within 2 msec. Surges of 0.15 amp/cm² (1.0 amp/in.²) for 100 msec result in better than 90% recovery in 10 msec.

Although few tests have been conducted at temperatures below −25°C, liquid system reserve batteries have operated as well at −55°C as at room temperature. Small vapor activated batteries have also been successfully activated and operated at −55°C. On the basis of work to date, the capabilities of AVA batteries appear to lie in the range

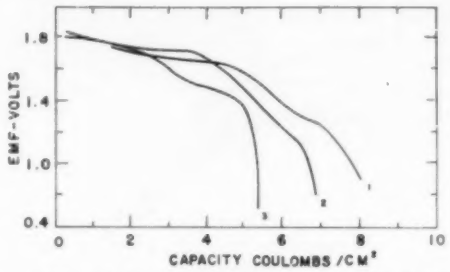

Fig. 7. Effect of temperature on discharge of Zn/NH_4SCN/PbO_2 AVA cells at 35.3 ma/cm² (228 ma/in.²). Curve 1 at 25°C, curve 2 at 50°C, curve 3 at 70°C.

of 1.0 wmin/cm³ (0.3 whr/in.³) for high rate discharges (over 25 ma/cm²) to more than 3.6 wmin/cm³ (1 whr/in.³) for low rate applications (under 3 ma/cm²). These are equivalent to a range of 0.6 to 2.5 wmin/g (5 to 20 whr/lb).

Acknowledgments

The development program has received support for the Department of Defense under several research and development contracts. The data reported in this paper were obtained in the course of work sponsored by the United States Army Signal Engineering Laboratories under Contracts DA-36-039 SC-71232 and DA-36-039 SC-72306.

The authors wish also to acknowledge the important roles in this program of C. Presgrave of G. and W. H. Corson, Inc., and of T. A. Hale, K. R. Scribner, J. R. Flynn, and V. M. Bryant, Jr., of the Eastman Kodak Company.

Manuscript received Nov. 25, 1957. This paper was prepared for delivery before the Buffalo Meeting, Oct. 6-10, 1957.

Any discussion of this paper will appear in a Discussion Section to be published in the December 1959 JOURNAL.

REFERENCES

1. E. C. Franklin, "The Nitrogen System of Compounds," Reinhold Publishing Co., New York (1935).
2. L. F. Audrieth and J. Kleinberg, "Non-Aqueous Solvents," John Wiley & Sons, Inc., New York (1953).
3. "Comprehensive Inorganic Chemistry," M. C. Sneed and R. C. Brasted, Editors, Vol. 5; "Nitrogen, Phosphorus, Arsenic, Antimony, and Bismuth" by H. H. Sisler; and "Nonaqueous Chemistry" by A. R. Pray, D. Van Nostrand Co., Inc., Princeton, N. J. (1956).
4. A. Seidell, "Solubilities of Inorganic and Metal-Organic Compounds," 3rd ed., Vol. I, D. Van Nostrand and Co., New York (1940) and "Supplement to the Third Edition" (1952).
5. H. W. Foote and M. A. Hunter, *J. Am. Chem. Soc.*, **42**, 69 (1920).
6. H. W. Foote and S. R. Brinkley, *ibid.*, **43**, 1018 (1921).
7. H. W. Foote, *J. Am. Chem. Soc.*, **43**, 1031 (1921).
8. H. Hunt and W. E. Larsen, *J. Phys. Chem.*, **38**, 801 (1934).
9. V. Pleskov, *Acta Physicochim. U. R. S. S.*, **5**, 509 (1936).
10. W. L. Jolly, *J. Chem. Ed.*, **33**, 512 (1956).
11. For example, G. W. Watt and D. M. Sewards, *This Journal*, **102**, 46 (1954) which also gives references to earlier papers.
12. L. J. Minnick and C. Presgrave (to G. and W. H. Corson, Inc.) U. S. Pat. 2,615,838, Oct. 28, 1952.

General and Intergranular Corrosion of Austenitic Stainless Steels in Acids

Effect of Cations in the Acids and the Influence of Heat Treatment and Grain Size of the Steel

Michael A. Streicher

Engineering Research Laboratory, Engineering Department, E. I. du Pont de Nemours & Co., Inc., Wilmington, Delaware

ABSTRACT

Corrosion of stainless steels by nitric acid is determined largely by the crystallography of grain boundaries. There is preferential attack even on annealed steels. Increasing the rate of dissolution, either by an anodic current or by oxidizing cations, intensifies intergranular penetration. The same crystallographic factors which determine preferential corrosion also determine the precipitation of chromium carbides. Their presence leads to a very great intensification of intergranular attack, as does sigma phase, even as an invisible, pre-precipitation constituent.

Oxidizing cations, such as Cr^{+6}, Ce^{+4}, and Fe^{+3}, increase the corrosion of stainless steels in nitric acid by cathodic depolarization, by shifting the open-circuit potential of cathodic areas toward more noble values and, probably, by depolarization of anodic areas.

The effect of surface finish on corrosion rate is largely a function of the true (absolute) area produced by various finishes.

Ferric ions in ferric sulfate-sulfuric acid solution greatly inhibit general, or grain-face, corrosion by anodic polarization. In place of the reduction of hydrogen ions and the evolution of hydrogen gas at cathodic areas, ferric ions are reduced. The consumption of ferric ions is electrochemically equivalent to the weight of steel dissolved. On steels containing intergranularly precipitated chromium carbides, intergranular attack leads to dislodgment of grains and a readily detectable weight loss.

Data obtained in sulfuric acid solutions containing ferric nitrate in place of ferric sulfate suggest that it may be possible to develop a 24-hr evaluation test with this solution.

The action of cupric sulfate in copper sulfate-sulfuric acid solution is similar to that of ferric ions. However, intergranular attack on susceptible steels does not dislodge grains readily, and, therefore, weight loss cannot be used for routine evaluation of the results.

Intergranular attack in this solution is greatly accelerated by metallic copper immersed simultaneously with the stainless steel specimen or in contact with it. This acceleration is a result of the formation of cuprous ions and of galvanic action by copper, which is the anode of this couple. The resulting galvanic current and the cuprous ions reduce anodic polarization most readily at grain boundaries containing chromium carbide precipitate and thereby greatly increase the rate of intergranular penetration. Sigma phase does not lead to accelerated intergranular attack in this solution.

The influence of grain size on intergranular corrosion depends on the method used for measurement, change in electrical resistance or weight-loss, and composition of the corroding acid solution.

Dissolution of stainless steels in all three acid solutions is predominantly under anodic control. The difference in grain surface corrosion and in intergranular penetration at susceptible boundaries is attributed primarily to a lower anodic polarizability of the metal in such grain boundary zones rather than to any difference which may exist in the open-circuit potentials of grain surfaces and grain boundaries.

The intensity of intergranular attack on stainless steels exposed to certain acid solutions may range from light etching of grain boundaries, which merely outlines the granular structure, to intense penetration, which may lead to complete loss of mechanical strength or even disintegration of the metal. Whether corrosion is predominantly by intergranular or by general attack depends on the difference in the rate of corrosion of the grain-boundary zones and of the grain faces. This difference in rates is determined by

the structure and composition of the grain boundaries and by the composition of the corroding solution.

In the present investigation a detailed study has been made of the type of intergranular attack produced by three acid solutions which are used, or have been proposed for use, in evaluation tests. These are nitric acid, ferric sulfate-sulfuric acid, and copper sulfate-sulfuric acid solutions. Special attention has been given to the electrochemical action of the cations encountered in these solutions, either as inhibitors of general corrosion or as corrosion products, which may accelerate or retard intergranular attack. Among the pertinent factors in the stainless steels, chromium carbides, sigma phase, and grain size have been investigated in their effect on intergranular attack.

It was essential to know whether or not a given specimen had been made susceptible previously to intergranular attack by heat treatments which formed intergranular precipitates of chromium carbides and/or sigma phase. The presence or absence of chromium carbide precipitate was determined by electrolytic etching in oxalic acid. This etch, originally described by Ellinger (1), has been developed into a standard testing method (2, 3). A 10% solution of oxalic acid is used for anodic etching at a current density of 1 amp/cm² for 1.5 min. In the absence of chromium carbides a "step structure" is formed, Figure 1A. Evidence of chromium carbide precipitate is shown by ditches at the grain boundaries. If the ditches do not envelope any one grain completely, the etch is classified as "dual structure," and if one or more grains are completely surrounded, as "ditch structure," Figure 1B. To detect susceptibility to intergranular attack associated with sigma phase, the steels were tested in nitric acid, since it was found that this is the only method which will detect the presence of certain kinds of sigma phase.

Corrosion in Nitric Acid

The investigations in nitric acid were made in boiling, 65% acid solution. This is the temperature and concentration of acid used in the standard nitric acid test (2) first proposed by Huey (4). In the standard test the weight loss of a specimen of known surface area (20-40 cm²) is determined after each of five 48-hr exposure periods. New acid is used for each of these periods. Tests are made in 1-liter wide-mouth Erlenmeyer flasks, containing 600 ml of acid. Evaporation is prevented by a "cold-finger" type of condenser and the specimens are held in glass cradles. (This apparatus was also used for tests with the other acids.) On a steel (Table I) which is resistant to accelerated intergranular attack, the corrosion rate (slope of annealed line, Fig. 2) is low and constant throughout the entire exposure period. The surface structure produced on this type of

Table I. Analyses of steels used

Steel AISI type	Code	Weight per cent					
		Cr	Ni	Mo	C	Si	Mn
304	FK-2	19.2	10.7	—	0.031	0.35	0.94
304	DT-2	18.3	10.7	—	0.06	0.45	0.098
304	HM-3	18.5	9.24	—	0.06	0.51	1.14
304	M304	18.3	9.3	—	0.063	0.37	0.80
316L	FI-4	16.2	13.2	2.2	0.020	0.47	1.6
316L	FH-5	17.7	13.2	2.40	0.026	—	—
316	M316	17.7	12.6	2.45	0.046	0.61	1.68
316L	FI-6	18.9	12.8	2.37	0.022	0.44	1.85
316L	EM-9	17.9	13.3	2.55	0.025	—	—
316L	FI-2	17.3	12.9	2.28	0.022	—	—
316L	FI-9	18.5	12.8	3.00	0.018	—	—
316	EW-6	17.4	12.7	1.89	0.053	0.44	1.60
316	GT-8	16.7	11.3	2.18	0.074	0.35	1.62

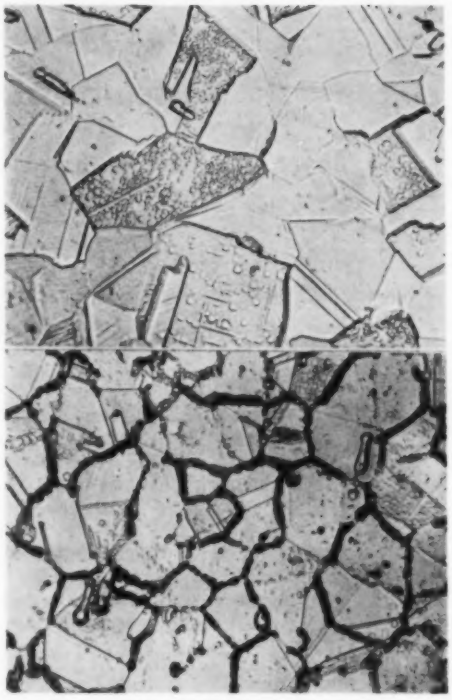

Fig. 1. Oxalic acid etch structure: A (top), annealed, step structure; B (bottom), heated 3 hr at 1250°F, ditch structure. Etched 1.5 min at 1 amp/cm². Steel AISI-304, FK-2 (analysis Table I). Magnification 500X before reduction for publication.

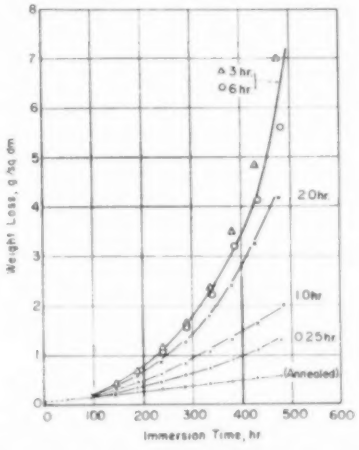

Fig. 2. Corrosion of AISI-304 stainless steel in boiling 65% nitric acid. Various degrees of susceptibility to intergranular attack produced by heating at 1250°F for periods indicated. Steel: FK-2, 0.031% C. (A weight loss of 1.0 g/dm² in 240 hr is equivalent to a corrosion rate of 0.0015 in./mo).

specimen during exposure to nitric acid is shown in Fig. 3A. It is apparent that even on a steel which is resistant to accelerated intergranular attack there is some etching at the grain boundaries which is so slow that it does not lead to undermining of these grains. In contrast, on susceptible specimens the attack at the grain boundaries leads to undermining and dislodgment of grains (Fig. 3B) and, consequently, to progressively increasing corrosion rates (slopes of tangents of curves in Fig. 2). The factors determining the rate of increase in slopes of these curves, such as composition of the steel, its heat treatment, and grain size, are dealt with throughout this discussion.

Influence of Surface Finish

The curves of Fig. 2 do not pass through the origin when extrapolated to zero exposure time, i.e., the corrosion rate at the beginning is high compared to the subsequent rate of attack. Specimens used for the tests of Fig. 2 were ground to an 80-grit finish. To determine whether this finish is responsible for the high initial corrosion rate, a number of specimens having other finishes, sand blasted, polished, and pickled, were exposed to nitric acid. Results have been plotted in Fig. 4 and show that both the high initial corrosion rate and the constant rate reached after 48-96 hr are a function of the type of surface finish.

On specimens having a smooth finish, produced by polishing or bright pickling, the corrosion rate is constant throughout the exposure period. Only when

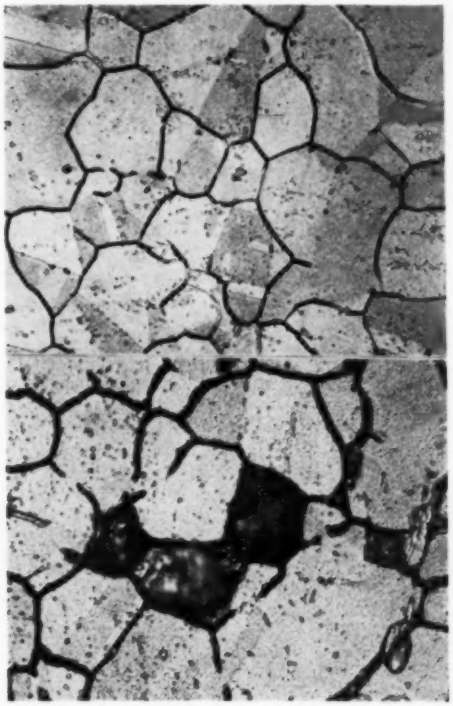

Fig. 3. Surface attack produced on AISI-304 steel after 80 hr of exposure to boiling 65% nitric acid. A (top), annealed; B (bottom), heated 3 hr at 1250°F. Steel: FK-2, 0.031% C. Magnification 500X before reduction for publication.

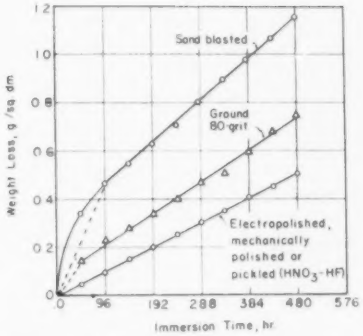

Fig. 4. Influence of surface finish on corrosion of AISI-304 steel in boiling 65% nitric acid. Annealed steel, heated 1 hr at 1950°F, W.Q.

the finishing operation produces sharp edges, as in grinding (abrading) or sand blasting, is there a high initial corrosion rate, which gradually decreases until it reaches a constant value.

Examination of the surface of the ground specimen at 750X shows that many edges and scratches on the ridges and valleys of the main grinding contours are eliminated during the first 50 hr of exposure. The main ridges remain, even after 500 hr of immersion, and suggest that the differences in corrosion rates during the period of changing rates and of constant slope (Fig. 4) are related to absolute areas. Thus, the slopes increase with the roughness of the surface finish. These observations are supported by some surface-area measurements made by O'Connor and Uhlig (5) on austenitic stainless steels. They found roughness factors (ratios of absolute to geometric areas) of 1.1 for electropolished, 1.4 for HNO_3-HF pickled, and 3.1 for (2/0) abraded finishes.

Unless otherwise noted, all specimens used in this investigation were given an 80-grit finish.

Stresses and metal deformation produced by surface treatments do not appear to have an appreciable effect on corrosion rates. The rate of the mechanically polished specimen is the same as that of the electropolished specimen. Also, it is of interest that the various surface finishes do not change the electrode potential of the steel when exposed to boiling 65% nitric acid. Measurements were made with the apparatus shown in Fig. 5.

Method of Measuring Electrode Potentials

The arrangement shown in Fig. 5 was used throughout this investigation to measure electrode potentials on stainless steels in boiling, concentrated acids. A 1-liter wide-mouth Erlenmeyer flask with a cold finger condenser was modified for this purpose. To make contact with the calomel cell a glass tube with a fritted glass filter at its end was sealed into the flask. This filter retarded movement of the acid electrolyte in and out of the flask. A glass tube was sealed into the condenser for the stainless steel wire used to make electrical contact with the specimen. This wire was welded to the specimen, covered with a plastic coating, and bent, as shown, to prevent condensate from running onto the specimen. At the top of the condenser, rubber tubing and a clamp were

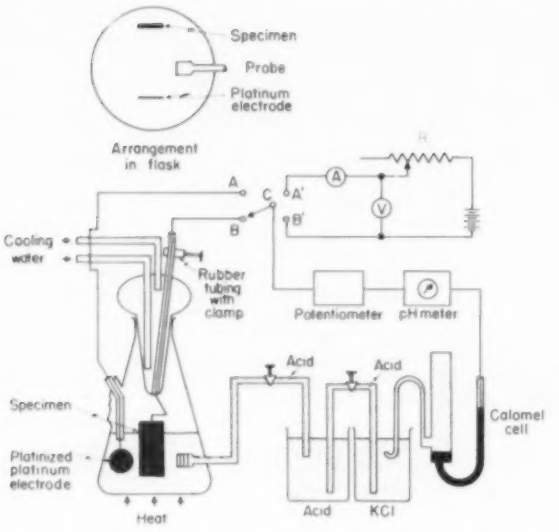

Fig. 5. Apparatus used for electrode potential measurements in boiling acids. As the reference cell, a saturated potassium chloride calomel cell was used.

used to prevent the loss of vapor from this glass tube. For anodic and cathodic polarization by an external current and for potential measurements, a platinized platinum electrode was inserted in the flask via a ground glass joint.

To prevent mutual contamination of acid electrolyte and the calomel cell, bridges were used. Only the flask was heated. The temperature of the calomel cell was 40°C. No temperature or junction potential corrections have been applied to the measurements reported.

Potential measurements on the stainless steel specimen or the platinum electrode were made by using a pH meter, with an impedance of 10^{10} to 10^{12} ohms, as a nil current indicator connected in series with a potentiometer (6). For polarization measurements, the circuit shown in Fig. 5 was used.

Effect of Corrosion Products

As the stainless steels dissolve, iron, chromium, and nickel corrosion products accumulate in the nitric acid solution. DeLong (7) has shown that, of

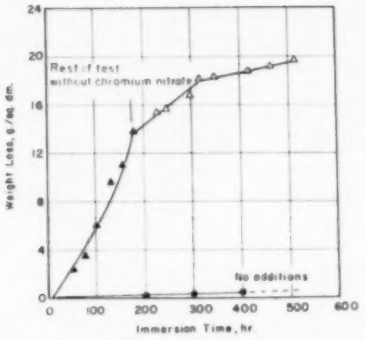

Fig. 6. Effect of chromium nitrate additions on the corrosion of AISI-304 in 65% boiling nitric acid. Steel: annealed condition, heated 1 hr at 1950°F, W.Q., HM-3. Addition: 1.26 g $Cr(NO_3)_3 \cdot 9H_2O$ in 600 ml acid for a solution containing 0.02% Cr (0.005 mole/liter). Solution changed every 24 hr.

these, only dissolved chromium affects corrosion in the concentrations likely to be encountered during evaluation tests. He found that concentrations greater than about 0.004% chromium (0.033 g Cr in 600 ml 65% nitric acid) greatly increase the rate of corrosion. Tests were made to determine the form and the mechanism of corrosion responsible for this great increase caused by dissolved chromium.

Previous investigators (8-11) have shown that acceleration is due to the action of chromium in the hexavalent state. When chromium dissolves in acids, it enters the solution as divalent ions, blue, which are rapidly converted to the trivalent state, green. These ions are then oxidized more gradually in nitric acid to the hexavalent state, orange. A green solution of 0.005 mole/l trivalent chromium in 65%, boiling nitric acid turns orange in 24 hr. For some of the tests described below, trivalent chromium was added to simulate as closely as possible the action of chromium dissolving from stainless steel.

A 1-cm^2 area was electropolished on the AISI-304 specimens for metallographic observation of the form of corrosion. New solutions were used every 24 hr. The weight-loss measurements have been plotted in Fig. 6, and microstructures are given in Fig. 7. Results on AISI-321 steel (not shown) were similar.

From these figures it is apparent that dissolved

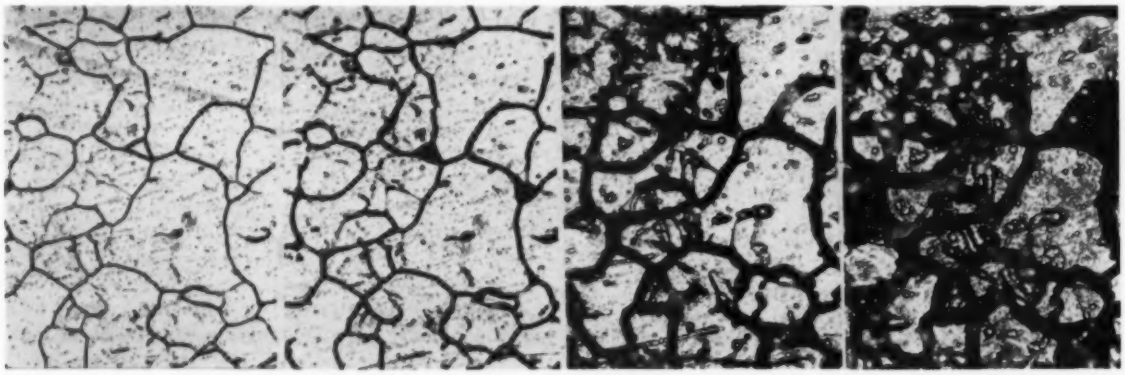

Fig. 7. Progressive attack of boiling 65% nitric acid containing dissolved chromium on annealed AISI-304 steel (HM-3). (Weight loss in Fig. 6.) Left, 15 hr; center left, 21 hr; center right, 47 hr; right, 96 hr. Magnification 250X before reduction for publication.

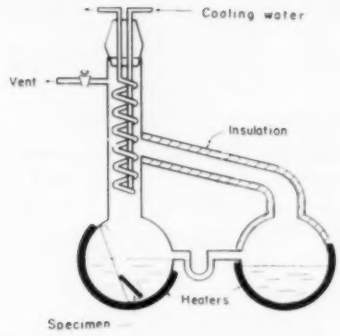

Fig. 8. Apparatus for continuous removal of soluble corrosion products from boiling solutions. Both 1-liter flasks are heated electrically. Corrosion products accumulate in specimen-free flask.

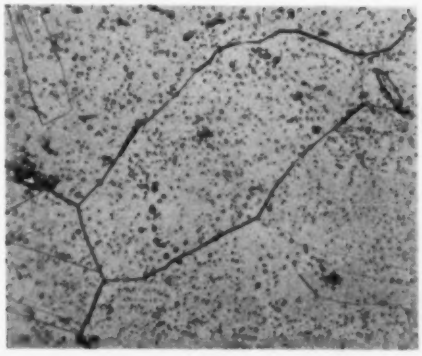

Fig. 9. Corrosion of annealed AISI-304 steel in pure nitric acid. Specimen exposed 254 hr to boiling 65% nitric acid in apparatus of Fig. 8. Magnification 500X before reduction for publication.

chromium greatly increases the weight loss of annealed stainless steels, largely as a result of accelerated intergranular attack. Grains are dislodged, even though both steels tested are in the annealed condition and do not contain any intergranularly precipitated chromium carbides or sigma phase. There is also some increase in general, or grain-face, corrosion, but most of the weight loss is due to grain dropping.

When a specimen which has been exposed to nitric acid containing chromium is immersed in pure nitric acid, the higher weight losses persist until these loosened layers have been removed completely. There is a gradual decrease in rate until the rate of the annealed steel is approached (Fig. 6).[1] Another factor which prolongs higher weight losses is the dissolution of the dislodged grains in the fresh nitric acid. Accumulation of hexavalent chromium is accelerated in this way.

Further tests on the effect of dissolved chromium were made to establish whether accelerated corrosion is by intergranular attack on other grades of stainless steels. Annealed specimens of AISI-304, 347, and 430 (17% Cr, no Ni) were immersed in boiling, 65% nitric acid containing direct additions of hexavalent chromium, 0.10 mole/l CrO_3. Within 2 hr very rapid intergranular attack produced dislodgment of appreciable numbers of grains on all three steels.

Continuous removal of corrosion products.—This intense intergranular attack on annealed steels produced by small amounts of added hexavalent chromium suggests that the chromium corrosion product which inevitably accumulates even during the 48-hr standard exposure periods used between renewal of acid may be the cause of grooving on annealed steel (Fig. 3A). The apparatus of Fig. 8 was used to determine whether there is intergranular grooving even when corrosion products are removed continuously. Its design is based on the principle of the multisample tester of DeLong (7). Each 1-liter flask contains about 500 ml of 65% nitric acid at the beginning of the test. The vapors from the solution containing the specimen (tester) are condensed and returned to this flask. Pure vapors from the other flask (boiler) are carried over to the cooling coil and condensed into the tester, causing a continuous overflow of solution containing corrosion products into the boiler, where they accumulate. This solution turns yellow during the test, while the solution with the specimen remains clear, even during a 500-hr test.

A metallographically polished specimen of annealed AISI-304 steel was exposed to 65% nitric acid for 516 hr in this apparatus without change of acid. The weight loss was 0.18 g. Analysis of the acid in the tester gave 1.1 ppm Fe, 0.12 ppm Ni, and less than 0.1 ppm Cr. Figure 9 shows the grooving at grain boundaries which took place even with continual removal of corrosion products.

In standard 48-hr flask tests the grain boundary grooves formed in this way accumulate chromium ion corrosion products, which then intensify the grooving action. The high corrosion rates observed on very small grained, annealed stainless steels are due to this type of action. Such steels have more grain boundaries per unit area of surface than large-grained steel. The grooving of very small grains may even lead to undermining and dislodgment of grains on annealed steels exposed to nitric acid solutions which are renewed every 48 hr.

Grain boundary grooves on annealed stainless steels may also be formed by making the steel anodic with an external current and an auxiliary electrode in 65% nitric acid (Fig. 10).[2] Longer etching or higher current densities make these grooves deeper and wider and lead to some grain dropping (Fig. 10B). Note the absence of grooves at the sides of twin boundaries (Fig. 10A). Preferential attack at grain boundaries of single-phase metals has also been found in other systems to be a function of the orientation of the two grains making up the boundary and its direction (12). Grooving in Fig. 3A and 9 shows evidence of this effect.

Mechanism of acceleration by oxidizing cations.—Hexavalent chromium is readily reduced at cathodic areas on steels exposed to acid solutions.

[1] Accelerated intergranular corrosion caused by precipitation of chromium carbides also is increased greatly by dissolved chromium in nitric acid. A concentration of 0.02% dissolved chromium increased the rate of a sensitized specimen by a factor of 10.

[2] These grooves are in contrast to the step structure produced on this same specimen by anodic etching in oxalic, sulfuric, and other acids.

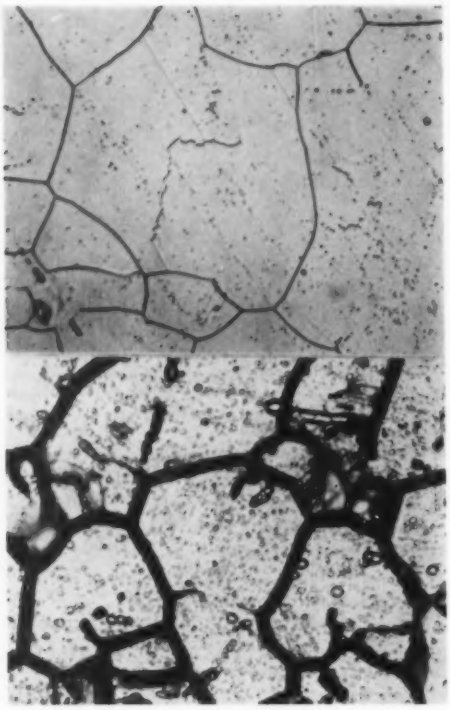

Fig. 10. Microstructure produced by anodic dissolution of annealed AISI-304 steel in 65% nitric acid. Etched at 0.02 amp/cm², temperature 25°C. A (top), 15 min; B (bottom) 60 min. Magnification 500X before reduction for publication.

$$Cr_2O_7^{=} + 14H^{+} + 6e = 2Cr^{+3} + 7H_2O$$

This reaction takes place more readily at cathodic points on the metal surface than does the reduction of hydrogen ions or of nitric acid. As a result, there is acceleration (depolarization) of the cathodic reaction. This makes possible a corresponding increase in the anodic, metal dissolution reaction. In this sense, the effect of oxidizing cations and of an anodic, external current is the same, i.e., the removal of electrons from the metal is accelerated. The result of this acceleration of dissolution, preferential grain boundary attack, is also the same in both cases (Fig. 7 and 10). The process is self-accelerating because hexavalent chromium ions accumulate more rapidly in the grooves, which tend to retard their diffusion into the solution.[8]

The effect of two other oxidizing cations, Fe^{+3} and Ce^{+4}, was also investigated. Weight-loss data obtained with ferric nitrate additions are plotted in Fig. 11A. Relatively large amounts are required before there is an appreciable increase in corrosion rate. As in the case of hexavalent chromium, the increase is largely a result of intergranular attack. Because of the high concentration of ferric ions required and the much greater effectiveness of dissolved chromium, their influence is not observed in nitric acid testing solutions containing only those ferric ions formed from dissolving stainless steels.

[8] Concentration of chromium-ion corrosion products in cavities is also responsible for accelerated attack at cross-sectional surfaces of bar stock, end-face corrosion. Hexavalent chromium collects in the small pits frequently formed when inclusions are removed by acid corrosion. These pits are then greatly enlarged by the rapid intergranular attack produced by the chromium ions.

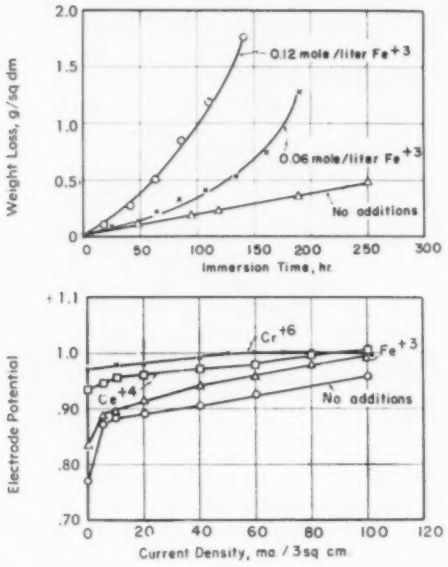

Fig. 11. Effect of cations in nitric acid on corrosion of stainless steel. A (top), acceleration of intergranular attack by ferric nitrate; Addition: $Fe(NO_3)_3 \cdot 9H_2O$, solution changed every 48 hr. B (bottom), anodic polarization of stainless steel. Concentration of cations: 0.10M. Additions: $Fe(NO_3)_3 \cdot 9H_2O$, CrO_3, and $Ce(HSO_4)_4$. Potential: against saturated KCl, calomel electrode, apparatus, Fig. 5.

What property of these ions determines the amount of acceleration, the oxidation potential, the valence change, or their influence on anodic and cathodic polarization? In another system in which oxidizing cations accelerate corrosion, iron dissolving in sulfuric acid, Gatos (6) found that the increase in corrosion was proportional to the concentration of the cation and its valence change in the reduction reaction. The rate of corrosion in this system depended on the rate of diffusion of the cations to the cathodic points on the surface of the metal rather than on a partially protective film on anodic areas. Since the diffusion rate was nearly the same for most cations investigated, it followed that the amount of acceleration was a function of the valence change of each ion. For the case of stainless steels in nitric acid, McIntosh (9) has suggested that the oxidation potential of the cations is the determining factor.

Polarization and corrosion rate tests were made to obtain data on this problem. The corrosion of annealed AISI-304 steel was determined in boiling, 65% nitric acid solutions, each of which contained 0.10 mole/l of a different oxidizing cation, hexavalent chromium, trivalent iron, and tetravalent cerium. Weight-loss measurements, together with other pertinent data, are given in Table II. These data show that the valence change involved in the cathodic reaction does not determine the corrosion rate, i.e., cathodic depolarization, while accelerating the rate of dissolution, is not the rate-controlling process. This indicates that the rate-controlling process is a combination of changes in the open-circuit potential of cathodic areas and, probably, in anodic polarization. The potentials of cathodic areas are changed in the cathodic direction to various de-

Table II. Effect of oxidizing cations on corrosion of AISI-304 steel in boiling 65% nitric acid

Cation*	(Concentration 0.10 mole/l) Electrode potential, Measured, Pt‡	Electrode potential, Measured, Stainless steel	Valence change	Weight loss, g/dm² 2 hr	Weight loss, g/dm² 8 hr**
HNO_3	+1.07 (1.20) +	+0.75 (0.95) +			
Fe^{+3}	+1.05	+0.79	1	0.0†	0.1
Cr^{+6}	+1.13	+0.97	3	1.4	10.3
Ce^{+4}	+1.22	+0.94	1	1.7	6.0

* Added as $Fe(NO_3)_3 \cdot 9H_2O$, CrO_3, and $Ce(HSO_4)_4$.
** After 8 hr the effect of Cr^{+6} is greater than that of Ce^{+4} because there is profuse grain dropping in the Cr^{+6} solution, while in Ce^{+4} solution there is less intergranular penetration, more widening of grain boundaries, and, therefore, almost no grain dropping.
† As is shown in Fig. 11A, there is acceleration of corrosion by ferric ions, but this is not sufficient to be detectable in a 2-hr exposure.
‡ Potential of platinized platinum electrode vs. saturated KCl calomel electrode.
+ Potential increases gradually with time at boiling temperature, 122°C.

grees by different cations; these changes increase the difference in the open-circuit potentials and, therefore, the corrosion rate (Table II).

A possible effect of the cations on the anodic polarization (formation, dissolution, and permeability of the protective film) is indicated by the data of Fig. 11B. As stainless steel is made anodic in nitric acid by an external current, its potential increases in the cathodic direction. However, the change in potential per milliampere of current depends greatly on the cations in the solution. The change in potential produced by a 100 ma current is 0.20 v for nitric acid without additions, 0.05 v for Cr^{+6}, 0.07 v for Ce^{+4}, and 0.16 v for Fe^{+3}. Thus, the ions which have the greatest effect on the corrosion rate also are most effective in reducing anodic polarization. These anodic polarization measurements suggest, but do not prove, the effect of cations on the anodic process, because the local cell current to which the external anodic currents of Fig. 11B are added also vary with the type of cation in the solution.[4]

These factors have been summarized in the schematic diagram of Fig. 12. Oxidizing cations increase the corrosion of stainless steel in nitric acid by cathodic depolarization (increase in rate of cathodic reaction), by shifting the open-circuit potential of cathodic areas toward more noble values and thereby increasing the open-circuit potential of the local cell,

[4] In ferric sulfate-sulfuric acid solution (see below) Cartledge (24) has found by radiotracer techniques that dissolved cations became part of the anodic film.

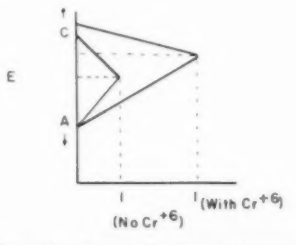

Fig. 12. Schematic potential-current diagram of local-cell action on stainless steel in nitric acid. Effect of dissolved chromium. "C" and "A" are open-circuit potentials of the local cathodic and anodic areas, and "I" is the corrosion current.

and, probably, by anodic depolarization (decreasing the protective properties of the anodic films).

Effect of Heat Treatment

Exposure of austenitic stainless steels to temperatures in the range of 1000°-1600°F may produce either or both of two types (chromium carbide and sigma phase) of susceptibility to intergranular attack, depending on the composition of the steel. The degree of susceptibility to intergranular attack increases with increasing temperature of heat treatment to a maximum at about 1250°F and then decreases with further increases in temperature. Heat treatments above 1700°F, with water quenching, do not result in appreciable susceptibility to intergranular attack in these steels (13).

The sigma phase responsible for susceptibility to intergranular attack may or may not be detectable in the microstructure. It can be revealed with certainty only by exposure of the steel to the nitric acid test. An example of this phenomenon is given by the steel whose microstructure is shown in Fig. 13. Because of the low carbon content there is no precipitation of chromium carbides after heating 1 hr at 1250°F, nor is there any visible formation of sigma phase. Yet the nitric acid corrosion rate is 35 times as great as that of an annealed specimen of the same heat of steel. While such examples are not common, similar behavior has been described by other investigators (14, 15).

In steels containing more than about 0.007-0.009% carbon, chromium carbides may be formed by heat treatments in the range of 1050°-1300°F. This lower limit of solubility was determined (14, 16) by heat treatments lasting from one day to three weeks.

The formation and growth of chromium carbides at grain boundaries can be shown by very gradual cooling of a large-grained specimen. Electrolytic etching reveals the dendritic impression in the steel left when the carbide is removed (Fig. 14A). An actual dendritic carbide, isolated from this steel, is shown in Fig. 14B. The carbide was isolated by the method of Mahla and Nielsen (17) who have made an extensive investigation of isolated carbides. A solution of bromine in anhydrous methanol was used to dissolve the stainless steel. The carbides were left

Fig. 13. Electrolytic etch of AISI-316L steel in 10% oxalic acid. Steel: FI-4 (0.020% C, 16.2% Cr) heated 1 hr at 1250°F. Etch: 1 amp/cm² for 1.5 min. Step structure: nitric acid corrosion rate 0.04 in./mo. Magnification 500X before reduction for publication.

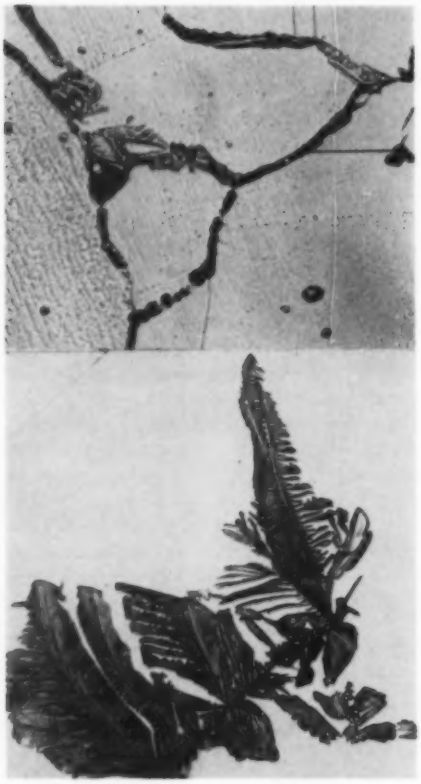

Fig. 14. Carbide precipitation in AISI-304 steel. A (top), etched electrolytically in oxalic acid. Traces of dendritic carbides (magnification 1000X before reduction for publication); B (bottom) electron photomicrograph of dendritic carbide isolated in bromine-methanol solution (magnification 5000X before reduction for publication). Steel: 0.05% C heated to 2000°F (1080°C) in evacuated, sealed quartz tube and furnace cooled.

behind in a residue layer, from which they were collected, washed, dried, and caught on a screen for examination in an electron microscope. As in the case of grain-boundary grooving of annealed steel, intergranular precipitation of chromium carbides depends on the structure of the grain boundaries. Thus, brief exposure at 1250°F produces carbides at certain preferred sites, and longer heating results in precipitation in most grain boundaries except twin boundaries. Prolonged heating (100 hr) precipitates carbides even at twin boundaries (18). This dependence of intergranular precipitation on the orientation of the grains has been observed in other alloys (19, 20).[5]

As the length of time of heat treatment at 1250°F is increased, more and more grains are completely enveloped by carbide precipitate. Upon subsequent exposure to boiling nitric acid, these grains are readily dislodged and the corrosion rate of the steel is increased (Fig. 2). It is apparent that a 1- or 2-hr sensitizing treatment of this steel at 1250°F does not produce the maximum possible amount of susceptibility to intergranular corrosion.

[5] During the formation and growth of chromium carbides the metal adjacent to the carbide is depleted in chromium. Since the carbides grow away from the boundary in very thin plates, the zone of metal depleted in chromium is parallel to the carbide and not to the grain boundary.

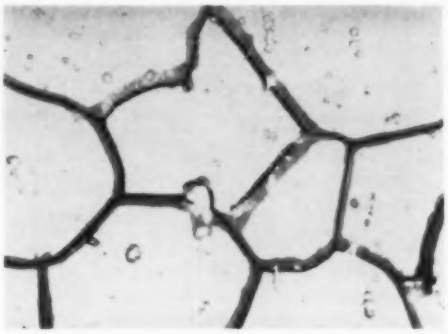

Fig. 15. Intergranular attack on AISI-316L steel in boiling 65% nitric acid. Print made from two superimposed negatives taken of the same surface area after 30 and 124 hr of exposure to acid. Narrow, dark lines show original location of grain boundaries. Steel: FH-5 (0.026% C) heated 1 hr at 1300°F. Magnification 500X before reduction for publication.

A further indication of the influence of grain orientation on intergranular precipitation and attack is given in metallographic studies of progressive corrosion. By photographing the same area of a corroding specimen after various periods of exposure to nitric acid, a series of negatives is obtained which shows the widening of grain boundary grooves. A print, made by superimposing a negative taken near the beginning of the test on one taken after considerable intergranular attack has taken place, shows the relative contributions to the grooves made by each grain (Fig. 15). In agreement with observations on intergranular precipitation, the amount of metal dissolved from various grains to make the grooves varies greatly. The grain in the center is oriented in such a way in relation to those adjacent that it contributes practically no metal to the grooves made in the exposed surface. Thus, the same crystallographic factors which determine preferential attack on annealed steel also determine the location of precipitates whose presence leads to a very great intensification of intergranular attack.

Susceptibility to intergranular attack on sensitized steel could not be detected by electrode potential measurements. Annealed and sensitized AISI-304 specimens had the same electrode potentials in boiling 65% nitric acid. This suggests that dissolution is under anodic control, i.e., the greater rate of intergranular attack on sensitized steel is a result of a lower polarizability as compared with that of the grain boundaries of annealed specimens.

Corrosion in Ferric Sulfate-Sulfuric Acid Solutions

Recent work (21) on the inhibition of corrosion of stainless steels in various acids by ferric salts has led to the development of a new test for evaluating the susceptibility of austenitic stainless steels to intergranular attack. This ferric sulfate-50% sulfuric acid test (22) is specific for revealing only the chromium carbide type of susceptibility to intergranular attack in unstabilized steels and requires only 120-hr testing time.

Mechanism of Ferric-Ion Inhibition

The minimum amount of ferric ions required for inhibition was determined for 50 and 60% solutions

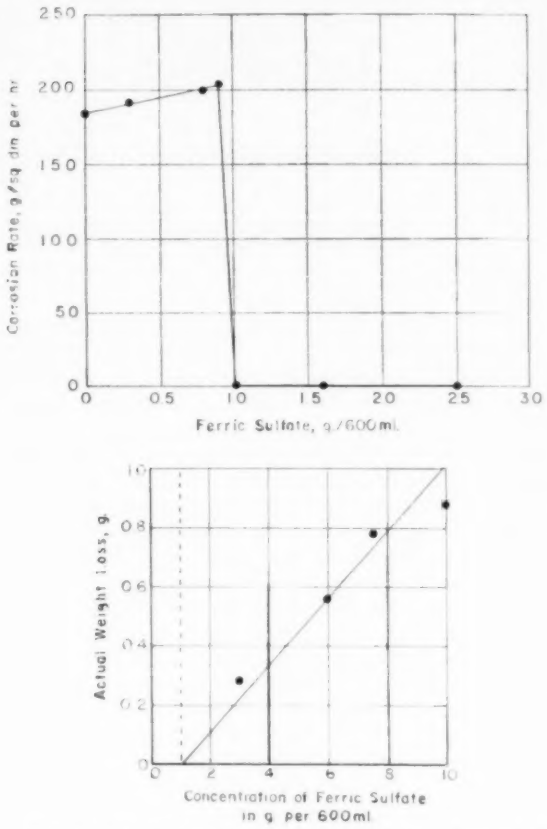

Fig. 16. Effect of ferric sulfate on corrosion of annealed AISI-304 steel in boiling 60% sulfuric acid. Ferric sulfate: 75% $Fe_2(SO_4)_3$. A (top), minimum amount of ferric sulfate required for inhibition; B (bottom), consumption of ferric sulfate. Weight loss of stainless steel at time of exhaustion of ferric sulfate as a function of amount of ferric sulfate added initially.

of boiling sulfuric acid by exposing specimens of AISI-304 stainless steel to a series of flasks to which various amounts of ferric sulfate had been added. At low concentrations of ferric ions there was no appreciable change in the very high, uninhibited corrosion rate (Fig. 16A). At a certain concentration (1 g ferric sulfate per 600 ml of 60% and 0.8 g in 50% acid) there was a sudden decrease in rate to a very low value. Corrosion was reduced from 200 to 0.037 g/dm²/hr in 60% acid.[6]

Clues to the mechanism of this process of inhibition are the absence of any hydrogen gas bubbles on the stainless steel, even though there is readily detectable corrosion, and the gradual dissolution of excess ferric sulfate in boiling acid solutions containing rapidly corroding (sensitized) stainless steel specimens. These observations suggest that ferric ions are consumed during inhibition.

When 18 Cr-8 Ni steel dissolves, divalent iron, chromium, and nickel are formed (reaction [1]). In acid solutions this anodic process is electrochemically equivalent to the discharge of hydrogen ions at cathodic areas (reaction [2]). However, in the presence of ferric ions, reaction [2] may be completely replaced by the reduction of ferric ions (reaction [3]) which results in consumption of inhibitor.

$$\left.\begin{matrix}\mathrm{Fe}\\ \mathrm{Cr}\\ \mathrm{Ni}\end{matrix}\right\} \xrightarrow{-e} \mathrm{Fe^{+2}} + \mathrm{Cr^{+2}} + \mathrm{Ni^{+2}} \qquad [1]$$

$$2\mathrm{H^{+}} + 2e \rightarrow 2\mathrm{H} \rightarrow \mathrm{H_2} \qquad [2]$$

$$\mathrm{Fe^{+3}} + e \rightarrow \mathrm{Fe^{+2}} \qquad [3]$$

The consumption of ferric ions to an amount just below the minimum required for inhibition is clearly indicated by the sudden onset of profuse evolution of hydrogen (change from reaction [3] to [2]).

To obtain data on the relationship of dissolution of stainless steel and the consumption of ferric ions, tests were made on coils of annealed stainless steel foil in a series of flasks containing 60% boiling sulfuric acid with various amounts of ferric sulfate in excess of the minimum amount (1 g/600 ml) needed for inhibition. This system was selected to obtain accurate weight loss-time data, which could be extrapolated 1 or 2 hr. Total testing time had to be restricted to about 7 hr because it was observed that there is gradual conversion of ferrous to ferric ions in boiling sulfuric acid solution.[7]

To expose large surface areas of steel which would provide readily detectable weight losses in periods of 0.5-7 hr the foil was made into cylindrical coils of about 600 cm² total surface area. From one to three coils were immersed in the flasks containing various amounts of ferric sulfate. The weight-loss-time data resulted in a straight line for all coils. At the instant of sudden activation (profuse hydrogen evolution) the total length of time of immersion was noted and used to determine the weight of metal dissolved by a small extrapolation of the weight loss-time line. In Fig. 16B these weight losses have been plotted against the total amount of ferric sulfate added at the beginning of the test.

The origin of the line in Fig. 16B is at 1 g ferric sulfate because the amount consumed is only that in excess of the minimum amount required for inhibition. Dissolution of 1 g of stainless steel is accompanied by the consumption of 9 g of ferric sulfate. This is in good agreement with the theoretical value of 9.7 g, derived[8] on the assumption that reactions [1] and [3] describe the process. This agreement between observed and theoretical amounts of ferric ion consumption, together with the fact that no hydrogen gas bubbles were observed in any of the solutions, some of which contained as much as 1500 cm²

[6] Sixty per cent acid was used for these tests to provide measurable corrosion rates in 7 hr or less. In the ferric sulfate-sulfuric acid test for detecting susceptibility to intergranular attack 50% acid is used (22). The minimum concentration of ferric ions required for inhibition depends on the alloy content of the steel and, therefore, may vary somewhat for different heats of 18-8 stainless steel (21). Larger concentrations of ferric ions are required to suppress corrosion of an active specimen than to prevent the onset of corrosion of an uncorroded specimen.

[7] Conversion of ferrous to ferric ions was detected by periodically exposing a stainless steel specimen to a boiling 50% solution of sulfuric acid containing 15 g per 600 ml of ferrous sulfate (colorless). This solution gradually turned yellow. When the specimen was immersed after 31 hr of boiling, it remained passive; i.e., at least 0.17 g per 600 ml of ferric ions (the minimum amount required for inhibition) had been formed.

[8] The stainless steel used was 18.9% Cr, 9.27% Ni, and, by difference, 71.8% Fe. One gram of this steel contains 0.018 moles of metal. Each mole of metal dissolving to divalent ions consumes two moles of ferric ions. The ferric sulfate used contained 20.8% iron by analysis, or one mole of ferric ions in 269 g of ferric sulfate. Therefore, the amount of ferric sulfate consumed during the dissolution of 1 g of steel is $2 \times 0.018 \times 269 = 9.7$ g.

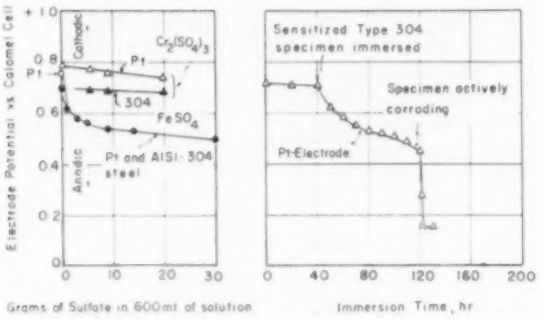

Fig. 17. Electrode potentials in boiling solutions of 50% sulfuric acid containing 15 g/600 ml of ferric sulfate. (For apparatus used see Fig. 5; all potentials measured against saturated potassium chloride calomel electrode.) A (left), effect of synthetic corrosion products on electrode potential; B (right), effect of corroding stainless steel specimen on potential of platinum electrode.

of corroding surface, shows that the reduction of ferric ions is electrochemically equivalent to the amount of metal dissolved. The corrosion current involved in reactions [1] and [3] in boiling 60% acid was derived from the weight loss, exposure time, and area of the specimen, and found to be 0.026 ma/cm^2.

Electrode potential measurements.—In 50% boiling sulfuric acid, 18 Cr-8 Ni steel has a potential of −0.34 v. With ferric ions the potential changes about 1 v in the noble direction to +0.70 v. When additions of small amounts of ferrous ions are made to the ferric sulfate-sulfuric acid solution, either as corrosion product from dissolving stainless steel or as an addition in the form of ferrous sulfate, the potential of stainless steel is the same as that of the platinum electrode, Fig. 17. Thus, the anodic areas on the steel are polarized to the potential of the cathodic areas on which the reduction of ferric ions takes place. The potential is the same for annealed and for sensitized steel and is independent of acid concentration (Table IV).

Neither ferrous ions nor other corrosion products affect corrosion in ferric sulfate-sulfuric acid solution (22). The effect of nickel and chromium sulfate additions on electrode potentials is shown in Fig. 17A. Divalent chromium (light blue) is rapidly changed to the trivalent (dark green) state in these solutions. Hexavalent chromium (orange-red), which accelerates corrosion of stainless steel, does not form in sulfuric acid during the dissolution process. This is in contrast to the behavior in nitric acid in which trivalent chromium is oxidized to the hexavalent state.

When ferrous ions accumulate from dissolving steel and reduction of ferric ions, the potential gradually changes in the anodic direction. As soon as the ferric ion concentration has been reduced to a value below that required for inhibition, the stainless steel becomes active and there is a further, rapid change to more negative potentials (Fig. 17B).

Rapid cathodic reduction of ferric ions in turn accelerates the anodic reaction, i.e., the dissolution of metal in pores of the protective film. The surge of metal (Fe, Cr, Ni) ions produced then makes possible the rapid formation of more film which heals the pores. [In the case of *iron* dissolving in sulfuric acid

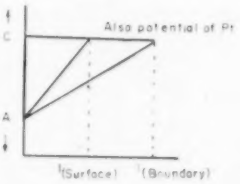

Fig. 18. Schematic potential-current diagram of local-cell action on stainless steel in ferric sulfate-sulfuric acid solution containing some ferrous ions. "C" and "A" are the open-circuit potentials of the local cathodic and anodic areas, and "I" is the corrosion current.

containing ferric ions the anodic corrosion product, ferrous ions, cannot form a protective film, and the result is an increase in the corrosion rate (6).] The passive state is dynamic. There is continual breakdown and repair of the surface. Ferric ions in solution and the ferrous ions formed by their reduction probably aid in the formation of this film (24).[9] There is also a possibility that film formation is promoted by oxygen evolved in the thermal reaction of water with ferric ions (25). The rate of dissolution of this film in the acid and/or the rate of diffusion of ions through the film determine the corrosion rate of the steel.[10]

The fact that the potential of annealed and of sensitized (chromium carbide type) steel is the same indicates that dissolution is under anodic control. The difference in grain face corrosion and intergranular penetration is primarily a result of the lower polarizability of the metal in grain boundary zones containing chromium carbide precipitate, rather than of any difference which may exist in open circuit potentials of grain centers and grain boundaries. This is also the case in nitric and in copper sulfate-sulfuric acid solution.[11]

A schematic diagram of local cell polarization is given in Fig. 18. The intersection of the polarization lines is the measured potential. Since the potential of stainless steel is the same as that of the platinized platinum electrode, the corrosion current "I" depends on the slope of the line representing anodic polarization. At grain boundaries containing chromium carbides and, therefore, a zone depleted in chromium, polarizability is less than at grain surfaces.

Intergranular Corrosion

Ferric ions greatly retard general, or grain face, corrosion (23). However, intergranular attack cannot be suppressed. As the concentration of sulfuric

[9] As a result, anodic polarization may be affected by cations in the solution. This may be different from polarization produced on stainless steel in pure sulfuric acid solutions by an anodic external current. Local cell polarization has, therefore, been described in terms of the simplified, schematic diagrams of the type of Fig. 18, rather than in reference to a specific polarization curve determined in pure acid solutions by means of an external current.

[10] In sulfuric acid solutions, without ferric ions, anodic polarization and consequent suppression of corrosion of stainless steel may be produced by means of an external electrical current or by aeration (26-29, 50, 55). Alloying additions of about 0.1% platinum and palladium to stainless steel have also been used to provide areas in the surface on which the rates of cathodic reactions are increased to permit more rapid formation of protective films on anodic areas (51).

Metal dissolution in aqueous media by diffusion of cations through protective films has been proposed by Petrocelli (48), Hoar and Evans (49), and Vetter (57).

[11] Support for this mechanism is given by electrode potential measurements made on grain surfaces and grain boundaries of large grained sensitized specimens using the technique described by Dix (53). There was no difference in these potentials in a solution of nitric-hydrofluoric acid. Similar measurements have been made by Standifer (54), who also found that the potentials of susceptible boundaries are the same as those of grain surfaces in several acids.

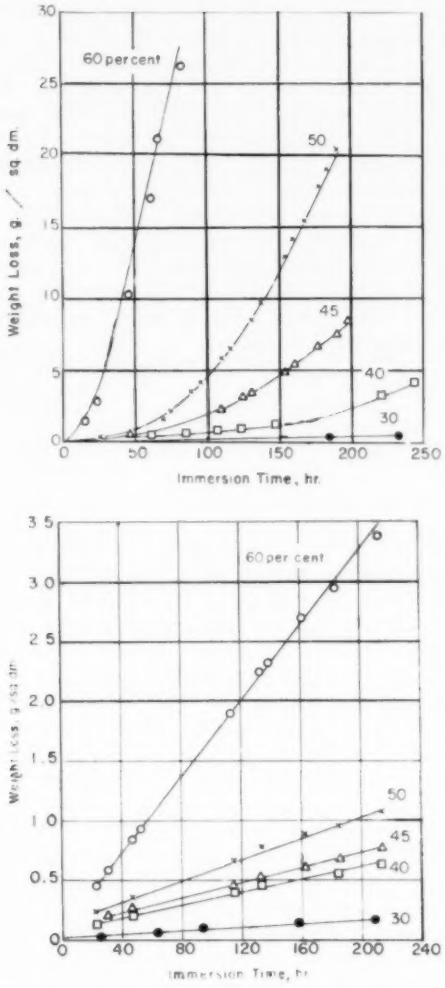

Fig. 19. Effect of concentration of sulfuric acid on corrosion of AISI-304 steel in boiling ferric sulfate-sulfuric acid solution (22). Solution: 600 ml with 15 g ferric sulfate (acid concentrations in weight per cent). Specimens: A (top), AISI-304 (M304, Table I) heated 1 hr at 1250°F; B (bottom), (M304, Table I) annealed.

acid is increased from 30 to 60% there is a large increase in intergranular corrosion of a steel containing chromium carbides (Fig. 19A). The morphology of intergranular penetration remains unchanged in this range of acid concentration (data in section on "Comparison of Types of Intergranular Attack"). General corrosion also increases as the acid concentration is increased (Fig. 19B). At a given length of exposure time, the ratio of intergranular to general corrosion is a measure of the resolving power or sensitivity of the solution to detect susceptibility to intergranular attack. Increases in acid concentration and testing time increase the ratio (22).

Intergranular corrosion in this solution leads to undermining and dislodgment of grains (Fig. 20) at a rate about twice that in the nitric acid test. This is shown by a comparison of ratios as given in Table III. On the AISI-304 steels the ratios obtained in 120 hr of exposure in the ferric sulfate-sulfuric acid solution are the same as those found after 240 hr of

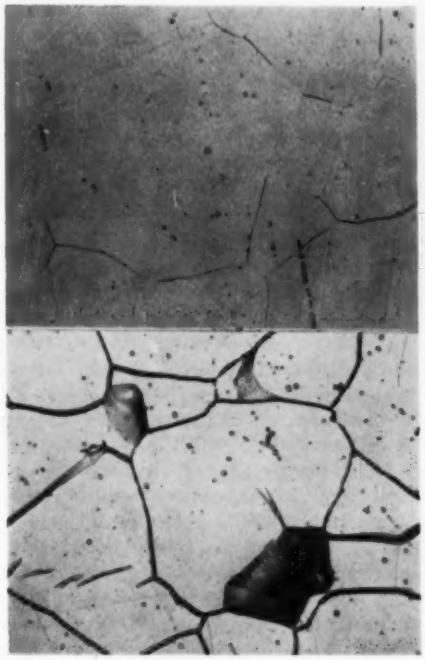

Fig. 20. Corrosion of AISI-316 steel in boiling ferric sulfate-sulfuric acid solution. Solution: 50% sulfuric acid containing 15 g/600 ml ferric sulfate. Steel: M316, analysis Table I. A (top), annealed, M316, after 20-hr exposure; B (bottom), sensitized, 1 hr 1250°F, after 20 hr exposure. Magnification 500X before reduction for publication.

testing in the nitric acid test. The conditions of acid concentration and testing time of the new evaluation test were selected on the basis of this type of data.

Table III also shows that on AISI-316 and 316L steels the ferric sulfate-sulfuric acid test does not reveal the type of susceptibility associated with sigma phase. Most of these steels have very high ratios in nitric acid but have a ratio of unity in the 120-hr ferric sulfate-sulfuric acid test. For example, steel FI-4, which does not contain any carbides after

Table III. Comparison of evaluation tests

(Types of susceptibility to intergranular attack and use of ferric sulfate and ferric nitrate)

Steel AISI	Code†	Ratio of weight losses* 65% nitric acid, 240 hr	50% sulfuric acid, Ferric sulfate, 120 hr	50% sulfuric acid, Ferric sulfate, 240 hr	50% sulfuric acid, Ferric nitrate(d), 24 hr
304	M304(a)	12.8	11.8	23.8	28.0
304	FK-2(a)	2.1	2.1	3.7	2.1
316L	FI-4(a)	35.6	1.4	1.7	1.0
316	M316(a)	19.0	7.8	18.5	—
316L	FI-6(b)	133.0‡	1.0	1.5	—
316L	EM-9(c)	3.3‡	1.0	1.2	—
316L	FI-2(b)	20.4‡	1.4	2.4	—
316L	FI-9(b)	210.0‡	1.3	2.2	—

* Weight loss of heat-treated specimen, (g/dm²) / Weight loss of annealed specimen, (g/dm²)

† (a) Heated 1 hr at 1250°F, W.Q.
(b) Heated 1 hr at 1300°F, W.Q.
(c) Heated 4 hr at 1600°F, W.Q.
(d) 35.5 g/liter $Fe(NO_3)_3 \cdot 9H_2O$

‡ Calculated from data given in Ref. (42).

heating 1 hr at 1250°F (Fig. 13), has a ratio of 35.6 in the nitric acid test as a result of severe intergranular corrosion of the sensitized specimen. In the ferric sulfate-sulfuric acid test there is essentially no intergranular attack on this steel even though there is some grain boundary grooving. This is a more severe form of the grooving shown on annealed AISI-316 steel in Fig. 20A.

Use of other ferric salts and other acids.—Corrosion and inhibition may be influenced greatly by the anion of the ferric compounds used for inhibition. Thus, ferric chloride and bromide readily break down passive films and lead to severe pitting (21, 30). The oxalate is decomposed in sulfuric acid solution, and the products of decomposition reduce ferric to ferrous ions.

Also, the anion of the ferric salt may affect the rate of intergranular attack. For example, ferric nitrate increases the rate of intergranular attack as compared with the rate obtained with ferric sulfate. The comparison of ratios in Table III suggests that a 24-hr test with the ferric nitrate inhibitor is equivalent in resolving power to a 120-hr ferric sulfate-sulfuric acid or a 240-hr nitric acid test. Thus, it may be possible to develop a 24-hr ferric nitrate-sulfuric acid test.

A further development of accelerated evaluation tests for susceptibility to intergranular attack may be possible by the combined use in these tests of ferric compounds and the very acid to which the steel is to be exposed in plant service. Ferric ions inhibit general corrosion in a number of acids, e.g., acetic, formic, oxalic, sulfamic, and sodium bisulfate (21). The use of ferric compounds in these acids makes it possible to use boiling solutions at acid concentrations selected to give the most rapid intergranular attack on susceptible steels. Thus, if a certain steel is to be used in acetic acid service, its susceptibility to intergranular attack might be determined by exposing it in boiling, ferric-ion inhibited, 20% acetic acid.

Corrosion in Copper Sulfate-Sulfuric Acid Solution

This combination of reagents, originally developed by Hatfield (31), has been widely used to determine the susceptibility of austenitic stainless steels to intergranular corrosion. Exposure to this solution at boiling temperatures produces intergranular attack only on steels containing intergranularly precipitated chromium carbides (13, 32, 33). The attacked zone at grain boundaries is such that the large majority of grains remain in place. Also, general corrosion on grain faces is very low. As a result, the change in weight, even on steels susceptible to intergranular attack, is very small and has not been used as a routine means of measuring the extent of intergranular corrosion.[12]

The most commonly used method for routine evaluation of this test consists of bending a 2-cm wide by 5- or 8-cm long specimen through 180° and examining the surface for cracks, which indicate intergranular attack. This qualitative evaluation method has actually been found to be a more sensitive indication of intergranular corrosion than measurement of changes in electrical resistance (33) or of weight loss. For resistance measurements, first used by Rutherford and Aborn (35), a modified Kelvin bridge, thin specimens, 4- to 10-cm long, and exposure periods of hundreds of hours are required.

A method of greatly accelerating intergranular attack in the copper sulfate-sulfuric acid solutions has recently been developed by Rocha (36). This consists of placing the stainless steel specimen in contact with copper metal chips during exposure in the test solution. As a result, the exposure time is reduced from 200 to 24 or 48 hr before evaluation by the bend test.

Intergranular Corrosion

A boiling solution of 15.7% sulfuric acid and 5.7% $CuSO_4$ (by weight) was used for all tests. This was prepared by adding 100 g $CuSO_4 \cdot 5H_2O$ and 100 ml H_2SO_4 (sp gr 1.84) to 840 ml of water (37). Apparatus was the same as that used for the nitric acid and the ferric sulfate-sulfuric acid solutions, i.e., a 1-liter Erlenmeyer flask, containing 600 ml of solution, with a cold finger condenser. To avoid accumulation of corrosion products frequent changes of solutions were made. For electrical resistance measurements the stainless steel specimens were machined and ground to a cross section of 0.6 x 0.15 cm and a length of 3 to 6 cm. Any heat treatments required were made on the specimens before machining.

Changes in electrical resistance of these specimens were measured with a precision Kelvin bridge. These resistances varied from 0.001 ohm on specimens before testing to about 0.06 ohm on specimens whose grain boundaries were extensively corroded. All resistance measurements were converted to per cent change in resistance. By determining this change for segments of various lengths of one specimen, it was found that the per cent change in resistance was independent of the length of specimens used in this investigation.

Before resistance measurements are made the specimens must be immersed in acetone to remove residual liquids and soluble solids from corroded grain boundaries

Dislodgment of grains in the cupric sulfate-sulfuric acid solution is very slow, especially from AISI-316 steels. Even though the grain boundaries may be penetrated enough to make a 6-cm long specimen bend under its own weight the surface may be almost unchanged in appearance. In the case of AISI-304 steels, grains are dislodged more readily and the specimens sometimes break in handling.

Effect of metallic copper.—Quantitative data were obtained on the acceleration of intergranular attack produced by immersion of metallic copper in the testing solution. Three types of tests were made: (*a*) simple immersion of stainless steel in cupric sulfate-sulfuric acid solution, (*b*) simultaneous immersion with metallic copper, but not in contact, and (*c*) immersion of steel in contact with copper. Contact with metallic copper was provided by partially filling the glass cradles, used to hold the steel specimen, with copper turnings. A weighed and measured cop-

[12] An intergranularly corroded specimen gives off a dull sound when dropped on a hard surface. This effect has been investigated by oscillographic analysis (34).

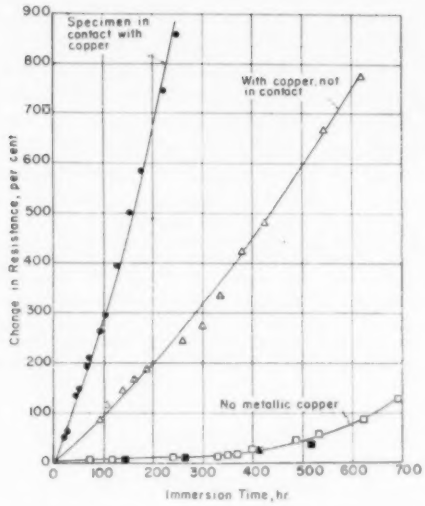
Specimen in contact with copper
With copper, not in contact
No metallic copper
Change in Resistance, per cent
Immersion Time, hr

Fig. 21. Change in electrical resistance of sensitized AISI-316 steel in boiling copper sulfate-sulfuric acid solution. Effect of metallic copper. Solution: 15.7% H_2SO_4 and 5.7% $CuSO_4$. Steel: AISI-316 (EW-6) heated 1 hr at 1250°F.

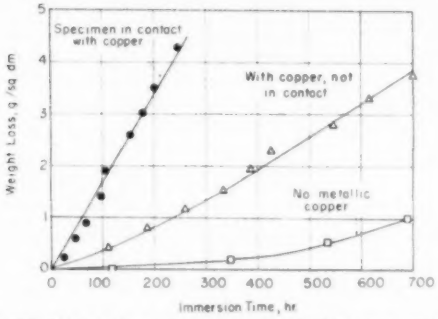

Fig. 22. Weight loss of sensitized AISI-316 steel in boiling copper sulfate-sulfuric acid solution. Same tests as Fig. 21.

per specimen was used for the simultaneous immersion tests.

The results of electrical resistance and weight-loss measurements are given in Fig. 21-23. It is apparent that without the use of metallic copper the rate of intergranular attack is very slow. After 240 hr the change in resistance is only 10% and the weight loss only 0.1 g/dm² (in a 120-hr exposure in 65% nitric acid the weight loss of this steel was 31.5 g/dm²). Simultaneous immersion of the copper, about 20 cm² in area, increases the rate of intergranular attack by a factor of 24 (at 240 hr of immersion) as determined by change in resistance (Fig. 21). Contact with the copper specimen produces a further increase in the rate of attack—by a factor of 85 over the copper-free test. These differences in rates of intergranular attack also are reflected in the weight losses (Fig. 22).

To determine whether this increase of corrosion by copper is a result of simple acceleration of the type of intergranular attack observed without immersion of copper, or the result of a change in the geometry of grain-boundary attack the per cent changes in resistance have been plotted against the weight losses (Fig. 23). In this graph the time factor has been eliminated. The resulting relationship of resistance change to weight loss is the same for all three tests. Thus, metallic copper increases corrosion by accelerating the type of intergranular attack produced in the absence of copper, rather than by changing the character of grain boundary attack.

A photomicrograph of intergranular attack produced in copper sulfate-sulfuric acid solution with the stainless steel in contact with copper is shown in Fig. 24. Even though the attacked grain-boundary zone is very narrow in comparison with that produced in nitric acid and ferric sulfate-sulfuric acid solutions (Fig. 3 and 20), there has been enough penetration to undermine and dislodge grains.

Effect of sensitizing time.—Increasing the heat treatment at 1250°F from 1 hr to 2 hr increases the amount of intergranularly precipitated chromium carbides and probably also the size of the carbides. Figure 25 indicates that the character of intergranular attack on specimens of the same heat of steel is changed by varying the length of time of sensitizing. Each specimen has its own resistance change vs. weight relationship. Greater amounts of carbide precipitate produce a more rapid increase in resistance than in weight loss in the cupric sulfate-sulfuric acid solution (without metallic copper). The rate of intergranular penetration increases more rapidly than does grain dropping.

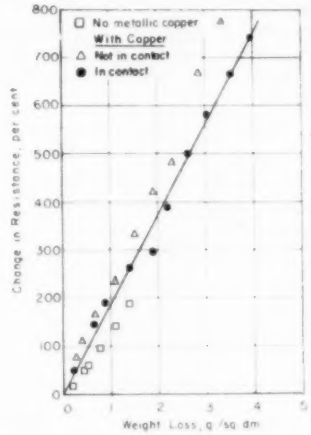

Fig. 23. Relationship of change in electrical resistance and weight loss of sensitized AISI-316 steel in boiling copper sulfate-sulfuric acid solution. Same tests as Fig. 21.

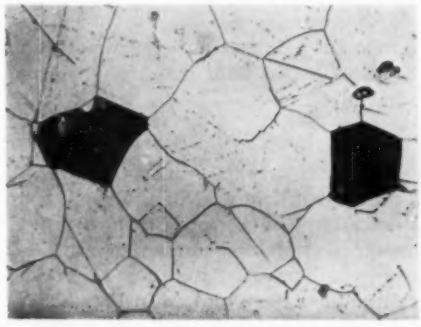

Fig. 24. Corrosion of sensitized AISI-316 steel in boiling copper sulfate-sulfuric acid solution. Specimen in contact with copper. Steel: AISI-316 (EW-6) heated 1 hr at 1250°F. Exposure: 23 hr. Magnification 500X before reduction for publication.

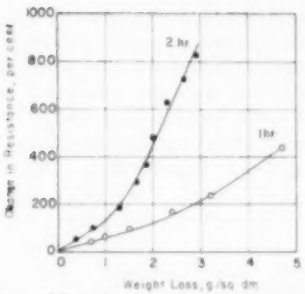

Fig. 25. Effect of length of time of heat treatment on intergranular penetration in boiling copper sulfate-sulfuric acid solution. AISI-316 (M 316) heated at 1250°F. As shown. Tests made without metallic copper.

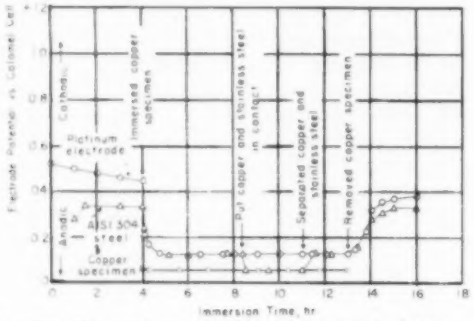

Fig. 26. Electrode potential measurements in boiling copper sulfate-sulfuric acid solutions. Effect of metallic copper. Solution: 15.7% sulfuric acid and 5.7% $CuSO_4$. (For apparatus used see Fig. 5; all potentials measured against saturated potassium chloride calomel electrode).

Tests have also been made in cupric sulfate-sulfuric acid solution on steels containing the sigma type of intergranular susceptibility. The results, discussed below, are in agreement with those of previous investigators (13, 32, 33) and show that the sigma type of susceptibility does not lead to accelerated intergranular attack in this solution.

Effect of dissolved iron.—Ferrous sulfate was added to copper sulfate solutions to give a concentration of 1.3 to 2.6 g/l of ferrous ions. Dissolved iron in this range of concentration was without effect on the weight loss of annealed or of sensitized steel, with or without metallic copper in the solution. However, in some tests dissolved iron reduced the change in resistance of sensitized specimens, which is in agreement with results of Brauns and Pier (39), who reported a decrease in intergranular attack (no metallic copper) as determined by the bend test, which indicates total penetration, as does the change in resistance.

Electrode Potential Measurements

Potential measurements in boiling solutions of copper sulfate-sulfuric acid of the same concentration as described above were made to provide data for an interpretation of the action of metallic copper and the mechanism of dissolution in this solution. Some results have been plotted in Fig. 26.

Initially, the potential of the platinized platinum electrode is about +0.53 v and that of a stainless steel specimen, +0.34 v. Immersion of a piece of copper (40 cm^2 surface area) in this solution, but not in contact with either the stainless or platinum electrode, very rapidly changes the potential of both electrodes in the anodic (active) direction to +0.13 v. Both electrodes now have the same potential, which is constant. The potential of the copper is constant at 0.06 v. When the copper is put in contact with the stainless electrode there is a further change in potential of the steel in the active direction to that of copper, which remains unchanged (large surface area). The potential of the solution (Pt electrode) remains unchanged. Breaking contact between the stainless steel electrode and the copper specimen reestablishes the potential of the stainless steel at the same value as that of the platinum electrode. Upon removal of the copper specimen the potentials of both platinum and stainless steel electrodes increase in the cathodic direction. As in the beginning, the platinum electrode assumes the more cathodic potential. These measurements are readily reproducible and are the same on annealed and on sensitized steel.

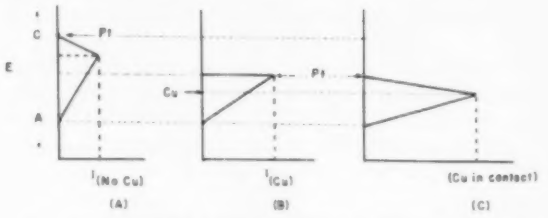

Fig. 27. Schematic potential-current diagrams of local-cell action on stainless steel in copper sulfate-sulfuric acid solution. Effect of metallic copper. "C" and "A" are the open-circuit potentials of the local cathodic and anodic areas, and "I" is the corrosion current. The electrode potentials of a platinized platinum electrode and the metallic copper, immersed together with the stainless steel, are indicated by arrows.

The action of metallic copper in this solution is shown by a comparison of weight-loss measurements obtained on copper in boiling sulfuric acid, with and without cupric sulfate. Without cupric sulfate the weight loss was about 0.3 g/dm^2 in 20 hr. Addition of cupric sulfate to make a 5.7% $CuSO_4$ solution increased this weight loss 40-fold by cupric-ion corrosion.

$$Cu + Cu^{+2} \rightarrow 2Cu^{+1}$$

Accumulation of cuprous ions in the cupric sulfate-sulfuric acid solution changes the potential in the anodic direction to the same value on both the platinum and stainless steel electrodes, which indicates that the local anodes are polarized to the potential of the cathodic areas. Thus, in copper sulfate-sulfuric acid solution, as well as in the other two acid solutions investigated, corrosion of stainless steel is controlled by the polarizability of anodic areas. These changes in potential are shown schematically in terms of local cell action in Fig. 27A and B.

When the copper specimen is put in contact with the stainless steel there is a further change in the potential of the steel, in the anodic direction, to that of the copper. (The potential of the platinum electrode remains constant.) This change indicates cathodic polarization of the steel.[13] Therefore, stainless

[13] Making an electrode a cathode by means of an external current either has no effect on its potential or changes it in the anodic direction. In turn, anodic polarization changes the potential in the cathodic direction.

steel is the cathode of the steel-copper galvanic couple.[14] There is a simultaneous reduction in anodic polarization, primarily at susceptible grain boundaries, and, consequently, an increase in corrosion rate, or corrosion current, in terms of the diagram in Fig. 27C. In this system cathodic polarization increases corrosion.[15] As suggested by Rocha (36) the copper contact produces dissolution of the stainless steel at a constant potential, i.e., the copper provides a very simple equivalent of a constant-potential instrument, a potentiostat.

Since copper is the anode of the galvanic couple with stainless steel, it might be expected that its rate of corrosion is increased. However, no increase was observed because of the very great difference in the corrosion rates of the stainless steel and the copper. The galvanic current produced by the couple doubles the corrosion rate of the stainless steel (Fig. 22). Only a small fraction of this is actually due to metal dissolution; most is a result of grain-dropping. The galvanic current passing to the stainless steel from the rapidly corroding copper (0.65 g/dm²/hr) produced such a small increment in this rate that it could not be detected.

Dissolution of stainless steel in cupric sulfate-sulfuric acid solution without metallic copper gradually changes the oxidation reduction potential of the solution in the anodic direction as cuprous ions are formed by reduction of cupric ions on the surface of the steel. However, in the presence of relatively large concentrations of dissolved ferrous ions this shift is suppressed. In agreement with Brauns and Pier (39) it was found that 1-3 g/l of ferrous ions retards or prevents the change of potential in the anodic direction. Ferrous ions were oxidized to the ferric state. A blue solution containing 1.3 g/l ferrous ions becomes blue-green in 12 hr at boiling temperature. When metallic copper was added, dissolved iron remained in the ferrous state and the potentials of copper and of stainless steel in contact with it were the same as in solutions without iron.

Comparison of Types of Intergranular Attack

In this concluding section the techniques described in the previous parts are used for a comparison and interpretation of the types of intergranular attack produced by various solutions. The data have been summarized in terms of criteria which can be used to compare the applicability of these corroding acids for routine evaluation tests. A description of experimental work undertaken to reveal the effect of grain size on intergranular corrosion concludes the discussion.

Effect of Acids

Some results obtained on AISI-304 and 316 steels in the three acid solutions discussed above are shown in Fig. 28. In these two graphs the effect of length of testing time has again been eliminated by plotting change in resistance against the weight loss of a given (sensitized) steel. Elimination of the testing time facilitates the comparison of types of intergranular attack, because the factors in the acids which determine the rate of intergranular penetration do not affect its character. Thus, it was shown (Fig. 23) that the very great acceleration of intergranular attack caused by the use of metallic copper in the copper sulfate-sulfuric acid test does not alter the characteristics of this attack. This is also the case for increasing acid concentration which greatly affects the rate of corrosion in the ferric sulfate-sulfuric acid solution (Fig. 19). The data on AISI-304 and 316 steels in Fig. 28, obtained in 15.7 and 50% acid, provide the evidence for this observation. Even though corrosion on the AISI-316 steel is increased 300-fold in 77 hr by this increase, the points for both concentrations fall on one line. A discussion of "characteristics of intergranular penetration" is given below.

The relationship of change in resistance and weight loss on intergranularly corroding specimens may be described with reference to an imaginary specimen suffering uniform general corrosion. Cal-

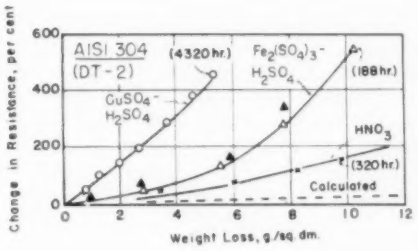

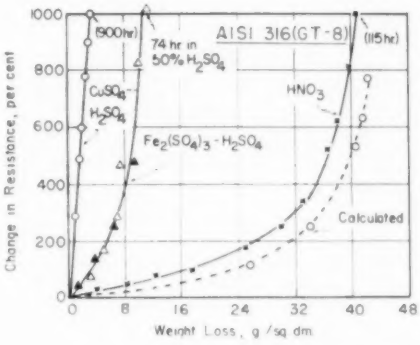

Fig. 28. Comparison of intergranular penetration and weight loss in three boiling acid solutions. Steels: A (top), AISI-304 (DT-2) heated 1 hr at 1250°F; B (bottom), AISI-316 (GT-8) heated 1 hr at 1950°F, then 1 hr at 1250°F. Solutions: O, 15.7% H_2SO_4 — 5.7% $CuSO_4$ (no metallic copper); △, 50% H_2SO_4 — $Fe_2(SO_4)_3$; ▲, 15.7% H_2SO_4 — $Fe_2(SO_4)_3$; ×, 65% HNO_3.

[14] Confirmation of this relationship in the copper-stainless steel couple was obtained in a test in which the current and its direction in this couple were measured. Specimens of copper and stainless steel, connected through a microammeter, were partially immersed in boiling sulfuric acid without cupric sulfate. The stainless steel dissolved with vigorous evolution of hydrogen and was the anode of the couple. When the couple was immersed in a second solution of sulfuric acid of the same concentration containing cupric sulfate, evolution of hydrogen on the stainless steel was suppressed. There was a reversal and a large decrease of the current between the specimens. The stainless steel became the cathode and the copper became the anode of the galvanic couple.

[15] This is in contrast to the behavior of some metals in nearly neutral solutions. Cathodic polarization frequently reduces corrosion in such systems (cathodic protection). On metals exposed to solutions in which they evolve hydrogen [steels in acids, aluminum in sodium hydroxide (38)] cathodic polarization usually does not affect the corrosion rate.

culations[16] were made of the per cent change in resistance as a function of the weight loss of such a stainless steel specimen (of similar cross-sectional area as those used in the laboratory tests) and have been plotted in Fig. 28. At a given weight loss the difference in per cent change in resistance between the calculated curve and one of the experimental curves is an indication of the extent of intergranular penetration beyond the metal surface produced by grain dropping. This difference in per cent resistance change is a measure of the grain boundary attack which has taken place, but which did not contribute to the weight loss. (The assumption is that the weight loss is very largely due to dislodged grains rather than to dissolved grain boundary material.)

Examination of the curves in Fig. 28 shows that intergranular penetration in addition to that indicated by weight loss measurements is greatest in copper sulfate-sulfuric acid solution and least in nitric acid. Also, this type of penetration is less for AISI-304 than for 316 steel in the two sulfuric acid solutions. These conclusions are in agreement with the qualitative observations made on corroded specimens. In the copper sulfate solution there is relatively little dislodgment of grains as compared with that produced in the other tests. Also, in copper sulfate-sulfuric acid solution grain dropping on AISI-304 steel is greater than on the 316 steel. On both steels there is more intergranular penetration beyond the surface in the ferric sulfate-sulfuric acid than in the nitric acid solution.

The slopes of the curves in Fig. 28 are determined by the ratio of intergranular penetration along susceptible grain boundaries to the rate of grain surface corrosion. If the rate of grain surface corrosion is low, there is little widening of grain boundary grooves following dissolution of the zone which contains chromium carbide or sigma phase constituent, and, therefore, the grains tend to remain in place (large slope). High rates of grain surface corrosion lead to widening of the attacked zone and to profuse grain dropping (low slope). In the narrow space formed by dissolution of the grain boundary zone the ratio of surface area to volume of solution is much greater than in the bulk solution. As a result, corrosion products may have a great effect on subsequent dissolution in these confined spaces.

Data on specimens corroding in ferric sulfate-sulfuric acid solution of various concentrations of acid support this view of the importance of the ratio of intergranular to grain surface corrosion. The resistance change-weight loss relationship in this solution is the same for 15.7 and 50% acid (Fig. 28). Thus, the ratio of intergranular penetration to grain surface corrosion should be independent of acid concentration. Evidence for this can be derived from the data plotted in Fig. 19, which shows the effect of acid concentration on the corrosion of annealed and of sensitized steel in ferric sulfate-sulfuric acid solutions. For this comparison the weight loss on sensitized specimens (Fig. 19A) may be used as a measure of intergranular penetration. From Fig. 28, it is apparent that the penetration measured by weight loss does not represent the total depth of penetration. Also, there is a relatively small amount of general corrosion reflected in this weight loss. However, these factors are eliminated by determining the ratio of intergranular to grain surface corrosion in solutions of various acid concentrations at the same stage of intergranular disintegration, i.e., at the same weight loss of the sensitized specimens, rather than at a certain time of immersion.

At a weight loss of 8.0 g/dm² the specimen (Fig. 19A) in 45% acid has corroded 192 hr. The weight loss of an annealed specimen in 45% acid after 192 hr is 0.70 g/dm², and the ratio of intergranular to grain surface corrosion is 8.0/0.70 = 11.4. Identical ratios are obtained in 50 and 60% acid. At a weight loss of 4.0 g/dm² the ratios are 5.7(40%), 7.25(45%), 7.25(50%), 7.25(60%). Thus, the ratio of intergranular to grain surface corrosion is independent of acid concentration.

The data of Fig. 23 show that the ratio of intergranular to grain-face corrosion in the copper sulfate-sulfuric acid solution is unaffected by the action of metallic copper.

In nitric acid, corrosion products, especially hexavalent chromium, greatly accelerate corrosion and cause widening of the spaces between the grains. Consequently, the depth of the layer of grains removed is almost equal to the depth of intergranular penetration (Fig. 28).

To compare corrosion currents and the corresponding electrode potentials in the three acid solutions, corrosion rates of annealed specimens have been converted to milliamperes per square centimeter, Table IV. Even though the corrosion current in ferric sulfate-sulfuric acid solutions varies by a factor of 88 in the range of 10-60% acid, the potential is essentially the same at all concentrations.

Effect of Chromium Carbide and Sigma Phase

The effect of length of time of sensitization on intergranular penetration and grain dropping de-

[16] The per cent change in resistance was derived from

$$\% \Delta R = \frac{R_f - R_o}{R_o}(100) = \frac{A_o - A_f}{A_f}(100)$$

where R_f, R_o, A_f, and A_o are the resistances and areas of cross sections of the specimens, at the beginning of the test and after exposure, f. To relate change in resistance to weight loss a specimen of 100 cm² surface area (neglecting the ends) 0.15 × 0.60 cm in cross section (66.6 cm long) was assumed. Using 8.04 g/cm³ as the density for 18 Cr-8 Ni stainless steel, the changes in weight for various changes in cross-sectional areas of the specimen was calculated. These same cross-sectional areas were used in the formula above to determine the accompanying change in resistance.

Table IV. Corrosion currents and electrode potentials of annealed AISI 304 (M304) steel in boiling acid solutions

Solution	Corrosion current,* ma/cm²	Electrode potential, (Sat. KCl electrode), v
Copper sulfate-15.7% sulfuric acid (in contact with copper)	0.00074	+0.06
Nitric acid (65%)	0.0040	+0.75–0.95
Ferric sulfate-sulfuric acid		
5.5 g/l Fe^{+3} + 1.15 g/l Fe^{+2}		
10% H_2SO_4	0.00043	+0.60†
30% H_2SO_4	0.0018	+0.60†
50% H_2SO_4	0.012	+0.59†
60% H_2SO_4	0.038	+0.61†

* Calculated from corrosion rates, which are constant with immersion time on annealed chromium carbide- and sigma phase-free) steel.

† Also the potential of platenized platinum electrode in these solutions.

pends on the solution to which the steel is exposed. Results obtained in copper sulfate-sulfuric acid solution have been plotted in Fig. 25. Intergranular penetration (per cent change in resistance) per gram of weight loss is greater on the specimen heated for 2 hr at 1250°F than for that heated 1 hr. Comparable tests have been made in ferric sulfate-sulfuric acid and in nitric acid solutions.

In ferric sulfate-sulfuric acid the difference in change in resistance between specimens heated 1 and 2 hr at 1250°F was only 35% at a weight loss of 8 g. This is much less than in the copper sulfate-sulfuric acid solution. Also, penetration per gram of weight loss was greater for the specimen heated 1 hr than for the 2-hr specimen. In nitric acid intergranular penetration and grain dropping were identical on both specimens. The data for the 1- and the 2-hr specimens, when plotted as in Fig. 25, fell on one curve. As expected, the rate of change in resistance and the rate of weight loss for a given length of exposure time was greatest in all three solutions for the specimen sensitized 2 hr.

These observations may also be interpreted in terms of the ratio of intergranular to grain face corrosion and the role of corrosion products. Increasing the length of sensitizing time from 1 to 2 hr increases the amount of chromium carbides formed and, to some extent, their size, i.e., the distance which they grow into the grains. There is some increase in widening of grooves and, therefore, an increase in grain dropping, and a consequent decrease of the slope of the resistance change-weight loss curve. In the ferric sulfate-sulfuric acid solution, in which corrosion products do not affect corrosion, there is such a decrease. In the copper sulfate-sulfuric acid solution increasing the length of sensitizing time increases intergranular penetration without a corresponding increase in grain dropping. In nitric acid, the accelerating effect of corrosion products obscures the influence of length of time of sensitizing. Again, grain boundaries are widened and lead to such rapid dislodgment that there is little penetration ahead of the surface produced by grain dropping.

For a comparison of the action of the acid solutions on various types of steels, the ratio of the corrosion rate (at a given exposure time) of a sensitized specimen to that of an annealed specimen of the same heat of steel has been applied. This ratio, which has already been used in connection with Table III, is a sensitive measure of the power of a solution to detect susceptibility to intergranular attack. In addition, it eliminates any changes in corrosion rates caused by small variations in alloy composition of the steels.

When these solutions are used for routine evaluation by means of weight-loss determinations, it usually is not necessary to test an annealed specimen along with the one being evaluated. The corrosion rate of the latter is compared with the maximum permissible rate established for the given solution and type of stainless steel. Selection of this maximum permissible rate is based, in part, on the known general or grain face corrosion.

There is one exception to this practice. In nitric-hydrofluoric acid solutions general corrosion is very sensitive to variations in alloy content (chromium) of the stainless steels. In the range of 16-19% Cr the corrosion rate of a group of AISI-316 steels varied from 2.7 to 0.8 in./mo; i.e., by a factor of 3. This solution has been employed occasionally as a qualitative method for detecting weld decay (32, 40, 41) and has been used in this investigation for comparison with the other three solutions. Because of the relatively large influence of small variations in chromium content on grain-face corrosion the ratio must be determined even for routine evaluation purposes.

A summary of results obtained on five different heats of steel is given in Table V. The susceptibility to intergranular attack in these steels varies from the pure chromium carbide type (AISI-304) to the pure sigma phase type (AISI-316L, FI-4). A combination of both types is illustrated by the two AISI-316 heats (M316, GT-8).

First, all specimens, except FI-4, show some completely encircled grains in the oxalic acid etch structure after heating 1 hr at 1250° (and 2 hr in the case of M316) and are, therefore, classed as "ditch" struc-

Table V. Comparison of tests

Test	Steel					
	AISI 304 (I-9)*	AISI 304 (FK-2)*	AISI 316 (GT-8)*	AISI 316 (M316)*	AISI 316† (M316)*	AISI 316L (FI-4)*
			Ratio**			
Oxalic acid						
Etch structure(a)	Ditch	Ditch	Ditch	Ditch	Ditch	Step
Nitric-hydrofluoric acid test(b)	4	1.5	9	6	40	1.0
Ferric sulfate-sulfuric acid test(c)	11	2	26(f)	8	34	1
Copper sulfate-sulfuric acid test(d)						
Exposure: 1000 hr						
Change in resistance, %	20	3	1475	40	568	1
Ratio of weight losses	4	2	34	7	20	1
Nitric acid test(e)	15	2	185(g)	19	141	36

* Refers to Laboratory Code, Analysis, Table I.
** Ratio of weight loss on sensitized to weight loss on annealed specimen.
† Sensitized 2 hr at 1250°F.
‡ (a) Standard oxalic acid etch of sensitized specimen.
(b) 10% HNO_3-3% HF at 65°C, 1-hr test.
(c) Ferric sulfate—50% sulfuric acid test, 120 hr.
(d) 5.7% $CuSO_4$-15.7% H_2SO_4 (no metallic copper).
(e) Standard 240-hr nitric acid test.
(f) 77-hr exposure.
(g) Only 120-hr exposure.

tures. The number of grains completely encircled varies from only a few grains on FK-2 to complete encirclement of almost all grains on I-9, GT-8, and M316. Only the FI-4 (0.020% C) steel is entirely free of chromium carbides after the sensitizing treatment (Fig. 13).

A comparison of the ratios obtained in nitric-hydrofluoric acid, ferric sulfate-sulfuric acid, and the 1000-hr cupric sulfate-sulfuric acid test shows that all these solutions give similar results. They reflect the chromium carbide type of intergranular susceptibility. The ratios of the FK-2 steel are smaller than those of the higher carbon, I-9 steel. Among the 316 steels the GT-8 heat is consistently higher than the M316 steel, which has been sensitized 1 hr. Extending the sensitizing treatment of M316 to 2 hr increases the ratio in all of these solutions. Also, the FI-4 steel, which is free of carbides, has a ratio of unity. In the copper sulfate test resistance measurement is a more sensitive indicator of intergranular attack than the ratio based on weight loss. The discrepancy between the ratio and the per cent change in resistance increases rapidly at the higher ratios.

In the *nitric acid* test the ratios on I-9 and FK-2 follow the trend of the other tests. However, on FI-4 there is a large increase in intergranular corrosion due to sigma phase, which is not detectable in the microstructure.[17] The relatively large ratios in nitric acid of the AISI-316 heats, especially GT-8,[18] are also caused by sigma phase in combination with chromium carbides.

All five tests reveal the presence of the chromium carbide type of susceptibility to intergranular attack. The sigma type is detected only in nitric acid.[19] Since the sigma type in 316 steel is known to cause intergranular attack only in nitric acid (42), one of the other quantitative evaluation tests could be used for routine evaluation of all stainless steels, except those AISI-316 and 316L steels which are intended for use in nitric acid. In determining which of these is the most promising, the following factors are of importance.

The most sensitive quantitative measure of intergranular attack in the copper sulfate-sulfuric acid test is the change in electrical resistance. Specialized apparatus is required for such measurements, and the test specimen must be relatively long and thin. Weight losses in this solution are relatively small and not nearly so sensitive as in the other solutions.[20] The nitric-hydrofluoric acid test is rapid (4 hr or less) (56), but requires testing of two specimens because evaluation is by ratio. Special equipment and care are required for handling hydrofluoric acid and holding the solution at a temperature considerably below the boiling point. For these, and other reasons, the 120-hr ferric sulfate-sulfuric acid test has been proposed to meet the need for a quantitative method of evaluating austenitic stainless steels for the chromium carbide type of susceptibility to intergranular attack in unstabilized stainless steels (22).

[17] An attempt was made to detect this phase by electrolytic etching in 15 other reagents, which included sulfuric, chromic, phosphoric, citric, and formic acid. In every case, a step structure similar to that obtained in the oxalic acid etch was the result. Intergranular attack in this steel in nitric acid is, therefore, associated with a preprecipitation form of the sigma constituent.

[18] Note that the ratio given in Table V is only for a 120-hr exposure in nitric acid. After the regular 240-hr test this ratio would be much greater.

[19] In terms of the polarization concepts developed above, this indicates that the presence of chromium carbides leads to a decrease in polarizability at grain boundaries in all five solutions. However, sigma phase, which is also a chromium-rich phase, occurring in 18 Cr-8 Ni-Mo steel, decreases polarizability of grain boundary zones only in nitric acid.

[20] For example, it was not possible to detect by weight loss or resistance change the relatively small variations in intergranular attack produced by various lengths of sensitizing heat treatments on FK-2 steel. In nitric acid these changes were readily found, as shown in Fig. 2.

Effect of Grain Size

Discussions of grain dropping and intergranular penetration, as given above, lead to the problem of the influence of grain geometry on these processes. Does the grain size of the steel affect the rate of intergranular corrosion? On the basis of corrosion tests in sulfuric acid, with and without copper sulfate, Newell (43) has concluded that susceptibility to intergranular attack increases with grain size. Rutherford and Aborn (35) and Ferri (44) have made resistance measurements on specimens exposed to copper sulfate-sulfuric acid solution, which also showed more rapid intergranular penetration on large than on small grained steel. On the basis of these observations some investigators (35, 43, 45, 46) have concluded that intergranular carbide precipitation per unit surface of grain boundary is a function of grain size. However, on steels corroding in nitric and other acids it has frequently been observed in the present investigation that small-grained steels drop grains after shorter exposure periods than large-grained specimens. Also, on specimens having grains of various sizes the smallest are the first ones to be dislodged. Furthermore, they are the most likely to be surrounded completely by ditching in the oxalic acid etch structures.

In order to obtain quantitative data on this problem, specimens having appreciably different grain sizes were required. Various combinations of mechanical deformation and heat treatments were tried to induce grain growth. These were unsuccessful. The only method found to produce exaggerated growth was a cyclic heat treatment. A group of AISI-304 specimens was welded into a stainless steel vessel and heated to 2200°F for 7 hr and then furnace cooled. This procedure was repeated three times. The over-all diameter of the grains was thus increased from 0.04 mm to 3 mm.

It was evident that there had been some decarburization of the specimens during these heat treatments. They were bright as a result of oxide removal by reaction with carbon in the steel. Examination of carbides isolated from these specimens, after sensitizing heat treatments, showed that these were entirely different in size and shape from those found in this steel before the high-temperature heat treatments. Thus, besides grain growth, there had been other changes which were known to affect intergranular penetration. (Figure 25 shows that a 2-hr sensitizing treatment results in a different type of intergranular attack than 1-hr treatment.) For these reasons, the data obtained on these specimens are not presented in detail but are used for qualitative comparison with those of another heat of steel in which a

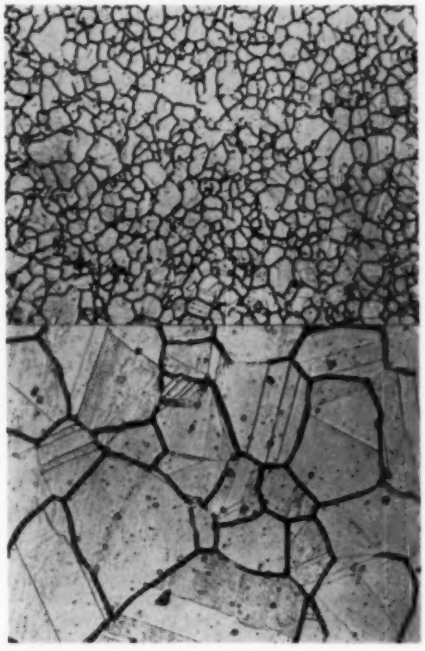

Fig. 29. Microstructure of AISI-316 steel used for grain size study. Steel: AISI-316 (GT-8, Table I). Etched electrolytically in oxalic acid. A (top), steel as received and heated 1 hr at 1250°F (unusually small grain size); B (bottom), heated first for 1 hr at 1950°F, W.Q., and then 1 hr at 1250°F. Magnification 500X before reduction for publication.

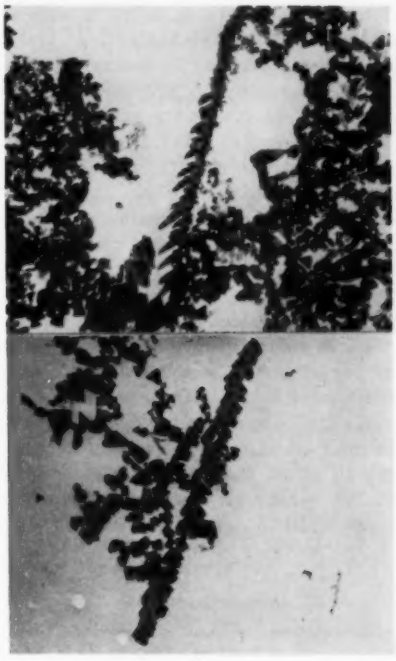

Fig. 30. Electron photomicrographs of carbides isolated from sensitized AISI-316 steel. Steel: GT-8, specimens same as Fig. 29. A (top), from small-grained specimen; B (bottom), from large-grained specimen. Magnification 20,000X before reduction for publication.

variation in grain size was induced without extensive heat treatments.

A heat of AISI-316 (GT-8) steel was found which had an unusually small, uniform grain size (Fig. 29A). This was readily changed to a normal grain size by a 1-hr heat treatment at 1950°F. The ratio of internal boundary area of the small-grained to the large-grained steel as determined by the method of random sectioning (47) was 5.7. Carbides were isolated from both types of specimens and examined in the electron microscope. The shapes and sizes of the carbides appear unchanged by this grain growth (Fig. 30A and B). As might be expected, the quantity of carbides remaining after some metal had been dissolved was much greater on the small-grained than on the large-grained specimen. Results obtained on sensitized large and small-grained specimens of this steel in three acid solutions have been plotted in Fig. 31.

The relatively high carbon content (0.074% C) of this steel leads to very high corrosion rates in all tests. An appreciable amount of the sigma type of susceptibility has also been formed during sensitization (Table V). The rates in nitric acid were so high that it was not possible to complete the standard 240-hr test because the ⅛-in. thick specimens became too thin.

In all three tests, Fig. 31, the small-grained specimens had a greater weight loss (corrosion rate) than the large-grained specimens, especially in the copper sulfate-sulfuric acid solution.[21] (This was also the case on the normal and large-grained AISI-304 steel.) However, changes in resistance are greater on the large-grained specimen in nitric acid and in ferric sulfate-sulfuric acid solution. In copper sulfate-sulfuric acid the small-grained specimen shows the greatest increase. This reversal may be due to an unusual amount of grain dropping, which is implied in the high weight loss in this solution. The grains are so small that there is profuse dropping even on an

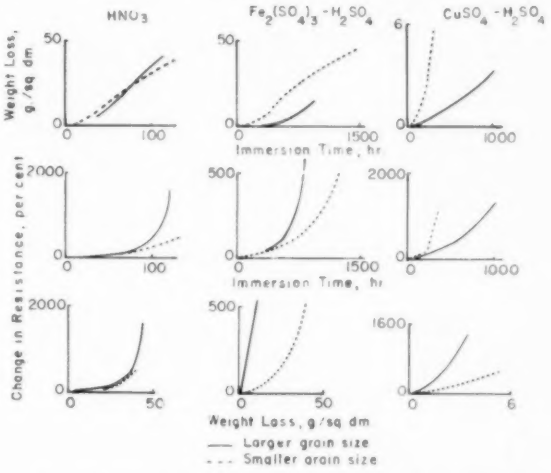

Fig. 31. Effect of grain size on intergranular corrosion of sensitized AISI-316 steel in three boiling acids. Steel: AISI-316 (GT-8) in two grain sizes as shown in Fig. 29. Specimens heated 1 hr at 1250°F. Solutions: 65% nitric acid; ferric sulfate, 15.7% sulfuric acid; 5.7% cupric sulfate, 15.7% sulfuric acid (no metallic copper).

[21] There is less difference between the two specimens in nitric acid than in the other solutions, and after about 80 hr the curves cross. Rapid accumulation of corrosion products and consequent acceleration by hexavalent chromium may have obscured the effect of grain size.

AISI-316 steel. Normal or large grains are not readily dislodged by this solution.

Despite these differences in behavior, the resistance change accompanying a given weight loss is greater on the large-grained specimen in all three solutions (bottom row, Fig. 31). Because small grains drop more readily, the results on the smaller steel are closer to the calculated curve.

In conclusion, the effect of grain size on corrosion depends on the method of measurement (weight loss or resistance change) and on the testing solution. While the total amount of intergranularly precipitated chromium carbides is greater in the small-grained than in the large-grained steel, the amount of carbide per unit area of internal grain surface is probably the same in both. Only when the diameter of the small grains approaches the width of the grain boundary zone containing chromium carbides will the grain size affect the amount of precipitate per unit area. The width of this zone depends, among other factors, on the length of time of the sensitizing treatment, i.e., the size of the carbides (cf. Fig. 14B and 30).

Acknowledgment

The writer wishes to thank S. J. Kucharsey for his assistance with this investigation.

Manuscript received April 16, 1958. This paper was prepared for delivery before the Ottawa Meeting, Sept. 28-Oct. 2, 1958.

Any discussion of this paper will appear in a Discussion Section to be published in the December 1959 JOURNAL.

REFERENCES

1. G. A. Ellinger, *Trans. Am. Soc. Metals*, **24**, 26 (1936).
2. ASTM Book of Standards, 1955, Part I, p. 1108, "Tentative Recommended Practice of Boiling Nitric Acid Test for Corrosion Resisting Steels," (A262-55T).
3. M. A. Streicher, *ASTM Bull.*, **188**, 35 (February 1953), *Werkstoffe u. Korrosion*, **5**, 363 (1954).
4. W. R. Huey, *Trans. Am. Soc. Steel Treating*, **18**, 1126 (1930).
5. T. L. O'Connor and H. H. Uhlig, *J. Phys. & Colloid Chem.*, **61**, 402 (1957).
6. H. C. Gatos, *Corrosion*, **12**, 322 (1956).
7. W. B. DeLong, "Symposium on Evaluation Tests for Stainless Steels," ASTM Special Tech. Publ. 93, 211 (1949).
8. M. M. Kurtepov, G. V. Akimov, and N. N. Bardizh, *Doklady Akad. Nauk SSSR*, **87**, 625 (1952).
9. A. B. McIntosh, *Chemistry & Industry*, **1957**, 687.
10. J. E. Truman, *J. Appl. Chem.*, **4**, 273 (1954).
11. M. M. Kurtepov and G. V. Akimov, *Doklady Akad. Nauk SSSR*, **87**, 93 (1952).
12. P. Lacombe, Physical Soc. Bristol Conference Report, 91 (1948).
13. M. H. Brown, W. B. DeLong, and W. R. Myers, "Symposium on Evaluation Tests for Stainless Steels," ASTM Special Tech. Publ. 93, 103 (1949).
14. J. J. Heger and J. L. Hamilton, *Corrosion*, **11**, 6 (1955).
15. A. J. Lena, Discussions in *Trans. ASM*, **45**, 446 (1953).
16. S. J. Rosenberg and C. R. Irish, *J. Research Nat. Bur. Standards*, **48**, 40 (1952).
17. E. M. Mahla and N. A. Nielsen, *Trans.* A.S.M., **43**, 290 (1951).
18. A. J. Lena, Private communication.
19. P. J. E. Forsyth, G. J. Metcalfe, R. King, and B. Chalmers, *Nature*, **158**, 875 (1946).
20. W. G. Gruhl and D. Ammann, *Acta Met.*, **3**, 347 (1955).
21. M. A. Streicher, *Corrosion*, **14**, 59 (1958); (to du Pont Co.) U. S. Pat. 2,793,190 and 2,793,191, May 21, 1957.
22. M. A. Streicher, ASTM Bulletin No. 229, p. 77, April 1958.
23. W. H. Hatfield, *Trans. Electrochem. Soc.*, **46**, 297 (1924).
24. G. H. Cartledge, *Nature*, **177**, 181 (1956), and *This Journal*, **104**, 420 (1957).
25. W. Good and W. A. B. Purdon, *Chemistry & Industry* (London), **1955**, 1594.
26. H. J. Rocha and G. Lennartz, *Arch. Eisenhüttenw.*, **26**, 117 (1955).
27. C. Carius, *ibid.*, **26**, 769 (1955).
28. C. Edeleanu, *Nature*, **173**, 739 (1954).
29. E. H. Phelps and D. C. Vreeland, *Corrosion*, **13**, 619 (1957).
30. M. A. Streicher, *This Journal*, **103**, 375 (1956).
31. J. H. G. Monypenny, "Stainless Iron and Steel," Vol. I, 99, Chapman and Hall, Ltd., London (1951).
32. W. O. Binder and C. M. Brown, "Symposium on Evaluation Tests for Stainless Steels," ASTM Special Tech. Publ. 93, 146-171 (1959).
33. H. Ebling and M. A. Scheil, "Symposium on Evaluation Tests for Stainless Steels," ASTM Special Tech. Publ. 93, 121-138 (1949).
34. O. Masi and A. Ferri, *Met. ital.*, **44**, 207 (1952).
35. J. B. Rutherford and R. H. Aborn, *Trans. Amer. Inst. Mining Met. Engrs.*, **100**, 293 (1932).
36. H. J. Rocha, Discussion in Reference (39).
37. ASTM Book of Standards, 1955, Part I, 1135, "Tentative Recommended Practice for Conducting the Acidified Copper Sulfate Test for Intergranular Attack in Austenitic Stainless Steels," (A393-55T).
38. M. A. Streicher, *J. (and Trans.) Electrochem. Soc.*, **93**, 285 (1948).
39. E. Brauns and G. Pier, *Stahl u. Eisen*, **75**, 579 (1955).
40. F. K. Bloom and M. E. Carruthers, "Symposium on Evaluation Tests for Stainless Steels," ASTM Special Tech. Publ. 93, 87-100 (1949).
41. H. Zitter, *Arch. Eisenhüttenw.*, **28**, 401 (1957).
42. D. Warren, Submitted to *Corrosion* (1959).
43. H. D. Newell, *Trans. Am. Soc. Steel Treating*, **19**, 673 (1932).
44. A. Ferri, *Met. ital.*, **43**, 432 (1951).
45. F. J. Phillips, *Trans. A.S.M.*, **39**, 891 (1947).
46. E. C. Bain, R. H. Aborn, and J. J. B. Rutherford, *Trans. Am. Soc. Steel Treating*, **21**, 481 (1933).
47. C. S. Smith and L. Guttman, *J. Metals*, **5**, 81 (1953).
48. J. V. Petrocelli, *This Journal*, **97**, 10 (1950).
49. T. P. Hoar and U. R. Evans, *ibid.*, **99**, 212 (1952).
50. I. D. G. Berwick and U. R. Evans, *J. Appl. Chem.*, **2**, 576 (1952).
51. N. D. Tomashov, G. P. Sinelshchikova, and M. A. Vedeneeva, *Zhur. Fiz. Khim.*, **23**, 3 (1949), discussed in Platinum Metals Review, **2**, 117 (1958).
52. G. Masing, T. Heumann, and H. Jesper, *Arch. Eisenhüttenw.*, **25**, 169 (1954).
53. E. H. Dix, *Trans. Am. Inst. Mining Met. Engrs.*, **137**, 11 (1940).
54. L. R. Standifer, Thesis, The Ohio State University, Columbus, Ohio (1952).
55. C. Carius, *Arch. Eisenhüttenw.*, **29**, 449 (1958).
56. D. Warren, *ASTM Bull.*, **230**, 45 (May 1958).
57. K. J. Vetter, *Z. Elektrochem.*, **62**, 642 (1958).

The Diffusion of Oxygen in Alpha and Beta Zircaloy 2 and Zircaloy 3 at High Temperatures

M. W. Mallett, W. M. Albrecht, and P. R. Wilson[1]

Battelle Memorial Institute, Columbus, Ohio

ABSTRACT

The diffusion rates of oxygen in alpha and beta Zircaloy 2 and Zircaloy 3 were determined in the range 1000°-1500°C. For alpha Zircaloy 2, the variation of the diffusion coefficient, D, in cm²/sec, with temperature is given by the equation

$$D_\alpha = 0.196 \exp(-41{,}000 \pm 1500/RT)$$

For beta Zircaloy 2,

$$D_\beta = 0.0453 \exp(-28{,}200 \pm 2400/RT)$$

Spot checks of the diffusion of oxygen in alpha and beta Zircaloy 3 to 1100° and 1400°C show that the rates are in close agreement with those for oxygen in Zircaloy 2.

The diffusion coefficients for oxygen in beta Zircaloy 2 and Zircaloy 3 are about 10 times greater than those for nitrogen in high-purity beta zirconium.

The water and steam corrosion of Zircaloy 2 has been investigated up to 400°C (1, 2). The corrosion reaction proceeds principally by formation of a surface film of ZrO_2. One of the processes that occurs during the reaction is the diffusion of oxygen in the metal. At the temperatures that have been investigated, the diffusion rates are very slow and do not contribute to the over-all corrosion process. However, at high temperatures above 1000°C or so, the rate of diffusion becomes appreciable and may play a large part in the over-all reaction. Therefore, as part of a study of the high-temperature corrosion of Zircaloy 2 and Zircaloy 3, the diffusion coefficients of oxygen in the alpha and beta phases of the materials were determined at 1000°-1500°C. Rather complete data were obtained for Zircaloy 2. The diffusion in Zircaloy 3 was spot checked to obtain a few rates for comparison with those for oxygen in Zircaloy 2.

Experimental

Materials

The Zircaloy 2 and Zircaloy 3 for this work were fabricated into 5/8-in.-diameter rods. Specimens for the experiments were machined from these rods. Analyses of both alloys were obtained by spectrographic, chemical, and vacuum-fusion techniques. Results are given in Table I.

Oxygen was prepared by the thermal decomposition of degassed potassium permanganate as described by Hoge (3). It was dried with a dry ice-acetone cold trap.

Zirconium-Oxygen Phase Diagram

Knowledge of the phase diagrams of the Zircaloy 2 and Zircaloy 3 oxygen systems should be known in preparing suitable diffusion specimens to determine diffusion coefficients, but no information is available on either system. However, it is believed that the zirconium-oxygen system (4) is very similar to the Zircaloy-oxygen systems since the basic structure of the alloys is not changed from that of zirconium, that is, alpha and beta Zircaloy alloys have the same structures as alpha and beta zirconium. Therefore, the zirconium-oxygen system was used as a source of oxygen-concentration data needed for diffusion studies of the Zircaloy materials. A partial phase diagram of the zirconium-oxygen system is reproduced in Fig. 1. The portion of the diagram of interest for this study is that from 1000° to 1500°C. In this range, the beta-alpha plus beta boundary represents the maximum solubility of oxygen in beta (solid solution) zirconium. The alpha plus beta-alpha boundary represents the lowest oxygen concentration required to maintain a single phase of alpha (solid solution) zirconium. The alpha-alpha plus ZrO_2 boundary represents the maximum solubility of oxygen in alpha zirconium.

Table I. Analyses of Zircaloy 2 and Zircaloy 3

Element	Amount present, wt %	
	Zircaloy 2	Zircaloy 3
Sn	1.5	0.22
Fe	0.20	0.34
Cr	0.05	0.03
Ni	0.03	0.005
Si	0.007	0.05
Al	0.006	0.005
Mn	0.002	0.01
Mg	0.002	0.001
Pb	0.002	—
O_2	0.089	0.14
N_2	0.003	0.01
H_2	0.002	0.003

[1] Present address: Department of Chemistry, University of Massachusetts, Amherst, Mass.

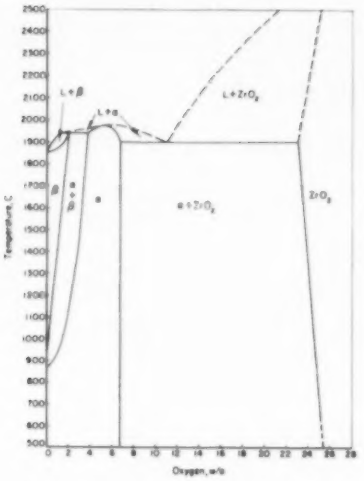

Fig. 1. Partial phase diagram of the zirconium-oxygen system.

Concentration-Gradient Technique

The concentration-gradient technique (5) was used to determine the diffusion coefficients for oxygen in beta-phase Zircaloy 2 and Zircaloy 3. Essentially, the method consists of analyzing the concentration gradient in a cylindrical specimen resulting from reaction with oxygen at a given temperature for a predetermined length of time. The diffusion coefficient was determined from the concentration gradient by a graphical method.

Specimens having gradients were prepared as follows. A Zircaloy 2 (or Zircaloy 3) cylinder about 1 cm in diameter and 4 cm long was dry abraded with 240-grit silicon carbide paper. After the dimensions of the cylinder were measured, the specimen was placed in the Vycor furnace tube of a modified Sieverts apparatus (2). The sample then was induction heated in a vacuum for 1 hr at the temperature of the run. Temperatures were measured under black-body conditions with an optical pyrometer. With the sample at the desired temperature, an amount of oxygen (based on the maximum solubility in beta phase at desired temperature) calculated to maintain a thin oxide film on the sample was added to the reaction chamber. The sample was heated for a length of time sufficient to prepare a suitable gradient; that is, enough oxygen was diffused to just begin to affect the core. At the end of this time, the sample was quenched as rapidly as possible. Temperatures below 500°C were attained in less than 30 sec. At 500°C and below, diffusion is extremely slow so that very little movement of oxygen occurred below this temperature. The film on the sample contained the phases shown in the phase diagram, Fig. 1. Proceeding from right to left on the diagram at the temperature of the run, the outer layer is ZrO_2; beneath this is a very thin layer of alpha solid solution. Beneath this is the beta core which contains the oxygen gradient being measured. It should be noted that two-phase regions are not produced by diffusion in a heterogeneous binary system (6).

Since diffusion occurs from the ends of the cylinder as well as the sides, lengths equal to the radius were cut from each end of the specimen and discarded. This insured that the remaining sample would have a concentration gradient as uniform as possible from end to end. The remainder of the sample was machined radially into layers of equal weight and each layer analyzed for oxygen by the vacuum-fusion method. Diffusion coefficients then were determined by the graphical method, using the average oxygen concentrations of the layers, the average radii, and the time. The thin surface layer, which contains alpha and oxide phases, was not used in the calculations.

Moving-Boundary Technique

The diffusion coefficients of oxygen in the alpha phase of Zircaloy 2 (and Zircaloy 3) were determined by the moving-boundary technique described by Jost (5).[2] This method was developed by Wagner for the case of diffusion into a heterogeneous system of given over-all concentration. The mathematical treatment of this case is based on the fact that a displacement, ξ, of the phase boundary produced by the diffusion of a single species is proportional to the square root of the time of diffusion, i.e.,

$$\xi = 2\gamma\sqrt{Dt} \qquad [1]$$

where ξ is the displacement of the phase boundary, cm; γ, a dimensionless parameter characteristic of the system; D, diffusion coefficient, cm^2/sec; and t, time, sec. The parameter, γ, is defined as follows:

$$\frac{C_\alpha - C_{\text{II, I}}}{C_{\text{II, I}} - C_0} = \sqrt{\pi}\,\gamma \exp\gamma^2 \operatorname{erf}\gamma \qquad [2]$$

where C_α, $C_{\text{II, I}}$, and C_0 are concentrations of the diffusing species at various phase boundaries. In the present case, for a given temperature, C_α is the maximum solubility of oxygen in the alpha phase, $C_{\text{II, I}}$ is the oxygen concentration at the alpha plus beta-alpha boundary, and C_0 is the oxygen concentration at the beta-alpha plus beta boundary. The term erf γ is the "gaussian error function." Values of erf γ may be found in Jost (7) and Carslaw and Jaeger (8). The value for γ was determined from Eq. [2] by a graphical method.

To determine the value of the diffusion coefficient, it is necessary to have values of ξ, t, and γ at a given temperature. The slope of the plot of ξ vs. $t^{1/2}$ is equal to $2\gamma\sqrt{D}$ from which D may be evaluated.

Experimental techniques used to obtain the moving-boundary measurements are as follows. A cylindrical specimen about 1 cm in diameter by 4 cm long was prepared as described above for the gradient method. A calculated quantity of oxygen, C_0, was then added in slight excess to saturate completely the beta phase at the experimental temperature. This sample was heated at temperature for 6 to 8 hr. The specimen then was quenched to room temperature. To check the homogeneity of the

[2] Jost presents the solution of Fick's law for movement of a boundary in a plate. Brief calculations showed that for small displacements of the boundary in a cylinder, the equations for plates could be used in calculating diffusion coefficients without introducing significant errors.

specimen, metallographic examination was made of a cross section. A uniform distribution of a few alpha grains in a beta zirconium matrix was observed. This would be expected since even slight lowering of the temperature would supersaturate the beta phase in respect to oxygen. The alpha grains must have formed during the 30-sec cooling required to reach a temperature below which diffusion was negligible. This cooling time introduces an error of not more than 10% in measuring the minimum diffusion time of 5 min. At maximum diffusion times (120 min) the error was less than 0.4%.

The surface oxide (excess oxygen) was abraded from the surface of the sample which was then cut into three cylinders. The cylinders were heated in an oxygen atmosphere at temperature for various periods of time. A calculated quantity of oxygen was reacted to maintain an oxide film at all times but to keep its thickness at a minimum. The thickness of the oxide was always less than 5% of the alpha layer and was ignored in all calculations. At the end of the heating period, the sample was quenched as rapidly as possible and cut in half diametrically. The cross section was examined metallographically to determine the movement of the alpha-beta boundary. The diameter of the beta core was measured and subtracted from the original diameter of the cylinder. From this, the displacement of the boundary was determined. Then, the diffusion coefficient was determined from the slope of a plot of the displacement, ξ, against $t^{1/2}$.

Results and Discussion

The diffusion coefficients for oxygen in alpha and beta Zircaloy 2 were determined in the range 1000°-1500°C at 100°C intervals. Experimental diffusion times ranged from 5 to 120 min. Attempts were made to obtain coefficients at 1600°C; however, no suitable gradients or moving boundaries could be prepared. The experimental times (less than 5 min) at 1600°C necessary to prepare optimum diffusion samples were so short that errors in the measurement of the time required to quench to room temperature would introduce large errors in the estimation of actual diffusion times. The data obtained on a gradient prepared in beta Zircaloy 2 at 1100°C for 35 min are shown in Fig. 2 The thicknesses of the machined layers and the average oxygen concentration of each layer are shown. The solid line is the theoretical curve derived from diffusion theory (5) for this gradient. It is seen that there is good agreement between the experimentally determined concentrations and the theoretical curve. Also, it was found that the terminal solubilities of oxygen in beta Zircaloy 2 (obtained from concentration gradients) agreed with those for oxygen in pure zirconium. It is seen from Table II that with the exception of the 1400°C value these solubilities show an average difference of only 0.03 wt %. This supports the earlier assumption that the Zircaloy(s)- and zirconium-oxygen phase relationships are closely similar. The 1100°C terminal oxygen solubility for beta Zircaloy 3 also agrees with zirconium data, but again the

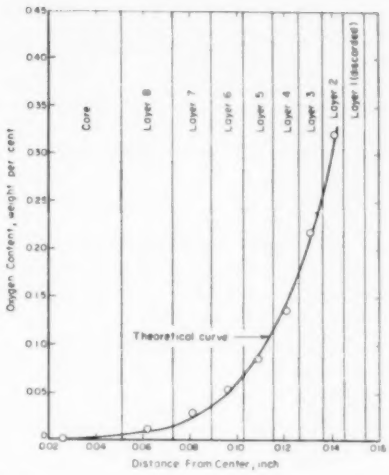

Fig. 2. Oxygen concentration gradient prepared in beta Zircaloy 2 at 1100°C for 35 min.

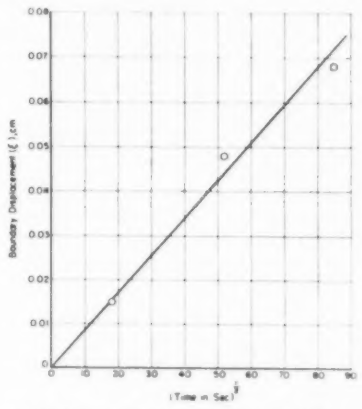

Fig. 3. Variation of displacement of alpha-beta boundary with time for oxygen in alpha Zircaloy 2 at 1200°C.

1400°C value shows a large discrepancy. The fact that the greatest differences were noted at 1400°C is believed to be coincidental rather than systemic. In Fig. 3 is shown a typical plot of the alpha-beta boundary displacement, ξ, against $t^{1/2}$ for alpha Zircaloy 2 at 1200°C. The slope of the line is equal to $2\gamma\sqrt{D}$. At 1200°C, the value of γ is 0.895. From

Table II. Terminal solubility of oxygen in beta Zircaloy 2 and beta Zircaloy 3

	Oxygen, wt %				
	Pure Zr*	Zircaloy 2		Zircaloy 3	
Temperature, °C	Solubility	Solubility	Difference†	Solubility	Difference†
1000	0.20	0.25	0.05	—	—
1100	0.38	0.44	0.06	0.42	0.04
1200	0.62	0.61	0.01	—	—
1300	0.83	0.80	0.03	—	—
1400	1.05	0.80	(0.25)	1.3	(0.25)
1500	1.29	1.3	0.01	—	—
	Average difference 0.03				

* From Ref. (4).
† Difference from pure zirconium.

Table III. Diffusion coefficients for oxygen in alpha and beta Zircaloy 2 and Zircaloy 3

Material	Diffusion coefficient, cm²/sec, at temperature indicated, °C					
	1000	1100	1200	1300	1400	1500
Zircaloy 2, alpha	1.8×10^{-8}	4.8×10^{-8}	2.3×10^{-7}	3.6×10^{-7}	7.9×10^{-7}	1.7×10^{-6}
Zircaloy 2, beta	8.2×10^{-7}	1.4×10^{-6}	2.4×10^{-6}	3.8×10^{-6}	8.1×10^{-6}	2.4×10^{-5}
Zircaloy 3, alpha	—	5.8×10^{-8}	—	—	1.4×10^{-6}	—
Zircaloy 3, beta	—	1.4×10^{-6}	—	—	6.5×10^{-6}	—

these values the diffusion coefficient was calculated. All the data are given in Table III. The diffusion coefficients for oxygen in alpha Zircaloy 2 range from 1.8×10^{-8} cm²/sec at 1000°C to 1.7×10^{-6} cm²/sec at 1500°C. Those for oxygen in beta Zircaloy 2 range from 8.2×10^{-7} cm²/sec at 1000°C to 2.4×10^{-5} cm²/sec at 1500°C.

In Fig. 4 and 5 are shown the variations of the diffusion coefficients with temperature for alpha Zircaloy 2 and beta Zircaloy 2, respectively. The logarithms of the diffusion coefficients are plotted against the reciprocal of temperature (Arrhenius-type plot). Equations for the best straight lines through the points were determined by the method of least squares. The equation for the diffusion coefficient, D, in cm²/sec, for oxygen in alpha Zircaloy 2 is

$$D = 0.196 \exp [(-41{,}000 \pm 1500)/RT] \quad [3]$$

For oxygen in beta Zircaloy 2,

$$D = 0.0453 \exp [(-28{,}200 \pm 2400)/RT] \quad [4]$$

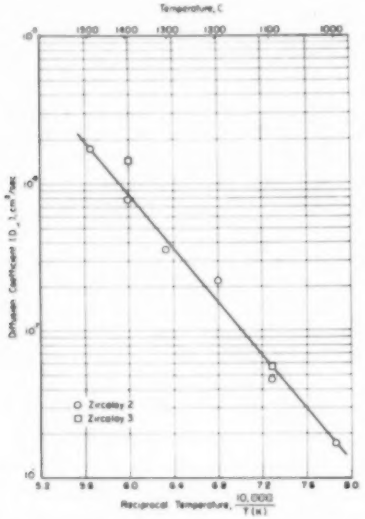

Fig. 4. Temperature variation of the diffusion coefficient for oxygen in alpha Zircaloy 2 and Zircaloy 3.

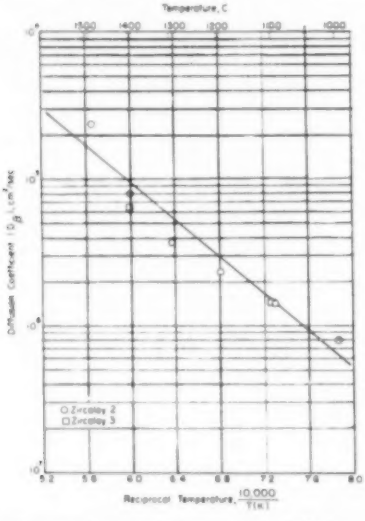

Fig. 5. Temperature variation of the diffusion coefficient for oxygen in beta Zircaloy 2 and Zircaloy 3.

The diffusion coefficients for oxygen in alpha and beta Zircaloy 3 were determined at 1100° and 1400°C. The values also are given in Table III and plotted in Fig. 4 and 5. It is seen that they are in good agreement with those for Zircaloy 2. Apparently, the alloying constituents in the range studied have very little effect on the diffusion of oxygen.

The diffusion coefficients for oxygen in beta Zircaloy 2 and Zircaloy 3 are greater (about 10 times) than those for nitrogen in high-purity beta zirconium (9). This difference probably arises from the differences in the size of the diffusing species, oxygen and nitrogen, and not from differences in the alloying constituents. The atomic radius of oxygen is 0.60Å and that of nitrogen is 0.71Å. Since oxygen is the smaller atom, it would be expected to diffuse faster.

Manuscript received Sept. 3, 1957. Work performed under subcontract to the Bettis Laboratory of the Atomic Energy Commission, operated by Westinghouse Electric Corporation. This paper was prepared for delivery before the Ottawa Meeting, Sept. 28-Oct. 2, 1958.

Any discussion of this paper will appear in a Discussion Section to be published in the December 1959 JOURNAL.

REFERENCES

1. D. E. Thomas, "Metallurgy of Zirconium," **VII-4** 608, McGraw Hill Book Co., New York (1955).
2. D. E. Thomas and S. Kass, Jr., *This Journal*, **104**, 261 (1957).
3. H. J. Hoge, *J. Research Nat. Bur. Standards*, **44**, 321 (1950).
4. R. F. Domagala and D. J. McPherson, *Trans. Am. Inst. Mining Met. Engrs.*, **200**, 238 (1954).
5. M. W. Mallett, E. M. Baroody, H. R. Nelson, and C. A. Papp, *This Journal*, **100**, 103 (1953).
6. F. N. Rhines, "Surface Treatment of Metals," p. 122, American Society for Metals, Cleveland, Ohio, (1941).
7. W. Jost, "Diffusion," p. 71, Academic Press, Inc., New York (1952).
8. H. Carslaw and J. C. Jaeger, "Conduction of Heat in Solids," Oxford University Press, London (1948).
9. M. W. Mallett, J. Belle, and B. B. Cleland, *This Journal*, **101**, 1 (1954).

Reaction of Aluminum and Carbon Tetrachloride, I

J. D. Minford, M. H. Brown, and R. H. Brown

Alcoa Research Laboratories, Aluminum Company of America, New Kensington, Pennsylvania

ABSTRACT

Many aluminum alloys are corroded severely by boiling CCl_4. Two of the products of the reaction are aluminum chloride and hexachloroethane. The presence of anhydrous aluminum chloride accelerates the reaction. A number of chemical agents can retard this reaction apparently by combining with aluminum chloride as it is produced. The reaction of aluminum alloys drops off rapidly as the magnesium content increases.

Aluminum reacts rapidly with boiling carbon tetrachloride to form aluminum chloride and hexachloroethane (1) as follows:

$$2Al + 6CCl_4 \rightarrow 2AlCl_3 + 3C_2Cl_6 \qquad [1]$$

Previous investigations have been concerned with the effect of impurities in the carbon tetrachloride and the relative rate of attack on different alloys. However, there has been little evidence to establish a suitable reaction mechanism. Since the use of aluminum with halogenated hydrocarbons has important commercial applications, a need exists for better understanding of the mechanism of the reaction.

Stern and Uhlig (2) investigated certain phases of the reaction between aluminum and boiling carbon tetrachloride and concluded that an induction period of about 70 min exists during which no reaction takes place. It was found that the length of the induction time could be increased in the presence of either water or carbon disulfide and decreased in the presence of the corrosion products (Eq. [1]). They also found no consistent difference in corrosion rates between cathode and anode from either galvanic coupling or an applied potential of 1.5 v. When they applied a potential of 1000 v, the anode corroded about 1 hr before the cathode, but this was described as being the result of a premature breakdown of the protective coating on the aluminum surface. These authors interpreted these results as excluding an electrochemical mechanism and concluded that the reaction proceeds by a "typical direct chemical reaction."

In a subsequent paper Stern and Uhlig (3) proposed that the reaction proceeded by a free radical mechanism. This conclusion was based on the fact that the reacting solution is colored and that water and oxygen, which increase the induction period, also are known to combine with free radicals. Also, substances such as quinone, 1, 4-napthoquinone, and nitrobenzene, which have been listed as free radical suppressors, act as inhibitors for this reaction. Additional experiments to supplement this data and determine the feasibility of this free radical mechanism will be presented in a subsequent paper (3a).

The importance of the practical application of aluminum with halogenated hydrocarbons has led to considerable investigation during the last seven years. As a result, significant data pertinent to the mechanism, not available in the literature, have been obtained.

Characteristics of the Reaction (99.99% Al)

Visible effects.—Most of the experiments were carried out in a 500-ml round-bottomed glass flask connected to a reflux condenser by a ground glass joint. Two hundred and fifty milliliters of carbon tetrachloride were placed in the flask and heated on an electric hot plate. The aluminum specimens (0.064 x ½ x 3 in.) were placed in the carbon tetrachloride after the boiling point was reached.

As previously reported (2) it was observed that the first sign of corrosion usually appeared as a small black spot of corrosion product on the surface of the specimen after about 30 min. These spots increased in number until the entire surface was covered. The solution turned a faint pink after several hours and gradually darkened, finally becoming black with the formation of a large amount of insoluble black corrosion product. When the solution was filtered to remove the black insoluble product and then evaporated, a yellow residue was left indicating that a soluble reaction product had been formed.

Weight loss vs. time relationships.—The weight loss data given in Table I show that very little corrosion occurred in the first hour, but following that it proceeded rapidly. This apparent induction period had been observed previously (2). As will be shown in the second paper (3a) the reaction proceeds from time zero.

Effect of temperature on reaction.—Zappi (4) has

Table I. Corrosion weight losses of 99.99% aluminum in boiling carbon tetrachloride

Specimen No.	Exposure time, hr	Weight loss, g
1	1.00	0.0024
2	1.75	0.1652
3	2.25	0.2146
4	3.00	0.4252
5	4.00	0.7257
6	4.50	1.0822
7	5.50	1.3862
8	6.50	1.6843
9	7.00	2.0022

Table II. Corrosion resistance of aluminum alloys to carbon tetrachloride at room temperature*

Alloy	CCl_4 purity	Time, mo	Weight loss, g	Observation
99.99% Al	Tech.	18	0.015†	No visual corrosion
99.99% Al	C. P.	18	0.012	No visual corrosion
3003	Tech.	18	0.002	No visual corrosion
3003	C. P.	18	0.007	No visual corrosion
5052	Tech.	18	0.006	No visual corrosion
5052	C. P.	18	0.009	No visual corrosion
5154	Tech.	18	0.008	No visual corrosion
5154	C. P.	18	0.005	No visual corrosion

* Aluminum alloys formed into storage containers with a weld midway up the side wall were half filled with carbon tetrachloride. The containers were stored in a tilted position so that only half of the weld bead was immersed.
† The weight losses represent averages from duplicate storage tests. The initial weights of the containers were about 270 g.
Note: The exposed area was 45 $in.^2$.

reported that no reaction occurred between aluminum and carbon tetrachloride at room temperature in a four-month test period. When aluminum was sealed in a tube with carbon tetrachloride and heated to 110°C, however, rapid reaction ensued.

Observations of the present authors indicate a rather critical temperature dependence for this reaction. The reaction proceeded rapidly at the boiling point of carbon tetrachloride (77°C), but very little reaction occurred at 50°C over a 60-day test period and none occurred in 18 months at room temperature (see Table II).

Yields of reaction products—Although Rhodes and Carty (1) stated that aluminum and carbon tetrachloride react to form aluminum chloride and hexachloroethane, two additional experiments were carried out to determine the yields based on the above reaction and to see if any additional reactions were involved.

The yield of the soluble fraction (assumed to be entirely hexachloroethane) in duplicate runs was 41.2 and 48.7% of the theoretical and the yield of insoluble fraction (assumed to be entirely aluminum chloride) was 83.8 and 100.6% of the theoretical. The theoretical yields were calculated from the weight loss of aluminum assuming that hexachloroethane and aluminum chloride were the only products formed according to the following reaction:

$$2Al + 6CCl_4 \rightarrow 3C_2Cl_6 + 2AlCl_3$$

Examination of fraction originally insoluble in carbon tetrachloride.—An x-ray diffraction analysis of the carbon tetrachloride insoluble fraction showed that aluminum chloride was the only identifiable component. Chemical analyses for aluminum and inorganic chlorides are shown in Table III.

The insoluble fraction does not appear to be pure aluminum chloride because the ratio of chlorine atoms to aluminum atoms was 2.74 instead of 3 as in pure aluminum chloride. In this case Stern (5) reported the Cl/Al ratio to be 2.8. These results indicate that some of the aluminum valence bonds were linked to some element other than chlorine. Since carbon and chlorine were the only elements present in addition to aluminum, it seems apparent that about 8.7% of the aluminum valence bonds were linked directly with carbon.

Table III. Chemical analysis of fraction originally insoluble

Sample No.	Al, %	Inorganic Cl, %	Ratio Cl atoms / Al atoms
1	18.6	67.3	2.74
2	18.9	68.1	2.74

The black carbon tetrachloride insoluble fraction almost completely dissolved in water with evolution of heat. A small quantity of the black material is insoluble in water. If this water insoluble material is dried and placed in carbon tetrachloride, it dissolves readily forming a dark brown colored solution. Upon evaporation of the carbon tetrachloride, a black resinous material is left behind. The carbon tetrachloride insoluble fraction contained 3.18% of this resinous material. Chemical analysis of the black resinous material revealed that its carbon content was 42.2%. These data are in accord with previously reported information (2).

The fact that this black resinous material is insoluble in carbon tetrachloride until it is treated with water suggests that an aluminum-carbon-chlorine complex is formed which is broken up by reaction with water. The formation of a resinous solid indicates that the complex must have a high molecular weight.

Examination of the fraction originally soluble in carbon tetrachloride—The carbon tetrachloride soluble fraction was a yellow solid. Chemical analysis showed that the aluminum content was less than 0.005%. An x-ray diffraction analysis of the soluble fraction revealed that it was mainly hexachloroethane. The soluble fraction also was analyzed by index of refraction measurements. In this method of structural determination, an equation developed by one of the authors was used (6).

$$n-1 = \frac{5.07}{\frac{m-1}{dA}}$$

Where n is the refractive index; m, the molecular weight; d, the density; and A, the sum of constants based on actual atomic volumes (A) of the atoms in the molecule ($A = 0.821$ for carbon, 1.800 for chlorine, and 0.436 for a double bond). For hexachloroethane, $A = (2)\ (0.821) + (6)\ (1.800) = 12.442$.

In using this method, the index of refraction for the structural formula in question is calculated using the measured density for the unknown. If the structural formula is correct, the calculated value of refractive index should agree with the observed value.

Since hexachloroethane is a solid it was necessary to dissolve the soluble fraction in a solvent to make the refractive index measurements. The solvent used was 1, 2, 4 trichlorobenzene. The value of m/A for the trichlorobenzene was determined experimentally as 14.19 by determining d and n in the equation $m/A = \frac{5.07d + (d-1)\ d}{n-1}$. When using a mix-

ture of two compounds the values of m and A should be average values based on the molecular percentages of the two components. The composition of the solution used was 22.3 mole % soluble fraction and 77.7 mole % trichlorobenzene.

If the soluble fraction was 100% hexachloroethane, the m/A value for the solution would be 15.25, whereas, the measured value was 15.17 ± 0.01. These results indicate that the soluble fraction was not pure hexachloroethane. It seems logical to assume that some of the hexachloroethane could have reacted with aluminum to form high molecular weight carbon-chlorine compounds. Several possible formulations of this type are given below along with the calculated m/A values if they replaced hexachloroethane completely in the trichlorobenzene solution.

Type of compound	Structure	m/A (calc.)
Straight chain polymer	$\begin{bmatrix} Cl\ Cl\ Cl\ Cl \\ -C\ -C\ -C\ -C- \\ Cl\ Cl\ Cl\ Cl \end{bmatrix}_n$	15.20
Branched chain polymer	$\begin{bmatrix} Cl \\ -C- \\ ' \end{bmatrix}_n$	15.10
Unsaturated straight chain polymer	$\begin{bmatrix} Cl & Cl \\ -C = C- \end{bmatrix}_n$	15.08
Unsaturated branched chain polymer	$\begin{bmatrix} & Cl \\ -C = C- \\ ' & \end{bmatrix}_n$	14.37

The evidence indicates that the small amount of impurity in the soluble fraction is not a straight chain polymer. The presence of branched chain, unsaturated straight chain, or unsaturated branched chain polymers could lower the m/A value from 15.25 for pure hexochloroethane to the 15.17 value actually measured.

Indications are that the impurities in the soluble fraction are intermediate compounds in the formation of the black resinous material since their carbon contents are between those of hexachloroethane and the black resinous material.

Table IV. Effect of reaction products on the corrosion of 99.99% aluminum in boiling carbon tetrachloride

Specimen No.	Conditions	Time, hr	Weight loss, g
1	Corrosion products from 1.6701 g spec.	1.00	0.3251
2	Corrosion products from 1.7359 g spec.	1.00	0.3774
3	Saturated with $AlCl_3$	0.25	0.0105
4	Saturated with $AlCl_3$	0.50	0.2738
5	Saturated with $AlCl_3$	1.00	0.6157
6	Saturated with $AlCl_3$	2.00	1.3378
7	Saturated with $AlCl_3$	3.25	1.6999
8	Saturated with $AlCl_3$	4.00	2.4072
9	Saturated with $AlCl_3$	4.50	2.7282
10	0.5% (by wt) hexachloroethane	4.00	0.9222
11	0.5% (by wt) hexachloroethane	4.50	1.1880
12	0.5% (by wt) hexachloroethane	5.50	1.5364
13	0.5% (by wt) hexachloroethane	6.50	1.8670

Effects of Reaction Product on Reaction

Tests were run exposing 99.99% aluminum specimens in solutions containing reaction products from previous exposures. The results given in Table IV show that the presence of reaction products increased the initial corrosion rate. Since aluminum chloride and hexachloroethane are the main reaction products, tests were run with additions of these two compounds to fresh carbon tetrachloride to determine their influence on the reaction. Since aluminum chloride is only slightly soluble in carbon tetrachloride, a saturated solution was used. An excess of anhydrous aluminum chloride was added to carbon tetrachloride and refluxed for 1 hr. The carbon tetrachloride then was decanted into another flask for the corrosion tests. It was observed that a faint pink color, which gradually darkened, developed in the boiling carbon tetrachloride saturated with aluminum chloride. No color developed when hexachloroethane was dissolved in boiling carbon tetrachloride.

The results of these tests are given in Table IV. This information in graphical form along with data from Table I is shown in Fig. 1. The presence of hexachloroethane had no detectable effect on the reaction, but the addition of aluminum chloride had a marked accelerating effect. This indicates that aluminum chloride acts as a reaction accelerator, probably through the formation of complexes with carbon tetrachloride.

Effective Retarding Agents

On the basis of the preceding discussion of factors that markedly affect the reaction of aluminum with carbon tetrachloride, it is obvious that aluminum chloride is one of the most potent promoters accelerating the reaction. The possibility was considered that chemical agents could retard this reaction by combining with the aluminum chloride to retard its effect on the reaction. In this manner, the stimulating effect normally produced on the carbon tetrachloride-aluminum reaction would be retarded.

Since benzoyl chloride has been reported in the literature to form a molecular complex with aluminum chloride (7), it should have a retarding effect

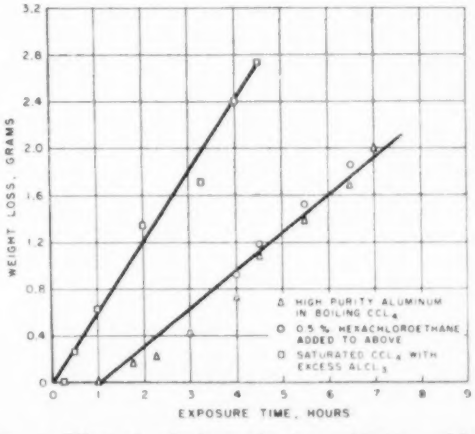

Fig. 1. Effect of anhydrous aluminum chloride and hexachloroethane additions.

on the reaction between aluminum and carbon tetrachloride by complexing the aluminum chloride and rendering the aluminum chloride unavailable for accelerating the reaction. Since significant retardation was obtained when 1% of freshly distilled benzoyl chloride was added to the carbon tetrachloride, the theory of an inhibitor operating by complexing the aluminum chloride was demonstrated.

It was also shown that the corrosiveness of carbon tetrachloride for aluminum was decidedly greater in the presence of a given added quantity of aluminum chloride than in the presence of the same quantity of aluminum chloride combined with benzoyl chloride in a molecular complex. The fact that aluminum reacted with somewhat greater rapidity in the presence of this complex than in the absence of any added aluminum chloride was attributed to the effect of some small amount of aluminum chloride that did not complex with the benzoyl chloride. This was further confirmed by the fact that the solution of carbon tetrachloride containing the complex became colored in a short time as if a relatively small amount of the total aluminum chloride had been separately added to the carbon tetrachloride (i.e., was not combined in the complex).

Additional support for the theory that retarding agents operate by complexing aluminum chloride was obtained by converting a corrosive carbon tetrachloride solution containing added aluminum chloride into a noncorrosive solution by removing the colored aluminum chloride-carbon tetrachloride complex that forms when aluminum chloride is heated with carbon tetrachloride. This was accomplished by the addition of any one of three different retarders (2, 5 hexanedione, ethyl acetoacetate, aluminum nitrate .$9H_2O$) in the following manner. Sufficient anhydrous aluminum chloride was added to refluxing carbon tetrachloride to produce the deep color associated with the beginning stages of the corrosion of aluminum in the halogenated hydrocarbon. If 1% by weight of either of three different retarding agents (i.e., an excess with respect to the amount of added aluminum chloride) was added, the characteristic color was rapidly removed and the carbon tetrachloride became noncorrosive to aluminum. Subsequent analysis disclosed that all the detectable aluminum chloride was now in the precipitate which formed simultaneously as the color of the solution disappeared. All compounds that were known to be effective retarding agents precipitated aluminum chloride in this manner. The explanation of the results of this type of experiment can be explained most satisfactorily in terms of the previously projected theory of complexing the aluminum chloride. It now appeared to be a logical step to search for new retarding agents among chemical compounds that offered the possibility of known or projected reactivity with aluminum chloride.

The possibility that acid anhydrides might have retardation properties was predicted on the basis of the use of anhydrides in organic syntheses with aluminum chloride acting as a catalyst through a complex intermediate. Both acetic anhydride and phthalic anhydride acted as effective retarding agents, although the possibility of conversion to the corresponding acid made their practical use questionable. Phthalic anhydride, however, proved to be equally effective as a retarder in the presence or absence of water in refluxing carbon tetrachloride. Phthalic acid, on the other hand, was ineffective as a retarding agent unless water was present in the carbon tetrachloride. The equilibrium established between the anhydride or the acid and water in carbon tetrachloride that affords such excellent retardation is not known at this time. Phthalic anhydride, itself, has proved to be the best retarder at the lowest levels (0.1-0.2% by weight) of all the retarding agents investigated.

One successful class of retarders for this reaction is the carbonyl compounds. Acetone is the simplest member of this series and its complexing with $AlCl_3$ has been reported (8). Acetone serves as an effective retarder at a concentration of 0.2% by weight. The difficulty of maintaining an adequate concentration of acetone is increased, however, because of its relatively low boiling point. A more effective carbonyl agent is 2,5-hexanedione. Although the ratio of C=O/C is the same as in acetone, some advantage is obtained through the lower volatility as well as in the possibility of chelation. Other effective carbonyl-type retarding agents that react with aluminum chloride are acetophenone (9, 10) and benzophenone (10). They offer the advantage of a lower volatility than acetone but require a larger addition of retarder because of the increased molecular weight. On the other hand, they are not so effective on a weight basis as 2,5-hexanedione but are considerably cheaper.

Other retarding agents related to the carbonyl compounds are the esters that contain the group

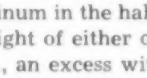

—C—O—R. A number of different esters have been reported to form complexes with aluminum chloride (11, 12). Ethyl acetate and ethyl acetoacetate both proved to be good retarders for this reaction. Ethyl acetate has the advantage of having about the same boiling point as carbon tetrachloride which might be desirable in certain industrial applications. Ethyl acetoacetate is the better retarder of the two as might be expected because of the combination of a carbonyl and an ester group as well as offering the possibility of chelation.

Some heterocyclic ring system compounds such as thiophene, pyrrole, and quinoline act as effective retarding agents. These compounds were selected for several reasons. For example, all of them enter into condensation reactions in the presence of aluminum chloride in which it is often necessary for the aluminum chloride to be present in a mole-for-mole ratio or greater. They might also work since onium-type compounds could be produced in such situations where a Lewis type acid, such as aluminum chloride, comes in contact with a Lewis type base such as the heterocyclic atom in these ring systems.

Several olefin-type compounds (cyclohexene and isoprene) in which no heterocyclic atom is present also were effective although to a lesser extent than the other retarders previously mentioned. There is a basis for selecting olefins since olefins formed by pyrolysis of paraffins in the presence of aluminum chloride polymerize and remain bound fast with the aluminum chloride according to Nenitzescu (13-15). The specificity of the olefinic linkage was demonstrated by showing that cyclohexane has no retardation effect. On the other hand, benzene does have some retardation effect although, as might be expected, it is not so good as cyclohexene; this is because the compound is aromatic and hence none of the bonds have 100% double bond character.

It has been shown that another halogenated hydrocarbon that could complex $AlCl_3$ was capable of retarding the reaction with carbon tetrachloride. Benzyl chloride, for example, will complex with aluminum chloride and will retard the reaction when present at a concentration of 1%. Benzyl chloride, itself, is reactive toward aluminum at its boiling point.

Two amines which retard the reaction (triethylamine, 2-methyl-2-amino-1 propanol) have the ability to remove almost quantitatively aluminum chloride from a carbon tetrachloride solution saturated with aluminum chloride. The response to the addition of the amine is immediate and can be followed by noting the loss of pink color in the solution as well as by analysis for the aluminum in filtered carbon tetrachloride solution. Other amine retarding agents are methylamine, diethylamine, trimethylamine, n-butylamine, 3-methoxypropylamine, and cyclohexylamine. One of the disadvantages of the amines as practical retarders is their separate reactivity with carbon tetrachloride to form voluminous precipitates; however, under some conditions amines may be practical.

The ability of 21 hydrated inorganic salts to retard this reaction has been noted. The salts tested were generally in four classifications: nitrates, sulfates, chlorides, and sulfides. Only the hydrated nitrate and sulfide salts were retarding agents. Unlike the anhydrous salt, the hydrated aluminum chloride did not accelerate the reaction rate. The attempt to relate this phenomena to the coordination number of the metal ion of the salt was unsuccessful. Likewise, when the equivalent of the total water of crystallization was added as water to the carbon tetrachloride, its retarding influence was not nearly as effective as the hydrated inorganic salt.

On the assumption that an agent that might chelate $AlCl_3$ would be an effective retarder, 8-hydroxyquinoline was added at levels of 1% or less. Comparison on a weight basis shows that 8-hydroxyquinoline is one of the two best retarders (the other is phthalic anhydride).

Table V. Effect of retarding agents on reactivity in carbon tetrachloride in contact with aluminum

Additive (1% by wt of each)	Reactivity (first visible attack) In CCl_4	In CCl_4 saturated with $AlCl_3$
None	1 hr	<5 min
Amines		
1, 6-hexanediamine	None (88 hr)	None (72 hr)
3-methoxypropylamine*	After 40 hr	After 72 hr
2-methyl-2-amino-1-propanol	None (88 hr)	None (264 hr)
Triethylamine	None (88 hr)	None (72 hr)
Carbonyls		
Acetone*	None (40 hr)	<20 hr
2, 5-hexanedione	None (576 hr)	After 72 hr
Esters		
Ethyl acetate*	None (336 hr)	After 21 hr
Ethyl acetoacetate	None (678 hr)	After 21 hr
Acid anhydrides		
Acetic anhydride	None (96 hr)	None (120 hr)
Phthalic anhydride	None (336 hr, 0.2%)	None (192 hr)
Organic acid + water		
Acetic acid + water	None (40 hr)	After 20 hr
Phthalic acid + water	None (144 hr)	None (144 hr)
Heterocyclic compounds		
Pyrrole	None (96 hr)	After 72 hr
Quinoline	None (96 hr)	After 66 hr
Thiophene	None (144 hr)	None (72 hr)
Olefins		
Cyclohexene	After 192 hr	After 35 min
Aromatic compounds		
1, 4 naphthaquinone*	None (40 hr)	None (68 hr)
Nitrobenzene*	None (216 hr)	Slight (120 hr)
Quinone*	Slight (40 hr)	None (68 hr)
1, 3, 5 trinitrobenzene	None (40 hr)	<16 hr
Inorganic salt		
Aluminum nitrate .9 H_2O	None (96 hr)	<6 hr
Water (equivalent to above)	Extensive (40 hr)	<6 hr
Chelating agent		
8-hydroxyquinoline	None (216 hr)	None (192 hr)

* These additives had been investigated previously (3).

Table VI. Effect of magnesium content in aluminum alloys on corrosion rate in boiling CCl_4

Alloy	Exposure time, hr	Specimen size, in.	Weight loss, g	Calc. vol. metal loss, $in.^3/in.^2/yr.$	Nominal magnesium content, %
Solution used—CCl_4					
99.99% Al	7.83	1/16 × 1/2 × 3	1.6950	12.1	0
99.99% Al	7.5	1/16 × 1/2 × 3	1.6111	12.0	0
99.99% Al	7.0	1/16 × 1/2 × 3	2.0022	16.1	0
3003-H14	16	1/16 × 1/2 × 3	2.2480	7.76	0
3004-H14	6.75 days	1/16 × 1/2 × 3	0.5377	0.183	1.0
5052-H34	6.75 days	1/16 × 1/2 × 3	0.3868	0.132	2.5
5356-H34	6 days	1/16 × 1/2 × 3	0.1891	0.0740	5.2
112	48	1/2 × 2	1.4946	1.263	0
195	48	1/4 × 1/2 × 3	1.0173	0.857	0
214	12.67 days	1/4 × 1/2 × 3	1.9174	0.256	3.8
220	7 days	1/4 × 1/2 × 3	0.0027	0.0009	10.0
220	7 days	1/4 × 1/2 × 3	0.0019	0.0006	10.0
356-T6	48	1/4 × 1/2 × 3	0.5668	0.482	0.3
Mg	6 days	1/16 × 1/2 × 3	0.0006	0.0007	100
Mg	3 days	1/16 × 1/2 × 3	0.0003	0.0002	100
Solution used—CCl_4 saturated with $AlCl_3$					
5356	17	1/16 × 1/2 × 3	0.1711	0.564	5.2
5356	24	1/16 × 1/2 × 3	0.2578	0.602	5.2
220	24	1/4 × 1/2 × 3	0.0122	0.0285	10.0
220	7 days	1/4 × 1/2 × 3	0.0586	0.0196	10.0
Mg	96	1/16 × 1/2 × 3	0.0024	0.0022	100
Mg	24	1/16 × 1/2 × 3	0.0096	0.0352	100
Solution used—CCl_4 plus 0.5% $AlCl_3$					
Mg	20.5	1/16 × 1/2 × 3	0.0289	0.124	100
Mg	96	1/16 × 1/2 × 3	0.0282	0.0260	100

Tests for Evaluating Effectiveness of Retarding Agents

Since some retarders seemed capable of protecting aluminum for almost indefinite periods of time, some means of accelerating the test was needed to determine the relative effectiveness of the retarders. Exposure of aluminum specimens to refluxing carbon tetrachloride saturated with aluminum chloride is a much more stringent test than exposing them to refluxing pure carbon tetrachloride. To establish the relative effectiveness of the best known retarders, the same concentration by weight of each retarder was added to carbon tetrachloride saturated with aluminum chloride at room temperature. In order to insure that uniform conditions were maintained, the carbon tetrachloride was degassed in a dry box with nitrogen flushing through both the solution and the box. The total volume of carbon tetrachloride to be employed was saturated with $AlCl_3$ inside the box. The carbon tetrachloride was transferred to reflux flasks inside the box and the retarder and specimens added before the flask was stoppered. The time necessary for corrosion to appear on the aluminum specimen exposed in the boiling solution was a measure of the relative efficiency of the retarder. For example, some of the retarders classified in order of decreasing effectiveness were as follows: phthalic anhydride, 8-hydroxyquinoline, 2,5-hexanedione, ethyl acetoacetate, ethyl acetate, aluminum nitrate·$9H_2O$, and cyclohexene. The first two retarders completely prevented reaction under this condition for the five day test period. The actual periods of retardation are given in Table V.

Reaction of Carbon Tetrachloride with Magnesium and Aluminum Alloys

Tests were run with magnesium and ten aluminum alloys. The results given in Table VI and Fig. 2 show that magnesium in aluminum alloys has a pronounced effect on the corrosion rate. The corrosion

Table VII. Effect of $AlCl_3$ and $MgCl_2$ on the corrosion of magnesium and aluminum alloys in CCl_4

Alloy	Exposure time, hr	Specimen size, in.	Additive	Weight loss, g	Calc. vol. metal loss, $in.^3/in.^2/yr.$
5356	17	1/16 × 1/2 × 3	Saturated with $AlCl_3$	0.1711	0.564
	24	1/16 × 1/2 × 3	Saturated with $AlCl_3$	0.2578	0.602
220	24	1/4 × 1/2 × 3	Saturated with $AlCl_3$	0.0122	0.0285
	7	1/4 × 1/2 × 3	Saturated with $AlCl_3$	0.0586	0.0196
Mg	96	1/16 × 1/2 × 3	Saturated with $AlCl_3$	0.0024	0.0022
	24	1/16 × 1/2 × 3	Saturated with $AlCl_3$	0.0096	0.0352
Mg	20.5	1/16 × 1/2 × 3	0.5% $AlCl_3$	0.0289	0.124
	96	1/16 × 1/2 × 3	0.5% $AlCl_3$	0.0282	0.0260
99.99% Al	3	1/16 × 1/2 × 3	0.5% $MgCl_2$	0.8544	16.0
	3	1/16 × 1/2 × 3	0.5% $MgCl_2$	1.3874	26.0
99.99% Al	3	1/16 × 1/2 × 3	0.25% Mg turnings	0.7757	14.5
	3	1/16 × 1/2 × 3	0.25% Mg turnings	0.4438	8.32

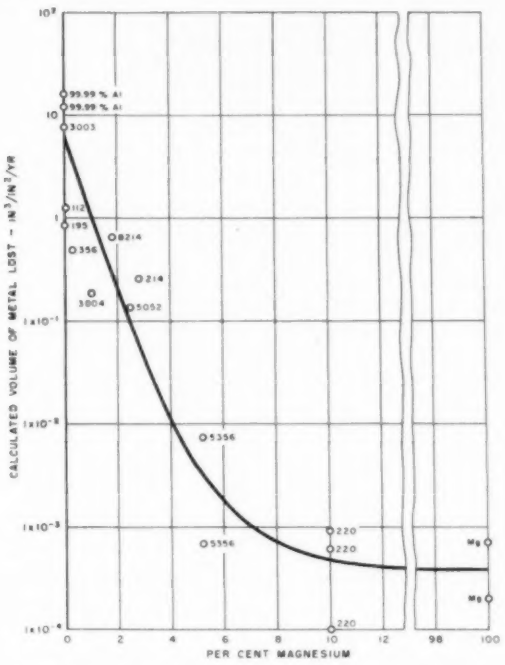

Fig. 2. Effect of magnesium content of aluminum alloys on corrosion rate in boiling CCl_4.

rate drops off rapidly as the magnesium content increases, becoming negligible for 220 cast aluminum alloy and magnesium. It should be pointed out that in Table VI and Fig. 2 varying exposure times were used to calculate the values of $in.^3/in.^2/yr$ and, hence, these values may not represent the true rates.

Tests also were run exposing magnesium and aluminum alloys 5356 and 220 to carbon tetrachloride saturated with aluminum chloride. The results given in Table VII show that the presence of aluminum chloride increased the corrosion rates of magnesium as well as the aluminum alloys. It was shown also that the presence of magnesium chloride or magnesium turnings had no significant effect on the corrosion of 99.99% aluminum in refluxing carbon tetrachloride. These results indicate that magnesium must be present as an alloying constituent in order to retard the reaction.

Conclusions

1. As reported by several others (1,2,5), many aluminum alloys are corroded severely by boiling carbon tetrachloride.

2. The reaction decreases rapidly when the temperature is dropped from the boiling point (77°C) to 50°C and is insignificant at room temperature. Some alloys show great resistance to carbon tetrachloride, even at the boiling point.

3. The addition of reaction products to carbon tetrachloride increases the initial reaction rate. Hexachloroethane had no effect on the reaction. Aluminum chloride, however, promotes the reaction and, when initially present, the reaction attains within a few minutes the same rate that is reached after several hours when starting with fresh carbon tetrachloride. This indicates that aluminum chloride acts as a reaction accelerator, probably through the formation of complexes with the carbon tetrachloride.

4. Chemical agents which can retard this reaction probably operate by combining with the aluminum chloride as it is produced. In this manner, the accelerating effect normally produced by the aluminum chloride is absent. Only anhydrous aluminum chloride accelerates corrosion.

5. Certain chemical agents that act as retarders for this reaction have shown the ability to decolorize a boiling solution of carbon tetrachloride containing aluminum chloride and to precipitate simultaneously and quantitatively in complexed form the aluminum chloride from the solution. Such a solution is noncorrosive if the retarder has been added in excess of that amount necessary to precipitate all the aluminum chloride.

6. Classes of retarding agent have been selected on the basis of known or projected reactivity with aluminum chloride. Some of the successful classes of retarders are acid anhydrides, amines, esters, heterocyclic compounds, halogenated hydrocarbons (which can complex aluminum chloride), ketones, olefins, and chelating agents in general. Certain hydrated nitrate and sulfide inorganic salts also were effective although the mechanism of their retardative ability is not clearly understood.

7. Reaction of aluminum alloys in boiling carbon tetrachloride drops off rapidly as the magnesium content increases. Addition of magnesium chloride or the presence of magnesium metal in carbon tetrachloride has no significant effect on the corrosion of high purity aluminum.

Manuscript received Nov. 13, 1957. This paper was prepared for delivery before the Buffalo Meeting, Oct. 6-10, 1957.

Any discussion of this paper will appear in a Discussion Section to be published in the December 1959 JOURNAL.

REFERENCES

1. F. H. Rhodes and J. T. Carty, *Ind. Eng. Chem.*, **17**, 909 (1925).
2. M. Stern and H. H. Uhlig, *This Journal*, **99**, 381, 389 (1952).
3. M. Stern and H. H. Uhlig, *ibid*, **100**, 543 (1953).
3a. R. H. Brown, E. H. Cook, M. H. Brown, and J. D. Minford, *ibid.*, **106**, 192 (1959).
4. E. V. Zappi, *Anales. soc. quim. argentina*, **2**, 217 (1914).
5. M. Stern, Thesis M.I.T. (1952).
6. M. H. Brown, Thesis Iowa State College (1949).
7. G. Perrier, *Compt. rend.*, **116**, 1298 (1893).
8. H. Funk, J. Schormuller, and W. Hensinger, *Z. anorg. u. allgem. chem.*, **204**, 361 (1932).
9. E. P. Kohler, *Am. Chem. J.* **27**, 241 (1902).
10. B. Menshutkin, *J. Russ, Phys. Chem. Soc.*, **42**, 1298 (1910).
11. J. W. Walker and A. Spencer, *J. Chem. Soc.*, **85**, 1106 (1904).
12. G. Gustavson, *Bull. Soc. Chem.* (2), **34**, 322 (1880).
13. C. D. Nenitzescu and I. P. Cantuniari, *Ber.*, **65**, 1449 (1932).
14. C. D. Nenitzescu and I. G. Gavat, *Ann.*, **519**, 260 (1935).
15. C. D. Nenitzescu and D. Curcaneanu, *Ber.*, **70**, 346 (1937).

Reaction of Aluminum and Carbon Tetrachloride, II

R. H. Brown, E. H. Cook, M. H. Brown, and J. D. Minford

Alcoa Research Laboratories, Aluminum Company of America, New Kensington, Pennsylvania

ABSTRACT

The mechanism of the reaction between aluminum and boiling carbon tetrachloride appears to be electrochemical. Conductivity measurements indicate that the reaction starts as soon as the aluminum is exposed to the boiling solution. The increase in the conductivity with time is caused by the presence of $AlCl_3$ and parallels the increase in weight of aluminum reacted as the reaction proceeds. The application of a cathodic current prevents attack of an aluminum specimen, indicating that the initial attack is caused by the presence of an ionic species. Trace amounts of the reaction product hexachloroethane were produced electrochemically in the absence of any aluminum.

Substances that retard the reaction apparently function by forming inactive complexes with the $AlCl_3$. The rate-determining step in the reaction does not appear to involve free radicals since the majority of the effective inhibitors failed to react with known free radicals.

It has been shown (1) that two of the products of the reaction between aluminum and carbon tetrachloride, are aluminum chloride and hexachloroethane. Evidence was also obtained for the presence of high molecular weight carbon-chlorine compounds soluble in carbon tetrachloride and high molecular weight carbon, chlorine, and aluminum compounds which were insoluble in carbon tetrachloride.

A rather critical temperature dependence can be shown for this reaction, ranging from rapid reaction at the boiling point to negligible reaction in eighteen months at room temperature.

The presence of the reaction products accelerates the reaction because of the presence of aluminum chloride. Hexachloroethane has no effect on the reaction. The aluminum chloride acts as a reaction accelerator probably through the formation of complexes with the carbon tetrachloride.

Chemical agents that act as retarders do so by reaction with the aluminum chloride as it is produced. This was demonstrated by quantitatively removing the aluminum chloride from a corrosive boiling carbon tetrachloride solution and rendering it noncorrosive in the process.

A number of classes of retarding agents were discovered on the basis of known or projected reactivity with aluminum chloride. Some of these were acid anhydrides, amines, esters, heterocyclic compounds, halogenated hydrocarbons (which can complex aluminum chloride), ketones, olefins, and chelating agents in general. Retardation was also secured with a number of hydrated inorganic nitrates and sulfides for less definitive reasons.

Reaction of aluminum alloys in boiling carbon tetrachloride drops off rapidly with increasing magnesium content. Magnesium metal or magnesium chloride has no significant effect on this reaction.

Studies of Conductivity

High-purity (99.99%) aluminum is attacked severely in boiling carbon tetrachloride but is resistant to carbon tetrachloride at room temperature. Since the conductivity of carbon tetrachloride is much higher at the boiling point than at room temperature, it was thought that a relationship might exist beween conductivity and corrosion.

The apparatus shown in Fig. 1 was used to measure conductivity. As shown in Fig. 2, the conductivity increased steadily for about 5 hr after aluminum specimens were immersed in boiling carbon tetrachloride, indicating that the conductivity increased as the corrosion products increased. On the basis of weight loss measurements, there would appear to be an induction period of about 1 hr; however, the more sensitive conductivity measurements show that the reaction starts soon after the aluminum is placed in the boiling carbon tetrachloride (see also Fig. 11). Since aluminum chloride and hexachloroethane were identified as two of

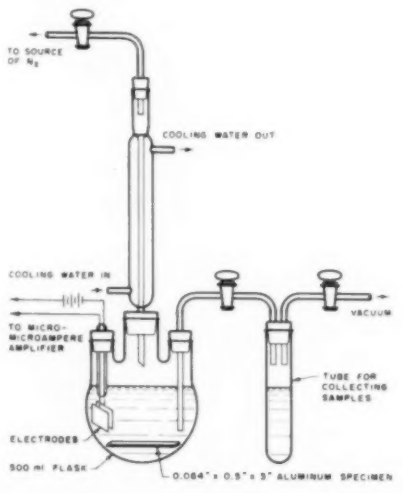

Fig. 1. Apparatus used for measuring conductivity and removing samples simultaneously.

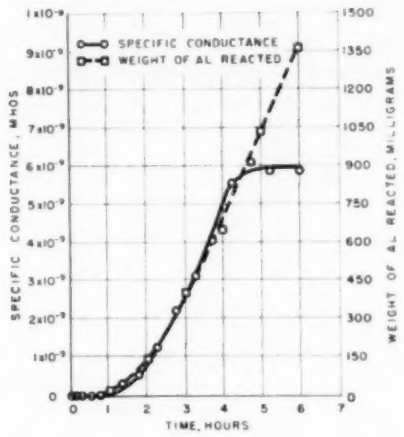

Fig. 2. Plot of specific conductance and weight of aluminum reacted vs. time.

the corrosion products, these compounds were added singly to determine the effect of each compound on conductivity. As shown in Fig. 3, aluminum chloride had a marked effect. The conductivity increased rapidly during the first 20 min and then leveled off. The reaction resulting when an aluminum specimen was added after the conductivity leveled off, caused the conductivity to rise to a value about ten times that of carbon tetrachloride saturated with aluminum chloride, indicating that additional ionized complexes are formed. No significant change in conductivity occurred when hexachloroethane was added to boiling carbon tetrachloride.

In another experiment, samples of solutions were withdrawn periodically and analyzed for aluminum at the same time as conductivity measurements were being made on the solution remaining in the flask. The results are shown in Table I and Fig. 2. The data show that the increase of conductivity and weight of aluminum reacted in the carbon tetrachloride roughly parallel each other in the first 4.5 hr. In Fig. 4,[1] a comparison of the curves of conductivity and total aluminum reacted shows that the aluminum reacted increases linearly with specific conductivity up to 5×10^{-9} mhos. The specific conductivity reaches a limiting value of about 6×10^{-9} mhos while the total aluminum reacted continues to increase. It can be seen in Fig. 5[2] that the reaction rate increases with increasing specific conductivity and levels off as the specific conductivity approaches 6×10^{-9} mhos. As shown in Fig. 6, the reaction rate increases with time up to 4 hr, where it reaches a constant value. As can be seen in Fig. 2, the specific conductance also reaches a limiting value after about 4 hr. These results which indicate a relationship between the reaction rate and specific conductivity suggest that ions may be involved in the reaction.

The conductance of a solution is proportional to the mobility and number of ions in the solution. The

[1] Figure 4 was plotted by taking points from the two curves on Fig. 2 for the same time, and plotting the points against each other.

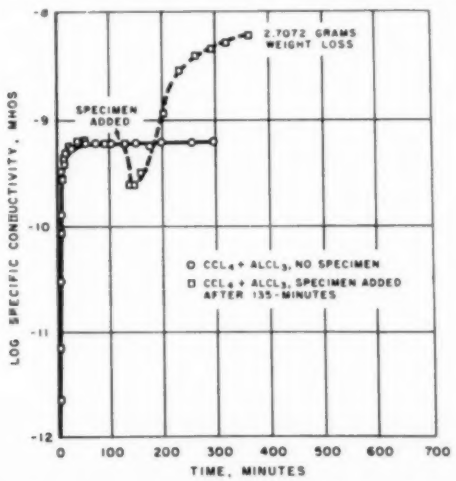
2.7072 GRAMS WEIGHT LOSS
SPECIMEN ADDED
LOG SPECIFIC CONDUCTIVITY, MHOS
O CCl_4 + $ALCl_3$, NO SPECIMEN
D CCl_4 + $ALCl_3$, SPECIMEN ADDED AFTER 135-MINUTES
TIME, MINUTES

Fig. 3. Conductivity measurements of boiling CCl_4 while $AlCl_3$ was going into solution.

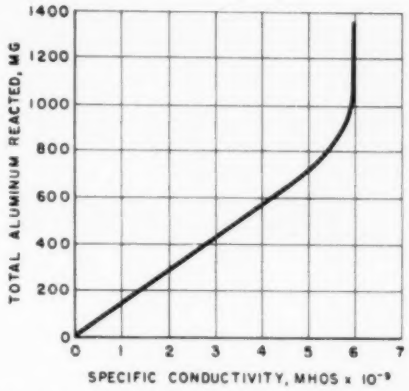

Fig. 4. Plot of total aluminum reacted vs. specific conductivity.

[2] The reaction rate was calculated from the slope of the weight of aluminum reacted vs. time curve shown in Fig. 2. The slope at a given time was plotted against the specific conductance value at the same time.

Table I. Data on per cent dissolved aluminum and conductivity

Time, min	Volume of* sample, ml	Weight of Al in samples, mg	Weight % Al dissolved in CCl_4	Total Al dissolved in CCl_4, mg	Specific conductivity, mhos
0	25	0	0	0	6.80×10^{-12}
10	—	—	—	—	1.78×10^{-11}
20	—	—	—	—	1.78×10^{-11}
30	—	—	—	—	4.40×10^{-11}
40	—	—	—	—	5.90×10^{-11}
50	—	—	—	—	9.15×10^{-11}
60	27.5	1.2	0.00274	21.8	—
80	—	—	—	—	3.15×10^{-10}
100	—	—	—	—	5.40×10^{-10}
120	27	8.1	0.0188	143	—
140	—	—	—	—	1.25×10^{-9}
160	—	—	—	—	2.24×10^{-9}
180	29	25.6	0.0553	403	—
200	—	—	—	—	3.12×10^{-9}
220	—	—	—	—	4.08×10^{-9}
240	28	41.2	0.0891	650	—
260	—	—	—	—	5.56×10^{-9}
280	—	—	—	—	6.10×10^{-9}
300	29	71.0	0.154	1033	—
330	—	—	—	—	5.87×10^{-9}
360	29	97.6	0.211	1367	5.87×10^{-9}

* Initial volume of CCl_4 = 500 cc.

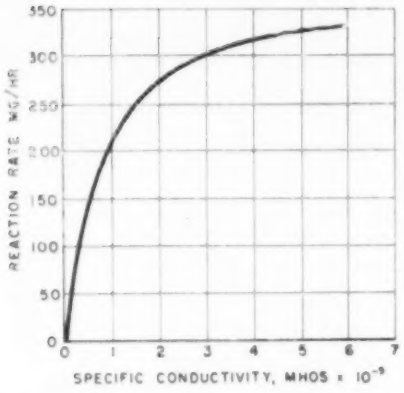

Fig. 5. Plot of reaction rate vs. specific conductivity

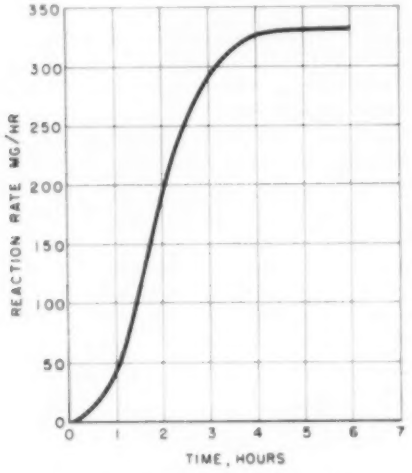

Fig. 6. Plot of reaction rate vs. time

slope of the line from a plot of log specific conductance vs. $1/T$ is the temperature coefficient. The smaller the temperature coefficient the greater the number of ions in a given solution. The relationship can be demonstrated by comparing the temperature coefficients for distilled water and the more highly ionized 0.01M KCl solution. The temperature coefficients are -0.208 for distilled water and -0.084 for 0.01M aqueous potassium chloride solution (2).

Figure 7 shows the effect on the temperature coefficient of carbon tetrachloride due to addition of aluminum chloride or corrosion products from the aluminum-carbon tetrachloride reaction. These results show that the addition of aluminum chloride to carbon tetrachloride decreases the temperature coefficient, indicating that the addition of aluminum chloride increases the number of ions. The presence of aluminum corrosion products further decreases the temperature coefficient indicating an additional increase in the number of ions. These results also suggest that an ionic mechanism may be involved.

The increase in conductivity with time that accompanies the reaction between aluminum and carbon tetrachloride is observed in other corrosion reactions occurring in aqueous solutions. Since conductance in solution depends on the presence of ions, this indicates that this reaction may proceed by

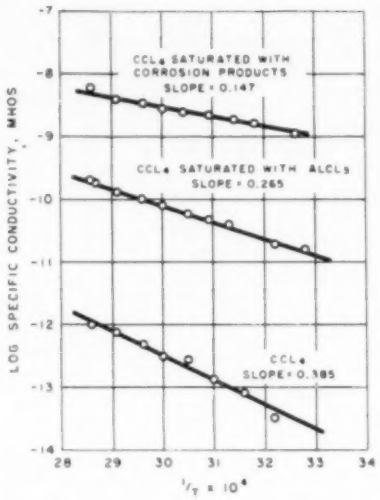
CCl₄ SATURATED WITH CORROSION PRODUCTS SLOPE = 0.147
CCl₄ SATURATED WITH AlCl₃ SLOPE = 0.265
CCl₄ SLOPE = 0.385
LOG SPECIFIC CONDUCTIVITY, MHOS
1/T x 10⁴

Fig. 7. Temperature coefficients for CCl_4 and CCl_4 saturated with $AlCl_3$ and corrosion products.

an electrochemical mechanism involving oxidation and reduction (3). For these reasons, electrochemical relationships that might be involved were further investigated. For example, if it could be shown that the reaction with carbon tetrachloride could be prevented by cathodically protecting the aluminum, this would support an electrochemical mechanism. However, it should be pointed out that the inability to protect the aluminum cathodically would not be sufficient to disprove such a mechanism. A reduction or an increase in the corrosion rate caused by the coupling to dissimilar metals or by an applied current would lend support to an ionic mechanism.

Effect of Galvanic Corrosion

A sample of high-purity sheet aluminum (99.99% Al) was coupled to a mild steel sheet specimen in boiling carbon tetrachloride. The electrodes were 1 in. apart. The exposed area of each specimen was approximately 3 in.^{2} and the initial galvanic current between the specimens was 2×10^{-11} amp. When the boiling carbon tetrachloride was saturated with aluminum chloride, in order to increase the conductance, the galvanic current increased over a 15-min period and leveled off at a value of 10×10^{-9} amp. During this time, the solution darkened, and the aluminum specimen became coated with corrosion product, while the steel specimen remained clean. The evidence of a current flow as a result of bimetallic coupling further indicated the analogy with similar reactions occurring in aqueous solutions. The fact that Stern and Uhlig (4) were unable to notice an increased weight loss effect from bimetallic coupling based on a 6-hr test in carbon tetrachloride is understandable in view of the very high solution resistance encountered between electrodes. The corrosion of aluminum in carbon tetrachloride could proceed by an electrochemical mechanism to give high corrosion rates if the local anodes and cathodes on the surface of the aluminum are only a few angstroms apart. This proximity of anode and cathode would enable the reaction to proceed at relatively

rapid rates even though the resistance of the solution were high.

Observations with an Applied Potential

Based on results with galvanic couples one would expect an externally applied current to protect an aluminum specimen cathodically in boiling carbon tetrachloride. To study the effects of an applied cathodic and anodic current on an aluminum specimen in carbon tetrachloride, a rather high emf source is required to overcome the resistance of the carbon tetrachloride. For the following experiment a potential source of 200 v d.c. was used.

To prevent attack on the portions of the electrodes in the vapor phase, the possibility of a coating resistant to boiling carbon tetrachloride and its vapors was investigated. It was found that an anodic coating (Alumilite[a] 204) prevented attack except at the edges of an aluminum sheet. By using round rods with rounded ends it was found that these anodic coatings almost completely retarded the attack. Round rods 99.99% Al, ¼ in. in diameter with rounded ends, were given Alumilite 204 treatment except for a band ½ in. long located ¼ in. from the end of the rod.

When an external potential was applied across two round aluminum rods (⅜ in. apart) of 99.99% Al in 400 cc of boiling carbon tetrachloride saturated with aluminum chloride, the corrosion of the cathode was slightly retarded, whereas the corrosion of the anode began almost immediately. A blank placed in the same solution clearly shows that the corrosion of the anode was accelerated and that of the cathode was slightly retarded (Fig. 8). Initially the current passing between the two electrodes was 10 x 10^{-5} amp. After about 200 min the rate of attack of the cathode increased and approached that of the anode. The current at this point increased to 110 x 10^{-5} amp. This increase in current was caused by an increase in solution conductivity because of the presence of aluminum corrosion products. At this point the solution was rather dark and the attack of both specimens was caused largely by local action rather than by the applied current. At the time the experiment was discontinued the current through the solution was 200 x 10^{-5} amp. This increase in current with a constant applied potential parallels the increase in conductivity which accompanies the corrosion of aluminum in boiling carbon tetrachloride.

[a] Trade name of Aluminum Company of America.

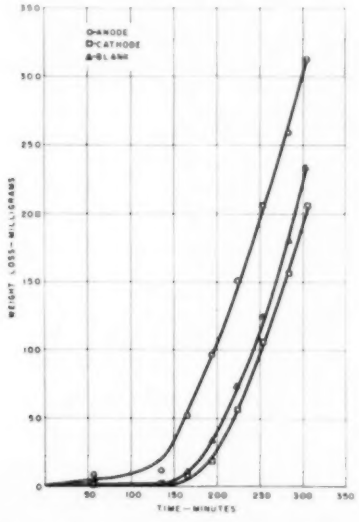

Fig. 8. Effect of an applied potential on aluminum rods in boiling carbon tetrachloride saturated with aluminum chloride.

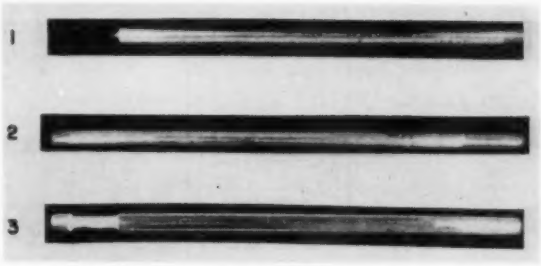

Fig. 9. Cathodic protection of aluminum in carbon tetrachloride: 1, An aluminum rod suspended in boiling carbon tetrachloride for four days (no cathodic current applied); 2, an aluminum rod suspended in boiling carbon tetrachloride for 28 days, with an applied cathodic current of 5 x 10^{-9} amperes. This specimen was completely protected; 3, The cathodically protected specimen 48 hr after the applied cathodic current had been removed.

In view of the above results, an experiment was devised to determine whether a specimen could be protected cathodically in boiling carbon tetrachloride. When an aluminum rod was suspended in boiling carbon tetrachloride, the unanodized portion completely reacted within four days, although the attack did not begin until about the third day (Fig. 9). This increase in induction time indicated the significance of eliminating corners and rough edges from the specimens.

When a potential of 220 v was applied across the aluminum rod and a cylindrical platinum gauze (the aluminum being the cathode), no attack of the aluminum specimens by boiling carbon tetrachloride was observed after 28 days (Fig. 9). The average current between the electrodes was 5 x 10^{-9} amp. This current was relatively constant over the 28-day time interval.

When the applied potential was removed, the corrosion of the aluminum began within 30 hr; in 48 hr the attack was severe (Fig. 9). This experiment was then repeated with lower currents and shorter periods of observation. The results indicate that cathodic protection was complete for the period of observation (Table II).

Table II. Cathodic protection of aluminum in boiling CCl_4

	Current, amp			Number of days the experiment was continued	Aluminum detected
	Initial	Maximum	Average		
(a)	"No Current"			3	Severe attack
(b)	8×10^{-11}	2.4×10^{-10}	2.2×10^{-10}	12	0.075 mg/l
(c)	2×10^{-10}	20×10^{-10}	10×10^{-10}	10	0.018 mg/l
(d)	6×10^{-10}	7×10^{-10}	6×10^{-10}	11	0.155 mg/l
(e)	5×10^{-9}	6×10^{-9}	5×10^{-9}	28	None detected

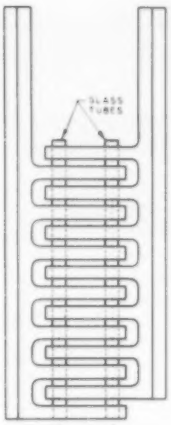

Fig. 10. Schematic diagram of carbon electrodes used for electrochemical production of hexachloroethane from carbon tetrachloride.

In the case of (*b*) and (*e*) (Table II), when the current was removed after the time of observation, corrosion began within 24 and 30 hr, respectively. All these results are indicative of an electrochemical mechanism for the attack of aluminum by carbon tetrachloride.

It was not possible to protect cathodically an aluminum rod in carbon tetrachloride saturated with aluminum chloride at the reflux temperature. It was estimated from the rate of attack of an aluminum specimen in this solution that a current density of at least 50 ma/cm^2 would be required to prevent attack of the aluminum. With the high resistance of the solution, such a current could be obtained only with excessively high applied potentials.

Thus, the reaction in carbon tetrachloride can be prevented for an indefinite period by cathodically protecting the aluminum with an applied potential. Therefore, it is concluded that the initial attack of the aluminum is caused by the presence of an ionic species.

During the corrosion of an aluminum specimen in boiling carbon tetrachloride, the energy supplied by the oxidation of the aluminum produces hexachloroethane as a reduction product. If reduction of the carbon tetrachloride to hexachloroethane can be produced in the absence of metallic aluminum by means of an applied potential, this fact would lend support to an electrochemical mechanism.

Graphite electrodes were constructed (Fig. 10) to give a large surface area and a small distance between anode and cathode. Each electrode consisted of seven plates (3 x 1¾ x ¼ in.) placed ½ in. apart. The electrodes were then placed so that the distance between each plate was about ⅛ in. Platinum was used to connect the electrode to the potential source.

Approximately 1 liter of carbon tetrachloride was added to the cell using aluminum chloride as the electrolyte. At a potential of 850 v the average current in the cell was 200 μa for a period of twelve days. At the end of the twelve-day period, the solution was filtered and the carbon tetrachloride evaporated on a water bath to a volume of about 50 cc. Because of the ease of sublimation of hexachloroethane, the remainder of the solution was evaporated at room temperature. The concentrated solution was yellow. When the solution was evaporated to dryness, an odor resembling hexachloroethane was detected in the residue (which also contained some aluminum chloride).

By means of infrared spectroscopy, hexachloroethane was detected, but special techniques were necessary. The hexachloroethane has two detectable absorption bands; one is rather weak while the stronger band is masked by carbon tetrachloride absorption. Because of the volatility of the product and its low yield, it was impossible to obtain a large enough sample to identify the weaker band of hexachloroethane. Consequently, the residue from the carbon tetrachloride evaporation was dissolved in spectral pure cyclohexane and submitted for analyses. Hexachloroethane was detected in this solution at the stronger wave length (12.77 μ). In an identical experiment in which there was no applied current, no hexachloroethane could be detected by the above procedure.

Relationship of Conductivity to Retarding Agents

Since the conductivity is markedly affected by the concentration of aluminum chloride in carbon tetrachloride solution, any factors that affect the aluminum chloride would also result in conductivity changes. Hence, the addition of retarding agents to colored carbon tetrachloride solutions containing anhydrous aluminum chloride should result in a subsequent drop of the conductivity to essentially the level of pure carbon tetrachloride (Fig. 11).

The results shown in Table III indicate that a good retarding agent can be generally predicted based on its ability to lower the conductivity of the corrosive carbon tetrachloride solution. Of all the retarding agents tested, only the addition of cyclohexene to the carbon tetrachloride-aluminum chloride solution failed to lower the conductivity by ap-

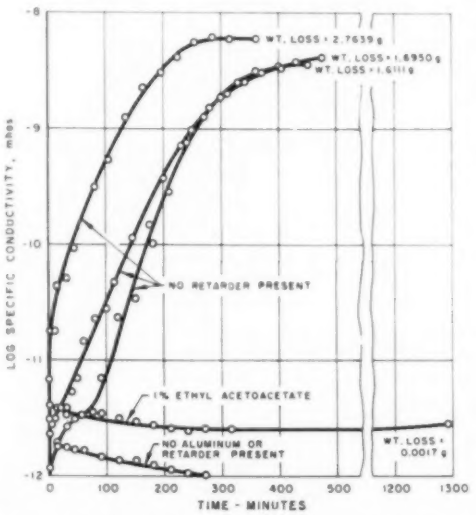

Fig. 11. Conductivity measurements on boiling carbon tetrachloride with and without aluminum specimens and retarders present.

Table III. Effect of retarding agents or reactivity and conductivity in carbon tetrachloride in contact with aluminum

Additive	Reactivity (first visible attack) in CCl_4	Initial specific conductivity, mhos in CCl_4 + additive	Initial specific conductivity, mhos in CCl_4 + additive + $AlCl_3$
None	1 hr	4×10^{-12}	2×10^{-10}
Amines			
1, 6 Hexanediamine	None (88 hr)	9×10^{-12}	Prevented by ppt
3-methoxypropylamine	After 40 hr	3×10^{-12}	2×10^{-11}
2-methyl-2-amino-1-propanol	None (88 hr)	7×10^{-12}	8×10^{-12}
Triethylamine	None (88 hr)	8×10^{-12}	2×10^{-11}
Carbonyls			
Acetone	None (40 hr)	2×10^{-12}	1×10^{-12}
2, 5 Hexanedione	None (576 hr)	4×10^{-12}	2×10^{-12}
Esters			
Ethyl acetate	None (336 hr)	2×10^{-12}	4×10^{-11}
Ethyl Acetoacetate	None (678 hr)	4×10^{-12}	3×10^{-11}
Acid Anhydrides			
Acetic anhydride	None (96 hr)	2×10^{-12}	4×10^{-11}
Phthalic anhydride	None (336 hr, 0.2%)	2×10^{-12}	8×10^{-12}
Organic Acid + Water			
Acetic acid + water	None (40 hr)	3×10^{-12}	8×10^{-12}
Phthalic acid + water	None (144 hr)	1×10^{-12}	8×10^{-12}
Heterocyclic Compounds			
Pyrrole	None (96 hr)	2×10^{-12}	3×10^{-12}
Quinoline	None (96 hr)	8×10^{-12}	3×10^{-12}
Thiophene	None (144 hr)	8×10^{-12}	2×10^{-11}
Olefins			
Cyclohexene	After 192 hr	3×10^{-12}	1×10^{-10}
Aromatic Compounds			
1, 4 Naphthaquinone	None (40 hr)	2×10^{-12}	2×10^{-12}
Nitrobenzene	None (216 hr)	9×10^{-12}	1×10^{-12}
Quinone	Slight (40 hr)	2×10^{-12}	4×10^{-12}
1, 3, 5 Trinitrobenzene	None (40 hr)	6×10^{-12}	2×10^{-11}
Inorganic Salt			
Aluminum nitrate·$9H_2O$	None (96 hr)	2×10^{-12}	5×10^{-12}
Water (equivalent to above)	Extensive (40 hr)	5×10^{-12}	2×10^{-12}
Chelating Agent			
8-Hydroxyquinoline	None (216 hr)	2×10^{-12}	1×10^{-11}

proximately a factor of ten or more. It should be pointed out that this particular agent was also considered least effective as a retarding agent when evaluated with a test specimen in a carbon tetrachloride solution initially saturated with anhydrous aluminum chloride. It can also be seen in Table III that the various retarding agents at 1% concentration have negligible effect on the conductivity of pure carbon tetrachloride. Accordingly, it is presumed that the conductivity changes are the result primarily of interaction of the colored ionized complex (between carbon tetrachloride and anhydrous aluminum chloride) and the retarding agent. It does not appear, however, that a direct proportional relationship exists between the ability of an agent to lower the conductivity a specific amount and its effectiveness as a retarding agent. For example, 8-hydroxyquinoline, 2,5 hexanedione, and phthalic anhydride are all highly effective retarding agents by actual test and do lower the conductivity of carbon tetrachloride-aluminum chloride solution but not to the same degree. For example these compounds lower the conductivity by factors of 20, 100, and 250, respectively.

One practical application of this relationship might be to follow the conductivity of a closed aluminum system containing inhibited carbon tetrachloride. A warning that the concentration of the retarding agent was inadequate would be indicated by a rise in conductivity. Addition of more retarding agent followed by a drop in the conductivity would mean the carbon tetrachloride was again adequately inhibited. Conceivably, this type of control could be exercised with other halogenated hydrocarbons where similar relationships between conductivity, aluminum chloride, and retarding agents might be established.

Discussion of Possible Alternate Free Radical Theory

As pointed out by Stern and Uhlig (5) several theoretical reasons indicate that the reaction may proceed by means of a free radical mechanism. It was concluded, therefore, that the reaction was initiated by free radicals whose formation accelerated with time until the rate of generation equaled the rate of destruction. This could be one of several possible explanations for the constant corrosion rate found for high-purity aluminum in carbon tetrachloride. However, an ionic mechanism would also be consistent with the observed data. In the following equilibrium,

$$AlCl_3 + CCl_4 \leftrightharpoons (CCl_3)^{\cdot} + (AlCl_4)^{-}$$

the concentration of the ionic species is so small that a steady-state condition would soon be obtained. In view of the complexity of the reaction, it would not be unreasonable to assume that some of the steps may involve free radicals. However, our data indicates that the rate-determining step is one involving an electrochemical mechanism.

Stern and Uhlig (5) have shown that certain free radical supressors are capable of retarding the aluminum-carbon tetrachloride reaction. If effective retarders do combine with free radicals, this would be another indication that the rate-controlling step is free radical in nature.

Tests for Free Radicals

The following experiments were carried out to determine whether or not free radicals are present in measurable quantities in boiling carbon tetrachloride. A solution of triphenylmethyl free radicals was prepared by dissolving 0.25 g triphenylchloromethane in 50 ml of benzene and adding 3 g of zinc filings and allowing the mixture to stand at room temperature for 6 hr in a sealed bottle. The presence of free triphenylmethyl radicals was indicated by the appearance of a yellowish-orange color. The free radicals form according to the reaction shown below:

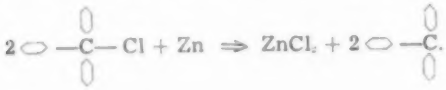

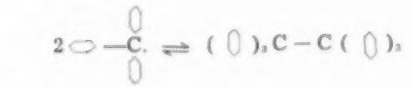

The solution of free radicals in benzene was decanted and added to 50 ml of carbon tetrachloride and the mixture refluxed under nitrogen for 10 min. The color did not fade during this period. The solution was then divided into two portions. One portion was placed in a bottle and sealed to exclude air. The color of this solution did not fade. The other portion was poured into an open beaker. The color of this solution faded completely within a few minutes indicating that the color was caused by the presence of free radicals and that the free radicals were destroyed by reaction with oxygen when the solution was exposed to air. One of the properties of triarylmethyl free radicals is the rapid absorption of atmospheric oxygen to form colorless triarylmethyl peroxides (6). If appreciable amounts of free radicals were present in the boiling carbon tetrachloride, it would be expected that the free radicals would be removed by the following reactions causing the color of the solution to fade in a short time:

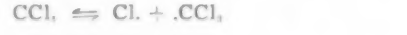

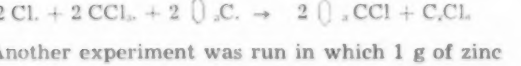

Another experiment was run in which 1 g of zinc filings, 50 ml of benzene and 50 ml of carbon tetrachloride were placed in a reflux flask and brought to the boiling point, 0.25 g of triphenylchloromethane was then added and the flask flushed with nitrogen. A dark yellow-orange color appeared in a short time. After refluxing for 10 min the solution was decanted and divided in two portions. One portion was sealed in a glass bottle and remained colored; the other portion was poured into an open beaker and became colorless within a few minutes. A blank was run in which 1 g of zinc filings, 50 ml of benzene, and 50 ml of carbon tetrachloride were refluxed for 30 min. This solution did not develop any color. The above results indicate that the rate of formation of free radicals from carbon tetrachloride was too low to prevent the formation of triphenylmethyl free radicals.

A number of the retarder materials investigated in this laboratory (1) as well as some mentioned by Stern and Uhlig (5) were tested for their ability to react with triphenylmethyl free radicals.

Some amines have already been mentioned as being reactive with aluminum chloride as well as carbon tetrachloride. The amine, 3-methoxypropylamine, does, in addition, react with triphenylmethyl free radicals almost as rapidly as the free radical reacts with air with the resultant solution becoming water clear. On the other hand, retarders containing carbonyl groups such as ethyl acetate, ethyl acetoacetate, 2,5-hexanedione, and phthalic anhydride which range from good to excellent as retarding agents do not react with solutions of this free radical species, and it is necessary to expose these solutions to air in order to decolorize them. Acetone was an exception to this rule.

Heterocyclic ring-type compound retarders such as thiophene did not react with the triphenylmethyl free radical. The olefin, cyclohexene, which is only a fair retarder for the carbon tetrachloride reaction, readily reacts with the colored free radical. The inorganic salt $Al(NO_3)_3 \cdot 9H_2O$, an effective retarder, can also decolorize the colored free radical solution.

Two of the free radical supressors mentioned by Stern and Uhlig (5), quinone and napthaquinone, could not be evaluated by this method since both materials give yellow colored solutions in benzene. However, nitrobenzene, another retarder mentioned by Stern and Uhlig, did react to the extent that small amounts of nitrobenzene lightened the deep yellow color of the free radical solution and air did not further lighten the color.

On the basis of the above results, it was concluded that the ability of a substance to react or not react with triphenylmethyl free radicals bears no relationship to its ability to retard the carbon tetrachloride-aluminum reaction. Therefore, the evidence indicates that the rate-determining step for this latter reaction is controlled largely by an electrochemical mechanism (7).

Results with Other Halogenated Hydrocarbons

This proposed electrochemical mechanism applies only to carbon tetrachloride and was not established for other halogenated hydrocarbons. High-purity aluminum specimens could not be cathodically protected in the case of the eight other halogenated hydrocarbons tested. From the initial high rates of attack, relatively high current densities would be required to achieve cathodic protection if the mechanism were electrochemical. These high current densities were not possible with the available equipment. The halogenated hydrocarbons were 2- chloro -2- methylbutane, 2-chloro -2- methylpropene, (1, 4-dichlorobutane), (1, 1, 2, 2- tetrachloroethane), α-chlorotoluene, methlychloroform, (1, 1, 2- trichloroethane), and 3- chloro -2- methylpropene. The inability to achieve cathodic protection in these cases

could be explained by (*a*) inability to achieve the minimum cathodic current required because of high solution resistance and limited emf source, or (*b*) the rate-controlling step being other than electrochemical.

Summary

1. Conductivity of a boiling carbon tetrachloride solution with high-purity aluminum present increases steadily as the reaction proceeds and after about 4-5 hr reaches a constant value.

2. Addition of hexachloroethane to boiling carbon tetrachloride has no effect on conductivity, but addition of aluminum chloride produces an immediate elevation of the conductivity. An additional elevation of the conductivity can be secured by reacting an aluminum specimen in this solution, suggesting that additional ionized complexes are formed.

3. Increase of conductivity in a corroding solution parallels the increase in weight per cent aluminum in solution which occurs as the reaction proceeds. However, the more sensitive conductivity measurements show that the reaction starts soon after the aluminum is placed in the boiling carbon tetrachloride; hence the induction period referred to in previous literature reports is only an "apparent induction time."

4. The fact that the reaction rate increases with increasing conductivity suggests an electrochemical mechanism. Changes in the temperature coefficient of the conductivity in the presence and absence of corrosion products also suggests this type of mechanism.

5. Cathodic protection successfully prevented the corrosion of high-purity aluminum in boiling carbon tetrachloride. This also supports an electrochemical mechanism since it must be concluded that the initial attack of the aluminum is caused by the presence of an ionic species.

6. Additional evidence for an electrochemical mechanism was obtained by producing an identifiable amount of hexachloroethane (a primary reaction product) by electrolysis of a carbon tetrachloride solution saturated with aluminum chloride.

7. The addition of retarding agents resulted in an alteration of the ionized aluminum chloride-carbon tetrachloride complex so that the conductivity dropped essentially to that of pure boiling carbon tetrachloride. There is no direct proportional relationship between the ability of an agent to lower the conductivity a specific amount and its effectiveness as a retarding agent. Following the pattern of conductivity in the carbon tetrachloride solution should, however, be indicative of the level of protection of a retarder agent added to the solution.

8. There was no apparent reaction between triphenylmethyl free radicals in benzene and boiling carbon tetrachloride, although a portion of the same solution reacted with the oxygen of the air. Similarly, triphenylmethyl free radicals could be made in the presence of boiling carbon tetrachloride, indicating that the rate of formation of free radicals in carbon tetrachloride, if present, was too low to prevent the formation of the triphenylmethyl free radicals by reaction.

9. Several of the retarder materials listed in previous publications were tested for their ability to react with triphenylmethyl free radicals. There was no relationship between the ability of a substance to retard this carbon tetrachloride-aluminum reaction and to react with triphenylmethyl free radicals.

Manuscript received Nov. 13, 1957. This paper was prepared for delivery before the Buffalo Meeting, Oct. 6-10, 1957.

Any discussion of this paper will appear in a Discussion Section to be published in the December 1959 JOURNAL.

REFERENCES

1. J. D. Minford, M. H. Brown, and R. H. Brown, *This Journal*, **106**, 185 (1959).
2. International Critical Tables VI, 152, 230.
3. L. P. Hammett, "Physical Organic Chemistry," p. 142, 310 f. McGraw-Hill Book Co., New York (1940).
4. M. Stern and H. H. Uhlig, *This Journal*, **99**, 381 (1952).
5. M. Stern and H. H. Uhlig, *ibid.*, **100**, 543 (1953).
6. M. Gomberg and L. H. Cone, *Ber.*, **37**, 3538 (1904).
7. E. R. Alexander, "Principles of Ionic Organic Reactions," p. 2, John Wiley & Sons, Inc. New York, (1950).

Copper-Activated Calcium Orthophosphate and Related Phosphors

Yasuo Uehara, Yoshimasa Kobuke, and Isoo Masuda

Matsuda Research Laboratory, Tokyo Shibaura Electric Co., Ltd., Kawasaki, Japan

ABSTRACT

The preparation and properties of copper-activated calcium orthophosphate and related phosphors are described. Copper-activated β-calcium orthophosphate phosphor fired in a reducing atmosphere produces a strong blue fluorescence peaked at 4800Å under excitation by 2537Å and cathode rays. With partial substitution of Ca by bivalent metals such as Be, Cd, and Sr the emission remains unchanged, while introduction of Mg and Zn gives a strong violet fluorescence peaked at about 4400Å and 4500Å, respectively. Phosphors containing boron produce a blue to greenish yellow fluorescence depending on the content of boron. All of these phosphors give a strong thermoluminescence. Only the blue fluorescent phosphor gives also a weak red emission stimulated by 3650Å radiation. Introduction of Mn or Sn as secondary activators into Cu-activated β-calcium orthophosphate or into the Cu-activated substituted phosphors gives rise to a red band due to Mn or Sn in addition to the original blue or violet band. The luminescent properties of zinc or cadmium orthophosphate are similar in some respects to those of zinc or cadmium sulfide phosphors.

Calcium metaphosphate and halophosphate activated with Cu have been reported to produce a weak blue fluorescence (1). According to the present investigation, calcium orthophosphate with added Cu and fired in air shows practically no fluorescence at room temperature under excitation by 2537Å, 3650Å, and cathode rays. However, calcium orthophosphate containing Cu which was fired in a reducing atmosphere was found to give a strong blue fluorescence under excitation by 2537Å and cathode rays. This phosphor also shows a strong blue thermoluminescence and a weak red emission stimulated by 3650Å. The present paper describes the preparation and properties of Cu-activated calcium orthophosphate fired in a reducing atmosphere and related phosphors.

Preparation and Structure of Phosphors

Calcium orthophosphate phosphors were prepared from dibasic calcium phosphate ($CaHPO_4$) and calcium carbonate. These materials were prepared from purified solutions of dibasic ammonium phosphate, calcium chloride, and ammonium carbonate. A solution of purified copper sulfate was added to a mixture of 2 mole dibasic calcium phosphate and 0.9 mole calcium carbonate. The blend was dried at about 200°C, then milled to assure intimate mixture. It was fired in a silica tube in an electrically heated furnace for about 30 min at 1100°C in air. The air-cooled powder was reground and fired in a reducing atmosphere for about 30 min at 1100°C, then cooled in the same atmosphere. As the reducing gas, a mixture of 75% nitrogen and 25% hydrogen was used for the most part. If pure hydrogen was used as a reducing gas, the resulting powder showed a grayish color and low fluorescent efficiency due to excessive reduction.

Optimal concentration of the activator was about 5×10^{-4} g-atom Cu for 1 mole calcium orthophosphate. Any departure of the activator concentration from its optimal value leads to a rapid decrease of the fluorescent intensity under excitation by 2537Å at room temperature, as shown in Fig. 1.

In order to obtain the brightest phosphor, it is preferable to use an amount of calcium carbonate about 10 mole % less than that required for the stoichiometric composition, as shown above. Even in this case, it was verified by x-ray analysis that the resulting phosphor has the calcium orthophosphate structure. Copper-activated calcium orthophosphate fired above about 1200°C in the same atmosphere shows only a weak blue fluorescence under excitation by 2537Å and cathode rays at room temperature, in contrast with the phosphor fired below about 1200°C. It was also verified by x-ray analysis that the former had α-form structure and the latter had β-form structure.

With partial substitution of bivalent metals such as Be, Mg, Zn, Cd, and Sr for Ca in the Cu-activated β-calcium orthophosphate, similarly efficient phosphors can be obtained. However, substitution of about 7 mole % Ca by Ba results in a weakly purple fluorescent phosphor. Phosphors containing Mn or Sn as secondary activators were prepared by

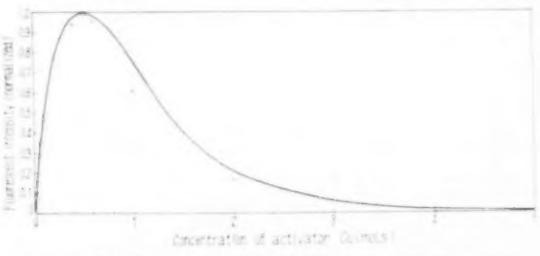

Fig. 1. Relative fluorescent intensity vs. activator concentration of Cu-activated β-calcium orthophosphate phosphors fired in a reducing atmosphere. Excitation with 2537Å at room temperature.

the same method as Cu-activated β-calcium orthophosphate.

Measurement Techniques

The spectral energy distribution of the phosphor excited by 2537Å was measured with a Zeiss three glass prism spectrograph which was equipped with an exit slit and a photomultiplier. This allowed its use as a constant deviation type monochrometer whose resolving power corresponded to a single 60° prism having 21-cm base length. The spectral sensitivity of this optical system was calibrated by use of a standard lamp.

In order to investigate the absorption characteristics of the phosphor, the spectral reflectance of a phosphor layer of about 2-mm thickness was measured relative to that of a plaque of smoked magnesium oxide whose spectral reflectance was measured previously. The spectral range from about 2300Å to the visible part of the spectrum was covered. This measurement was carried out with a Beckmann-type monochrometer combined with a photomultiplier. As a light source a low pressure hydrogen lamp was used. The arrangement of the optical system was similar to that reported by Botden and Kröger (2). In the measurement of the spectral reflectance, various cut-off filters were used to eliminate the fluorescent radiation from the reflected light. Using this apparatus, the quantum efficiency of fluorescence also was measured. The detailed method of the measurement and measured results for various phosphors, except some typical phosphors which are described below, will be published elsewhere.

Decay characteristics of Cu-activated β-calcium orthophosphate excited by cathode rays at room temperature were measured with a demountable cathode ray tube. The phosphor was placed as a uniform layer of powder in a shallow, nickel plated brass cup. A square wave of voltage from a Hewlett Packard 212A pulse generator was fed to the grid of the electron gun of the cathode-ray tube. The pulse width and frequency of excitation were variable. The emitted light was received by a RCA 1P21 photomultiplier through a glass window of the cathode-ray tube. Its output was fed to the vertical amplifier of a Tektronix 545 oscilloscope.

The decay characteristics of the persistent phosphorescence with 2537Å excitation at 297°-298°K were measured with a Brown Electronik Recording Electrometer in combination with a photomultiplier. Periods of constant excitation by 2537Å varied from 10 sec to 6 hr. Curves of the decay characteristics were recorded with the recording electrometer for periods of time from 1 to 100 min after the end of excitation.

The buildup and decay characteristics of thermoluminescence with a thin layer of the phosphor which was excited by 2537Å at about 280°K and then heated at about 465°K were measured by using the recording electrometer combined with a photomultiplier. However, the rate of buildup of thermoluminescence was too fast to be measured accurately by this method, and only the rate of decay could be determined.

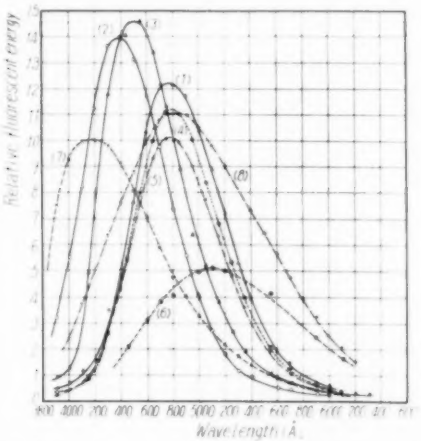

Fig. 2. Spectral energy distribution of Cu-activated calcium orthophosphate and substituted orthophosphates fired in reducing atmospheres, in comparison with tungstate phosphors. All phosphors excited with the same intensity of 2537Å at room temperature. Curve 1, 2.9 CaO · P_2O_5: 5 x 10^{-3} Cu; curve 2, 2.5 CaO · 0.4 MgO · P_2O_5 x 10^{-3} Cu; curve 3, 2.7 CaO · 0.2 ZnO · P_2O_5:5 x 10^{-3} Cu; curve 4, 2.7 CaO · 0.2 CdO · P_2O_5 x 10^{-3} Cu; curve 5, 2.7 CaO · 0.2 SrO · P_2O_5 x 10^{-3} Cu; curve 6, 2.9 CaO · 0.15 B_2O_3 · P_2O_5 x 10^{-3} Cu; curve 7, $CaWO_4$; curve 8, $MgWO_4$.

Phosphor Characteristics

Emission under excitation by 2537Å, 3650Å, and cathode rays.—Cu-activated β-calcium orthophosphate fired in a reducing atmosphere shows a strong blue fluorescence peaked at 4800Å under excitation by 2537Å and cathode rays, while with 3650Å excitation it produces only an extremely weak blue fluorescence at room temperature. The spectral energy distribution of this phosphor excited by 2537Å at room temperature is shown by curve 1 in Fig. 2, compared with that of calcium tungstate (curve 7) and magnesium tungstate (curve 8). All the curves shown in Fig. 2 were obtained under conditions of constant 2537Å intensity and identical geometry of the optical system.

Cu-activated β-calcium orthophosphate fired in air shows practically no fluorescence at room or low temperature under excitation by 2537Å, 3650Å, and cathode rays, as mentioned before, but it produces a very weak blue fluorescence at temperatures higher than about 500°K with 2537Å excitation. Cu-activated α-calcium orthophosphate fired in a reducing atmosphere shows only a weak blue fluorescence under excitation by 2537Å and cathode rays at room temperature, as mentioned before. Therefore, only Cu-activated β-calcium orthophosphate fired in a reducing atmosphere can give an efficient fluorescence.

Partial substitution of Be, Cd, and Sr for Ca in Cu-activated β-calcium orthophosphate fired in a reducing atmosphere has very little effect on the intensity and color of fluorescence. The substituted orthophosphate phosphors containing 0.2 g-atoms of the bivalent metals mentioned above still produce a fairly strong fluorescence, but as the amount of bivalent metals is further increased, the intensity of the fluorescence gradually decreases. The spectral energy distribution curves of the substituted

phosphors containing 0.2 g-atoms of Cd and Sr are shown by curves 4 and 5 in Fig. 2.

Partial substitution of Mg and Zn for Ca in Cu-activated β-calcium orthophosphate shifts the peak of emission toward shorter wave lengths and increases the efficiency of fluorescence. The peak position of the substituted phosphors containing 0.4 g-atoms of Mg and 0.2 g-atoms of Zn are 4400Å and 4500Å, respectively, as shown by curves 2 and 3 in Fig. 2. The band widths of the phosphors mentioned above are very narrow compared with that of calcium or magnesium tungstate. Fluorescent lamps made with these phosphors show a very saturated blue or violet color and the average output in 20-w fluorescent lamps made with Cu-activated β-calcium orthophosphate was 370 lumens at 100 hr.

If boron compounds such as ammonium borate or boric oxide are introduced into Cu-activated β-calcium orthophosphate in amounts of 0.1 mole, the color of fluorescence is practically identical with that of the original phosphor, but as the amount of boric oxide is further increased, the color of the fluorescence shifts gradually from blue to green and finally to greenish yellow with about 0.4 mole of boric oxide. Besides, the intensity of the fluorescence is lowered as the amount of boric oxide is increased. The phosphor containing about 0.15 mole of boric oxide gives a very broad band peaked at 5100Å, as shown by curve 6 in Fig. 2.

Copper-activated orthophosphates of Be, Mg, Sr, and Ba which were prepared by firing at 850°-950°C in air for 30 min and then in a reducing gas for 30 min show essentially no fluorescence under excitation by 2537Å, 3650Å, and cathode rays at any temperature ranging from room to liquid air temperature. However, Cu-activated zinc orthophosphate fired in a reducing atmosphere at 850°C gives a green fluorescence of moderate intensity at room temperature with 3650Å excitation and a very weak green fluorescence with 2537Å excitation, but not with cathode ray excitation. At liquid air temperature, the fluorescence increases in intensity without change of color. Pure zinc orthophosphate without added activator and fired in a reducing atmosphere at 800°C, also produces a weak green emission peaked at 5000Å at room temperature but only with 3650Å excitation. At liquid air temperature, it shows a green fluorescence of moderate intensity under excitation by both 3650Å and 2537Å.

Copper-activated cadmium orthophosphate fired in a reducing atmosphere at 850°-900°C gives a weak orange fluorescence at liquid air temperature only with 2537Å excitation, but it does not fluoresce at room temperature under excitation by either 2537Å, 3650Å, or cathode rays. However, pure cadmium orthophosphate without added impurities and fired at 900°C in a reducing atmosphere or in nitrogen gives a weak whitish yellow fluorescence at room temperature with 2537Å excitation. At liquid air temperature, the fluorescence increases in intensity. Pure cadmium orthophosphate fired in air at 850°C for 30 min shows a weak whitish yellow fluorescence at liquid air temperature under excitation by 2537Å and 3650Å. At room temperature, it shows no fluorescence under excitation by 2537Å, 3650Å, and cathode rays.

Introduction of Mn, in addition to Cu, into β-calcium orthophosphate fired in a reducing atmosphere produces a whitish purple fluorescence which consists of a blue band and a sensitized red band. Calcium orthophosphate doubly activated with Cu and Sn and fired in a reducing atmosphere produces a blue to whitish red fluorescence depending on the Sn concentration. With partial substitution of Mg and Zn for Ca in β-calcium orthophosphate containing Mn or Sn, in addition to Cu, the peaks of the red band due to Mn or Sn, as well as that of the blue or violet band due to Cu, are shifted toward shorter wave lengths. As a typical example, the spectral energy distribution of β-calcium orthophosphate doubly activated with Cu and Sn, calcium magnesium orthophosphate containing 0.2 g-atoms of Mg and 2.7 g-atoms of Ca and doubly activated with Cu and Sn, and calcium orthophosphate doubly activated with Cu and Mn are shown by curves 1, 2, and 3 in Fig. 3. These curves were obtained under the same conditions as those for Fig. 2 and the ordinate scale is the same as that of Fig. 2.

The peak positions of the red bands of β-calcium orthophosphate doubly activated with Cu and Sn, and with Cu and Mn are about 6300Å and 6600Å, respectively, as seen in Fig. 3, and they are in good agreement with those of the corresponding bands of β-calcium orthophosphate activated with Sn alone and with Sn and Mn which have already been reported by Butler (3).

As clearly seen in Fig. 2, the peak intensity of calcium orthophosphate, calcium·magnesium orthophosphate, and calcium·zinc orthophosphate activated with Cu is larger than that of calcium or magnesium tungstate. The measured quantum efficiency of fluorescence of Cu-activated calcium·magnesium orthophosphate and calcium orthophosphate was about 0.9 and 0.8, respectively, with 2537Å excitation at room temperature. Considering a rather large absorption of the phosphors in the visible part of the spectrum, a correction for absorption loss must be made in order to evaluate the intrinsic quantum efficiency of fluorescence. Ac-

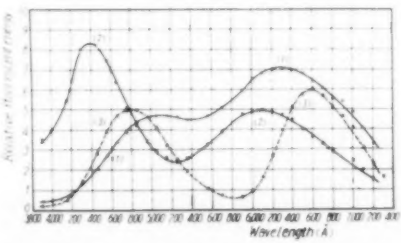

Fig. 3. Spectral energy distribution of orthophosphates doubly activated with Cu and Sn or Mn and fired in reducing atmospheres. All phosphors excited with the same intensity of 2537Å at room temperature. Curve 1, 2.9 CaO · P_2O_5:5 x 10^{-3} Cu + 5 x 10^{-3} Sn; curve 2, 2.7 CaO · 0.2 MgO · P_2O_5 x 10^{-3} Cu + 5 x 10^{-3} Sn; curve 3, 2.9 CaO · P_2O_5:5 x 10^{-3} Cu + 3 x 10^{-2} Mn.

cording to Bril and Klasens (4), the intrinsic quantum efficiency of fluorescence, νi, is given by

$$\nu i = \frac{2}{1 + R\infty}\,\nu m,$$

where νm is the measured quantum efficiency of fluorescence and $R\infty$ is the reflectance of the phosphor layer having practically infinite thickness. Since the value of $R\infty$ for both Cu-activated calcium·magnesium orthophosphate and calcium·orthophosphate was about 0.8 over the wide range of the visible part of the spectrum, a value close to unity was obtained for the intrinsic quantum efficiency of Cu-activated calcium·magnesium orthophosphate with 2537Å excitation at room temperature. The intrinsic quantum efficiency of Cu-activated β-calcium orthophosphate evaluated by the same method was about 0.9 with 2537Å excitation at room temperature, and a value of about 0.1 with 3650Å excitation at about 600°K was estimated.

Temperature dependence of fluorescent intensity.—The temperature dependence of fluorescent intensity of a typical β-calcium orthophosphate activated with 0.5 mole % Cu and fired in a reducing atmosphere is shown in Fig. 4. Curves 1 and 2 were obtained under excitation by 2537Å and 3650Å, respectively, and show a remarkable difference in behavior.

Although the emission peak of Cu-activated calcium orthophosphate shifts slightly toward shorter wave lengths at temperatures higher than room temperature, the effect of variation of the peak position on the measured intensity of fluorescence at higher temperatures will be small. Since the intensity of exciting radiation used in this measurement is rather weak, the intensity of fluorescence at various temperatures will be proportional to the quantum efficiency of fluorescence at the corresponding temperatures. The units of the ordinate in Fig. 4 are given so that the curves shown in this diagram express the temperature dependence of the intrinsic quantum efficiency of fluorescence.

The temperature dependence curves of fluorescent intensity of the Cu-activated phosphors substituted with Be, Mg, Zn, Cd, and Sr were similar to that of Cu-activated β-calcium orthophosphate.

Absorption.—The reflection spectra of typical phosphors measured at room temperature are

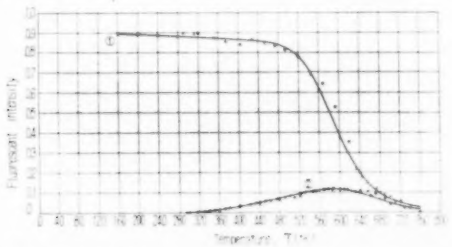

Fig. 4. Temperature dependence of β-calcium orthophosphate activated with 0.5 mole % Cu and fired in a reducing atmosphere. (Ordinate is equivalent to the intrinsic quantum efficiency of fluorescence). Curve 1, 2537Å excitation; curve 2, 3650Å excitation.

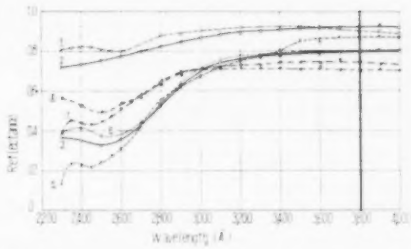

Fig. 5. Reflection spectra of pure and Cu-activated calcium orthophosphates and related phosphors at room temperature. Curve 1, β—2.9 CaO · P_2O_5 fired in a reducing atmosphere; curve 2, β—2.9 CaO · P_2O_5 fired in air; curve 3, β—2.9 CaO · P_2O_5:5 x 10^{-3} Cu fired in a reducing atmosphere; curve 4, α—2.9 CaO · P_2O_5:5 x 10^{-3} Cu fired in a reducing atmosphere; curve 5, β—2.9 CaO · P_2O_5:5 x 10^{-3} Cu fired in air; curve 6, β—2.5 CaO · 0.4 MgO · P_2O_5:5 x 10^{-3} Cu fired in a reducing atmosphere; curve 7, β—2.9 CaO · 0.15 B_2O_3 · P_2O_5:5 x 10^{-3} Cu fired in a reducing atmosphere.

illustrated in Fig. 5. Pure calcium orthophosphates fired in air or in a reducing atmosphere give rather flat reflection curves throughout the measured range of the spectrum, as shown by curves 1 and 2 in Fig. 5.

Copper-activated β-calcium orthophosphate fired in a reducing atmosphere gives a pronounced absorption band ranging from about 3100Å down to the short wave-length region of the spectrum and peaking at about 2550Å, as shown by curve 3 in Fig. 5. The reflection spectra of this phosphor measured at higher temperatures were practically identical with curve 3 in Fig. 5. Therefore, the temperature dependence of fluorescent intensity shown in Fig. 4 will be essentially independent of the absorption transition probability in the activator center.

The absorption of Cu-activated α-calcium orthophosphate shown by curve 4 in Fig. 5 is shallower than that of Cu-activated β-calcium orthophosphate in the shorter wave-length region below about 3000Å, but in the long wave-length region the situation is reverse. The shallowness of the absorption in the α-form, as well as the difference in structure, may be responsible for the low efficiency of its fluorescence. It is interesting that the absorption of Cu-activated β-calcium orthophosphate fired in air is stronger than that of the phosphor fired in a reducing atmosphere, at least in the shorter wave-length region below about 2700Å, as shown by curve 5 in Fig. 5. This fact, together with the temperature dependence of fluorescent intensity mentioned before, suggests that the trapping or quenching effect of this phosphor is much stronger than that of the phosphor fired in a reducing atmosphere.

The effect of the introduction of Mg or boron in Cu-activated calcium orthophosphate is shown by curves 6 and 7 in Fig. 5.

The measured reflection spectra of pure zinc orthophosphate and cadmium orthophosphate, which were prepared by firing in air or nitrogen, showed a flat and strong absorption with absorption edges at about 3900Å and 3200Å, respectively. The interesting fact was found that the characteristic ab-

sorption of these phosphors was decreased by the introduction of Cu or by firing in a reducing atmosphere. Detailed quantitative results will be published elsewhere.

The properties of zinc and cadmium orthophosphate phosphors, for example, absorption and emission characteristics, thus resemble those of zinc sulfide phosphors.

Although the detailed results of the reflection spectra of bivalent metal phosphates (except for a series of calcium orthophosphates) will be published elsewhere, it will be noted here that all curves of the reflection spectra of magnesium, strontium, and barium orthophosphate with added copper and fired in a reducing atmosphere were similar in shape to those of pure calcium orthophosphate (curves 1 and 2 in Fig. 5), but they were deeper in absorption. The average reflectance of these phosphors in the spectral region from 2300Å to 4000Å was about 0.7, 0.65, and 0.55, respectively. The detailed hue of color of these powders depends on the nature of the matrix. The natural color of the magnesium, strontium, and barium orthophosphates is reddish, grayish, and reddish, respectively.

Decay characteristics of phosphorescence.—The measured decay characteristics of the phosphorescence of Cu-activated β-calcium orthophosphate were of a monomolecular type under excitation by both 2537Å and cathode rays. The measured decay constants of this phosphor were 0.13 μsec for a fast component of afterglow and 1.6 μsec for a slow component under excitation by cathode rays of about 5 kv and 0.07 μsec pulse width at room temperature.

The measured decay constants for the components of the persistent phosphorescence with 2537Å excitation were 3.87 hr, 24.6 min, 4.13 min, and 0.931 min at 297°-298°K and their relative light sums were 100, 19.7, 6.9, and 3.9, respectively. The intensity of the persistent phosphorescence is extremely weak and the initial intensity of the most persistent component of the phosphorescence was of the order of 10^{-4} compared with the fluorescent intensity at about 300°K. The color of the phosphorescent light was identical with that of the fluorescent light.

Thermoluminescence.—Copper-activated β-calcium orthophosphate fired in a reducing atmosphere shows a strong blue thermoluminescence when it is heated after a previous exposure to 2537Å radiation for more than 10 min, and even after storage in the dark for times longer than about 10 hr at about 280°K. The intensity of thermoluminescence is dependent on the intensity of 2537Å, time of exposure to 2537Å, and temperature during excitation as well as the heating temperature. When the excitation by 2537Å is made at low temperature such as liquid air temperature or at higher temperatures than about 500°K, the phosphor shows no thermoluminescence. The brightest thermoluminescence was obtained after excitation by 2537Å at about 280°K. The phosphor excited with 3650Å showed no thermoluminescence.

The decay characteristics of thermoluminescence at a constant heating temperature were exponential. The decay constant of thermoluminescence measured at 465°K was about 10 sec. The rise time was very fast compared with the decay time. The characteristics of thermoluminescence of Cu-activated orthophosphate phosphors containing Be, Mg, Zn, Cd, Sr, and boron are similar to those of Cu-activated β-calcium orthophosphate, and only detailed behaviors are dependent on the amount of the added elements.

Stimulation by 3650Å radiation.—When Cu-activated β-calcium orthophosphate fired in a reducing atmosphere was first excited to saturation with 2537Å and then irradiated with 3650Å, it produced a weak red emission. The peak of the red emission was judged to be in the spectral range from 6000Å to 6500Å, according to visual inspection. The intensity of the red emission depended on the duration and intensity of the 2537Å excitation and on the intensity of the 3650Å radiation, but it was insensitive to the time of storage after exposure to 2537Å radiation as well as thermoluminescence. Indeed, we could observe the red emission after more than 10 hr following the excitation at about 280°K. This duration time for the stimulated red emission together with the thermoluminescence is of the same order as that of the most persistent component of the phosphorescence, whose decay constant is 3.87 hr at about 298°K. The red emission showed a very fast rise time, but its decay time was as long as minutes under stimulation by 3650Å of moderate intensity at room temperature. The brightest red emission was observed under excitation by 2537Å at about 280°K.

The blue fluorescent orthophosphate phosphors containing Be, Cd, Sr, or boron also gave the stimulated red emission, but the violet fluorescent orthophosphate phosphors containing Mg or Zn did not produce the red emission at all over a wide range of temperatures at which excitation was made with 2537Å.

In order to investigate the effect of impurities on the stimulation, a number of compounds of elements were added in the preparation of Cu-activated β-calcium orthophosphate. Introduction of about 0.01 mole of compounds of Ce, Zr, Mo, Ni, Se, V, Cr, Au, U, Co, Sn, and Mn per mole of Cu-activated β-calcium orthophosphate suppressed the red emission. On the other hand, introduction of K, Na, As, and boron compounds enhanced the red emission. However, if the amount of these added impurities except boron exceeded about 0.1 mole per mole of the matrix, the red emission was also suppressed completely.

Discussion

Although the properties of the phosphors here described are more complicated than those of the usual oxide-type phosphors, it does not seem to be difficult to give a straightforward theoretical interpretation, at least qualitatively. Quantitative explantations have already been formulated by one (6) of the present authors, and detailed results will be published in the near future. Therefore, only a qualitative discussion for the observed results is given here.

It is reasonable to suppose that the activator of Cu-activated β-calcium orthophosphate fired in a reducing atmosphere is different from that of the phosphor fired in air, because their respective characteristics of emission and absorption are quite different. Considering the firing process, it is natural to assume that the activator center of the phosphor fired in air may be formed by a Cu^{++}ion, while that of the phosphor fired in a reducing atmosphere may be ascribed to a Cu^{+}ion. Indeed no paramagnetic resonance absorption was detected in Cu-activated β-calcium orthophosphate fired in a reducing atmosphere.[1] The grayish color of the phosphor prepared by firing in pure hydrogen may be attributed to colloidal copper formed through a process of reduction from Cu^{+} ion to Cu atom as may be understood from the following consideration. Referring to the color of the magnesium, strontium, and barium orthophosphates mentioned before, we assume that the copper added to these phosphates is dispersed uniformly in the matrix in the form of neutral atoms, and we can then expect a pronounced characteristic absorption due to the Cu atoms in the near u.v. or visible region of the spectrum which, however, is contrary to the observed results. Therefore, the natural color of these phosphates may be attributed to the colloidal copper dispersed in the matrix. For the same reason, the grayish color of Cu-activated calcium orthophosphate fired in pure hydrogen may be ascribed to the same origin, as mentioned before.

Referring to the position of the activator in Cu-activated calcium orthophosphate, and assuming that the activators occupy interstitial sites in the lattice, we cannot find any convincing reason why copper cannot be introduced into the matrix of magnesium, strontium, or barium phosphate as an effective activator. However, the experimental results mentioned above will be explained by assuming that the activator in Cu-activated calcium orthophosphate can replace Ca^{++}ions at lattice sites in the form of Cu^{++} or Cu^{+}ions, as suggested above. If we consider the Cu^{+}ion to be the activator in Cu-activated β-calcium orthophosphate fired in a reducing atmosphere, we must assume that a vacancy of a single O^{--}ion may be generated by the replacement of two Ca^{++}ions by Cu^{+}ions in order to satisfy the condition of charge neutrality in the phosphor.

According to the above consideration concerning the activator center in Cu-activated β-calcium orthophosphate fired in a reducing atmosphere, the allowed transition of $^1S_0 \rightarrow {}^3P_1^\circ$ may be responsible for the absorption band peaking at about 2550Å, and also the transition $^1S_0 \rightarrow {}^3D_{1,2,3}$ or $^1D_2$ for the weak absorption in the spectral range above about 3100Å. Although the latter transition is originally forbidden in a free Cu^{+}ion, we can expect that it will be allowed by the interactions between the activator center and lattice ions. If the trapping state for the most persistent component of phosphorescence, thermoluminescence, and stimulation is attributed to the $^3P_2^\circ$ or $^3P_0^\circ$ states because of their similar decay constants, the stimulation by 3650Å may be caused by the absorption transition $^3P_2^\circ$ or $^3P_0^\circ \rightarrow {}^1P_1^\circ$ and the red emission by the transition $^1P_1^\circ \rightarrow {}^1S_0$ which is allowed. This absorption transition in a free Cu^{+}ion is originally forbidden because of the same odd parity of the spectrum terms. However, if we assume that it will be allowed by the interactions between the activator center and Ca^{++}ions in the lattice, we can explain the experimental result that no stimulated red emission could be observed in the phosphors containing Mg or Zn in the following way. The transition $^3P_2^\circ,0 \rightarrow {}^1P_0^\circ$ may become completely forbidden in the phosphor containing Mg or Zn because of the small interactions between the activator center and Mg^{++} or Zn^{++} ions which have smaller ionic radii than Ca^{++} ions; thus it results in complete suppression of the red emission. Incidentally, the effect of the introduction of boron on the stimulated red emission will be explained satisfactorily in a similar way. The observed peak position of the emission band peaking at a longer wave length and the large width of the emission band of the phosphor containing boron in contrast with those of the phosphor containing Mg or Zn suggests large interactions in the activator center. Thus we can expect an enhanced red emission of the phosphor containing boron in accordance with the observed result.

The experimental result that neither thermoluminescence nor stimulation could be observed under excitation by 2537Å at lower or higher temperatures, as mentioned before, suggests that some activation energy will be necessary for the transition $^3P_1^\circ \rightarrow {}^3P_2^\circ,0$ in the activator center.

The effect of boron introduced in the phosphor on the fluorescence and stimulated red emission is quite different compared with that of the other elements, as mentioned before. We are inclined to believe that boron may replace phosphorus in the matrix.

Acknowledgment

The authors wish to express their sincere thanks to Dr. Tsuneo Harada for his continuous support and encouragement. Part of this paper was presented at the Annual Meeting of the Japan Chemical Society in Tokyo, April 1-5, 1955.

Manuscript received April 28, 1958.

Any discussion of this paper will appear in a Discussion Section to be published in the December 1959 JOURNAL.

REFERENCES

1. F. A. Kröger, "Some Aspects of the Luminescence of Solids," p. 268, Elsevier Publishing Co., Inc., New York (1948); A. H. McKeag and P. W. Ranby, U. S. Patent 2,664,401.
2. T. H. J. Botden and F. A. Kröger, *Physica*, **15**, 747 (1949).
3. K. H. Butler, *This Journal*, **100**, 250 (1953).
4. A. Bril and H. A. Klasens, *Philips Tech. Rev.*, **15**, 63 (1953).
5. Y. Uehara, Y. Kobuke, I. Masuda, K. Maed, and M. Yamanaka, presented at the Second Symposium of the Atomic Power Commission, Tokyo, Feb. 7-9, 1958.
6. Y. Uehara, paper presented at the Annual Meeting of the Chemical Society of Japan, Tokyo, April 1-5, 1955; Kyoto, April 2-6, 1956; Tokyo, April 4-8, 1957.

[1] The authors are obliged to Professor Hidetaro Abe of Ochanomizu University, Tokyo, for this measurement.

Crystal Growth of Electrodeposited Zinc

An Electron Diffraction and Electron Microscopic Study

Ryoitiro Sato

Mitsubishi Metal Mining and Metallurgical Laboratory, Omiya City, Saitama Prefecture, Japan

ABSTRACT

Crystallographic aspects of zinc electrodeposited on to polycrystalline cathode from $ZnSO_4 + H_2SO_4 + H_2O$ baths with or without organic colloids have been investigated by electron diffraction (reflection method) and electron microscopy (replica method). At the initial stage of deposition, the zinc layer always consists of fine-grained crystallites oriented at random. As the zinc layer becomes thicker, some of these crystallites grow larger to yield a fiber orientation depending on the depositing condition. For such relatively thick zinc layers deposited under various degrees of influence of hydrogen and/or organic colloids, the orientation and texture are interpreted from standpoint of crystal growth.

Electron diffraction investigations of crystal growth of a variety of metals at the cathode during electrodeposition have so far been carried out by many authors (1-10). Although a comprehensive interpretation of their results is given by Finch, *et al.* (7), crystal growth of metals of lower symmetry has not yet been sufficiently explained, contrary to that of cubic metals. For this reason, zinc, a hexagonal metal, was chosen for this investigation, and it has been approached first in a study of crystal growth on a polycrystalline cathode.

Although addition of organic colloids to the electrolytic bath is of great technical importance, the crystallographic aspects of their effects have been studied little by means of electron diffraction. Again, zinc, which has moderate inhibitor sensitivity (11, 12), is suitable for such a study.

Thus, this paper reports electron diffraction (reflection method) and electron microscopic (replica method) investigations of zinc films electrodeposited under the following conditions: insoluble anode, polycrystalline cathode, and $ZnSO_4 + H_2SO_4 + H_2O$ baths (with or without addition of various organic colloids).

Experimental

The aqueous solution of $ZnSO_4 \cdot 7H_2O$ was purified by zinc dust. The organic colloids used were proteins (glue, gelatin, and albumin), a gum (gum arabic), and carbohydrates (dextrin, soluble starch, and saponin).

Electrodeposition was carried out in a 300-ml beaker, using a platinum plate as anode (1 cm x 1 cm x 0.2 mm) and a mechanically polished plate of α-brass as cathode (1 cm x 1 cm x 1 mm). These were separated by 4 cm. Depositing time varied from several seconds to 20 min. Immediately after taking out the cathode, it was washed successively with running water, distilled water, and acetone. To avoid chemical change of the cathode after the deposition, the procedure was carried out rapidly.

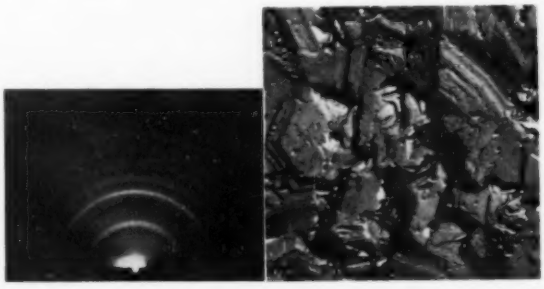

Fig. 1a (left). Electron diffraction pattern; Fig. 1b (right). Electron micrograph, magnification 5,000X. Bath: Zn 50 g/l; room temperature; $D_k = 3.5$ amp/dm^2; $C_{eff} = \sim 100\%$; θ (mean thickness) $= 38 \times 10^3$ Å. Hydrated basic zinc sulfate covering zinc layer.

The accelerating voltage of the electron beams for diffraction work was 35-50 kv. The sample to plate distance was 30 cm. To obtain the electron micrographs of the surface of the deposited layer, a two-stage replica method (acetylcellulose-carbon, followed by shadowing with Ge) was adopted. Usually the cathode which had served as the sample for the electron diffraction was itself subsequently observed by the electron microscope.

Results and Discussion

Experiments Using Baths Containing No Organic Colloids

(I) In some cases a diffraction pattern due to a substance other than zinc was obtained (Fig. 1a). In the corresponding electron micrograph (Fig. 1b) the substance covering the zinc layer is observed. Since the pattern is more marked with the baths containing comparatively low concentrations of the free acid, the substance is probably soluble in sulfuric acid. The analysis of the pattern is given in Table I. The data of hydrated basic zinc sulfate ($4ZnO \cdot SO_3 \cdot 7H_2O$) (13) agree fairly well with the analysis of Table I. The pattern appears invariably

Table I. Analysis of the Debye-Scherrer rings of Fig. 1a

Spacing, Å	Intensity
4.3	m
3.7	m
2.8	st
2.6	st
2.47	w
2.15	w
1.79	w
1.57	st
1.35	m
1.18	m
1.02	m
0.90	m

as Debye-Scherrer rings, showing no particular orientation relationship of the substance to the underlying zinc layer.

(II) In the zinc patterns obtained, almost always two blurred halos are observed, the one at the inside of the innermost ring of zinc and the other between the (10.2)-ring and the (11.0)-ring (e.g., Fig. 2a, 4a, and 5a). The same pair of halos appeared also in the pattern from the zinc layer deposited from a cyanide bath. The halos can be ascribed neither to minute crystallites of hydrated basic zinc sulfate nor to those of zinc oxide, which might be formed by oxidation of the deposited zinc.

(III) In the zinc patterns the (00.2)-ring is usually imperceptible. This anomaly in intensity of the diffraction patterns shows that the crystallites of the deposit are flat plates parallel to the basal plane (14). This is supported by the corresponding electron micrographs (e.g., Fig. 3b, 4b, and 5b).

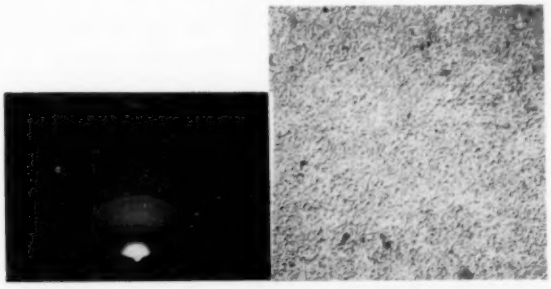

Fig. 2a (left). Electron diffraction pattern; Fig. 2b (right). Electron micrograph, magnification 10,000X. Zn 100 g/l + H_2SO_4 100 g/l; room temperature; D_k = 4 amp/dm²; θ = 700 Å. Random orientation.

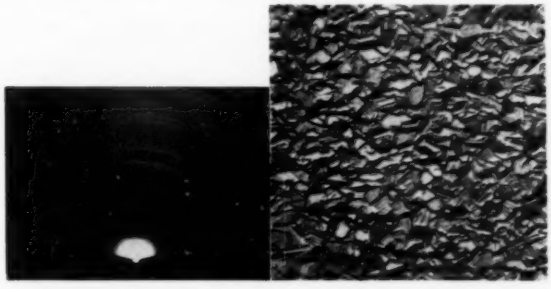

Fig. 3a (left). Electron diffraction pattern; Fig. 3b (right). Electron micrograph, magnification 5,000X. Zn 100 g/l + H_2SO_4 100 g/l; room temperature; D_k = 4 amp/dm²; θ = 6.3 x 10⁵ Å. Random orientation.

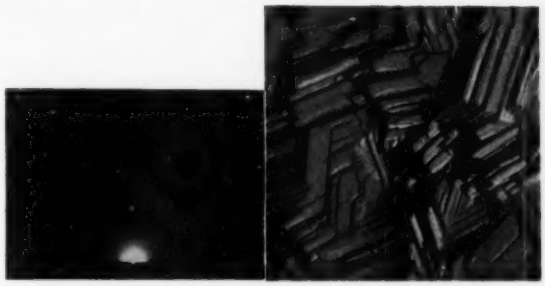

Fig. 4a (left). Electron diffraction pattern; Fig. 4b (right) electron micrograph, magnification 5,000X. Zn 100 g/l + H_2SO_4 100 g/l; room temperature; D_k = 4 amp/dm²; C_{eff} = 92%; θ = 54 x 10⁵ Å. Plane of orientation : (11.l), l ≈ 4.

Fig. 5a (left). Electron diffraction pattern; Fig. 5b (right) electron micrograph, magnification 5,000X. Zn 10 g/l + H_2SO_4 100 g/l; room temperature; D_k = 3 amp/dm²; C_{eff} = 58%; θ = 50 x 10⁵ Å. Plane of orientation : (10.l), l ≈ 1.

(IV) All of the zinc patterns show that the zinc crystallites take a fiber orientation (including random orientation), whose axis stands upright to the cathode surface. To denote such a fiber orientation, its "plane of orientation," i.e., the crystallographic plane of zinc which tends to lie parallel to the surface, is used in the following descriptions.

(V) With various bath compositions and depositing conditions, the zinc layer deposited in initial stages (up to several thousand angstroms in thickness) consists invariably of fine-grained crystallites (approximate dimension : 300Å in Fig. 2b, and 5000Å in Fig. 3b), and the tendency for a fiber orientation is very weak (Fig. 2a and 3a). This is in harmony with the results of Finch, *et al.* (7).

(VI) With continued deposition, the crystallites grow larger and a fiber orientation characteristic of the bath composition appears (Fig 4a, 4b, 5a, and 5b). According to Bauer (15), this kind of orientation should be called orientation due to crystal growth (vide infra). Table II gives a summary of the orientations. Variations in the temperature and in the current density within the ranges of the experimental conditions of plating had no noticeable effects on the plane of orientation.

(VII) According to Table II, except for deposits from baths having relatively high ratios of H_2SO_4/Zn, (11.l)-orientation (Fig. 4a and 4b) is invariably obtained. The occurrence of this orientation may be explained as follows. Since the surface of the growing layer is not atomically flat parallel to the cathode surface (as evidenced by the electron

micrographs, as well as by the spotty nature of the diffraction patterns), the zinc ions are carried to the surface from any direction in the bath. Under such a condition, among the many crystallites which were oriented randomly in the initial stage of the deposition, only those having by chance an orientation favorable to growth do grow and become predominant over those having unfavorable orientations. This favorable orientation is most likely determined by the relation of the growth velocities (or the surface energies) of various crystallographic planes. Thus, it is supposed that every crystallite near the surface of the relatively thick zinc layer has a tendency to be bounded by three crystallographic planes, i.e., the plane of the lowest outward velocity (basal plane) and a pair of planes of the second lowest outward velocity. If for the latter planes two prismatic planes of the first order, (10.0), [or two pyramidal planes of the first order, (10.1)] are assumed, the occurrence of the (11.l)-orientation is readily understood (Fig. 6). Although the value of l (not necessarily an integer) should be determined by the competition in the growth of the basal plane and the above prismatic (or pyramidal) plane, the quantitative data on their outward velocities of growth are not available. In this connection, the reversed order of the outward velocities of growth due to Stranski, *et al.* (16-19), together with the order of the reticular densities, are listed in Table III for various crystallographic planes of close-packed hexagonal metal. The morphology observed in the electron micrographs of Fig. 4b seems to support the point of view of this paragraph. Finch, *et al.* (7) postponed the explanation for their observation of (11.2)-orientation of electrodeposited cadmium. This may also be accounted for along the above line (15).

(VIII) As seen from Table II, when the ratio H_2SO_4/Zn of the bath is relatively high, the (11.l)-orientation is replaced by the (10.l)-orientation (Fig. 5a and 5b). This change may be related to the increased hydrogen evolution which occurs with these baths. Straumanis made observations on

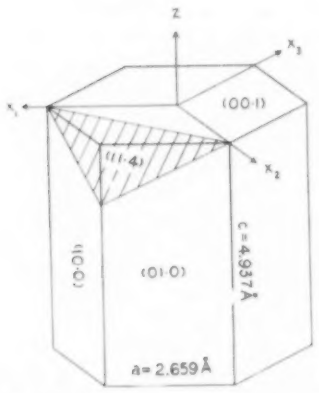

Fig. 6. Explanation of the occurrence of the (11.l)-orientation. Only (00.1) and (10.0) are depicted as the permanent faces determining the plane of orientation. l is assumed to be 4.

Table II. Plane of orientation characteristic of the bath composition

Bath composition, g/l	Plane of orientation
Zn 50 Zn 50, H_2SO_4 50 Zn 100, H_2SO_4 100 Zn 100, H_2SO_4 200	(11.l), $l \approx 4$, with angular tolerance of about ±15°
Zn 10, H_2SO_4 50 Zn 10, H_2SO_4 100	(10.l), $l \approx 1$, with angular tolerance of about ±15°

Mean thickness (θ), 10-100 × 10^3Å; temperature, room temperature—80°C; current density (D_k), 1-15 amp/dm².

the crystal growth of zinc, which was formed by evaporation in hydrogen atmospheres (21). According to him, under hydrogen pressures lower than ~4 mm Hg the permanent crystallographic faces of zinc are: (00.1) (basal planes), (10.0) (prismatic planes of the first order), (10.1) (pyramidal planes of the first order), and (11.0) (prismatic planes of the second order). When his results are compared with the theory of Stranski, *et al.* (16-19), it seems that differences in growth velocities of the planes of lower indices of zinc (except for the basal plane) are slight, and that even a reversal of the velocities can be effected by the presence of hydrogen. Such a reversal of growth velocities of planes resulting from adsorption of impurity is discussed by Smekal (19). In (VII) the occurrence of the (11.l)-orientation was explained by assuming that the permanent faces of zinc are the basal plane and a pair of prismatic (or pyramidal) planes of the first order. Now, taking into account the consideration regarding the reversal of the growth velocities of the planes, if a pair of prismatic planes of the second order is substituted for the pair of the first order, the (10.l)-orientation is reasonably reached in the same manner as in (VII).

Results and Discussion

Experiments Using Baths Containing Organic Colloids

The effects on the zinc plating by minor quantities of addition agents, which eventually lead to structural modifications of the deposited layer, are caused by complex factors such as a change in viscosity of the bath, cathode polarization, hydrogen overvoltage, current efficiency, etc. However, the

Table III. Relative velocities of growth and relative reticular densities of planes of close-packed hexagonal metal

(*hk.l*)	Reversed order of the outward velocities of growth	Order of reticular densities
(00.1)	1	1
(10.0)	2	3*
(10.1)	4	5
(10.2)	3	
(10.3)	6	
(11.0)	5	2
(11.2)		4*

* For zinc the third and the fourth are reversed, owing to its deviation of c/a ratio (1.857) (20) from the ideal value (1.633).

most essential function of an addition agent on the deposited layer seems to lie in its adsorption on the surface of the layer. A simple measure of adsorbability of an organic colloid is the well-known "gold number," which refers to the protective action of the colloid on red gold sol. Note that a lower value of gold number means a higher adsorbability (or protective action) of the colloid. The gold numbers of the organic colloids used in the present experiments are listed in Table IV (22). Their values were estimated roughly by using the red gold sol prepared by utilizing the reducing flame of coal gas (23). The obtained values fell in the ranges shown in Table IV.

As mentioned earlier, the (11.*l*)-orientation is characteristic of the zinc layer electrodeposited from the baths of $ZnSO_4 + H_2SO_4 + H_2O$ system, except for the baths of relatively higher values of the ratio H_2SO_4/Zn. Consequently, in most of the following experiments to clarify the effects of organic colloids on the structure of deposited zinc, the concentrations of zinc and sulfuric acid were chosen both as 100 g/l, since, with no addition agents, this is a bath which leads invariably to the (11.*l*)-orientation (Table II). The temperature of the bath, the current density for the deposition, and the mean thickness of the deposited layer were room temperature, ~4 amp/dm^2, and $20 - 60 \times 10^3$ Å, respectively. The results of the electron diffraction investigations are summarized in Fig. 7, and some of the electron micrographs are reproduced in Fig. 8b and 9-12.

(I) It is generally accepted that the flatness of the surface of the electrodeposited layer becomes improved by adding an organic colloid to the bath, as the result of its ability to increase cathode polarization and, therefore, throwing power of the bath. Although such a tendency is actually observed with the naked eye with baths of relatively low concentrations of an organic colloid which is a protein or carbohydrate (roughly up to 50 mg/l), the surface is liable to become inhomogeneous with higher concentrations of the colloid. This seems due to the adherence of hydrogen bubbles to the surface, resulting from the increased viscosity of the bath. Gum arabic shows a somewhat different behavior; it makes the surface inhomogeneous at a concentration as low as 10 mg/l and yields a fine-grained surface of blackish appearance at 500 mg/l (Fig. 8b). Unfortunately, it is impossible to obtain

Table IV. Gold numbers of biocolloids used (22)

Colloid		Gold number, mg sol/100 cm^3
Protein	Glue	0.05-0.1
	Gelatin	0.05-0.1
	Albumin	0.3-2
Gum	Gum arabic	1.5-2.5
Carbohydrate	Dextrin	20-70
	Starch	50-250
	Saponin	230

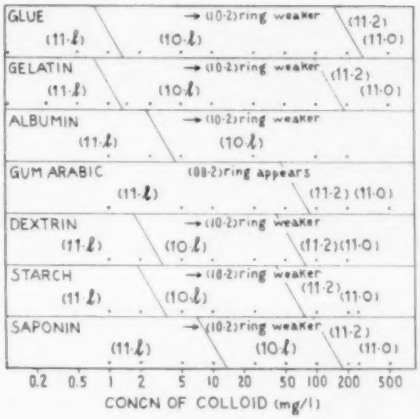

Fig. 7. Effects of organic colloids on plane of orientation. Each fiber orientation involves angular tolerance of about ±15°. Bath : Zn 100 g/l + H_2SO_4 100 g/l + organic colloid; room temperature; D_k : ~ 4 amp/dm^2; θ : 20-60 x 10^3 Å. The zinc layers deposited from the baths containing the addition agent concentrations marked by the dots were investigated by electron diffraction and microscopy.

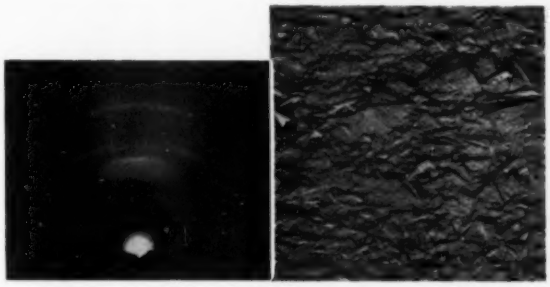

Fig. 8a (left). Electron diffraction pattern; Fig. 8b (right). Electron micrograph, magnification 5,000X. Zn 100 g/l + H_2SO_4 100 g/l + gum arabic 500 mg/l; room temperature; D_k = 4 amp/dm^2; C_{eff} = 45%; θ = 24 x 10^3 Å. Plane of orientation : (11.0).

precise values of current efficiency, since the weight increase of the cathode on deposition is usually only several milligrams. It is roughly 92% in the case of no colloids and decreases with the concentration of a colloid down to 65-80% with 200 mg/l addition.

(II) As before, the (00.2)-ring is generally barely perceptible, showing the flatness of the crystallites parallel to the basal plane (layer structure). With the addition of a protein or carbohydrate, besides the low intensity of the (00.2)-ring, the (10.2)-ring shows a tendency to decrease in intensity with increasing concentration. Since among the planes of lower indices, which yield strong reflections, the (10.2)-plane makes a relatively low angle with the basal plane, this is accounted for by the further predominance of the layer structure and agrees with the discussion by Smekal (19) on crystal growth under the presence of impurity. This change of the degree of layer structure with the concentration of addition agent is also morphologically observed in a series of electron micrographs in the case of dextrin (Fig. 4b and 9-12). With gum arabic such a change of the layer structure is not observed. Moreover, it is

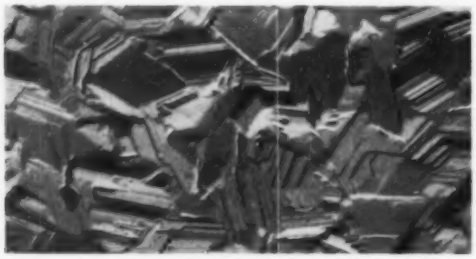

Fig. 9

Fig. 10

Fig. 11

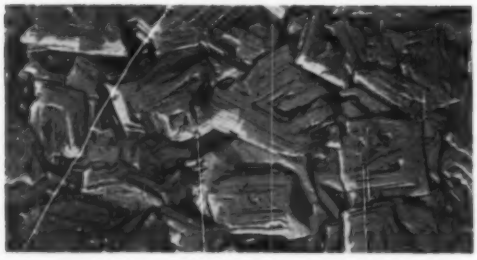

Fig. 12

Fig. 9-12. Electron micrographs, each magnification 5,000X. Zn 100 g/l + H_2SO_4 100 g/l + dextrin (2 mg/l, 10 mg/l, 25 mg/l, and 200 mg/l, respectively); room temperature; $D_k = \sim 4$ amp/dm^2; $C_{rr} = 88, 86, 82$, and 70%, respectively; $\theta = \sim 40 \times 10^5$ A. Plane of orientation : (11.l), (10.l), (10.l), and (11.0), respectively.

remarkable that the (00.2)-ring appears with 10-50 mg/l of gum arabic (Fig. 7). This seems to have some relation to the inhomogeneity of the zinc layer, which has been touched on just above.

(III) Figure 7 shows changes of plane of orientation with concentration of the seven addition agents. Apart from the case of gum arabic, the following sequence of changes is general:

$$(11.l), l = 4 \rightarrow (10.l), l = 1 \rightarrow (11.2) \rightarrow (11.0)$$

each fiber orientation involving a considerable angular tolerance of about $\pm 15°$. To the first, (11.l) $\rightarrow$ (10.l), the discussion made in (VIII) above applies, if it is assumed that the role of hydrogen is now played by organic colloid. This line of consideration is also preferable for elucidation of the predominance of the layer structure with increasing addition agent, which was touched on in (II). The final (11.0)-orientation (Fig. 8a) is an orientation, where the most densely packed atom rows in the most densely packed lattice plane (basal plane) stand upright to the cathode surface. When the concentration of addition agent is sufficiently high, resulting in high viscosity of the bath and low current efficiency for the deposition, the supply of zinc ions to the hollows of the surface and the mobility of zinc ions at the surface are both supposed to be insufficient. It should be understood that the (11.0)-orientation derives from such a situation. The (11.2)-orientation is most likely a transient stage before reaching the final (11.0)-orientation. With gum arabic it is remarkable that the plane of orientation changes from (11.l) directly to (11.2) $\rightarrow$ (11.0).

(IV) In Fig. 12 a square structure is noticeable. This structure is also observed with high concentrations of others carbohydrates, starch, and saponin. In these cases the plane of orientation is (11.0), and flat plates thin in the direction of c-axis, which lies parallel to the cathode surface, are supposed to be piled up to form a block. If such a block is oriented to an adjacent block of the same nature so as to form twinning on (10.2)-plane, the square structure should appear. It is well known that the twinning plane of close-packed hexagonal metals, such as zinc, is (10.2) (24). For zinc, (10.2) makes 47° 0′ with (00.1), the doubled value of which is near 90°. With proteins this square structure is less noticeable and with gum arabic is never encountered.

(V) In comparing Fig. 7 with Table IV, a reasonable correlation between the gold number of a colloid and its ability to change the orientation of deposited zinc is found in three proteins and in three carbohydrates. However, in spite of the much higher values of the gold number of carbohydrates as compared with those of proteins, they are not so ineffective in changing the orientation. This might be accounted for by the difference of their states of hydration and electric charge in the bath. Elucidation in detail must be postponed. An exceptionally weak ability of gum arabic to change the orientation is remarkable, together with its peculiarity in many aspects mentioned in the foregoing paragraphs.

Conclusion

It has been shown that many experimental results concerning the orientation and texture of electrodeposited zinc layer can be reasonably interpreted from the standpoint of development of crystallographic planes under various degrees of influence of hydrogen and/or organic colloids. However, the interpretation is considerably simplified. The fiber orientations observed in the present study invariably involve some tolerance. This implies that the crystallographic planes other

than those which determine the orientation are not necessarily excluded, presumably owing to slight differences among the surface energies of many crystallographic planes. This situation is reflected in the fine structure of the diffraction spots, which is to reveal the external crystallographic planes. Close examination of the fine structure of the spots shows that it is too complex to permit a simple interpretation, although generally the nature of the fine structure does not contradict the line of consideration described so far.

Acknowledgments

The author wishes to acknowledge with grateful thanks the support and permission to publish this article of Mr. S. Yamagata and Mr. M. Kamada, Director and Assistant Director of our Laboratory, respectively, and Mr. H. Kurama, Manager of our Research Section. The author thanks sincerely Dr. H. Hagihara, Kobayasi Institute of Physical Research, for his interest and discussions. His heartful thanks are due to Messrs. B. Ishii and Y. Kikuchi for their assistance.

Manuscript received June 23, 1958.

Any discussion of this paper will appear in a Discussion Section to be published in the December 1959 JOURNAL.

REFERENCES

1. G. P. Thompson, *Proc. Roy. Soc.*, **133**, 1 (1931).
2. G. I. Finch and C. H. Sun, *Trans. Faraday Soc.*, **32**, 852 (1936).
3. W. Cochrane, *Proc. Phys. Soc.*, **48**, 723 (1936).
4. A. G. Quarrell, *ibid.*, **49**, 3 (1937).
5. G. I. Finch and A. I. Williams, *Trans. Faraday Soc.*, **33**, 564 (1937).
6. G. I. Finch, A. G. Quarrell, and H. Wilman, *Discussions Faraday Soc.*, "The Structure of Metallic Coatings, Films and Surfaces," 1058 **1935**.
7. G. I. Finch, H. Wilman, and L. Yang, *ibid.*, "Electrode Processes," 144 **1947**.
8. G. I. Finch, *Z. Elektrochem.*, **54**, 457 (1950).
9. L. Yang, *This Journal*, **101**, 456 (1954).
10. S. Yoshioka and H. Yamamoto, *J. Metal Finishing Soc. Japan*, **6**, 110 (1955) (in Japanese).
11. H. Fischer, *Z. Elektrochem.*, **49**, 342 (1943); **49**, 376 (1943).
12. H. Fischer, "Elektrolytische Abscheidung und Elektrokristallisation von Metallen," Springer-Verlag, Berlin (1954).
13. A. S. T. M., "X-Ray Powder Data File," 3-0797.
14. J. M. Bijvoet, N. H. Kolkmeijer, and C. H. MacGillavry, "Röntgenanalyse von Krystallen," p. 94, Julius Springer, Berlin (1940).
15. E. Bauer, *Z. Krist.*, **107**, 265 (1956); **107**, 290 (1956).
16. I. N. Stranski and R. Kaishew, *ibid.*, **78**, 373 (1931).
17. I. N. Stranski and L. Krastanow, *ibid.*, **83**, 155 (1932).
18. I. N. Stranski, *Discussions Faraday Soc.*, "Crystal Growth," 13 **1949**.
19. A. Smekal, "Strukturempfindliche Eigenschaften der Kristalle" in "Handbuch der Physik," Vol. 24/2 (Aufbau der zusammenhängenden Materie), Julius Springer, Berlin (1933).
20. R. W. G. Wyckoff, "Crystal Structures," Vol. 1, Interscience Publishers, Inc., New York (1948).
21. M. Straumanis, *Z. phys. Chem.*, **B13**, 316 (1931); **B19**, 63 (1932).
22. A. Kuhn, "Kolloidchemisches Taschenbuch," Leipzig (1944).
23. Z. Samesima, *J. Chem. Soc. Japan*, **54**, 695 (1933) (in Japanese).
24. C. S. Barrett, "Structure of Metals," McGraw-Hill Book Co., Inc., New York (1952).

Changes in Trapping Levels of Zinc Sulfide Phosphors Resulting from Positive Ion Bombardment

William T. Allen[1] and C. H. Bachman

Department of Physics, Syracuse University, Syracuse, New York

ABSTRACT

Utilizing a decay method which consisted of measuring the amount of visible light emitted by the ZnS:Ag phosphor 5.0 msec after excitation by weak ultraviolet, studies were made of the changes in trap distribution on the surface of phosphor crystals which previously had been bombarded by Ar^+, H_2^+, and O_2^+ ions. Interpretation of results was limited to first order kinetics.

The results showed that bombardment by ions caused an increase in the number of traps at the lowest trapping level, 0.28 ev deep, as well as the creation of new traps at depths slightly greater and slightly less than 0.28 ev. This effect was independent of the ion used for bombardment.

In addition, ion bombardment caused new traps to appear at deeper trapping levels: 0.37 ev for Ar^+ ion bombardment, 0.38 ev for H_2^+ ion bombardment, and 0.39 ev for O_2^+ ion bombardment. For the latter, the peak in the difference curve is quite sharp and clearly located at 345°K, locating its depth at 0.39 ev. This corresponds to the next trapping level with increasing depth reported in the literature and thus may indicate that this trapping level is caused by the presence of oxygen in ZnS phosphors.

Ion bombardment, as a cause of deterioration in zinc sulfide phosphors, has been studied by many authors (1-8). In recent years, all research has been done with the working hypothesis that the reduced luminescence is caused by the creation of electronic levels between the valence band and the conduction band, such states making possible direct transition from the conduction band to the valence band.

It was considered desirable to investigate the dis-

[1] Present address: Franklin and Marshall College, Lancaster, Pa.

tribution of states between the valence band and the conduction band and the distribution of the states as a result of ion bombardment on the surface of the crystals.

The Lambe-Klick model (9) for luminescence in zinc sulfide was assumed valid. The depth of a state was designated as the energy difference between the state and the top of the valence band. States with depths less than 1 electron volt (ev) can influence the decay of a phosphor and customarily are called traps.

The usual method for investigating trap distributions is by the use of glow curves, a technique developed by Randall and Wilkins (10). In measuring a glow curve, the phosphor is first cooled to a very low temperature, so that electrons in the traps are stabilized, that is to say, their half-life is much longer than the time required to perform the experiment. Then the phosphor is excited at this low temperature by irradiation with ultraviolet (u.v.) light in order to fill the traps. If, now, the phosphor is warmed at a slow rate, traps filled with holes will be emptied. These holes, thermally excited to the valence band, will be attracted to the luminescent centers. The electron and hole are now in a position to recombine, giving up one photon of visible light, and the phosphor will glow as a result of a great number of these recombinations.

The temperature at which a particular trapping level becomes unstable depends on its depth, the deeper traps becoming unstable as the temperature gets higher. A curve of light output vs. temperature is called a glow curve and can be assumed to represent a trap depth distribution. For example, if a phosphor contains traps at two different depths, then the glow curve will have two different peaks, each representing one of the trapping levels.

Using glow curve techniques, Bube (11) has found that traps are present in ZnS at five distinct trapping levels. These are revealed by five distinct glow peaks at −120°C, −60°C, −25°C, −15°C, and 90°C. Any change in the methods of preparation or in the activator used will not alter the temperature at which these peaks exist but will change the relative heights of the peaks, and hence, the relative numbers of traps represented by each peak.

In the past few years, studies have been made to improve the interpretation of glow curves by considering the second order kinetics or retrapping. Such analyses not only involve consideration of holes thermally excited to the valence band finding their way to luminescent centers, but also holes thermally excited to the valence band and then retrapped and excited again to the valence band one or more times before finding their way to luminescent centers. Satisfactory interpretation of glow curves where more than one level of trap is present and where second order kinetics are considered is very difficult to achieve. It is customary in the literature to present glow curves showing light ouput as a function of temperature at a particular heating rate and leave it for the reader to interpret.

Very roughly, it can be said that if T is the temperature of a glow peak (10), then $E = 20\ kT$, where E is the trap depth and k is Boltzmann's constant. This could mean that a peak occurring at room temperature will represent a trap depth of approximately 0.5 ev.

A decay measurement consists of exciting the phosphor with u.v., cutting off this excitation, and measuring the phosphorescent light output of the phosphor as a function of time, the temperature remaining constant.

In the present investigation a problem arose in that impinging ions with energies of the order of 10 kev do not penetrate the crystal sufficiently so that changes can be observed by the use of glow curves. This is because in the excitation which precedes the warming in a glow curve measurement, the phosphor is maintained for at least several minutes under u.v. radiation, and traps are filled as deeply into the crystal as the u.v. can penetrate. Glow curve measurements are then essentially the determination of trap distributions throughout the volume of the crystal. Any change, therefore, in the distribution of traps in the surface will be largely masked by the response of the remainder of the crystal which has not been damaged.

Young (4) has shown that the deterioration of the phosphor lies in a very thin surface layer, its thickness being of the order of 0.1μ for bombardment by ions of energies in the order of 10 kev. Since the phosphor crystals ordinarily used in television screens have diameters of about 10μ, the volume of the layer is the order of 1% of the volume of the crystals, and for this reason ion bombardment by ions, the energies of which are in the order of 10 kev, does not affect glow curves of the phosphors appreciably.

However, it was observed that a phosphor damaged by ion bombardment exhibits increased phosphorescence when irradiated by low intensity u.v. for times in the order of hundredths of a second. This is because the excitation is only sufficient to fill traps on the surface of the phosphor crystal, and such surface traps are filled preferentially. This observation led to a technique in which observations of the decay characteristics yield information concerning the trap distribution.

Theory for Decay Measurements

Let P be the probability that a hole in a single trapping level of depth E will escape, then,

$$P = \frac{1}{t_d} = G\left[\exp\left(-\frac{E}{kT}\right)\right] \qquad [1]$$

where t_d is the decay time, i.e., the time for the number of holes in a trapping level to reduce to $1/e$ of its value at cutoff, E is the trap depth, k is Boltzmann's constant, T is the temperature in degrees Kelvin, and G is a constant of the order of 10^{s} given by Randall and Wilkins (10) and represents the vibration frequency of an atom in the lattice (10^{12} vib./sec) multiplied by the probability that a hole in a trapping state having received enough energy from the lattice to undergo a transition to the valence band will do so.

Figure 1 shows a plot of p_t/p_{t_0} vs. time, where p_t is the density of holes in traps at any time, and p_{t_0} is the density of holes in this trapping level at cutoff. The observed visible light, I, is proportional to the

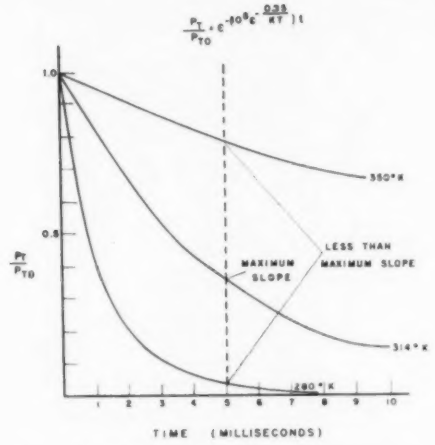

Fig. 1. P_T/P_{T_0} vs. time for various temperatures

rate of change of p_T with respect to time, or is proportional to the slope of the p_T/p_{T_0} vs. time curve. If measurements are made at a particular time, say 5 msec after cutoff, it can be seen that the maximum slope occurs at neither a high nor a low temperature, but somewhere between. Location of the temperature at which a peak occurs can be done in the following way:

If we consider a single trapping level of depth E, then from Eq. [1]

$$p_T = p_{T_0} \exp\left\{-G\left[\exp\left(-\frac{E}{kT}\right)\right]t\right\} \qquad [2]$$

The light output I due to this single trapping level as a function of time after cutoff is equal to

$$I = V\frac{\partial p_T}{\partial t} = S\,p_{T_0}\exp\left\{-\left[\frac{E}{kT} + Gt\exp\left(-\frac{E}{kT}\right)\right]\right\} \qquad [3]$$

where V and S are proportionality constants.

I will be a maximum value when

$$\frac{\partial I}{\partial T} = 0 = Up_{T_0}\exp\left\{-\left[\frac{E}{kT} + Gt\exp\left(-\frac{E}{kT}\right)\right]\right\}$$
$$\left\{\frac{E}{kT^2} - Gt\left[\exp\left(-\frac{E}{kT}\right)\right]\frac{E}{kT^2}\right\} \qquad [4]$$

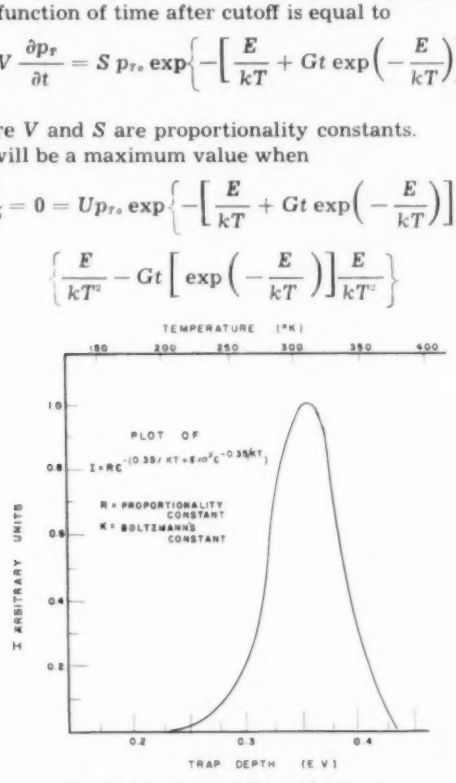

Fig. 2. I vs. temperature at 5.0 msec

where U is a proportionality constant.

$$\exp\left(-\frac{E}{kT}\right) = \frac{1}{Gt}$$

Hence a peak occurs at

$$E = (\log Gt)\,kT = 2.3\,(\log_{10} Gt)\,kT \qquad [5]$$

Thus if measurements are made 5 msec after cutoff, I will be a maximum, or a peak should occur at

$$E = 13.1\,kT \qquad [6]$$

Figure 2 is a plot of I vs. T as a result of holes trapped at a single trapping level of depth arbitrarily chosen to be 0.35 ev. It should be noted that the curve peaks rather sharply at its maximum point and also that it is not completely symmetrical in that it approaches zero much faster at high temperatures than at low temperatures.

It is interesting to compare Eq. [5] with the results obtained by Randall and Wilkins (10). If, in performing a glow curve experiment, the rising in temperature is suddenly stopped at a glow curve peak, then the visible light, according to Randall and Wilkins, will be emitted, but will decay to $1/e$ of its value in a certain amount of time in the order of 10 sec. Substituting $t = 10$ sec in Eq. [5], we have

$$E = (2.3\,\log_{10} 10^8)\,(10\,kT)$$
$$E = (2.3)\,(9\,kT) = 20.7\,kT \qquad [7]$$

or almost exactly the formula given by Randall and Wilkins.

If, during excitation, u.v. light irradiates the phosphor for an amount of time sufficient to allow the emitted light to reach a constant value, an equilibrium exists between the holes in the traps and the holes in the valence band, that is to say, the number of holes entering the traps must equal the number of holes which are thermally ejected from the traps. This can be expressed by the following equation, which should be valid if we consider only one trapping level at cutoff.

$$pb\,(\tau - p_{T_0}) = p_{T_0}\,G\left[\exp\left(-\frac{E}{kT}\right)\right] \qquad [8]$$

where p is the density of holes in the valence band, τ is the density of traps, p_{T_0} is the density of holes in the traps at cutoff, $(\tau - p_{T_0})$ is the density of empty traps, and b is a constant representing the product of the capture cross section of a trap and the velocity of a hole in the valence band.

Solving for p_{T_0}

$$p_{T_0} = \frac{\tau}{1 - \dfrac{G}{pb}\left[\exp\left(-\dfrac{E}{kT}\right)\right]} \qquad [9]$$

showing that at cutoff p_{T_0} is proportional to the number of traps. Since according to Eq. [3], I is proportional to p_{T_0} then it also, by Eq. [9] is proportional to τ, the density of traps.

It is obvious that by plotting I vs. temperature, where measurements are made 5 msec after cutoff, a curve possessing peaks should be obtained from Eq. [6]. The height of a peak should give a qualitative indication of the density of traps at a particular trapping level, according to Eq. [9]. Since the

heights of the peaks can at best only be compared qualitatively and since the efficiency of the phosphor decreases markedly at higher temperatures, it was decided to measure I/I_o instead of I, where I_o is the visible light output of the phosphor at cutoff. The I/I_o vs. temperature curves therefore should be similar to glow curves except that there should be a shift in the position of the peaks. The amount of such shift can be obtained by dividing Eq. [6] by Eq. [8]

$$\frac{T_{I/I_o}}{T_\alpha} = 1.58 \qquad [10]$$

Thus peaks determined by the decay method should be at temperatures about 60% higher than those from glow curves.

Since ion damage occurs very near the surface of phosphor crystals, it is of importance that a method be utilized which measures only surface effects. In the method of glow curves, every effort must be made to saturate all of the traps as deeply into the crystals as possible in order that the glow will consist of a measurable amount of light. If, however, I/I_o measurements are made, weak u.v. can be used, and allowed to fall onto the phosphor for a small amount of time, so that only surface traps are preferentially filled during irradiation and can be detected during decay.

The above derivation assumed only first order kinetics, i.e., retrapping is not considered. The reason for this is that there is no way of determining the ratio of the number of filled traps to the total number of traps for any trap depth at cutoff (p_α/τ), since the phosphor is flashed with ultraviolet for a brief period of time and the traps are not saturated. Also (p_α/τ) is not constant at all distances from the surface of the crystal, and an average value of (p_α/τ) would require information not available at the present writing.

Procedure

Description of Phosphor Used

The ZnS phosphor was provided by the General Electric Company and was the blue component of phosphor used for the luminescent screens in earlier television tubes. This phosphor contained 0.015% chlorine by weight, 0.015% sodium by weight, and 0.04% ZnO by weight. The average particle size was 9μ. The phosphor contained 0.05% silver by weight as activator, which was introduced into the crystal with a sodium chloride flux (amounts of retained sodium and chlorine listed above) by heating to about 1000°C for about a half hour. The phosphor was examined by standard x-ray diffraction methods and found to be completely hexagonal.

The phosphor was water settled to a thickness of 0.01 g/cm^2 on aluminum slides 20 mils thick, measuring 15 x 30 mm. Previous to settling, the slides and the beakers used were carefully boiled in detergent and rinsed several times in doubly distilled water. The water used for settling was also doubly distilled.

Description of Equipment Used for Ion Bombardment

The ion bombardment equipment is shown in Fig. 3. The main part of the bell jar can be maintained at a relatively high vacuum (10^{-4} mm or better), and the small discharge chamber can be maintained at about 20μ.

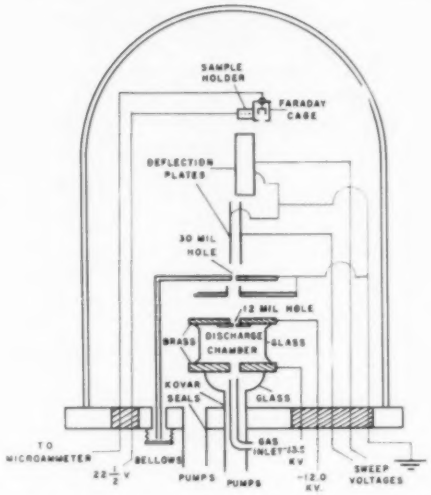

Fig. 3. Apparatus for bombarding phosphors with ions

The center support of the system is a length of heavy cane glass, and all electrical connections are fastened to the cane by means of ring stand clamps.

The output of a 30-kv power supply is applied across a string of 30, 1-megohm resistors. The positive end of the string is grounded and the negative end of the string is connected to the bottom plate of the discharge chamber. A center tap is connected through a 10 megohm resistor to the top plate of the discharge chamber.

With the pressure at 20μ and a voltage applied to the top and bottom plates of the discharge chamber, a discharge results causing positive ions to be produced. The electric field between the plates causes the ions to be accelerated upwards. A ½-in. hole, drilled in the top plate of the chamber is covered by a piece of 5-mil thick tantalum in which a 12-mil hole is drilled. Ions, produced in the chamber, pass through the hole and are accelerated by the electric field in the space between the top plate of the chamber and the next plate, which is at ground potential. Immediately above this plate is a thin sheet of aluminum, 10-mils thick, in the middle of which is drilled an aperture 1½ mm in diameter for the purpose of controlling the diameter of the beam. As an aid to lining up the apparatus, the position of this aperture can be controlled from outside of the bell jar by means of a metal bellows.

The ions proceed upward through two sets of parallel plates, arranged so that one set of plates is perpendicular to the other, but with one pair displaced laterally to allow removal of neutral particles. The electric field between these plates controls the lateral position of the beam at all times, as voltages of from 0 to 10,000 v can be applied to one plate of each set, the other remaining at ground potential. Sweep voltages of 3 and 1/10 cps are used. The sample is mounted with the phosphor facing downward or toward the beam. The sample holder and sample are operated at −22.5 v when the beam, aimed into the hole of the Faraday cage, is being measured in

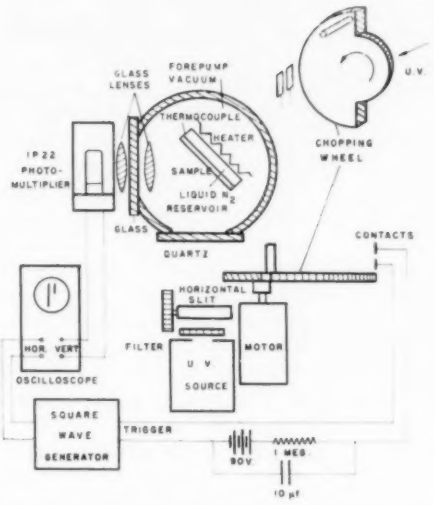

Fig. 4. Apparatus for measuring I/I_0 vs. temperature

order to retard the emission of secondary electrons from the inside of the Faraday cage, but are operated at ground potential when the beam is bombarding the sample.

Apparatus for measuring amount of fluorescent light emitted by the phosphor after a given amount of time.—This apparatus is shown in Fig. 4. The u.v. radiation is produced by the standard Beckman u.v. accessory kit which is intended for use with the Beckman DU spectrophotometer. This source is a hydrogen arc which is rich in u.v. at all wave lengths from 2000 to 4000Å.

First the light is passed through a Corning 9863 filter which passes most of the u.v. emitted by the hydrogen arc, but cuts out the visible light. The light then is passed through a narrow slit, which can be varied in width. Next, the beam is chopped by a wheel rotating at about 25 rps, so that u.v. light passes for 20 msec and is cut off for an equal amount of time. The time required for the intensity of the u.v. to reduce to a negligible value is measured by using a photomultiplier tube and an oscilloscope. This time is less than 50 μsec, which is 1% of the time during which the measurements were made. The chopped beam passes through a quartz window into a chamber maintained at forepump vacuum and onto the phosphor sample which is placed at a 45° angle to the beam.

The sample is so arranged that its temperature can be varied from −150° to +200°C and is in a vacuum in order to avoid the formation of frost on the sample when at low temperatures. All temperatures are measured using a copper-constantan thermocouple and a L&N thermocouple potentiometer. Melting ice is used as a temperature reference junction. The emitted visible light from the phosphor is collected by a lens within the vacuum chamber, transmitted through the glass window, and converged by a second lens onto an RCA 1P22 photomultiplier tube. The electrical signal from the photomultiplier tube is applied with amplification to the vertical plates of an oscilloscope.

The chopping wheel carried a small metal protrusion so arranged that at the time of u.v. light cutoff an electrical contact is made with two wires, thus triggering a Tektronix #162 wave form generator. The wave form generator gives a square pulse 5 msec in duration every time it is triggered. This pulse is then applied to the horizontal plates of the oscilloscope.

The pattern on the screen of the oscilloscope consists of two vertical lines. The vertical deflection is dependent on the light output of the phosphor. The first vertical line indicates the light output under u.v. irradiation. The second, displaced to the right, gives the light output during the 5 msec pulse. By setting the vertical amplifier of the oscilloscope so that top termination of the first vertical line is at 100 on the screen scale and so that the beam is a zero when no u.v. light shines on the phosphor, the termination of the second line immediately gives the percentage of light emitted from the phosphor 5 msec after cutoff.

It was necessary to insure that the u.v. light falling on the phosphor was constant and equal for all samples measured. Before and after each run, a phototube was placed in the vacuum chamber at the exact point where the phosphor was placed during a run, and it was found that, if a half-hour warmup was allowed, the light output never varied more than 1%.

Ion-burning of samples.—With the sample in place and the system evacuated, potentials are applied to create the ion beam. This is deflected into the Faraday cage for current measurement, after which the sweep voltages are applied to the deflection plates, so that the beam now traces a square raster on the phosphor sample. Bombardment is allowed to continue for a length of time dependent on the number of particles per square centimeter desired.

The beam is redirected into the Faraday cage for a check on intensity. The beam current is assumed to be constant throughout the bombardment if the measurements made before and after bombardment are equal.

The sample is then examined under u.v. light and the unaffected portion, which fluoresces brighter than the affected part, is scraped off. The bare aluminum is painted with aquadag to reduce reflected u.v. light. The area of the affected portion is measured so that with measurements of beam current and time of bombardment, the density of particles per square centimeter can be computed.

Measurements.—With the samples in place the chamber is evacuated and the sample is cooled to −150°C by pouring liquid nitrogen into the reservoir The chopping wheel is then rotated at about 25 rps, and the triggered pulse generator is activated.

The heater coils are activated then so that the temperature of the sample increases at no more than 4°C/min. This is sufficiently slow so that glow curve effects can be neglected. The temperature is measured at all times with the thermocouple potentiometer and measurements of I/I_0 are made every 0.25 mv. This amounts to taking a measurement every 10°C at low temperatures and every 4°C at high temperatures.

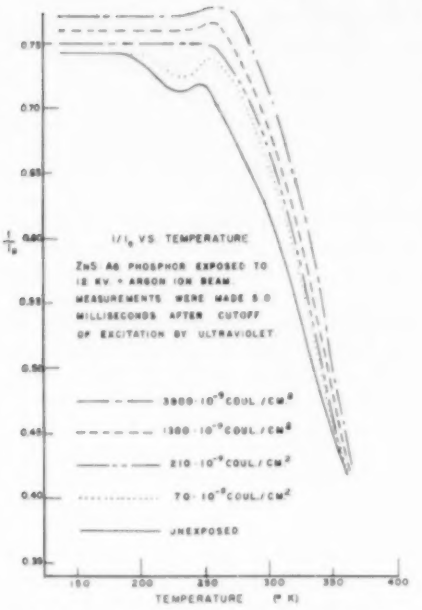
I/I0 VS. TEMPERATURE
ZnS Ag PHOSPHOR EXPOSED TO 12 KV + ARGON ION BEAM. MEASUREMENTS WERE MADE 5.0 MILLISECONDS AFTER CUTOFF OF EXCITATION BY ULTRAVIOLET
3800·10⁻⁹ COUL/CM²
1300·10⁻⁹ COUL/CM²
210·10⁻⁹ COUL/CM²
70·10⁻⁹ COUL/CM²
UNEXPOSED
TEMPERATURE (°K)

Fig. 5. I/I_0 vs. temperature for argon bombardment

Experimental Results

The curves shown in Fig. 5 represent I/I_0 measurements made on ZnS:Ag phosphor which had been previously bombarded by 12 kv ions of Ar^+.

There are significant differences in the I/I_0 vs. temperature curves for varying degrees of ion bombardment. Whereas the difference in I/I_0 is as much as 12% for some temperatures, it does not always appear to be significant, due to the large negative slope of these curves. For this reason the I/I_0 vs. temperature curve for the unbombarded phosphor was subtracted from the I/I_0 curve for the bombarded phosphor. In this way, it was possible to emphasize the difference in the decay as a result of bombardment. The difference curves are shown in Fig. 6 for argon bombardment; Fig. 7 and 8 show similar difference curves for samples which had been bombarded with H_2^+ and O_2^+ ions.

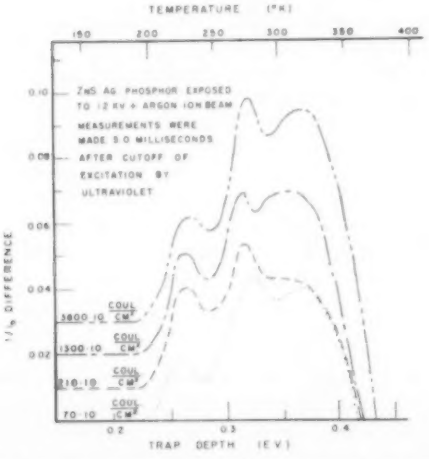
TEMPERATURE (°K)
ZnS Ag PHOSPHOR EXPOSED TO 12 KV + ARGON ION BEAM MEASUREMENTS WERE MADE 5.0 MILLISECONDS AFTER CUTOFF OF EXCITATION BY ULTRAVIOLET
I/I0 DIFFERENCE
3800·10⁻⁹ COUL/CM²
1300·10⁻⁹ COUL/CM²
210·10⁻⁹ COUL/CM²
70·10⁻⁹ COUL/CM²
TRAP DEPTH (E.V.)

Fig. 6. I/I_0 vs. temperature (difference curve) for argon

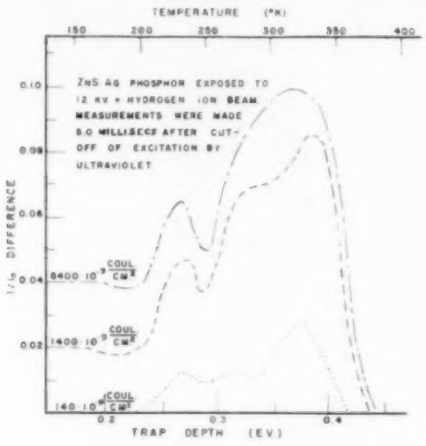
TEMPERATURE (°K)
ZnS Ag PHOSPHOR EXPOSED TO 12 KV + HYDROGEN ION BEAM MEASUREMENTS WERE MADE 5.0 MILLISECS AFTER CUTOFF OF EXCITATION BY ULTRAVIOLET
I/I0 DIFFERENCE
6400·10⁻⁹ COUL/CM²
1400·10⁻⁹ COUL/CM²
140·10⁻⁹ COUL/CM²
TRAP DEPTH (E.V.)

Fig. 7. I/I_0 vs. temperature (difference curve) for hydrogen

In the I/I_0 vs. temperature curve for the standard unbombarded phosphor, it is observed that a peak exists at 250°K. Since this is the lowest observable peak, it is assumed to be due to the trapping level represented by the glow curve peak at −120°C or 153°K. This means that experimentally the ratio

$$\frac{T_{I/I_0}}{T_a} = \frac{250^\circ}{153^\circ} = 1.63 \qquad [11]$$

which agrees very closely with Eq. [10], where the ratio is 1.58. This discrepancy of about 3% is perhaps explained by retrapping or second order kinetics. Since the saturation of traps in this decay method is not attempted, one would expect the percentage of unfilled traps to be higher than that encountered in glow curve measurements. Therefore, the probability of trapping would be somewhat larger since holes excited to the valence band would encounter a greater number of empty traps in which to be trapped. In general the retrapping effect shifts the peak to higher temperatures, as holes which are retrapped on the low temperature side of the peak predicted by first order theory do not recombine with electrons at centers to emit visible light. Also on the high temperature side of the peak predicted

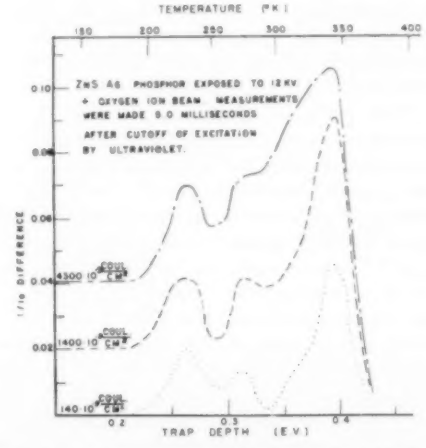
TEMPERATURE (°K)
ZnS Ag PHOSPHOR EXPOSED TO 12 KV + OXYGEN ION BEAM MEASUREMENTS WERE MADE 5.0 MILLISECONDS AFTER CUTOFF OF EXCITATION BY ULTRAVIOLET
I/I0 DIFFERENCE
4300·10⁻⁹ COUL/CM²
1400·10⁻⁹ COUL/CM²
140·10⁻⁹ COUL/CM²
TRAP DEPTH (E.V.)

Fig. 8. I/I_0 vs. temperature (difference curve) for oxygen

by first order theory, the probability of holes being thermally ejected from traps becomes very large since it is an exponential function of temperature, whereas the probability of recombination with empty traps is only proportional to the number of empty traps. Accordingly the value of I/I_o at temperatures below the peak predicted by first order theory should be reduced and at temperatures above the peak predicted by first order theory, I/I_o should remain about the same. In this way retrapping will tend to cause a peak to shift slightly to the higher temperature.

From the I/I_o difference vs. temperature curves, Fig. 6-8, one can conclude the following:

1. In general, the heights of the I/I_o difference vs. temperature curves are dependent on the degrees of bombardment. It appears that small ion exposures are very efficient in creating traps, whereas increased ion exposures yield diminishing changes in the I/I_o difference vs. temperature curves. There is an apparent saturation of traps at this depth.

2. All I/I_o difference vs. temperature curves show two peaks, located at 230° and 290°K, that are equally distant from the 250°K peak in the I/I_o vs. temperature curve. The closeness of these two peaks to the 250°K peak indicates that possibly the new traps at these two levels are related to the 250°K peak. If bombardment by ions had only increased the population in the trapping level represented by the 250°K peak, then the I/I_o difference vs. temperature curve would have shown a single peak at 250°K. However, if the bombardment had produced new trapping levels not only at the discrete trap depth represented by the 250°K peak but also at levels slightly greater and smaller in depth, then the difference curve would show two peaks on either side of 250°K. This was observed.

It is evident that traps at a depth of 0.28 ev which are represented in the I/I_o vs. temperature curve by a peak at 250°K are not only increased in number, since the height of the I/I_o vs. temperature curve was shown in Eq. [9] to be proportional to the number of traps at a particular level, but also, following bombardment, traps exist at depths slightly greater and slightly less than 0.28 ev.

This is not in agreement with work by Martin (8) who found that this trapping level in ZnS:Ag was decreased rather than increased by ion bombardment. He used 45 kev hydrogen ions and measured trap distribution by use of glow curves.

3. In all of the I/I_o difference vs. temperature curves, another large peak appeared at a somewhat higher temperature. As can be seen in Fig. 6-8, this was dependent on the ion used for bombardment, as the peak in the argon curves was at 315°K, in the hydrogen curves at 330°K, and in the oxygen curves at 345°K, corresponding to trap depths of 0.37, 0.38, and 0.39 ev, respectively.

It is interesting to note that the distinct oxygen peak a 345°K corresponded almost exactly to the predicted second peak at 344°K. Although this certainly is not conclusive evidence, it is clearly indicative that this trap depth of 0.39 ev might be caused by oxygen in the ZnS:Ag crystal replacing sulfur in the lattice either substitutionally or interstitially.

4. Values of I/I_o were increased at low temperatures as a result of ion bombardment. This might indicate trapping levels of depths below 0.28 ev, but such have not been reported previously in the literature. Such values of I/I_o, which at low temperatures are constant with respect to temperature, but which increase as a result of ion bombardment, may be explained in two different ways.

First, it is possible to assume that, since surfaces are being studied, other trapping levels can exist and these can have a depth distribution which is constant. This assumption appears unlikely as traps are associated with particular kinds of imperfections in the lattice and would be preferentially located at particular levels.

Second, it should be noted that the theoretical curve of I vs. T in Fig. 2 is not symmetrical, but has a tail which is significantly large at low temperatures. It is possible that the tails of many of these curves added together give what appears to be a higher value of I/I_o constant with respect to temperature.

If the destruction of luminescence is simply a matter of producing levels between the valence band and the conduction band so that radiationless or infrared emitting transitions can take place, then the number of paths for the recombination of electrons and holes will be increased, and the time t_e for the density of holes in the valence band to drop to $1/e$ of its initial value will be decreased. In all of the measurements made, t_e was always observed to increase as a result of ion bombardment. The data gathered at low temperatures indicate that: (a) these levels were not produced; (b) these levels may be produced, but their effect is overcompensated by the destruction of centers; and (c) these levels may be produced but their effect is overcompensated by the low temperature tail of the curve I vs. T, shown in Eq. [2].

Manuscript received June 11, 1958. This paper has been scheduled for presentation at the Philadelphia Meeting, May 3-7, 1959. The work on this paper was sponsored by the office of Ordnance Research, Department of the Army.

Any discussion of this paper will appear in a Discussion Section to be published in the December 1959 JOURNAL.

REFERENCES

1. B. Stech, *Z. Naturforsch.*, **7a**, 175 (1952).
2. W. Hanle and K. H. Rau, *Z. Phys.*, **133**, 297 (1952).
3. A. W. Smith and J. Turkevich, *Phys. Rev.*, **94**, 857 (1954).
4. J. R. Young, *J. Appl. Phys.*, **26**, 1302 (1955).
5. W. Berthold, *Naturwissenschaften*, **42**, 436 (1955).
6. H. P. Gilfrich, *Z. Phys.*, **145**, 241 (1956).
7. A. W. Smith, *Phys. Rev.*, **101**, 1263 (1956).
8. W. Martin, *Z. Phys.*, **147**, 582 (1957).
9. J. Lambe and C. C. Klick, *Phys. Rev.*, **98**, 909 (1955).
10. J. T. Randall and M. H. F. Wilkins, *Proc. Roy. Soc.*, **A184**, 366 (1945).
11. R. H. Bube, *Phys. Rec.*, **90**, 70 (1953).

Influence of Firing Conditions, Composition, and Screening Media on the Zeta Potentials of ZnS Phosphors as Related to Adherence to Glass Surfaces

Boris Levy[1]

Electron Tube Division, Radio Corporation of America, Lancaster, Pennsylvania

ABSTRACT

Zeta potentials were determined by the streaming potential method as a function of firing conditions, flux, activator, phosphor coating, and type and concentration of screening media. The effect of these factors on adherence was determined by the jet impingement method. Positive zeta potentials were obtained in $Ba(Ac)_2$ solutions and in H_2O during all stages of phosphor preparation prior to the coating operation. Either positive or negative potentials are obtained with the finished phosphor depending on the type of coating used. Firing conditions also have been found to be important in determining the sign of the zeta potential. A general trend toward enhanced wet adherence with decreasing negative zeta potential and increasing positive zeta potential has been noted.

The influence of electrolyte concentration on the zeta potentials of ZnS powders was measured with solutions of the following materials: $Ba(Ac)_2$, K_2SiO_3, $Ba(Ac)_2$-K_2SiO_3 mixtures, $(NH_4)_2Cr_2O_7$, polyvinyl alcohol, and mixtures of $(NH_4)_2Cr_2O_7$ and polyvinyl alcohol.

Adherence of a phosphor to a glass faceplate is one of the important factors involved in the manufacture of television tubes. The phosphor is commonly applied to the glass by either a settling (1) or slurry technique (2). Both methods involve the preparation of a phosphor suspension containing water, an electrolyte, and a bonding agent, but the nature of the electrolyte and bonding agent differs for the two methods. Different phosphors, or even the same phosphor handled in slightly different manners often have wide variations in screening properties. The concentrations of electrolyte and bonding agent also have marked effects on screen characteristics.

Hazel and co-workers have demonstrated a correlation between zeta or electrokinetic potential and adherence in settled screens (3-5). They found a decrease in the magnitude of the zeta potential with increasing concentration of either $Ba(Ac)_2$ or K_2SiO_3-$Ba(Ac)_2$ mixtures. Similar results were obtained with powdered glass. In the systems in which the potential of the phosphor and glass were negative, measurements of the adherence of the phosphor to glass surfaces indicated enhanced adherence with a decrease in the magnitude of the zeta potential. The explanation offered by Hazel was that the repulsive forces between the two similarly charged surfaces were reduced, thereby giving the silicate a chance to bind the phosphor to the glass in a more compact network.

The present study is an outgrowth of Hazel's work in that it attempts to discover the factors of importance in a phosphor preparation and handling that influence the electrical properties of its surface. To this end streaming potential experiments were performed at various stages of phosphor preparation and under a variety of conditions that might occur in screen application. Attempts were made to correlate the results with adherence measurements.

Experimental

Materials.—Measurements are made on either commercial RCA phosphor powders or on specially prepared samples as described in Table I. Demineralized water is used in the preparation of all solutions used in the measurements. Reagent-grade $Ba(Ac)_2$, KCl, and $(NH_4)_2Cr_2O_7$ are used. The potassium silicate solutions are prepared from Sylvania PS5 (0.96M K_2O-3.05M SiO_2), and the polyvinyl alcohol (PVA) solutions are prepared from du Pont Elvanol #52-22.

Apparatus.—The streaming-potential apparatus used in these experiments combines several of the features used by Gaudin and Fuerstenau (10) and by Hazel and his co-workers (3-5). Calomel electrodes, as used by Hazel, are employed for most of the potential measurements when a L&N Type K potentiometer and galvanometer are used in the measuring circuit. Perforated platinum electrodes, sealed to the ends of specially ground 24/40 standard taper joints, are used for the conductivity measurements. The joints are ground in such a way that a piece of filter paper can be placed over the ends of the electrodes without interfering with the fit of the joints. The filter paper helps to confine the powdered sample in the streaming potential cell between the platinum electrodes. When preparing the streaming potential cell one of the 24/40 joints is sealed with Apiezon W wax and a suspension of powder

[1] Present address: Radiation and Nucleonics Laboratory, Materials Engineering Departments, Westinghouse Electric Corporation, Engineering Center, East Pittsburgh, Pa.

Table I. Streaming potential measurements in 5.8×10^{-4}M $Ba(Ac)_2$ and relative wet adherence measurements
Experiments with firing conditions

Test No.	Description of sample	Zeta potential, mv	Relative wet adherence
1	RCA 33-Z-10; ZnS prepared by ppt. from $ZnSO_4$ solution with H_2S. Lot #1877	+13.1	1.3
2	RCA 33-Z-19 Lot #1869	+13.6	1.6
3	RCA 33-Z-19 Lot #1784	+14.3	1.5
4	RCA 33-Z-19 Lot #1869 fired in H_2S for 1 hr at 1000°C, flushed with N_2	−6.50	
5	Sample and firing as Test 4	−6.73	
6	RCA 33-Z-19 Lot #1869 fired in H_2S for 1 hr at 1000°C, flushed with N_2	+9.41	2.1
7	Same sample and firing as Test 6	+10.7	
8	RCA 33-Z-19 Lot #1869 fired in H_2S for 1 hr at 1000°C, flushed with N_2 (more extended N_2 flushing than with previous samples)	−3.64	1.3
9	Same sample and firing as Test 8	−2.62	1.6
10	RCA 33-Z-19 Lot #1869 fired in H_2S for 1 hr at 1000°C, flushed with N_2. Samples 10-12 were fired in the same furnace simultaneously, with Test 10 in the hottest region, Test 11 in the next hottest, and Test 12 in the coolest region	−8.49	0.96
11		−3.24	1.5
12		−2.89	1.6
13	RCA 33-Z-19 Lot #1869 fired in H_2S for 1 hr at 975°C, N_2 for ½ hr at 975°C, cooled in N_2	−3.53	
14	RCA 33-Z-19 Lot #1869 fired in H_2S for 1½ hr at 975°C, cooled in H_2S	+18.5	2.6
15	Fired same as Test 13	−4.62	1.8
16	Fired same as Test 13, but at 1100°C	+4.43	3.3
16a	Fired same as Test 13, but at 1100°C	+13.1	1.3
17	Repeat of Test 16 (new H_2S cylinder)	−6.17	1.8
18	Fired same as Test 14, but at 1100°C	+6.09	2.5
19	Starting material Test 14, heated in vacuum furnace for 2 hr at 160°C	+12.7	1.8
20	Starting material Test 15, rinsed with dilute NH_4OH, dried	+2.28	1.8
21	RCA 33-Z-19 Lot #1869 plus 2% NaCl, no Ag, fired at 975°C for 1¼ hr in air, covered, washed with H_2O	+16.9	1.8
22	RCA 33-Z-19 Lot #1869 plus 2% NaCl plus 0.015% Ag fired at 975°C for 1¼ hr in air, covered, washed with H_2O	+16.8	1.6
23	RCA 33-Z-19 Lot #1869 plus 4% NH_4Cl plus 0.015% Ag fired at 975°C for 1¼ hr in air, covered, washed with H_2O	+18.9	1.8
24	RCA 33-Z-19 Lot #1869 plus 2% $CaCl_2$ plus 0.015% Ag fired at 975°C for 1¼ hr in air, covered, not washed	+20.3	3.3
25	RCA 33-Z-19 Lot #1869 plus 4% NH_4 plus 0.015% Ag fired at 975°C for 1¼ hr in air, covered, washed with H_2O	+18.7	2.2
26	RCA 33-Z-19 Lot #1869 fired at 975°C for 1¼ hr in air, open tube	+24.9	1.9
27	RCA 33-Z-19 Lot #1869 fired at 975°C for 1¼ hr in N_2, cooled in N_2	+16.3	1.6

Table I. Streaming potential measurements in 5.8×10^{-4}M $Ba(Ac)_2$ and relative wet adherence measurements
Experiments with firing conditions (*Continued*)

Test No.	Description of sample	Zeta potential, mv	Relative wet adherence
28	RCA 33-Z-19 Lot #1869 fired at 975°C for 1¼ hr in air, flushed with N_2	+25.1	2.2
	Experiments at various stages of phosphor preparation		
29	RCA Phosphor 33-Z-265, uncoated, ZnS:0.015% Ag (100 g) coated with 3 cc of 5% silicate* + 0.1 g $ZnSO_4$ specially prepared	+10.2	1.9
30	RCA Phosphor 33-Z-265, uncoated, (100 g) coated with 5 cc of 5% silicate* + 0.1 g $ZnSO_4$	−19.8	2.3
31	RCA Phosphor 33-Z-265, uncoated, (100 g) coated with 15 cc of 5% silicate* + 0.1 g $ZnSO_4$	−31.4	2.7
32	RCA Phosphor 33-Z-265, standard product, (100 g) coated with 3 cc of 5% silicate* + 0.1 g $ZnSO_4$	−19.4	1.5
33	RCA Phosphor 33-Z-265, uncoated, with 0.5% ZnS	Positive in H_2O	2.2
34	RCA Phosphor 33-Z-265, uncoated, coated with CaCdZn hydroxy apatite	Negative in H_2O	2.3
35	RCA Phosphor 33-Z-265, uncoated, factory product	+27.4	1.9
36	RCA Phosphor 33-Z-285, ZnS:0.01% Ag coated with CaCdZn hydroxy apatite	−8.28	2.3
37	RCA Phosphor 33-Z-285, ZnS:0.01% Ag coated 0.1% $Mg(BO_2)_2$, 0.2% BaO, 0.2% SiO_2	−23.0	1.2
38	RCA 33-Z-285, ZnS:0.01% Ag coated with 0.75% $Mg(BO_2)_2$, 0.2% BaO, 0.2% SiO_2	−13.7	2.6
39	RCA 33-Z-386A, (ZnCd)S: 0.003% Ag coated with CaCdZn hydroxy apatite	−3.38	4.1

* 5% by volume silicate solution prepared from a stock solution containing 0.96M K_2O and 3.05M SiO_2.

poured into the open end of the cell. Suction is applied in order to achieve a tight packing. The other electrode then is sealed into place. Occasionally, when a pH meter or an electrometer is used, the platinum electrodes are employed for the potential measurements.

Experimental procedure.—In the streaming-potential experiments, care is taken to rinse out all sections of the apparatus with the liquid being used in the experiments. Measurements are made at several pressures (10-50 cm Hg) and with the liquid flowing in both directions. Potential and conductance measurements are made at each pressure, and sufficient time is allowed for the system to come to equilibrium before each measurement is made. The system is then disassembled, rinsed with 0.010M KCl, and reassembled in order to determine the cell constant of the streaming potential cell under flow conditions analogous to those used in streaming potential determinations.

The formula used to calculate zeta potentials from the experimental data is:

$$\zeta = \frac{4\pi\eta K}{D} \cdot \frac{E}{P}$$

where ζ is zeta potential (mv); η, viscosity of the solution, (poise); D, dielectric constant of the solution; K, specific conductance of the solution within the plug (ohms^{-1}); E, streaming potential (mv); and P, driving pressure (dynes/cm).[2]

Assuming that the viscosity (η) and the dielectric (D) of the solution do not differ appreciably from pure water, the following formula is used for the calculation at 25°C:

$$\zeta = 9.69 \times 10^4 \frac{KE}{P}$$

Experimental Results

Effect of firing conditions.—The first experiments performed in this investigation were made with precipitated ZnS (Table I). Because the surface condition of the powder is of paramount importance in streaming potential measurements, some way of removing adsorbed ions on the ZnS was thought desirable. The ZnS used in these experiments was prepared by bubbling H_2S into a solution of $ZnSO_4$. Under these conditions one may reasonably expect that adsorbed Zn^{++} and $SO_4^{=}$ ions will be present on the ZnS surface. If an excess of Zn^{++} ions are on the surface, there will also be a possibility of ZnO formation. The method of obtaining ZnS free of $SO_4^{=}$, Zn^{++}, and ZnO recommended by Larach and Thomsen (11) was used in this study. It consists of firing precipitated ZnS in H_2S at ~1000°C.

Streaming potential measurements on the ZnS powder prepared in this manner initially gave negative zeta potentials in 5.8×10^{-4}M $Ba(Ac)_2$ (Table I, Test No. 4 and 5). Changes in sign, of this nature, indicate rather radical changes in the condition of the surface. Further investigation of firing conditions showed that it is possible to obtain either positive or negative zeta potentials with a given sample of ZnS. For negative zeta potentials, the method used should be:

Method A

1. Fire ZnS in H_2S at 975°C for 1 hr.
2. With the sample at 975°C, flow N_2 through the furnace for ½ hr.
3. Allow the sample to cool in a N_2 atmosphere.

For positive zeta potential the ZnS sample is:

Method B

1. Fired in H_2S at 975°C for 1½ hr, and
2. Allowed to come to room temperature in an H_2S atmosphere.

These results were found to be reproducible as may be seen in Table I. When the H_2S used in the firing was taken from an almost empty cylinder, Method A yielded phosphors having a positive zeta potential (Test 16). Negative phosphors were always obtained when fresh cylinders of H_2S were used on the samples fired according to Method A. Impurities in the H_2S cylinder (definite infrared spectrum evidence for CH_2Cl_2 was found) which become more pronounced as the cylinder is almost empty may be the cause of the positive zeta potentials obtained when samples were fired by Method A (Test 16). Since O_2 is a usual contaminent in nitrogen cylinders, it is possible that ZnO or chemisorbed O_2 may be formed on the surface of the powder when Method A is used. Method B will probably result in adsorbed H_2S.

The ZnS transition temperature for the transformation from cubic to hexagonal form occurs at 1020°C. Tests 16, 17, and 18 were fired at 1100°C. The other firings were below this temperature. There is some indication that crystal habit affects the zeta potential, but it is felt that not enough experiments were performed above the transition temperature to come to any definite conclusions concerning this point.

Several attempts were made to treat a sample that had been fired by Method A with H_2S in order to cause the streaming potential to become positive. Hydrogen sulfide was allowed to come in contact with dry phosphor and with phosphor-water suspensions. The sign of the potential remained unaltered in all cases. Samples fired by Method B were vacuum heated to 160°C in an unsuccessful attempt to remove adsorbed H_2S and cause the samples to revert to negative potentials (Test 19).

Samples of ZnS that were prepared by Method A and had negative zeta potentials were rinsed with a dilute NH_4OH solution (Test 20). This treatment caused the streaming potential to become positive. X-ray analysis of the ZnS samples before and after treatment with the NH_4OH solution revealed several unidentified lines in the sample treated with the NH_4OH that were not present in the untreated sample. NH_4OH treatment commonly is used commercially to neutralize any excess H_2SO_4, formed during the precipitation of the ZnS, that has not been removed by water rinsing.

Streaming potential measurements at various stages of phosphor preparation.—Streaming potential experiments were performed next on a ZnS phosphor during various stages of preparation. Experiments on several lots of precipitated ZnS all resulted in positive zeta potentials in $Ba(Ac)_2$ (5.84×10^{-4}M) (Tests 1, 2, and 3). When various fluxes such as NH_4Cl, NaCl, and $CaCl_2$ were used to incorporate the Ag activator into the ZnS, the zeta potential still remained positive (Tests 21 through 25). It was not until the phosphor was coated with silicate that the zeta potential became negative in the $Ba(Ac)_2$ solution (Test 32). A phosphor that had been fluxed with the NaCl and activated with 0.015% Ag was coated with ZnS. The coating was applied by bubbling H_2S into a suspension of the uncoated phosphor resulting in the formation of an amorphous layer of ZnS on the surface. This phosphor was found to have a positive zeta potential in H_2O (Test 33). CaCdZn hydroxyapatite coatings give negative potentials (Tests 34, 36, and 39). Several experiments were performed using various amounts of silicate coating, and the results indicate that the magnitude of the negative potential increases with increased amounts of silicate (Tests 30, 31, and 32). Tests 37 and 38 show that $Mg(Bo_2)_2$ coatings give negative zeta potentials with the RCA 33-Z-285 phosphor.

Streaming potential experiments on a ZnS:0.015% Ag, *uncoated phosphor* (33-Z-265 *uncoated*).—(*a*)

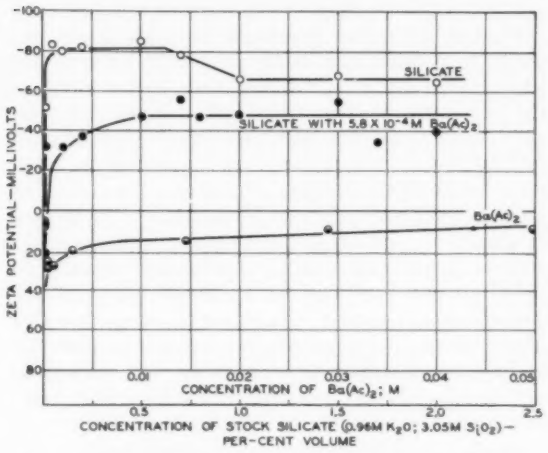
ZETA POTENTIAL—MILLIVOLTS
SILICATE
SILICATE WITH 5.8 X 10⁻⁴M Ba(Ac)₂
Ba(Ac)₂
CONCENTRATION OF Ba(Ac)₂; M
CONCENTRATION OF STOCK SILICATE (0.96M K₂O; 3.05M Si(O₂)— PER-CENT VOLUME

Fig. 1. Zeta potential of RCA phosphor 33-Z-265, uncoated (ZnS:0.015% Ag) as a function of (a) $Ba(Ac)_2$ concentration, (b) silicate concentration, (c) silicate concentration with 5.8×10^{-4}M $Ba(Ac)_2$.

$Ba(Ac)_2$ solution: The results of these experiments are shown in Fig. 1 where the calculated zeta potentials are plotted as a function of the molar concentration of $Ba(Ac)_2$. It is seen that the zeta potential starts at a value of +30 mv at the lowest concentration and falls to a plateau value of about +10 mv at higher concentrations.

(*b*) Silicate: In Fig. 1 the zeta potential is plotted as a function of silicate concentration. The zeta potential starts out with positive values at low silicate concentrations, goes through zero, and continues to increase in magnitude until it reaches a value of about −80 mv. It remains fairly steady at this value and then proceeds to decrease in magnitude in the conventional manner to a plateau value of about −65 mv.

(*c*) $Ba(Ac)_2$-silicate system, $Ba(Ac)_2$ conc. held constant at 5.8×10^{-4}M: These results are also given in Fig. 1. A comparison of the curves in Fig. 1 shows that the added $Ba(Ac)_2$ has the effect of lowering the magnitude of the zeta potential over those obtained with silicate dose.

Several experiments were performed using 9.93×10^{-4}M $Ba(Ac)_2$ plus 0.05% silicate and 0.2% silicate. The zeta potentials were −6.32 and −23.6 mv, respectively, indicating that additional $Ba(Ac)_2$ further suppresses the magnitude of the potentials as compared to that obtained with silicate.

(*d*) Polyvinyl alcohol-ammonium dichromate system: Streaming potential experiments with PVA have been performed on the regular product 33-Z-265 phosphor (ZnS:0.015% Ag, silicate coated) and on uncoated 33-Z-265 phosphor. The results, given in Table II, show that the PVA does not change the sign of the zeta potential of these phosphors from that in pure water. As will be remembered, potassium silicate solutions caused a reversal from positive to negative in the sign of the zeta potential of the uncoated phosphor.

With $(NH_4)_2Cr_2O_7$ as the streaming electrolyte, the same phosphors gave unusual results. Particular difficulty was encountered with the uncoated phosphor. The streaming potential was found to start out positive and to drop rapidly in magnitude. In some cases when the direction of liquid flow was reversed, the measured potential did not reverse sign in the normal manner. The coated 33-Z-265 also showed some tendency toward a decrease in magnitude of the zeta potential with time, but to a much smaller degree than the uncoated material. The zeta potential of the coated phosphor was negative in all cases and ranged from about −25 to −13 mv with time. The concentrations of $(NH_4)_2Cr_2O_7$ used were 0.001 and 0.0005 wt %.

Table II

RCA Phosphor No.	Per cent of PVA	Zeta potential, mv
33-Z-265 uncoated	0.149	+9.77
33-Z-265	0.149	−12.21
33-Z-265 uncoated	0.0149	+13.89

Experiments using PVA (0.0149 wt %) plus $(NH_4)_2Cr_2O_7$ (0.0005 wt %) were performed on the coated and uncoated phosphor. The coated 33-Z-265 had zeta potentials that ranged with time from −8 to −3.5 mv. The potential of uncoated 33-Z-265 ranged from +31 to +6.5 mv. These changes in zeta potential with time are probably due to chemical interaction of the $(NH_4)_2Cr_2O_7$ with the phosphor and could possibly be used as a means of estimating how well a phosphor has been coated.

Adherence measurements.—Table I and Fig. 2 give zeta potential and adherence data on a number of samples prepared by various firing conditions and with different fluxes and coatings. A water jet impingement method (12) for evaluating wet adherence was used. It consists of first dispersing the sample to be tested in a solution containing 9.25×10^{-5}M $Ba(Ac)_2$ and 0.22% stock potassium silicate and then allowing the sample to settle to the bottom of the vessel. After the prescribed time (20 min) has elapsed, a glass capillary tube with an inner diameter of 1.2 mm is immersed into the vessel and a jet of water allowed to impinge through a given height of liquid (1 in.) onto the settled powder. The geometry and hydrostatic pressure applied to the capillary

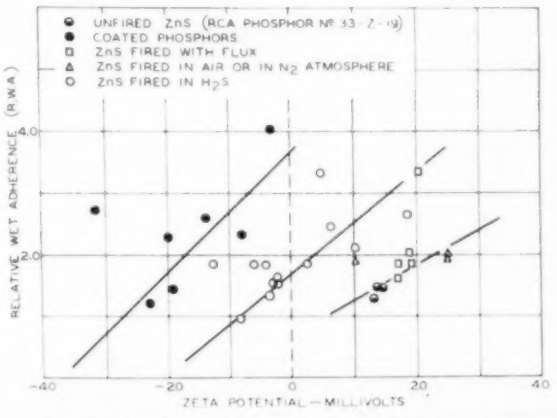
UNFIRED ZnS (RCA PHOSPHOR № 33-Z-19)
COATED PHOSPHORS
ZnS FIRED WITH FLUX
ZnS FIRED IN AIR OR IN N₂ ATMOSPHERE
ZnS FIRED IN H₂S
RELATIVE WET ADHERENCE (RWA)
ZETA POTENTIAL—MILLIVOLTS

Fig. 2. Correlation between zeta potential and relative wet adherence.

Table III

Conc. $Ba(Ac)_2$, M	Hole diameter*, mm: Standard phosphor	Uncoated phosphor
1.06×10^{-3}	8.2	17.2
8.57×10^{-4}	9.3	22.3
8.57×10^{-5}	28.7	38.5
8.57×10^{-6}		39.3

* Large hole diameter indicates poor adherence.

are kept constant (jet-flow rate equals 153 cc/min). The data in Table I for relative wet adherence (RWA) are the reciprocal of the eroded area produced by the water jet on the sample being studied, divided by the reciprocal of the area obtained with a standard sample, and multiplied by 4.05 (the RWA of the standard phosphor).

Wet-adherence measurements using the jet-impingement technique, but with the data reported in terms of eroded hole diameter, were performed on the uncoated 33-Z-265 phosphor as a function of $Ba(Ac)_2$ concentration. The concentration of the silicate was 0.81% of the stock solution. Results are given in Table III.

It is apparent that the uncoated 33-Z-265 phosphor has comparatively poor wet adherence. The fact that the jet impingement test with the uncoated phosphor results in hole diameters that increase with decreasing concentration indicates that it has a negative zeta potential when suspended in the silicate for the wet adherence test. The streaming potential experiments confirm this assumption.

Discussion

The results of the experiments on the effect of firing conditions on the sign of the zeta potential indicate the importance of surface conditions. The difference in sign between ZnS samples that have been fired in H_2S and flushed with N_2 (negative zeta potential) and those fired in H_2S and allowed to cool in H_2S (positive zeta potential) may possibly be due to adsorbed H_2S, in the latter case, and O_2 adsorption or ZnO formation, due to impurities in the N_2, in the former case.

Samples allowed to cool in H_2S may be expected to behave quite differently from those cooled in N_2. Undoubtedly, H_2S will be adsorbed which, when placed in H_2O, will have the opportunity of dissociating into H^+ and HS^- ions. If the H^+ ions remain adsorbed, the diffuse part of the double layer must have an excess of negative charge. This negative charge will result in the observed positive values for the streaming potential and zeta potential. It was not possible to detect any differences in pH of water suspensions of ZnS samples prepared by the methods mentioned above, probably because the concentration of HS^- ions discharged from the surface of the powder cooled in H_2S was too small to be effective.

It is difficult to establish from the experiments that have been performed thus far whether the impurities in the N_2 contribute measurably to the resulting zeta potentials. The negative zeta potentials obtained by firing in H_2S and flushing with N_2 may be due to ZnO or O_2 on a ZnS substrate, or simply to ZnS.

The NH_4OH treatment of the sample that had been treated by Method A caused the potential to become positive. Because zinc complexes with NH_3, an adsorbed zinc-ammonia complex may be the cause of the sign reversal. The x-ray data indicate the possible formation of a new species in the NH_4OH treated sample, but the intensity is too low to allow for positive identification.

The streaming potential experiments performed at various stages of phosphor preparation also indicate the importance of surface conditions as compared to bulk modification of a ZnS powder. Thus, the streaming potential was found to remain positive during all stages of phosphor preparation until the coating operation. Additions of various fluxes, as well as Ag activator, resulted in powders with positive potentials. All of the streaming-potential experiments performed by various workers on phosphors have been with finished products (3-5). In all cases but one, negative potentials were obtained. Hazel and Schnabel (4) found that du Pont #1630 (ZnS; ZnCdS) had a positive potential in the absence of K_2SiO_3. They suggest that the positive potential was due to the flux or other impurities. The present findings indicate that the positive potentials are not due to the flux, because the original ZnS starting material has a positive potential. A ZnS coated ZnS:0.015% Ag phosphor was found to have a positive potential. Silicate coatings result in negative potentials with the magnitude of the potential increasing with heavier coatings. The ZnS coated phosphors have all of the free-flowing characteristics that have been found desirable in phosphor coatings that have negative potentials. This information permits the selection of a coating with either a positive or negative potential should a particular screen-application technique indicate one or the other to be most desirable.

Streaming-potential experiments on the ZnS: 0.015% Ag uncoated phosphor (33-Z-265) as a function of $Ba(Ac)_2$ concentration, silicate concentration, and $Ba(Ac)_2$-silicate mixtures are shown in Fig. 1. The curve for zeta potential vs. $Ba(Ac)_2$ concentration shows the usual reduction of the zeta potential with increased concentration of electrolyte as a result of condensation of the diffuse part of the electrical double layer. As may be seen from the curve for zeta potential vs. silicate concentration there is a reversal in the sign of the zeta potential from positive to negative with increasing silicate concentration. The region of rapid increase in negative values of the zeta potential with increasing silicate concentration may indicate only partial coating of the phosphor with silicate. From 0.05 to 0.7% silicate, the phosphor may be completely coated with silicate. It is only at concentrations higher than 0.7% stock silicate that compression of the electrical double layer, caused by additional adsorption of ions into the inner Helmholtz plane and, consequently, reduction in magnitude of the zeta potential, becomes predominant. With an ordinary electrolyte, the zeta potential falls to values considerably lower than the −64.5 mv at 2.0% stock silicate found in the present system. This reduction may be due to the tendency

of the silicate ions to associate into micells which will result in only a relatively small increase in the concentration of free ions with an increase in silicate concentration.

Comparison of the curve for zeta potential vs. silicate concentration with the curve for zeta potential vs. silicate concentration plus 5.8×10^{-4}M $Ba(Ac)_2$ shows that the added $Ba(Ac)_2$ (5.8×10^{-4}M) has the effect of lowering the magnitude of the zeta potential and of shifting the curve toward the higher concentration range. A possible explanation is that the silicate is forced to compete with the Ba^{++} ions for adsorption sites, despite the fact that different charge types are involved. For example, an adsorbed silicate ion at a positively charged site may prevent adsorption of a Ba^{++} ion at an adjacent negatively charged site by steric hindrance. The silicate ions overbalance the Ba^{++} ions because they cause a phosphor that has positive zeta potentials in H_2O or in $Ba(Ac)_2$ solutions to become negative. The lowered magnitude of the negative zeta potential in $Ba(Ac)_2$ as compared to that found with silicate alone indicates partial adsorption of the Ba^{++} ions in the inner Helmholtz plane in the region of low silicate concentration. Another mechanism that would contribute to the lowered potentials would be strongly adsorbed Ba^{++} ions on top of the adsorbed silicate ions. The drop in the zeta potential, after the maximum value of the negative potential has been obtained, is less pronounced than for the silicate system. This difference is to be expected because the $Ba(Ac)_2$ will tend to gel the silicate system at these higher concentrations, in effect reducing the number of ions available to cause compression of the electrical double layer and, therefore, reduction of the zeta potential.

The experiments with PVA and ammonium dichromate indicate that the PVA does not change the sign of the potential of the uncoated phosphor as compared to that found with water, and also that some reaction occurs between the phosphor and the ammonium dichromate. Perhaps the ZnS is oxidized to the sulfate. The silicate coated phosphor is more resistant to attack by the dichromate, as is evident from the smaller zeta potential change with time as compared to that observed for the uncoated material. Streaming potential measurements on systems of this type may be useful in studying chemical reactions which would otherwise remain undetectable.

Attempts to correlate wet-adherence measurements, performed in 9.25×10^{-5}M $Ba(Ac)_2$ and 0.22% stock silicate, with zeta potential data have not been completely successful. This variance may be due largely to the tendency of the silicate, used in making the RWA measurements, to coat the sample and at least partially mask the electrical properties of the original material. Thus, while there is a trend toward increasing RWA with decreasing zeta potential, the results are not conclusive as there is considerable scatter in the experimental data (Table I and Fig. 2). The best correlation is found with the coated phosphors that have negative zeta potentials in 5.8×10^{-4}M $Ba(Ac)_2$. Thus far, no attempt has been made to study the effect of shape and size distribution on the relative wet adherence and the zeta potential. Because the samples studied were prepared under different conditions of firing, fluxing, activation, and coating, the lack of correlation is not surprising. If the samples are grouped according to treatment when the data are plotted, as has been done in Fig. 2, fair correlation is obtained. It should be re-emphasized, however, that the best correlation between zeta potential and wet adherence is found if the same sample is used and its zeta potential is altered by changing the concentration of the electrolyte.

Conclusions

1. The zeta potential of ZnS may be altered in sign depending on firing technique. Apparently, adsorbed H_2S plays an important role.
2. NH_4OH washing can change the zeta potential of a ZnS sample that has been fired in H_2S and flushed with N_2 from negative to positive. The change is due possibly to an adsorbed zinc ammonia complex.
3. ZnS phosphors have positive zeta potentials during all stages of preparation prior to the coating operation. Silicate coatings yield negative potentials, while ZnS coatings yield positive potentials. These experiments illustrate the importance of surface conditions as compared to bulk properties in determining the zeta potential.
4. The influence of electrolyte concentration on the zeta potential of a ZnS:0.015% Ag, uncoated phosphor has been determined with $Ba(Ac)_2$, potassium silicate, and $Ba(Ac)_2$-potassium silicate mixtures. Similar experiments were performed in the PVA-ammonium dichromate system for the coated as well as the uncoated phosphor. The dichromate interacts chemically with the phosphor, causing rapid changes in the zeta potential.
5. Zeta potential data have been correlated with adhesion measurements.

Acknowledgment

The author is happy to acknowledge the assistance of L. E. Whitmer and Dr. S. A. Harper, who prepared many of the samples used in these experiments. Mrs. K. Maisane performed a major share of the streaming potential experiments concerned with the effect of electrolyte concentration, and her help is gratefully appreciated. Dr. D. J. Donahue and Dr. R. N. Summergrad assisted in many instances with helpful discussion and suggestions.

Manuscript received May 19, 1958. This paper was prepared for delivery before the New York Meeting, April 27-May 1, 1958.

Any discussion of this paper will appear in a Discussion Section to be published in the December 1959 JOURNAL.

REFERENCES

1. M. Sadowsky, *J. (and Trans.) Electrochem. Soc.*, **95**, 112 (1949).
2. D. J. Donahue, *RCA Engineer*, **1**, No. 3, 10 (1955).
3. R. Edelberg and J. F. Hazel, *J. (and Trans.) Electrochem. Soc.*, **96**, 13 (1949).
4. J F. Hazel and G. L. Schnable, *This Journal*, **100**, 65 (1953).
5. J. F. Hazel and G. L. Schnable, *J. Phys. Chem.*, **58**, 812 (1954).
6. See *Electrical Phenomena at Interfaces*, The Macmillan Company, New York, 1951, J. A. V. Butler, Chap. II and III.

7. J. J. Bikerman, *Trans. Faraday Soc.*, **36**, 154 (1940).
8. D. R. Briggs, *J. Phys. Chem.*, **33**, 641 (1928).
9. J. Th. G. Overbeek and P. W. O. Wijga, *Rec. Trav. chim.*, **65**, 556 (1946).
10. A. M. Gaudin and D. W. Fuerstenau, *Mining Engineering*, January 1955, pp. 1-7.
11. S. Larach and S. M. Thomsen, *Anal. Chem.*, **26**, 1600 (1954).
12. A. S. T. M., F-1 subcommittee No. 7 on Luminescent Materials is currently considering a number of methods of measuring wet adherence one of which is the method being used by RCA, briefly described in this paper.

Associated Donor-Acceptor Luminescent Centers in Zinc Sulfide Phosphors

E. F. Apple and F. E. Williams

Research Laboratory, General Electric Company, Schenectady, New York

ABSTRACT

Zinc sulfide activated with copper or silver and coactivated with gallium or indium shows two emission bands. The shorter wave-length band does not involve the ground state of the coactivator or donor, whereas the longer wave-length band does. Both bands involve the ground state of the activator or acceptor. The factors contributing to the emission intensities from the various associated donor-acceptor pairs are discussed theoretically. The dependences on temperature and on concentrations of activator and coactivator are in accord with the longer wave-length band involving a highly associated donor-acceptor pair. In addition, the energy levels of the donors, as obtained from thermoluminescent data, are correlated on the basis of the model with the differences in the transition energies of the two emission bands of these phosphors.

Zinc sulfide phosphors coactivated with Group III elements of the Periodic Table have been reported to have a long wave-length emission band in addition to the short wave-length emission band associated with activation by Group I elements and with self-activation. Kröger and Dikhoff (1), for example, reported long wave-length emission in phosphors coactivated with Sc, Ga, or In. The emission bands peaked at 5250Å with Sc, 5700Å with Ga, and 6800Å with In and were relatively independent of the identity of the activator. They also observed that the substitution of ZnS in part by CdS had less effect on the long wave-length emission spectra than on the short wave-length emission spectra. Klasens (2) attributed these long wave-length bands to the radiative recombination of a free hole with an electron trapped at the coactivator. Froelich (3) reported long wave-length emission for Cu and self-activated ZnS phosphors which were coactivated with quite high concentrations of Al. Emission peaks are at 5880 and 5000Å, respectively. Apple (4) has reported that the crystalline structure influences the relative intensities of the two emission bands observed with ZnS: x(Cu, Ag, Au), y(Ga, In) phosphors in which $x < y$. The long wave-length emission was found to be enhanced in hexagonal ZnS. He has suggested that this effect may be related to a change in association of activator and coactivator.

In this investigation a comprehensive study of ZnS:x(Cu or Ag), y(Ga or In) was made. The spectra of the long wave-length emission are found to depend on the identities of both activator and coactivator. The relative intensities of the long and short wave-length emission depend on concentrations of activator and coactivator and on temperature of excitation. These experimental results are explained by means of a model for the long wave-length emission center consisting of a highly associated activator-coactivator center. This center is similar to the associated donor-acceptor system proposed by Prener and Williams (5) to explain the short wave-length emission by radiative transitions from excited states of the donor to the ground state of the acceptor but is different in that the donor and acceptor responsible for the long wave-length emission are more closely associated so that radiative transitions occur from the ground state of the donor to the ground state of the acceptor.

Experimental Results

The phosphor mixes usually were made by adding aqueous solutions of activator and coactivator to a water slurry of ZnS (G.E. luminescent grade); in a few cases the activator and coactivator were added as the solid ternary sulfides, i.e., $CuGaS_2$, $CuInS_2$, or $AgGaS_2$ in the absence of water. The mixes were fired in an H_2S stream either at 950°C to give a cubic material or at 1150°C to give a hexagonal phosphor. The H_2S used was bubbled through $Ba(OH)_2$ solution, then through drying columns containing silica gel and P_2O_5 and a cold trap held at −50°C before coming in contact with the sample.

Emission spectra of the phosphors under 3650Å excitation[1] are shown in Fig. 1-4. Concentrations are given in gram-atoms added per mole ZnS, but the amounts of activator and Ga present after firing were equivalent to the amounts added, whereas the

[1] Essentially 3650A radiation was obtained from a G.E. mercury lamp, #H100-FL4, in conjunction with Corning #5840 and Kopp #41 uv filters. The spectra were recorded on an automatic spectroradiometer which plots radiant energy flux vs. wave length.

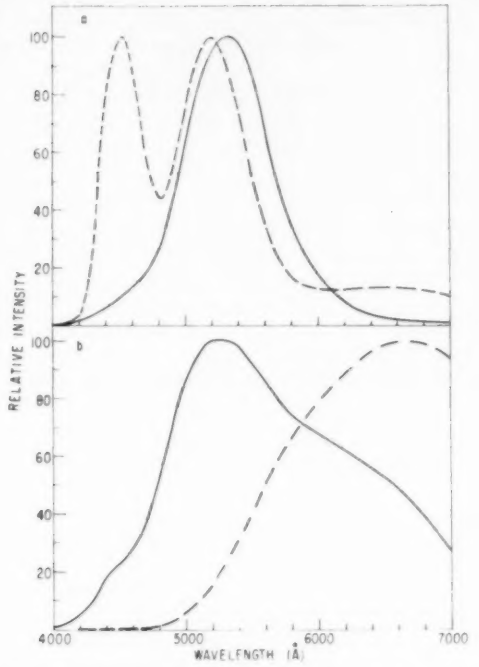

Fig. 1. Emission spectra of ZnS:10^{-4} Cu, 10^{-4} Ga; a, cubic structure; b, hexagonal structure; 3650Å excitation; ——— room temperature - - - - - —196°C.

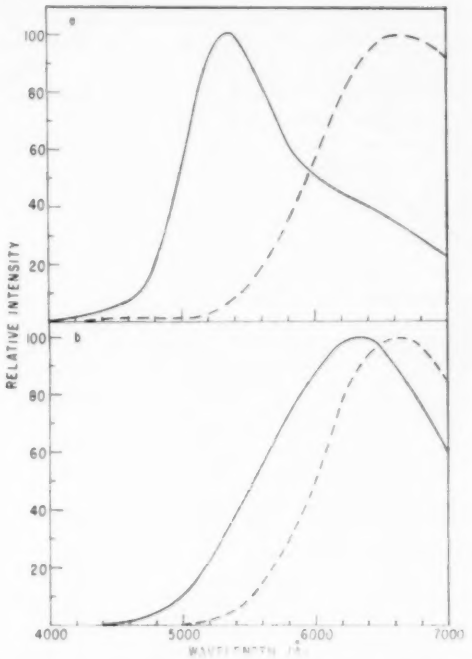

Fig. 2. Emission spectra of ZnS:10^{-4} Cu, 2×10^{-4} In; captions as in Fig. 1.

final In concentration, because of volatization, was approximately equal to the concentration of activator present. Although most of the phosphors were prepared in purified H_2S, they could be made equally well in sealed, evacuated quartz tubes, S_2($p = 30$ atm), N_2, or H_2, provided that water and oxygen were excluded in the phosphor preparation.

This class of phosphors clearly shows two emission bands.[2] The shorter wave-length emission, which is in the blue with Ag and in the green with Cu, is dependent on the identity of the activator only, while the longer wave-length emission, which is in the yellow with Ag and orange with Cu, depends on the identity of both activator and coactivator. For example, the longer wave-length emission peaks at 5900Å in ZnS:Ag,Ga and at 6150Å in ZnS:Ag,In.

The relative intensities of the two bands are determined by such parameters as concentration of activator and coactivator, temperature during excitation, identity of coactivator, crystal structure, and firing temperature.

An increase in concentration of activator and coactivator causes an increase in the long to short wave-length emission ratio. For example, consider the emission in cubic ZnS:Cu,In. Below 10^{-5} Cu and In, virtually no contribution from the orange band is observed under excitation at room temperature. Increase in concentration of Cu and In from 10^{-5} causes an increase in the orange emission until at 3×10^{-4} Cu and In the intensity of the orange band is about equal to that of the green band and above this concentration, the orange band predominates. In Ga-coactivated phosphors, the shorter wave-length band predominates in samples containing up to about 10^{-2} Cu and Ga. Related to the concentration effect is the dependence of the longer to shorter wave-length emission ratio on firing temperature. In cubic ZnS: 10^{-4} Cu, 2×10^{-4} In, this ratio at room temperature is 0.31, 0.27, 0.26 for samples fired at and air-cooled from 600°, 700°, and 900°C, respectively.

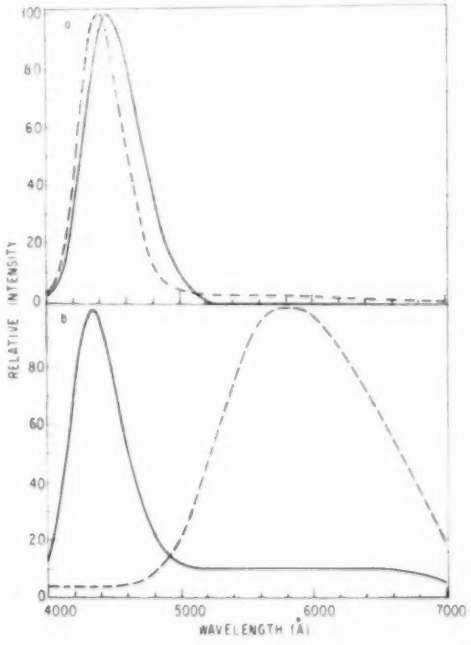

Fig. 3. Emission spectra of ZnS:10^{-4} Ag, 10^{-4} Ga; captions as in Fig. 1.

[2] The additional band at 4500Å observed only in cubic ZnS:Cu, Ga is not discussed in this paper.

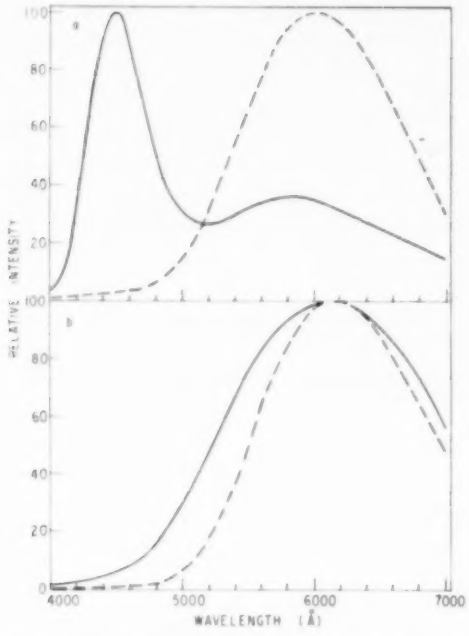

Fig. 4. Emission spectra of ZnS:10^{-4} Ag, 2×10^{-4} In; captions as in Fig. 1.

As is evident from Fig. 1-4 the longer wave-length emission is favored under excitation at lower temperatures. The temperature dependence of emission of the phosphors was determined by recording the spectra as the sample contained on a large Cu block in vacuum was cooled slowly from about 275°C to room temperature. Below room temperature, the block was cooled by the addition of small quantities of liquid nitrogen. The temperature change during measurement of the spectrum was in no case greater than 5°C. Figure 5 shows some of the spectra obtained on hexagonal ZnS:10^{-4} Cu, 2×10^{-4} In at the temperatures indicated. Even at 255°C, where temperature quenching has begun, the contribution of the orange band is considerable. The slight shift in the spectra at lower temperatures is due in part to the disappearance of the green band below −140°C. Cubic ZnS:10^{-4} Cu, 2×10^{-4} In shows the same general temperature dependence, but above 100°C the orange contribution to the spectra is small and the change from predominantly orange to green emission occurs at −35° to 0°C. The green-orange change in emission occurs at lower temperatures as the concentration of Cu and In is decreased. This is observed for both cubic and hexagonal phosphors. Figure 6 shows the temperature dependence of emission for hexagonal ZnS:10^{-4} Cu, 10^{-4} Ga. Above 100°C, the contribution from the orange band is again very small. These data indicate that the temperature dependence of emission at a given concentration of activator and coactivator is determined by the identity of the coactivator. In ZnS:Ag,Ga or In, the data were limited to below about 80°C where temperature quenching of luminescence begins. Consequently, the yellow to blue emission shift was not observed in hexagonal ZnS:Ag,In.

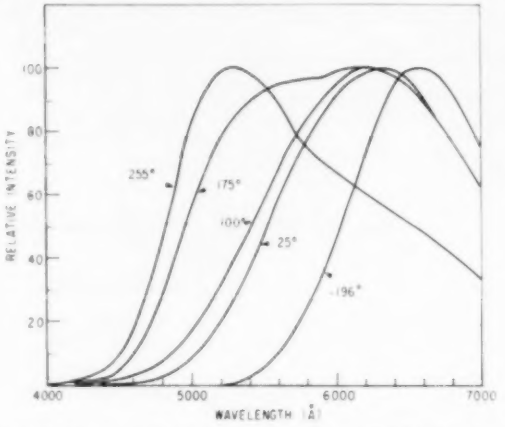

Fig. 5. Emission spectra of hexagonal ZnS:10^{-4} Cu, 2×10^{-4} In at indicated temperature using 3650Å excitation.

The effect of structure of the ZnS in luminescence has been mentioned heretofore in connection with the concentration- and temperature-dependent properties of the phosphors. At a given concentration of activator and coactivator, the longer wave-length emission is enhanced in the hexagonal phase of ZnS as, again, is shown in Fig. 1-4. On annealing a hexagonal phosphor for an extended time at 800°-900°C, the shorter wave-length emission typical of cubic phosphors increases concurrently with increase in the amount of cubic phase present. The effect is reversible with change in structure. Also, phosphors with emission spectra characteristic of those prepared at 1150°C can be made at temperatures as low as 600°C provided hexagonal ZnS is used in preparation of the phosphor mixes. The structure of these phosphors remains hexagonal during the 1-hr firing period at 600°C.

Glow curves were obtained on samples previously excited by a BH-4 lamp at −195°C for a 5-min period, and then heated at a rate of 10°C/min. The glow intensity was measured with an RCA 5819 PM tube with S-4 response. Glow peaks apparently resulting from In occur at −140° and −60°C. The thermoluminescence changes from the longer to the shorter wave-length emission during these glow experiments. The high-temperature glow peak at 100°-

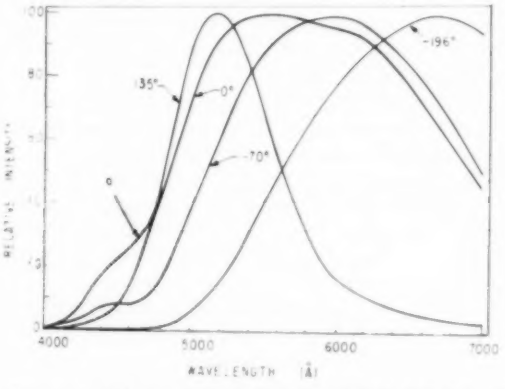

Fig. 6. Emission spectra of hexagonal ZnS:10^{-4} Cu, 10^{-4} Ga at indicated temperature using 3650Å excitation.

140°C observed with Cu-activated materials changes position with change in concentration.

Theoretical Analysis

As a consequence of the association of activator and coactivator impurities into donor-acceptor pairs, a unique impurity system is not expected in these phosphors, but rather a distribution of diatomic centers each characterized by a different interimpurity distance is expected. These pairs will each have a different energy level structure and transition probabilities for excitation and emission.

Prener and Williams (5) have proposed a model for the luminescent center defined in this paper as the short wave-length luminescent center. In this model, the transitions responsible for the short wave-length emission occur between excited states of the donor and the ground state of the acceptor in an associated, but not nearest neighbor, coactivator-activator pair. Because excited states of the donor are involved, the emission is independent of the chemical identity of the coactivator. Recently, Williams (6) extended the original concept of associated pairs at second, third, and fourth nearest-neighbor sites to more widely separated pairs of nonrandomly distributed donors and acceptors contributing to short wave-length emission. The present analysis is consistent with the short wave-length emission involving pairs with sufficiently great interimpurity spacing such that only radiative transitions from excited donor states to the ground state of the acceptor can occur with appreciable probability. The ground state of the donor for these pairs will function as an electron trap. These pairs will be designated *s*-type and are shown on the left of the band model in Fig. 7. The emission process also is indicated with the transition probability A_s.

We propose that the long wave-length emission arises from coactivator-activator pairs sufficiently closely associated so that radiative transitions may occur directly from the ground state of the donor to the ground state of the acceptor. The probability of this transition depends, of course, on overlap of the ground state donor and acceptor wave functions. Because the energies of the ground states are dependent on the identities of donor and acceptor, respectively, the transition energy for the long wave-length emission will be dependent on the chemical identities of both the coactivator and the activator. These pairs will be designated as *l*-type and are shown on the right in Fig. 7 along with the emission process indicated by the transition probability A_l.

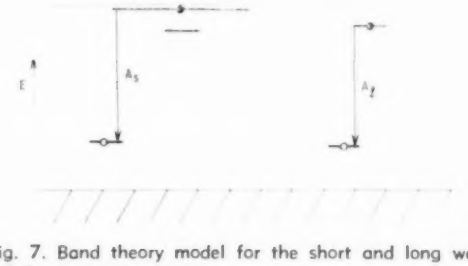

Fig. 7. Band theory model for the short and long wave-length luminescent centers.

The relative intensities of the short and long wave-length emission bands can be analyzed theoretically most readily for temperatures sufficiently great so that thermal equilibrium applies among the electron states and separately among the hole states. The ratio of intensities from *s*- and from *l*-type centers will then be of the following form:

$$\frac{I_s}{I_l} = \frac{\rho_s}{\rho_l} \cdot \frac{P(\epsilon_s)}{P(\epsilon_l)} \cdot \frac{A_s}{A_l} \cdot \frac{\alpha_s}{\alpha_l} \qquad [1]$$

where the ρ's, P's, A's, and α's are, respectively, the densities of states, occupational probabilities for each state, transition probabilities for emission, and fractions of pairs responsible for the *s*- and *l*-type emission.

Because the *s*-centers are believed to comprise all the coactivator-activator pairs in which any excited donor state has a finite matrix element for a radiative transition with the ground state of the acceptor and since there are many excited donor states characterized by different spatial extensions of their wave functions, a distribution of pairs with different interimpurity spacings is expected to contribute to α_s. On the other hand, the *l*-centers probably comprise a unique pair, or at most a narrow distribution of pairs, because the interimpurity spacing must be such that a finite matrix element for a radiation transition exists between the ground states of the donor and acceptor. Only a small fraction α_l of the pairs are consistent with this requirement. In the following analysis the ratio α_s/α_l will be determined theoretically in an approximation consistent with being large compared to unity. From the formula of Prener (7), we obtain:

$$\frac{\alpha_s}{\alpha_l} = \frac{\sum_{l+1}^{s} \alpha_m}{\alpha_l} = \frac{\sum_{l+1}^{s} Ac\, Z_m e^{e^2/Kr_m kT_D} e^{-c\sum_1^m Z_j}}{Ac\, Z_l\, e^{e^2/Kr_l kT_D} e^{-c\sum_1^l Z_j}} \qquad [2]$$

where Z_j is the number of sites of the jth type and T_D is the temperature during preparation below which diffusion over interimpurity distances cannot occur. We then make a continuum approximation (8) for the pairs of the *s*-type and replace the sums by integrals. In this approximation $(Z_{l+1} - Z_l) \rightarrow dZ = 4\pi r^2 dr$, and

$$\frac{\alpha_s}{\alpha_l} = 4\pi Z_l^{-1} e^{c\sum_1^l Z_j} \int_{r_l}^{\infty} r^2 e^{\frac{e^2}{KkT_D}\left(\frac{1}{r} - \frac{1}{r_l}\right)} e^{-\frac{4}{3}\pi r^3 c}\, dr \qquad [3]$$

For $T_D \approx 10^3$ °K and $l \geqq 3 (r_l \geqq 7\text{A})$, the factor $e^{\frac{e^2}{KkT_D}\left(\frac{1}{r} - \frac{1}{r_l}\right)}$ is a sufficiently slowly varying function of r from r_l to ∞ so that a weighted average value can be removed from the integrand. The result is integrated and the relation $\frac{4}{3}\pi r_l^3 = \sum_1^l Z_j$ between the continuum approximation and the lattice is utilized to yield the following approximate relation:

$$\frac{\alpha_s}{\alpha_l} = c^{-1} Z_l^{-1} \left[e^{\frac{e^2}{KkT_D}\left(\frac{1}{r_s} - \frac{1}{r_l}\right)} \right] \qquad [4]$$

in which r_s can be interpreted as a weighted average interimpurity distance for the *s*-type centers. The factor α_s/α_l will favor *s*-type emission and is clearly

dependent on the concentration c of activators and coactivators.

On the other hand, the factor in Eq. [1] which takes account of the occupational probabilities of emitting states of the s- and l-type centers favors l-type emission and is strongly temperature-dependent. This is evident from Fig. 7 and also from the equilibrium approximation. For ordinary excitation intensities the fraction of centers excited simultaneously will be sufficiently small so that Boltzmann statistics may be used. The difference in emission spectra of the two bands is a measure of the difference in energies of the states of the two types of centers. We may write, therefore

$$\frac{P(\epsilon_s)}{P(\epsilon_l)} \simeq e^{-\frac{hc}{kT}\left(\frac{1}{\lambda_s}-\frac{1}{\lambda_l}\right)} \qquad [5]$$

This formula will be in error by the difference in polarization energy of the two types of centers following emission. This error may be as great as the difference between the thermal depth and the optical depth of the donor. At low temperatures the occupational probabilities will not be determined by equilibrium considerations but rather by detailed balance between excitation and emission within each coactivator-activator pair. Under these conditions Eq. [5] will not apply, and an appreciable fraction of s-type pairs will no longer contribute to emission at low temperatures in the steady state because of electron trapping in the ground state of the donor of these pairs.

The ratio of densities of states ρ_s/ρ_l and transition probabilities for emission A_s/A_l are both expected to be of the order of unity and not appreciably dependent on temperature or concentration of luminescent centers. In the l-type center, emission is exclusively from the ground state of the donor so that ρ_l is obviously unity. The excited states in the highly associated l-type pair have been perturbed back to the conduction band edge (5). In an s-type center the lower excited states which give a finite matrix element for radiative recombination with the positive hole in the associated acceptor contribute to ρ_s, the higher excited states having been perturbed back into the conduction band (5). Since the s-type centers comprise a distribution of pairs with different interimpurity spacings $r_m > r_l$, the identities of the excited states contributing to ρ_s will vary with r_m; however, their number is expected to be a constant small integer. The magnitudes of the matrix elements A for radiative recombination with the positive hole in the associated acceptor should be comparable for s- and l-type emission.

In addition, the ratio I_s/I_l has been investigated with the assumption that the transitions between the unperturbed conduction band states and the ground state of the acceptor are responsible for s-type emission. With this assumption, the same dependence on temperature and impurity concentration is obtained as in the foregoing analysis. However, a pronounced dependence of I_s/I_l on excitation intensity is obtained because I_s is proportional to both the concentration of the electrons in the conduction band and the concentration of empty acceptors, whereas I_l is proportional only to the concentration of empty acceptors. This is not the case with the analysis based on s-type emission involving excited donor or perturbed conduction band states since, for this analysis, both I_s and I_l are proportional only to the concentration of empty acceptors.

The model illustrated in Fig. 7, in addition to providing the basis for the preceding analysis of the relative intensities of the short and long wave-length emission bands, provides a basis for relating the transition energies for emission to other luminescent properties. For example, the ground state of the donor in the s-type center is an electron trap, and therefore, the depth of the trap should be approximately equal to the difference in transition energies for the two emission bands.

$$E_T \simeq hc\left(\frac{1}{\lambda_s}-\frac{1}{\lambda_l}\right) \qquad [6]$$

This relation is more nearly correct for the optical, rather than the thermal, trap depth. In addition, this relation is based on the assumption that the energies of the ground states of the donor and acceptor are independent of whether the association is into s-type or l-type pairs.

Since the energies of the states of the donor and acceptor do depend on association, the accuracy with which Eq. [6] is in accord with experiment permits placing an approximate limit on the degree of association of the l-type pairs. Williams (9) recently has examined theoretically the donor-acceptor pair system, which is a two-particle system consisting of an electron and a positive hole bound in the field of a finite dipole. The analysis is similar to the Heitler-London treatment of the hydrogen molecule and takes account of the overlap of the donor and acceptor wave functions. This overlap was neglected in the analysis of Hoogenstraaten (10). The transition energy for emission E_s for pairs characterized by the interimpurity spacing r_l and by radial wave functions for the separated donor and acceptor of the form $a^{-3/2}\,e^{-r/a}$ is:

$$E_s = -\frac{e^2}{Ka}\,e^{-2r_l/a}\left[\frac{a}{r_l}+\frac{5}{8}-\frac{3}{4}\frac{r_l}{a}-\frac{1}{6}\frac{r_l^2}{a^2}\right] - \frac{e^2}{12a}\left(\frac{1}{K_s}-\frac{1}{K}\right)e^{-2r_l/a}\left[4\frac{r_l^2}{a^2}+18\frac{r_l}{a}+9\right] + \frac{e^2}{K_s r_l} - E_D - E_A + E_G \qquad [7]$$

where E_D and E_A are the ionization energies for the separated donor and acceptor, K and K_s are the static and optical dielectric constants, and E_G is the band gap. For pairs consisting of donors and acceptors both located at sites of the same sign and with $E_D \geqq 0.5$ ev and $E_A \geqq 0.5$ ev, the perturbation of the ground states and consequent increase in E_s will be quite accurately e^2/Kr_l. The error involved in using Eq. [6] to calculate thermal trap depths tends to cancel the error involved in assuming the energies of the donor and acceptor states to be independent of degree of association.

Interpretation of Experimental Results

The longer wave-length emission is attributed to radiative transitions involving the ground states of highly associated donor-acceptor pairs and consequently should depend on the chemical identity of

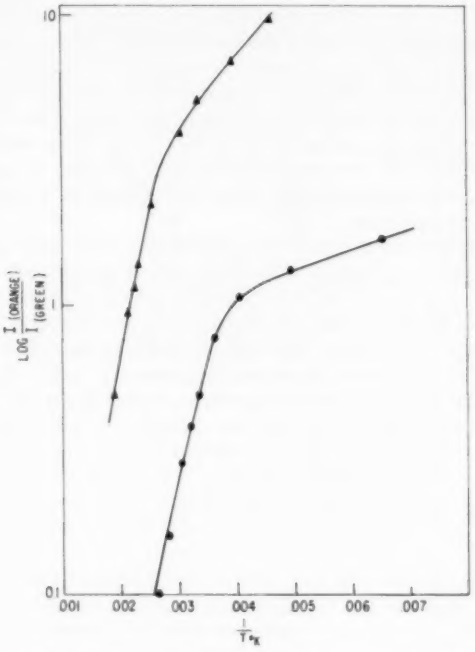

Fig. 8. log I orange/I green vs. 1/T ——— 3650Å excitation; ▲, hexagonal ZnS:10^{-4} Cu, 2 × 10^{-4} In; ●, hexagonal ZnS:10^{-4} Cu, 10^{-4} Ga.

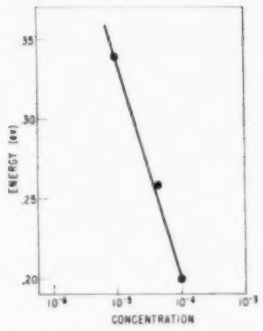

Fig. 9. E (slope from Fig. 8) vs. log concentration Cu in ZnS:Cu, In.

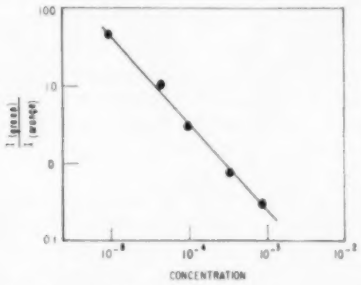

Fig. 10. log I orange/I green vs. log concentration Cu in cubic ZnS:Cu, In.

both donor and acceptor. This has been observed experimentally as has already been pointed out with ZnS:Ag,Ga and ZnS:Ag,In. In ZnS:Cu,Ga and ZnS:Cu,In, the difference in spectral distributions of the long wave-length emissions is less marked but present.

In addition, the model for the long wave-length center is in agreement with the fact that the temperature dependent properties are determined primarily by the identity of the coactivator, since the energy level of the activator for both the short and long wave emission is nearly identical, whereas different energies are associated with the Ga and In levels. The latter was pointed out by Hoogenstraaten (10) for the trap depths for Ga and In. This was confirmed in the glow curve measurements of the present study. In Fig. 8 the log of the ratio of orange to green intensities is plotted against the reciprocal of the absolute temperature for hexagonal ZnS:10^{-4} Cu, Ga and hexagonal ZnS:10^{-4} Cu, 2 x 10^{-4} In. The slopes of these plots are the differences in energies of the *s*- and *l*-type centers in their emitting states and are approximately the difference in energies of the donor levels responsible for the short and long wave-length emissions. The total quantum efficiency does not decrease in this temperature interval, and the effects of competing nonradiative processes can therefore be neglected. The nonlinear portions of the plots observed at lower temperatures indicate the absence of thermal equilibrium. The slope is 0.12 ev for ZnS:Cu,Ga and 0.20 ev for ZnS:Cu,In. Although these energies are lower than the values of the trap depths, i.e., 0.50 ev for In and 0.42 ev for Ga, the energy differences are in the right direction and the 0.08 ev difference between Ga and In is the same as the difference in energies reported for the trap depths (10). With decrease in concentration of activator and coactivator, the energies become larger as is shown in Fig. 9. This effect of concentration is qualitatively in accord with the changes in energy level structures of the two types of centers predicted by Eq. [7] since the contribution from each pair changes with concentration.

Using Eq. [6], the trap depths for In and Ga as calculated from emission spectra of Cu-activated materials are 0.47 ev for In and 0.44 for Ga which compare favorably with the thermal trap depths described above. In the case of Ag-activated phosphors, however, the values obtained are 0.80 for In and 0.72 for Ga. The difference in calculated trap depths is 0.08 ev, however.

Equation [4] predicts a slope of minus one between log I_s/I_l and log C, and Fig. 10 shows such a dependence in the cubic ZnS:Cu,In system.

The ratio I_s/I_l was found to be approximately independent of excitation intensity. This experimental result is consistent with the prediction of the theoretical analysis in the Theoretical Analysis Section based on *s*-emission involving excited donor states of donor-acceptor pairs, and is contrary to the results of the analysis based on *s*-emission involving conduction electrons.

In the section on Experimental Results it was pointed out that a higher concentration of Ga than of In is necessary to make the long wave-length emission predominate. Superficially, this might seem in conflict with the model since Ga has the shallower trap depth and consequent greater spatial extension of its wave functions so that sufficient overlap for radiative transitions to a less closely associated ac-

Table I

	I, ev	II, ev	III, ev	IV, ev
Hex. ZnS:Cu, Ga	2.39	0.42	1.97	1.89
Hex. ZnS:Cu, In	2.39	0.50	1.89	1.88
Hex. ZnS:Ag, Ga	2.78	0.42	2.36	2.10
Hex. ZnS:Ag, In	2.78	0.50	2.28	2.02

I. Energy of short wave-length emission peak.
II. Trap depth of coactivator (10).
III. I-II calculated energy for long wave-length emission.
IV. Observed energy at long wave-length emission peak.

ceptor at a lower concentration would be expected. However, as is evident from Eq. [5] the ratio of occupational probabilities $P(\epsilon_s)/P(\epsilon_l)$ not only strongly favors the long wave-length emission but also is strongly dependent on the energy of the ground state of the donor. The Ga, compared to In, is less favored by this factor to emit in the long wave-length band so that an increased concentration of Ga over In is necessary to attain comparable values of I_s/I_l in these two materials.

In Table I, the energy at the long wave-length emission peak is compared to that calculated from thermal and optical data involving the trap depth of the coactivator and the emission peak of the short wave-length process, respectively. The difference in these two values should give approximately the energy of the long wave-length emission in accordance with Eq. [6]. In the Cu-activated materials, this relation is satisfied but with Ag-activated phosphors the calculated and observed values differ by 0.26 ev in both cases.[a] Because of this approximate agreement of Eq. [6] with experiment a lower limit on the value of l is suggested. From Eq. [7] an increase in the transition energy E_l for nearest-neighbor pairs ($l = 1$) of 3/4 ev is predicted for these phosphors; an increase of 1/2 ev for second-nearest neighbors pairs ($l = 2$); and an increase of 2/5 ev for third-nearest neighbors pairs ($l = 3$). Only $l \geq 4$ is consistent with the success of Eq. [6]. In addition, the interimpurity distance r_l is different for the cubic and hexagonal structures if $l \geq 3$, and this may account in part for the dependence on crystal structure of the relative intensities of the short and long wave-length bands.

An interesting sequel to the work reported here is a preliminary study of the effect of Cd substitution on ZnS phosphors showing the long wave-length emission. In hexagonal ZnS:10^{-4}Cu,In, substitution of up to 15 mole % CdS causes an increase in the ratio of intensities of the short wave-length to long wave-length emission at room temperature. These data are consistent with the analysis of the occupational probabilities of electrons in the emitting states of the s- and l-type centers as discussed in this paper. Up to 15% CdS substitution essentially decreases the depth of the ground state of the donor and thus increases the competition of the short wave-length process with the long wave-length process. A more detailed account of this work will appear in a future communication.

In summary, the long wave-length emission bands observed in ZnS:(Cu or Ag), (Ga or In) phosphors are attributed to transitions between the ground state of the donor and the ground state of the acceptor in highly associated coactivator-activator pairs. The short wave-length emission apparently involves transitions between excited donor states and the ground state of the acceptor in less highly associated pairs characterized by a distribution of interimpurity distances. The spectra and the dependence on temperature and on pair concentration of the intensities of the short and long wave-length bands are in accord with this model.

It is predicted that at low temperatures the centers responsible for the long wave-length emission should be capable of excitation at longer wave lengths than the short wave-length centers, and excitation of single crystals under these conditions with polarized light should yield polarized long wave-length emission since the highly associated pairs have a strong anisotropy.

[a] It should be pointed out that observed and calculated values of the long wave-length emission in ZnS:Au, In agree very well.

Acknowledgment

We wish to acknowledge the contributions from the following people: Mrs. D. J. Weil for sample preparation; Dr. J. S. Prener for suggestions and critical review; Dr. P. D. Johnson for glow-curve measurements; Dr. F. J. Studer for measurement of emission spectra.

Manuscript received Aug. 4, 1958. This paper was prepared for delivery before the New York Meeting, April 27-May 1, 1958.

Any discussion of this paper will appear in a Discussion Section to be published in the December 1959 JOURNAL.

REFERENCES

1. F. A. Kröger and J. Dikhoff, *Physica*, **16**, 297 (1950).
2. H. A. Klasens, *This Journal*, **100**, 72 (1953).
3. H. C. Froelich, *ibid.*, **100**, 496 (1953).
4. E. F. Apple, *ibid.*, **105**, 251 (1958).
5. J. S. Prener and F. E. Williams, *Phys. Rev.*, **101**, 1427 (1956); *This Journal*, **103**, 342 (1956); *J. phys. radium*, **17**, 667 (1956).
6. F. E. Williams, *J. Opt. Soc. Amer.*, **47**, 869 (1957).
7. J. S. Prener, *J. Chem. Phys.*, **25**, 1294 (1956).
8. H. Reiss, *ibid.*, **25**, 400 (1956).
9. F. E. Williams, To be published.
10. W. Hoogenstraaten, Thesis, University of Amsterdam, February 1958.

Effect of Various Etches on Recombination Centers at Germanium Surfaces

George Wallis[1] **and Shyh Wang**[2]

Sylvania Electric Products, Inc., Woburn, Massachusetts

ABSTRACT

Germanium samples were etched with CP-4, hydrogen peroxide, iodine A, electrolytic, and silver etch. The density, energy levels, and capture probabilities of the recombination centers were measured before and after the etched samples were baked. It was found that iodine A and electrolytic etches produce recombination centers of one type, and the remaining etches, centers of another type. Baking converted the centers found on iodine A etched surfaces into the type of centers that are characteristic of surfaces etched with CP-4, hydrogen peroxide, and silver etches. When surfaces were prepared with an etch other than iodine A, baking increased the density but did not affect the types of the centers. The different etches did not produce significant differences in maximum surface recombination velocity either before or after baking.

During recent years, it has become evident that the recombination process on germanium surfaces is described fully by the Shockley-Read theory (1). Good theoretical fits to experimental results can be obtained if it is assumed that the recombination centers are at discrete energy levels, and it has been our experience that within experimental error the same type of recombination centers is found on CP-4 etched surfaces irrespective of conductivity type. The present work was undertaken in order to find out what effect different etches have on the recombination centers. The etches under investigation were CP-4, hydrogen peroxide etch, iodine A etch, electrolytic etch, and silver etch (see appendix). Our results indicate that under favorable conditions all of the above etches produce comparable densities of recombination centers. However, iodine A and the electrolytic etch produce recombination centers of one type while the remaining etches produce centers of a different type. As far as maximum surface recombination velocity is concerned, a range of values between 100 and 200 cm/sec was found for all etches. Baking of the etched samples under atmospheric conditions at 100°C for periods in excess of 16 hr increased the density of recombination centers by varying amounts. In addition, baking converted the type of recombination center found on iodine A etched surfaces into the type characteristic of CP-4, hydrogen peroxide, and silver etch. Baking did not change the type of recombination center when the surfaces were treated previously with any etch other than iodine A.

Theory and Procedure

Previous investigation of the fast states at a CP-4 etched germanium surface has indicated that the following simple model is adequate (2). The fast states are located at four discrete energy levels within the forbidden gap, as shown in Fig. 1. Each of the levels is associated with four parameters, i.e., energy, density, capture probability for holes, and capture probability for electrons. The levels near the two band edges have a larger density than the levels near the center of the gap; however, the levels near the band edges have much smaller capture probabilities for electrons and/or holes. When the surface potential (energy difference between Fermi-level and intrinsic Fermi-level at surface) is in a range $-6\ kT$ to $+2\ kT$, the field effect is controlled by all four levels, but the surface recombination process is controlled primarily by the two levels near the center of the gap. The latter therefore will be referred to as surface recombination centers. It turns out that within experimental error the parameters in the theoretical expression for surface recombination velocity are the same for either recombination level. Hence, the two levels are regarded as constituting one type of recombination centers, having the same capture probabilities for holes and electrons. In view of these simplifications, we are concerned with ten rather than sixteen parameters, i.e., the densities and energies of the four levels, and the capture probabilities for holes and electrons of the pair of recombination centers.

When a freshly etched sample is exposed to various ambient atmospheres, some of these parameters

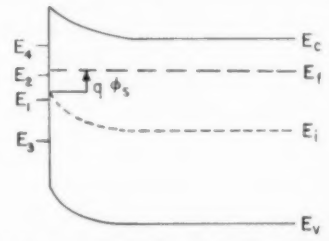

Fig. 1. Band structure of Ge near surface. E_1, E_2, E_3, and E_4 are the energy levels of the four groups of fast states at the germanium-oxide interface.

[1] Present address: Clevite Transistor Products, Waltham, Mass.

[2] Present address: Department of Electrical Engineering, University of California, Berkeley, Calif.

evidently change. A consistent interpretation is possible if it is assumed that only the densities of the pair of recombination centers change, and that they change in such a way that the ratio of the densities remains constant.

In the presence of a single type of recombination center with energy level E_t and capture probabilities for electrons c_n and for holes c_p, the photoconductance G_L of a thin sample[3] is given by

$$G_L = k\tau_{eff} = k\{1/\tau + N_t\,(c_p c_n)^{1/2}\,(n_s + p_s)/an_i[C + \cosh q\,(\phi_s - \phi_s)/kT]\}^{-1} \quad [1]$$

where k is a proportionality constant; τ_{eff} and τ are the effective and the bulk lifetime, respectively; N_t is the density of the centers; n_s and p_s are the equilibrium electron and hole concentrations; n_i is the intrinsic carrier concentration; a is the thickness of a sample; ϕ_s is the surface potential; $2q\phi_s/kT = \ln (c_p/c_n)$; $C = \cosh (E_i - E_t - q\phi_s)/kT$; and E_i is the intrinsic Fermi level. The effective lifetime is related to the surface recombination velocity v_s by the equation $\tau_{eff} = [1/\tau + 2v_s/a]^{-1}$.

A range of ϕ_s values can be obtained by exposing a sample to a Brattain-Bardeen cycle (3) of dry oxygen, sparked oxygen, and wet nitrogen. During the cycle, a series of simultaneous measurements of G_L and ϕ_s can be made. The determination of C and ϕ_s from the experimental curves of G_L vs. ϕ_s is straightforward provided N_t, C, and ϕ_s remain constant during a cycle. We believe that C and ϕ_s satisfy this condition. However, N_t did not remain constant on the freshly etched surfaces under discussion. Hence, C and ϕ_s had to be determined by a less direct method (4) which is independent of N_t.

When a small a-c field is applied normal to the surface of a sample, the change in photoconductance ΔG_L may be expressed as

$$\frac{\Delta G_L}{G_L} = (\tau_{eff}/\tau - 1)\,\frac{\sinh q\,(\phi_s - \phi_s)/kT}{C + \cosh q\,(\phi_s - \phi_s)/kT}\,\frac{q\Delta\phi_s}{2kT} \quad [2]$$

This equation contains the same parameters C and ϕ_s as Eq. [1], but it does not contain N_t explicitly. The change in surface potential with field, $\Delta\phi_s$, can be calculated from the field effect conductance, ΔG_s, for a given value of ϕ_s by use of the expression

$$\Delta G_s = \frac{\partial G_s}{\partial \phi_s}\,\Delta\phi_s \quad [3]$$

where $\partial G_s/\partial\phi_s$ is a known function of ϕ_s.

Experimentally, a series of simultaneous measurements of the following four quantities is made during a Brattain-Bardeen cycle: (a) surface potential ϕ_s, calculated from the d-c surface conductance; (b) field effect conductance, ΔG_s, for a small a-c field applied normal to the surface; (c) the a-c photoconductance G_L which results when a region of the sample is illuminated with chopped light from a water filtered light source;[4] (d) the change in conductance ΔG with an a-c field of the same strength as in (b), measured in the presence of d-c light of the same intensity as the chopped light in (c). ΔG (4) is found to be the sum of the change in photoconductance ΔG_L and the dark field-effect conductance ΔG_s.

From these four quantities, a plot of $\Delta G_L/G_L$ vs. ϕ_s may be constructed which can be fitted by Eq. [2] by means of the adjustable parameters C and ϕ_s. Relative changes in the density of the recombination centers can be deduced by comparing the experimental plot of G_L vs. ϕ_s with Eq. [1] into which the previously derived values of C and ϕ_s have been substituted.

Finally, the densities of the recombination centers and the other two surface states are deduced as follows. In the field-effect experiment, the total charge, induced by the a-c field, is the sum of the charge in the space charge region, ΔQ_{sc}, and the charge in the surface states, ΔQ_{ss}. The total induced charge is known, and ΔQ_{sc} can be computed for each experimental point from the equation

$$\Delta Q_{sc} = \frac{\partial Q_{sc}}{\partial \phi_s}\,\Delta\phi_s \quad [4]$$

where $\partial Q_{sc}/\partial\phi_s$ is a known function of ϕ_s, and $\Delta\phi_s$ is obtained from the field effect by use of Eq. [3]. Hence, one can construct a curve of ΔQ_{ss} vs. ϕ_s. From the latter, the density of each of the surface states can be deduced by curve fitting to the equation

$$\Delta Q_{ss} = q\sum_{n=1}^{4} N_{tn}\,\frac{\exp y_n}{(1 + \exp y_n)^2}\,\frac{q\Delta\phi_s}{kT} \quad [5]$$

where $y_n = (E_{tn} - E_i - q\phi_s)/kT$, and the summation is over the four states.

All samples used in this work were cut from a single crystal of n-type Ge. The resistivity of the samples was 18 ohm-cm and the bulk lifetime about 1000 μsec. All samples were oriented along the same plane (321) in order to exclude possible structural effects. The thickness of the samples was between 7 and 25 mil. Samples were hand polished, and their ends plated with Rh. Ohmic contacts were soldered to the plated ends, and two further contacts which served as voltage probes were soldered to one side of the samples. During an etch, the plated and soldered areas were masked by Apiezon W wax. After etching, the samples were rinsed in distilled water, the wax was dissolved in Triad,[5] and the Triad in turn was rinsed off with acetone, alcohol, and distilled water, in this order. After the last rinse was dried off, the sample was mounted in a glass holder and placed in a double-walled glass tube. Water from a thermostatically controlled tank was pumped through the region between the two walls. Thus, the temperature of the sample during a cycle was kept at 29° ± 0.05°C. Furthermore, the water served to filter out penetrating light.

The d-c conductance was measured to five significant figures. From the conductance, the surface potential was calculated without taking Schrieffer's correction (5) into consideration. The field-effect measurements were made with a 32 cps sinusoidal voltage, using essentially Low's circuit (6). The peak field strength was 4000 v/cm. The photoconductance

[3] The thickness a of the sample must be less than a diffusion length.

[4] The theoretical expressions hold only if injection is limited to the surface. Hence, nonpenetrating light must be used.

[5] Detrex Chemical Industries, Inc., Detroit, Mich.

Table I

Etch		$(v_s)_{max.}$ cm/sec.	$q\phi_o/kT = \frac{1}{2}\ln(c_p/c_n)$	C	$(N_{to})_1 \times 10^{-10}$, cm^{-2}	$(E_{t1}-E_i)/kT$	$(E_{t2}-E_i)/kT$	$\sigma_p \times 10^{16}$, cm^2	$\sigma_n \times 10^{16}$, cm^2	$(N_t)_2 \times 10^{-12}$, cm^{-2}
CP-4	Pre-bake	150	1.1	8	4.6	−1.7	3.9	27.6	3.1	0.7
	Post bake	306	1.1	6	8.2	−1.4	3.6	25.5	2.8	2.2
H_2O_2	Pre-bake	235	1.1	7	6.3	−1.5	3.7	30.0	3.3	0.8
	Post bake	535	1.4	7	12.9	−1.2	4.0	44.2	2.7	2.1
Iodine A	Pre-bake	162	1.9	8	4.6	−0.9	4.7	67.1	1.5	1.1
	Post bake	403	0.9	7	18.1	−1.7	3.5	14.7	2.5	2.2
Electrolytic	Pre-bake	131	1.9	8	2.5	−0.9	4.7	106.0	2.4	0.9
	Post bake	1100	1.9	6	16.7	−0.6	4.4	101.0	2.3	2.1
Silver	Pre-bake	170	1.1	10	7.3	−1.7	3.9	27.6	3.1	0.8
	Post bake	600	1.4	8	19.7	−1.4	3.6	25.5	2.8	—

Summary of results: $(N_{to})_1$ refers to the density of recombination centers below the intrinsic Fermi level and was measured at $\phi_s = \phi_o$. The density of the recombination centers above the intrinsic Fermi level was found to be $(N_{to})_2 = \frac{1}{2}(N_{to})_1$. $(N_t)_2$ refers to the density of the levels near the valence band which are seen in the field effect but are found to have a negligible effect on surface recombination. The values of $(N_t)_2$ were computed on the assumption that the level is located at $E_t - E_i = -6.8$ kT. The contribution of $(N_t)_2$ to the field effect was negligible on the silver-etched baked surface. The capture cross sections σ_p and σ_n for holes and electrons, respectively, refer to the recombination centers. They are related to the corresponding capture probabilities c_p and c_n by the equations $c_p = v_t\sigma_p$, $c_n = v_t\sigma_n$, where v_t is the thermal velocity 10^7cm/sec at room temperature.

was measured with light from a tungsten lamp chopped at 60 cps. The injection never exceeded 10% of the equilibrium bulk majority carrier concentration. Usually the photoconductance measurement was checked by a direct measurement of effective lifetime by means of the photoconductive decay method. The surface potential was changed by exposing the sample to Brattain-Bardeen cycles of sparked oxygen, dry oxygen or nitrogen, and nitrogen bubbled slowly through distilled water. The oxygen was sparked with a Tesla coil for short periods of time (usually less than a second). The gases were preheated to the temperature of the sample. Measurements were made before and after the samples were baked in a dry room atmosphere at 100°C for a period of 16 hr or more.

Results and Discussion

A summary of the results is presented in Table I. In Fig. 2, we show experimental points of $\Delta G_L/G_L$ and theoretical fits (solid lines) plotted as a function of ϕ_s for surfaces freshly etched with silver etch, electrolytic etch, iodine A etch, and H_2O_2 etch. Corresponding plots for CP-4 have been shown in a previous paper (2). It will be noticed that the theoretical plots (based on Eq. [2]) fit the experimental points quite closely throughout the experimental range of ϕ_s. Notice, also, that there appear to exist two distinct values of ϕ_o, i.e., 1.1 kT and 1.9 kT. The significance of these two values is discussed below. With ϕ_o given by the value of ϕ_s at which $\Delta G_L/G_L$ vanishes, C was the only parameter in each fit. From ϕ_o and C, the energy levels of the recombination centers were deduced for each curve.

Figure 3 presents curves of surface recombination velocity v_s vs. ϕ_s for the same surfaces as the curves in Fig. 2. For comparison's sake, we have added a theoretical curve (dashed line) based on Eq. [1], with the parameters C and ϕ_o, appropriate for the H_2O_2-etched surface and with $(N_t)_1$ and $(N_t)_2$ assumed constant. The experimental curve (triangles) is much flatter and rises beyond the maximum of the theoretical curve. The discrepancies between the experimental and theoretical curves are due entirely to changes in $(N_t)_1$ and $(N_t)_2$ during the cycle. If we had failed to take these changes into consideration,

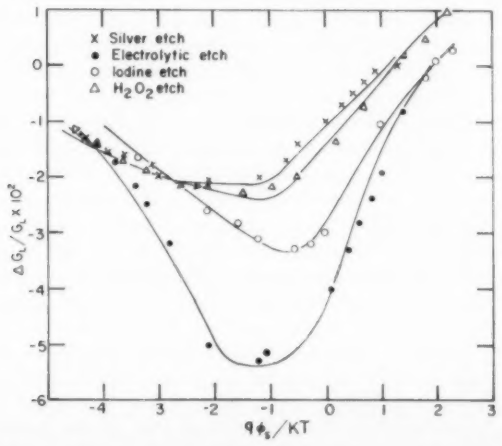

Fig. 2. $\Delta G_L/G_L$ vs. $q\phi_s/kT$ for variously etched Ge surfaces. Solid lines represent theoretical fits to the experimental data.

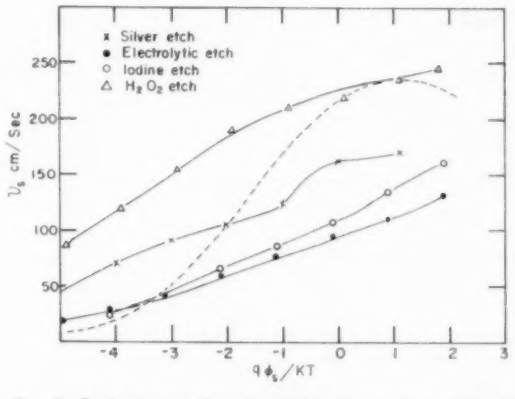

Fig. 3. Surface recombination velocity, v_s, vs. surface potential $q\phi_s/kT$ for the same surfaces as in Fig. 2. Solid lines represent the experimental data. Dashed curve was computed from Eq. [1] for the hydrogen peroxide-etched surface, with the parameters C and ϕ_o as deduced from the corresponding plot in Fig. 2, and with $(N_t)_1$ and $(N_t)_2$ assumed constant.

and if we had attempted to analyze the v_s vs. ϕ_s curves on the basis of Eq. [1], we would have obtained much larger values of C and ϕ_o. These values would have been inconsistent with the experimental $\Delta G_L/G_L$ curves.

By comparison of experimental and theoretical curves of v_s vs. ϕ_s, one can deduce whether relative changes in the density of the two recombination centers have taken place during a Brattain-Bardeen cycle. Typical relative changes for an H_2O_2 etched surface several days after etching (solid line) and after baking (dashed curve) are shown in Fig. 4. N_{t_o} is the density at the time ϕ_s was measured. N_t is not a function of ϕ_s but has been plotted against ϕ_s merely for convenience. For each curve, the extreme point at the left represents the density of centers immediately after oxygen was sparked. The extreme points at the right were in both cases taken in an ambient of wet nitrogen. Evidently, the baked surface was far more stable than the unbaked surface. Comparable amounts of sparking increased the density of centers on the unbaked surface by a factor of ten, as compared to an increase of less than two for the baked surface. Upon sparking, the unbaked surface became more p-type than the baked surface. On the other hand, in wet nitrogen, the unbaked surface became somewhat less n-type than the baked surface. Therefore, baking appears to make the surface more n-type. Moreover, the same Brattain-Bardeen cycle swung the surface potential of the unbaked surface through a larger range than that of the baked surface. Although these results were not strictly reproducible, these tendencies usually have been observed.

Figure 5 shows plots of $kT\Delta Q_{ss}/q\Delta\phi_s$ vs. ϕ_s for the same surfaces as in Fig. 2. The points were computed from the experimental plots of ΔG_s vs. ϕ_s, as described above. The theoretical fits are based on Eq. [7] which contains eight parameters, i.e., the densities and energies of the four levels. The energy levels near the band edges were far enough removed

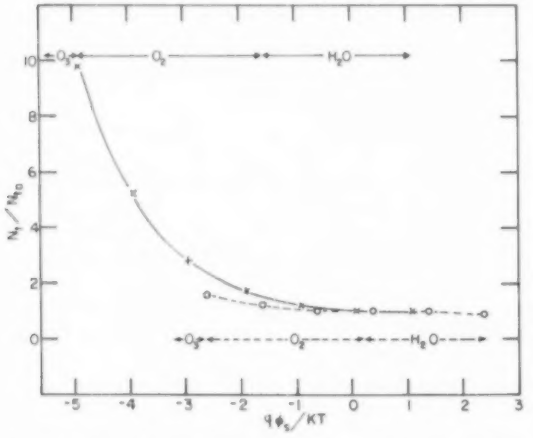

Fig. 4. Normalized density of the recombination centers, N_t/N_{t_o} vs. surface potential, $q\phi_s/kT$, for the hydrogen peroxide-etched surface during a Brattain-Bardeen cycle. Normalization was arbitrarily carried out at the point $\phi_s = \phi_o$. The solid curve refers to the freshly etched sample, and the dashed curve refers to the same sample after baking.

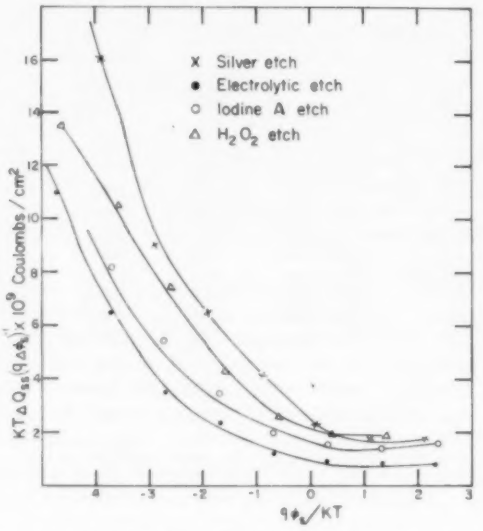

Fig. 5. Change of charge in the fast states per unit change in surface potential, $kT\Delta Q_{ss}/q\Delta\phi_s$, vs. surface potential, $q\phi_s/kT$, for the surfaces shown in Fig. 2 and 3. Solid curves represent theoretical fits to the experimental data.

from our range of ϕ_s values so that the two respective terms $N_{t_o} \exp y_n (1 + \exp y_n)^{-2}$, $n = 3,4$, could be replaced by $(N_t)_2 \exp y_2 = A_2 \exp(-q\phi_s/kT)$, where $A_2 = (N_t)_2 \exp(E_{t_2} - E_i)/kT$ for the level near the valence band $(E_{t_2} - E_i < 0)$, and by $(N_t)_1 \exp(-y_1) = A_1 \exp q\phi_s/kT$, where $A_1 = (N_t)_1 \exp -(E_{t_1} - E_i)/kT$ for the level near the conduction band $(E_{t_1} - E_i > 0)$. For the energy levels of the states near the center of the forbidden gap (recombination centers), we used the values deduced from Fig. 2. As previously stated, it was assumed that the ratio of the densities of the two recombination centers remained constant during a Brattain-Bardeen cycle. The relative changes in the density of either recombination center were read off from plots such as Fig. 4. Thus, the solid lines in Fig. 5 represent four parameter fits, the parameters being the densities $(N_{t_o})_1$ and $(N_{t_o})_2$ of the recombination centers and A_2 and A_1 of the centers near the band edges. The density $(N_{t_o})_1$ of the recombination center below the center of the gap, $E_{t_1} - E_i < 0$, has been found generally to be larger than the density $(N_{t_o})_2$ of the other recombination center. Almost invariably, the best fits were obtained by setting $(N_{t_o})_1 = 2\,(N_{t_o})_2$. The values for the density N_{t_2} of the fast states near the valence band were calculated from A_2 on the assumption (2) that the states were located at the level $E_t - E_i = -6.8\,kT$. This level could not be determined with great accuracy. The level near the conduction band contributed relatively little to the field effect. Hence, there is considerable uncertainty about the values of A_1, and since, in addition, there is some doubt about the location of the level, we did not calculate the corresponding densities.

Before the data can be discussed, one must make an estimate of the errors involved in the measurements. No over-all estimates can be given because the accuracy of the different measurements is not the same throughout the experimental range of ϕ_s.

For instance, near the minimum in surface conductance, a large change in ϕ_s corresponds to a small change in surface conductance so that accurate determination of ϕ_s is very difficult. However, when $\phi_s - \phi_{min}$[6] becomes larger than kT, the situation is reversed: a small change in ϕ_s corresponds to a larger change in surface conductance so that fairly accurate determination of ϕ_s becomes possible. On the other hand, the determination of ΔG_L is less accurate near $\phi_s = \phi_o$ than it is for other regions of ϕ_s since it represents the difference between two large quantities, i.e., ΔG and ΔG_s.

We estimate that our values of ϕ_o are reliable to $\pm 0.3\ kT$, the uncertainty being due to inaccuracy in the measurement of ϕ_s and ΔG_L. Values of C were obtained from fits to the $\Delta G_L/G_L$ vs. ϕ_s curves and are estimated to be accurate to 20%. The energy levels were calculated from the values of C and ϕ_o and are reliable to about $\pm 0.5\ kT$. The densities of the recombination centers were obtained from a comparison of three curves, i.e., $\Delta G_L/G_L$ vs. ϕ_s, ΔG_s vs. ϕ_s, and G_L vs. ϕ_s. Moreover, the values are quite sensitive to the exact values for the energy levels. Therefore, they are probably only reliable to about 50%. Finally, the error in the values of $\sqrt{c_p c_n}$ involving C and N_t is also of the order of 50%.

We can summarize the results as follows:

(i) The values of ϕ_o in Table I fall into two groups: one around 1.1 kT and the other around 1.9 kT. With an estimated error of $\pm 0.3\ kT$, one might at first sight hesitate as to whether this difference in ϕ_o should be interpreted as a single level or several levels. However, repeated experiments with electrolytically etched surfaces consistently gave larger values of ϕ_o than were obtained on CP-4 etched surfaces. Hence, we conclude that recombination centers exist at two types of discrete levels, a pair of "CP-4 levels" with a ϕ_o of about 1.1 kT and a pair of "electrolytic levels" with a ϕ_o of about 1.9 kT. It is seen from the table that the pair of "electrolytic levels" are separated by about the same energy interval as the pair of "CP-4 levels" but are displaced from the latter by about 0.8 kT. The capture probabilities for electrons, c_n, have approximately the same value for the two types of levels. However, the capture probabilities for holes, c_p, of the "electrolytic levels" are larger than those of the "CP-4 levels" by a factor of about three.

(ii) After samples etched with iodine A were baked, the initial "electrolytic levels" were found to have been replaced by CP-4 levels. On surfaces prepared with any of the other etches, the same type of centers were observed before and after baking. In all cases, the density of the recombination centers was larger after baking than before baking. The increase in the density of recombination centers during baking appears to take place in a few hours. Further baking at the same temperature has little effect on the density of the centers. This seems to argue for the existence of an equilibrium concentration of recombination centers.

If the baked samples are allowed to stand in a dry atmosphere at room temperature for several days, the density of the centers usually decreases somewhat from the high value immediately after baking. However, the density of centers never recovers to the initial value before baking.

(iii) When a sample is exposed to sparked oxygen, the changes in the density of recombination centers depend on three factors, (*a*) intensity of the spark, (*b*) duration of the sparking, (*c*) history of the sample. The changes are largest for freshly etched samples, and they are small for aged and baked samples. On freshly etched samples, the density of recombination centers often is increased by an order of magnitude when the ambient oxygen is sparked for a fraction of a second. No comparable increases in density have ever been observed after baking. Whereas recovery after baking is very slow and the decrease in density is small, after sparking the recovery is almost complete after about half an hour.

(iv) Exposure of a freshly etched sample to water vapor increases the density of recombination centers by amounts depending on (*a*) humidity, (*b*) length of exposure, and (*c*) history of the sample. The changes are quite gradual, but they can get as large as a factor of twenty if the sample is kept in a humid atmosphere for several hours.

When the humid atmosphere is replaced by a dry ambient, a slow recovery in the density of recombination centers usually is observed. Frequently, the density recovers to a value somewhat smaller than the value before exposure to water vapor. Sometimes, however, no change in density is apparent for an hour or more. A detailed study of these effects has not been made yet.

(v) Irrespective of which of the etches was used, the surface potential of a newly etched sample in a dry oxygen atmosphere was usually near the intrinsic Fermi level, but its exact value depended on the washing procedure after etching. After baking, the surface potential was invariably such as to make the surface more n-type. This is in agreement with the observation of other workers (7) according to which oxidation of a sample tends to make the surface n-type. We have also observed in agreement with other authors (7) that comparable Brattain-Bardeen cycles produce large changes in surface potential on some surfaces and small changes on others. There is an indication that baking and aging of the surface tends to cut down the range over which the surface potential can be changed. When a baked surface is rinsed in distilled water, the range over which the surface potential can be changed is increased and the density in recombination centers is decreased.

Baking, exposure to sparked oxygen, and exposure to water vapor all tend to increase the density of recombination centers and to decrease the range of surface potential. Baking and exposure to sparked oxygen clearly promote oxidation of the Ge surface. The effect of water vapor is more complicated. In part, water vapor may be expected to dissolve small amounts of soluble oxide. In part, water vapor appears to promote the oxidation of insoluble GeO to soluble GeO_2. Thus, our results strongly suggest that

[6] ϕ_{min} is the value of ϕ_s for minimum conductance and is given by $kT/q \ln(bn_o/p_o)$ where b is the ratio of electron to hole mobility.

the density of the recombination centers depends on the condition of the oxide films.

The recombination levels probably arise wherever there is a mismatch between the bulk Ge and the oxide film, at the edges and corners and at imperfections of any kind. Since the oxide films appear to be largely amorphous (8), epitaxical growth probably is confined to small regions where the films nucleate, and regions of mismatch abound. A further important source for imperfections may be the lack of stoichiometry in the film. For instance, surplus oxygen atoms at the interface could provide recombination levels. Another source of recombination centers may be fluorine which is believed to be present in the films (8). In general, it can be said that the density of the recombination centers is probably a measure of the amount of disorder at the germanium-oxide interface. We conclude, therefore, that such oxidation processes as baking, exposure to water vapor, and exposure to sparked oxygen all increase the degree of disorder at the interface. During subsequent exposure to a dry ambient, some degree of order is gradually restored. This throws an interesting light on the details of the oxidation process.

The results in (ii) suggest that not only the density but also the type of recombination centers depend on the oxide film. Any correlation between the type of recombination center and some property of the oxide film is extremely difficult as the following remarks show. Since the centers are probably at the germanium-oxide interface, one would expect that they would be affected only by a few monolayers of film nearest the interface. It is possible that these first monolayers are not representative of the rest of the film. In addition, the oxide films are probably inhomogeneous; both monoxide and dioxide as well as impurity atoms from the etching solution may be present in varying amounts (8). It should also be emphasized that the condition of the first few monolayers at the time of an experimental run may be different from their condition immediately after the etch. A time interval of at least several hours between etch and first run was required to mount the sample and allow it to get into thermal equilibrium with the tube. During most of this time, the sample was kept in a dry atmosphere, but it is nevertheless possible that changes occurred in the oxide film. Further changes undoubtedly occurred during the Brattain-Bardeen cycle. Whether, and to what extent, the few monolayers nearest the germanium-oxide interface were affected presumably depended on the thickness and porosity of the remainder of the film.

It is possible that both types of centers are present simultaneously on an etched surface. Usually, one type of center will be dominant, but in some cases, both may contribute to the recombination process in appreciable amounts. In such cases, our interpretation in terms of a single type of recombination center would be an oversimplification, and the parameters derived on the basis of such an interpretation would, in fact, represent averages over both types of centers. If this is the correct interpretation, it must, however, be assumed that the relative contributions of the two types of centers remained approximately constant during a Brattain-Bardeen cycle. Otherwise, the $\Delta G_L/G_L$ curves could not have been fitted with single values of C and ϕ_s throughout a cycle.

So far, the discussion has been limited to the centers near the intrinsic Fermi level which largely control the recombination process. The existence of another pair of levels near the band edges is indicated clearly by the field effect. The density of these levels is usually an order of magnitude larger than the density of levels near the center of the gap. However, their capture probabilities for electrons and/or holes are so small that their net effect on the recombination process is negligible in the range of surface potential which was used in this work. Likewise, the range of surface potential was too small to ascertain the energy of the levels with any accuracy. On relatively freshly etched surfaces the density of the levels near the band edges was increased by baking. It is possible that some changes in density also occurred during exposure to a Brattain-Bardeen cycle. However, in the analysis, we assumed that the density of the states near the band edges remained constant during a cycle so as not to introduce further parameters. From the quality of the fits in Fig. 4, it appears that, if changes in density did occur, they were relatively small.

Extensive work on the recombination centers on CP-4 etched surfaces has been reported by Brattain and Garrett (9) and by Many and Gerlich (10). The same levels were seen also in field effect measurements by Montgomery and Brown (11) and by Bardeen, *et al.* (12). All of these authors agree that there exists a discrete level near the conduction band and a discrete level near the valence band. There is, however, some disagreement as to whether the levels near the center of the gap are continuously distributed or discrete. Continuous distributions are assumed by Brattain and Garrett, Montgomery and Brown, and by Bardeen, *et al.* Two discrete levels are assumed by Many and Gerlich and by the authors. It is agreed generally that the field effect data at room temperature can be interpreted equally well on either assumption. The low temperature field-effect data of Montgomery and Brown also could be interpreted in terms of discrete levels provided the assumption is made that the density of the levels was smaller at low temperatures than it was at high temperatures. This assumption would explain the small slope of their low-temperature curve of change of charge in surface states vs. surface potential. Surface recombination velocity data have been fitted most closely when discrete levels were assumed.

A comparison of our results and those of Many and Gerlich will be made after a brief description of their procedures and underlying assumptions. Whereas we obtained variations in ϕ_s by exposing the sample to the Brattain-Bardeen cycle, Many and Gerlich varied ϕ_s by the application of high a-c fields normal to the two surfaces of a sample. Measurements of surface conductivity and effective lifetime were made at peak field, peaks of different ampli-

tudes corresponding to different values of ϕ_s. During a run, a sample was kept in a constant atmosphere. In analyzing their data, Many and Gerlich used essentially Eq. [1] and assumed that N_t as well as C and ϕ_s remained constant during a run. By contrast, our analysis was based on Eqs. [2] and [3] and the assumption that C and ϕ_s, but not N_t, remained constant during a run.

Both procedures are open to criticism. Many and Gerlich's assumption that N_t remains constant during a run may not be entirely correct in view of the observations by Statz, *et al.* (13) according to which large applied fields appear to produce changes in the density of surface states. It is frequently difficult to tell from an analysis of the v_s vs. ϕ_s curves whether changes in the density of recombination centers have, in fact, occurred during a run. On the other hand, our assumption that C and ϕ_s remain constant during a Brattain-Bardeen cycle also may be questioned. Indeed, Many and Gerlich conclude that the C and ϕ_s values on a CP-4 etched surface vary through a range larger than the experimental error, and that the values depend both on the history of the sample and on the ambient atmosphere. This would mean that several types of recombination centers can exist on CP-4 etched surfaces, with one type being dominant under one set of ambient conditions, and another type dominant under different ambient conditions. Such a view would present two difficulties:

1. According to Many and Gerlich, $C = 6$ in nitrogen and $C = 12$ in oxygen and sparked oxygen. In the part of the ambient cycle in which we changed from oxygen to nitrogen, the fit to the $\Delta G_l/G_l$ curve is quite sensitive to C, and a change in the value of C by 50% should have been easily detectable. No such changes have been found.

2. During repeated cycles, ϕ_s was found sometimes immediately after the oxygen was sparked, and sometimes, at a considerable time after sparking, during which time the sample stood in a dry oxygen or nitrogen atmosphere. Occasionally, ϕ_s was found in a cycle from which the sparking of oxygen was omitted. Since, according to Many and Gerlich, $\phi_s = 0.35\ kT$ in oxygen and nitrogen and $\phi_s = 0.97\ kT$ in sparked oxygen, one would expect to measure different ϕ_s values depending on the details of the cycle. Within experimental error, we have found no such dependence. Thus, we conclude that we observed during a Brattain-Bardeen cycle either a single type of recombination center or, conceivably, two types of centers whose relative contributions to the recombination process remained approximately constant during the cycle.

Possible explanations for the discrepancies between our results and those of Many and Gerlich are the following. The dependence of C and ϕ_s on an ambient gas may show up only after extended exposure of a sample to the gas. Alternatively, it is possible that once a surface has acquired the recombination centers characteristic of sparked oxygen, it becomes immune to the growth of other types of centers upon subsequent exposure to different ambients.

Another difference between the work of Many and Gerlich and ours is concerned with the interpretation of the parameter $C = \cosh\ (E_t - E_i - q\phi_s)/kT$. The v_s vs. ϕ_s curve has the same shape irrespective of whether recombination centers are located at the level $E_t - E_i = q\phi_s + kT$ arcosh C or at the level $E_t - E_i = q\phi_s - kT$ arcosh C or at both levels. Since ϕ_s/kT is assumed to be temperature independent, the correct level could be deduced in principle from the measurement of C at two different temperatures. Temperature measurements were made by Many and Gerlich, and the results suggest that the recombination center lies at the level $E_t - E_i = q\phi_s + kT$ arcosh C. However, the results are not sufficiently accurate to make this conclusion altogether convincing. We rather incline to the view that recombination centers are located at both levels because the field effect measurements indicate that there exist fast states at both these levels. As far as the principal conclusions of this work are concerned, it does not matter whether one or both of the levels act as recombination centers.

A numerical comparison of results for CP-4 etched surfaces follows. Many and Gerlich find ϕ_s to have a range of values between 0.35 and 1.70 kT under the ambient conditions: vacuum, oxygen, nitrogen, hydrogen, and sparked oxygen. This is to be compared to our value of $1.1 \pm 0.3\ kT$. Many and Gerlich's values for C under the above ambient conditions range from 6.1 to 29.0, while the values found by us for all etches before and after baking are in the range 8 ± 2. From their values of C and ϕ_s, Many and Gerlich calculate that the recombination centers are located at a range of $E_t - E_i$ between 2.9 and 6 kT compared to our corresponding range $3.9 \pm 0.5\ kT$. From their field-effect measurements, Many and Gerlich find another state at about $-1\ kT$. Our corresponding value is $-1.7 \pm 0.5\ kT$. If Montgomery and Brown (11) interpret their field-effect data on the basis of discrete levels, they also find these levels at 3.9 kT and $-1\ kT$. In the calculation of ϕ_s, Many and Gerlich used the Schrieffer correction whereas Montgomery and Brown and the authors did not. Within the range of ϕ_s under discussion, the Schrieffer correction is not important.

The effect of various etches on surface recombination velocity has also been investigated by McKelvey and Longini (14). Their results indicate that progressively larger surface recombination velocities are obtained on n-type germanium with silver, hydrogen peroxide, CP-4, and electrolytic etches. However, large spreads in surface recombination velocity were produced in repeated treatments with a particular etch, and the spreads for different etches were found to overlap. These results cannot be strictly compared with ours because simultaneous measurements of surface potential were not made. However, if McKelvey and Longini made their measurements on thoroughly dried samples and in a dry atmosphere, it is probable that their results represent only 50% or less of the respective maximum surface recombination velocities, corresponding to $\phi_s - \phi_s > 3\ kT$. If this assumption is made, our values of surface recombination velocity (see Table I) are consistent with their range of values. Unlike McKelvey and Longini, we did not observe that some etches produce consistently smaller surface recombination velocities than others.

Acknowledgments

The authors are grateful to P. Wang and J. Flynn for assistance with the chemical aspects of this work and for valuable discussions.

Manuscript received May 15, 1958. This paper was prepared for delivery before the New York Meeting, April 27-May 1, 1958.

Any discussion of this paper will appear in a Discussion Section to be published in the December 1959 JOURNAL.

REFERENCES

1. W. Shockley and W. T. Read, *Phys. Rev.*, **87**, 835 (1952); See also D. T. Stevenson and R. J. Keyes, *Physica*, **20**, 1041 (1954).
2. S. Wang and G. Wallis, *Phys. Rev.*, **107**, 947 (1957).
3. W. H. Brattain and J. Bardeen, *Bell System Tech. J.*, **32**, 1 (1953).
4. S. Wang and G. Wallis, *Phys. Rev.*, **105**, 1459 (1957).
5. J. R. Schrieffer, *ibid.*, **97**, 641 (1955).
6. C. G. E. Low, *Proc. Phys., Soc. (London)*, **B68**, 10 (1955).
7. M. Lasser, C. Wysocki, and B. Bernstein, *Phys. Rev.*, **105**, 491 (1957).
8. S. G. Ellis, *J. Appl. Phys.*, **28**, 1262 (1957).
9. W. H. Brattain and C. G. B. Garrett, *Bell System Tech. J.*, **35**, 1019 (1956); C. G. B. Garrett and W. H. Brattain, *ibid.*, **35**, 1041 (1956).
10. A. Many and D. Gerlich, *Phys. Rev.*, **107**, 404 (1957).
11. H. C. Montgomery and W. L. Brown, *ibid.*, **103**, 865 (1956).
12. J. Bardeen, R. E. Coovert, S. R. Morrison, J. R. Schrieffer, and R. Sun, *Phys. Rev.*, **104**, 47 (1956).
13. H. Statz, G. A. de Mars, L. Davis, Jr., and A. Adams, Jr., "Semiconductor Surface Physics," p. 139, University of Pennsylvania Press, Philadelphia (1957).
14. J. P. McKelvey and R. L. Longini, *J. Appl. Phys.*, **25**, 634 (1954).

APPENDIX

The composition of the five etches used in this work are given below. The reagents are: 70% HNO_3, 48% HF, 30% H_2O_2, 100% HAc.

CP-4: 50 cc HNO_3, 30 cc HAc, 30 cc HF, 0.6 cc bromine.
Hydrogen peroxide: 10 cc HF, 20 cc H_2O_2, 20 cc H_2O.
Iodine A: 30 cc HNO_3, 33 cc HAc, 15 cc HF, 90 mg iodine.
Electrolytic: 2M KOH, 3 v.
Silver: 20 cc HNO_3, 40 cc H_2O, 40 cc. HF, 2 g $AgNO_3$.

Principles and Applications of the Iodide Process

A. C. Loonam

Consulting Engineer, 70 East 45th Street, New York, New York

ABSTRACT

The thermodynamic factors favoring deposition of elements from vapors of their iodides are the low heats of formation of those iodides and the ease with which diatomic iodine dissociates at moderately high temperatures. The vapor pressure of the element and the stability of its lower iodides determine the temperature and pressure range in which deposition can occur. The lower pressure limit for deposition at a given temperature is set by the vapor pressure of the deposited element and the upper limit by the stabilities of the lower iodides. At very low pressures, deposition is a first order heterogeneous reaction, every iodide molecule which strikes the surface adding to the deposit. As the pressure is increased, the deposition rate falls off and eventually becomes zero order, the rate being governed by that at which I atoms evaporate from the saturated surface. At higher pressures the deposition reaction is diffusion-controlled. Factors influencing the character of the deposits, the removal of impurities, and the deposition of alloys are discussed.

The iodide process was introduced by van Arkel and de Boer in 1925 (1). Shapiro (2) gave an excellent account of the development of the process through about 1954. Much of the information in the Government reports to which he referred has since appeared in the technical literature or in patents.

The elements which have been deposited by the iodide process and convenient temperatures for their deposition are listed in Table I.

Some Fundamentals of the Process

To be capable of being refined by the van Arkel-de Boer process, an element must fulfill two requirements:

1. It must be capable of existing in a solid or liquid state at some condition of temperature and pressure in equilibrium with gas containing a high atomic ratio of iodine to element. Thus, both Ti and Zr are in equilibrium with gases containing ratios of I to metal of 80 and higher at temperatures of 1100°C and above at low pressures. It is desirable that the element have a high melting point and a low vapor pressure to permit deposition as the more convenient solid at pressures where high efficiency can be obtained; but neither is essential as shown by the deposition of molten U and the fact that the relatively volatile Si can be deposited from the vapor of its tetraiodide just as well as the much less volatile Zr.

Table I. Elements prepared by thermal dissociation of their iodides

Element	Deposition temperature, °C	Element	Deposition temperature, °C
Be	700-900	Si	1000
Cr	1100	Th	1700
Cu	900	Ti	1400
Fe	1100	U	1100
Hf	1600	V	1200
Ni	1030	Zr	1400
Pa	—		

2. The element must be capable of reacting readily with the gaseous products of the deposition reaction at the same pressure and another temperature to yield a gaseous product with a low atomic ratio of I to element. For example, crude Ti and Zr react readily with I at temperatures in the neighborhood of 200°C to produce gaseous TiI_4 and ZrI_4.

These two statements are perfectly general. It is not essential that the deposition temperature be higher than that of the crude. In an excellent recent paper, Schäfer and Morcher (3) showed that Si can be made to travel either up or down a temperature gradient via the vapors of its iodides by varying the pressure, high pressures favoring transport down the gradient owing to the reversible reaction

$$SiI_4 + Si = 2SiI_2 \qquad [1]$$

and low pressures favoring transport up the gradient via dissociation of SiI_2 and SiI_4

$$SiI_2 = Si + 2I \qquad [2]$$

$$SiI_4 = Si + 4I \qquad [3]$$

In both cases the Si is transported from the region where a gas with a low atomic ratio of I to Si is in equilibrium with the element to the region in which this ratio is higher.

Theoretically, at least, a pressure gradient should have the same general effect as a temperature gradient. Thus, at a suitable temperature, a relatively low pressure should cause reaction [1] to proceed as written, while increasing the pressure should cause it to reverse, thus making Si travel up the pressure gradient. Conversely, reactions [2] and [3] take place at low pressures, but are reversed at higher pressures with the result that Si travels down the pressure gradient.

However, all applications of the iodide process to date have been based on formation or supply of iodide vapors at low temperatures and pressures and their dissociation at high temperatures at essentially the same pressure, i.e., transport up a temperature gradient. Accordingly, this discussion is confined to that phase of the subject.

Thermodynamics of the Process

The most important thermodynamic factors in the iodide process are the low heats of formation of the iodides and the ease with which diatomic iodine dissociates. The latter, data for which are given in Table II, is perhaps the more important of the two factors because, especially with the higher valence elements, it produces a large increase in the number of moles of gas when the iodides dissociate. Accordingly, the dissociation reactions have large positive entropies and, even though the heats of formation of the iodides are moderately high, the free energies of dissociation decrease rapidly with increasing temperature. Thus, $\Delta S°$ at 25°C for the reaction

$$ZrI_{4(g)} = Zr_{(c)} + 4I_{(g)}$$

is about +75 e.u. Furthermore, the expression for the equilibrium constant for this reaction contains the pressure of atomic I to the 4th power, so that even if the value of this constant is rather small, it can still mean that a respectable pressure of I vapor exists in equilibrium with the metal.

Table II. Dissociation of diatomic iodine

Temp., °C	K*	Percent dissociated at 1 atm	100 mm	10 mm	1 mm	0.1 mm
600	2.10×10^{-4}	0.72	2.00	6.31	19.6	53.4
800	1.09×10^{-2}	5.2	14.2	41.4	82.1	97.7
1000	0.166	19.9	48.9	87.1	98.4	
1100	0.482	32.8	69.1	95.0		
1200	1.22	48.3	83.5	97.9		
1300	2.73	63.7	91.6			

* Equilibrium constant, $(pI)^2/pI_2$; p in atmospheres.

It follows from the foregoing that the process should become less well adapted in going from tetraiodides to tri-, di-, and monoiodides. Although, as will be seen later, other factors are also important, this is generally true. It is the author's opinion that monomeric monoiodides which have respectable stabilities in the vapor state cannot be decomposed by dissociation to give solid or liquid metal. Since there is only one mole of gas on each side of the reaction equation, there is no pronounced increase in entropy and therefore no marked reduction in free energy upon heating. The fact that deposition of Ag from AgI vapor has not been reported is to be expected on this basis. It also follows that an element forming a stable gaseous monomeric monoiodide cannot be deposited by dissociation. Indeed, it can readily be shown that deposition of a metal by dissociation of a gaseous iodide, MI_n, requires that the equilibrium constant at the deposition temperature for the reaction,

$$MI_{(g)} = M_{(c,\ l)} + I_{(g)}$$

be greater than $(n\text{-}1)$, i.e., MI must be definitely unstable and to a greater extent the greater the value of n.

The author believes that the monoiodides of Al and perhaps those of the rare earth metals are sufficiently stable to prevent deposition by dissociation. Like Al, such metals probably could be transported down a temperature gradient by disproportionation. In this connection it is to be expected that a high heat of vaporization of the element to be deposited would favor instability of a monoiodide, causing it to break down to the condensed element and gaseous atomic I.

However, if the monoiodide is polymeric in the vapor state, conditions would be quite different. Thus, Brewer and Lofgren's (4) results indicate that the cuprous halides exist as trimers in the vapor state. The condition is now

$$Cu_3I_{3(g)} = 3Cu_{(c)} + 3I_{(g)}$$

indicating a considerable entropy increase. The fact that deposition of Cu from its iodide has been reported therefore is excellent independent evidence of the soundness of these workers' views.

The fact that many of the transition metals are deposited readily from the vapors of their diiodides

may be attributed to the low heats of formation of these vapors resulting from their relatively high heats of vaporization. A comparatively small entropy increase therefore is sufficient to promote instability on heating. There is also good evidence that they are dimeric so that the entropy situation becomes similar to that of the tetraiodides with the advantage that two atoms of metal are deposited for every iodide molecule decomposing.

It is readily apparent that there must be, at any given temperature, a lower pressure limit below which deposition cannot take place. This is at the point where the rate of deposition just equals the rate of evaporation of the deposited element due to its own vapor pressure. At lower pressures the rate of evaporation will exceed that of deposition and there will be a net loss or "chewing" of the deposit.

It is not so readily apparent that an upper pressure limit can also exist. This happens with tri- and higher iodides if subiodides above the mono compound have appreciable stabilities in the gaseous state. Under such conditions there must be a pressure at which the atomic ratio of I to element in the gases in equilibrium with the deposit just equals that in the iodide used for transport. There is therefore no deposition at this point. Reduction of the pressure below this value results in deposition, while an increase produces attack or chewing. The author discovered this situation in the deposition of Ti from TiI, many years ago (5), a fact later confirmed by Runnalls and Pidgeon (6) who located this point at a TiI, pressure of 38 mm Hg at 1500°C. Schäfer and Morcher (3) located it at several temperatures in the Si-SiI, system, e.g., 15 mm of SiI, at 1160°, calling it "the critical decomposition pressure"; while Emelyanov, Bystrov, and Evstyukhin (7) found it in the Zr-ZrI, system.

Plotting of the percentage iodide decomposition at equilibrium against the pressure in such a system yields a curve which starts at zero at the pressure corresponding to the lower deposition limit, rises to a maximum, falls off to zero again at the upper deposition limit, and then passes into the region of negative decomposition or attack. Such a curve for deposition of Sn from SnI, at 1300°C is shown in Fig. 1.

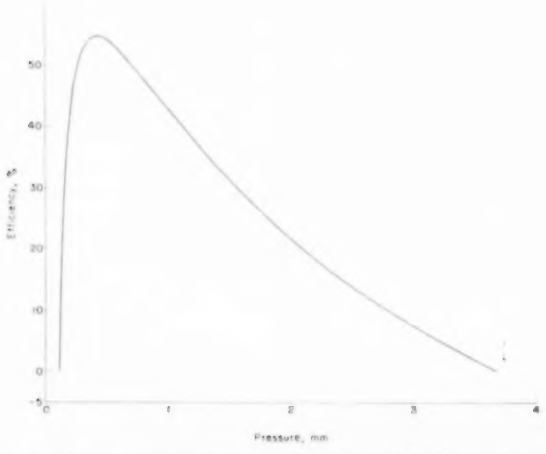

Fig. 1. Equilibrium efficiency deposition of Sn from SnI, at 1300°C.

In general, the value of the upper critical pressure increases with temperature. It can also be raised by reducing the ratio of I to element in the gas contacting the deposition surface and indeed may disappear altogether, but the fact remains that there will be no net decomposition of the highest iodide at pressures above its upper deposition limit. In this connection, it is important to note that, given a fixed temperature and pressure in the presence of deposit and I gases alone, the equilibrium composition of the gases will be the same regardless of the starting material.

In systems where lower iodides do not exist, the decomposition efficiency-pressure curve starts at zero and rises to a maximum as before, but then falls more slowly, approaching the zero axis asymptotically.

Given sufficient reliable thermodynamic data, it is relatively easy to calculate whether a given element can be deposited from the vapors of its iodides and, if so, the pressures and temperatures at which it can occur and the equilibrium efficiencies obtainable. At present, however, although the situation is slowly improving, no such fund of data is available for any element. It is therefore necessary to resort to estimates and even educated guesses. On the basis of these and also by analogy with other cases the author believes that B, C, Co, Ge, Mo, Nb, Ta, Sn, and perhaps Re, can be deposited from the vapors of their iodides. This statement does not mean that all of these elements can be refined by the van Arkel-de Boer process. In some cases, e.g., carbon, it would be necessary to prepare the iodide by an external process.

Kinetics of the Deposition Reaction

The writer believes that in the region represented by the lefthand leg of the curve in Fig. 1 and at low pressure, i.e., in the free molecule region where the Knudsen number (the ratio of the mean free path to the diameter of the deposition surface) is greater than about 10, the deposition reaction is a heterogeneous one, the rate being given by the Knudsen equation with an accommodation efficiency of unity, i.e., every iodide molecule which strikes the surface adds to the deposit. The reaction is therefore first order modified perhaps by the rate of evaporation of the metal itself, the activation energy is zero, and the deposition rate is proportional to the exposed surface area. This high efficiency is in accord with the findings of Holden and Kopelman (8) and Döring and Molière (9) with Zr. The author calculated the vapor pressure of TiI, from Fast's deposition rate at a bulb temperature of 50°C on this basis, and obtained a value which, when combined with that at the melting point derived from the data of Blocher and Campbell, yielded a figure for the heat of fusion of TiI, only 1.3% lower than that determined calorimetrically. Furthermore, calculation of the vapor pressure of ZrI, from Fast's rate of deposition of Zr at 150°C gave a value equal to 72% of that given by Rahlfs and Fischer's simple log $P - 1/T$ equation (10) and

120% of that obtained from the free energy equation using what is believed to be an accurate expression for the specific heat difference. Finally, rates of deposition of chromium from CrI_2 vapor were very close to 1.4 times those to be expected on the basis of measurements of the vapor pressure of the iodide if it were a monomer in the gaseous state and almost exactly that to be expected if it were a dimer, thus providing evidence that the latter is the case. Indeed, measurement of the rate of deposition of a metal is recommended as a method for determining the vapor pressure of its iodides at low pressures (11).

Since the primary deposition reaction is so highly efficient, it follows that it must be at least nonendothermic and more probably strongly exothermic. In the author's opinion the only one which can fulfill this requirement is the direct reaction of the incident molecule with the deposition surface to produce an atom of deposit and a chemisorbed monolayer of I atoms, i.e.

$$MI_n(g) = M_{(c)} + nI_{(ads)}$$

Such a mechanism would require heats of adsorption of I atoms on Ti and Zr of at least 42 and 50 kcal, respectively. They could be considerably higher than these values and still be consistent with that of 53.7 kcal found by Van Praagh and Rideal (12) for I atoms on Pt. The author believes that the chemisorbed I is mobile at deposition temperatures and that it evaporates at a rate consistent with its heat of adsorption.

On the basis of this mechanism, the deposition reaction should be first order with 100% efficiency so long as a large part of the deposition surface is free of adsorbed I, the rate of evaporation of I atoms just equalling that of deposition. On continued increase in pressure, however, the chemisorbed I layer covers a larger and larger fraction of the surface until ultimately it forms a complete monolayer. At this point the deposition reaction should become zero order, the deposition rate being governed solely by the rate of evaporation of the I. There is meager evidence that the point of complete surface coverage is identical with the maximum in the equilibrium efficiency curve of Fig. 1.

It is to be expected that any free I striking the deposition surface will also deposit with 100% efficiency. If its pressure and therefore its deposition rate is high enough to cause formation of the monolayer, it should reduce the rate of metal deposition, but it should have little or no effect at lower pressures.

It is believed that the foregoing mechanism applies to cases, such as the deposition of Cr from Cr_2I_6, in which lower iodides do not play any part. If, on the other hand, lower iodides can be formed, the reaction also approaches zero order, but attack of the metal begins via the I monolayer. This is in accord with the results of Langmuir on the reaction of oxygen with tungsten. He found (13) that at low pressure, oxygen formed a chemisorbed monolayer of atoms on the tungsten surface which evaporated as atoms at high temperature and was not readily reduced by hydrogen or other reducing agents. Furthermore, it showed no tendency to form WO_3. On raising the pressure of oxygen above that required to form the monolayer, however, formation of WO_3 set in.

The foregoing picture applies only to the free molecule region. As the pressure is increased with suitable adjustment of the temperature to maintain deposition, a point is ultimately reached where diffusion becomes an important, and ultimately, the controlling factor, the deposition rate being governed by that at which the iodide molecules diffuse to the deposition surface through the adjacent stationary gas film and the I atoms diffuse away.

Schäfer, Jacob, and Etzel have recently published two important papers on this phase of the subject (14, 15), in the first of which they discuss the theory of the transport of condensed phases through a temperature gradient via reversible gaseous reactions, and in the second of which they give experimental data for the transport of Fe and Ni via the vapors of their iodides and present calculations showing that the results can be accounted for by assuming equilibrium at both ends of the gradient with transport by diffusion. They secured good agreement between experimental and calculated results on the basis of diffusion coefficients derived from kinetic theory. They bring out that their treatment holds only within a definite pressure range. Presumably at lower pressures the foregoing free molecule form of transport applies, while at higher pressures transport is promoted by convection. Schäfer and Morcher (3) also discuss this subject.

One consequence of diffusion control is that the rate of deposition on a cylindrical surface, such as a filament coaxial with a cylinder of crude, becomes constant per unit length and independent of filament diameter. Shapiro and others (2) analyzed this situation and showed that the rate should be not quite independent of filament diameter, but inversely proportional to the log of the ratio of the inside diameter of the cylinder of crude to the diameter of the filament, similar to the conduction of heat radially through a cylindrical wall. In the corresponding heat transfer case, Kyte, Madden, and Piret found (16) that the ratio of the effective diameter of the stationary gas film to that of the filament was an inverse function of the Grashof and Prandtl numbers and the ratio of diameter to the length of the filament. They also took the mean free paths of the gas molecules into account at low pressures and small filament diameters.

Some of the foregoing statements regarding conditions in the range where diffusion is controlling must be accepted with qualifications. The one that the deposition rate on a filament is nearly independent of diameter is true only for relatively large diameters. That this must be so follows from the simple fact that, given any reasonable rate of deposition per unit length of, say a ½-in. filament and indefinitely reducing the diameter, a point must be reached where the original deposition rate cannot possibly be maintained because an insufficient number of iodide molecules strike the surface.

The surface reaction then becomes controlling and the rate proportional to the square of the diameter. A relation beween the deposition rate as a function of diameter and the Knudsen number probably exists for any given temperature, although the change in the diffusion gradient would also have to be taken into account.

The assumption of equilibrium at both ends of a temperature gradient is probably valid for systems in which both temperatures are high and also at the high temperature ends of other systems, but it certainly is not valid in the refining of Ti, Zr, and probably Hf with crude temperatures of 100°-200°C. These processes depend on the dynamic formation of the volatile tetraiodides instead of the much less volatile di- and triiodides which are in thermodynamic equilibrium with the metals. Under equilibrium conditions it is necessary to go to temperatures above 400°C to secure adequate vapor and dissociation pressures of the lower iodides.

These metals therefore have two distinct ranges of crude temperatures in which the process can be operated and which, as will be seen later, can yield deposits of quite different properties. As Fast has shown with Ti (17) and Döring and Molière with Zr (9), a temperature range of zero or low deposition rate can be found between them under suitable conditions, the lower limit of this gap being determined by the upper pressure deposition limit of the tetraiodides and the rate at which they are reduced, and the upper limit by the vapor and dissociation pressures of the lower iodides. Incidentally, the author believes that the tetraiodides are the primary products of the reaction of I with these metals at low temperatures and that formation of lower iodides is a secondary reaction.

Finally, the assumption of a simple diffusion gradient in the cases of Ti and Zr may be an oversimplification. In the range between 200° and 1400°C, two potentially important processes can take place in the gas phase, namely combination of I atoms at temperatures below about 900° and tetraiodide dissociation above 1000°C. There is reason to believe that both processes should be active even at the low pressure ordinarily prevailing. It is known that such reversible reactions markedly increase the thermal conductivity of a gas and they could have similar effects on other transport properties. It is possible that relatively few tetraiodide molecules reach the deposition surface at high surface temperatures and pressures where diffusion is controlling.

As Shapiro showed when he compared the rate of deposition of Zr from cut up crystal bar with that from Kroll process sponge (2), the reactivity of the crude can also be rate-controlling.

Removal of Impurities

In general, the purpose of an iodide process is to secure a high purity product. The elimination of impurities is therefore of the utmost importance. Both equilibrium and dynamic considerations are important in this connection.

If the iodide to be dissociated is prepared in a separate operation, it can be purified by any of the usual methods, filtration, fractional condensation, crystallization from a solvent, sublimation, fractional distillation, and even zone refining (18-20). Furthermore, these unit operations can be modified to meet special requirements. Thus KI has been added to a mixture of TiI_4 and AlI_3, which have very similar boiling points, to form $KAlI_4$ which is not volatile at a low red heat and from which the TiI_4 can be readily boiled away (21). Again, Zr and Hf have been separated by taking advantage of the difference in reducibility of their tetraiodides to less volatile lower iodides (22). Finally, U and Zr have been separated in a mixture of iodides produced by iodination of reactor fuel by fractionally condensing the less volatile U iodide and allowing the ZrI_4 to pass on (23).

One is somewhat more restricted when the operation is confined to a single unit as in the de Boer-van Arkel process, but even here advantage can be taken of a number of equilibrium and dynamic effects. In this connection, it is worth noting that I does not react with C or the oxides of any of the heavy polyvalent metals except perhaps those of Cd and Hg at any reasonable temperature. Indeed, the reverse is the case. The iodides of these metals can readily be roasted to oxide and iodine vapor in air or oxygen.

Probably the elements most readily refined by the de Boer-van Arkel process are Ti, Zr, and Hf. At the low crude temperatures possible when transfer takes place via the volatile tetraiodides, nitrides, carbonitrides, silicides, and perhaps other intermetallic compounds, as well as oxides and carbides, are unattacked, while the iodides of divalent metals have negligible vapor pressures if they are formed.

To secure the maximum benefit of these advantages, it is necessary to maintain a low temperature of the crude metal. This material can have considerable resistance to heat flow and, if reasonably thick, the surface facing that on which deposition is taking place can have a temperature at which the divalent iodides have large vapor pressures, carbonitrides and silicon are attacked by iodine, and even carbon monoxide can be formed by reaction of liberated carbon with oxides with consequent transfer of both components. Carbon monoxide can exist in equilibrium with iodine and iodide vapors at high temperatures.

Close control of the temperature of the crude may permit some interesting separations. Thus, Fast (24) secured no appreciable deposit from ZrI_4 at a bulb temperature of 100°C because of the low vapor pressure of the iodide, but he secured a considerable deposit of Ti from TiI_4 at a bulb temperature of 50° (17). Possibly Zr and Hf might be separated similarly.

One apparently neglected field has been the introduction of foreign substances into the units to aid in separations. This would seem to have definite possibilities. Thus, following Blumenthal and Smith (21), KI might be introduced into a Ti unit to prevent transfer of Al and other metals. Similar separations might be made among the fourth group

metals. Thus, KI does not form a complex with TiI_4 but it may with ZrI_4 or HfI_4. It is worth noting in this connection that there is less tendency to complex formation in the tetraiodide-alkali iodide systems than in the corresponding chloride systems, but that the tendency increases with the atomic weight of the alkali metal. Thus, K_2SnCl_6 is well known, but only Rb_2SnI_6 and Cs_2SnI_6 are known in the anhydrous state.

Another possibility is the introduction of an oxide. Chaigneau recently published two papers on the preparation of a large number of iodides by reaction of the corresponding oxides with AlI_3 at moderate temperatures (25, 26). Of the 29 oxides tried, 26, including TiO_2 and ZrO_2, yielded pure iodides; only one, Cb_2O_5, yielded an appreciable quantity of oxyiodide; and two, Cr_2O_3 and B_2O_3, did not react. There was no report on SiO_2.

Presumably, then, the presence of TiO_2 in a Ti bulb could prevent transfer of Al if the reaction rate were fast enough. Indeed, it should be possible to make up a list of elements in order of ease of conversion of their oxides to iodides with the alkali metals at the top and B and Al near the bottom.

Formation of stable "intermetallic" compounds does not appear promising from a thermodynamic standpoint because of the presence of free I in the system. However, empirical research could disclose compounds of value because of the slowness with which they react. Thus, addition of C might reduce the rate of transfer of strong carbide formers, while Ti might prevent transfer of N.

Application of the de Boer-van Arkel process to the divalent transition metals as well as U, and, to some extent, Th, presents greater difficulties because the high crude temperatures necessary to secure useful iodide pressures promote attack on nitrides and other relatively inert compounds as well as formation of CO by reaction of C with the generally less stable oxides. Furthermore, all iodides have appreciable vapor pressures at these temperatures, making separations more difficult.

Another factor of importance in the case of Cr, V, Fe, Co, and Ni is that their diiodides have appreciable dissociation pressures in the temperature range where their vapor pressures are appreciable (15, 27-29). Accordingly, the I pressure gradient is from that at the deposition surface to a finite value and not to zero at the crude. This could mean that, if there were any considerable temperature gradient in the crude metal, the vapor pressure of the iodide would tend to be fixed by the cold end of that gradient and the minimum I pressure by the hot end. This would reduce diffusion of both components with a consequent reduction in deposition rate.

However, the situation is by no means entirely unfavorable, as shown by the appearance of iodide chromium on the market. Because of the instability of the iodide vapors, deposition surface temperatures can be considerably lower than for the Ti group metals (cf Table I).

When operated under optimum conditions, the process can yield products of extraordinarily high purity. On the basis of his experiments with spent uranium reactor fuel, Robb (23) concluded that the process is capable of producing better decontamination than any of the known pyrometallurgical processes under study and that theoretical considerations and study of the vapor pressures of the pertinent iodides indicate that separation from every fission product should be possible. Additional evidence to this effect is the recent production of ultra pure Si (19, 20, 30).

Finally, one curious fact is that a sample of iodide Cr, analyzed by the radioactivation method at Oak Ridge, was found to contain less I than one of chromate electrolytic metal analyzed at the same time (31).

Character of the Deposits

One generalization which has appeared in the study of the iodide process is that diiodides, such as FeI_2 and CrI_2, tend to yield spiny, noncompact, noncoherent deposits. Compact deposits can be secured by proper choice of conditions, but even then the coherence is low because of low adhesion between the individual grains. On the other hand, the tetraiodides of Ti, Zr, and Hf, readily give compact, coherent deposits which can be mechanically worked directly.

Factors responsible for this situation are:

1. The high-temperature gradient in the deposition of Ti, Zr, and Hf from their tetraiodides and the fact that, for Ti and Zr at least, there is a temperature at which deposition changes to attack. Accordingly, a "sprout" or protuberance cannot grow very far, and the growing deposit maintains a reasonably smooth surface. With the divalent metals on the other hand, there are no lower iodides to produce a deposition limit, and the low volatility of their diiodides requires a high crude temperature, thereby reducing the temperature gradient. Furthermore, because of the high temperature of the crude, the gases leaving are nearly in thermodynamic equilibrium with it, thereby reducing the concentration gradient. Hence, a sprout can grow quite a distance without being attacked.

In support of this viewpoint are the facts that Ti deposited at high crude temperatures, where the temperature gradient is less and lower iodides participate in the transport, is much less compact than that deposited at low crude temperatures, and that Th, which requires relatively high crude temperatures because of the low volatility of its tetraiodide (bp 839°C) also gives noncoherent deposits according to Veigel, Sherwood, and Campbell (32).

2. The greater volatility of the divalent transition metals. At 1300°C, the vapor pressure of Cr is 417 times and that of Fe 90 times that of Ti, the most volatile of the fourth group transition metals. Accordingly, these metals have a much greater tendency to sublime from the high temperatures of crevices in the deposits to the ends of sprouts. The monoiodides of the divalent metals could enhance the rate of this transport down the temperature gradient. As pointed out they can be more stable than those of the tetravalent metals without preventing deposition.

Deposition of Alloys

Alloys can be deposited by the iodide process. De Boer and Fast (33-35) prepared alloys of Zr with Sn and Al, as well as Ti-Zr and Zr-Hf alloys over their entire composition ranges, while Shapiro (2) prepared alloys of Zr with Cr, Fe, Ni, and Sn. Very recently, Robb (23) reported deposition of U-Zr alloys ranging in Zr content from 16 to 97% from a 40% Zr-60% U alloy by changing conditions.

Factors of importance in the preparation of alloys are: (*a*) relative stability of the iodides; (*b*) relative volatility of the iodides; (*c*) relative volatility of the metals. By employing a high filament temperature, de Boer and Fast (33) prepared Fe-free Zr from a contaminated feed, the volatilized Fe collecting on the cooler electrode. High transfer efficiencies of Fe have, however, been obtained under other conditions (2); (*d*) thermodynamic activity of the second metal in the alloy. If extensive solid solutions or stable compounds are formed, even metals which cannot be deposited in the pure state from their iodides can be codeposited as alloys as shown by the foregoing preparation of Zr-Al alloys.

This whole subject may be summed up in the statement that, if alloys are desired, conditions for obtaining high purity should be avoided. Of course, the converse is also true.

Acknowledgment

The author wishes to thank the Chilean Iodine Educational Bureau, Inc., for permission to present this paper and for its sponsorship of studies of the iodide process at Battelle Memorial Institute, as well as Drs. Ivor E. Campbell and John M. Blocher, Jr., and others of the Battelle staff for many pleasant and illuminating discussions of the process.

Manuscript received July 2, 1958. This paper was prepared for delivery before the New York Meeting, April 27-May 1, 1958.

Any discussion of this paper will appear in a Discussion Section to be published in the December 1959 JOURNAL.

REFERENCES

1. A. E. van Arkel and J. H. de Boer, *Z. anorg. u. allgem. Chem.*, **148**, 345 (1925).
2. Z. M. Shapiro, Chapter 5 in "The Metallurgy of Zirconium," B. Lustman and F. Kerze, Jr., McGraw-Hill Book Co., New York (1955).
3. Harald Schäfer and Bernhard Morcher, *Z. anorg. u. allgem. Chem.*, **290**, 279 (1957).
4. Leo Brewer and Norman L. Lofgren, *J. Am. Chem. Soc.*, **72**, 3038 (1950).
5. A. C. Loonam, U. S. Pat. 2,694,654, Nov. 16, 1954.
6. O. J. C. Runnalls and L. M. Pidgeon, *Trans. Am. Inst. Mining Met. Eng.*, **194**, 843 (1952).
7. V. S. Emelyanov, P. D. Bystrov, and A. I. Evstyukhin, *J. Nuclear Energy*, **4**, 253 (1957).
8. Robert B. Holden and Bernard Kopelman, *This Journal*, **100**, 120 (1953).
9. H. Döring and K. Molière, *Z. Elektrochem.*, **56**, 403 (1952).
10. O. Rahlfs and W. Fischer, *Z. anorg. u. allgem. Chem.*, **211**, 349 (1933).
11. J. M. Blocher, Jr., Personal communication.
12. Gordon Van Praagh and Eric K. Rideal, *Proc. Roy. Soc. (London)*, **A134**, 385 (1931).
13. Irving Langmuir, *J. Chem. Soc.*, **1940**, 511.
14. Harald Schäfer, Herbert Jacob, and Karl Etzel, *Z. anorg. u. allgem. Chem.*, **286**, 27 (1956).
15. *Ibid.*, pp. 42-55.
16. J. R. Kyte, A. J. Madden, and Edgar L. Piret, *Chem. Eng. Progr.*, **49**, 653 (1953).
17. J. D. Fast, *Z. anorg. u. allgem. Chem.*, **241**, 42 (1939).
18. A. C. Loonam, U. S. Patents 2,694,652-3-4, Nov. 16, 1954.
19. B. Rubin, G. H. Moates, and J. R. Weiner, *This Journal*, **104**, 656 (1957).
20. G. Szekely, *ibid.*, 663.
21. W. B. Blumenthal and H. Smith, *Ind. Eng. Chem.*, **42**, 249 (1950).
22. Commonwealth Scientific and Industrial Research Organization, Australian Pat. 4831/54, Nov. 22, 1954.
23. W. L. Robb, Knolls Atomic Power Laboratory Report KAPL-1788, May 1, 1957.
24. J. D. Fast, *Z. anorg. u. allgem. Chem.*, **239**, 145 (1938).
25. Marcel Chaigneau, *Compt. rend.*, **242**, 263 (1956).
26. Marcel Chaigneau, *Bull. soc. chim. France*, **1957**, 886.
27. J. W. Nash, H. R. Ogden, R. E. Durtschi, and I. E. Campbell, *This Journal*, **100**, 272 (1953).
28. H. Schäfer and W. J. Hones, *Z. anorg. u. allgem. Chem.*, **288**, 62 (1956).
29. T. L. Allen, *J. Am. Chem. Soc.*, **78**, 5476 (1956).
30. C. S. Herrick and J. G. Krieble, Report No. 57-RL-1825, General Electric Research Laboratory, Schenectady, October 1957.
31. J. M. Blocher, Jr., Discussion, Symposium on Ductile Chromium, American Society for Metals, Philadelphia, Pa., October 18, 1955.
32. N. D. Veigel, E. M. Sherwood, and I. E. Campbell, *This Journal*, **102**, 687 (1955).
33. J. H. de Boer and J. D. Fast, *Z. anorg. u. allgem. Chem.*, **187**, 177 (1930).
34. *Ibid.* 193.
35. J. D. Fast, *Rec. trav. chim.*, **58**, 973 (1939).

Techniques and Results of Zone Refining Some Metals

J. H. Wernick, D. Dorsi, and J. J. Byrnes

Bell Telephone Laboratories, Inc., Murray Hill, New Jersey

ABSTRACT

Techniques and results are given for the floating zone refining of Ni, Ti, V, and for boat zone refining of Al and Au. These elements have been purified by zone melting. A considerable amount of purification was obtained by volatilization during floating zone melting.

The need for purer metals for basic research and development purposes is great. Because of these needs, we have zone refined a number of metals by floating zone and boat techniques. Some of the results are discussed here.

Floating Zone Refining Equipment

The floating zone refining was done in vacuum in a vapor plating unit[1] adapted for this work. It is similar to the unit used by Buehler (1). Figure 1 shows a schematic drawing of the equipment. The liquid nitrogen trap, diffusion, and mechanical pumps are not shown. The ends of the rod to be zone refined are placed in quartz holders which in turn are held in the yoke by chucks made of stainless steel. The upper chuck (Fig. 2) is so designed that, as the chuck body moves upward, the steel balls prevent the chuck body from returning to its original position.[2] This prevents squeezing out of the molten zone after melting. The yoke is attached to a water-cooled push-rod which passes through an O-ring vacuum seal (Fig. 3) on the base plate. The high-frequency power leads pass through a coaxial vacuum seal, the details of which are shown in Fig. 4. The pressure attained prior to heating is 10^{-6} mm Hg and rises to 10^{-5} mm Hg during refining.

Radio frequency power is obtained from an Ecco 10-kw output generator at a frequency of either 5 mc or 450 kc. The tank circuit for the 450-kc frequency is located within the unit, whereas the tank circuit for 5 mc is located under the base plate of the vacuum system to minimize power loss (Fig. 1). A frequency of about 5 mc was used exclusively for

[1] Consolidated Electrodynamics Corporation LCI-18 Vacuum Coater.

[2] This chuck, as well as the mechanical feed mechanism, was designed by J. J. Gillich.

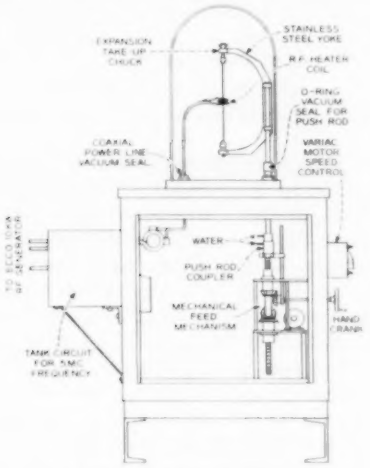

Fig. 1. Vacuum floating zone refiner

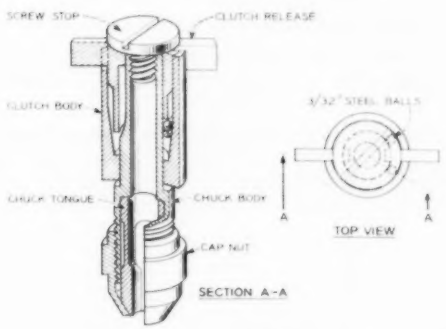

Fig. 2. Expansion take-up chuck

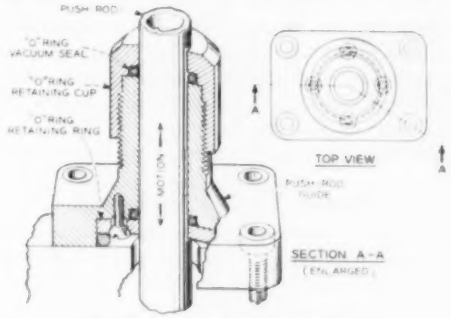

Fig. 3. Vacuum seal for push rod

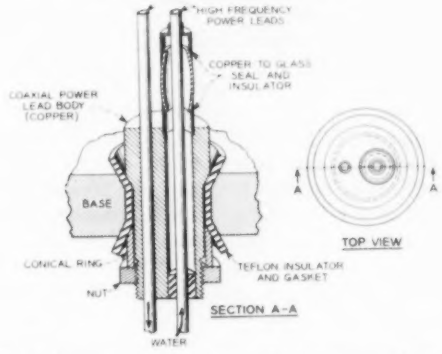

Fig. 4. Vacuum seal for coaxial high frequency leads

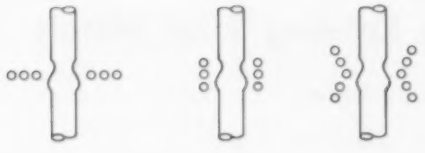

(a) (b) (c)

Fig. 5. Induction work coils for (a) Ni, (b) Ti, and (c) V

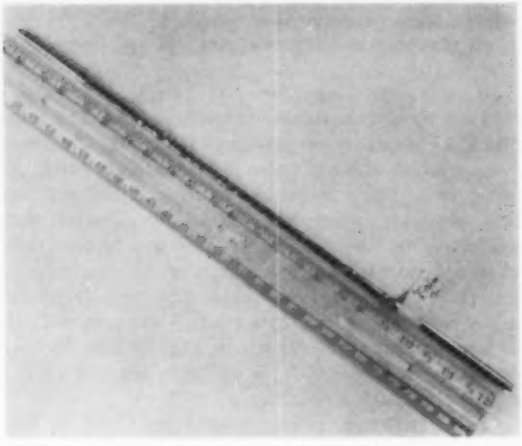

Fig. 6. Zone melted 3/16 in. D Ni rod

the floating zone refining of metals, although a frequency of 450 kc could also be used.

The work coils are made of 3/16 in. D copper tubing, and those used for Ni, Ti, and V (a, b, and c, respectively) are illustrated in Fig. 5. Some trial and error effort is involved in determining the proper coil, because one needs a sufficient concentration of power and yet obtain a stable zone. The zone travel rate was 0.07 in./min for these elements, and the zone lengths varied from ¼ to ⅜ in. For the case of Ni, the zone melted bar was more uniform in cross section when the zone traveled from top to bottom.

Floating Zone Melting Results

Figures 6, 7, and 8 are photographs of zone melted Ni, Ti, and V rods. The starting high purity Ni was obtained from K. M. Olsen and was made by a crucible melting technique(2). The analytical data for this Ni are shown in Table I (2). Examination of the phase diagrams of Ni with the metal impurities indicates that the equilibrium distribution coefficients for these impurities in Ni are not too different from unity.

The zone refined Ni (2¼ in./hr travel rate) was evaluated by measuring the residual resistances, at liquid He temperature, of sections of the zone refined ingot, as described by Kunzler and Wernick (3). A decrease in the residual resistance indicates purification. Figure 9 shows the resistance ratio $R_{4.2°K}/R_{273°K}$ (residual resistance) as a function of position along the bar. The control data are for the unmelted sections at the ends. Note that crucibleless zone melting, after four passes, resulted in purification, mainly by volatilization of volatile impurities, as indicated by the absence of appreciable pile up of impurities at either end.

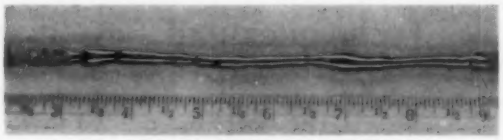

Fig. 7. Zone melted ¼ in. D Ti rod

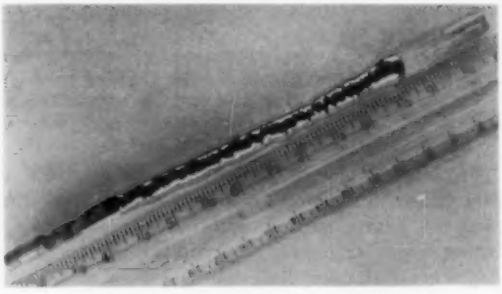

Fig. 8. Zone melted ⅜ in. D V rod

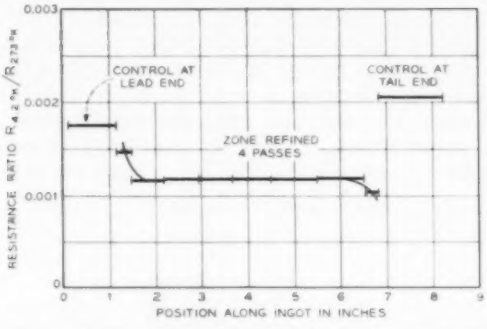

Fig. 9. Low-temperature resistivity of floating zone refined Ni

The zone melted Ti bar (6 passes, 1¼ in./hr travel rate) was analyzed spectroscopically. Titanium is not cubic, and residual resistance measurements for determining purity would be difficult to interpret unless one has a single crystal. Quantitative analytical data are shown in Table II. It appears that purification was mainly due to volatilization, as indicated by the absence of appreciable pile up of impurities at either end. No carbon and oxygen analyses were obtained.

The qualitative spectroscopic data for zone melted V (6 passes, 2¼ in./hr travel rate) are shown in Table III. Purification was obtained both by movement of impurities and by volatilization.

Boat Zone Melting Results for Al and Au

The zone refining of aluminum in Al_2O_3 boats has been discussed by Albert, *et al.* (4), Caron (5),

Table I. Analysis of BTL nickel used for zone refining

Element	% by weight
Fe	<0.005
Si	<0.005
Cu	<0.001
Mg	<0.005
C	0.001
S	0.001
O	0.0015
H	0.0001
N	0.0001

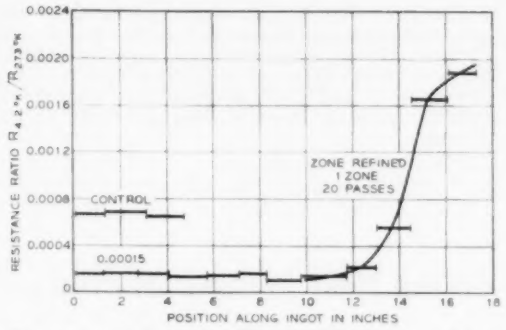

Fig. 10. Low-temperature resistivity of zone refined Al 99.999+%.

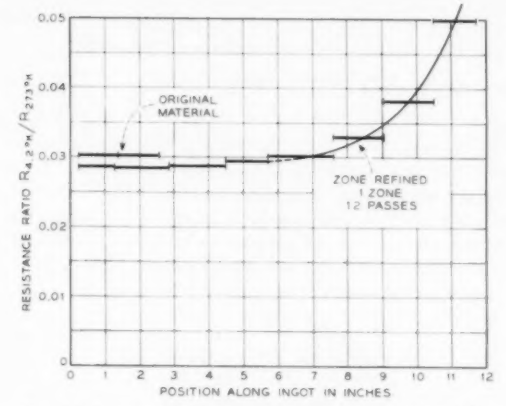

Fig. 11. Low-temperature resistivity of zone refined Au

Table II. Spectrochemical quantitative analysis of floating zone refined titanium

	Original	Lead section	End section
Ni	0.062	0.018	0.0051
Mn	0.015	N.D.	N.D.
Mg	0.010	0.0043	0.0043
Fe	0.042	0.0087	0.017
Si	0.24	0.062	0.11
Cu	0.006	0.0008	0.0007
Ca	0.033	0.014	0.014
Al	0.0088	N.D.	N.D.
Mg	(<0.005) *	N.D.	N.D.

N.D., not detected.
* Qualitative estimate.

Table III. Qualitative spectroscopic analytical data for zone melted vanadium (in weight per cent)

Element	Control (unmelted) portion	Lead section	Center section	End section
Al	<0.001	<0.03	N.D.*	N.D.
Ca	<0.001	<0.03	N.D.	N.D.
Co	<0.03	<0.001	<0.001	<0.005
Cr	<0.03	<0.001	<0.001	<0.001
Cu	<0.005	<0.001	<0.001	<0.001
Fe	<0.03	<0.005	<0.001	<0.001
Mg	<0.001	<0.005	<0.001	N.D.
Mn	<0.03	<0.001	N.D.	N.D.
Si	<0.03	0.01-0.3	0.01-0.3	<0.03
Ti	N.D.	<0.005	N.D.	N.D.
W	0.03	0.03	0.03	0.03

* N.D., not detected.
Alkaline earth elements not detected.

Montariol (6), and in graphite boats by Demmler (7). We have zone refined Al in graphite boats[5] in a flowing purified argon atmosphere (4.9 in./hr travel rate). The graphite boat is first degassed *in vacuo* at a temperature estimated to be 1200°C. The argon is cleaned by passing it through a bed of drying agent, Linde Molecular sieve, and then through a bed of steel wool held at 600°C. Induction heating (450 kc) was used for zone refining. Mass transfer during zone refining is excessive, and it is prevented by tilting the refiner. This also aids in maintaining a zone of given size during refining. Figure 10 shows a plot of resistance ratio vs. distance along the length of a zone refined bar.[6] Also shown are the resistance ratio data for an annealed section of the original ½ in. D rod (marked control). It is apparent that zone refining was effective in increasing the purity of the 99.999+% Al. Table IV compares the reciprocal resistance ratios of zone refined Alcoa 99.99+% and AIAG 99.999+% Al ingots. The impure ends were not removed at any time during refining.

Gold was also zone refined by induction heating in a degassed graphite boat in a flowing argon atmosphere (3.6 in./hr travel rate). The residual resistance data for an ingot are shown in Fig. 11. Note that some zone refining was accomplished, but that there was also some impurity pickup from the surroundings, as indicated by the rather large pile-up of impurities at the impure end. The nature and source of the external impurities are not known at present.

[5] A limited discussion of this work appears in Ref. 3.

[6] The starting 99.999% Al used for this zone refining work was kindly furnished by Aluminium-Industrie-Aktien-Gesselschaft, Neuhausen am Rheinfall, Switzerland. The American supplier for this material is United Mineral and Chemical Corp., New York, N. Y.

Acknowledgments

The authors wish to thank J. E. Kunzler for advice concerning the residual resistance measurements; K. E. Benson for experimental assistance; E. K. Jaycox and D. Babusci for the spectroscopic analysis; and E. Buehler for suggesting the yoke design for the floating zone apparatus.

Manuscript received Aug. 13, 1958. This paper was prepared for delivery before the New York Meeting, April 27-May 1, 1958.

Table IV. Resistance ratios for zone refined Al

Starting material	Original $R_{273°K}/R_{4.2°K}$	Zone refined $R_{273°K}/R_{4.2°K}$	Atmosphere	Passes	Boat
Alcoa 99.99+ (Ref. 3)	800	5000	Argon (purified)	20	Graphite
AIAG 99.999+%	1500	6600	Argon (purified)	20	Graphite

Any discussion of this paper will appear in a Discussion Section to be published in the December 1959 JOURNAL.

REFERENCES

1. E. Buehler, to be published in Transactions of the Metallurgical Society, AIME.
2. K. M. Olsen, *Metal Prog.*, **72**, 105 (1957).
3. J. E. Kunzler and J. H. Wernick, Transactions of the Metallurgical Society, AIME, **212**, 856 (1958).
4. P. Albert, F. Montariol, R. Reich, and G. Chaudron, in "Radioisotope Conference," p. 75, Vol. 2, J. E. Johnson, Editor, Academic Press, New York (1954).
5. M. Caron, Proceedings of a Meeting Held by Commissions 1 and 2 of International Institute of Refrigeration in Louvain, Belgium, Sept. 4-7, 51 (1956).
6. F. Montariol, *ibid.*, p. 63.
7. A. W. Demmler, Jr., *Trans. Am. Inst. Mining Met. Engrs.*, **206**, 958 (1956).

Effects of Electrolytes and of Gelatin on the Half-Wave Potentials of Carbon Tetrachloride, Dibromoacetate, and p-Dinitrobenzene

Leif E. I. Hummelstedt and L. B. Rogers

Department of Chemistry and Laboratory for Nuclear Science, Massachusetts Institute of Technology, Cambridge, Massachusetts

ABSTRACT

Polarograms were obtained in media in which reductions of each compound occurred on both sides of the electrocapillary maximum. Capillary-active anions retarded the less cathodic reduction steps and capillary-active tetramethylammonium ion facilitated the second reduction steps of carbon tetrachloride and the dibromoacetate ion. Capillary-inactive calcium ion had little effect on the halogenated compounds, but it greatly facilitated the second reduction of p-dinitrobenzene thereby suggesting ion-pair formation with the known divalent intermediate

Gelatin, for the first time, was found to shift a reduction to less cathodic values. This occurred only in acidic media when the reduction took place on the negative branch of the electrocapillary curve. The shift was attributed to the presence of protonated gelatin in the double layer.

In an earlier study of the effect of added electrolyte on the half-wave potentials of carbon tetrachloride (1), the possibility existed that the observed changes, which had been attributed to changes in the double layer at the electrode surface, might have been due to changes in junction potential. In the present study, the effects of electrolytes were re-examined using a large concentration of a relatively inert electrolyte in order to minimize changes in junction potential. By examining two different waves of the same compound, each on a different side of the electrocapillary maximum, it was possible to isolate selective influences. By using a single medium for studying carbon tetrachloride, dibromoacetic acid, and p-dinitrobenzene, it was possible to distinguish further between different types of electrolyte effects.

Experimental Details

Apparatus.—Polarograms were obtained using a Sargent Model XXI recording polarograph. The initial and final potentials of each polarogram were measured with a Rubicon or a Sargent potentiometer. All measurements were made against an external saturated calomel electrode (S.C.E) which was connected to the polarographic cell by means of a salt bridge which contained 1*M* potassium chloride. The end of the salt bridge which dipped into the sample was closed by a Vycor plug, the other, by an agar plug. The capillary used throughout the experiments had a value for $m^{2/3}t^{1/6}$ of 1.32 $mg^{2/3}$ $sec^{-1/2}$ at -0.800 v vs. S.C.E. in 0.9*M* potassium chloride. The resistance of the polarographic cell circuit was measured using an Industrial Instruments Company conductivity bridge, Model RC-1B. The pH measurements were made using a glass electrode in conjunction with a Beckman H or G pH meter.

Reagents and solutions.—Most of the chemicals were analytical reagent grade. However, the dibromoacetic acid was a research sample kindly furnished by Dr. Vernon Stenger of the Dow Chemical Company. The tetramethylammonium chloride was the polarographic grade of Southwestern Analytical Chemicals. The p-dinitrobenzene, after recrystallization from ethanol, had a melting point of 173.2°-173.7°C.

Carbon tetrachloride and dibromoacetic acid were added in the form of methanol solutions to solutions of background electrolyte. The p-dinitrobenzene was added as either a methanol or ethanol solution. Most of the experiments were performed using a high concentration of lithium chloride (2.0*M*) as supporting electrolyte in 41% methanol. Other electrolytes were added to such a solution as solids. To make the background alkaline, the pH was adjusted by adding sodium hydroxide; to make it acidic, a phthalate buffer was prepared in the manner described by Pearson (2). In adjusting the apparent pH of some of these buffers in different concentrations of alcohol, hydrochloric acid was added. Gelatin was added as an aqueous 0.50% solution.

Procedures.—The polarographic solutions, which were generally 50 ml, were deaerated with prepurified nitrogen that had been passed through a portion of the supporting electrolyte before entering the polarographic cell. Usually 15 min of deaeration was sufficient to remove the oxygen. In working with carbon tetrachloride, the supporting electrolyte was first deaerated for 15 min, whereupon 1.00 ml of the stock solution containing carbon tetrachloride was added and the solution deaerated for an additional period of 1.5 min.

All data were corrected for residual current and *IR* drop. All experiments were performed using a mercury height of 102 cm and a thermostatic bath held at 24.0°C. Electrocapillary curves were determined from recordings for at least 100 drops at each potential.

Results

Effect of Monovalent Ions

Figure 1a shows the effect of potassium thiocyanate and tetramethylammonium chloride, respectively, on the half-wave potentials of carbon tetrachloride solutions in alkaline 2.0*M* lithium chloride containing 41% by volume of methanol. It is apparent that the addition of relatively small amounts of potassium thiocyanate shifted the first wave of carbon tetrachloride in a more cathodic direction, while the second was shifted slightly in the opposite direction. Addition of tetramethylammonium chloride, on the other hand, had no effect on the first wave, while the second was shifted to markedly less cathodic potentials. Addition of an equimolar mixture of potassium thiocyanate and tetramethylammonium chloride simultaneously shifted the first wave toward more cathodic potentials and the second wave toward less cathodic. The shifts observed for the mixture were about half those for the separate components (−0.066 v vs. −0.116 v and +0.181 v vs +0.274 v).

The results of a similar experiment using dibromoacetic acid, a compound extensively studied by Elving, *et al.* (3) are shown in Fig. 1b. The shift in half-wave potential for the second wave was smaller than that for the corresponding wave for carbon tetrachloride, probably because the former is closer to the electrocapillary maximum. The importance of such a factor is qualitatively illustrated by the data of Elving, *et al.* (4) on α-bromo-n-butyric acid. Comparison of Fig. 2 with Fig. 1a and 1b shows that the electrocapillary maximum lay as expected between the two polarographic waves of both carbon tetrachloride and the dibromoacetate ion. Electrocapillary curves for separate additions of either potassium thiocyanate or tetramethylammonium chloride had maxima which fell in the same region of potential as those in Fig. 2.

In an earlier study of carbon tetrachloride by Lothe and Rogers (1) similar shifts in polarographic waves were demonstrated, but contributions from changes in junction potential were present because a high concentration of background electrolyte had not been used. In order to check the constancy of the liquid junction potential in the present study polarograms of 2 x 10^{-3}*M* thallium (I) were run in the same background medium. On addition of a mixture giving 0.05*M* potassium thiocyanate and 0.05*M* tetramethylammonium chloride, the half-wave potential remained constant at −0.447 v; an increase in concentration to 0.20*M* caused only a slight shift to −0.454 v (further complexing of thallium?). The largest effect of the "active" salts on the half-wave potentials of carbon tetrachloride occurred for additions of 0.05*M* or less for which the 2*M* lithium chloride did indeed hold the liquid junction potential constant.

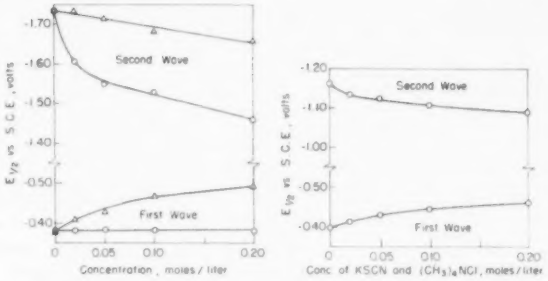

Fig. 1. Effect of electrolytes on the half-wave potentials of carbon tetrachloride and dibromoacetate in solutions of 2.0M lithium chloride and 41% methanol having an apparent pH of 10.9: (a) (left), addition of KSCN (△) and $(CH_3)_4NCl$ (○) to 10^{-3}M carbon tetrachloride; (b) (right), addition of an equimolar mixture of KSCN and $(CH_3)_4NCl$ to 1.7×10^{-3}M dibromoacetate.

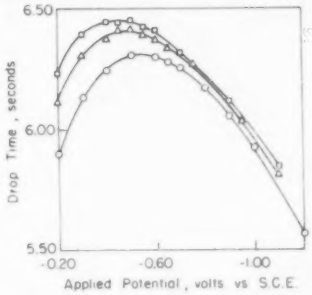

Fig. 2. Drop time as function of applied potential in 2.0M lithium chloride and 41% methanol with different additions of an equimolar mixture of KSCN and $(CH_3)_4NCl$ (□—no addition; △—0.05M; ○—0.20M). Apparent pH, 10.9.

To evaluate the effect of competition of lithium and chloride ions for positions at the interface, additions of an equimolar mixture of potassium thiocyanate and tetramethylammonium chloride were made to solutions of carbon tetrachloride containing lower initial concentrations of background electrolytes. A change from 2.0*M* to 1.0*M* lithium chloride resulted in a slightly greater shift in each half-wave potential in the range up to 0.05*M* of each electrolyte but, for larger additions, virtually the same shifts were found as those shown for the more concentrated lithium chloride. When 0.60*M* potassium nitrate was substituted for lithium chloride as a supporting electrolyte, the second wave could not be measured because of decomposition of the background. However, the shift of the first wave was practically identical with that observed for 1.0*M* lithium chloride.

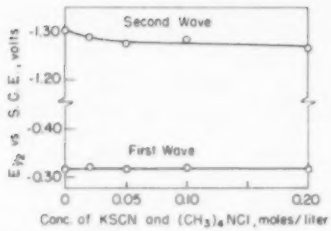

Fig. 3. Effect of an equimolar mixture of KSCN and $(CH_3)_4NCl$ on the half-wave potentials of 10^{-4}M p-dinitrobenzene in solutions of 2.0M lithium chloride and 41% methanols having an apparent pH of 10.9.

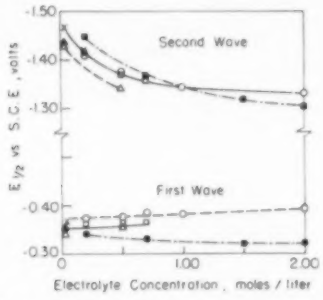

Fig. 4. Effect of electrolytes on the half-wave potentials of 10^{-4}M p-dinitrobenzene in 41% methanol. □—KCl, ○—KSCN, △—$(CH_3)_4NCl$, ×—KI, ▲—$(CH_3)_4NI$, ■—LiCl. The apparent pH is approximately 11.9 except for solutions containing LiCl which caused a decrease to 10.9. ——— "Inactive" ions; - - - "Active" ions; - . - . - LiCl curves.

After the similarities of carbon tetrachloride and dibromoacetic acid had been established, p-dinitrobenzene was studied because it represented a different type of reducible group. In the case of an organic halide the transfer of one electron (possibly two) is followed by rapid elimination of a halide ion. The first wave of p-dinitrobenzene in alkaline solution corresponds to a two-electron change with formation of a relatively stable divalent ion; the second wave to formation of p-hydroxylaminoaniline (5). Hence, the organic halides involve electron-transfer to neutral (or monovalent) species whereas the second alkaline reduction step of p-dinitrobenzene goes through a stable divalent intermediate.

Figure 3 indicates that the first wave of p-dinitrobenzene in 2*M* lithium chloride was unaffected by an equimolar mixture of potassium thiocyanate and tetramethylammonium chloride whereas the second wave was shifted, but only slightly, toward less cathodic potentials.

In the absence of 2*M* lithium chloride (Fig. 4) the second wave was shifted considerably by an increase in ionic strength. Potassium chloride, potassium thiocyanate, and potassium iodide behaved the same. Points for tetramethylammonium chloride and tetramethylammonium iodide fell at less cathodic potentials, indicating that the tetramethylammonium ion had a greater effect than potassium. In going from 0.2 to 2.0*M* lithium chloride, the apparent *p*H decreased from 11.55 to 10.90, a change that was confirmed using a hydrogen electrode (6). Correction for the change in pH would make the lithium curve essentially parallel to, but more cathodic than, the potassium curve, indicating that lithium by itself was less effective than potassium.

Lithium chloride also caused a small amount of shift in the first wave which, according to Holleck and Exner (5), should be practically independent of the pH in the alkaline range. It is possible that a shift of this magnitude (0.02 v) could be caused by a change in liquid junction potential. Although all the electrolytes had only a small effect, values for the first half-wave potential in the presence of thiocyanate or iodide are consistently more negative than the corresponding values for chloride, in accord with known differences in capillary activity of those anions (7).

Agreement between the present study and the earlier one by Holleck and Exner (5) was good for the first wave. However, their values for the second wave were more cathodic (nearly −1.6 v vs. −1.3 v) in spite of the fact that their lower concentration of methanol (20%) would normally be expected to result in a less cathodic wave. Figure 4 shows that a difference in ionic strength is the chief source of the discrepancy since they did not use as highly concentrated background electrolyte.

Though the above discussion refers only to two waves of p-dinitrobenzene, Holleck and Exner (5) showed that this compound has three polarographic waves at intermediate values of pH. At high values of pH the middle wave is not present but, under the conditions of the present experiment, a small wave was still visible at about −0.88 v. Unfortunately this wave was too small to permit accurate half-wave measurements, so changes in its position were not included in the study. As a further complication, a new wave was observed to grow in at slightly more positive potentials when the solution was allowed to stand a few hours before a polarogram was run. It was established that p-nitroanisole was the compound produced in alkaline methanol.

Effects of Divalent Ions

Prior studies on the reduction of ketones (8) and nitrate ion (9) have indicated that di- and trivalent cations resulted in a less cathodic half-wave potential than monovalent ions of comparable concentration. It was surprising, therefore, to find that the addition of calcium chloride in an amount sufficient to produce a 0.05*M* solution had little effect on the first and second waves of carbon tetrachloride and dibromoacetic acid. In contrast, the second wave for p-dinitrobenzene shifted +56 mv although the first wave remained constant. Barium chloride was also tried and gave a shift of +23 mv for the second wave, but unfortunately a precipitate formed which decreased the concentration of barium by an unknown amount. The fact that calcium exerted little effect on the second waves of the halides (compared to tetra alkylammonium ion) is probably due to its lack of electrocapillary activity (10).

The greater effect of calcium ion on the second wave of p-dinitrobenzene appears to be due to ion-

pair formation with the stable divalent intermediate. Ion-pair formation would decrease the effective negative field around the nitro body and would facilitate further reduction. The acidic reduction of p-dinitrobenzene as well as the acidic and alkaline reductions of o-dinitrobenzene, none of which involve a stable charged intermediate (5), show little effect of calcium (6). The fact that changes in the concentrations of lithium and potassium ions had nearly the same effect as changes in tetramethylammonium ion, plus the fact that doubly charged calcium had a much greater effect than any monovalent cation, suggests that the shift is associated with charge rather than electrocapillary activity.

Effect of Gelatin

In early exploratory runs with p-dinitrobenzene in acidic solutions, gelatin exhibited unusual effects which made further investigation seem worthwhile. In acidic media, p-dinitrobenzene is reduced in two steps, the first corresponding to formation of p-hydroxylaminonitrobenzene and the second to p-hydroxylaminoaniline (5).

Two series of runs were made in different concentrations of ethanol. In one the apparent *p*H of the buffer was adjusted to 4.1 by the addition of hydrochloric acid, while in the second the electrolyte concentration was held constant and the apparent pH allowed to increase with alcohol concentration. At the lowest ethanol concentration (8%) a maximum was formed on the second wave of p-dinitrobenzene unless 0.002% gelating was present. Hence, the half-wave potential of the second wave in the absence of gelatin was somewhat uncertain in 8% ethanol. At higher ethanol concentrations no maxima were observed even in the absence of gelatin.

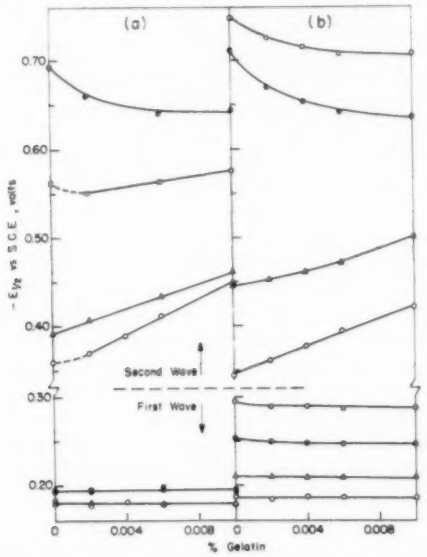

Fig. 5. Effect of gelatin on the half-wave potentials of 10^{-4}M p-dinitrobenzene in 0.07M phthalate buffers of varying ethanol concentration (O—8%; △—29%; ∅—49%; □—73%). (a) Apparent pH maintained constant at 4.1 by adding HCl when increasing the ethanol concentration. (b) Apparent pH allowed to increase with ethanol concentration.

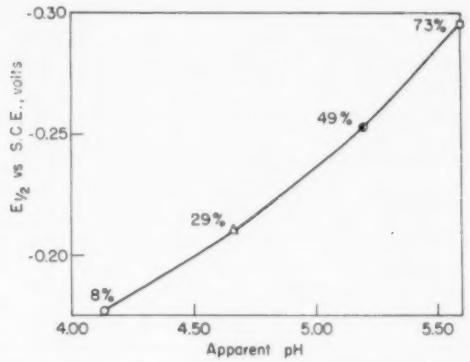

Fig. 6. Changes in the half-wave potential of the first wave of 10^{-4}M p-dinitrobenzene as function of the apparent pH of solutions of different ethanol content with 0.07M potassium acid phthalate as supporting electrolyte.

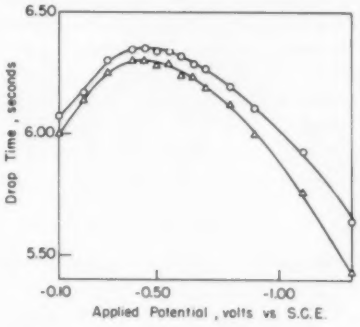

Fig. 7. Effect of gelatin on the electrocapillary curve in 0.07M potassium acid phthalate and 29% ethanol (O—no gelatin added; △—0.01% gelatin present).

As shown in Fig. 5a and 5b gelatin had no effect on the first wave. This probably indicates that this wave is more nearly reversible in character than the second. The shift observed for the half-wave potential as a function of alcohol in Fig. 5b is largely due to a change in *p*H, though Fig. 6 shows the change to be somewhat greater than expected, i.e., 85 mv per unit of apparent pH. This undoubtedly reflects a change in the composition of the solvent and in the resulting junction potential. This solvent effect is also indicated by the slight cathodic shift of the first wave with increasing ethanol concentration, at constant apparent pH, shown in Fig. 5a.

The behavior of the second wave with a change in concentration of gelatin was complex. At the 8 and 29% levels of alcohol, the difficulty of reduction increased almost linearly with concentration. At the 49% level, reduction was facilitated, an effect not previously reported for gelatin. This must have been due to superposition of a second factor which counteracted the generally observed retardation. Electrocapillary data of the type shown in Fig. 7 showed that these reductions were taking place on the negative branch of the electrocapillary curve. Hence, the acceleration is probably due to protonated gelatin in the double layer.

At the 73% level, the effect of gelatin differed in the two series. In Fig. 5a where the reduction fell

only slightly on the negative side of the electrocapillary maximum (due to a large increase in ionic strength when a large amount of hydrochloric acid had to be added to attain an apparent pH of 4.1), the retarding effect was predominant. In Fig. 5b, the positive-ion effect was still predominant, but smaller, even though the reduction took place at a more cathodic potential than in 49% alcohol. This probably reflects less extensive protonation of the gelatin in the lower dielectric medium, as well as a possible denaturization.

Confirmation of the protonation hypothesis may be found by noting in Table I that, at pH 10.9 where protonation was very slight, the retarding effect was always observed regardless of position of the reduction relative to the electrocapillary maximum. This indicates that the positive-ion effect was indeed the cause of the reversal observed in acidic medium. The only reservations that must be made are: (*a*) the fact that the reduction mechanism for p-dinitrobenzene differs in acidic and alkaline media, and (*b*) a small positive shift was observed for the second wave of carbon tetrachloride. However, the latter data are very uncertain due to superposition of the carbon tetrachloride reduction on that of the background electrolyte.

Discussion

The present study confirms the importance of the position of a polarographic wave relative to the electrocapillary maximum in determining whether one can expect anion or cation effects on the half-wave potential of an electron-transfer controlled reaction (1). Although Ashworth (8) was one of the first to report the influence of cations on irreversible organic reductions (benzophenone and fluorenone) and the fact that similar compounds may react differently to the same ion, the conditions under which the two ketones were examined were not strictly comparable. Thus, his results are difficult to analyze. The present study indicates that one may be able to differentiate between different roles played by the electrolytes. In one case the effect may be a general one and probably depends only on the presence of excess anions or cations sufficiently close to the electrode surface to change the potential at the point where reduction takes place. [There is evidence that tetraalkylammonium ions are not appreciably solvated and are electrocapillary active (11).] Therefore, calcium ion, in spite of its greater charge, may have had less effect on the halide reductions because its solvated ion is not appreciably concentrated by adsorption at the interface. The comparatively small effects in 2*M* lithium chloride of capillary-active monovalent ions on p-dinitrobenzene may be the result of the more nearly reversible character of the waves (especially the first).

Table I. Effect of gelatin on the half-wave potentials of carbon tetrachloride, dibromoacetate, and p-dinitrobenzene in 2.0*M* lithium chloride and 41% methanol of apparent pH 10.9

	Carbon tetrachloride		Dibromoacetate		p-Dinitrobenzene	
Gelatin, %	First wave	Second wave	First wave	Second wave	First wave	Second wave
0	−0.39	−1.71*	−0.414	−1.179	−0.315	−1.284
0.01	−0.42	−1.68*	−0.443	−1.194	−0.318	−1.316

* Values for the second wave of carbon tetrachloride are uncertain due to superposition of the reduction on that of the background electrolyte.

The large effect of calcium on the alkaline reduction of p-dinitrobenzene was discussed earlier. Although this may be a specific effect of calcium ion, it appears more probable that the specificity is associated with the divalent intermediate formed in this particular mechanism. However, electrocapillary-inactive ions may exert an additional characteristic influence. Unfortunately, the alkaline reduction of p-dinitrobenzene did not lend itself to such a study because most difficultly reducible multivalent cations form hydroxide complexes or precipitates. However, good examples of specific cation effects have been reported for the electrochemical reduction of nitrate which is affected by a number of multivalent cations in addition to calcium. Collat and Lingane (12) found the products to be quite different if obtained in the presence of uranyl ion instead of lanthanum (III). In fact, somewhat different yields of products resulted in shifting from lanthanum (III) to cerium (III).

The half-wave potentials for irreversible reactions are usually affected by changes in concentration of the reducible substance so the concentration was held constant. However, the volatility of carbon tetrachloride made difficult the maintenance of a constant concentration throughout a series of experiments, so the effect of a change in concentration on the half-wave potential was briefly investigated. A change from 4.1×10^{-4} to 4.1×10^{-5} *M* caused a shift in half-wave potential of about +10 mv, an insignificant amount compared to most of the shifts that were observed.

It was recognized that the results obtained with solutions at apparent pH 10.9 would be open to some question because of the absence of a buffer. Unfortunately, higher concentrations of sodium hydroxide, which would have been better buffers, would also have prevented the study of the calcium effect by precipitating the hydroxide. As a compromise, the concentration of sodium hydroxide used was 0.007*M* which would serve rather well as a buffer for the pH-sensitive reduction of 1×10^{-4} *M* p-dinitrobenzene. The calculated pH of 11.85 was actually observed in the absence of a large concentration of background electrolyte, but the presence of 2.0*M* lithium chloride caused a decrease in apparent pH to 10.9. This decrease was checked and substantially confirmed using a hydrogen electrode although there was a small sodium and lithium error (6).

Acknowledgment

The authors are grateful to Dr. Vernon Stenger for providing the dibromoacetic acid, to Dr. William H. Reinmuth for many stimulating discussions and the opportunity to read one of his manuscripts during its preparation. This work was supported in part by the Atomic Energy Commission.

Manuscript received March 28, 1958.

Any discussion of this paper will appear in a Discussion Section to be published in the December 1959 JOURNAL.

REFERENCES

1. J. L. Lothe and L. B. Rogers, *This Journal*, **101**, 258 (1954).
2. J. Pearson, *Trans. Faraday Soc.*, **44**, 683 (1948).
3. P. J. Elving, I. Rosenthal, and M. K. Kramer, *J. Am. Chem. Soc.*, **73**, 1717 (1951).
4. P. J. Elving, J. C. Komyathy, R. E. Van Atta, C.-S. Tang, and I. Rosenthal, *Anal. Chem.*, **23**, 1218 (1951).
5. L. Holleck and H. J. Exner, *Z. Elektrochem.*, **56**, 677 (1952).
6. R. F. Breese, Private communication.
7. D. C. Grahame, *Chem. Revs.*, **41**, p. 451, Table I, (1947).
8. M. Ashworth, *Collection Czech. Chem. Commun.*, **13**, 229 (1948).
9. M. Tokuoka and J. Ruzicka, *ibid.*, **6**, 339 (1934).
10. W. H. Reinmuth, Private communication.
11. G. Sutra, *J. Chim. Phys.*, **43**, 189, 279 (1946); *see also*: G. Darmois and E. Darmois, *Compt. rend.*, **238**, 971 (1954).
12. J. W. Collat and J. J. Lingane, *J. Am. Chem. Soc.*, **76**, 4214 (1954).

Kinetics of the Cathodic Reduction of Anions: Germanium Oxides

Mino Green[1] and P. H. Robinson

Lincoln Laboratory, Massachusetts Institute of Technology, Lexington, Massachusetts

ABSTRACT

The electrochemical cell Hg(Na)|GeO_3, NaOH(aq)|Pt, gives GeH_4, Ge, and H_2 as end products at the cathode. GeH_4 yields have been obtained with a current efficiency of >40% and a mass conversion efficiency of >80%. The partial currents of GeH_4, Ge, and H_2 have been measured as a function of electrolyte composition, cathode potential, and cathode diffusion boundary layer thickness. A highly reducing reactive intermediate has been detected in solution with a mean life of ~4 min. The value of the Tafel slope for GeH_4 evolution was found to be -56 ± 2 mv per decade. The mechanism for the over-all reaction $GeO_3^= + 7\ H_2O + 8\ e^- \rightarrow GeH_4 + 10\ OH^-$ is discussed and the most likely mechanisms up to the rate-determining step are narrowed down to three possible cases. Further experiments for the final determination of the rate-determining step are suggested.

The work reported here had two main objects: (*a*) the determination of the optimum conditions for the electrochemical preparation of germane, GeH_4; and (*b*) an investigation of the kinetics and mechanism of the cathodic reduction of anions in the light of recent advances in the theory of electrode processes, e.g., Ref. (1). It has been found that the system Na(Hg)|NaOH, GeO_2(aq)|Pt, anode, gives high yields of GeH_4 and therefore it is this system which is discussed here.

Experimental

Materials.—Unless otherwise specified reagent grade chemicals were used. The GeO_2 used contained less than 1 ppm w/w total metallic impurities. The Hg used was triply distilled and all other metallic electrodes used were designated "spectroscopically pure."

Estimation of GeH_4-H_2 *ratios.*—The gaseous product from the cathode was a mixture of GeH_4 and H_2; no other gaseous species were detected, nor were there any other volatile hydrides of Ge. The GeH_4-H_2 ratio was determined using a Rayleigh-Zeiss interferometer. The essentials of the analytical method, which depended on measuring the differences between the refractive indexes of hydrogen and a GeH_4-H_2 mixture, have been reported elsewhere (2). The procedure has been modified somewhat to extend the range to 100% GeH_4: the accuracy of the method was ± 0.004 mole fraction GeH_4.

[1] Present address: Zenith Radio Corporation, Chicago, Ill.

Cell assembly.—The assembly of Fig. 1 was used where quantitative gas collection was required. The system was cooled by flowing water. Current was obtained from a 110 ± 1 v d-c generator and the other circuitry was conventional. The anode con-

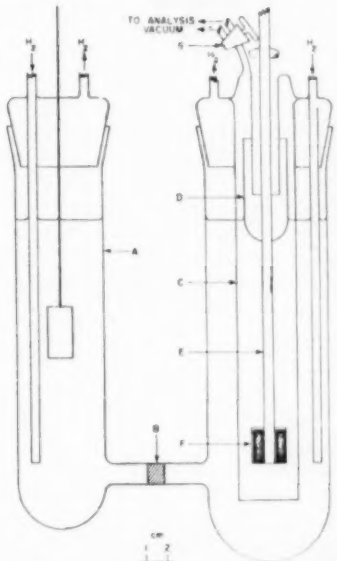

Fig. 1. Cell assembly: A, anode compartment; B, porous disk (medium); C, gas collecting bell; D, Hg-liquid seal; E, "Teflon" shaft; F, Hg cathode.

sisted of Pt(A = 4 cm^2) and the cathode was contained in a cup attached to a Teflon rod. Electrical contact was made to the mercury in the cup by means of a platinum wire which passed down the center of the stirring rod. The exposed area of mercury was about 0.8 cm^2, and the volume of mercury was about 0.5 cc. The cathode could be spun to speeds up to 800 rpm. Gas produced at the cathode was collected in the bell. No corrosion of the glass cup containing the cathode was observed.

A typical run was performed as follows: Current corresponding to the desired current density at the cathode was passed through the cell. The cathode was "run-in" for a suitable time after which liquid was drawn up in the bell to the stopcock, S. At this point the current was recorded continuously on a strip-chart recorder. One determination was completed when the liquid in the bell was displaced by gas down to the level of the cathode surface. Then the gas was transferred to the evacuated collecting bulb via a mixed calcium chloride-barium oxide drying column. The run-in of the cathode was necessary since the sodium first formed at the cathode dissolved in the mercury (fresh Hg used for each run), and only after the cathode reached a certain Na-Hg composition did gas evolution occur. After a further period of electrolysis a determination of composition, etc., was made and this was repeated. The second determination usually gave the same results as the first, indicating that the cathode had reached a limiting Na concentration for both cases. If the second determination did not give the same values as the first, a further determination was carried out and this invariably gave, within experimental error, the same values as the preceding run. Since reproducible yield results were obtained in the manner just outlined, it is reasonable to assume that no error arises out of the possible solubility of GeH, in the electrolyte. The temperature near the cathode was 25° ± 3°C for all current densities up to ~ 2 amp-cm^{-2}; for higher current densities (not used in kinetic analysis) the cathode rose to somewhat higher temperatures.

The information available from each run was: the amount and composition of the evolved gas, the rpm of the cathode, and the total coulombs passed. The volume of the bell (about 80 cc) was determined by weighing the amount of Hg required to fill it to the point where cathode/electrolyte contact was broken. The number of moles of GeH, produced was calculated taking into account the temperature, atmospheric pressure, and water vapor pressure above the particular electrolyte being used. The coulombs passed were measured by graphical integration of the current-time recording. The rotary speed of the cathode was measured by a stroboscopic illumination method.

Determination of cathode potential.—The potential of the cathode with current passing was determined in an H-shaped cell, using the cathode and Luggin arrangement of Fig. 2. The object of this Luggin capillary arrangement, used by Piontelli and Polli (3), was to avoid measuring any resistive potential drop in the solution. The geometrical surface

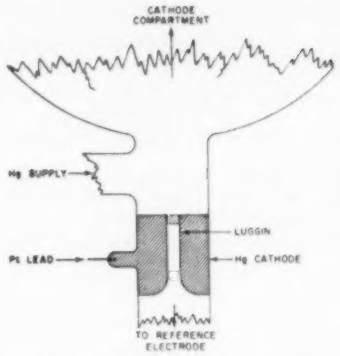

Fig. 2. Backside Luggin capillary arrangement

area of the cathode was 0.31 cm^2 and the outside diameter of the Luggin was 0.02 cm with a wall thickness of about 0.004 cm. In a measurement of cathode potential the Hg was always kept filled to the tip of the Luggin; any excess Hg passed out through the Luggin. Measurements of potential were made at the lowest current density first. The cathode potential measured was in each case the steady-state value, i.e., a run-in period was necessary to allow the Na concentration of the cathode to reach its limiting value (cf. above).

Cathode potential measurements were made in NaOH and also in solutions of GeO_2 and NaOH. Yield values also were determined in the case of GeO_2/NaOH solutions in a cell similar to that shown in Fig. 1 but with the cathode at the bottom of the cathode compartment and identical in construction with that shown in Fig. 2 but without a Luggin. The aim of making the two arrangements identical was to obtain the same hydrodynamical conditions at the cathode. Note that there was no rotation of the cathode in either case; in fact, nearly all the electrolysis data reported here refer to a stationary cathode. It was shown that the cathode potential depended only on the partial current of hydrogen; this enabled an evaluation of the cathode potential if the hydrogen current was known.

Measurement of the lifetime of an intermediate product.—Some of the results reported below pointed to the possible production of an intermediate product which was sufficiently long lived so that there could be substantial diffusion of this material from the cathode into solution. If such an intermediate product were present in solution, it would be a stronger reducing agent than Ge. ($GeO_2 + 4H^+ + 4e_0^- = Ge + 2H_2O$: $e = -[0.15 + 0.059\,pH + 0.015\ pG]$, where pG is the negative of the logarithm of the GeO_2 concentration.) Thus, if Ge/GeO_2 is added to an acid solution containing vanadium(III) and vanadium(II) ions ($V^{3+} + e^- = V^{2+}$; $e^0 = -0.255$) no reduction of vanadium (III) will take place, if the conditions of the experiment are such that $e_{GeO_2,Ge}$ and $e_{V^{3+}/V^{2+}}$ are more positive than −0.15 v and more negative than about −0.2 v, respectively. But if this supposedly highly reducing intermediate product were added, a reduction of vanadium(III) might well occur.

A solution of known concentration of vanadyl sulphate in 8*N* HCl was reduced to the V^{2+} state with

Table I. Dependence of mean values* of ϕ, i_{GeH_4} and i_{Ge}, on current density and electrolyte composition

Composition†	ϕ‡	i_{GeH_4}	i_{Ge}
	c.d. = 3.10^{-2} amp-cm^{-2}		
2.0(2.5)	4.83×10^{-3}	1.2×10^{-4}	2.32×10^{-2}
	c.d. = 1.10^{-1} amp-cm^{-2}		
2.0(2.5)	0.0488	5.04×10^{-3}	7.06×10^{-2}
	c.d. = 8×10^{-1} amp-cm^{-2}		
2.0(2.5)	0.172	0.314	0.120
	c.d. = 1.2 amp-cm^{-2}		
5.5(1.6)	0.0900	0.294	0.170
3.0(1.6)	0.1200	0.378	0.188
2.0(1.6)	0.1199	0.361	0.169
2.0(2.0)	0.1498	0.436	0.144
3.0(2.0)	0.1384	0.402	0.151
5.5(2.0)	0.1261	0.378	0.118
8.0(2.0)	0.0820	0.251	0.215
3.0(2.8)	0.1839	0.521	0.106
5.5(2.8)	0.1479	0.412	0.206
8.0(2.8)	0.1175	0.346	0.188
	c.d. = 2.4 amp-cm^{-2}		
2.0(1.0)	0.0605	0.398	—
2.1(1.0)	0.0584	0.427	0.237
2.1(1.0)	(S)0.0422	0.384	0.264
3.0(1.0)	0.0568	0.360	—
4.0(1.0)	0.0421	0.322	—
5.0(1.0)	0.0398	0.302	—
6.0(1.0)	0.0340	0.281	—
7.0(1.0)	0.0278	0.235	—
8.0(1.0)	0.0192	0.166	—
9.0(1.0)	0.0113	0.086	—
10.0(1.0)	0.0099	0.084	—
5.5(1.3)	0.0611	0.427	0.245
2.25(1.4)	0.1026	0.650	0.293
2.0(1.5)	0.1100	0.778	0.0564
4.0(1.5)	0.0885	0.576	0.344
7.0(1.5)	0.0490	0.403	0.0451
9.0(1.5)	0.0300	0.218	—
4.6(1.8)	0.1010	0.641	0.301
2.0(2.0)	0.1367	0.713	—
3.0(2.0)	0.1310	0.749	—
5.0(2.0)	0.1160	0.806	—
7.0(2.0)	0.0755	0.552	0.158
8.0(2.0)	0.0625	0.458	0.212
2.4(2.1)	0.1444	0.811	0.383
2.0(2.25)	0.1623	0.902	0.301
2.0(2.4)	0.1610	0.960	0.185
3.0(2.4)	0.1563	0.917	—
5.0(2.4)	0.1344	0.794	—
7.0(2.4)	0.1010	0.593	0.484
9.0(2.4)	0.0750	0.497	0.362
2.0(2.5)	0.1734	0.907	0.414
2.5(2.5)	0.1630	0.924	0.266
8.0(2.5)	0.0820	0.578	0.204
9.5(2.5)	0.0615	0.442	0.262
3.0(2.6)	0.1605	0.924	0.269
7.0(2.6)	0.1020	0.655	0.299
8.5(2.6)	0.0860	0.590	0.240
2.0(2.7)	0.1832	1.018	—
3.0(2.7)	0.1730	0.974	0.258
4.0(2.7)	0.1495	0.847	—
5.5(2.7)	0.1309	0.890	0.0234
5.5(2.7)	(S)0.1315	0.706	0.152
7.0(2.7)	0.1164	0.742	0.241
10.0(2.7)	0.0667	0.439	0.152
2.75(2.75)	0.1724	0.931	0.392
3.4(2.8)	0.1630	0.924	0.293
3.8(2.8)	0.1600	0.922	0.399
2.0(3.0)	0.1914	1.034	—
3.0(3.0)	0.1728	1.010	—
3.5(3.0)	0.1730	0.936	0.343
4.0(3.0)	0.1612	0.972	—
5.0(3.0)	0.1507	0.991	—
7.0(3.0)	0.1200	1.013	—
8.0(3.0)	0.1030	0.898	—
10.0(3.0)	0.0738	0.631	—
4.5(3.1)	0.1640	0.888	0.369
	c.d. = 4.8 amp-cm^{-2}		
2.0(1.6)	0.0986	1.440	0.0890
3.0(1.6)	0.0970	1.272	0.566
5.5(1.6)	0.0592	0.965	0.0638
2.0(2.0)	0.1184	1.704	0.276
3.0(2.0)	0.1090	1.709	0.725
5.5(2.0)	0.0929	1.248	0.624
8.0(2.0)	0.0346	0.504	—
3.0(2.8)	0.1445	1.632	0.576
5.5(2.8)	0.1289	1.656	0.320
8.0(2.8)	0.0782	1.277	0.450

* Maximum errors in ϕ, i_{GeH_4}, and i_{Ge} are about ±0.5%, ±1.5%, and ±3%, respectively.
† Composition is given as normality NaOH and GeO_2 g/100 ml in brackets.
‡ Mole fraction GeH_4 in $GeH_4 - H_2$ mixture.
(S) Electrode rotated at ~250 rpm. Electrode stationary in all other cases.

Sn. This solution then was placed in a small beaker, and with nitrogen bubbling through the solution the oxidation-reduction potential of the V^{2+}/V^{3+} couple at a platinum electrode was measured against a calomel reference electrode. Then oxygen was bubbled through the solution until most, but not all, of the V^{2+} had been oxidized, as shown by the potential of the platinum electrode (from which the V^{2+}/V^{3+} ratio could be determined). All of the solution (about 10 ml) from the cathode compartment of a small electrolysis cell which had been in operation for about 20 min was drained off, filtered, and equal aliquots of the filtrate added to the $V^{2+} - V^{3+}$ containing solution at regular time intervals. The change in potential of the $V^{2+} - V^{3+}$ solution was measured each time; these changes occurred in a few seconds, and each time the potential remained constant at the new value. From these measurements it was possible to calculate (see later) the reducing power of the solution at each addition and thus to obtain a measure of the lifetime of the strongly reducing substance in the GeO_2/NaOH solution. The same experiments were repeated but without GeO_2 in the NaOH solution; this time material from the cathode compartment did not affect the V^{2+}/V^{3+} couple. Finally powdered Ge was added to the $V^{2+} - V^{3+}$ solution to determine its effect on the redox potential; it was undetectable.

Diffusion layer thickness.—A small quantity ($\sim 10^{-3}$ *M*) of tagged $Hg(CN)_2$ was added to the electrolyte in the cathode compartment of a cell similar to that shown in Fig. 1 but containing no bell and no stirring arrangement. $Hg(CN)_2$ is reduced readily at a Hg cathode and, since the concentration of the tracer is small, its partial current density can confidently be expected to be its limiting current. Hence a determination of the rate of removal of $Hg(CN)_2$ from

solution can be used to calculate the effective thickness of the diffusion layer, δ. Thus,

$$\frac{1}{\delta} = \frac{S}{DtA} \ln (n_o/n)$$

where S is the volume of solution in the cathode compartment; D is the diffusion coefficient for $Hg(CN)_2$; t is time of electrolysis; A is the surface area of the electrode; and n_o and n are the initial and final radioactivity of the solution, respectively.

Results

Partial currents.—The partial currents for the products of electrolysis, GeH_4, Ge, and H_2 are given in Table I and Fig. 3 and 4. The variation of ϕ, mole fraction of GeH_4 in the gas, with the nature of the cathode material was examined; results are shown in Table II. There is no simple relation apparent between yield and the hydrogen overpotential.

Cathode potential.—Hydrogen overpotential measurements on the cathode as a function of current density, 10^{-2} to 1 amp-cm^{-2}, in solutions of 2 and 10N NaOH are shown in Fig. 5. The Tafel b-function obtained is in agreement with the over-all results of Bockris and Watson (4) obtained at lower current densities and for more dilute NaOH solutions. Cathode potential measurements also were made with a solution of 2N NaOH containing 2 g GeO_2/100 ml; a plot of the cathode potential against the current density for hydrogen evolution gave a curve identical with curve 1 in Fig. 5. Thus the cathode potential in the presence of GeO_2 can be defined as long as the hydrogen current is known.

Table II. Yield, ϕ, at different cathodes
Electrolyte composition: 10N NaOH, 2 g GeO_2/100 ml

Cathode material	Current density, amp-cm^{-2}	ϕ
Hg (Na)	0.90	0.19
Pb	0.88	0.0460
Th	0.90	0.019
Ge (p-type)	8.0	0.0102
Ge (n-type)	8.0	0.0058
Ta	1.45	0.0006
Pt	0.25	<0.0005

ϕ = mole fraction GeH_4 in $GeH_4 - H_2$ mixtures.

A plot of i_{GeH_4} vs. cathode potential (Fig. 8) yields a Tafel slope of -56 ± 2 mv per decade. It is quite possible, however, that the appropriate current to use is not i_{GeH_4}, since, as has been noted above, an intermediate product (abb. I.P.) diffuses away from the cathode. If the I.P. occurs before the rate-determining step, then η vs. i_{GeH_4} is the correct way to obtain the overpotential for the GeH, production process. If, on the other hand, the I.P. occurs after the rate-determining transition state, then the current of material going through the rate-determining transition state will be

$$I = i_{GeH_4} + (8/m) i_{Ge}$$

where m is the number of stages of reduction (from $GeO_3^{=}$) that the I.P. has gone through. This presupposes that i_{Ge} is due to the I. P., and this interpretation of the facts is suggested by the result that, as stirring at the cathode is increased, i_{GeH_4} decreases and i_{Ge} increases. Furthermore, if Ge were produced at the cathode, the comparative yield of GeH, would be very much lower since Ge electrodes give very low GeH, yields (whence the reaction Ge → GeH, would appear to go with difficulty). Since no plot of η vs. ln I for values of m from 1 to 4 yields a single Tafel slope, it is suggested that the I.P. occurs before the rate-determining transition state.

Intermediate product.—The reducing power of solution drawn from the cathode compartment is shown as a function of time in Fig. 6. The initial concentration of V^{2+}, $(a_{V^{2+}})_{t=0}$, was known and $(a_{V^{2+}})_{t=0} << (a_{V^{3+}})_{t=0}$, i.e., 10^{-4} N: 1N; since the over-all change in $a_{V^{2+}}$ was from 10^{-4} N to 1.8×10^{-4} N the concentration of the V^{3+} can be taken as constant. Thus the change in potential, ΔE, due to reduction of

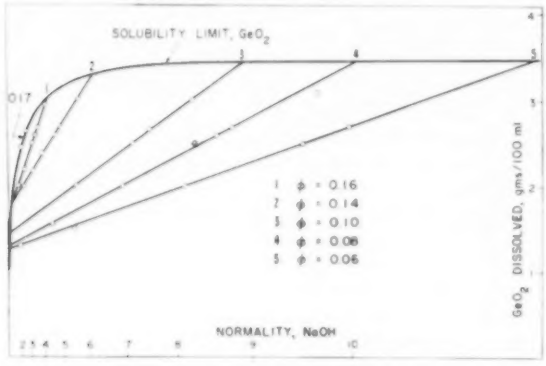

Fig. 3. Lines of constant yield, ϕ, current density 2.4 amp-cm^{-2}

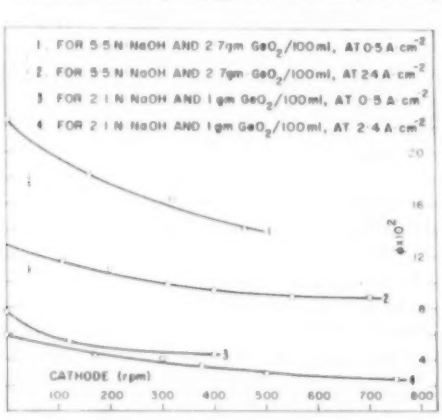
1. FOR 5.5 N NaOH AND 2.7 gm GeO2/100 ml, AT 0.5 A cm-2
2. FOR 5.5 N NaOH AND 2.7 gm GeO2/100 ml, AT 2.4 A cm-2
3. FOR 2.1 N NaOH AND 1 gm GeO2/100 ml, AT 0.5 A cm-2
4. FOR 2.1 N NaOH AND 1 gm GeO2/100 ml, AT 2.4 A cm-2
φ %
CATHODE (rpm)

Fig. 4. Variation of ϕ with cathode rotation

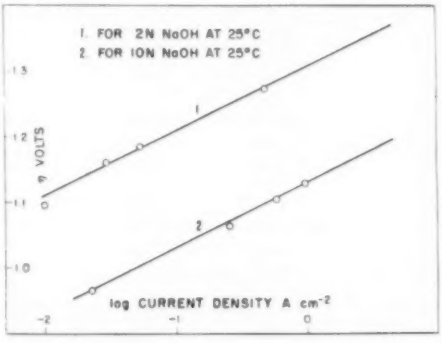

Fig. 5. η vs. $\log_{10}$ current density

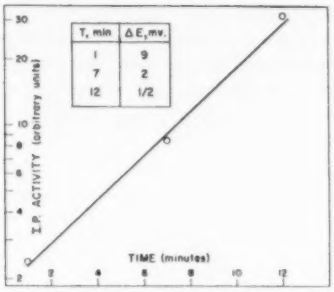

Fig. 6. Decay of intermediate product

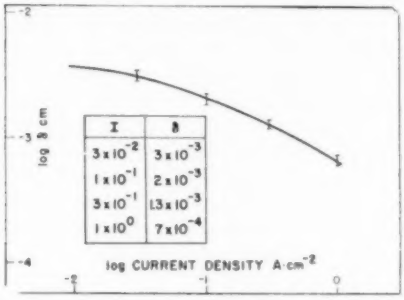

Fig. 7. Change of diffusion layer thickness with current density.

V^{2+}, by reactive intermediate at a time t' after removal from the cathode compartment is,

$$\Delta E = RT/F \ln [(a_{V^{2+}})_{t=t'}/(a_{V^{2+}})_{t=0}]$$

The concentration of the intermediate product is proportional to the amount of V^{2+} reduced, i.e., $\propto [(a_{V^{2+}})_{t=t'} - (a_{V^{2+}})_{t=0}]$. Upon a further addition of reactive intermediate, the new V^{2+} concentration can be determined from the potential change and so the concentration of reactive intermediate at time t'' was

$$\propto [(a_{V^{2+}})_{t=t''} - (a_{V^{2+}})_{t=t'}], \text{ etc.}$$

The slope of the line of $\log_{10} [(\Delta a_{V^{2+}})_{\Delta t}]$ vs. t (Fig. 6) gave a mean life for the intermediate product of 4.3 min: this presupposes a monomolecular decay process.

The nature of the intermediate product has not been established by direct chemical means. However, it has been shown that the intermediate product does not give rise to H_2 in solution. An electrolysis cell with a U-shaped cathode compartment was used; the cathode was in one limb and the other limb was filled completely with electrolyte. Convective mixing was relatively unhampered as shown by the Ge particles first formed near the cathode appearing in the opposite limb in ~ 1 min. There was no accumulation of H_2 gas in the sealed limb after prolonged electrolysis.

Diffusion layer.—The measurement of diffusion layer thickness for various current densities in 2*N* NaOH solution, using tagged $Hg(CN)_2$, is shown in Fig. 7. The presence of GeO_2 in solution could not be tolerated since the Ge metal produced might well adsorb some of the $Hg(CN)_2$. That $Hg(CN)_2$ is the only diffusing mercury species has been established by Tomes (5). Its diffusion coefficient in 10^{-2} *N* NaOH is (6) 1.56×10^{-5} cm^2 sec^{-1} at 28°C. The diffusion coefficient for $Hg(CN)_2$ in more concentrated solutions of NaOH has been calculated from this value assuming Stokes law applies, values for the viscosity of aqueous solutions of NaOH being available (7). The applicability of Stokes law for the diffusion of zinc sulfate and zinc acetate in various concentrations of NaOH solution has been tested by Brasher and Jones (8) and has been found to be valid: it is therefore reasonable to assume that $Hg(CN)_2$ in NaOH solutions also obeys Stokes law.

Discussion

The experiments of Pugh (9) and Carpéni (10) have shown that, when GeO_2 is dissolved in NaOH solutions of pH $\geq$ 13, the Ge will be present as $GeO_3^=$; all the solutions used in this study were of pH > 14.

Transport to the cathode.—The variation of ϕ with current density and cathode stirring rate suggests that the over-all electrochemical process is not entirely activation controlled; thus it is necessary to consider the diffusion of various ions toward and away from the cathode. The primary species moving to the cathode are Na^+ and $GeO_3^=$. Na^+ ions move to the cathode under a favorable potential gradient and $GeO_3^=$ ions approach the cathode by diffusion and convection in an adverse potential gradient. Wagner (11) has treated these cases in a theoretical study of the electroreduction of anions in solutions of high electrolyte concentration. The solution of the diffusion equation for the discharge of Na^+ shows that the Na^+ concentration at the cathode does not rise above 1.1 times the bulk Na^+ concentration for the highest current densities employed in this study. The Na^+ concentration is enhanced at the cathode since discharged Na^+ ions react with water; the change in water concentration at the cathode is insignificant. The transport rate per unit time per unit area along the x-coordinate (which is normal to the surface of the electrode and is measured from the cathode) of ions of type i to the cathode under steady-state conditions, is given by (11)

$$\frac{1}{A}\frac{dn_i}{dt} = -c_i D_i \left(\frac{\partial \ln c_i}{\partial x} + \frac{z_i F}{RT}\frac{\partial \Psi}{\partial x} \right) \quad [1]$$

where the symbols are: dn_i/dt, number of moles of i passing cross section, A, per unit time; D_i, diffusion coefficient of ions of type i; c_i, their concentration; z_i, their valence; F, the Faraday; Ψ, electrical potential; R, gas constant; and T, absolute temperature. It is reasonable to make the simplifying assumption that the cathode is covered by a static diffusion layer, thickness δ, beyond which concentration differences are negligible owing to convective mixing: concentration changes will occur only between $x = 0$ and $x = \delta$. In Eq. [1] the first term on the right hand side accounts for transport due to a concentration gradient, and the second term accounts for electrolyte migration. As Wagner points out, if the potential difference across the diffusion layer is $< RT/F$ (0.025 v at room temperature) then the potential gradient will have little effect on anion migration. The value of $(\partial\Psi/\partial x)\delta$ was always <0.025 v in the systems studied. This argument assumes an

essentially linear potential gradient across δ. The validity of this assumption is not in question except at short distances from the electrode, $<10^{-6}$ cm (δ is typically 10^{-4} cm) when deviations from local charge neutrality can occur, i.e., the region of the Stern double layer. Since all the solutions used were concentrated electrolytes it is known that (12) a diffuse layer (i.e., Gouy layer) was not present, so Eq. [1] will be applicable up to the outer Helmholtz plane of the cathode.

The transport of ions from the bulk of the electrolyte to the outer Helmholtz plane has been considered thus far. An outline of the derivation of the equation for electron transfer to an anion follows. Consider the electrochemical reaction

$$A^{z-} + e^- \rightarrow A^{(z+1)-} \qquad [2]$$

For zero applied p.d. the initial state for this reaction is A^{z-} ions in the outer Helmholtz plane and electrons in the cathode. The final state is $A^{(z+1)-}$ anions partially adsorbed on the cathode. When a p.d. η is applied across the Helmholtz double layer the change in Galvani p.d. is η and if the dipole distribution in the Helmholtz double layer is taken to be unchanged, and the fractional surface coverage due to $A^{(z+1)-}$ is far from unity or close to unity (i.e, 0.9) then η may be equated to the Volta p.d. across the Helmholtz double layer. That is, η is due to the building up of excess, equal and opposite charge, on either side of the Helmholtz double layer. This is the usual assumption made in current theories of hydrogen overpotential and seems to be in accord with the facts. If the potential in the outer Helmholtz plane is arbitrarily taken as zero, then an applied (negative) potential η will increase the potential energy of the electrons in the cathode by an amount $F\eta$ per mole. That is, the potential energy of the initial state is increased by amount $F\eta$ per mole. The potential energy of the final state is raised by $(d_o - d/d)F\eta$ per mole, where d_o is the thickness of the Helmholtz double layer and d is the distance from the metal side of the Helmholtz double layer to the species $A^{(z+1)-}$. Thus the applied p.d. will have reduced the activation energy for the forward path of reaction [2] by

$$\beta F\eta(d/d_o) \qquad [3]$$

where β is the Tafel symmetry factor [discussed fully by Bockris (1)]. Since d_o is taken to be 5 to 10 times greater than $(d_o - d)$, the term (d/d_o) in Eq. [3] can be neglected. Whence, in the form usual for electron transfer reactions from the cathode, the forward velocity of reaction [2] is given by

$$i = i_o \exp(-\beta F\eta/RT) \qquad [4]$$

The limiting current, i_l, for $GeO_3^=$ calculated from Eq. [1], using a typical set of values, shows for all but the highest current densities that $i << i_l$: this gives rise to two limiting cases for GeH_4 evolution,

$$i_{GeH_4} = i_o[\exp(-\alpha\eta F/RT)] \qquad [5]$$

and

$$i_{GeH_4} = i_l[1 - \exp(\eta 8F/RT)] \qquad [6]$$

where, for the GeH_4 formation reaction, i_o is the exchange current and α is the Tafel transfer coefficient. Eqs. [5] and [6] are for activation and diffusion controlled processes, respectively. A plot of log i_{GeH_4} vs. cathode potential (Fig. 8) obeys the form of Eq. [5] over a range of >0.2 v and four decades of current density. Thus it is concluded that the GeH_4 formation reaction is largely activation controlled.

Consecutive electrode processes.—The $GeO_3^=$ reduction process is taken to be a sequence of consecutive reactions. The method of handling such reactions is outlined below. Christiansen (13) has shown how the steady-state reaction rate for an open sequence of reactions can be represented in terms of the rate constants of the elementary reactions and the concentration of the stable components. In a sequence of reactions such as

$$A_1 \underset{s_{-1}}{\overset{s_1}{\rightleftharpoons}} X_1 + B_1\,,\ X_1 + A_2 \underset{s_{-2}}{\overset{s_2}{\rightleftharpoons}} X_2 + B_2 \ldots \text{ etc.} \qquad [7]$$

where the A's and B's are stable components and the X's are reactive intermediates and s and s_- are the forward and reverse reaction rates, respectively. A set of quantities ω are defined such that:

$$\omega_1 = s_1 = k_1 c_{A_1}$$

$$\omega_{-1} = \frac{s_{-1}}{c_{X_1}} = k_{-1} c_{B_1}$$

$$\omega_{-n} = s_{-n} = k_{-n} c_{B_n}$$

The principle of detailed balance is assumed, whence the over-all reaction rate, S, is given by:

$$S = s_1 - s_{-1} = s_2 - s_{-2} \ldots = \omega_1 - \omega_{-1} c_{X_1} = \omega_2 c_{X_1} - \omega_{-2} c_{X_2} \ldots$$

This gives rise to an expression for S which can be written generally as:

$$S = \frac{\prod_{k=1}^{k=n} \omega_k}{\sum_{m=2}^{m=n+1} \prod_{k=m}^{n} \omega_k \prod_{l=1}^{l=m-2} \omega_{-l}} \qquad [8]$$

where m goes from 2 to $n + 1$ and $\prod_a^b = 1$ if $b < a$.

Bockris (14) first applied this method to the calculation of the over-all rate of electrochemical reac-

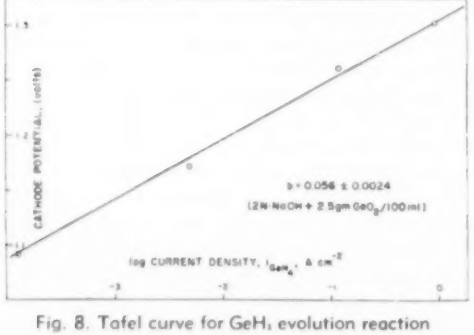

Fig. 8. Tafel curve for GeH_4 evolution reaction

tions for oxygen evolution. The essential change to be made from the application to chemical kinetics is that the rate constants in reactions involving charge transfers are potential dependent. Thus, for a cathodic reaction, the rate constant for a partial cathodic reaction becomes

$$\vec{\bar{k}} = \vec{k} \exp\left[-\beta \Delta\xi \, nF/RT\right] \qquad [9]$$

where $\vec{\bar{k}}$ and $\vec{k}$ are the electrochemical and chemical rate constants, respectively; $\Delta\xi$ is the Galvani p.d. between the electrode and the solution; and n is the number of electrons transferred. Correspondingly for the partial anodic reaction

$$\overleftarrow{\bar{k}} = \overleftarrow{k} \exp\left[(1-\beta)\, \Delta\xi \, nF/RT\right] \qquad [10]$$

These rate constants, utilized in partial reactions which involve charge transfer, give rise to potential terms in the final expression for the over-all reaction, and hence allow the evaluation of $\partial\Delta\xi/\partial \ln n_i$, i.e., the Tafel slope, b, characteristic of a given reaction mechanism. Thus a typical reaction sequence is examined for each partial reaction, in turn, being the rate-determining step (r.d.s.). In each case it can be taken that the reactions preceding the r.d.s. are fast, so that $k_+/k_- = K$, an "equilibrium" constant. Further, if $k_{+\text{r.d.s.}} \to k_{-\text{r.d.s.}} \to 0$, and $k_{+\text{r.d.s.}} \geqq 10\, k_{-\text{r.d.s.}}$, then all terms involving $k_{-\text{r.d.s.}}$ in the denominator of Eq. [8] can be neglected. This gives rise to a simple expression for the over-all rate which involves only one rate constant, i.e., $k_{+\text{r.d.s.}}$, and Eq. [8] can be written for the ith rate-determining step:

$$S = \prod_{k=1}^{k=i} \omega_k \Big/ \prod_{k=1}^{k=(i-1)} \omega_k \qquad [11]$$

This expression is used here in the evolution of various reaction paths.

Mechanism of $GeO_3^=$ → GeH_4 *reaction.*—The final chemical products occurring at the cathode are H_2, Ge, and GeH_4. The reduction of $GeO_3^=$ to give GeH_4 can be represented by the over-all stoichiometric equation,

$$GeO_3^= + 7H_2O + 8\, e^- \to GeH_4 + 10\, OH^-$$

The over-all reduction reaction is taken to occur in a set of simple consecutive reactions, i.e., it is taken to be an open sequence of reactions. Since it is unlikely that the first step in the reduction of the $GeO_3^=$ ion can occur in two different, and approximately equally probable ways, the production of Ge must be taken to be due to a branch reaction in the $GeO_3^=$ → GeH_4 reaction sequence. If absorbed hydrogen atoms are used at any stage in the reduction of $GeO_3^=$ ions, then the $GeO_3^=$ → GeH_4 reaction sequence is complex, and H_2 evolution can be considered to be a branch reaction. But, if $GeO_3^=$ → GeH_4 does not involve the use of absorbed hydrogen atoms, then H_2 evolution is a process which occurs in parallel with the $GeO_3^=$ reduction process.

If atomic hydrogen is used in the reduction process it must be treated as one of the "stable" products, A, in the reaction sequence, Eq. [7]. Since the reaction which produces atomic hydrogen cannot be treated as in equilibrium as compared with the r.d.s. of the $GeO_3^=$ → GeH, reaction an expression for the steady-state concentration of atomic hydrogen is required. Bockris and Watson (4) have shown that the reaction of sodium atoms with water is the rate-determining step in the hydrogen evolution reaction on mercury cathodes in aqueous NaOH solutions. Whence, assuming the reaction

$$Na + H_2O \to Na^+ + OH^- + H$$

The surface concentration of atomic hydrogen will be directly proportional to the surface sodium atom concentration (the activity of water is taken to be large and invariant). Furthermore, these workers found that the surface activity of sodium atoms is proportional to exp $(-F\eta/2RT)$; thus,

$$c_H = C \exp\left(-F\eta/2RT\right) \qquad [12]$$

where C is a constant at constant electrolyte composition.

Unfortunately the work of Bockris and Watson (4) is not completely convincing, e.g., these workers accept the experimental fact that the reaction rate of sodium atoms with water depends on the square root of the sodium concentration but do not show in their proposed reaction mechanism how this comes about. Also, they assume that barium amalgams behave in a similar way, but Kaplsan and Jofa (15) have shown that for Ba the reaction rate with water is proportional to $[Ba]^{1/4}$. Bockris and Watson, however, present cogent reasons for rejecting all other simple reaction paths for the hydrogen evolution reaction of sodium amalgam electrodes in NaOH solution other than the mechanism mentioned above. Thus in the absence of evidence to the contrary the mechanism of Bockris and Watson must be accepted, bearing in mind that the analysis given below would have to be re-examined in the light of any new and contrary development arising out of this point.

Table III. Potential dependent factors introduced into Eq. [11] by an elementary reaction. $x \equiv \eta F/RT$ (when $\beta = \frac{1}{2}$)

Reaction	Factor r.d.s.	Factor Equil.
1. $A^{z-} + e^- \to A^{(z+1)-}$	$e^{-x/2}$	e^{-x}
2. $A^{z-} + H \to HA^{z-}$	$e^{-x/2}$	$e^{-x/2}$
3. $A^{z-} + H + e^- \to HA^{(z+1)-}$	e^{-x}	$e^{-3x/2}$

By means of Eqs. [11] and [12] Table III lists the factor that an elementary reaction will introduce into the final expression for S, depending on whether the reaction is rate determining or precedes the r.d.s. whence it is treated as being in equilibrium. The Tafel slope for the $GeO_3^=$ → GeH_4 reaction is $-RT/F$, from experiment. Use of Eq. [11] shows that each successive stage of reduction leads to a smaller Tafel slope. Thus the possible reaction paths up to the rate-determining step which give a Tafel slope of $-RT/F$ can be written, viz:

(i) $$GeO_3^= + e^- \xrightarrow{\text{fast}} GeO_3^-$$

$$GeO_3^- + H_2O \xrightarrow{\text{slow}} H\,GeO_3^- + OH^-$$

(ii) $$GeO_3^{=} + H \xrightarrow{\text{fast}} H\,GeO_3^{-}$$

$$H\,GeO_3^{-} + H_2O \xrightarrow{\text{slow}} H_2GeO_2^{-} + OH^{-}$$

or,

$$(H\,GeO_3^{-} \xrightarrow{\text{slow}} GeO_2^{-} + OH^{-})$$

(iii) $$GeO_2^{=} + H \xrightarrow{\text{fast}} GeO_2^{-} + OH^{-}$$

$$GeO_2^{-} + H_2O \xrightarrow{\text{slow}} H\,GeO_2 + OH^{-}$$

(iv) $$GeO_3^{=} + H + e \xrightarrow{\text{slow}} H\,GeO_3^{=}$$

(v) $$GeO_3^{=} + H + e \xrightarrow{\text{slow}} GeO_2^{=} + OH^{-}$$

Since an intermediate product of high reducing power appears to diffuse away from the electrode before the r.d.s., from (i) to (v), this must be GeO_3^{2-}, $HGeO_3^{2-}$, or GeO_2^{-}. Thus the reactions (iv) and (v) are excluded as possible reaction paths since $GeO_3^{=}$ is the only Ge species before the rate-determining transition state. It is not possible to say on the basis of the work done here which of the remaining possibilities, (i), (ii), or (iii) is the actual mechanism. However, it should be possible to distinguish between reduction by electron transfer and reduction by atomic hydrogen on the basis of two further experiments, viz., (*a*) reduction in divalent alkali metal solutions, rather than NaOH, where $c_H \propto \exp(-\eta F/RT)$ should give different Tafel slopes if atomic hydrogen is involved in the reduction; (*b*) reduction at high current densities where the surface concentration of atomic hydrogen reaches a limiting value (4) should give $\partial\eta/\partial \ln i \rightarrow 0$ if atomic hydrogen is used in the r.d.s.; otherwise there should be no variation in the Tafel slope with current density.

Acknowledgment

The authors are pleased to acknowledge their thanks to Professor Carl Wagner and Professor J. O'M. Bockris for their interest and helpful suggestions. The method for determining the diffusion layer thickness was based on a suggestion of Professor Wagner's.

Manuscript received March 14, 1958. The research reported in this document was supported jointly by the Army, Navy, and Air Force under contract with M.I.T.

Any discussion of this paper will appear in a Discussion Section to be published in the December 1959 JOURNAL.

REFERENCES

1. J. O'M. Bockris, "Modern Aspects of Electrochemistry," p. 180, Butterworths Scientific Publications, London (1954).
1a. *Ibid.*, p. 190.
2. M. Green and P. H. Robinson, *Anal. Chem.*, **25**, 1913 (1953).
3. R. Piontelli and G. Polli, *Gazz. Chim. Ital.*, **78**, 717 (1948); R. Piontelli, *Z. Elektrochem.*, **55**, 128 (1951).
4. J. O'M. Bockris and R. G. H. Watson, *J. Chim. Phys.*, **49**, 070 (1952).
5. J. Tomes, *Collection Szechoslav. Chem. Communs.*, **9**, 12, 81, 150 (1937); see also I. M. Kolthoff and J. J. Lingane, "Polarography," p. 232, Interscience Publishers, New York (1952).
6. J. Newman, Private communication.
7. "International Critical Tables," New York, **5**, 15 (1926).
8. D. M. Brasher and F. R. Jones, *Trans. Faraday Soc.*, **42**, 775 (1946).
9. W. Pugh, *J. Chem. Soc.*, **1929**, 1537.
10. G. Carpéni, *Bull. Soc. Chem., France*, **15**, 629 (1948).
11. C. Wagner, *This Journal*, **101**, 181 (1954).
12. D. C. Grahame, *Chem. Revs.*, **41**, 441 (1947).
13. J. A. Christiansen, *Z. Physik. Chem.* (*B*), **28**, 303 (1935); *ibid.*, **33**, 145 (1936).
14. J. O'M. Bockris, *J. Chem. Phys.*, **24**, 817 (1956).
15. O. L. Kaplsan and Z. A. Jofa, *Zhur. Fiz Khim.*, **26**, 193 (1952); *ibid.*, **26**, 201 (1952).

The Electrical Conductivity of Sweat

II. The Interionic Attraction Factor and the Conductivity of Undiluted Sweat in the Study of Cystic Fibrosis

Andre J. deBethune and Truman S. Licht

Department of Chemistry, Boston College, Chestnut Hill, Massachusetts

and Milton Stern and Harry Shwachman

Division of Laboratories and Research, Children's Medical Center, and Department of Pediatrics, Harvard Medical School, Boston, Massachusetts

ABSTRACT

The electrical conductivity of sweat is a useful criterion for the study and diagnosis of *cystic fibrosis*. The sweat conductivity usually is determined from measurements on diluted sweat solutions. A method of calculation is presented to account for the interionic attraction effects due to the greater ionic strength in the undiluted parent sweat sample. This introduces a correction of the order of 10% in the conductivity based on the dependence of equivalent conductance on ionic strength. Experimental verification of the correction is given for synthetic mixtures of sodium and potassium chlorides and for a natural sweat sample. Sweat conductivity data obtained from a study of 77 control subjects and 47 cystic fibrosis patients are summarized, after application of this correction.

In a study of the electrolyte content of thermally induced eccrine sweat, Licht, Stern, and Shwachman (1) described a technique for the measurement of the electrical conductivity of sweat. They reported values of sweat conductivity for subjects with and without the disease *cystic fibrosis* and showed that for cystic fibrosis patients a threefold elevation of sweat conductivity was obtained which was significant enough to be used as a diagnostic criterion.

The method of obtaining sweat samples by collection on a weighed gauze pad and elution of electrolytes with distilled water necessitates that chemical and physical tests be performed on diluted solutions. As pointed out in (1) calculation of sweat conductivity from data obtained in diluted sweat solutions, without taking into account the interionic attraction effects due to greater ionic strength in the parent sample, results in conductivities approximately 10% too high. While this error is of no significance when sweat conductivity is used as a diagnostic criterion for cystic fibrosis, it does become important when sweat conductivities are correlated with ionic composition, a study which is currently in progress and will be reported elsewhere. The present paper attempts to develop a method of calculation which introduces a correction for the dependence of equivalent conductance on ionic strength. Conductivity data are presented for sodium and potassium chloride mixtures and for pure sweat and diluted sweat solutions which show that sweat conductivities calculated by this corrected method are reliable within 2 to 3%. Sweat conductivities presented in (1) from a study of 77 control subjects and 47 cystic fibrosis patients are recalculated. Availability of these more accurate values will permit correlation with analytical information and aid in the further elucidation of the electrolyte constitution of sweat.

Experimental

The thermal induction of sweat by placing the subject in a plastic bag, the collection of sweat on a weighed gauze pad, and the subsequent measurement of the diluted sweat sample in a special 3-ml conductivity cell with the Serfass conductance bridge has been described in (1). To establish the validity of the interionic attraction factor (described below), it was necessary to collect pure sweat not exposed to air long enough for evaporation to occur. Using a 1-ml pipette as a capillary tube, drops of pure sweat were collected. The volumes of such samples ranged from 0.2 to 1 ml and their conductivity could be measured directly in a Sunderman conductivity pipette[1] with a cell constant of 12.7 cm^{-1}. This pipette, which has a nominal capacity of 0.5 ml, could be used for measuring as little as 0.2 ml by floating the sample on top of mercury (mercury in the stem only). Five to fiftyfold dilutions were prepared with conductivity water and the conductivity again measured. The specific conductance of mixtures of sodium and potassium chloride in the range of pure and diluted sweat samples were measured also.

Theoretical

In (1), the sweat conductivity (i.e., the specific conductance of sweat in micromhos per centimeter),

[1] Available from Arthur H. Thomas Co., Philadelphia, Pa.

to be here denoted by L_s', was calculated from experimental observables by the relation

$$L_s' = (J_s - J_b)KF \qquad [1]$$

where J_s and J_b are the observed conductances in micromhos at 25°C of the diluted sweat solutions and blank solutions, respectively; K is the cell constant in cm^{-1}; F, the dilution factor, is the volume ratio of diluted to undiluted sweat. The grouping $(J_s - J_b)K = L_d$ is the observed conductivity of the diluted sweat solution. Multiplication by the dilution factor F is based on the tacit assumption that conductivity is a linear function of concentration.

This assumption is approximately valid for strong electrolytes over narrow concentration ranges and corresponds to the hypothesis that ionic mobilities and equivalent ionic conductances are constants independent of ionic strength. In point of fact, interionic attraction effects lead to a decrease of ionic mobilities and ionic conductances with increasing ionic strength (2-4).

Over the range of dilution factors F (5-fold to 58-fold) utilized in (1), the equivalent conductances of sodium, potassium, and chloride ions drop by about 5 to 15% in going from the diluted to the parent sweat sample, and the sweat conductivities calculated by Eq. [1] are too high by the same amount.

It is therefore desirable to correct the sweat conductivities L_s'. This can be done by the equation

$$L_s = L_dFS = L_s'S \qquad [2]$$

where L_s is the "corrected" sweat conductivity, and the interionic attraction factor S accounts for the drop-off of the equivalent conductances with increasing ionic strength.

The conductivity L of any electrolyte (in micromhos per centimeter) is equal to the summation of terms of the form $c_j\Lambda_j$ where c_j is the number of milliequivalents per liter and Λ_j is the equivalent conductance of the j^{th} electrolyte. By taking the ratio of L_s to L_dF, it can be shown that the factor S is given by

$$S = \Sigma(x_j\Lambda_j)_s/\Sigma(x_j\Lambda_j)_d \qquad [3]$$

where x_j is the equivalent fraction of the j^{th} electrolyte in the total electrolyte content (normality of j/ total normality of all electrolytes). In both cases, the Λ_j's are determined by the total ionic environment (5, 6), i.e., by the total ionic strength, of the liquid: either the parent sweat sample s or the diluted sweat sample d.

The composition of sweat (1, 7-10) is such that 60-90% of the conductivity may be attributed to sodium and potassium chlorides, the remainder being due chiefly to calcium, sulfate, and lactate. The pH ranges from 4 to 7. Sodium chloride constitutes 50-90% of the sum of the sodium and potassium chloride normality. It was therefore decided, as an approximation, to restrict the summations in [3] to the two salts j = NaCl, and KCl. Since Λ values for the mixtures of these salts were not readily available, the Λ's of the pure salts were used (4a, 11). It was postulated that *the Λ of a salt in a mixture is equal to the Λ of the same pure salt at the same total ionic strength.* This postulate was verified experimentally by us for synthetic mixtures of sodium and potassium chlorides in the total chloride concentration range of 2 to 100 mEq/l, and shown to be valid within the experimental error of the measured conductivity (1%) (Table I). The calculated values in Table I were computed from

$$L(\mu mho/cm) = (c\Lambda)_{KCl} + (c\Lambda)_{NaCl} \qquad [4]$$

where the c's are in milliequivalents per liter, and the Λ's are chosen in accordance with the *ionic strength postulate* stated above.

Table I. Conductivity of NaCl—KCl mixtures (25°C)

c (KCl), mEq/l	c (NaCl), mEq/l	L (observed), μmho/cm	L (calculated, Eq. [4]), μmho/cm
100	0	(12,896)	12,896
0	100	10,590	10,674
50	50	11,790	11,785
25	75	11,200	11,230
10	0	1414	1413
0	10	1178	1185
5	5	1288	1299
2.5	7.5	1266	1242
1	1	268	268.5

In 1911, Bray and Hunt (12) determined the conductivities of mixtures of sodium chloride and hydrochloric acid. Their observed conductivities agreed with values calculated from the ionic strength postulate within about 1% up to ionic strengths of about 0.1M. Deviations due to the "mixture effect" (5,6) of cations of widely different mobilities with a common anion are to be expected and tend to make the conductivity calculated from the ionic strength postulate slightly high. Bray and Hunt consistently observed a small but systematic deviation in this direction. In their work, this deviation reached a maximum in equimolar mixtures of the two electrolytes, dropping off as the mixtures approached either one or the other pure electrolyte. These maximum mixture effect deviations attained the values: 2.0% in a mixture of 100 mEq/l of HCl and NaCl; 1.1%, in 20 mEq/l of each; 0.68%, in 5 mEq/l of each. Since the mobilities of potassium and sodium ions are much closer than those of hydrogen and sodium ions, the mixture effect should be smaller in sweat and in the synthetic mixtures akin to sweat investigated in the present study than it was in Bray and Hunt's studies. It was felt by us that the mixture effect could be neglected safely, and that the ionic strength postulate should be reliable within 1% or better in the present instance.

The calculation of the interionic attraction factor S is best illustrated by an example. Consider a "parent sweat sample" initially 0.100N in chloride ion. By a 50-fold dilution, this is reduced to 0.002N in the "diluted sweat solution." The Λ's of pure KCl and NaCl at 25°C are, respectively, 128.96 and 106.74 mho cm^2 Eq^{-1} at 0.1N, and 145.80 and 122.70

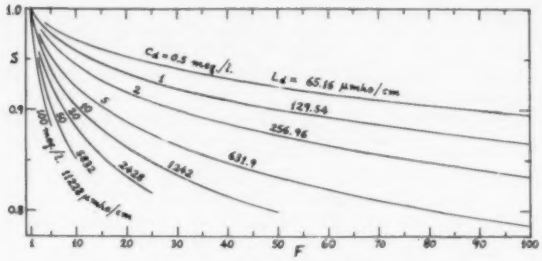

Fig. 1. Interionic attraction factor S for a 25 eq. % KCl : 75 eq. % NaCl mixture as a function of dilution factor F, diluted sweat sample electrolyte concentration c_d (in milliequivalents per liter), and diluted sample conductivity L_d (in micromhos per centimeter at 25°C).

at 0.002*N* (4, 11). The *S* factor calculated from Eq. [3] then takes on the value 0.884, 0.881, 0.878, 0.874, and 0.870, as the equivalent ratio of KCl:NaCl goes from 100:0 to 75:25, 50:50, 25:75, and 0:100, respectively. At less than 50-fold dilution, the spread in *S* values is even less. Thus the *S* factor is an insensitive function of the actual KCl to NaCl ratio. The 25KCl : 75NaCl equivalent ratio was arbitrarily selected as representative of the bulk of sweat samples, and was used in the construction of the family of *S* curves plotted in Fig. 1. Here, the *S* factor is given as a function of two variables, the total chloride concentration c_d of the diluted sample (in mEq/l), and the dilution factor *F*. In addition, each curve (of constant c_d) is identified by the appropriate value of L_d, the diluted sample conductivity (in micromhos per centimeter at 25°C) calculated from Eq. [4].

In practice, the interionic attraction factor *S* is determined as follows. The available empirical data on any actual sweat sample are, as already noted, the diluted sweat conductivity $L_d = (J_o - J_b)K$ and the dilution factor *F*. The value of *S* is then read off the curves of Fig. 1, at the proper value of *F*, by visual interpolation between the several L_d values. The final "corrected" sweat conductivity L_s is then calculated as $(J_o - J_b)KFS$.

Sweat Conductivity

To establish the validity of the interionic attraction factor *S*, pure sweat samples were collected from three subjects as described above and the conductivity of undiluted and diluted portions measured. Table II shows the data obtained for one of these samples from a cystic fibrosis patient whose undiluted sweat conductivity was measured directly as 15,500 μmho/cm. The sample was diluted five to fifty-fold, and the conductivity measured again. The uncorrected "sweat conductivities" L_s' calculated by Eq. [1] ranged from 17,150 to 18,320, about 11 to 18% high. Application of the *S* factor (Fig. 1) yielded "corrected sweat conductivities" L_s ranging from 15,300 to 16,030, i.e., from 1.3% low to 3.4% high, the average error being 2.2% for the dilutions of this one sample. On all three subjects, uncorrected conductivities L_s' ranged from 7 to 23% high; values corrected by use of the *S* factor ranged from 2.7% low to 5.7% high, the average error being 3.3%.

Table II. Comparison of observed and calculated sweat conductivities for a pure and diluted sweat sample (25.0°C, cell constant $K = 12.7\ cm^{-1}$) (CF Subject No. 1693)

L_d (observed), μmho/cm	*F*	*S*	L_s' (uncorrected), μmho/cm	L_s (corrected), μmho/cm
15,500*	1*	1*	15,500*	15,500*
3430	5	0.918	17,150	15,740
1780	10	0.893	17,780	15,880
916	20	0.875	18,320	16,030
352	50	0.87	17,590	15,300

* Pure undiluted sweat.

Table III. Typical sweat conductivity data for subjects with and without cystic fibrosis (25°C)

Subject No.	L_d (observed), μmho/cm	Dilution factor, *F*	Interionic attraction factor, *S*	Sweat conductivity: L_s' (uncorrected), μmho/cm	Sweat conductivity: L_s (corrected), μmho/cm
A. For Children with Cystic Fibrosis					
474	229	47.43	0.879	10,860	9540
505	1274	10.60	0.897	13,510	12,110
532	550	21.31	0.896	11,720	10,500
646	2655	5.36	0.920	14,240	13,090
654	481	35.49	0.871	17,060	14,860
B. Healthy Children and those with Miscellaneous Diseases (Control Group)					
513	215	20.55	0.927	4420	4100
520	477	11.48	0.941	5480	5150
526	286	12.95	0.933	3710	3460
650	103	57.69	0.912	5940	5420
651	733	4.68	0.955	3430	3270

C. Summary of Sweat Conductivity Data

Group	No. in group	Sweat conductivity: Mean, μmho/cm	Group standard deviation, μmho/cm	Range, μmho/cm
Cystic fibrosis	47	(uncorrected) $L_s' = 16{,}150$	3500	9000-24,640
		(corrected) $L_s = 14{,}380$	3130	8030-21,260
Control group	77	(uncorrected) $L_s' = 5560$	2360	2080-14,380
		(corrected) $L_s = 5080$	2160	1970-13,340

In Table III, typical sweat conductivity data, originally presented in (1), are recalculated from Eq. [2] employing the interionic attraction factor. The mean, group standard deviation, and range of sweat conductivities for 77 subjects in a control group and 47 patients with cystic fibrosis are presented in summary. It is noted that a significant change in conductivity values occurs as a result of the application of the *S* factor. The corrected values can be used as a basis for a further correlation between conductivity and electrolyte content currently in progress.

Acknowledgment

The authors wish to express their thanks to the International Nickel Company, Inc., of New York, and to the National Cystic Fibrosis Research Foundation for Grants-in-Aid in support of this work.

Manuscript received April 29, 1958.

Any discussion of this paper will appear in a Discussion Section to be published in the December 1959 JOURNAL.

REFERENCES

1. T. S. Licht, M. Stern, and H. Shwachman, *Clinical Chem.*, **3**, 37 (1957).
2. P. Debye and E. Hückel, *Physik Z.*, **24**, 185, 305 (1923).
3. L. Onsager, *ibid.*, **27**, 388 (1926); **28** 277 (1928).
4. D. A. MacInnes, "The Principles of Electrochemistry," p. 339, Reinhold Publishing Co., New York (1939).
5. L. Onsager and R. M. Fuoss, *J. Phys. Chem.*, **36**, 2689 (1932).
6. H. S. Harned and B. B. Owen, "The Physical Chemistry of Electrolytic Solutions," 3rd. ed., Reinhold Publishing Co., New York (1958).
7. S. Robinson and A. H. Robinson, *Physiol. Rev.*, **34**, 202 (1954).
8. S. Rothman, "Physiology and Biochemistry of the Skin," University of Chicago Press, Chicago (1954).
9. Y. Kuno, "Human Perspiration," p. 224, Charles C. Thomas, Springfield, Ill. (1956).
10. H. Shwachman, M. Stern, R. R. Dooley, and E. A. Higgins, *Clinical Chem.*, **2**, 393 (1956).
11. F. H. MacDougall, "Physical Chemistry," 3rd ed., p. 504, MacMillan Co., New York (1952).
12. W. C. Bray and F. L. Hunt, *J. Am. Chem. Soc.*, **33**, 788 (1911).

The System LiF-LiCl, LiF-NaCl, LiF-KCl

H. M. Haendler, P. S. Sennett, and C. M. Wheeler, Jr.

Department of Chemistry, University of New Hampshire, Durham, New Hampshire

ABSTRACT

Liquid-solid equilibrium data for the systems LiF-LiCl, LiF-NaCl, LiF-KCl were obtained through the concentration range 0-100 mole % LiF. These data were used to test the formula

$$T_{calc} = T_m \left(\frac{1 + x^2 \Delta F^\circ / L}{1 - \frac{2RT_m \ln (1 - X)}{L}} \right)$$

for the prediction of liquidus temperatures. Activities were calculated from experimental data by

$$a_{M_1A_1} = (1 - X)_{M_1} \cdot (1 - X)_{A_1} e^{X_{M_2} \cdot X_{A_2} \cdot \Delta F^\circ / RT}$$

It was shown that the activities of salt components can be calculated by this formula, if the difference in the sum of lattice energies of the reactants and products of mixing is not too large.

Although phase relationships in fused salt systems have been studied for many years, it is only recently that the practical applications of these relationships have become apparent. One promising new application is in the purification and separation of metals by extraction with fused salt media (1). Of particular interest are systems containing fused LiF as one of the components. Botschwar (2) and Bergman (3) have published data for the system LiF-LiCl. However these phase diagrams are not in agreement, exhibiting a difference in liquidus temperatures over a wide concentration range and a substantial difference in the eutectic temperature and composition. Flood (4) has reported data for the system LiF-KCl over a limited concentration range. The work reported in this paper defines more accurately the system LiF-LiCl and extends the reported data for the system LiF-KCl through the entire concentration range, 0-100 mole % LiF. This paper also presents new data for the system LiF-NaCl.

In addition to determining phase diagrams for binary systems of fused salt systems, it is also of interest to use these data where possible to determine the activities of the salt components in the binary systems. An important contribution to this problem has been made by Flood (4, 5). His equations have been tested with the data reported in this work. For systems with components of similar lattice energies, Flood's equations for the determination of activities and prediction of liquidus temperatures are much better than the Clausius-Clapeyron equation for ideal solutions, when the Temkin model for ideal solutions is used.

Experimental

All chemicals were reagent grade and were used after drying without further purification. Mixtures were prepared by accurate weighing of components and melting in a nickel sample holder. A gas stirring device, described by Campbell and Prodan (6), was used for the LiF-LiCl system and the NaCl-rich portion of the LiF-NaCl system. A nickel stirring paddle connected to a variable speed motor was used for the LiF_7rich portion of the LiF-NaCl system and the entire LiF-KCl system.

Temperatures were measured using chromel-alumel thermocouples, calibrated at the melting point of Bureau of Standards samples of aluminum and zinc. The emf of the thermocouple was measured by a L&N Type G two point recording potentiometer and a Rubicon Type B potentiometer.

The samples were heated for ½ to 1 hr at 100° above the expected freezing point. When supercooling was not a problem, the current through the furnace was completely turned off and the sample was

allowed to cool at the rate of about 20°C/min. When supercooling was encountered, the cooling rate was adjusted to 5°C/min.

There was no evidence that the nickel sample holder reacted appreciably with the melt. The pure salts apparently attacked the cell to a lesser extent than did mixtures of intermediate composition. As an example of the extent of corrosion, electrolytic determination of nickel present in the LiF-LiCl system at 10 mole % LiF, gave 0.08, 0.07, and 0.08% nickel in three determinations. X-ray powder pattern data also substantiated these results.

Results

The system LiF-LiCl.—Temperature-composition data were obtained for the LiF-LiCl system over the concentration range 0 to 100 mole % LiF. An eutectic composition of 30.5 mole % LiF was observed, melting at 501°C. Botschwar (2) reported 20 mole % LiF at a eutectic temperature 485°C, Bergman (3) reported 30.5 mole % LiF, 484°C. There was no evidence of compound formation or of solid solutions. The experimental data are recorded in Table I. Figure 1 is a plot of these data. Also plotted are the theoretical liquidus curves for solutions of this system, as calculated from the Clausius-Clapeyron equation.

The System LiF-NaCl.—Temperature-composition data were obtained for the LiF-NaCl system over the concentration range 0 to 100 mole % LiF. The eutectic for this system occurs at 41.5 mole % LiF and 680°C. The phase diagram for this system is similar to that for the LiF-LiCl system, exhibiting a single eutectic, with no evidence of compound formation or solid solutions.

The 50-90 mole % LiF region of this system presented considerable experimental difficulties because of supercooling. Supercooling apparently did not occur in any other composition range. Thermal analysis of mixtures in this range were performed initially using a cell with an air stirring device. Data using this equipment were not reproducible and varied consistently by 10°C from the data reported here. When a more vigorous mechanical stirring device was used, supercooling became small enough so that reproducible results were obtained. The results obtained while using the mechanical stirrer are included in Table II since their reproducibility is considerably better. The values included in Table II and plotted in Fig. 2 for 50-90 mole % LiF are averages of three determinations with a maximum difference of ±2°C.

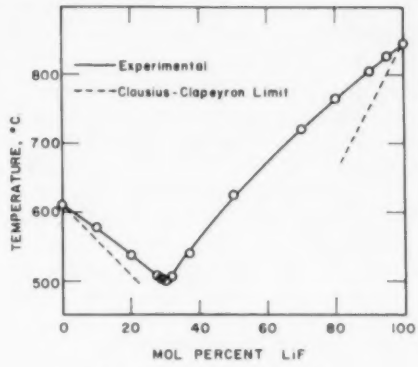

Fig. 1. The system LiF-LiCl

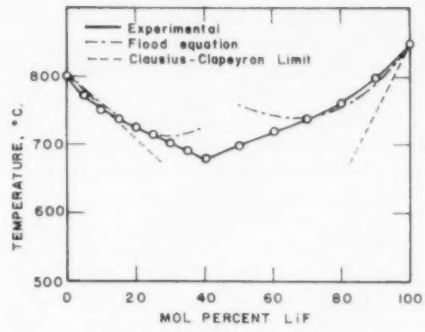

Fig. 2. The system LiF-NaCl

Table II records the experimental data for the system LiF-NaCl. Figure 2 includes a plot of these experimental data and the theoretical liquidus curves for ideal solutions of this system as calculated from the Clausius-Clapeyron equation and Flood's equation.

The System LiF-KCl.—The temperature-composition data obtained for this system in the concentration range 0-100 mole % LiF are listed in Table III.

A plot of these data is shown in Fig. 3, with the theoretical liquidus curves for this system as pre-

Table I. System LiF-LiCl

Composition, mole % LiF	Temperature, °C Liquidus	Eutectic
0.0 (100% LiCl)	—	610
10.0	577	500
20.0	538	499
27.4	509	501
29.0	504	501
30.0	—	501
32.0	509	501
36.9	543	502
50.0	626	502
70.0	723	502
80.0	769	502
90.0	805	502
95.0	830	—
100.0	—	848

Table II. System LiF-NaCl

Composition, mole % LiF	Temperature, °C Liquidus	Eutectic
0.0 (100% NaCl)	—	802
5.0	775	676
10.0	752	679
15.0	742	679
20.0	729	681
25.0	717	681
30.0	704	681
35.0	694	680
40.0	—	681
50.0	700	—
60.0	720	—
70.0	740	—
80.0	764	680
90.0	800	680
100.0	—	848

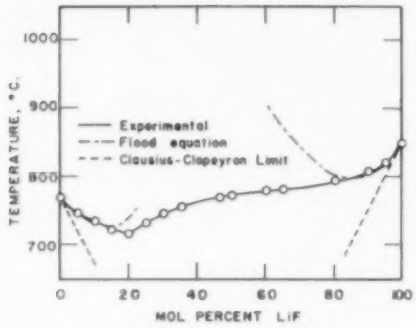

Fig. 3. The system LiF-KCl

dicted by the equations of Clausius-Clapeyron and Flood. This system forms a eutectic at 20 mole % LiF and 715°C. Flood (4) does not list specific eutectic data for this system, but his phase diagram shows eutectic behavior consistent with that which was observed in this work. As will be noted in Fig. 3, the liquidus curve for the potassium chloride side of the eutectic is fairly regular with a slight curvature. On the lithium fluoride side of the eutectic, however, the liquidus curve exhibits a point of inflection. The shape of this curve and its deviation from the general shape of the corresponding curve in the previous two systems can be accounted for in two ways.

The first possible explanation of this curve is that the two components tend toward the formation of an equimolar binary compound. This would account for the abrupt change in the freezing point near the eutectic and the slow change of freezing point with composition in the 40-80 mole % LiF region.

A second explanation for the shape of this type of phase diagram is given by Sidgwick and Ewbank (7). Curves of this shape are due to a submerged miscibility gap. This miscibility gap is unstable with respect to the liquidus curve, that is, it occurs at a lower temperature than the liquidus curve. Presumably if the melt could be supercooled below the liquidus temperature, two liquid phases in metastable equilibrium would appear. This can actually be accomplished in systems where the miscibility gap is not far below the liquidus temperature. It is assumed that solid solubility in these systems is negligible since none of the experimental data indicated any solid solution formation.

Table III. System LiF-KCl

Composition, mole % LiF	Temperature, °C Liquidus	Eutectic
0.0 (100% KCl)	—	772
5.0	747	—
10.0	736	716
15.0	722	714
20.0	—	716
25.0	732	—
30.0	747	—
35.0	755	—
46.4	767	714
50.0	772	—
60.0	780	—
65.0	783	—
80.0	795	713
90.0	805	712
95.0	819	—
100.0	—	848

Discussion

From a comparison of Fig. 1, 2, and 3 it can be seen that the deviations from ideality on the lithium fluoride side of the eutectic increases in the order LiCl-NaCl-KCl. The most pronounced deviation occurs in the LiF-KCl system on the lithium fluoride side of the eutectic. Of the three systems studied, it is to be expected, based on the influence of ionic sizes and radius ratios, that the maximum deviation from ideality would appear in this system. The apparent tendency toward the formation of two immiscible liquid solutions is consistent with the higher lattice energy of lithium fluoride and the consequent higher attractive forces operative in the fused salt media.

An improvement over the Clausius-Clapeyron equation for calculating the liquidus temperature is given by Flood's equation (4).

$$T_{calc} = T_m \left(\frac{1 + X^2 \Delta F^\circ / L}{1 - \frac{2RT_m \ln (1 - X)}{L}} \right) \qquad [1]$$

Using the solution reaction of KCl in LiF as an example, the terms of this equation have the following meaning: where ΔF° is standard free energy change of the reaction

$$KCl + LiF \rightarrow LiCl + KF$$

L is molar heat of fusion of major component (LiF); T_{calc}, liquidus temperature of melt of mole fraction X; T_m, melting temperature (degrees Absolute) of major component; X, mole fraction of minor component (KCl), M_2A_2; $1 - X$, mole fraction of major component, M_1A_1.

It is of interest to determine the activities of the salt components of the two binary systems LiF-NaCl and LiF-KCl. The major component of the binary salt mixtures may be considered the solvent. The activity of the solvent is related to the depression in freezing point of the solvent by the equation (negligible solid solubility assumed)

$$\ln a_{M_1A_1} = \frac{L}{R} \left(\frac{1}{T_m} - \frac{1}{T} \right) \qquad [2]$$

where $a_{M_1A_1}$ is the activity of the major component M_1A_1; L is the heat of fusion of the major component, considered to be constant; T_m is the melting point of the major component in the pure state; and T°K is the experimentally observed temperature for a solution of mole fraction $1 - X$.

The activity coefficient $\gamma_{M_1A_1} = \dfrac{a_{M_1A_1}}{(1 - X)_{M_1}(1 - X)_{A_1}}$.

The value of $a_{M_1A_1}$ is calculated from Eq. [2]. The activity coefficients calculated in this fashion will be called γ exp in this paper.

These equations permit the calculation of activities and activity coefficients from liquidus curve temperatures. The equations developed by Flood are intended to provide a means of theoretically calculating the activities and liquidus temperatures for a

binary system, using free energy, heat of fusion, and concentration data.

For the mixing $M_1A_1 + M_2A_2 = M_2A_1 + M_1A_2$, the activity of M_1A_1 may be calculated using Flood's simplified formula

$$a_{M_1A_1} = (1-X)_{M_1} \cdot (1-X)_{A_1} \cdot e^{X_{M_2} \cdot X_{A_2} \cdot \Delta F^\circ / RT}$$

where ΔF° is the standard free energy change for the reaction as written.

The activity coefficient may be calculated using

$$\ln \gamma\, M_1A_1 = X_{M_2} \cdot X_{A_2} \cdot \Delta F^\circ / RT$$

The quantitative comparison between calculated and experimentally determined activity, activity coefficient, and liquidus temperature values is given in Table IV-VII.

Table IV. System LiF-KCl (LiF as solvent)

	T°K		a		γ	
$(1-X)_{LiF}$	exp.	calc.	exp.	calc.	exp.	calc.
1	1121					
0.95	1092	1089	0.93	0.92	1.03	1.02
0.90	1078	1073	0.89	0.87	1.10	1.08
0.80	1068	1074	0.86	0.87	1.34	1.38
0.65	1056	1143	0.84	1.15	1.99	2.71
0.60	1053	1178	0.83	1.32	2.30	3.69
0.50	1045	1258	0.81	1.96	3.24	7.85
0.46	1040	1288	0.80	2.33	3.78	11.00
0.35	1028	1370	0.77	4.22	6.28	34.90
0.30	1020	1435	0.75	5.61	8.33	62.70
0.25	1005	1423	0.71	4.10	11.36	65.90

Table V. System LiF-KCl (KCl as solvent)

	T°K		a		γ	
$(1-X)_{KCl}$	exp.	calc.	exp.	calc.	exp.	calc.
1	1045					
0.95	1020	1016	0.93	0.92	1.03	1.02
0.90	1009	1002	0.90	0.88	1.11	1.09
0.85	995	998	0.86	0.87	1.19	1.21

Table VI. LiF-NaCl (LiF as solvent)

	T°		a		γ	
$(1-X)_{LiF}$	exp.	calc.	exp.	calc.	exp.	calc.
1	1121					
0.90	1073	1060	0.88	0.89	1.08	1.04
0.80	1037	1027	0.79	0.76	1.23	1.19
0.70	1013	1015	0.74	0.74	1.51	1.51
0.60	993	1018	0.69	0.76	1.91	2.15
0.50	973	1029	0.64	0.82	2.56	3.29

Table VII. LiF-NaCl (NaCl as solvent)

	T°		a		γ	
$(1-X)_{NaCl}$	exp.	calc.	exp.	calc.	exp.	calc.
1	1075					
0.95	1048	1046	0.92	0.91	1.02	1.01
0.90	1025	1024	0.85	0.85	1.05	1.05
0.85	1015	1006	0.82	0.80	1.13	1.11
0.80	1002	996	0.79	0.77	1.23	1.24
0.75	990	990	0.75	0.75	1.33	1.34
0.70	977	987	0.72	0.75	1.47	1.53
0.65	967	988	0.69	0.76	1.63	1.80

Free energies of formation and heats of fusion were taken from National Bureau of Standards Circular 500.

The development of Flood's equation assumes that the entropy condition of the fused salt melt is that of an ideal ion mixture; each cation is surrounded by anions and vice versa; the cations as well as the anions are statistically distributed at random. In addition it is assumed that the heat of mixing is equal to zero. Thus the calculated liquidus temperature and activities of the components are related through the free energy change of mixing to the entropy condition of the mixture.

In a system such as LiF + NaCl = LiCl + Na F the difference in lattice energies of the reactants and products of mixing is much less than for the system Li F + K Cl = LiCl + KF. One may suppose, then, that the entropy condition required by Flood's treatment would more nearly be approximated by the LiF-NaCl system. Consequently liquidus temperature calculated by his equation should more closely correspond to the experimental temperatures for this system than for the LiF-KCl system, in which a greater difference in lattice energies is observed. This is the case and is evident from the plots in Fig. 2 and 3. The theoretically calculated liquidus curve for the LiF-NaCl system is in fair agreement with the experimental curve over a wide concentration range. However, in the LiF-KCl system large positive deviations are observed at concentrations greater than 25 mole % LiF. Apparently due to the strong interionic forces between the Li^+ and F^- ions, the random distribution of cations and anions of the Li^+, F^-, K^+, Cl^- mixture is not realized in these more concentrated solutions. In the LiF-NaCl system the bond energies of the products of mixing more nearly equal those of the reactants. This should provide for a more random distribution of the Li^+, F^-, Na^+, Cl^- ions and consequently for better agreement between theoretical and experimental activities and liquidus temperatures.

Flood (4) has shown that the activities of salt components with lower lattice energies can be calculated accurately with his simplified theoretical formula. The data and calculations reported here for the LiF-NaCl system indicate that the formula can also be used with fair results for a system in which the lattice energies of the components are large, providing the difference in the sum of lattice energies of reactants and products of mixing is not too great. For systems in which the difference in lattice energies of the components is large, the formula fails for solutions of even moderate concentrations.

Acknowledgment

This research was supported in part by the Atomic Energy Commission.

Manuscript received March 7, 1958.

Any discussion of this paper will appear in a Discussion Section to be published in the December 1959 JOURNAL.

REFERENCES

1. D. W. Bareis, R. H. Wiswall, Jr., and W. E. Winsche, *Nucleonics*, **12**, 16 (1954).

2. A. A. Botschwar, *Z. anorg. Chem.*, **210**, 163 (1933).
3. A. G. Bergman and E. I. Banashek, *Izvest. Saktora Fiz-Khim. Anal., Akad. Nauk. S.S.S.R.*, **23**, 201 (1953); *C. A.*, **48**, 9170a (1954).
4. H. Flood, O. Fykse, and S. Urnes, *Z. Elektrochem.*, **59**, 364 (1955).
5. H. Flood, T. Forland, and K. Grjotheim, *Z. anorg. Chem.*, **276**, 289 (1954).
6. A. N. Campbell and L. A. Prodan, *J. Am. Chem. Soc.*, **70**, 553 (1948).
7. N. W. Sidgwick and E. K. Ewbank. *J. Chem. Soc.*, **119**, 979 (1921).

Technical Notes

Study of Magnetic Oxides by Cathode Rays

S. Yamaguchi

Scientific Research Institute, Tokyo, Japan

The path of cathode rays is deflected by a magnetic field (Lorentz effect). This effect is observable in the electron diffraction pattern obtained from a ferromagnetic substance. In the present study, the magnetic states of two ferromagnetic oxides were investigated by means of electron diffraction.

The two specimens employed were ferromagnetic pure nickel oxide (NiO) and an oxide permanent magnet of practical use (Fe_2O_3:NiO:ZnO = 50:15:35 by weight). The weight of the specimen used for the experiment was about 1 mg.

In Fig. 1, the diffraction rings from a powder of the nickel oxide and those from a nonferromagnetic gold foil are photographed on the same dry plate by means of double exposure. In this procedure, the wave length of the electron beam applied and the position of the photographic plate were kept fixed. It is noticeable in Fig. 1 that the diffraction rings from these two substances are not co-centric. This implies that the paths of the electrons are magnetically perturbed by the ferromagnetic specimen.

In Fig. 2, the diffraction rings from a nonferromagnetic aluminum oxide (böhmite) (1) and those from the gold foil are photographed by the same process as for Fig. 1. In this photograph all the diffraction rings are co-centric, i.e., there is no magnetic effect on the electrons. Figure 2 corresponds to the result of a blank test for magnetic analysis.

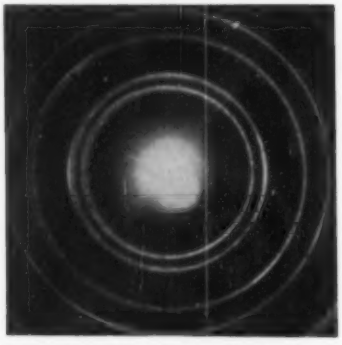

Fig. 1. Superposition of the diffraction patterns from nickel oxide and from gold. Diffraction rings of the former and those of the latter are excentric as the result of Lorentz effect. Wave length, 0.0292Å. Camera length, 495 mm. Positive enlarged 2.1 times.

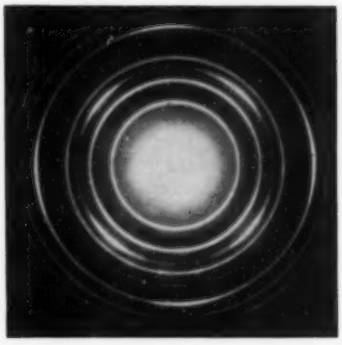

Fig. 2. Superposition of the diffraction patterns from bohmite and from gold. All the rings are co-centric. No Lorentz effect.

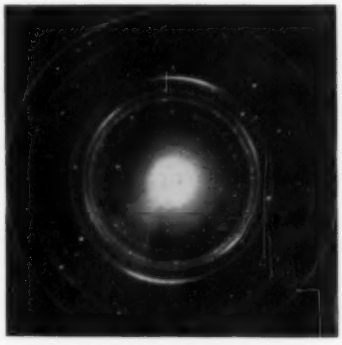

Fig. 3. Superposition of the diffraction patterns from the oxide magnet (Fe_2O_3-NiO-ZnO) and from gold. Lorentz effect. Wave length, 0.0302Å.

The diffraction pattern of Fig. 3 was observed from a powder of the oxide permanent magnet and from the gold foil in the same way as for Fig. 1 and 2. In Fig. 3, the diffraction rings of the oxide and those of gold are not co-centric.

From the diffraction figures thus prepared, it is possible to estimate the strength H of the magnetic field given by the ferromagnetic oxide.

$$H = \frac{m}{e}\frac{v}{lL} \cdot \Delta x$$

or

$$H = \frac{h}{e\lambda lL} \cdot \Delta x \qquad [1]$$

where e is electron charge (1.6×10^{-20} CGSEMU); m, electron mass; v, velocity of electrons; L, camera length (495 mm); h, Planck's constant (6.6×10^{-27} erg sec); l, width of the magnetic field (about 0.5 mm); λ, wave length of the electron wave; and Δx, observed deflection of the electron beam.

In Fig. 1 and Fig. 3,

$$\Delta x = 0.2 \text{ mm } (\lambda = 0.0292\text{Å})$$

and

$$\Delta x = 0.1 \text{ mm } (\lambda = 0.0302\text{Å}),$$

respectively.

According to Eq. [1], therefore,

$$H = 11.4 \text{ and } 5.53 \text{ gauss, respectively.}$$

It is thus possible to investigate ferromagnetic oxides magnetochemically as well as crystallographically by means of electron diffraction.

Manuscript received Sept. 30, 1957.

Any discussion of this paper will appear in a Discussion Section to be published in the December 1959 JOURNAL.

REFERENCE

1. S. Yamaguchi, *Z. anal. Chem.*, **155**, 21 (1957).

The Mechanism of Blackening of Nickel Anodes

Thomas C. Franklin and Jack Goodwyn

Chemistry Department, Baylor University, Waco, Texas

In the process of depositing black nickel using a nickel wire anode and cathode and a modification of the bath used by Moline (1) it was noted that the anode as well as the cathode became black. Meyer (2) gave the composition of solutions in which nickel may be blackened without passing current, but no mention was made of the composition of the black coating nor of the mechanism of its formation. Since the solutions used by Meyer and Moline were similar, the coatings were assumed to be the same. This paper describes an investigation on the composition of the black deposit and the mechanism by which it was formed.

Experimental Methods and Results

Composition of the anode coating.—The bath used contained $NiSO_4 \cdot 6H_2O$, 70 g/l; $(NH_4)_2SO_4$, 37 g/l; $ZnSO_4 \cdot 7H_2O$, 34.3 g/l; and KSCN, 17.9 g/l, and was operated at a pH of 5.0, a temperature of 30°C, and a current density of 11 amp/m^2. All chemicals were reagent grade. To determine which component of this bath caused the blackening of the anode, an aqueous solution of each component was prepared, adjusted to a pH of 5.0 with HCl, and a small piece of nickel wire was placed in each solution. The nickel wire in the solution containing potassium thiocyanate darkened in two days. When the pH was lowered to 2.0, the solution darkened the wire in 7 hr. With current passing, both solutions darkened the anode within 6 min. None of the solutions containing the other components blackened the nickel wire. The odor of H_2S was noticed above those test tubes containing potassium thiocyanate.

To identify the reaction which liberated the H_2S, a series of test tubes was prepared with moistened lead acetate paper fastened over the mouth of each test tube. Each tube contained 20 ml of water, 1 g of potassium thiocyanate, and 2 ml of concentrated HCl. To these test tubes 1 g portions of different substances were added and the results were noted. These results are summarized in Table I.

The yellow solid which settled out of the blank solution (No. 1) was a polymerization product of thiocyanic acid (3). Metal ions evidently retard this polymerization as evidenced by the fact that 12 days were required for the formation of crystals in the solutions containing the cobalt and nickel ions and that 15 days were required with zinc ions present. The blackening of the lead acetate paper above test tubes 1, 4, 6, and 7 was due to H_2S from the hydrolysis of thiocyanic acid. The fact that H_2S was generated more rapidly in the solutions con-

Table I. Effect of various materials on acidified potassium thiocyanate solutions

	Material added	Results observed
1.	None	Lead acetate paper blackened in 5 days. Yellow crystals precipitated in 12 hr
2.	Nickel wire	Lead acetate paper blackened in 3 hr
3.	Tin (II) chloride	Lead acetate paper blackened in 3 hr. Brown precipitate formed in solution
4	Zinc chloride	Only slight darkening of lead acetate paper in 3 days. Crystals formed in solution in 15 days
5.	Copper (II) chloride	Black precipitate [copper(II) thiocyanate] formed in the solution immediately
6.	Cobalt (II) chloride	Slight darkening of lead acetate paper in 3 days. Crystals formed in solution in 12 days
7.	Nickel (II) chloride	Slight darkening of lead acetate paper in 3 days. Crystals formed in solution in 12 days

taining the metal ions than in the blank was due to the inhibition of the polymerization by the metal ions thus making the hydrolysis the major reaction. In the presence of the reducing agents, tin (II) chloride and nickel wire, the evolution of H_2S was much more rapid and proceeded by a reduction similar to the following:

$$2CNS^- + 2Sn^{++} \rightarrow SnS_2 + 2CN^- + Sn^{++++}$$

Both chemical tests and x-ray diffraction showed the presence of nickel sulfide in the anode coating.

Mechanism of formation of the anode coatings.— An examination of the data shows that the reduction of the thiocyanic acid by nickel wire produced a coating in 7 hr while the anodic reaction produced a coating in 6 min. It seems unreasonable that the nickel anode was the reducing agent. Therefore it was postulated that the nickel anode was oxidized to nickel (I) and these ions then acted as the reducing agent on the thiocyanate ion. Kleinberg (4) has postulated a similar mechanism for the anodic dissolution of magnesium in the presence of oxidizing agents.

Because of the formation of nickel (II) sulfide on the anode, it was impossible to check coulometrically the valence of nickel as it went into solution in the presence of the thiocyanate ion. To avoid this difficulty, the nickel was anodically oxidized in solutions containing potassium bromate in place of the thiocyanate. Thus the valence could be checked and any bromine produced by the reduction of the bromate could be detected by odor and by its ability to bleach methyl red indicator. The electrolysis was carried out in a 400 ml beaker containing a 100 ml porous porcelain cup as the anode compartment. Sulfuric acid was used rather than HCl in order to prevent reaction between the chloride and bromate ions. An oxy-hydrogen coulometer, modeled after that of Lingane (5), was used. The potassium bromate was added in the form of a 0.1177M solution. A nickel wire of the same diameter and length as the anode was placed in a solution identical in composition to the anode solution and was left there for the duration of each electrolysis. The small change in weight of this blank was subtracted from the change in weight of the anode to give the exact loss of weight due to electrolytic oxidation. Results are given in Table II.

As can be seen, the valence of nickel anodically dissolved in H_2SO_4 averaged 2.02 ± 0.03. However, in the presence of potassium bromate, the valence of the nickel going into solution dropped below two (runs 3-7 and 15-23). It will be noticed that on repeated use of the bromate solution the valence rose toward two as the bromate concentration was lowered. The introduction of a fresh solution or the addition of more bromate always caused the valence to drop. At the completion of each electrolysis, it was found that the anolyte had a distinct odor of bromine and that it would bleach methyl-red readily. It was not possible to make an extended study since slight changes in current density or in pH caused oxygen to be evolved at the anode.

In order to establish further the existence of nickel (I) as an intermediate in the anodic dissolution of nickel, the nickel was oxidized anodically at low current densities (0.13 amp/m^2) in acetonitrile containing tetramethylammonium chloride as a supporting electrolyte. In this solvent corrosion was not possible. The apparatus was an H-tube with the compartments separated by means of a fine porosity sintered glass disk. The temperature was maintained at 7°C in order to minimize electro-osmosis. Results are summarized in Table III. In all cases it can be seen that part of the nickel dissolves as nickel (I).

Table II. Effect of potassium bromate on the anodic dissolution of nickel in sulfuric acid solution

Run No.	Electrolyte	Current density, amp/m^2	Change in wt of anode, g	Loss in wt of blank, g	Dissolution time, min	N-number of Faradays per mole	Remarks
1	0.171*N* H_2SO_4	8.40	0.0121	0.0012	30	2.00	
2	0.171*N* H_2SO_4	8.40	0.0084	0.0010	20	1.98	
3	0.171*N* H_2SO_4 + 5 ml $KBrO_3$	8.40	0.0153	0.0005	30	1.48	
4	0.171*N* H_2SO_4 + 5 ml $KBrO_3$	8.40	0.0105	0.0010	20	1.54	
5	0.171*N* H_2SO_4 + 5 ml $KBrO_3$	4.54	0.0093	0.0012	30	1.41	
6	0.171*N* H_2SO_4 + 5 ml $KBrO_3$	8.40	0.0218	0.0044	70	1.17	
7	0.171*N* H_2SO_4 + 5 ml $KBrO_3$	8.40	0.0187	0.0027	60	1.17	
8	0.1676*N* H_2SO_4	4.72	0.0080	0.0005	40	2.02	
9	0.1676*N* H_2SO_4	4.44	0.0078	0.0006	40	1.97	
10	0.1*N* H_2SO_4	2.83	0.0045	0.0003	40	2.05	
11	0.0378*N* H_2SO_4	2.88	0.0050	0.0004	40	1.98	
12	0.0378*N* H_2SO_4	2.88	0.0051	0.0007	40	2.06	
13	0.0378*N* H_2SO_4	4.60	0.0077	0.0004	40	2.05	
14	0.0378*N* H_2SO_4	4.60	0.0059	—	30	2.06	
15	0.1046*N* H_2SO_4 + 5 ml $KBrO_3$	2.77	0.0082	0.0015	50	1.64	
16	0.1046*N* H_2SO_4 + 5 ml $KBrO_3$	2.62	0.0072	0.0014	50	1.78	Soln. 15 reused
17	0.1046*N* H_2SO_4 + 5 ml $KBrO_3$	2.43	0.0060	0.0020	40	1.93	Soln. 16 reused
18	0.1046*N* H_2SO_4 + 5 ml $KBrO_3$	2.52	0.0070	0.0012	40	1.40	Soln. 17 + 5 ml of $KBrO_3$
19	0.1046*N* H_2SO_4 + 5 ml $KBrO_3$	2.52	0.0069	0.0012	40	1.42	Soln. 18 reused
20	0.1676*N* H_2SO_4 + 5 ml $KBrO_3$	4.05	0.0100	0.0017	40	1.56	
21	0.1676*N* H_2SO_4 + 5 ml $KBrO_3$	4.20	0.0095	0.0025	40	1.90	Soln. 20 reused
22	0.1676*N* H_2SO_4 + 5 ml $KBrO_3$	4.56	0.0110	0.0017	40	1.59	Fresh soln.
23	0.1676*N* H_2SO_4 + 5 ml $KBrO_3$	4.47	0.0112	0.0011	40	1.44	Fresh soln.

Table III. Anodic dissolution of nickel in acetonitrile containing tetramethyl ammonium chloride

Total weight loss, g	N-number of Faradays per mole
0.0213	1.85
0.0230	1.67
0.0285	1.35

From these experiments it was concluded that the black coating formed on nickel anodes in baths containing thiocyanate was nickel sulfide formed by the following series of reactions:

$$Ni \rightarrow Ni^{+} + e$$

$$2Ni^{+} + CNS^{-} \rightarrow NiS + CN^{-} + Ni^{++}$$

These reactions might also be expected to occur to some extent at the cathode in black nickel plating baths. It is known that these black cathodic plates contain nickel sulfide. Sanborn and Orlemann (6) have shown the formation of an intermediate Ni (I) ion during the electrolytic reduction of Ni (II) in concentrated salt solutions. Therefore it is reasonable to expect that part of the nickel sulfide arises from the above reactions.

Acknowledgment

This work was sponsored by the Office of Ordnance Research, U. S. Army.

Manuscript received Oct. 28, 1957.

Any discussion of this paper will appear in a Discussion Section to be published in the December 1959 JOURNAL.

REFERENCES

1. W. E. Moline, *Proc. Am. Electroplater's Soc.*, **1943**, 21.
2. W. R. Meyer, *ibid.*, **1943**, 90.
3. N. V Sidgwick, "The Organic Chemistry of Nitrogen," p. 333, Oxford University Press, London (1937).
4. Jacob Kleinberg, *J. Am. Chem. Soc.*, **76**, 363 (1954).
5. J. J. Lingane, *ibid.*, **67**, 1916 (1945).
6. R. H. Sanborn and E. F. Orlemann, *ibid.*, **78**, 4852 (1956).

ZnS Phosphors with P, As, Sb Coactivators

E. F. Apple

Research Laboratory, General Electric Company, Schenectady, New York

In ZnS:P,Cl and ZnS:As,Cl phosphors (1, 2) it is thought that both the Group V element and chlorine occupy S sites in the ZnS lattice. This configuration gives rise to an acceptor-donor luminescent system in which P and As are acceptors or activators and chlorine is a donor or coactivator (3). Emission spectra under 3650Å excitation show a broad band in the yellow with P and a broad band in the yellow-orange with As.

If P or As or Sb is incorporated in ZnS along with Cu, only the blue and green emissions typical of Cu-activated ZnS are observed. These phosphors, which contain (before firing) from 5×10^{-6} to 5×10^{-4} g-atoms Cu/mole ZnS with equal to five times as much Group V element, are prepared in an H_2S stream or in a sealed, evacuated quartz tube at 950°C. Figure 1 shows the emission spectra of ZnS: 10^{-4} Cu, 5×10^{-4} As both under 3650Å and cathode-ray excitation. The spectra of corresponding ZnS:Cu,P and ZnS:Cu,Sb phosphors are almost identical with those shown. Note that under cathode-ray excitation the blue band disappears almost completely. This blue emission, which peaks at about 4450Å, is probably the "Cu-blue" emission previously described in the literature (4, 5). The self-activated blue emission in cubic ZnS peaks at 4600°-4700Å and has a much broader half-width than the blue emission band in ZnS:Cu,As. Increasing the temperature of preparation of ZnS:Cu,As causes an increase in the blue emission and decrease in the green emission intensity. It should be mentioned that ZnS:Cu, ZnS:P, ZnS:As, or ZnS:Sb are all practically nonluminescent when prepared in H_2S at 950°C.

The absence of the P-yellow and As-orange emissions in ZnS:Cu, P and ZnS:Cu, As, respectively, indicates that in the presence of Cu the Group V element assumes a different role than when in the presence of halogens. Because of the similarity in emission to ZnS:Cu,Al, in which Al is a donor, it is concluded that the Group V elements are donors (coactivators) when incorporated in ZnS along with Cu, the acceptor or activator. It is probable that the Group V element occupies a Zn

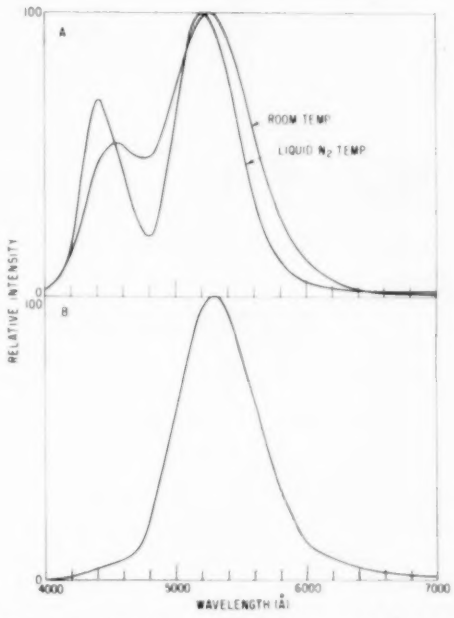

Fig. 1. ZnS: 10^{-4} Cu, 5×10^{-4} g-atoms As/mole ZnS; fired in H_2S at 950°C. A, 3650Å excitation; B, CR excitation (15 kv, 3μa/cm²).

site when incorporated as a donor, a situation not unexpected; As and Sb occupy metal lattice sites in several ternary sulfides whose structures are related to the zinc blende or wurtzite modifications of ZnS. Phosphors with Group V coactivators have slightly weaker emissions and shorter afterglows than those with Group III coactivators such as Al. Also, Group V elements do not give rise to the self-activated blue center in ZnS.

In covalent compounds, Sb (or As) usually forms only three strong bonds and usually has only three nearest neighbors. For instance, Cu_3SbS_3 has the zinc blende structure in which the Cu and Sb atoms occupy metal sites and one quarter of the S sites are vacant. $CuSbS_2$ has a more complicated structure, related to the wurtzite structure, in which each Sb atom forms three strong pyramidal bonds and Cu four tetrahedral bonds to S atoms. Sb_2S_3 itself has a chain structure in which each Sb atom has three nearest-neighbor S atoms. Arsenic forms similar compounds with correspondingly complex structures (6). In contrast, $CuAlS_2$ and Al_2S_3 both have structures in which the metal atoms are tetrahedrally bonded to four equidistant S atoms (7). In addition to effects on luminescent processes, the differences in bonding between ternary sulfides of Al and As or Sb may be responsible for the more limited solubilities of added impurities in the phosphors containing Cu along with the Group V element. ZnS phosphors containing more than 10^{-3} g-atoms Cu/mole ZnS and equal to five times as much P, As, or Sb, have a very gray body color, and are only weakly luminescent. Presumably, a multiphase system exists. However, ZnS:Cu,Al or $ZnS:CuGaS_2$ phosphors containing 10^{-3} Cu have a light body color, exhibit a fairly bright green luminescence, and are single phase systems (8, 9).

In summary, it has been shown that P, As, and Sb may, under special conditions, function as coactivators in ZnS phosphors. Whether the Group V element acts as an activator and substitutes on S sites or a coactivator and substitutes on Zn sites depends on which type of compensating impurity is incorporated simultaneously. In the presence of halogen, the substitution occurs at S sites, whereas with Cu it occurs at Zn sites.

Preliminary experiments indicate that P, As, and Sb are also coactivators in ZnS phosphors containing Ag or Au activators.

Manuscript received Sept. 25, 1958.

Any discussion of this paper will appear in a Discussion Section to be published in the December 1959 JOURNAL.

REFERENCES

1. A. H. McKeag and P. W. Ranby, *This Journal*, **96**, 85 (1949).
2. J. S. Prener, *ibid.*, **98**, 406 (1951).
3. J. S. Prener and F. E. Williams, *ibid.*, **103**, 342 (1956).
4. F. A. Kröger and N. W. Smit, *Physica*, **16**, 317 (1950).
5. F. A. Kröger and J. Dikhoff, *ibid.*, **16**, 297 (1950).
6. A. F. Wells, "Structural Inorganic Chemistry," pp. 402-405, Oxford Press (1950).
7. H. Hahn, G. Frank, W. Klinger, A. Meyer, and G. Störger, *Z. anorg. u. allgem. Chem.*, **271**, 153 (1953).
8. H. C. Froelich, *This Journal*, **100**, 496 (1953).
9. E. F. Apple, *ibid.*, **105**, 251 (1958).

Brief Communication

Titanium Coatings on Molybdenum Wire

Robert L. Bronnes

Philips Laboratories, Irvington-on-Hudson, New York

In an electron tube, the level of primary grid emission is dependent on many factors, including grid and cathode temperatures, rate of supply of evaporation products from emitter material in the cathode, and evolution of gases. Espersen and Rogers of these Laboratories have shown that the emission level may be lowered by controlling grid temperatures and by choosing grid materials which are not readily activated by contamination with evaporation products from the cathode (1). Titanium, in comparison to molybdenum and other commonly used grid materials, is remarkably insensitive to such activation, but does not have sufficient high-temperature rigidity to maintain the anode-grid-cathode spacings. In order to combine the low-level emission characteristics of titanium with the rigidity of molybdenum, a method was developed for depositing a layer of titanium on molybdenum by the evaporation of metallic titanium.

Apparatus and Method

The materials required are 0.010-in. molybdenum wire, 0.010-in. titanium wire, and a 0.020-in. helical tungsten wire heater coil having a diameter of 0.5-in. and 8 complete turns, 1-in. long. The steps required are:

1. Degrease the molybdenum, tungsten, and titanium wires in acetone.

2. Hydrogen-fire the molybdenum and tungsten wires at 1100°C for 30 min to remove surface contamination and reduce surface oxides.

3. Mount the molybdenum wire vertically on a bulb stem inside the tungsten coil. Approximately 50 mg of titanium wire are wrapped uniformly around the tungsten coil.

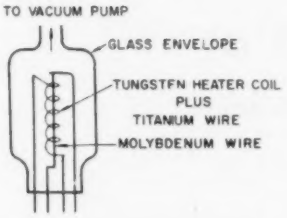

Fig. 1. Evaporation assembly

Fig. 2. Titanium coated molybdenum wire. Original magnification 900X.

4. Thoroughly degrease the assembly in trichlorethylene vapor.

5. Seal the assembly in a glass envelope (Fig. 1), mount on a vacuum pump, evacuate, and bake-out at 450°C for 1 hr. A vacuum of ca 2 x 10^{-7} mm Hg should be obtained.

6. Raise the temperature of the molybdenum wire to 1600°C[1] for degassing, while maintaining a vacuum of at least 6 x 10^{-5} mm Hg. Degas until a vacuum of ca 2 x 10^{-6} mm Hg is obtained. Note power requirements.

7. Lower the temperature of the molybdenum wire to 900°C. A vacuum of ca 6 x 10^{-7} mm Hg should be obtained. Note power requirements.

8. While the temperature of the molybdenum wire is held at 900°C, slowly raise the temperature of the tungsten heater coil to a few degrees above the melting point of titanium. Maintain a vacuum of ca 6 x 10^{-5} mm Hg, and hold at this temperature for 5 min. After the heater coil has cooled down, a vacuum of ca 6 x 10^{-7} mm Hg should be obtained. Since the glass envelope will become opaque during the evaporation of titanium, the temperature of the molybdenum wire can be maintained only by reference to the power requirements noted in Step No. 7.

9. Raise the temperature of the molybdenum wire to 1600°C by using the power requirements noted in Step No. 6. Hold for 1 min.

10. Allow the assembly to cool down and remove from the vacuum pump.

[1] All temperatures are uncorrected, as measured with a L&N optical pyrometer.

Results and Discussion

Smooth, uniform coatings have been obtained by this method with good reproducibility of results. Bonding occurs during deposition and during final heating by the formation of a molybdenum-titanium alloy. The titanium coating and alloyed region are clearly visible in Fig. 2.

If the parts have been carefully processed and a good vacuum maintained, the coatings will be of good physical integrity, firmly bonded and adherent to the molybdenum, and sufficiently ductile so that rupturing will not occur on moderate flexing.

While this process has been described as a laboratory procedure, it is possible to modify the apparatus to permit continuous processing of wire in any desired lengths.

Manuscript received Oct. 20, 1958.

Any discussion of this paper will appear in a Discussion Section to be published in the December 1959 JOURNAL.

REFERENCE

1. G. A. Espersen and J. W. Rogers, IRE Transactions of the Professional Group on Electron Devices, Vol. ED-3, No. 2, pp. 100-107, April, 1956.

Manuscripts and Abstracts for Fall 1959 Meeting

Papers are now being solicited for the Fall Meeting of the Society, to be held at the Deshler-Hilton Hotel in Columbus, Ohio, October 18, 19, 20, 21, and 22, 1959. Technical sessions probably will be scheduled on Batteries, Corrosion (including a joint Corrosion—Electronics-Semiconductors session), Electrodeposition (including symposia on "Electrodeposition from Organic Solvents" and "Electro- and Chemical-Polishing"), Electronics (Semiconductors), Electro-Organics, and Electrothermics and Metallurgy.

To be considered for this meeting, triplicate copies of abstracts *(not exceeding 75 words in length)* must be received at Society Headquarters, 1860 Broadway, New York 23, N. Y., *not later than June 1, 1959. Please indicate on abstract for which Division's symposium the paper is to be scheduled, and underline the name of the author who will present the paper.* Complete manuscripts should be sent in triplicate to the Managing Editor of the JOURNAL at the same address.

* * *

The Spring 1960 Meeting will be held in Chicago, Ill., May 1, 2, 3, 4, and 5, 1960, at the Lasalle Hotel. Sessions will be announced in a later issue.

FUTURE MEETINGS OF
The Electrochemical Society

Philadelphia, Pa., May 3, 4, 5, 6, and 7, 1959

Headquarters at the Sheraton Hotel

Sessions will be scheduled on

Electric Insulation, Electronics (Including

Luminescence, Semiconductors, Thermionics, and Devices), Electrothermics and Metallurgy,

Industrial Electrolytics, and Theoretical Electrochemistry

* * *

Columbus, Ohio, October 18, 19, 20, 21, and 22, 1959

Headquarters at the Deshler-Hilton Hotel

Sessions probably will be scheduled on

Batteries, Corrosion (including a joint Corrosion—Electronics-Semiconductors session),

Electrodeposition (including symposia on "Electrodeposition from Organic Solvents"

and "Electro- and Chemical-Polishing"),

Electronics (Semiconductors), Electro-Organics,

and Electrothermics and Metallurgy

* * *

Chicago, Ill., May 1, 2, 3, 4, and 5, 1960

Headquarters at the Lasalle Hotel

* * *

Houston, Texas, October 9, 10, 11, 12, and 13, 1960

Headquarters at the Shamrock Hotel

* * *

Papers are now being solicited for the meeting to be held in Columbus, Ohio, October 18-22, 1959. Triplicate copies of each abstract (*not exceeding 75 words in length*) are due at Society Headquarters, 1860 Broadway, New York 23, N. Y., *not later than June 1, 1959* in order to be included in the program. *Please indicate on abstract for which Division's symposium the paper is to be scheduled, and underline the name of the author who will present the paper.* Complete manuscripts should be sent in triplicate to the Managing Editor of the JOURNAL at 1860 Broadway, New York 23, N. Y.

Philadelphia Program

THE ELECTROCHEMICAL SOCIETY

One Hundred and Fifteenth Meeting

May 3, 4, 5, 6, and 7, 1959

Sunday through Thursday

CONDENSED TECHNICAL PROGRAM

Monday, May 4, 1959

Electric Insulation (Abs. 1-7) 9:45 A.M.-12:00 M.; 2:00-3:30 P.M. (Constitution and Independence Rooms, 3rd Floor)

Electronics—Luminescence (Abs. 39-54) 9:00 A.M.-12:05 P.M.; 2:00-4:55 P.M. (Pennsylvania Ballroom, West, 3rd Floor)

Electronics—Semiconductors (Abs. 72-82) 9:30 A.M.-12:00 M.; 2:25-5:15 P.M. (West Ballroom, 2nd Floor)

Electrothermics and Metallurgy (Abs. 104-120) 9:30 A.M.-12:00 M.; 2:00-4:30 P.M. (Hall of Flags, West, Concourse) 2:00-5:05 P.M. (Hall of Flags, East, Concourse)

Industrial Electrolytic (Abs. 151-161) 9:00-11:30 A.M.; 2:30-5:00 P.M. (East Ballroom, 2nd Floor)

Theoretical Electrochemistry (Abs. 172-175) 10:00 A.M.-12:00 M.; 2:00-5:00 P.M. (Pennsylvania Ballroom, East, 3rd Floor)

Tuesday, May 5, 1959

Electric Insulation (Abs. 9-18) 9:00 A.M.-12:00 M.; 2:00-4:00 P.M. (Constitution and Independence Rooms, 3rd Floor)

Electronics—Luminescence (Abs. 55-65) 9:00-11:55 A.M.; 2:00-5:00 P.M. (Pennsylvania Ballroom, West, 3rd Floor)

Electronics—Semiconductors (Abs. 83-93) 9:00 A.M.-12:10 P.M.; 2:00-5:15 P.M. (West Ballroom, 2nd Floor)

Electrothermics and Metallurgy (Abs. 121-127) 9:00-11:30 A.M.; 2:00-4:00 P.M. (Hall of Flags, East and West, Concourse)

Industrial Electrolytic (Abs. 162-171) 8:30-11:30 A.M.; 2:30-5:00 P.M. (East Ballroom, 2nd Floor)

Theoretical Electrochemistry (Abs. 176-182) 9:00 A.M.-12:00 M.; 2:00-5:00 P.M. (Pennsylvania Ballroom, East, 3rd Floor)

Wednesday, May 6, 1959

Electric Insulation (Abs. 19-29) 9:00 A.M.-12:00 M.; 2:00-4:30 P.M. (Pennsylvania Ballroom, East, 3rd Floor)

Electronics—Luminescence and Semiconductor (Abs. 66-71) 9:00 A.M.-12:10 P.M. (West Ballroom, 2nd Floor)

Electronics—Thermionics (Abs. 94-103) 9:30 A.M.-12:00 M.; 2:00-4:30 P.M. (Hall of Fame, West, Concourse)

Electrothermics and Metallurgy (Abs. 128-138) 9:00-11:30 A.M.; 2:00-5:00 P.M. (East Ballroom, 2nd Floor)

Theoretical Electrochemistry (Abs. 183-188) 9:00 A.M.-12:00 M.; 2:00-4:45 P.M. (Pennsylvania Ballroom, West, 3rd Floor)

Thursday, May 7, 1959

Electric Insulation (Abs. 30-38) 9:00-11:30 A.M.; 2:00-4:00 P.M. (Independence Room, 3rd Floor)

Electrothermics and Metallurgy (Abs. 139-150) 9:00 A.M.-12:00 M.; 2:00-5:00 P.M. (Constitution Room, 3rd Floor)

Theoretical Electrochemistry (Abs. 189-205) 9:00-11:10 A.M.; 2:00-4:30 P.M. (Pennsylvania Ballroom, East, 3rd Floor)

GENERAL INFORMATION

Convention Headquarters will be the Sheraton Hotel, 1725 Pennsylvania Boulevard, Philadelphia 3, Pa.

Rates per day for rooms (with bath) are: single room $8.50, 8.85, 11.50, 13.50, 15.50; Double-bed room $13.00, 15.00; Double room, twin beds $15.00, 17.00, 19.00, 22.00; Suite—parlor, bed room, 2 baths $30.50, 33.50, 40.50, 41.00.

Requests for room reservations at the Headquarters Hotel should be mailed to Lloyd B. Carswell, General Manager, Sheraton Hotel, 1725 Pennsylvania Boulevard, Philadelphia 3, Pa. BE SURE to state your intention to attend The Electrochemical Society meeting. Early reservations are advised. If your wife will be attending, be sure to indicate this on your request for reservation.

Within several blocks of the Headquarters Hotel are: Hotel Robert Morris, 17th and Arch Sts., single room $6.50 and up; double-bed room from $9.50; twin-bed room from $10.00. Central YMCA, 1421 Arch St., single room $2.00-$2.50.

Requests for room reservations should be mailed directly to hotel of choice. BE SURE to state your intention to attend The Electrochemical Society meeting.

The office of the Secretary will be in Parlor A (Third floor)

Ladies' Headquarters will be in Parlor C-D (Third floor)

The Local Section Headquarters and Press Room will be in Parlor B (Third floor)

All technical sessions will be held on the Concourse, Second, and Third Floors.

REGISTRATION

The registration desk will be on the Grand Ballroom floor (Second floor) Following is the registration schedule:

Sunday, May 3—3:00 to 9:00 P.M.
Monday, May 4—8:00 A.M. to 4:00 P.M.
Tuesday, May 5—8:00 A.M. to 4:00 P.M.
Wednesday, May 6—8:00 A.M. to 4:00 P.M.
Thursday, May 7—8:00 A.M. to 12:00 M.

Registration fees are:

Members	$ 7.00
Nonmembers	13.00*
Ladies	5.00
Thursday only	5.00
Students	2.00

*If a nonmember fills out an application blank and is subsequently elected to membership in the Society, the difference between the nonmember and member registration fee will be applied to his first year's dues.

INFORMATION ABOUT PHILADELPHIA

The Sheraton Hotel is in the heart of the fabulous Penn Center Plaza and is conveniently located for all activities. The hotel's 1000-car garage is directly across the street and has an underground entrance to the hotel.

Information about places of interest, theatrical and other attractions, and restaurants will be available at the ticket desk, or you may write to the Philadelphia Convention and Visitors Bureau, Penn Square Building, Philadelphia 7, Pa.

SYMPOSIA AND ROUND TABLE

The Electric Insulation Division has scheduled a symposium on Liquid Dielectrics—Gassing of Oils and Aging Studies, Factors Influencing Electrical Breakdown, and Conductivity Mechanisms, sponsored by the

National Science, Foundation, Office of Naval Research, and The ECS, as well as General Symposia.

The Electronics Division—Luminescence Group has scheduled four General Symposia and a Round Table as well as a Joint Symposia with the Semiconductor Group on Electroluminescent Devices.

The Electronics Division—Semiconductor Group has scheduled symposia on Bulk Properties, Surfaces and Junctions, Semiconducting Compounds, and Diffusion Techniques, as well as a Joint Symposium with the Luminescent Group on Electroluminescent Devices.

The Electronics Division—Thermionics Group has scheduled two symposia.

The Electrothermics and Metallurgy Division has scheduled symposia on miscellaneous topics, Constitution and Thermodynamics, New Equipment Developments in the Field of High-Temperature Technology, Mechanical Properties of Intermetallic Compounds, Refractory Compounds, and Effects of Impurities on Reactive Metals.

The Industrial Electrolytic Division has scheduled symposia on Electrolysis in Molten Electrolytes and General Sessions.

The Theoretical Electrochemistry Division has scheduled a symposium on Electrode Processes sponsored by the U. S. Air Force, Office of Scientific Research, and the ECS.

GENERAL FUNCTIONS

Symposia Chairmen Breakfasts

On **Monday, Tuesday, Wednesday,** and **Thursday,** May 4, 5, 6, and 7, special breakfasts will be held for symposia chairmen. On the day on which he presides at a symposium each chairman should be at the Café Carême, 2nd floor, by 7:45 A.M.

Monday Electronics Division Cocktail Party

Monday from 5:15-6:30 P.M. the Electronics Division will hold a cocktail party in the East Ballroom and Assembly (2nd floor). Admission by ticket.

Monday Evening Mixer

On Monday, May 4, all those registered at the meeting are invited to attend the get-acquainted Mixer in the Ballroom East and Assembly (2nd floor) from 8:00 P.M. on. Beer, soft drinks, and snacks will be served on a complimentary basis; a bar will be available for the purchase of other beverages.

Admission is by registration badge. This will be a good opportunity to meet old friends, make new ones, and plan your convention activities.

Tuesday Society Luncheon and Business Meeting

The Electrochemical Society Luncheon and Business Meeting will be held on Tuesday, May 5, at 12:15 P.M. in the East Ballroom (2nd floor). An outstanding speaker will be featured.

Tuesday Evening Reception and Banquet

A reception honoring President Sherlock Swann and the new Honorary Members of the Society will be held at 6:30 P.M. on Tuesday, May 5, in the Balloom Assembly (2nd floor). Cocktails will be served from 6:30 P.M. to 7:30 P.M., followed by dinner at 7:30 P.M. in the Grand Ballroom. Dr. Swann will deliver the Presidential Address and will introduce the newly elected Honorary Members and present Certificates of Honorary Membership to them. (Dress optional).

Wednesday Evening Cruise and Buffet Supper

On Wednesday evening, May 6, a unique, informal, relaxing, and fun program has been planned. A famous river boat has been chartered to provide a cruise on the Delaware River. A buffet supper with entertainment and surprises will round out the evening, returning about eleven o'clock. This evening's function should allow everyone to relax after several days of scientific pursuit. Transportation will be available from the Sheraton Hotel to place of debarkation and return. Definite information regarding time and place will be available at the ticket desk. Make this evening a MUST during your convention stay.

LADIES' PROGRAM

A friendly invitation is extended to all the ladies attending the convention to make Parlor C-D on the 3rd floor of the Sheraton Hotel their headquarters during their stay in Philadelphia.

The morning coffee hour will be held each day, Monday through Thursday, and visitors are cordially invited to come and become acquainted. Members of the Ladies' Committee will be there to give information or to assist in any way to make the stay a pleasant one.

The visitor's cooperation would be greatly appreciated if they would let the committee know as early as possible which trips they wish to make. This will enable the committee to make reservations in sufficient time to assure their participation and enjoyment.

Monday morning, May 4.—Coffee hour will be held from 9:30 to 10:30 A.M. in Parlor C-D. The rest of the morning is left open for individual shopping or sightseeing.

Monday afternoon, May 4.—At 2:00 P. M. a bus will leave for a tour of historic Philadelphia, including Independence Hall, the Liberty Bell, Betsy Ross house, Christ Church, and Elfreth's Alley.

Or an ALTERNATE TRIP for those who attended the Ottawa meeting and others who are interested in the University of Pennsylvania's Robert Tait McKenzie exhibit has been arranged and transportation provided. This trip also starts at 2:00 P.M.

Monday evening, May 4.—The ladies are invited to attend the Mixer at 8:00 P.M. in the East Ballroom (see General Functions).

Tuesday morning and afternoon, May 5.—Coffee hour will be held from 9:00 to 10:00 A.M. in Parlor C-D.

At 10:20 A.M. buses will leave for luncheon at the Dupont Country Club in Wilmington, Del. At 1:30 the buses will resume their trip to the Henry Francis du Pont Winterthur Museum and Gardens. At this famous museum we will see twenty rooms taken from early American houses as well as Mr. du Pont's spring flower and azalea gardens. The buses will leave at 4:00 P.M. to return to the hotel. A limited number of reservations are available for this trip and reservations will be required not later than 9:00 A.M. Tuesday morning.

Tuesday evening, May 5—The ladies are invited to attend the Reception and Banquet at 6:30 P.M. in the Grand Ballroom. Tickets should be purchased at the ticket desk on registration floor.

Wednesday morning and afternoon, May 6—Coffee hour in Parlor C-D from 9:30 to 10:00 A.M.

Buses will leave the hotel at 10:50 A.M. for a trip through suburban Philadelphia with a visit to Morris Arboretum in Chestnut Hill. The arboretum was turned over to the Botany Department of the University of Pennsylvania by the will of Miss Lydia Morris, a descendant of Samuel B. Morris of Revolutionary fame, and contains specimens gathered both here and abroad. Luncheon will be at the Philadelphia Cricket Club, after which the group will visit the widely known stained glass studio of Henry Lee Willets. An illustrated lecture will be given by Mr. Willets. Buses will return to the hotel arriving at about 4:00 P.M.

Wednesday evening, May 6—The ladies are invited to "come aboard" for the cruise on the Delaware, during which supper and entertainment are provided. Tickets must be purchased in advance at the ticket desk. (See General Functions)

Thursday morning, May 7.—Coffee hour from 9:30 to 10:30 A.M. in Parlor C-D. The day is left free for individual plans.

LUNCHEONS AND BUSINESS MEETINGS OF DIVISIONS

Electronics Division Luncheon and Business Meeting, Monday, May 4, at 12:30 P.M. in the Hall of Flags, East, Concourse.

Industrial Electrolytic Division Luncheon and Business Meeting, Monday, May 4, at 12:30 P.M., in the East Ballroom, 2nd floor.

Electrothermics and Metallurgy Division Business Meeting on Tuesday, May 5, at 11:00 A.M., in the Hall of Flags, Concourse.

Electric Insulation Division Luncheon and Business Meeting, Wednesday, May 6, at 12:15 P.M., in the Constitution Room, 3rd floor.

Theoretical Electrochemistry Division Luncheon, Wednesday, May 6, at 12:15 P.M. in the Hall of Flags, Concourse.

Theoretical Electrochemistry Division Business Meeting, Thursday, May 7, at 11:30 A.M., in the Pennsylvania Ballroom, East, 3rd floor.

BOARD AND COMMITTEE MEETINGS

Sunday, May 3, 2:00 P.M.—Meeting of the **Board of Directors** in the Connie Mack Room, 3rd floor.

Sunday, May 3, 7:30 P.M.—Meeting of the **Investment Advisory Panel** in the Connie Mack Room, 3rd floor.

Monday, May 4, 5:00 P.M.—Meeting of the **Membership Committee** in Room 556-8, 5th floor.

Tuesday, May 5, 5:00 P.M.—Meeting of the **Editorial Staff** of the *Journal* in Room 556-8, 5th floor.

Wednesday, May 6, 5:00 P.M.—Meeting of the **Council of Local Sections** in Room 556-8, 5th floor.

Thursday, May 7, 12:00 M.—Meeting of General Chairmen of Future Meetings. Meet at the Office of the Secretary (Parlor A, 3rd floor) at 12:00 M. Luncheon will be arranged.

COST OF VARIOUS FUNCTIONS

(other than registration)

Tickets for all functions will be sold at a separate desk near registration center. Please secure tickets as early as possible. Deadlines for each function will be posted at ticket desk.

Symposia Chairmen breakfasts-Standard Menu prices	
Monday P.M. Electronics Division Cocktail Party	$3.00
Monday evening Mixer	Complimentary
Division Luncheons	4.00
Tuesday Society Luncheon	4.25
Tuesday Reception and Banquet	8.00
Wednesday Cruise and Buffet Supper	4.50
Ladies' Functions	Largely complimentary

JOURNALS

Copies of the January, February, March, and April issues of the "Journal of The Electrochemical Society" will be available at the registration desk. The price of a single copy of the **Journal** is $1.25 to members and $1.75 to nonmembers.

EXTENDED ABSTRACTS

The Electronics Division and the Theoretical Electrochemistry Division are making available extended abstract booklets containing 1000-word abstracts of most of the papers presented at the Philadelphia Meeting. Copies of these two booklets will be available at the registration desk.

The Electric Insulation Division will probably have an extended abstract booklet also.

DISCUSSION

No recordings will be made of oral discussions. Those contributing to the discussion of a paper and desiring their remarks to be published will be supplied by the symposium chairman with a printed form on which any discussion may be written. These forms should be given to the Secretary-Treasurer of the Division or to the Managing Editor of the JOURNAL after the session; they can be mailed to the Managing Editor of the JOURNAL, 1860 Broadway, New York 23, N. Y. The discussion will then be referred to the author for reply. Publication of the discussion and the comments of the author depends on publication of the article in the JOURNAL.

Written discussion should be submitted within two months following publication of the article in the JOURNAL. A Discussion Section is published semi-annually in the JOURNAL.

EMPLOYMENT POSTERS

Companies which desire to recruit employees at the Philadelphia Meeting will have posters to this effect on a bulletin board near the registration desk.

FALL MEETING
at the
Deshler-Hilton Hotel
COLUMBUS, OHIO
October 18, 19, 20, 21 and 22, 1959

Sessions probably will be scheduled on
Batteries
Corrosion (including a joint **Corrosion—Electronics—Semiconductors** session)
Electrodeposition (including symposia on "Electrodeposition from Organic Solvents" and "Electro- and Chemical-Polishing")
Electronics (Semiconductors)
Electro-Organics
Electrothermics and Metallurgy

Abstracts for the Fall Meeting *(not exceeding 75 words in length)* must reach Society Headquarters, 1860 Broadway, New York 23, N. Y., not later than June 1, 1959 in order to be included in the program.

Indicate on abstract for which Division's symposium the paper is to be scheduled, and underline the name of the author who will present the paper.

ELECTRIC INSULATION

Monday, May 4, 1959
Liquid Dielectrics
Gassing of Oils and Aging Studies
Sponsored by the National Science Foundation, Office of Naval Research, and The ECS
with H. Basseches presiding
(CONSTITUTION AND INDEPENDENCE ROOMS, 3rd Floor)

9:45 A.M.—Welcome by H. Basseches

10:00 A.M.—"Influence of the Constitution of Oils on Their Gassing under Electric Stress" by E. H. Reynolds and S. C. Clarke (Abstract No. 1)

10:30 A.M.—"A New Explanation of Gas Evolution in Electrically Stressed Oil Impregnated Paper Insulation" by Z. Krasucki, H. F. Church, and C. G. Garton (Abstract No. 2)

11:00 A.M.—"The Chemistry of Cable-Oil Deterioration" by George Feick, W. F. Olds, and E. D. Eich (Abstract No. 3)

11:30 A.M.—"Ultraviolet Irradiation of Chlorinated Biphenyl" by H. M. Stahr (Abstract No. 4)

Electric Insulation
Monday, May 4, 1959
Liquid Dielectrics (cont'd)
Gassing of Oils and Aging Studies (cont'd)
Sponsored by the National Science Foundation, Office of Naval Research, and the ECS
with H. Basseches presiding

MEETING ROOM SCHEDULES

Meeting	Monday A.M.	Monday P.M.	Tuesday A.M.	Tuesday P.M.	Wednesday A.M.	Wednesday P.M.	Thursday A.M.	Thursday P.M.
Electric Insulation	D&E	D&E	D&E	D&E	C	C	E	E
Electronics—Luminescence	B	B	B	B				
—Semiconductors	A	A	A	A				
—Devices					A			
—Thermionics					F	F		
Electrothermics and Metallurgy	F	F	F&G	F&G	H	H	D	D
Electrothermics and Metallurgy		G						
Industrial Electrolytic	H	H	H	H				
Theoretical	C	C	C	C	B	B	C	C

A = West Ballroom, 2nd floor
B = Pennsylvania Ballroom, West, 3rd floor
C = Pennsylvania Ballroom, East, 3rd floor
D = Constitution Room, 3rd floor
E = Independence Room, 3rd floor
F = Hall of Flags, West, Concourse
G = Hall of Flags, East, Concourse
H = East Ballroom, 2nd floor

(CONSTITUTION AND INDEPENDENCE ROOMS, 3rd Floor)

2:00 P.M.—"Correlation between Dielectric Losses and Chemical Stability of Mineral Oils" by T. Salomon (Abstract No. 5)
2:30 P.M.—"The Dependence of the Dielectric Power Factor of Insulating Oils on the Water and Gas Content" by K. Brinkmann (Abstract No. 6)
3:00 P.M.—"A Method for the Determination of the Aging of Insulating Oils" by R. Strigel (Abstract No. 7)

Electric Insulation
Tuesday, May 5, 1959
Liquid Dielectrics (cont'd)
Factors Influencing Electric Breakdown
Sponsored by the National Science Foundation, Office of Naval Research, and The ECS
with T. D. Callinan presiding

(CONSTITUTION AND INDEPENDENCE ROOMS, 3rd Floor)

9:00 A.M.—"Effect of Dissolved Gases on the Electric Conduction and Breakdown of Insulating Oil" by H. Tropper (Abstract No. 9)
9:30 A.M.—"The Influence on the Oil Breakdown Strength of the Gas Pressure in Equilibrium with the Oil" by P. G. Priaroggia and G. L. Palandri (Abstract No. 10)
10:00 A.M.—"Effects of Hydrostatic Pressure, Temperature, and Voltage Duration on the Electric Strengths of Hydrocarbon Liquids" by K. C. Kao and J. B. Higham (Abstract No. 11)
10:30 A. M.—"Measurement of the Breakdown in Insulating Oil" by E. Baumann (Abstract No. 12)
11:00 A.M.—"A New Statistical Theory of the Breakdown Process and the Reinterpretation of Pulse Breakdown Measurements in Liquid Hydrocarbons" by T. J. Lewis (Abstract No. 13)
11:30 A.M.—"Influence of Electrode Surface Conditions on the Electrical Strength of Liquified Gases" by T. J. Lewis (Abstract No. 14)
12:15 P.M.—Society Luncheon and Business Meeting in the East Ballroom (2nd Floor).

Electric Insulation
Tuesday, May 5, 1959
Liquid Dielectrics (cont'd)
Factors Influencing Electrical Breakdown (cont'd)
Sponsored by the National Science Foundation, Office of Naval Research, and The ECS
with T. D. Callinan presiding

(CONSTITUTION AND INDEPENDENCE ROOMS, 3rd Floor)

2:00 P.M.—"Recent Investigations of the Development of a Discharge during an Electric Breakdown in Oil in a Nonuniform Field" by R. Strigel (Abstract No. 15)
2:30 P.M.—"Prebreakdown Discharges in Insulating Liquids" by T. W. Dakin and D. Berg (Abstract No. 16)
3:00 P.M.—"Recent Developments in the Chemistry of Active Nitrogen" by R. A. Back and C. A. Winkler (Abstract No. 17)
3:30 P.M.—"Molecular Structure and the Electrical Strength of Liquid Hydrocarbons" by T. J. Lewis (Abstract No. 18)

Electric Insulation
Wednesday, May 6, 1959
Liquid Dielectrics (cont'd)
Conductivity Mechanisms
Sponsored by the National Science Foundation, Office of Naval Research, and The ECS
with L. J. Frisco presiding

(PENNSYLVANIA BALLROOM, EAST, 3rd Floor)

9:00 A.M.—"Electrical Conduction in Hexane under Pulse Conditions" by K. A. Macfadyen and G. C. Helliwell (Abstract No. 19)
9:30 A.M.—"High-Field Conduction Currents in Liquid Hexane under Pulse Conditions" by A. H. Sharbaugh and P. K. Watson (Abstract No. 20)
10:00 A.M.—"Equilibrium Space Charge at the Contact of a Metal and a Pure, High-Insulating Liquid and Its Influence on High-Field Conductivity" by M. J. Morant (Abstract No. 21)
10:30 A.M.—"Electron Drift Mobility in Liquid n-Hexane" by O. H. LeBlanc, Jr. (Abstract No. 22)
11:00 A.M.—"Particle Separations by Nonuniform Electric Fields in Liquid Dielectrics, Batch Methods" by H. A. Pohl and J. P. Schwar (Abstract No. 23)
11:30 A.M.—"Continuous Separations of Suspensions by Nonuniform Electric Fields in Liquid Dielectrics" by H. A. Pohl and C. E. Plymale (Abstract No. 24)
12:15 A. M.—Electric Insulation Division Luncheon and Business Meeting in the Constitution Room (3rd floor). C. P. Smyth, Department of Chemistry, Princeton University, Princeton, N. J., is speaker.

Electric Insulation
Wednesday, May 6, 1959
Liquid Dielectrics (cont'd)
Conductivity Mechanisms (cont'd)
Sponsored by the National Science Foundation, Office of Naval Research, and The ECS
with L. J. Frisco presiding

(PENNSYLVANIA BALLROOM, EAST, 3rd Floor)

2:00 P.M.—"Temperature and Space Charge Effects in Liquid Hydrocarbons" by R. Coelho and M. Bono (Abstract No. 25)
2:30 P.M.—"Flash Conductivity in Organic Solution" by H. T. Witt (Abstract No. 26)
3:00 P.M.—"Demonstration of Physical Properties of Water by D-C Conductivity of Undesiccated Insulating Liquids (Fields below 2 kv/cm)" by R. Guizonnier (Abstract No. 27)
3:30 P.M.—"The Wien Effect and Ionic Association" by Andrew Patterson, Jr., and Harlow Freitag (Abstract No. 28)
4:00 P.M.—"Nonuniform Field Effects in Poorly Conducting Media" by H. A. Pohl (Abstract No.29)

Electric Insulation (cont'd)
Thursday, May 7, 1959
with B. R. Eichbaum presiding

(INDEPENDENCE ROOM, 3rd Floor)

9:00 A.M.—"High-Temperature Silicone Laminates" by W. Elsfelder (Abstract No. 30)
9:30 A.M.—"Silver Migration—A Cause of Component Failure" by A. A. Cortesi (Abstract No. 31)
10:00 A.M.—"A Universal Meter for Measuring Voltages at High Impedances, Microamperes, and Insulation Resistance" by W. R. Clark, R. E. Watson, and G. C. Mergner (Abstract No. 32)
10:30 A.M.—"Electrical Properties of Waxes" by T. D. Callinan (Abstract No. 33)
11:00 A.M.—"Domain Structure and Optical Properties of Transport Ferrimagnetic Crystals" by J. F. Dillon, Jr. (Abstract No. 34)

Electric Insulation (cont'd)
Thursday, May 7, 1959
with B. R. Eichbaum presiding

(INDEPENDENCE ROOM, 3rd Floor)

2:00 P.M.—"Piezoelectric and Dielectric Properties of Ceramics in the Potassium-Sodium Niobate System" by L. Egerton and D. M. Dillon (Abstract No. 35)
2:30 P.M.—"Influence of Processing Techniques on the Dielectric Properties of Titanates and Zirconates" by Lawrence Kopell (Abstract No. 36)
3:00 P.M.—"Factors Involved in the Application of Ceramic Insulation" by J. S. White and N. J. Norante (Abstract No. 37)
3:30 P.M.—"Properties of Some Special Purpose Glasses" by G. W. McLellan (Abstract No. 38)

ELECTRONICS—LUMINESCENCE

Monday, May 4, 1959
with Ephraim Banks presiding

(PENNSYLVANIA BALLROOM, WEST 3rd Floor)

9:00 A.M.—Keynote Address—"Luminescent Centers in ZnS Phosphors" by J. S. Prener (Invited Paper) (Abstract No. 39)
9:45 A.M.—"Copper- and Tin-Activated Alkaline Earth Halophosphate Phosphors" by B. E. Hunt and A. H. McKeag (Abstract No. 40)
10:05 A.M.—"Luminescence of Copper-Activated Calcium and Strontium Orthophosphates" by W. L. Wanmaker and C. Bakker (Abstract No. 41)
10:25 A.M.—"Tin-Activated Pyrophosphate Phosphors" by R. C. Ropp and R. W. Mooney (Abstract No. 42)
10:45 A.M.—"Phase Equilibria and Fluorescence in the System $Zn(PO_3)_2 - Mg(PO_3)_2$" by J. F. Sarver and F. A. Hummel (Abstract No. 43)
11:05 A.M.—"Calcium Halophosphate Phosphors, II.

Theoretical Optics of Lamp Coatings" by K. H. Butler (Abstract No. 44)
11:25 A.M.—"Calcium Halophosphate Phosphors, III. Effect of Particle Size on Optical Constants" by M. J. B. Thomas (Abstract No. 45)
11:45 A.M.—"Calcium Halophosphate Phosphors, IV. Influence of Particle Size on Lamp Performance" by H. H. Homer (Abstract No. 46)
12:15 P.M.—Electronics Division Luncheon and Business Meeting in the Hall of Flags, East, Concourse.

Electronics—Luminescence (cont'd)
Monday, May 4, 1959
with C. H. Haake presiding
(PENNSYLVANIA BALLROOM, WEST, 3rd Floor)

2:00 P.M.—"Voltage Dependence and Particle Size Distribution of Electroluminescent Phosphors" by W. Lehmann (Abstract No. 47)
2:25 P.M.—"The Action of Iron-Group Elements in Electroluminescent Zinc Sulfide Phosphors" by Paul Goldberg (Abstract No. 48)
2:50 P.M.—"Microscopic Observations on Electroluminescent Phosphors" by Alfred Kremheller (Abstract No. 49)
3:15 P.M.—"Changes in Trapping Levels of Zinc Sulfide Phosphors Resulting from Positive Ion Bombardment" by W. T. Allen and C. H. Bachman (Abstract No. 50)
3:40 P.M.—"Some New Features of Phosphors Showing the Electro-Enhancement Effect" by F. Pingault and G. Destriau (Abstract No. 51)
3:55 P.M.—"A General Effect of Coactivators of Mn in CdZnS:Mn, X Phosphors Showing the Electro-Enhancement Effect" by G. Destriau (Abstract No. 52)
4:15 P.M.—"Field Enhancement of the Light Emitted by Alpha-Scintillations" by J. Mattler (Abstract No. 53)
4:35 P.M.—"On the Origin of Complex Output Wave Forms of A-C Electroluminescence" by E. E. Loebner and I. J. Hegyi (Abstract No. 54)

Electronics—Luminescence (cont'd)
Tuesday, May 5, 1959
with Simon Larach presiding
(PENNSYLVANIA BALLROOM, WEST, 3rd Floor)

9:00 A.M.—"Influence of Hydrogen on Red ZnS-Cu Fluorescence" by W. van Gool and A.P.D.M. Cleiren (Abstract No. 55)
9:25 A.M.—"Associated Donor-Acceptor Luminescent Centers in (Zn,Cd)S Phosphors" by E. F. Apple and D. J. Weil (Abstract No. 56)
9:50 A.M.—"Effect of Sulfur Pressure and Donors on the Infrared Emission Intensity in ZnS:Cu" by J. S. Prener, E. F. Apple, and D. J. Weil (Abstract No. 57)
10:15 A.M.—"Antistokes Fluorescence in (Zn,Cd)S" by R. M. Potter (Abstract No. 58)
10:40 A.M.—"Hydrothermal Preparation of Two-Component Solid Solutions from II-VI Compounds" by Alfred Kremheller, A. K. Levine, and G. Gashurov (Abstract No. 59)
11:05 A.M.—"Polarization of Luminescence of ZnS and CdS Single Crystals" by A. Lempicki (Abstract No. 60)
11:30 A.M.—"On the Polarization of Fluorescence in CdS and ZnS Single Crystals" by J. L. Birman (Abstract No. 61)

Electronics—Luminescence (cont'd)
Tuesday, May 5, 1959
with Ralph Potter presiding
(PENNSYLVANIA BALLROOM, WEST, 3rd Floor)

2:00 P.M.—"The Fluorescence of Some Binary and Ternary Germanates" by H. Koelmans and C. M. C. Verhagen (Abstract No. 62)
2:20 P.M.—"Two Unusual Effects Observed with CaO:Mn, Li Phosphors" by P. M. Jaffe (Abstract No. 63)
2:40 P.M.—"Tin-Activated Calcium-Silicate Phosphors" by R. W. Mooney (Abstract No. 64)
3:00 P.M.—"The Calcium Silicate Mn + Pb Phosphor; Phase Relationship and Preparation" by D. E. Harrison and M. V. Hoffman (Abstract No. 65)

Round-Table Discussion

3:30-5:00 P.M.—Round-table discussion with Nathan Melamed, moderator

ELECTRONICS-LUMINESCENCE & SEMICONDUCTOR GROUPS

Joint Symposium
Wednesday, May 6, 1959
Electroluminescent Devices
with Henry Ivey presiding
(WEST BALLROOM, 2nd Floor)

9:00 A.M.—Keynote Address—"Solid-State Opto-Electronics" by E. E. Loebner (Abstract No. 66)
10:00 A.M.—"Analysis of Characteristics of Electroluminescent Lamps with Conductive Grid Structures" by R. J. Coerdt (Abstract No. 67)
10:25 A.M.—"An Improved Electroluminescent Display Panel" by R. R. Chamberlin (Abstract No. 68)
10:55 A.M.—"An Electroluminescent Symbolic Indicator" by R. C. Lyman (Abstract No. 69)
11:20 A.M.—"Preparation and Performance of Sintered CdS Layers" by R. R. Billups, W. L. Gardner, and M. D. Zimmerman (Abstract No. 70)
11:45 A.M.—"A Discussion of Photoconductive Response" by Arthur Bramley (Abstract No. 71)

ELECTRONICS—SEMICONDUCTORS

Monday, May 4, 1959
Bulk Properties
with N. B. Hannay presiding
(WEST BALLROOM, 2nd Floor)

9:30 A.M.—"Electromagnetic Levitation of a Floating Zone" by K. M. Arnold, B. W. Levinger, and H. F. Matare (Abstract No. 72)
9:50 A.M.—"Bulk Properties of High-Resistivity P-Type Silicon" by C. A. Klein and W. D. Straub (Abstract No. 73)
10:20 A.M.—"The Semiconductivity of Organic Compounds" by Leroy Schieler and P. L. Nichols, Jr. (Abstract No. 74)
11:00 A. M.—"Temperature Dependence of the Solid Solubility and the Distribution Coefficient of Various Impurities in Ge and Si" by F. A. Trumbore and C. D. Thurmond (Abstract No. 75)
11:30 A.M.—Recent News Papers. Titles and short abstracts will be available at the Registration Desk.
12:30 P.M.—Electronics Division Luncheon and Business Meeting in the Hall of Flags, East, Concourse.

Electronics—Semiconductors (cont'd)
Monday, May 4, 1959
Surfaces and Junctions
with R. N. Hall presiding
(WEST BALLROOM, 2nd Floor)

2:25 P.M.—"Intrinsic Regions in Si Produced by Li Ion Drift" by E. M. Pell (Abstract No. 78)
2:55 P.M.—"Influence of Surface Treatment on Performance of Silicon Current Limiters" by T. M. Buck, W. H. Jackson, and F. S. McKim (Abstract No. 79)
3:30 P.M.—"Studies of Surface Conductivity and Recombination in Silicon" by C. G. Peattie and W. R. Savage (Abstract No. 80)
3:55 P.M.—"Alloy Junctions in Gallium Arsenide" by S. M. Ku and H. T. Minden (Abstract No. 81)
4:25 P.M.—"Very Low Voltage D-C Electroquenchable Phosphors" by L. W. Hershinger and M. E. Lasser (Abstract No. 82)
4:50 P.M.—Recent News Papers. Titles and short abstracts will be available at the Registration Desk.

Electronics—Semiconductors (cont'd)
Tuesday, May 5, 1959
Semiconducting Compounds
with A. C. Beer presiding
(WEST BALLROOM, 2nd Floor)

9:00 A. M.—"Determination of Impurities in III-V Semiconducting Compounds" by F. J. Reid, S. E. Blum, and R. K. Willardson (Abstract No. 83)
9:50 A.M.—"High-Purity Single Crystals of Indium Antimonide" by R. C. Bourke, S. E. Miller, and W. P. Allred (Abstract No. 84)
10:10 A.M.—"Preparation and Properties of AlSb" by W. P. Allred, W. L. Mefferd, and R. K. Willardson (Abstract No. 85)

10:55 A.M.—"Purification and Crystal Growth of Zinc Arsenides" by V. J. Lyons and G. A. Silvey (Abstract No. 86)
11:25 A.M.—"Rare Earth Compound Semiconductors" by J. F. Miller, F. J. Reid, and R. C. Himes (Abstract No. 87)
11:50 A.M.—Recent News Papers. Titles and short abstracts will be available at the Registration Desk.
12:15 P.M.—Society Luncheon and Business Meeting in the East Ballroom, 2nd floor.

Electronics—Semiconductors (cont'd)
Tuesday, May 5, 1959
Diffusion Techniques
with S. J. Angello presiding
(WEST BALLROOM, 2nd Floor)

2:00 P.M.—"Diffusion in Silicon by the Box Method" by L. A. D'Asaro (Abstract No. 88)
2:30 P.M.—"Application of Oxide Masking to Silicon Diffused Transistors" by R. H. Lanzl (Abstract No. 89)
3:00 P.M.—"Penetration of an Oxide Film on Silicon by P_2O_5" by C. T. Sah, H. Sello, and D. Tremere (Abstract No. 90)
3:35 P.M.—"Evaluation of Impurity Distributions" by K. Lehovec, C. Pihl, and C. Wrigley (Abstract No. 91)
4:05 P.M.—"Gaseous Diffusion of Phosphorus in Germanium" by K. Lehovec, C. Pihl, and C. Wrigley (Abstract No. 92)
4:30 P.M.—"Polishing and Etching of a III-V Binary Semiconductor, Gallium Arsenide" by J. G. Harper and M. S. Astor (Abstract No. 93)
4:55 P. M.—Recent News Papers. Titles and short abstracts will be available at the Registration Desk.

ELECTRONICS—SEMICONDUCTOR & LUMINESCENCE GROUPS

Joint Symposium
Wednesday, May 6, 1959
Electroluminescent Devices
with Henry Ivey presiding
(WEST BALLROOM, 2nd Floor)

9:00 A.M.—*See* Electronics—Luminescence & Semiconductor Program, Abstracts 66-71.

ELECTRONICS—THERMIONICS

Wednesday, May 6, 1959
with W. G. Shepherd presiding
(HALL OF FLAGS, WEST, Concourse)

9:30 A.M.—Keynote address by J. S. Wagener (Abstract No. 94)
10:00 A.M.—"Measurement of Adsorbed and Desorbed Gases in Vacuum Tubes by Mass Spectrometric Techniques" by J. E. Turnbull (Abstract No. 95)
10:30 A.M.—"Determination of Residual Amounts of Organic Contaminants in Electron Tubes by Radiotracer Technique" by H. A. Stern (Abstract No. 96)
11:00 A.M.—"Methods of Cathode Temperature Measurement in Commercial Tubes" by J. H. Affleck (Abstract No. 97)
11:30 A.M.—"Diffusion of Thorium in Dispenser Cathodes" by D. L. Goldwater and W. E. Danforth (Abstract No. 98)

Electronics—Thermionics (cont'd)
Wednesday, May 6, 1959
with W. G. Shepherd presiding
(HALL OF FLAGS, WEST, Concourse)

2:00 P.M.—"Oxygen in High-Purity Cathode Nickel Alloys" by H. E. Kern, C. W. Caldwell, E. T. Graney, A. L. Beach, and W. G. Guldner (Abstract No. 99)
2:30 P.M.—"Gettering Properties of Titanium-Zirconium Alloys" by V. L. Stout and M. G. Gibbons (Abstract No. 100)
3:00 P.M.—"Electrolysis and the Activation Processes in the Oxide Coated Cathode" by D. E. Anderson (Abstract No. 101)
3:30 P.M.—"Proposed New Model for the Cause of Flicker Noise in Oxide Coated Cathodes" by R. R. Johnson (Abstract No. 102)
4:00 P.M.—"A Study of Tungsten, Magnesium, and Aluminum as Nickel Additives for Oxide Cathode Use" by H. B. Frost and R. C. Gee (Abstract No. 103)

ELECTROTHERMICS AND METALLURGY

Monday, May 4, 1959
Miscellaneous Topics
with A. U. Seybolt presiding
(HALL OF FLAGS, WEST, Concourse)

9:30 A.M.—"The Production of Thorium Powder by Calcium Reduction of Thorium Oxide" by N. Fuhrman, R. B. Holden, and C. I. Whitman (Abstract No. 104)
10:00 A.M.—"Super Pure Aluminum" by R. R. Haberecht (Abstract No. 105)
10:30 A.M.—"Oxide Nucleation and the Substructure of Iron" by E. A. Gulbransen and K. F. Andrew (Abstract No. 106)
11:00 A.M.—"Oxidation Studies on the Nickel Chromium and Nickel-Chromium-Aluminum Heater Alloys" by E. A. Gulbransen and K. F. Andrew (Abstract No. 107)
11:30 A.M.—"A Study of the Factors Affecting the Electrical Characteristics of Sintered Tantalum Anodes" by G. L. Martin, C. J. B. Fincham, and E. E. Chadsey, Jr. (Abstract No. 108)

Electrothermics and Metallurgy
Monday, May 4, 1959
Constitution and Thermodynamics
with J. H. Westbrook presiding
(HALL OF FLAGS, WEST, Concourse)

2:00 P.M.—"Equilibrium Reduction of Tungsten Oxides by Hydrogen" by R. C. Griffis (Abstract No. 109)
2:30 P.M.—"Electrode Potential Measurements of the Liquid Al-Ag and Al-Ag-Pb Systems between 690° and 1000°C" by T. C. Wilder and J. F. Elliott (Abstract No. 110)
3:00 P. M.—"Some Observations on the Effect of the Interaction of Tantalum with Oxygen, Nitrogen, and Hydrogen" by R. Bakish (Abstract No. 111)
3:30 P.M.—"The Nature of Alumina in Quenched Cryolite-Alumina Melts" by P. A. Foster, Jr. (Abstract No. 112)
4:00 P.M.—"On the Solubilities of a Certain Gas in Refactory Metals at Elevated Temperatures" by Charles London, Richard Beck, Rudolph Speiser, *et al.* (Abstract No. 113)

Electrothermics and Metallurgy
Monday, May 4, 1959
New Equipment Developments in the Field of High-Temperature Technology
with J. M. Blocher, Jr., presiding
(HALL OF FLAGS, EAST, Concourse)

2:00 P.M.—Introductory Remarks by J. M. Blocher, Jr.
2:10 P.M.—"Arc-Image Furnace for High Thermal Flux" by F. C. Todd (Abstract No. 114)
2:35 P.M.—"Imaging Furnace Developments for High-Temperature Research" by P. E. Glaser (Abstract No. 115)
3:00 P. M.—"The Plasma Torch" by M. L. Thorpe (Abstract No. 116)
3:25 P.M.—"The High-Intensity Arc; An Aid in the Development of Ceramic Compositions for High-Temperature Applications" by C. E. Shulze (Abstract No. 117)
3:50 P.M.—"The Design and Operation of an Improved Consumable Electrode Vacuum Arc Melting Furnace" by K. L. Bryant, Jr., and A. L. Feild, Jr. (Abstract No. 118)
4:15 P.M.—"High-Temperature Laboratory Furnaces for Sintering Single-Crystal Growth and Button Melting of Tungsten" by H. G. Sell (Abstract No. 119)
4:40 P.M.—"An Electron Bombardment Annealing Furnace" by B. S. Chandrasekhar and P. A. Flinn (Abstract No. 120)

Electrothermics and Metallurgy
Tuesday, May 5, 1959
Mechanical Properties of Intermetallic Compounds
with R. W. Guard presiding
(HALL OF FLAGS, EAST & WEST, Concourse)

9:00 A.M.—"Review of the Mechanical Properties of Intermetallic Compounds" by J. H. Westbrook (Abstract No. 121)
10:00 A.M.—"The Electronic Factor in Mechanical Strength" by G.-M. Schwab (Abstract No. 122)
10:30 A.M.—"Influence of Temperature on Mechanical Properties of Intermetallic Compounds" by E. M. Savitskii (Abstract No. 123)

11:00 A.M.—Electrothermics and Metallurgy Division Business Meeting in the Hall of Flags, Concourse
12:15 P.M.—Society Luncheon and Business Meeting in the East Ballroom, 2nd Floor.

Electrothermics and Metallurgy
Tuesday, May 5, 1959
Mechanical Properties of Intermetallic Compounds (cont'd)
with E. M. Sherwood presiding
(HALL OF FLAGS, EAST & WEST, Concourse)

2:00 P.M.—"Techniques for High-Temperature Tensile and Torsional Testing of Brittle Refractory Materials" by L. Green, Jr., M. L. Stehsel, and C. E. Waller (Abstract No. 124)
2:30 P.M.—"Fractographic Study of NiAl" by A. M. Turkalo and R. W. Guard (Abstract No. 125)
3:00 P.M.—"Extrusion of Intermetallic Compounds" by D. L. Wood (Abstract No. 126)
3:30 P.M.—"Ordered Lattices from Fused Salt Electrolysis, I. Ordered Alloys of Chromium" by R. S. Dean, W. W. Gullett, F. X. McCawley, and L. D. Resnick (Abstract No. 127)

Electrothermics and Metallurgy
Wednesday, May 6, 1959
Mechanical Properties of Intermetallic Compounds (cont'd)
with A. Lawley presiding
(EAST BALLROOM, 2nd Floor)

9:00 A.M.—"The Interaction between Dislocations and the Superlattice" by Norman Brown (Abstract No. 128)
9:30 A.M.—"Deformation Modes in Face-Centered Cubic Superlattice Alloys" by Tadami Taoka, Ryukicki Honda, and Ko Yasukochi (Abstract No. 129)
10:00 A.M.—"Electron Microscope Observations of the Domain Structure in Ordered Copper-Gold Alloy" by D. W. Pashley and A. E. B. Presland (Abstract No. 130)
10:30 A.M.—"Effects of Radiation on the Properties of TiAl" by E. M. Grala and J. B. McAndrew (Abstract No. 131)
11:00 A.M.—"Plastic Deformation of InSb" by J. J. Duga (Abstract No. 132)

Electrothermics and Metallurgy
Wednesday, May 6, 1959
Mechanical Properties of Intermetallic Compounds (cont'd)
with J. H. Westbrook presiding
(EAST BALLROOM, 2nd Floor)

2:00 P.M.—"Mechanical Properties of Some Transition Element Beryllides" by A. J. Stonehouse, R. M. Paine, and W. W. Beaver (Abstract No. 133)
2:30 P.M.—"Plasticity of the Complex-Cubic Gamma 2 Phase of the Copper-Aluminum System" by A. J. Birkle, W. L. Krubsack, and D. J. Mack (Abstract No. 134)
3:00 P.M.—"Intermetallic Compounds of the Transition Metals and Their High-Temperature Properties" by R. D. Grinthal (Abstract No. 135)
3:30 P.M.—"The Mechanical Properties of Some Intermetallic Compounds of Iron and Nickel" by I. Kornilov (Abstract No. 136)
4:00 P.M.—"Investigation of NiAl and Ni_2Al" by E. M. Grala (Abstract No. 137)
4:30 P.M.—"Mechanical and Electromechanical Properties of Indium Antimonide" by R. F. Potter and J. H. Wasilik (Abstract No. 138)

Electrothermics and Metallurgy
Thursday, May 7, 1959
Refractory Compounds
with G. M. Butler presiding
(CONSTITUTION ROOM, 3rd Floor)

9:00 A. M.—"Structures and Structural Relations of Borides, Carbides, Nitrides, Silicides, and Sulfides" by Erwin Parthe (Abstract No. 139)
9:30 A.M.—"Fabrication, Properties, and Applications of Some Metallic Silicides" by R. D. Grinthal (Abstract No. 140)
10:00 A.M.—"Micro Techniques for Studying Electrical Properties of Metalloids" by W. R. Eubank, L. E. Pruitt, and H. Thurnauer (Abstract No. 141)
10:30 A.M.—"An Investigation of the Compound Silicon Boride (SiB_6)" by C. F. Cline (Abstract No. 142)
11:00 A.M.—"Carbide Coatings for Graphite" by J. M. Blocher, Jr., and I. E. Campbell (Abstract No. 143)
11:30 A.M.—"Some Properties of Aluminum Nitride" by K. M. Taylor and Camille Lenie (Abstract No. 144)

Electrothermics and Metallurgy
Thursday, May 7, 1959
Effects of Impurities on Reactive Metals
with S. J. Noesen presiding
(CONSTITUTION ROOM, 3rd Floor)

2:00 P.M.—"The Effect of Gettering Additions to Niobium" by R. H. Hiltz, Jr. (Abstract No. 145)
2:30 P.M.—"The Effects of Interstitial Impurities and Process Schedules on Some Mechanical Properties of Arc-Cast Molybdenum and Molybdenum-Base Alloys" by H. M. McCullough and A. L. Feild, Jr. (Abstract No. 146)
3:00 P.M.—"Purification of Tantalum Obtained by Vacuum Arc Melting" by M. L. Torti (Abstract No. 147)
3:30 P.M.—"The Effect of Dissolved Hydrogen on the Physical and Thermodynamic Properties of β-Phase Titanium and Zirconium" by A. D. McQuillan (Abstract No. 148)
4:00 P.M.—"Melting and Fabrication of Ductile Vanadium Metal" by J. W. Armstrong (Abstract No. 149)
4:30 P. M.—"The Properties of Titanium-Columbium-Aluminum Alloys" by John Suiter (Abstract No. 150)

INDUSTRIAL ELECTROLYTIC

Monday, May 4, 1959
Electrolysis in Molten Electrolytes
with J. C. Cole, presiding
(EAST BALLROOM, 2nd Floor)

9:00 A.M.—"A Study of the Production of Metallic Sodium from the Sodium Amalgam" by S. Okada, S. Yoshizawa, and N. Watanabe (Abstract No. 151)
9:30 A.M.—"Electrolytic Production of Boron" by G. T. Miller (Abstract No. 152)
10:00 A.M.—"Ion Transfer in a Double Chamber Fused Salt Cell" by E. A. Maduk and W. E. Haupin (Abstract No. 153)
10:30 A.M.—"A Contribution to the Study of the Polarization Phenomena in Aluminum Cells" by R. Piontelli (Abstract No. 154)
11:00 A.M.—"A Pneumatic Force Balance System for Measuring Large Cell Line Current" by H. C. Behrens (Abstract No. 155)
12:30 P.M.—Industrial Electrolytic Division Luncheon and Business Meeting in the East Ballroom, 2nd floor. Presentation of the Annual Chlor-Alkali Report by N. J. Ehlers and C. A. Hampel (Abstract No. 156)

Industrial Electrolytic
Monday, May 4, 1959
Electrolysis in Molten Electrolytes (cont'd)
with N. J. Ehlers, presiding
(EAST BALLROOM, 2nd Floor)

2:30 P.M.—"Electrolysis of Lithium Chloride in the 1000-Amp Cell" by G. T. Motock (Abstract No. 157)
3:00 P.M.—"Exchange Current Measurements of Electrode Reactions in Molten LiCl-KCl Eutectic" by H. A. Laitinen, R. P. Tischer, and D. K. Roe (Abstract No. 158)
3:30 P.M.—"A Transparent Laboratory Cell for the Study of Molten Salt Electrolysis" by A. W. Dauer (Abstract No. 159)
4:00 P.M.—"High-Temperature Reference Electrodes" by M. F. Rey and G. P. Danner (Abstract No. 160)
4:30 P.M.—"The Use of Cs_2UCl_6 and Cs_2PuCl_6 as Starting Materials for U and Pu Metal Preparation" by D. M. Gruen (Abstract No. 161)

Industrial Electrolytic
Tuesday, May 5, 1959
General Session
with W. D. Sherrow presiding
(EAST BALLROOM, 2nd Floor)

8:30 A.M.—"Caustic Potash from Mercury Cells" by C. B. Handelin (Abstract No. 162)
9:00 A.M.—"Hydrochloric Acid Electrolysis" by F. M. Berkey (Abstract No. 163)
9:30 A.M.—"Day-Kesting Chlorine Dioxide Process" by Robert Spitzer and G. A. Day (Abstract No. 164)
10:00 A.M.—"Development of Equations for Calculation of *IR* Drop in Electrolytic Cell Electrodes" by C. W. Raetzsch and D. E. Tunison (Abstract No. 165)
10:30 A.M.—"Oscillographic Studies of Anode Passivity" by G. P. Martusevich and C. L. Mantell (Abstract No. 166)

Industrial Electrolytic
Tuesday, May 5, 1959
General Session
with R. F. Bechtold presiding
(EAST BALLROOM, 2nd Floor)

2:30 P.M.—"Anode Design for Mercury Cells" by W. C. Gardiner and W. J. Sakowski (Abstract No. 167)
3:00 P.M.—"Effects of Graphite Oil-Level and Density on Hooker Cell Operation" by W. J. Baker (Abstract No. 168)
3:30 P.M.—"The Solvay and Company Mercury Cell V-200" by A. G. Basilevsky (Abstract No. 169)
4:00 P.M.—"Diamond Alkali Company's Rectangular-Diaphragm Cell at 34,000 Amp" by R. H. Parsons (Abstract No. 170)
4:30 P.M.—"High-Pressure Electrolytic Hydrogen Oxygen Generator" by Robert Spitzer (Abstract No. 171)

THEORETICAL ELECTROCHEMISTRY

Monday, May 4, 1959
Symposium on Electrode Processes
Sponsored Jointly by the U. S. Air Force, Office of Scientific Research, and The ECS
with Paul Delahay presiding
(PENNSYLVANIA BALLROOM, EAST, 3rd Floor)

10:00 A.M.—Introductory Remarks by Paul Delahay
10:05 A.M.—"Adsorption of Ions at the Metal-Solution Interface and Its Influence on Electrode Kinetics" by A. N. Frumkin (Invited Paper) (Abstract No. 172)

Theoretical Electrochemistry
Monday, May 4, 1959
Symposium on Electrode Processes (cont'd)
with C. W. Tobias presiding
(PENNSYLVANIA BALLROOM, EAST, 3rd Floor)

2:00 P.M.—"Mechanism of Hydrogen Electrode Reaction" by Juro Horiuti (Invited Paper) (Abstract No. 173)
3:00 P.M.—"Determination of Electrochemical Reaction Mechanisms by the Electrochemical Reaction Order" by K. Vetter (Invited Paper) (Abstract No. 174)
4:00 P.M.—"A Contribution to the Study of the Electrode Behavior of Metallic Single Crystals" by R. Piontelli, G. Poli, and G. Seravalle (Invited Paper) (Abstract No. 175)

Theoretical Electrochemistry
Tuesday, May 5, 1959
Symposium on Electrode Processes (cont'd)
Sponsored Jointly by the U. S. Air Force, Office of Scientific Research, and The ECS
with Ralph Roberts presiding
(PENNSYLVANIA BALLROOM, EAST, 3rd Floor)

9:00 A.M.—"Double Layer and Rate of Electrode Processes" by L. Gierst (Invited Paper) (Abstract No. 176)
10:00 A.M.—"Acousto-Electrochemical Effects in Electrode Systems" by Ernest Yeager (Invited Paper) (Abstract No. 177)
11:00 A.M.—"The Electrodeposition and Dissolution of Metals" by J. O'M. Bockris (Invited Paper) (Abstract No. 178)
12:15 P.M.—Society Luncheon and Business Meeting in the East Ballroom, 2nd floor.

Theoretical Electrochemistry
Tuesday, May 5, 1959
Symposium on Electrode Processes (cont'd)
with C. V. King presiding
(PENNSYLVANIA BALLROOM, EAST, 3rd Floor)

2:00 P.M.—"Effect of Specific Adsorption of Anions on the Kinetics of Anodic Dissolution of Some Metals" by J. Kolotyrkin (Invited Paper) (Abstract No. 179)
3:00 P.M.—"Search for Specific Adsorption of Cesium Ions in the Absence of Specifically Adsorbed Anions" by D. C. Grahame, A. E. Higinbotham, and F. R. M. Deane (Invited Paper) (Abstract No. 180)
3:30 P.M.—"Kinetic Parameters of Very Rapid Metal Ion-Amalgam Electrode Reactions" by J. E. B. Randles (Invited Paper) (Abstract No. 181)
4:15 P.M.—"Faradaic Impedance in Anodic Formation of Halogens" by J. Llopis, J. Fernandez-Biarge, and M. Perez-Fernandez (Invited Paper) (Abstract No. 182)

Theoretical Electrochemistry
Wednesday, May 6, 1959
Symposium on Electrode Processes (cont'd)
Sponsored Jointly by the U. S. Air Force, Office of Scientific Research, and The ECS
with Ernest Yeager presiding
(PENNSYLVANIA BALLROOM, WEST, 3rd Floor)

9:00 A.M.—"A Theory of Electron Transfer Processes at Electrodes" by R. A. Marcus (Invited Paper) (Abstract No. 183)
10:00 A.M.—"Effect of Quaternary Ammonium Ions on the Rate of the V^{2+}/V^{3+} Reaction at a Mercury Electrode" by K. M. Joshi, Wolfgang Mehl, and Roger Parsons (Invited Paper) (Abstract No. 184)
11:00 A.M.—"Isotopic Effects in Electrode Reactions" by B. E. Conway (Invited Paper) (Abstract No. 185)
12:15 P.M.—Theoretical Electrochemistry Division Luncheon in the Hall of Flags, East, Concourse.

Theoretical Electrochemistry
Wednesday, May 6, 1959
Symposium on Electrode Processes (cont'd)
with Paul Delahay presiding
(PENNSYLVANIA BALLROOM, WEST, 3rd Floor)

2:00 P.M.—"On the Theory of Convective Diffusion" by B. Levich (Invited Paper) (Abstract No. 186)
3:00 P.M.—"Kinetics of Hydrogen Evolution and Dissolution at Activated Platinum Metals" by Manfred Breiter (Invited Paper) (Abstract No. 187)
3:45 P.M.—"Use of Faradaic Rectification for the Study of Electrode Processes" by G. C. Barker (Invited Paper) (Abstract No. 188)
4:30 P.M.—Concluding Remarks by Paul Delahay

Theoretical Electrochemistry
Thursday, May 7, 1959
with Walter Hamer presiding
(PENNSYLVANIA BALLROOM, EAST, 3rd Floor)

9:00 A.M.—"Electrode Kinetics and Electrostatic Interaction in the Double Layer" by P. Rüetschi (Abstract No. 189)
9:15 A.M.—"Surface Coverage during Hydrogen and Oxygen Evolution" by P. Rüetschi, J. B. Ockerman, and R. Amlie (Abstract No. 190)
9:30 A.M.—"The Oxygen Evolution Reaction at Gold Anodes, II. Overpotential Measurements and Reaction Mechanism in Sulfuric Acid Solutions" by Sidney Barnartt (Abstract No. 191)
9:50 A.M.—"Surface-to-Volume Considerations in the Palladium-Hydrogen System" by J. P. Hoare (Abstract No. 192)
10:10 A.M.—"Temperature Coefficient of Electrode Potentials: Isothermal and Thermal Coefficients; Standard Ionic Entropy of Electrochemical Transport of the Hydrogen Ion" by A. J. deBethune, T. S. Licht, and N. Swendeman (Abstract No. 193)
10:30 A.M.—"An Absolute Null Electrode from Double-Layer Capacity Measurements" by R. B. Stein (Abstract No. 194)
10:50 A.M.—"The Mechanism of Electrode Reaction, I. Discharge of Pb^{++} in Fused NaCl-KCl" by R. B. Stein (Abstract No. 195)
11:30 A.M.—Theoretical Electrochemistry Division Business Meeting in Pennsylvania Ballroom, East, 3rd floor.

Theoretical Electrochemistry
Thursday, May 7, 1959
with Ralph Roberts presiding
(PENNSYLVANIA BALLROOM, EAST, 3rd Floor)

2:00 P.M.—"Molten Salt Thermocells" by B. R. Sundheim (Abstract No. 196)
2:15 P.M.—"The Effect of Electrolytes on the Streaming Currents of Bulk Metals" by L. Rice and N. Hackerman (Abstract No. 197)
2:30 P.M.—"The Relation between the Kinetics of Self-Discharge of the Nickel-Nickel Oxide Electrode and Electrode Composition over a Range of Temperatures" by B. E. Conway and P. Bourgault (Abstract No. 198)
2:45 P.M.—"Cathode Polarization in the Electrodeposition of Metals and Alloys" by T. L. Rama Char (Abstract No. 199)
3:00 P.M.—"The Significance of the Flade Potential" by M. J. Pryor (Abstract No. 200)

3:15 P.M.—"Electrochemical Calorimetry, II. The Absolute Entropy of the Cupric Ion" by J. M. Sherfey and Abner Brenner (Abstract No. 201)
3:30 P.M.—"The Anodic Behavior of Nickel" by J. C. Banter, Ernest Yeager, and F. Hovorka (Abstract No. 202)
3:45 P.M.—"Some Aspects of the Nonaqueous Chemistry of the Uranium Chlorides" by R. E. Panzer and J. F. Suttle (Abstract No. 203)
4:00 P.M.—"Mass Transfer and Current Distribution under Free Convection Conditions" by Kameo Asada, Fumio Hine, Shiro Yoshizawa, and Shinzo Okada (Abstract No. 204)
4:15 P.M.—"Mass Transfer at the Streaming Mercury Electrode" by Kameo Asada, Fumio Hine, Shiro Yoshizawa, and Shinzo Okada (Abstract No. 205)

ABSTRACTS

In the Index to Authors, the Abstract Number is the number listed in the right-hand column.

ELECTRIC INSULATION

Abstract No. 1

Influence of the Constitution of Oils on Their Gassing under Electric Stress

E. H. Reynolds and **S. C. Clarke,** Research Organization, British Insulated Callender's Cables Ltd., 38 Wood Lane, London 12, England

It has long been regarded as important to control the "gassing" characteristics of hydrocarbon oils to be used in impregnated paper dielectrics. This paper describes the apparatus and techniques for quantitative study of this phenomenon at a stressed oil/gas interface. Results under different atmospheres with low viscosity oils of varying constitution are presented. In particular the effects of natural and synthetic aromatic constituents of different ring structures are compared, and the superior nascent hydrogen absorption characteristics of alkyl naphthalenes is demonstrated.

Abstract No. 2

A New Explanation of Gas Evolution in Electrically Stressed Oil Impregnated Paper Insulation

Z. Krasucki, H. F. Church, and **C. G. Garton,** The British Electrical and Allied Industries Research Assn., Surrey England

In void-free oil impregnated paper, gas evolution starts at a critical stress which is markedly dependent on the degree of dryness of the paper. The gas first formed arises from decomposition of water in the cellulose, the nature of the impregnant having little effect. Subsequent more rapid gassing resulting from decomposition of the oil is a secondary process depending on ionization within gas bubbles previously formed. Study of the fundamental primary process is continuing.

Abstract No. 3

The Chemistry of Cable-Oil Deterioration

George Feick and **W. F. Olds,** Arthur D. Little, Inc., Cambridge, Mass., and **E. D. Eich,** Anaconda Wire and Cable Co., Hastings-on-Hudson, N. Y.

The known chemistry of cable-oil deterioration is reviewed, and some of the current theories are examined. It is shown that none of these is adequate to explain all the observed facts. A new theory of oil deterioration, based on the known electron transfer of organic peroxides, is advanced and compared with the available data. The results of some experiments suggested by the theory are discussed.

Abstract No. 4

Ultraviolet Irradiation of Chlorinated Biphenyl

H. M. Stahr, General Electric Co., Hudson Falls, N. Y.

Chlorinated biphenyls are used widely as dielectric liquids. In particular, the trichlorinated biphenyl, a mixture of chlorobiphenyls having an average composition of three chlorine atoms per molecule and commonly known as Aroclor 1242 or Pyranol 1499, is in use as a capacitor impregnant. As part of a study of the chemical, physical, and electrical properties of dielectric liquids, it was of interest to determine the effect of u.v. light on this material. Changes in conductivity, power factor, free chlorides, acidity, and color have been observed on u.v. exposure. These changes were studied as a function of time and intensity of irradiation. The effect of conventional light sources has also been investigated, and artificial light sources which have no deleterious effect have been found. It is suggested that u.v. degradation frequently may be an important variable in very precise studies of the electrical properties of dielectric liquids.

Abstract No. 5

Correlation between Dielectric Losses and Chemical Stability of Mineral Oils

T. Salomon, Institut Francais du Petrole,4 Place Bir-Hacheim, Rueil-Malmaison, S and O, Paris, France

It is well established that the dielectric losses of a new mineral oil are lower when the chemical stability is increased, but the determination of dielectric losses alone is not sufficient to characterize the performance of an oil in operation. A better correlation between dielectric losses and chemical stability is obtained when following the increase in dielectric losses with the progress of the artificial oxidation of the oils.

Two different techniques have been used for this study: that of Masson, measuring the resistivity of the oil in cc, and that of Bruckmann, measuring the loss angle increase in ac. Results obtained are compared with those found in a normal aging test, characterizing the oil stability by the increase in acidity and in sludge. It is shown that a good correlation can be established between the two techniques applied, chemical and electrical, for well refined oils. The impurities present in the oils have a great importance as they may sometimes produce a bigger change in the electrical properties of the oils than in their chemical properties.

Abstract No. 6

The Dependence of the Dielectric Power Factor of Insulating Oils on the Water and Gas Content

K. Brinkmann, Geschäftsführer der Kabelwerk Vohwinkel G.m.b.H., Wipperfürth, Rhld., Germany

The dielectric power factor of insulating oils depends on many factors of which, in particular, the water and gas content are of primary importance. In order to investigate this dependence a number of insulating oils were dried and degassified at different pressures down to their vapor pressure, and the dielectric properties were measured. New results gained on dielectric power factor at different water contents and after varying degree of degassification are communicated. Further, some phenomena which occurred in the course of such measurements are reported.

Abstract No. 7

A Method for the Determination of the Aging of Insulating Oils

R. Strigel, Technische Universitat Berlin, Jebenstrasse 1, Berlin-Charlottenburg 2, Germany

Nacke has demonstrated that a numeric can be obtained from the frequency behavior of the phase angle difference of insulating oils and that the degree of aging and refining of the oils can be inferred quantitatively from this numeric. Experimental investigations conducted by Wermann indicated the above results in general. However, these experiments required considerable work. This work can be minimized when other indicators are used which are based likewise on the modification of the dipole properties with aging.

There is no Abstract No. 8

Abstract No. 9

Effect of Dissolved Gases on the Electric Conduction and Breakdown of Insulating Oil

H. Tropper, Queen Mary College, University of London, Mile End Rd., London, E.1, England

Results are given of a number of investigations, some still in progress, concerned with the effect of dissolved gases on the electric conduction and breakdown processes. Most of the work has been done on insulating

oil, although, for comparison, results for a few simple hydrocarbons are included. Samples of varying gas content were tested with electrodes of different metals and over a range of hydrostatic pressures. Factors influencing the "conditioning" were examined in detail.

Abstract No. 10

The Influence on the Oil Breakdown Strength of the Gas Pressure in Equilibrium with the Oil

P. Priaroggia and **G. L. Palandri,** Societa Italiana Pirelli, Milan, Italy

A laboratory investigation on the influence of gas pressure on the electrical breakdown of thin oil as used in oil-filled cables was carried out between a gas pressure of about 5.10^{-4} mm Hg and about 1000 mm Hg. The testing cell consisted of a glass container enclosing a platinum sphere gap (0.5 mm). Tests were carried out at ambient temperature. The result of this investigation showed that the breakdown strength of the oil, provided a perfect equilibrium is reached between the gas dissolved in the oil and the one remaining in the cell above the oil surface, is absolutely independent of the gas pressure.

Abstract No. 11

Effects of Hydrostatic Pressure, Temperature, and Voltage Duration on the Electric Strengths of Hydrocarbon Liquids

K. C. Kao (present address: English Electric Co. Ltd., Stafford, England) and **J. B. Higham** (present address: Pilkington Brothers Ltd., St. Helens, Lanc., England) Electrical Engineering Dept., University of Birmingham, Birmingham, England

A special feature of the investigation is that most of the results are for fresh liquids and electrodes. The electric strengths of simple hydrocarbons and of transformer oil have been found to be dependent on applied hydrostatic pressure under all conditions investigated, including conditions of extreme cleanliness and for voltage pulses lasting only one microsecond. It has been concluded that electric breakdown is partly governed by dielectric layers on the cathode, which change with successive breakdowns, and that breakdown first takes place in a bubble of gas or vapor which has been caused to elongate in the direction of the field.

Abstract No. 12

Measurement of the Breakdown in Insulating Oil

E. Baumann, Technischen Hochschule Fridericiana Karlsruhe, Kaiserstrasse 12, Karlsruhe, Germany

In this paper some results concerning the solubility of water in insulating oil, in the range 50-300 ppm, are given. Measurements of breakdown at a-c, d-c, and pulse-voltage with different shapes of electrodes are given. This paper will also show results of a-c breakdown tests as a function of the rate of use of voltage. All these measurements were undertaken depending on the varying percentage of water contained in the oil, far below 50 ppm. The results are shown for different temperatures. Automatic apparatus and statistical methods have been applied to discover small variations of the breakdown, which might have been caused by only a few ppm of water in the oil.

Abstract No. 13

A New Statistical Theory of the Breakdown Process and the Reinterpretation of Pulse Breakdown Measurements in Liquid Hydrocarbons

T. J. Lewis, Queen Mary College, University of London, Mile End Rd., London, E.1, England

Hitherto it has been accepted that breakdown under pulse conditions occurs in liquid hydrocarbons with an insignificant statistical time-lag. Theories have been developed in which the whole of any time-lag measured has been assigned to a formative time, but these theories are not at all satisfactory. The paper shows that (*a*) significant statistical time-lag does in fact exist, provided the experimental procedure is correct, and (*b*) a proper statistical analysis of the previous pulse measurements together with a statistical theory of breakdown shows that these measurements provide clear evidence for, rather than against, a statistical time-lag.

Abstract No. 14

Influence of Electrode Surface Conditions on the Electrical Strength of Liquified Gases

T. J. Lewis, Queen Mary College, University of London, Mile End Rd., London, E.1, England

The strengths of liquified argon, oxygen, and nitrogen are of the order of 1 mv/cm but are found to depend to a marked degree on the nature of the electrode surfaces. The strength can be changed in a regular manner (sometimes by as much as 50%) by changing both the electrode metal and the degree of surface oxidation. The important discovery is that the anode as well as the cathode has a strong influence on the strength. This surprising result has as yet no obvious explanation in terms of usual breakdown mechanisms, but may be very significant, not only for theories of breakdown in these liquids but for hydrocarbon liquids as well.

Abstract No. 15

Recent Investigations of the Development of a Discharge during an Electric Breakdown in Oil in a Nonuniform Field

R. Strigel, Technische Universitat Berlin, Jebenstrasse 1, Berlin-Charlottenburg 2, Germany

When photographic paper is placed perpendicularly to the direction of the principal field at varying distance in a point-plate spark gap, the space-time development and structure of the discharge channels can be inferred from the discharge traces on the paper. Such investigations have been carried out by Tetzner. They indicate that the channels starting from the point behave very differently in regard to development, rate of growth, and state of ionization when a positive or negative potential is impressed on the point.

Abstract No. 16

Prebreakdown Discharges in Insulating Liquids

T. W. Dakin and **D. Berg,** Westinghouse Electric Corp., East Pittsburgh, Pa.

This paper describes an investigation of small discharges which occur at voltage gradients less than the breakdown of liquid dielectric gaps. The occurrence and distribution of the discharges are observed by photographic and photomultiplier tube detector techniques. Both hydrocarbon and askarel transformer liquids are included in the study. The effects of voltage gradient and duration, degassing, electrode preparation, and pressure are all shown. The origin of these discharges and their relation to liquid gap breakdown is discussed.

Abstract No. 17

Recent Developments in the Chemistry of Active Nitrogen

R. A. Back and **C. A. Winkler,** McGill University, Montreal, Canada

The chemistry of active nitrogen is reviewed, and the nature of the chemically reactive species is discussed. The mechanisms by which nitrogen atoms may react are considered "Direct reaction"

$$N + M \rightarrow [N\text{-}M] \rightarrow \text{reaction products}$$

appears to be operative in many reactions. At low temperatures, direct reaction may be accompanied by "catalytic recombination" of nitrogen atoms,

$$N + [N\text{-}M] \rightarrow N_2 + M$$

The reagent M may be decomposed in this highly exothermic process, and, in some cases, this "destructive catalytic recombination" appears to be the main mode of reaction of active nitrogen. There is some evidence, particularly in reactions with nitric oxide and ammonia, which strongly suggests that some chemically

reactive species other than nitrogen atoms is present in active nitrogen. Recent physical measurements, which confirm this conclusion, are discussed.

Abstract No. 18

Molecular Structure and the Electrical Strength of Liquid Hydrocarbons

T. J. Lewis, Queen Mary College, University of London, Mile End Rd., London, E.1, England

It is suggested that electrons moving through hydrocarbon liquids are able to excite molecular vibrations of infrared frequencies and that this provides an effective energy loss mechanism. The relative magnitudes of this loss may be estimated for a wide range of hydrocarbons and other liquids and can be used in a criterion of breakdown. Thus the electrical strengths of these liquids measured under standard conditions may then be compared with their molecular structures. A good correlation is found.

Abstract No. 19

Electrical Conduction in Hexane under Pulse Conditions

K. A. Macfadyen and **G. C. Helliwell,** Dept. of Physics, The University, Edgbaston, Birmington 15, England

Three different methods of measuring the conduction between electrodes in a liquid dielectric during a 5 μsec pulse of voltage have been examined. One method has been developed to detect currents of about 10^{-5} amp. Further increase in sensitivity seems possible. Currents of about 10^{-5} amp have been detected in purified hexane at about 200 kv/cm, but the pretreatment of the electrodes greatly influences this. Larger currents (of the order of 10^{-4} amp) have been measured after a breakdown has occurred, even though the liquid is renewed. D-C measurements showed currents of about two orders of magnitude lower.

Abstract No. 20

High-Field Conduction Currents in Liquid Hexane under Pulse Conditions

A. H. Sharbaugh and **P. K. Watson,** General Electric Co., Schenectady, N. Y.

In this paper we present an extension of our previously described pulse technique to the measurement of high-field conduction in insulating liquids. In the past this phenomenon has been widely investigated with d.c., but conflicting results have been reported. It is clear that this lack of agreement of the many existing d-c results is caused by a polarization process. It is also evident that the use of short pulses of voltage (10^{-6}—10^{-3} sec) overcomes this trouble and, furthermore, permits a study of the time dependence of this phenomenon. Results obtained on n-hexane are presented. It is planned to extend these measurements to the study of other liquids.

Abstract No. 21

Equilibrium Space Charge at the Contact of a Metal and a Pure, High-Insulating Liquid and Its Influence on High-Field Conductivity

M. J. Morant, Queen Mary College, University of London, Mile End Rd., London, E.1, England

The high-field conduction of a highly purified insulating liquid such as hexane may be influenced largely by electron emission from the cathode. Theoretical interpretations of such emission have neglected the influence of an electronic space charge at the contact of a metal and such a liquid. This would be expected in equilibrium to be similar to that at a metal-semiconductor contact. A novel electrostatic method is described which, it is believed, can measure directly the potential of such an electronic double layer at the contact.

Abstract No. 22

Electron Drift Mobility in Liquid n-Hexane

O. H. LeBlanc, Jr., Research Lab., General Electric Co., Schenectady, N. Y.

The drift mobilities of electrons in several hydrocarbon liquids at low field strengths have been measured using a technique involving injection of electron pulses from a photosensitive cathode. Liquid n-hexane has been studied in detail, and for this case the data can be represented by $\mu = \mu_0 \exp(-\Delta\epsilon/kT)$, where $\mu_0 = 0.3$ cm^2/v-sec and $\Delta\epsilon = 0.14$ e.v. These results indicate that the charge carrier involved in conduction is neither a free electron nor a negative molecular ion. We propose that the carrier is an electron whose drift is modulated by shallow traps of 0.14 e.v. average depth.

Abstract No. 23

Particle Separations by Nonuniform Electric Fields in Liquid Dielectrics, Batch Methods

H. A. Pohl and **J. P. Schwar,** Plastics Lab., Princeton University, Princeton, N. J.

The motion of suspended solids caused by nonuniform electric fields is called dielectrophoresis. Several quantitative aspects of dielectrophoresis in batch processes are described in this paper. The yield of solids removed from a quiescent suspension is shown to depend markedly on the difference of the dielectric constant between solid and liquid. A critical upper field intensity was discovered to exist, above which precipitation ceases. The yield is also seen to decrease on increase of volume fraction of suspended solids in the range 1 to 50% v/v.

Abstract No. 24

Continuous Separations of Suspensions by Nonuniform Electric Fields in Liquid Dielectrics

H. A. Pohl and **C. E. Plymale,** Plastics Lab., Princeton University, Princeton, N. J.

Suspensions of various solids in organic (dielectric) liquids can be treated continuously by pulsating d-c or a-c nonuniform electric fields of modest strength to clarify or enrich the suspensions. The method and its important variables are described in this paper. It is found, for example, that there exists a critical lower voltage and a critical upper voltage between which operation must take place if appreciable separation is to occur. Best results are obtained if the dielectric constant of the solid exceeds that of the liquid.

Abstract No. 25

Temperature and Space Charge Effects in Liquid Hydrocarbons

R. Coelho and **M. Bono,** Lab. for Insulation Research, Massachusetts Institute of Technology, Cambridge, Mass.

Preliminary results on the residual d-c conduction in n-heptane and n-hexane under highly inhomogeneous field conditions are presented. The temperature dependence of the residual current is significantly different for the two polarities of the test cell within the temperature range investigated. Additional results supporting the findings were obtained when only one electrode was heated. Under either polarity, field-emission induced by a space charge layer seems to take place. The temperature dependence of the density distribution in the space charge layer is discussed and a simple model is proposed to explain the observations.

Abstract No. 26

Flash Conductivity in Organic Solutions

H. T. Witt, University of Marburg, Marburg, Germany

A method is described by which it is possible to detect short-lived charged primary products (ions, electrons) produced in photochemical reactions. The photochemical reaction is initiated in an electric field of approximately 1000 v/cm of a light flash. The produced changes are measured by the current impulse which occurs between the electrodes. The method is applicable for organic solutions which have a very small conductivity in the dark, like hexane, benzene, toluene, etc. The method was used to detect light-produced short-lived radical ions of triphenyl-amine and similar substances in hexane.

Abstract No. 27

Demonstration of Physical Properties of Water by D-C Conductivity of Undesiccated Insulating Lnquids (Fields below 2 kv/cm)

R.Guizonnier, University of Bordeaux, Bordeaux France.

The law of insulating liquids $i_s = A_s e^{-W/kT}$, where $W = 0.41$ e.v., is found to apply to pure water. In addition there is demonstrated the freezing point of water near 0°. An indication from electrometric readings of a polarizing emf tends to be that of pure water under the same conditions.

Abstract No. 28

The Wien Effect and Ionic Association

Andrew Patterson, Jr., and **Harlow Freitag,** Sterling Chemistry Lab., Yale University, New Haven, Conn.

The high-field conductance (Wien effect) of electrolytic solutions can be determined theoretically using the Onsager-Kim theory for strong electrolytes and the Onsager theory for weak electrolytes. The results are valid for any degree of association of the solute and for any field strength from zero to infinity. The Onsager-Kim theory has been verified by experiment. A modification of the theory of Onsager for small degrees of association agrees favorably with experiment with the possible exception of a time dependent effect.

Abstract No. 29

Nonuniform Field Effects in Poorly Conducting Media

H. A. Pohl, Plastics Lab., Princeton University, Princeton, N. J.

A simplified theory of the behavior of suspended polymer particles in a real dielectric is presented. It is shown that the dielectrophoresis is affected by the presence of conduction in real dielectric liquids. The initial attraction to the central electrode due to the nonuniform fields and its polarizing induction felt by all particles is gradually overcome by the repulsive effects of charge accumulated on the particles due to ionic conduction in the liquid. The "reversal time" for the particle motion is calculated and shown to be in reasonable agreement with experiment.

Abstract No. 30

High-Temperature Silicone Laminates

W. Elsfelder, Silicone Insulation, Inc., 1383 Seabury Ave., Bronx 61, N. Y.

Mechanical, electrical, and thermal stabilities of various silicone laminates are presented. Typical applications for specific silicone laminates are discussed.

Abstract No. 31

Silver Migration—A Cause of Component Failure

A. A. Cortesi, International Business Machines Corp., Poughkeepsie, N. Y.

Experimental results obtained from an extensive study of silver migration and its relation to component failure are described. General conditions under which migration is likely to occur, such as voltage gradient, humidity, temperature, and electrode spacing, are discussed. The relative susceptibility to silver migration of various insulating materials as found from this study is discussed in detail and recommendations are presented concerning insulation in components. During the investigation, an epoxy coating was found that would inhibit the migration process.

Abstract No. 32

A Universal Meter for Measuring Voltages at High Impedances, Microamperes, and Insulation Resistance

W. R. Clark, R. E. Watson, and **G. C. Mergner,** Leeds and Northrup Co., Philadelphia 44, Pa.

This paper describes a multipurpose instrument which can measure direct voltages in high impedance circuits, small direct currents, and high resistance with good accuracy. The basic detector is a chopper-type stabilized feed back amplifier which is entirely a-c powered.

Abstract No. 33

Electrical Properties of Waxes

T. D. Callinan, IBM Research Center, Yorktown Heights, N. Y.

The dielectric constant power factor and dielectric loss factor of select waxes have been determined. Among the materials studied are carnauba and montan wax.

Abstract No. 34

Domain Structure and Optical Properties of Transport Ferrimagnetic Crystals

J. F. Dillon, Jr., Bell Telephone Labs., Inc., Murray Hill, N. J.

Thin sections cut from single crystals of a number of ferrimagnetic compounds have been found to be reasonably transparent to visible light. The plane of polarization of light passing through such crystals undergoes a nonreciprocal rotation. Measurements of this rotation as well as of the absorption within the visible, with particular reference to ferrimagnetic garnets, are presented. One of the striking results of these optical properties is that the magnetic domain can be observed with an ordinary polarizing microscope. The character of the domains is discussed. Motion pictures are shown illustrating the effects of external fields as well as those of changes in temperature.

Abstract No. 35

Piezoelectric and Dielectric Properties of Ceramics in the Potassium-Sodium Niobate System

L. Egerton and **D. M. Dillon,** Bell Telephone Labs., Inc., Murray Hill, N. J.

Dense ceramic bodies have been prepared over a wide compositional range in the potassium-sodium niobate system. Dielectric constants are relatively low and the losses relatively high for ceramic bodies in this system. Low dielectric constants and fairly high activities of compositions near the equimolar range make these materials of interest for delay-line use, especially where thin sections are required, such as in certain high-frequency applications.

Abstract No. 36

Influence of Processing Techniques on the Dielectric Properties of Titanates and Zirconates

Lawrence Kopell, Erie Technical Ceramics, Erie, Pa.

Additions of small and large quantities of various oxide additions are made to titanates and zirconates, and their effects on dielectric qualities are noted. Some of the necessary techniques which affect the dielectric characteristics are discussed.

Abstract No. 37

Factors Involved in the Application of Ceramic Insulation

J. S. White and **N. J. Norante,** Refractories Div., Carborundum Co., Latrobe, Pa.

The dielectric and physical properties of various ceramic insulating materials are presented to aid in the selection of the proper insulation for specific applications.

Abstract No. 38

Properties of Some Special Purpose Glasses

G. W. McLellan, Corning Glass Works, Corning, N. Y.

Glasses can be manufactured having many different combinations of chemical, electrical, and optical properties. Many glasses have been formulated with particular attention to only one or possibly two properties. Glasses to be discussed are: Fused silica, 96% silica, photosentitive, radiation shielding, radiation darkening, sealing.

ELECTRONICS—LUMINESCENCE

Abstract No. 39

Luminescent Centers in ZnS Phosphors

J. S. Prener, Research Labs., General Electric Co., Schenectady, N. Y.

Present knowledge of the defects in ZnS responsible for the fluorescence in the visible and infrared regions of the spectrum is reviewed. The role of vacancies and associated defects in luminescence is discussed.

Abstract No. 40

Copper- and Tin-Activated Alkaline Earth Halophosphate Phosphors

B. E. Hunt and **A. H. McKeag,** Research Labs., General Electric Co. Ltd., Wembley, Middlesex, England.

New copper- and tin-activated halophosphate phosphors are described, which are of potential practical importance. They include copper- and tin-activated barium chlorophosphates with good thermal characteristics. Copper-activated barium chlorophosphate shows a moderate red fluorescence, under long u.v. excitation, at ambient temperatures, which becomes brighter at higher temperatures due to a marked color shift toward the yellow. The same matrix, activated with tin, shows a strong pale green emission under 2537Å excitation, which is also shifted to shorter wave lengths at elevated temperatures.

Abstract No. 41

Luminescence of Copper-Activated Calcium and Strontium Orthophosphates

W. L. Wanmaker and **C. Bakker,** Phosphor Div., N. V. Philips' Gloeilampenfabrieken, Eindhoven, The Netherlands.

Copper proved to produce a strong luminescence in $Ca_3(PO_4)_2$ and $Sr_3(PO_4)_2$, with a maximum (under excitation with 2537Å) at 4700Å and 4950Å, respectively. The introduction of the activator ion is facilitated (especially with the Sr compound) by the addition of Al or other ions such Zn, Cd, and Mg. With Mn, sensitization occurs, giving rise to a red emission peak. The emission bands of the phosphors are narrow, and the temperature of the fluorescence intensity is good.

Abstract No. 42

Tin-Activated Pyrophosphate Phosphors

R. C. Ropp and **R. W. Mooney,** Sylvania Electric Products Inc., Towanda, Pa.

The preparation and properties of the Group II metal pyrophosphates activated by tin are described. It is shown that the fluorescent emission is strongly dependent on the matrix shifting toward higher wave lengths with increasing size of the cation of the pyrophosphate. Excitation and emission spectra of many of the phosphors are given. The most useful of these phosphors is $Sr_2P_2O_7$:Sn, a very efficient blue phosphor emitting at 452 μ.

Abstract No. 43

Phase Equilibria and Fluorescence in the System $Zn(PO_3)_2 - Mg(PO_3)_2$

J. F. Sarver and **F. A. Hummel,** Dept. of Ceramic Technology, College of Mineral Industries, The Pennsylvania State University, University Park, Pa.

The equilibrium diagram for the system $Zn(PO_3)_2$-$Mg(PO_3)_2$ was established as a solid solution type by quenching and solid-state methods. About 10 mole % $Mg(PO_3)_2$ was soluble in β-$Zn(PO_3)_2$ at 850°C, but less than 2 mole % was soluble in α-$Zn(PO_3)_2$ at 650°C. Solid solution of $Zn(PO_3)_2$ in $Mg(PO_3)_2$ was extensive, ranging from approximately 35 to 100 mole % $Mg(PO_3)_2$. The cathodoluminescence of compositions in the three solid solution series was examined for peak emission and brightness when activated with manganese. A shift in the position of the emission peak from 6000 to 6200Å in the magnesium metaphosphate solid solution series has been interpreted in terms of the difference in influence between magnesium and zinc ions on the polarizability of oxygen ions in the neighborhood of the manganese activator.

Abstract No. 44

Calcium Halophosphate Phosphors, II. Theoretical Optics of Lamp Coatings

K. H. Butler, Sylvania Lighting Products, Division of Sylvania Electric Products Inc., 60 Boston St., Salem, Mass.

The basic theory of light scattering by particles has been applied to the problem of the coating of fluorescent lamps. The effects of size and size distribution of particles on the reflectance and transmittance of a single layer of the coating and on the absorption of the light emitted by the phosphor layer have been calculated. The effect of variation of the ultraviolet absorption and scattering coefficients on phosphor performance has also been calculated and shown to be vital factors in lamp performance.

Abstract No. 45

Calcium Halophosphate Phosphors, III. Effect of Particle Size on Optical Constants

M. J. B. Thomas, Sylvania Lighting Products, Division of Sylvania Electric Products Inc., 60 Boston St., Salem, Mass.

Reflectance measurements on phosphors with various particle size characteristics have been made. Comparison of these data with the theory show that the scattering constant, while nearly independent of wave length, is directly dependent on particle size. The absorption constant, however, is independent of particle size but strongly dependent on wave length. Reasonable estimates of the ratio of its absorption constant to the scattering constant at various wave lengths for a specific sample therefore can be made from simple reflectance data.

Abstract No. 46

Calcium Halophosphate Phosphors, IV. Influence of Particle Size on Lamp Performance

H. H. Homer, Sylvania Lighting Products, Division of Sylvania Electric Products Inc., 60 Boston St., Salem, Mass.

The milling of phosphors to reduce particle size is a standard technique of the lamp industry despite the fact that it reduces lumen output. Various explanations have been offered for the cause of this reduction in efficiency. A study has been made of various particle size fractions before and after milling to determine the influence of particle size on lamp performance. Indications are that the performance data can be traced to the presence or absence of a superfine fraction in the phosphor.

Abstract No. 47

Voltage Dependence and Particle Size Distribution of Electroluminescent Phosphors

W. Lehmann, Lamp Div., Westinghouse Electric Corp., Bloomfield, N. J.

The dependence of the brightness, L, of electroluminscent zinc sulfides on the voltage, V, can be described by $L = L_o \exp[-(V_o/V)^{1/2}]$ only if the phosphor has a certain "statistical" particle size distribution. The narrower this distribution, the more the $L(V)$ dependence approaches $L = L_o \exp[-(V_o/V)]$. Experimental results on separated phosphor fractions, single particles, and thin films are presented. A correlation between the above two equations exists by means of the common "statistical" particle size distribution.

Abstract No. 48

The Action of Iron-Group Elements in Electroluminescent Zinc Sulfide Phosphors

Paul Goldberg, Research Labs., Sylvania Electric Products Inc., Bayside. N. Y.

Iron-group elements are found to introduce marked changes in the behavior of electroluminescent zinc

sulfide phosphors. At low and intermediate concentrations of the elements, the following results are found: (*a*) changes in shape of the emittance-frequency and emittance-voltage characteristics; (*b*) simplification of the brightness wave forms; and (*c*) enhancement of emittance in blue-emitting phosphors. This behavior can be understood in terms of the recombination processes of electrons and holes and the dielectric properties of the phosphors.

Abstract No. 49

Microscopic Observations on Electroluminescent Phosphors

Alfred Kremheller, Research Labs., Sylvania Electric Products Inc., Bayside, N. Y.

The electroluminescent brightness of single phosphor particles is studied microscopically in liquid dielectric cells. A simple visual technique in conjunction with the microscope permits one to analyze the brightness distribution within and among electroluminescent particles. Some results are presented on the influence of particle orientation, electrode contact, external irradiation, milling, acid etching, and processing temperature on the particle brightness.

Abstract No. 50

Changes in Trapping Levels of Zinc Sulfide Phosphors Resulting from Positive Ion Bombardment

W. T. Allen (Present address: Franklin and Marshall College, Lancaster, Pa.) and **C. H. Bachman,** Syracuse University, Syracuse, N. Y.

A decay technique for measuring trap distribution difference of a surface layer (100 lattice spacings thick) is described. Utilizing this method, changes in the trap distribution of zinc sulfide phosphor crystals resulting from bombardment by 12 kv positive ion of hydrogen, oxygen, and argon were measured. These data indicate increased trapping at all levels and greatly increased trapping at the discrete levels previously reported for zinc sulfide in the literature.

Abstract No. 51

Some New Features of Phosphors Showing the Electro-Enhancement Effect

F. Pingault and **G. Destriau,** Faculté des Sciences, Paris, France.

Irradiation of such phosphors with infrared radiation gives a permanent enhancement of the sensitivity to x-rays similar to that produced by an electric field. As a matter of fact, infrared radiation and electric field act in the same manner, both giving either permanent quenching with most phosphors or enhancement with CdZnS:Mn,X phosphors irradiated with x-rays.

Abstract No. 52

A General Effect of Coactivators of Mn in CdZnS:Mn,X Phosphors Showing the Electro-Enhancement Effect

G. Destriau, Faculté des Sciences, Paris, France.

It was reported two years ago that small gold additions are able to improve the enhancement of CdZnS:Mn phosphors. It has now been found that many other "coactivators" can produce similar results.

Abstract No. 53

Field Enhancement of the Light Emitted by α-Scintillations

J. Mattler, Faculté des Sciences, Paris, France.

With some Mn-activated sulfide phosphors, the light emitted under α-particle irradiation is strongly enhanced when an electric field is simultaneously applied. This electroenhancement effect was studied as a function of phosphor composition, field strength, and temperature (between $-150°$ and $+100°C$). Oscilloscopic study of the scintillations indicates that the field increases neither the height nor the width of the individual light pulses; the increased output seems to arise from the background luminescence accompanying the scintillations.

Abstract No. 54

On the Origin of Complex Output of Wave-Forms of A-C Electroluminescence

E. E. Loebner and **I. J. Hegyi,** RCA Labs., Radio Corp. of America, Princeton, N. J.

Striated single crystals of GaP grown from a solution of GaP and GaN in gallium show brightness waves of a-c electroluminescence so far only observed in ZnS-type phosphors. By varying the amplitude of the sinusoidal excitation field, we can obtain one, two, or three luminance peaks per half cycle. We have shown that this behavior results from the superposition of three phenomena, all in phase with the voltage and current. These effects are: (*a*) low-field electroluminescence, (*b*) field quenching of electroluminescence and (*c*) high-field electroluminescence. A study of striated single crystals of ZnS confirms qualitatively the same behavior.

Abstract No. 55

Influence of Hydrogen on Red ZnS-Cu Fluorescence

W. van Gool and **A. P. D. M. Cleiren,** Philips Research Labs., N. V. Philips' Gloeilampenfabrieken, Eindhoven, The Netherlands

Self-coactivated ZnS-Cu phosphors were made by firing in different atmospheres. When H_2S/H_2 mixtures were used the red fluorescence decreased with increasing amounts of hydrogen. With A/S_2 or with N_2/S_2 atmospheres no red fluorescence was obtained. From these experiments the conclusion is reached that hydrogen forms a part of the center responsible for the red fluorescence. No definite model of these centers can be given at this moment.

Abstract No. 56

Associated Donor-Acceptor Luminescent Centers in (Zn,Cd)S Phosphors

E. F. Apple and **D. J. Weil,** Research Lab., General Electric Co., Schenectady, N. Y.

ZnS phosphors with Ga or In donors and Cu or Ag acceptors exhibit two emission bands whose relative intensities depend on the concentration of donor and acceptor, temperature, donor identity, and crystal structure. Substitution of Cd (up to 20%) for Zn causes a gradual increase in the relative intensity of the short wave-length emission band. This effect is explained by use of the associated donor-acceptor models already proposed for the two luminescent centers involved.

Abstract No. 57

Effect of Sulfur Pressure and Donors on the Infrared Emission Intensity in ZnS:Cu

J. S. Prener, E. F. Apple, and **D. J. Weil,** Research Lab., General Electric Co., Schenectady, N. Y.

The intensity of the infrared emission in ZnS:Cu has been studied as a function of sulfur pressure over the sample at elevated temperatures and donor impurity concentration. The intensity, measured at 77°K, increases with increasing sulfur pressure until a saturation value is reached. It decreases with increasing donor impurity concentration. The results are interpreted using a model in which ZnS:Cu is p-type at high sulfur pressures and sulfur vacancies give rise to donor levels.

Abstract No. 58

Antistokes Fluorescence in (Zn, Cd)S

R. M. Potter, Lamp Research Lab., Lamp Div., General Electric Co., Nela Park, Cleveland 12, Ohio

Materials of composition $Zn_x\ Cd_{1-x}S$: Ag, Cu, where $x = 0.00$ to 0.75, show appreciable antistokes fluorescence. Simultaneous excitation in two spectral regions is necessary: (*a*) in the long-wavelength tail of the copper excitation band, and (*b*) in the near infrared in either of two bands. The first band is broad and extends from about 0.6μ to 0.9μ, and the second is

narrow, peaking at about 1.3μ. The mechanism is shown to involve excitation of copper centers, followed by infrared excitation of holes, with subsequent recombination taking place in silver centers.

Abstract No. 59

Hydrothermal Preparation of Two-Component Solid Solutions from II-VI Compounds

Alfred Kremheller, A. K. Levine, and **G. Gashurov,** Research Labs., Sylvania Electric Products Inc., Bayside, N. Y.

The hydrothermal synthesis of binary solid solutions of inorganic phosphors and photoconductors is described. This processing method is based on the high reactivity between the components which are kept in an aqueous solution at high temperature and pressures up to several hundred atmospheres. The hydrothermal method offers the advantages of a sealed system and easily reproducible experimental conditions. Some binary solid solutions which have never been prepared previously could be synthesized readily by this technique.

Abstract No. 60

Polarization of Luminescence of ZnS and CdS Single Crystals

A. Lempicki, Research Labs., Sylvania Electric Products Inc., Bayside, N. Y.

We have studied the polarization of luminescence of Zn and Cd sulfide synthetic crystals. Up to 50% polarization of emission was observed on some specimens. The magnitudes differ considerably depending on the crystal structure and doping. The direction of preferential polarization of emission was always found to be perpendicular to the "c" axis of the crystals and remains the same even if the exciting light was unpolarized. Contrary to halide crystals the results cannot be accounted for by anisotropic dipoles arranged along some preferred direction in the lattice. This indicates that the centers in ZnS and CdS are of more complicated nature.

Abstract No. 61

On the Polarization of Fluorescence in CdS and ZnS Single Crystals

J. L. Birman, Research Labs., Sylvania Electric Products Inc., Bayside, N. Y.

The polarization of the fluorescence at 6200Å in CdS and at 4500 and 5800Å in ZnS is reported in the preceding paper, along with the failure of various simple dipole theories to account for these results. Since a dipole model was able to account for color centers in the halides and the localized centers in diamond, it was indicated that the CdS and ZnS centers in question may be of an essentially different type. We shall suggest that the 6200Å emission in CdS and probably the 4500Å in ZnS be interpreted on the basis of the Lambe-Klick model and make certain predictions based on this explanation, which, if verified, will substantiate the interpretation. The 5800Å Mn emission in ZnS apparently requires a more complex interpretation which is not surprising in view of the complexity of the ground and excited states of Mn^{++}.

Abstract No. 62

The Fluorescence of Some Binary and Ternary Germanates

H. Koelmans and **C. M. C. Verhagen,** Philips Research Labs., N. V. Philips' Gloeilampenfabrieken, Eindhoven, The Netherlands

The fluorescence of binary and ternary germanates of Ca, Sr, Ba, Mg, and Zn with different activators was investigated. Germanate-phosphors activated with Pb, Ti, and Mn are described. The ternary composition phase diagrams are given together with the x-ray powder diagrams of 23 hitherto unknown germanates.

Abstract No. 63

Two Unusual Effects Observed with CaO:Mn, Li Phosphors

P. M. Jaffe, Research Dept., Westinghouse Electric Corp., Bloomfield, N. J.

Two rather unusual effects have been observed for hydrogen-fired calcium oxide containing manganese and lithium: (*A*) the phosphor as removed from the furnace has a red emission under 2537Å excitation and is dead under 3650Å. Applying pressure to the phosphor (grinding, rubbing, etc.) causes the intensity of the red emission to decrease while a relatively strong blue emission band appears under 2537Å. (*B*) Excitation of the ground sample first by 2537Å and then by 3650Å now results in a transitory red emission which decreases rapidly to zero.

Abstract No. 64

Tin-Activated Calcium-Silicate Phosphors

R. W. Mooney, Sylvania Electric Products Inc., Towanda, Pa.

The preparation and properties of several calcium silicates activated by tin are described. It is shown that a wide variety of phosphors are obtained depending on the ratio of calcium to silica and the firing temperature. Excitation and emission spectra are given for many of these phosphors. The more efficient phosphors discovered were a tin-activated calcium orthosilicate, Ca_2SiO_4:Sn, emitting at 452 μ; and a tin-activated calcium metasilicate, $CaSiO_3$:Sn, emitting at 520 μ.

Abstract No. 65

The Calcium Silicate Mn + Pb Phosphor; Phase Relationships and Preparation

D. E. Harrison and **M. V. Hoffman,** Lamp Wire & Phosphors Dept., General Electric Co., Cleveland, Ohio

Phase relationships were examined in the vicinity of $CaSiO_3$ in the system $CaSiO_3$-$MnSiO_3$-$PbSiO_3$. Lead solid solutions in $CaSiO_3$ lower the wollastonite to pseudowollastonite inversion temperature. The addition of $MnSiO_3$ to (Ca, Pb) SiO_3 markedly lowers the solubility of lead in $(Ca,Mn,Pb)SiO_3$ and causes a change in structure from pseudowollastonite to wollastonite. Application of the phase data is used to demonstrate how the synthesis technique can be varied to produce major differences in particle size of the phosphor.

ELECTRONICS—LUMINESCENCE & SEMICONDUCTOR

Abstract No. 66

Solid-State Opto-Electronics

E. E. Loebner, RCA Labs., Radio Corp. of America, Princeton, N. J.

In solid-state opto-electronics photons and electrons are used in solids to generate, convert, and control power and to detect, transmit, amplify, process, and display information. A review of electroluminescent and photoconductive elements associated in relatively simple devices is followed by a discussion of applications in more complex data control, handling, and processing devices. An analogy between biological systems and opto-electronic decision networks is discussed.

Abstract No. 67

Analysis of Characteristics of Electroluminescent Lamps with Conductive Grid Structures

R. J. Coerdt, Large Lamp Dept., General Electric Co., Cleveland, Ohio

Improved high-frequency performance of EL lamps may be obtained by using a network of conductive grid lines over the transparent conductive electrode of the lamp, thus affording a more efficient and uniform distribution of power to the field responsive lamp elements. This paper discusses the operating characteristics of lamps made both with and without such a grid system. Brightness and voltage variations and their effect on lamp performance are

described. Lamps having the same total area but different shapes are analyzed and performance described in terms of lamp length/width ratio.

Abstract No. 68

An Improved Electroluminescent Display Panel

R. R. Chamberlin, National Cash Register Co., Dayton, Ohio

A new method for constructing an electroluminescent display panel with improved contrast is presented. To overcome the lack of contrast inherent in conventional panels, display panels have been made using a layer of discrete phosphor particles backed by a light absorbing layer. Samples of the new panels will be shown together with display panels of conventional design. Data on source requirements and contrast ratios for both these and conventional display panels are given.

Abstract No. 69

An Electroluminescent Symbolic Indicator

R. C. Lyman, New Products Engineering Dept., Westinghouse Electric Corp., Cheswick, Pa.

Flat electroluminescent panels are especially well suited to use as symbolic or graphic visual indicators. A panel having a metallic back electrode evaporated in many separate segments can display a variety of precoded patterns by selective excitation of the segment areas. It has many advantages including greater efficiency and wider viewing angle than conventional indicators. An electroluminescent symbolic indicator of this type, now being used in an optimizing process control system, is described and shown. The circuitry used for control is described also.

Abstract No. 70

Preparation and Performance of Sintered CdS Layers*

R. R. Billups, W. L. Gardner, and **M. D. Zimmerman,** Lincoln Lab., Massachusetts Institute of Technology, Cambridge 39, Mass.

The technique of making the sintered CdS layers and their properties is discussed. The characteristics of the photoconductive layer depend on the activation, sintering parameters, and the type electrode used. Sintered CdS layers activated with copper and chlorine have light-to-dark current ratios as high as 10^6. The electrical response is fast, being in the order of a microsecond; however, the optical response is of the order of milliseconds. Sintered layers with these characteristics are being utilized in light amplifiers, display devices and computer components such as photorectifier arrays.

* The work reported here was performed at Lincoln Laboratory, a technical center operated by Massachusetts Institute of Technology with the joint support of the Army, Navy, and Air Force, under contract.

Abstract No. 71

A Discussion of Photoconductive Response

Arthur Bramley, Bramley Consultants, Passaic, N. J. (Consultant to Stromberg-Carlson, San Diego, Calif.)

Characteristics are presented for photoconductor types which are of special interest in switching, particularly those used in light amplifiers. Both surface and volume conductivity are discussed, and an attempt is made to correlate their mechanism of operation. Observations are given on the differences in the behavior of ordinary sintered CdS photoconductors and the same photoconductors impregnated with Araldite. These differences refer to rectification and the relation of conductivity (particularly transient effects) to the incident light sum.

ELECTRONICS—SEMICONDUCTOR

Abstract No. 72

Electromagnetic Levitation of a Floating Zone

K. M. Arnold, B. W. Levinger, and **H. F. Matare,** Research Labs., Sylvania Electric Products Inc., Bayside, N. Y.

The problem of increasing the maximum diameter of a semiconductor rod, which may be subjected to a "floating zone" purification or single-crystal growth, is solved by applying electromagnetic forces to hold the molten zone together. In distinction to other methods the melting field is separated from the levitation field by a two-coil, two-frequency system. Silicon rods up to 1 in. in diameter have been zone refined and converted into single crystals.

Abstract No. 73

Bulk Properties of High-Resistivity P-Type Silicon

C. A. Klein and **W. D. Straub,** Research Div., Raytheon Manufacturing Co., Waltham, Mass.

Hall coefficient R and conductivity σ of p-type silicon samples having N_A-N_D values ranging from less than 10^{15} to a few 10^{15} cm^{-3} were measured carefully as a function of temperature between 25° and 400°K. The Hall mobilties at 300°K were found to lie between 340 and 360 cm^2/v-sec indicating that even for the purest samples the mobility ratio has a value less than unity at room temperature. At low temperatures mobilities of more than 10^{-5} cm^2/v-sec were observed, implying that galvanomagnetic fine structure effects should occur. The Hall coefficient factor was then obtained by an analysis of the 1/Re data based on theoretical considerations of the carrier density in p-type silicon. It is believed that the approach leads to accurate determinations of the total impurity concentration in our samples.

Abstract No. 74

The Semiconductivity of Organic Compounds

Leroy Schieler and **P. L. Nichols, Jr.,** Jet Propulsion Lab., California Institute of Technology, Pasadena, Calif.

The semiconductivity of organic compounds has been investigated by measurement of the a-c and d-c conductivity of single-crystal material over a wide range of temperatures and frequencies. On the basis of these experiments, it is concluded that organic compounds must be considered intrinsic rather than impurity semiconductors. As a consequence of the electropositive nature of aromatic compounds, the electrons have a high probability of being trapped, and most of the current is carried by holes. This trapping process gives rise to a polarization which complicates the measurement of conductivity by a-c methods and results in an anomalously high resistance in d-c measurements. Some possible applications of organic semiconductors in electronic applications are discussed.

Abstract No. 75

Temperature Dependence of the Solid Solubility and the Distribution Coefficient of Various Impurities in Ge and Si

F. A. Trumbore and **C. D. Thurmond,** Bell Telephone Labs., Inc., Murray Hill, N. J.

For certain impurity elements in Ge and Si, the experimentally determined solidus and liquidus curves yield a distribution coefficient, the logarithm of which is markedly nonlinear when plotted against the reciprocal of the absolute temperature. This "anomalous" behavior is explained in terms of the effects of the ionization of donor and acceptor impurities and of departures from ideal solution behavior in the liquid state. The binding energies of a number of Group III, IV, and V elements in Ge are estimated.

Abstract No. 76

There is no Abstract No. 76

Abstract No. 77

There is no Abstract No. 77

Abstract No. 78

Intrinsic Regions in Si Produced by Li Ion Drift

E. M. Pell, Research Lab., General Electric Co., Schenectady, N. Y.

The electric field in a reverse-biased Si n-p junction can be used to drift Li ions in such a way that an intrinsic region is produced. High reverse voltage junctions and analog transistors have been achieved with this technique. By measuring rates of capacitance change as a function of temperature, ion binding energies between the Li and both oxygen and Group III acceptor elements have been measured.

Abstract No. 79

Influence of Surface Treatment on Performance of Silicon Current Limiters

T. M. Buck, W. H. Jackson, and **F. S. McKim,** Bell Telephone Labs., Inc., Murray Hill, N. J.

The silicon current limiters under study operate on the field-effect principle and have a very thin conducting channel on one side of a p-n junction. Conditions on the surface of this channel play a large part in determining the characteristics of the device. Changes in the electrical parameters were correlated with known changes in surface conductivity and surface potential produced by various surface treatments. The best limiter characteristics resulted from strong inversion treatments.

Abstract No. 80

Studies of Surface Conductivity and Recombination in Silicon

C. G. Peattie and **W. R. Savage,** Texas Instruments, Inc., 6000 Lemmon Ave., Dallas 29, Texas

Field effect (a.c.) studies show 4200 ohm-cm, p-type silicon to emerge from CP-4 etch with either an n- or a p-type surface. Evacuation results in an intrinsic or a p-type surface. Pressures of 60% relative humidity air as low as 40 μ produce an n-type surface. Surface recombination studies and reverse current measurements of rectifiers made from this silicon are correlated with these results.

Abstract No. 81

Alloy Junctions in Gallium Arsenide

S. M. Ku and **H. T. Minden,** Sylvania Electric Products Inc., Bayside, N. Y.

Alloy p-n junctions have been prepared on n-type gallium arsenide, using gallium metal as the alloying agent. The gallium was doped with 10% zinc which acts as an acceptor impurity. The alloying was done in an argon atmosphere at temperatures between 800°-900°C. No flux was used. Best results were obtained when the wafer was cooled, after alloying, at a rate of about 1°/min. The excess gallium was etched away and solder contacts were made to plated areas on both sides of the junction. Metallographs and photomicrographs showed a typical recrystallized region. Rectification was observed only on units which were prepared with doped gallium. Etching the completed unit improved the rectification characteristic.

Abstract No. 82

Very Low Voltage D-C Electroquenchable Phosphors

L. W. Hershinger and **M. E. Lasser,** Research Div., Philco Corp., Philadelphia 34, Pa.

It has been discovered that the application of about 1 v d.c. is sufficient to quench the fluorescence of phosphors of the ZnS group. The effect is found to be independent of the technique used to prepare the phosphor, providing only that the phosphor layer is conductive. The quenching effect takes place at one of the electrodes and arises because charges created by the exciting radiation are extracted at the electrode.

Abstract No. 83

Determination of Impurities in III-V Semiconducting Compounds

F. J. Reid, S. E. Blum, and **R. K. Willardson,** Battelle Memorial Institute, Columbus, Ohio

The chemical and physical methods generally used to determine impurities in III-V compounds are reviewed and their limitations discussed. Electrical measurements and other techniques are used to determine impurity concentrations below the detection limits of the classical methods. Carrier concentrations, carrier mobilities, and the magnetic field dependence of the Hall coefficient are used to identify the impurities and determine their concentrations.

Abstract No. 84

High-Purity Single Crystals of Indium Antimonide*

R. C. Bourke, S. E. Miller, and **W. P. Allred,** Battelle Memorial Institute, Columbus, 1 Ohio

A combination zone-refining and crystal-pulling technique has been developed. The indium antimonide is purified by multiple zone passes, and crystals are then pulled from the high-purity sections of the ingot. The same hydrogen atmosphere is used for both the zone-refining and the pulling operations. Large, high-purity, single crystals of indium antimonide with electron mobilities of over 450,000 cm²/v-sec at 80°K can be pulled consistently. The crystals have extremely low dislocation densities as shown by etch-pit studies.

* This research was supported by the U. S. Air Force, through the Office of Scientific Research of the Air Research and Development Command.

Abstract No. 85

Preparation and Properties of AlSb*

W. P. Allred, W. L. Mefferd, and **R. K. Willardson,** Battelle Memorial Institute, Columbus 1, Ohio

An improved method of growing single crystals of AlSb is presented. Previously, oxide from the aluminum produced particles on the surface of the AlSb melt and inhibited the growth of single crystals. This oxide has been eliminated by a vacuum heat-treating technique, which also removes volatile impurities. Effects of carrier density on the mobility of positive carriers, magnetic field dependence of the Hall coefficient, and damage from fast neutron bombardment were investigated.

* This research was supported in whole or in part by the U. S. Air Force, monitored by the Aeronautical Research Lab., Wright Air Development Center.

Abstract No. 86

Purification and Crystal Growth of Zinc Arsenides

V. J. Lyons and **G. A. Silvey,** Research Center, International Business Machines Corp., Poughkeepsie, N. Y.

Three standard methods have been employed to produce single crystals of the semiconducting compounds $ZnAs_2$ and Zn_3As_2. Details of the methods are presented together with experimental results. Methods for arsenic and zinc purification as well as general preparative techniques are described. The dissociation pressure of $ZnAs_2$ has been measured in the temperature range 600°-770°C. Conductivity type changes in $ZnAs_2$ have been obtained by doping of the melt with suitable impurity elements. Crystallographic data relating to monoclinic $ZnAs_2$ and tetragonal Zn_3As_2 have been determined. Recent infrared spectra and electrical properties of the compounds are discussed.

Abstract No. 87

Rare Earth Compound Semiconductors*

J. F. Miller, F. J. Reid, and **R. C. Himes,** Battelle Memorial Institute, Columbus 1, Ohio

Compounds of a number of rare earth elements (including yttrium) with elements of chemical group

VIB have been prepared by direct reaction of the elements. Electrical characteristics measured on the selenides and tellurides suggest semiconducting behavior, with the possibility of obtaining a wide range of properties. All the compounds prepared possess high melting points (1700°-2100°C) and exhibit good thermal stability.

* This investigation was supported by the Rare Earth Research Group (Davison Chemical Co., Electro Metallurgical Co., Heavy Minerals Co., Lindsay Chemical Div. of American Potash and Chemical Corp., Mallinckrodt Chemical Works, Rare Earths and Thorium Div. of Michigan Chemical Corp., and Molybdenum Corp. of America).

Abstract No. 88

Diffusion in Silicon by the Box Method

L. A. D'Asaro, Bell Telephone Labs., Inc., Murray Hill, N. J.

A single-step process for impurity diffusion into silicon is described. The source of impurity and the sample to be diffused are placed in a box which can be opened or closed readily. The surface concentration of the impurity in the silicon can be varied over several orders of magnitude by a controlled variation in the nature of the source. A discussion is given of the conditions under which the effect of the finite leak rate of the box is negligible. Specific experimental results are reported for the diffusion of boron and phosphorus. This technique enables the formation of double diffused structures by a novel method.

Abstract No. 89

Application of Oxide Masking to Silicon Diffused Transistors

R. H. Lanzl, General Electric Co., Syracuse, N. Y.

This paper is concerned with the use of oxide masking to increase the design flexibility of simultaneous double diffused transistors. Particular emphasis is placed on improvements in low collector saturation resistance for high-frequency power and switching transistors. Some aspects of design advantages that may be obtained in voltage breakdown, input resistance, and contact formation to diffused layers are discussed. A summary of electrical characteristics of typical devices is presented.

Abstract No. 90

Penetration of an Oxide Film on Silicon by P_2O_5

C. T. Sah, H. Sello, and **D. Tremere,** Shockley Transistor Corp., A Subsidiary of Beckman Instruments, Inc., Mountain View, Calif.

Experimental relationships are found for diffusion temperature, diffusion time, and oxide thickness at the point where the oxide film fails to mask against P_2O_5. Diffusion time ranges from 5 to 240 min, diffusion temperature ranges from 850° to 1250°C, and oxide film thickness from 0.08 to 0.9 microns. Results are discussed in terms of a simple diffusion mechanism.

Abstract No. 91

Evaluation of Impurity Distributions

K. Lehovec, C. Pihl, and **C. Wrigley,** Sprague Electric Co., North Adams, Mass.

Impurity distributions produced by gaseous indiffusion have been evaluated by measurements of breakdown voltage and of capacitance on diodes placed in jet etched indentations of various depths. Error sources of this evaluation method and their elimination are discussed. An empirical relation between breakdown voltage and impurity concentration for a surface barrier diode is given in the range where the built in potential exceeds the breakdown potential. A theoretical interpretation is presented.

Abstract No. 92

Gaseous Diffusion of Phosphorus in Germanium

K. Lehovec, C. Pihl, and **C. Wrigley,** Sprague Electric Co., North Adams, Mass.

The distribution of impurities in germanium exposed to a phosphorus atmosphere has been measured as a function of germanium temperature, phosphorus vapor pressure, and diffusion time. A relation to thermal conversion is discussed. Similar data are presented for the germanium-indium system. A theoretical analysis is presented.

Abstract No. 93

Polishing and Etching of a III-V Binary Semiconductor, Gallium Arsenide

J. G. Harper and **M. S. Astor,** Central Research Labs., Texas Instruments, Inc., Dallas, Texas

A III-V binary semiconductor, gallium arsenide, has been polished and etched by various methods to obtain information about structural features. Methods of observing macrostructural features such as grain boundaries and twin boundaries are presented. In addition, microstructural features consisting of subgrains and dislocation etch pits can be observed also.

Gallium arsenide has been polished by hand, chemically, and electrolytically. It has been etched chemically, electrolytically, and thermally. Chemical methods of polishing and etching, in general, give a good indication of dislocation etch pit densities and other structural features. Dislocation etch pit densities obtained by this method may be used with reliability. Electrolytic polishing and etching is feasible with low resistivity n-type material and medium resistivity p-type material. The etch pits formed are well defined in shape and screw dislocation etch pits can be distinguished from edge dislocation etch pits. The most reproducible data are obtained by this method. Thermal etching has been accomplished but does not appear to be a feasible method of obtaining reliable information about microstructural features.

ELECTRONICS—THERMIONICS

Abstract No. 94

Keynote Address

J. S. Wagener, Kemet Co., A Division of Union Carbide Corp., Cleveland, Ohio

(No abstract received)

Abstract No. 95

Measurement of Adsorbed and Desorbed Gases in Vacuum Tubes by Mass Spectrometric Techniques

J. E. Turnbull, Electron Tube Div., Radio Corp. of America, Lancaster, Pa.

(No abstract received)

Abstract No. 96

Determination of Residual Amounts of Organic Contaminants in Electron Tubes by Radiotracer Technique

H. A. Stern, Electron Tube Div., Radio Corp. of America, Lancaster, Pa.

Radiotracer technique is employed to study organic contamination and its effects on cathode environment. Degreasing operations, backstreaming of diffusion pump oil, adsorption, and retention of carbon dioxide by tube components and the pyrolysis or decomposition of organic binders and lacquers are studied easily by labeling the organic constituent with radioactive carbon 14. Ultimate objectives are to: (*a*) define the levels of contamination; (*b*) develop processing to minimize the contamination; (*c*) determine the effect of the contaminate on cathode life.

Abstract No. 97

Methods of Cathode Temperature Measurement in Commercial Tubes

J. H. Affleck, Power Tube Dept., General Electric Co., Schenectady, N. Y.

Conventional methods of determining the cathode temperatures in commercial tubes are reviewed and discussed. These methods are only applicable in spe-

cial cases where thermocouples may be used or the cathode is visible. However, the determination of cathode temperature by the retarding potential method requires no special modification of the tube. Data are presented demonstrating the validity and practicality of this method. The limitations of this technique are discussed.

Abstract No. 98

Diffusion of Thorium in Dispenser Cathodes

D. L. Goldwater and **W. E. Danforth,** Bartol Research Foundation, Swarthmore, Pa.

A simple mathematical model for the diffusion of thorium to the surface of an impregnated matrix cathode has been considered. In clean diode tests, it is believed that the dispensing rate is substantially in equilibrium with evaporation from the surface. Measurements of the evaporation of thorium from these cathodes are considered in the light of the mathematical treatment, leading to suggestions as to means of improvement, i.e., making the dispensing rate more constant in time.

Abstract No. 99

Oxygen in High-Purity Cathode Nickel Alloys

H. E. Kern, C. W. Caldwell, E. T. Graney, A. L. Beach, and **W. G. Guldner, Bell** Telephone Labs., Inc., Murray Hill, N. J.

The residual oxygen content of several high-purity single additive cathode nickel alloys is shown to be related to the concentration and chemical activity of the reducing agent additive. For high-purity nickels containing no reducing additives, the oxygen content is about an order of magnitude higher than for active additive nickels. Low thermionic emission is obtained from oxide coatings on these pure nickels. Removal by suitable heat treatment produces a pure nickel cathode with total thermionic emission comparable to that of active additive nickel alloys. Emission measurements obtained on a series of high-purity nickels containing various amounts of oxygen indicate a critical dependence of thermionic emission on oxygen content of the nickel base.

Abstract No. 100

Gettering Properties of Titanium-Zirconium Alloys

V. L. Stout and **M. G. Gibbons,** Research Labs., General Electric Co., Schenectady, N. Y.

(No abstract received)

Abstract No. 101

Electrolysis and the Activation Processes in the Oxide Coated Cathode

D. E. Anderson, University of Minnesota, Minneapolis, Minn.

It has been demonstrated that passage of continuous current through the oxide coated cathode results in an enhancement of the thermionic properties of the cathode which persists even when current drain is discontinued. This activity develops in several minutes following application of the continuous current drain, while the permanent enhancement requires tens of hours to develop completely. Data are interpreted in terms of a model in which donors are produced irreversibly by electrolysis of the surface layers of the oxide particles with eventual saturation of the bulk of the particles by diffusion.

Abstract No. 102

Proposed New Model for the Cause of Flicker Noise in Oxide Coated Cathodes

R. R. Johnson, University of Minnesota, Minneapolis, Minn.

A model is proposed to explain the cause of flicker noise in oxide coated cathodes. The model is based on the diffusion of donors through a narrow surface depletion layer. A frequency spectrum is predicted which deviates from the 1/f dependence at low frequencies. This departure has also been measured in 2 x 2 diodes; compared with the theoretical values good agreement was obtained. By measuring the spectrum it has been possible to determine some of the parameters involved in the time constant of the model.

Abstract No. 103

A Study of Tungsten, Magnesium, and Aluminum as Nickel Additives for Oxide Cathode Use

H. B. Frost and **R. C. Gee,** Bell Telephone Labs., Inc., Murray Hill, N. J.

Seven single-additive alloys—three tungsten and two each of magnesium and aluminum—have been compared as oxide cathode base materials with 220 alloy and pure nickel. The specially prepared materials have no more than 50 ppm of any one impurity. Life tests of tetrodes for 20,000 hr show that tungsten and magnesium can provide satisfactory cathode emission without cathode interface impedance, although tungsten alloys are slow to activate at low (660°C) temperatures.

ELECTROTHERMICS AND METALLURGY

Abstract No. 104

The Production of Thorium Powder by Calcium Reduction of Thorium Oxide

N. Fuhrman, (Present address: Research Lab., Lansdale Tube Co., Division of Philco Corp., Lansdale, Pa.) **R. B. Holden,** (Present address: Metallurgical Labs., Olin Mathieson Chemical Corp., New Haven, Conn.) and **C. I. Whitman,** Sylvania-Corning Nuclear Corp., Bayside, N. Y.

A process for the preparation of high-purity thorium powder by calcium reduction of thorium oxide has been developed. Calcined thorium oxide is reduced in an inert atmosphere at 950°C with high-purity calcium metal in the presence of calcium chloride. The reduction vessel is fabricated of Type 446 stainless steel to avoid pick up of iron and nickel impurities and permit break out of the reduction cake. The thorium powder so produced has essentially the same purity as the thorium oxide starting material.

Abstract No. 105

Super Pure Aluminum

R. R. Haberecht, P. R. Mallory & Co. Inc., Indianapolis, Ind.

High-purity aluminum (99.99%) as starting material was refined by the zone refining method followed by a special method of vacuum melting to result in a metallic impurity range of 1-3 ppm and a carbon content of 5 ppm or less. Compared to 99.99% Al, this super pure aluminum shows considerable improvement in corrosion properties, in alkaline and various acid solutions. The super pure aluminum deteriorates in water at 200°C and corresponding pressure. Hardness and strength are markedly lower than that of the 99.99% material. Methods of removing carbon from aluminum are discussed.

Abstract No. 106

Oxide Nucleation and the Substructure of Iron

E. A. Gulbransen and **K. F. Andrew,** Research Labs., Westinghouse Electric Corp., Pittsburgh 35, Pa.

Electron optical studies were made of the initial stage of reaction of oxygen with pure iron. Oxidation occurred in a discontinuous manner with the oxide structure orienting to the metal grain. The sites for oxide nucleation depend upon the initial pretreatment atmosphere. Thus, a vacuum annealing treatment showed a random arrangement of nucleation sites, while a hydrogen annealing treatment showed a highly ordered arrangement of nucleation sites. Since iron was embrittled by annealing in dry and moist hydrogen and not by vacuum annealing, the nucleation sites probably show the substructure of iron responsible for embrittlement.

Abstract No. 107

Oxidation Studies on the Nickel Chromium and Nickel-Chromium-Aluminum Heater Alloys

E. A. Gulbransen and **K. F. Andrew,** Research Labs., Westinghouse Electric Corp., Pittsburgh 35, Pa.

A systematic study was made of the oxidation resistance of four 80Ni-20Cr heater alloys and one 4Al-19Cr-77Ni alloy. Kinetic and crystal structure studies were made over the temperature range of 500° to 1100°C. The adhesion of the oxide film to the alloy was tested by the strain oxidation technique and the over-all performance was evaluated by the ASTM useful life tests.

The rate of oxidation of the several alloys could not be correlated with the ASTM useful life results while the strain oxidation tests could be correlated with the ASTM useful life tests. Cr_2O_3 was the major oxide formed on the 80Ni-20Cr alloys at 1100°C. Although Al_2O_3 and Cr_2O_3 were observed below 1000°C on the 4Al-19Cr-77Ni alloy, no Al_2O_3 was observed in the oxide scale at 1100°C. A thermodynamic and kinetic interpretation was made of the results.

Abstract No. 108

A Study of the Factors Affecting the Electrical Characteristics of Sintered Tantalum Anodes

G. L. Martin, C. J. B. Fincham, and **E. E. Chadsey, Jr.,** National Research Corp., 70 Memorial Drive, Cambridge 42, Mass.

Measurements were made of the electrical characteristics (d-c leakage, capacitance, and dissipation factor) of anodically oxidized sintered tantalum pellets, which were made from several types of tantalum powder of varying purity and different particle shapes and size distributions. The effects of varying the pressed density of the anodes and the time and temperature of sintering were studied systematically, and the results were correlated in the form of empirical equations.

Abstract No. 109

Equilibrium Reduction of Tungsten Oxides by Hydrogen

R. C. Griffis, Lamp Metals and Components Dept., General Electric Co., 21800 Tungsten Rd., Cleveland 17, Ohio

A complete study has been made of the heterogeneous equilibrium involving the four tungsten oxides, water and hydrogen, using a modified static equilibrium apparatus. These data show that the initial results, previously reported, are in error due to thermal diffusion. The new data were used to compute the standard heats of formation and entropies of the solid oxide species.

Abstract No. 110

Electrode Potential Measurements of the Liquid Al-Ag and Al-Ag-Pb Systems between 690° and 1000°C

T. C. Wilder and **J. F. Elliott,** Dept. of Metallurgy, Massachusetts Institute of Technology, Cambridge 39, Mass.

The thermodynamic behavior of aluminum in the Al-Ag binary and the Al-Ag-Pb ternary has been measured between 690° and 1000°C with the cell

$$Al(1)|Al(KCl + NaCl)|Al(\text{in liquid Ag-Pb})$$

Activities and values of F_i^{MX}, H_i^M and S_i^{MX} have been computed for the three components. The molar properties F^{MX}, H^M, and S^{MX} have also been derived. The boundary of the two phase (liquid) region of the ternary has been redetermined. Some experimental problems encountered in building reversible electrode potential cells are considered.

Abstract No. 111

Some Observations on the Effect of the Interaction of Tantalum with Oxygen, Nitrogen, and Hydrogen

R. Bakish, Sprague Electric Co., North Adams, Mass. (Present address: Rare Metals Div., Ciba Ltd., Basle, Switzerland)

Experiments and results on the interaction of tantalum with O_2, N_2, and H_2 are presented. The {100} is shown to be the habit plane of the segregation of the reaction products which appear to be Ta_2O_5, TaN, and βTaH, respectively. The role of the gas-metal interaction on the fracture behavior of single crystals has been evaluated. The observed {100} and {110} cleavage-type fractures as induced by this interaction are discussed and a hypothesis to explain occurrence advanced. Markings observed on cleavage faces are described.

Abstract No. 112

The Nature of Alumina in Quenched Cryolite-Alumina Melts

P. A. Foster, Jr., Alcoa Research Labs., Aluminum Co. of America, P.O. Box 772, New Kensington, Pa.

The equilibrium primary phases that precipitate from cryolite-alumina melts are cryolite, to the left of the eutectic, and corundum, to the right of the eutectic. No solid solubility of alumina in the cryolite phase was found. Evidence is presented in the form of photomicrographs and x-ray powder patterns that a new alumina phase is obtained by extremely rapid quenching of the liquid. The x-ray pattern of this phase is similar to the aluminum silicate, mullite. It is thought to result from the disproportionation of an oxyfluoride complex in the melt and is perhaps a skeletal arrangement with some of the characteristics of the oxyfluoride precursor. This new alumina phase is metastable and transforms through eta-alumina to corundum on heating.

Abstract No. 113

On the Solubilities of a Certain Gas in Refractory Metals at Elevated Temperatures

Charles London and **Richard Beck,** Denver Research Institute, University of Denver, Denver, Colo., and **Rudolph Speiser,** *et al.,* Dept. of Metallurgy, Ohio State University, Columbus, Ohio

(No abstract received)

Abstract No. 114

Arc-Image Furnace for High Thermal Flux*

F. C. Todd, Southwest Research Institute, Dept of Physics, 8500 Culebra Rd., San Antonio 6, Texas

An arc-image furnace was constructed with two parabolic mirrors which has a ⅝-in. diameter image of a Gaertner-type, blown arc. Test specimens are radiated in controlled atmospheres with pressures from one micron to a few atmospheres. The arc is operated in air at pressures up to 150 psig. Thermal fluxes of over 4000 BTU/ft²sec are roughly calculated.

* Supported by NASA and Sandia Corporation.

Abstract No. 115

Imaging Furnace Developments for High-Temperature Research

P. E. Glaser, Arthur D. Little, Inc., 30 Memorial Drive, Cambridge 44, Mass.

The principles of imaging furnaces using the sun or a high-intensity electric arc are presented. The performance of imaging furnaces with the two energy sources are contrasted, and the relative advantages of each source are pointed out. Advances in instrumentation for measuring and controlling temperature and heat flux are described. Means for changing the atmosphere surrounding the sample are discussed. The function of a flux distributor to obtain larger, uniformly heated area is explained.

Abstract No. 116

The Plasma Torch

M. L. Thorpe, Thermal Dynamics Corp., Hanover, N. H.

The Plasma Jet, a new heat source for industry, consists of an arc contained within a water-cooled tube.

Gas is blown through the arc and heated to temperatures in excess of 60,000°F or as low as 500°F. A brief review of related arc theory will precede a description of Plasma Jet apparatus available for research, development, and industrial uses. A comparison with existing high-temperature sources such as flames; resistance, arc, arc-image, and solar furnaces is made. Recent advances in plasma spray techniques are described along with heating, welding, chemical, melting, and cutting applications.

Abstract No. 117

The High-Intensity Arc; An Aid in the Development of Ceramic Compositions for High-Temperature Applications

C. E. Shulze, Research and Development Div., The Carborundum Co., Niagara Falls, N. Y.

The use of the high-intensity arc is discussed as a means of testing ceramic materials for high-temperature applications. The free burning arc and the plasma jet provide means for subjecting ½-in. diameter cylinder shaped specimens to jet velocities either subsonic or supersonic. Specimens' surface temperatures in excess of 5000°F are reached during a test period of 30 sec. A short 16-mm film is included.

Abstract No. 118

The Design and Operation of an Improved Consumable Electrode Vacuum Arc Melting Furnace

K.L. Bryant, Jr., and **A. L. Feild, Jr.** (present address of A.L.F.: Universal-Cyclops Steel Corp., Bridgeville, Pa.) Central Research Dept., Experimental Station, E. I. du Pont de Nemours & Co., Inc., Wilmington 98, Del.

A laboratory consumable electrode vacuum arc melting furnace was constructed incorporating an extremely sensitive electrode drive and arc voltage control system based on hydraulic operation. Instantaneous system response to voltage changes has resulted in improved vacuum melting characteristics for a variety of refractory metals and their alloys. Silicon rectifiers were employed successfully as a power supply. Other operational features superior to those of conventional laboratory furnaces are discussed, including the use of a remote control console and d-c transformers for measuring rectifier currents.

Abstract No. 119

High-Temperature Laboratory Furnaces for Sintering Single-Crystal Growth and Button Melting of Tungsten

H. G. Sell, Lamp Div., Westinghouse Electric Corp., Bloomfield, N. J.

Two inductively heated tungsten muffle furnaces for inert gas or vacuum sintering of tungsten at temperatures up to 3000°C are described. The advantage of this type of furnace is uniformity of heating and easy control. Further described is a small electron bombardment furnace for melting tungsten and tungsten alloy buttons. This furnace produces tungsten buttons of extremely high purity. For the growth of single crystals of tungsten the design and functioning of a magnetically driven electron bombardment type furnace is discussed. Results are presented.

Abstract No. 120

An Electron Bombardment Annealing Furnace

B. S. Chandrasekhar and **P. A. Flinn,** Research Lab., Westinghouse Electric Corp., Beulah Rd., Churchill Boro., Pittsburgh 35, Pa.

An electron bombardment furnace has been constructed for annealing refractory metal samples in high vacuum at temperatures up to about 2800°C. The furnace is designed to accept small rods or plates, not over about 3 in. in the largest dimension. Provision is included for quenching in water (or other liquid) directly from the annealing temperature. The maximum power input to the sample is about 600 w.

Abstract No. 121

Review of the Mechanical Properties of Intermetallic Compounds

J. H. Westbrook, Research Lab., General Electric Co., Schenectady, N. Y.

Intermetallic compounds are here regarded as comprising all intermediate phases between true metals. This definition, therefore, includes the so-called superlattices but excludes such compounds as the borides and carbides. The existing knowledge of the mechanical behavior of such compounds is reviewed. The treatment is of necessity largely phenomenological but includes such systematization as is now possible.

Abstract No. 122

The Electronic Factor in Mechanical Strength

G.-M. Schwab, Physics-Chemistry Institute, University of Munich, Sophienstrasse 11, Munich, Germany

It has been shown for Hume-Rothery alloys that the hardness increases within the α-phase with increasing electron concentration, reaches a sharp maximum at the γ-phase, and decreases vs. the phases ϵ and η. Because hardness depends on temperature, the temperature coefficient has been measured nearly up to the melting points. It was found that at high temperatures the activation energy of plastic gliding shows the same variation as hardness itself. It is concluded that the work for formation of a dislocation, presupposing the intermediate stretching of atomic distances, is greatest in alloys with nearly complete Brillouin-zones.

Abstract No. 123

Influence of Temperature on Mechanical Properties of Intermetallic Compounds

E. M. Savitskii, Institute of Metallurgy, Academy of Science, U.S.S.R., Moscow

(No abstract received)

Abstract No. 124

Techniques for High-Temperature Tensile and Torsional Testing of Brittle Refractory Materials

L. Green, Jr., M. L. Stehsel, and **C. E. Waller,** Aerojet-General Corp., Azusa, Calif.

An optical technique employed for measurement and recording of small tensile strains of brittle refractory specimens at temperatures up to 2500°C in an inert atmosphere is described, and typical stress-vs.-strain and creep data thus derived are illustrated. Modifications of this method permitting vacuum operation at temperatures in excess of 3000°C and preliminary data so obtained are discussed. Equipment for measurement and recording of torsional stress-vs.-strain, creep, and stress-relaxation properties of specimens in inert atmosphere and at temperatures up to 2800°C is described, together with typical results.

Abstract No. 125

Fractographic Study of NiAl

A. M. Turkalo and **R. W. Guard,** Research Lab., General Electric Co., Schenectady, N. Y.

The application of the electron microscope to the study of fracture surfaces offers several advantages over optical methods. The greater magnification and depth of field permits the observation of details of the fracture surface not possible by other methods. In the present work the surfaces of fractured specimens of NiAl and NiAl plus Ni_2Al are examined using several methods of replication. The appearances of cleavage and grain boundary fractures are described. These are compared with the observations on iron and similar metals. For the two phase systems the effect of a ductile second phase on the fracture path is described.

Abstract No. 126

Extrusion of Intermetallic Compounds

D. L. Wood, Research Lab., General Electric Co., Schenectady, N. Y.

Extrusion permits formation of useful sample shapes in certain intermetallic compounds which cannot otherwise be fabricated. Extrusion conditions for a variety of compounds are reported and related to other physical properties. Resulting mechanical properties and microstructures are described.

Abstract No. 127

Ordered Lattices from Fused Salt Electrolysis I. Ordered Alloys of Chromium

R. S. Dean, W. W. Gullett, F. X. McCawley, and **L. D. Resnick,** Chicago Development Corp., Riverdale, Md.

Alloys of chromium with cobalt and with iron formed by fused salt electrolysis have the atoms in ordered arrangements not previously observed. The electrolysis method produces alloys whose magnetic and mechanical properties are markedly different from those of ordered alloys prepared by normal melting or by powder metallurgy techniques.

Abstract No. 128

The Interaction between Dislocations and the Superlattice

Norman Brown, University of Pennsylvania, Philadelphia, Pa.

The structure of the superdislocation in the superlattice is examined with respect to its orientation, extension, and width of the antiphase boundary. The magnitudes of the stresses to move dislocations in the superlattice are considered from the various ways that slip produces disorder. The effects on properties such as yield point, work hardening, creep, and internal friction have been observed. The interaction also affects the behavior of the quenched state.

Abstract No. 129

Deformation Modes in Face-Centered Cubic Superlattice Alloys

Tadami Taoka and **Ryukicki Honda,** National Research Institute for Metals, Meguro-ku, Tokyo, Japan, and **Ko Yasukochi,** Faculty of Science, University of Tokyo, Bunkyo-ku, Tokyo, Japan

An essential difference is found between slip patterns in different states of superlattice alloys, Cu_3Au, Ni_3Mn, etc., namely an elementary structure in the ordered state, but the usual coarse slip in the disordered state. Changes of saturation magnetization of ordered Ni_3Mn and Pt_3Co alloys caused by plastic deformation are observed. These effects suggest a formation of new disordered phases with Curie points different from those of the ordered state, by a mechanism of homogeneous slip on successive planes, instead of inhomogeneous slip.

Abstract No. 130

Electron Microscope Observations of the Domain Structure in Ordered Copper-Gold Alloy

D. W. Pashley and **A. E. B. Presland,** T.I. Research Labs., Hinxton Hall, Cambridge, England

Thin single-crystal films of CuAu are prepared by an evaporation technique. These are examined by transmission in the electron microscope, while they are being annealed, so that the ordering process is observed directly as it takes place. A continuous change occurs in the arrangement of domain boundaries, from the irregular CuAu I structure to the regular periodic CuAu II structure. A study is made of the influence of dislocations on this process and on the final arrangement of domain boundaries in the CuAu II structure.

Abstract No. 131

Effects of Radiation on the Properties of TiAl

E. M. Grala and **J. B. McAndrew,** Armour Research Foundation, Illinois Institute of Technology, Chicago, Ill.

The effect of irradiation on the physical and mechanical properties of the ordered TiAl phase was investigated. The purpose of this research was to determine if the alloy could be disordered by irradiation and whether brittleness of the alloy is reduced by such irradiation. Significant changes in the electrical resistivity and hardness were accomplished by an exposure of 10^{20} nvt. The impact strength of TiAl was reduced considerably. An activation energy for the recovery of the hardness of the irradiated material was found to be 49 kcal/mole.

Abstract No. 132

Plastic Deformation of InSb*

J. J. Duga, Physical Chemistry Div., Battelle Memorial Institute, Columbus, Ohio

The deformation-induced changes in the transport properties of InSb are seen to be strongly dependent on the mode of deformation. Plastic bending results in the introduction of edge-type dislocations which act as acceptor centers in n-type material, thereby reducing the carrier concentration and mobility. The decrease in the electron mobility following uniaxial compression, on the other hand, is associated principally with the creation of ionized vacancies and interstitials. Various scattering mechanisms for the charge carriers are proposed and the experimental data are interpreted in terms of them.

* Supported by the Office of Naval Research.

Abstract No. 133

Mechanical Properties of Some Transition Element Beryllides

A. J. Stonehouse, R. M. Paine, and **W. W. Beaver,** Research and Development Dept., Brush Beryllium Co., 4301 Perkins Ave., Cleveland, Ohio

(No abstract received)

Abstract No. 134

Plasticity of the Complex-Cubic Gamma 2 Phase of the Copper-Aluminum System

A. J. Birkle, W. L. Krubsack, and **D. J. Mack,** Dept. of Mining and Metallurgy, University of Wisconsin, Madison Wisc.

Compression tests on polycrystalline material and hot hardness tests on polycrystalline and single crystals showed the gamma 2 phase to be brittle until about 650°C when it quite suddenly became plastic. Electrical resistance vs. temperature curves showed a rapid change in slope at the same temperature. X-ray diffraction studies of quenched specimens showed a previously unreported phase change at this same temperature. The sudden onset of plasticity is believed associated with this phase change.

Abstract No. 135

Intermetallic Compounds of the Transition Metals and Their High-Temperature Properties

R. D. Grinthal, American Electro Metal Div., Firth-Sterling Steel Co., Inc., Yonkers, N. Y.

General description is given of an investigation of intermetallic compounds for use at elevated temperature as structural materials. Data are presented on several aluminides, and the effect of addition of a third metal to a binary compound is discussed. Information about Cr_2Ti and the effect of copper and molybdenum additions is presented. Some rare earth intermetallic compounds are also described.

Abstract No. 136

The Mechanical Properties of Some Intermetallic Compounds of Iron and Nickel

I. Kornilov, Academy of Sciences, U.S.S.R., Moscow

(No abstract received)

Abstract No. 137

Investigation of NiAl and Ni_2Al

E. M. Grala Armour Research Foundation, Illinois Institute of Technology, Chicago, Ill.

An investigation was made to determine the effects of composition and homogenization heat treatments on the hardness and tensile properties of the NiAl and Ni_2Al intermetallic phase. Relatively small changes in composition within the NiAl phase resulted in appreciable hardness and strength changes. None of the as-cast or homogenized NiAl alloys showed any measurable tensile ductility at room temperature. NiAl alloys containing up to 31.5% aluminum (stoichiometric) exhibited considerable ductility in the 1500°F tensile tests. The tensile strengths at room and elevated temperatures and ductility of the intermetallic Ni_2Al were found to be very sensitive to composition, structure, and grain size.

Abstract No. 138

Mechanical and Electromechanical Properties of Indium Antimonide

R. F. Potter, Naval Ordnance Lab., Corona, Calif., and **J. H. Wasilik,** Solid State Physics Section, National Bureau of Standards, Washington, D. C.

Properties investigated include the elastic content, anelastic effects, and piezo resistivity.

Abstract No. 139

Structures and Structural Relations of Borides, Carbides, Nitrides, Silicides, and Sulfides

Erwin Parthe, Massachusetts Institute of Technology, Cambridge, Mass.

The available data on the crystal structures of borides, carbides, nitrides, silicides, and sulfides are used to develop criteria for the stability of these compounds. Carbides and nitrides belong to the Hagg compounds, while the silicides and borides form their own group. The formation of particular structures is influenced to a high degree by radius ratio and valence electron concentration. Sulfides show, in general, a higher degree of heteropolar bonding and therefore choose a different kind of structure.

Abstract No. 140

Fabrication, Properties, and Applications of Some Metallic Silicides

R. D. Grinthal, American Electro Metals Div., Firth-Sterling Steel Co., Yonkers, N. Y.

General discussion is given of the production of silicide powders and fabrication methods employed to produce parts. Physical and mechanical properties of some metallic silicides at room and elevated temperatures are given. Effect of addition of a third metal to binary silicide systems, solid solution formation between silicides in pseudo-binary systems, and applications of some of these materials in the high-temperature and nuclear fields are discussed.

Abstract No. 141

Micro Techniques for Studying Electrical Properties of Metalloids

W. R. Eubank, L. E. Pruitt, and **H. Thurnauer,** Ceramic Section, Central Research Dept., Minnesota Mining & Manufacturing Co., Minneapolis, Minn.

Sufficiently large test specimens of metalloids are difficult to prepare in conventional sizes. Therefore techniques have been developed for determining the electrical properties of small test samples of either multi- or single crystals. A micromanipulator test apparatus with platinum probes for determining resistance as a function of temperature over the range liquid nitrogen temperature to 1000°C is described. Methods of sample preparation including mounting and attaching of electrodes are considered. Employing this technique, plots of log R vs. $1/T$ for a number of refractory borides and silicides have been made. A spring-loaded crystal holder with three pairs of copper electrodes for studying crystals as small as one mil in diameter has been constructed. Resistivity and mobility measurements for characterizing semiconductors are discussed.

Abstract No. 142

An Investigation of the Compound Silicon Boride (SiB_6)

C. F. Cline, Research and Development Div., The Carborundum Co., Niagara Falls, N. Y.

Single crystals of the compound silicon hexaboride have been prepared. Laue, rotation, and Weissenberg photographs indicate an orthorhombic cell with lattice parameters $a = 14.39 \pm 0.01$, $b = 18.27 \pm 0.01$, $c = 9.88 \pm 0.01$. The pycnometer density is 2.43 g/cm³. The average electrical resistivity of single crystals, based on a probe technique, is 0.2 ohm-cm. The melting point is 1950°C. SiB_6 has a Knoop hardness, with a 100-g load, of 1910 kg/mm².

Abstract No. 143

Carbide Coatings for Graphite

J. M. Blocher, Jr., and **I. E. Campbell,** (Present address: National Steel Corp., Weirton, W. Va.) Battelle Memorial Institute, 505 King Ave., Columbus 1, Ohio

A technique has been developed for the uniform coating of extended graphite surfaces with metal carbides by reaction with metal halide vapors in a pressure-temperature range unfavorable for the deposition of metal but favorable for carbide formation. In this range, the rate of diffusion of carbon through the carbide can be made to limit the coating rate, and uniform coatings are obtained over a wide range of vapor flow conditions. The application of this method to NbC, SiC, TaC, TiC, and ZrC coatings is discussed.

Abstract No. 144

Some Properties of Aluminum Nitride

K. M. Taylor and **Camille Lenie,** Carborundum Co., Niagara Falls, N. Y.

This paper describes the preparation and properties of crystalline and hot-pressed aluminum nitride. Fine particle size powder was produced by direct combination of the elements. Crystals, up to 25 mm long, were grown by refurnacing the powder at high temperatures. The crystals were found to have a number of interesting properties, including relative chemical inertness. Data on strength, corrosion resistance, and electrical properties are given for the hot-pressed material.

Abstract No. 145

The Effect of Gettering Additions to Niobium

R. H. Hiltz, Jr., Thompson Products, Inc., Cleveland, Ohio

The detrimental effect of the interstitial elements, oxygen and nitrogen, in niobium has been of major concern during the metals development. The addition of gettering elements during melting potentially offers a twofold advantage: the removal of interstitials from solution and the formation of a hard particle dispersion in the matrix. Binary alloys of niobium containing 1 at.% of five gettering elements were prepared and evaluated. Data are presented for the relative efficiency of oxygen removal, partition of removed oxygen between slag and entrapped particles, effect of oxygen removal on hardness and lattice spacings, and the oxygen compound produced in each case.

Abstract No. 146

The Effects of Interstitial Impurities and Process Schedules on Some Mechanical Properties of Arc-Cast Molybdenum and Molybdenum-Base Alloys

H. M. McCullough and **A. L. Feild, Jr.,** Universal-Cyclops Steel Corp., Bridgeville, Pa.

Effects on some common mechanical properties of the residual interstitial impurities carbon, oxygen, and

nitrogen present in pure and alloy arc-cast molybdenum are presented as a function of prior working history and heat treatment. A comparison of chemical, fractographic, and metallographic analyses for representative materials of commercially acceptable impurity levels is made and limitations discussed. The influence of interstitial impurities on the recrystallization temperature of pure and alloy arc-cast molybdenum is examined as a function of important process variables.

Abstract No. 147

Purification of Tantalum Obtained by Vacuum Arc Melting

M. L. Torti, National Research Corp., 70 Memorial Dr., Cambridge 42, Mass.

High-purity tantalum powder was consolidated by a single, vacuum, consumable-arc melting operation yielding ingots of considerably higher purity. Interstitial and metallic impurity analyses are presented for a large number of heats made under consistent conditions of ingot and electrode size, arc current, and furnace pressure. The effect of carbon addition to an oxygen-rich starting material was investigated, and the optimum carbon-oxygen ratio for maximum refinement has been approximately located. Under these conditions, the oxygen content is reduced by approximately one order of magnitude.

Abstract No. 148

The Effect of Dissolved Hydrogen on the Physical and Thermodynamic Properties of β-Phase Titanium and Zirconium

A. D. McQuillan, University of Birmingham, Birmingham, England

The ability of β-phase titanium and zirconium to dissolve up to 50 at. % hydrogen is a remarkable property of the elements which has, so far, received no explanation in terms of electric structure. In attempting to gain some insight into the electronic nature of the phenomenon, a number of physical and thermodynamic properties of hydrogen solutions have been measured. One of the more surprising effects observed is a pronounced decrease in electrical resistivity of the hydrogen-metal solutions with increasing hydrogen content. The existence of the effect cannot be explained readily in terms of the currently accepted picture of the electronic structure of the metals, and it is for this reason that the work described here has been chosen as the starting point for an extensive program aimed at elucidating the electronic structure of all the early transition metals.

Abstract No. 149

Melting and Fabrication of Ductile Vanadium Metal

J. W. Armstrong, Vanadium Corp. of America, Cambridge, Ohio

The melting and fabrication of calcium-reduced vanadium metal has reached a semicommercial stage. Consumable-electrode vacuum arc melting is being used to make ingots up to 6 in. in diameter for fabrication into bars, wire, and flat rolled products. Double melting has been found effective for lowering the oxygen content to sufficiently low levels. Several solutions to the problem of protecting the metal against contamination by oxygen and nitrogen during heating for hot working have been developed. Successful techniques for hot forging and rolling, warm extrusion and rolling, cold swaging, and drawing have been developed.

Abstract No. 150

The Properties of Titanium-Columbium-Aluminum Alloys

John Suiter, Physical Metallurgy Section, Baillieu Lab., University of Melbourne, Victoria, Australia

It is shown that although columbium increases the strength of the titanium-aluminum alloys at low temperatures it has little effect on strength at temperatures above 500°C. Results are also presented showing the effect of heat treatment and of small additions of oxygen on mechanical properties. Mechanical properties of titanium-columbium-aluminum alloy at room temperature are given.

INDUSTRIAL ELECTROLYTIC

Abstract No. 151

A Study of the Production of Metallic Sodium from the Sodium Amalgam

S. Okada, S. Yoshizawa, and **N. Watanabe,** Dept. of Industrial Chemistry, Faculty of Engineering, Kyoto University, Kyoto, Japan

Metallic sodium was produced from sodium amalgam by electrolysis in a molten salt bath at 240° to 270°C, using a 500-800 amp experimental cell (sodium cell) which had three rotating anodic disks. The electrolyte was the mixture of 76 mole % NaOH, 10 mole % NaBr, and 14 mole % NaI, of which the total charge was about 24 kg; the amalgam containing 0.2 to 0.6 wt % sodium was recovered in two amalgam cells from the electrolysis of 15 wt % aqueous sodium hydroxide solution. The anodic disks were made of nickel plates, 5 mm thick and 400 mm in diameter.

Two amalgam cells and the sodium cell were connected electrically in series and the electric current flowing through the two amalgam cells was controlled by shunt to obtain a desired amalgam concentration. The sodium cell voltage was 1.2 to 1.9 v.

In order to protect the deposited metal from oxidation, hydrogen gas was passed through the sodium cell. The cathode deposits were caught and weighed every hour. Furthermore, sodium contents in amalgam were determined at both the inlet and the outlet in the sodium cell.

As 10 to 20% mercury contaminated the deposited sodium metal, it was purified by filtration. By this procedure the mercury content in the cathode metal was reduced to about 1%. Furthermore, it was lowered to 0.01% by the passage over metallic calcium at 370°-390°C. Current efficiencies were 40-70%.

Abstract No. 152

Electrolytic Production of Boron

G. T. Miller, Hooker Chemical Corp., Niagara Falls, N. Y.

Elemental boron was produced by the fused salt electrolysis of potassium fluoborate. A study was made of anode and cathode materials of construction, particularly the effect of various grades of graphite as anode materials. The effect of additives to the electrolyte (including potassium, aluminum, calcium, vanadium, nickel, Inconel, water, and sulfate ion) on boron yield and purity was investigated. A method of passivating elemental boron was developed.

Abstract No. 153

Ion Transfer in a Double Chamber Fused Salt Cell

E. A. Maduk and **W. E. Haupin,** Process Metallurgy Div., Alcoa Research Labs., Aluminum Co. of America, P.O. Box 772, New Kensington, Pa.

Alkali and alkali earth metal ion transfer from the reduction to the refining compartment is a serious problem in the operation of a combined aluminum reduction-refining cell. The theory of this phenomenon and attempts to overcome it are discussed.

Abstract No. 154

A Contribution to the Study of the Polarization Phenomena in Aluminum Cells

R. Piontelli, Laboratorio di Chimica Fisica, Elettrochimica e Metallurgia, Politecnico de Milano, Milan, Italy

After a presentation of the general aspects of the problems, the experimental work of the author and his associates on cathodic and anodic overvoltages and concentration polarization in aluminum cells is sum-

marized. The main theoretical conclusions of these results and of those available in the literature are discussed.

Abstract No. 155

A Pneumatic Force Balance System for Measuring Large Cell Line Currents

H. C. Behrens, Texas Div., Dow Chemical Co., Freeport, Texas

An entirely new concept of measurement has been developed for measurement of cell line currents up to and beyond 100,000 amp. Through the use of the "force balance" principle, a pneumatic device has measured large currents with good accuracy, stability, and ultimate sensitivity for many months. The device is isolated from high potentials and is linear in calibration. Additional pneumatic devices have been used to provide measurements of voltage, a suppressed range of current, ampere-hours, kilowatts, and kilowatt-hours.

Abstract No. 156

Report of the Chlor-Alkali Committee of the Industrial Electrolytic Division for the Year 1958

N. J. Ehlers, Columbia-Southern Chemical Corp., 420 Fort Duquesne Blvd., Pittsburgh 22, Pa., and **C. A. Hampel,** 8501 Harding Ave., Skokie, Ill.

Production facilities for chlorine and alkali are reviewed with indications of market and end use patterns. New plants and expansions during the year and technical and outstanding commercial developments are noted.

Abstract No. 157

Electrolysis of Lithium Chloride in the 1000-Amp Cell

G. T. Motock, Energy Div., Olin Mathieson Chemical Corp., P.O. Box 438, Niagara Falls, N. Y.

Electrolytic production of lithium from molten LiCl-KCl eutectic was performed at temperatures 400°-550°C, cell amp 1000-3500, and volts at 5-9. High-purity metal was collected continuously and used directly without prior solidification. Chlorine is used either directly or neutralized and discarded. Operating characteristic relationships were determined for: preparation of fused salts, variation of cell potential with temperature and amperes, cathode and anode current densities, current and chemical efficiencies, power consumption, material, and heat balance.

Abstract No. 158

Exchange Current Measurements of Electrode Reactions in Molten LiCl-KCl Eutectic

H. A. Laitinen, R. P. Tischer, and **D. K. Roe,** Dept. of Chemistry, and Chemical Engrg., University of Illinois, Urbana, Ill.

Kinetic parameters of several metal-metal ion couples have been determined in molten KCl-LiCl eutectic. Both the double pulse (constant current) method of Gerischer and Krause and the voltage step method of Vielstich and Delahay have been used, with good agreement. The systems studied include cadium, zinc, bismuth, and lead. In each case the electron transfer is relatively rapid and the cathodic transfer coefficient is small (<0.25).

Abstract No. 159

A Transparent Laboratory Cell for the Study of Molten Salt Electrolysis

A. W. Dauer, Texas Div., Magnesium Dept., Dow Chemical Co., Freeport, Texas

Information obtained from the usual opaque laboratory cell is derived from measurements of voltage and amperage and analyses of products and electrolyte. A transparent cell permits observing also the size and nature of product deposits, movements of bubbles and electrolyte, and formation of films. These supplemental observations aid gathering and speed the interpreting of data. The construction and operation of a transparent molten salt cell used to investigate magnesium electrolysis are described.

Abstract No. 160

High-Temperature Reference Electrodes

M. F. Rey and **G. P. Danner,** Laboratoire de recherches de la Société d'Electro-Chimie, d'Electro-Métallurgie et des Aciéries Electriques d'Ugine, 82, rue Arago, Saint-Ouen (Seine), France

In high-temperature electrochemical studies, good reference electrodes are needed. They must be reversible and present sufficient stability and reproductibility. Other important factors are: easy handling and good resistance to thermal, mechanical, and chemical conditions. Below 900°C, reference electrodes presenting these qualities are now available, but, at higher temperature, new difficulties appear in the construction of electrodes and new solutions must be found. The authors expose some of their own solutions and describe reference electrodes working at temperature higher than 1000°C.

Abstract No. 161

The Use of Cs_2UCl_6 and Cs_2PuCl_6 as Starting Materials for U and Pu Metal Preparation*

D. M. Gruen, Argonne National Lab., Lemont, Ill.

Conventional methods for the preparation of U and Pu metals involve UF_4 and PuF_4 as starting materials. In the case of Pu metal, it is desirable to eliminate F from the system because of the neutron hazard associated with the $[\alpha, n]$ reaction on F. The compound Cs_2PuCl_6 has been found to have a solubility of 0.003 m/l in 12M HCl. This compound is a nonhygroscopic free flowing powder and would appear to be a suitable starting material for the preparation of Pu metal. Experiments are described in which Pu metal was made in the liquid state by electrolysis of solutions of Cs_2PuCl_6 in molten CsCl at 700°C. The use of Cs_2UCl_6 for the preparation of U metal will be described.

* Based on work performed under the auspices of the U.S.A.E.C.

Abstract No. 162

Caustic Potash from Mercury Cells

C. B. Handelin, Dow Chemical Co., Western Div., P.O. Box 351, Pittsburg, Calif.

Operation of horizontal, Krebs-type mercury cells for the commercial production of caustic potash are described in some detail. Typical operating data are presented. A brief process description is given. This type of cell is also operated to produce caustic soda. Differences in operation between caustic soda and caustic potash are highlighted and discussed. Information on cell maintenance and repair is presented.

Abstract No. 163

Hydrochloric Acid Electrolysis

F. M. Berkey, Engineering Sales Dept., Monsanto Chemical Co., Lindbergh and Olive St. Rd., St. Louis 24, Mo.

Hydrochloric acid is often a by-product of no value and difficult to dispose of. Several oxidation and electrolysis processes have been tried to recover chlorine from HCl. Of these, direct electrolysis seems best technically and economically. Characteristics and performance of the first U.S. commercial installation of the de Nora electrolyzer are described. The de Nora electrolyzer produces pure chlorine and hydrogen with low power consumption and is particularly recommended for captive chlorine uses where by-product HCl is available.

Abstract No. 164

Day-Kesting Chlorine Dioxide Process

Robert Spitzer, M. H. Treadwell Co. Inc., 140 Cedar St., New York 6, N. Y., and **G. A. Day,** Brown Co., Berlin, N. H.

A method of producing chlorine dioxide by means of a cyclic electrolytic process is explained. This method was developed independently by Day in the

United States and by Kesting in Germany. Experience in a number of operating plants indicates the lowest operating cost of any method of manufacture. The electrolytic production of sodium chlorate, as applicable to this process, is described.

Abstract No. 165

Development of Equations for Calculation of *IR* Drop in Electrolytic Cell Electrodes

C. W. Raetzsch and **D. E. Tunison,** Development Dept., Columbia-Southern Chemical Corp., Corpus Christi, Texas

The *IR* losses which occur are an important consideration in the study and design of electrolytic cells. Calculation of the voltage drop in electrodes is often somewhat involved, and suitable equations are apparently not available in the literature. This paper presents the development of equations which can be used to calculate the voltage drop to any point along an electrode or to calculate the average voltage drop in an electrode. Various electrode configurations are considered.

Abstract No. 166

Oscillographic Studies of Anode Passivity

G. P. Martusevich and **C. L. Mantell,** Amco Research, Inc., 400 Middlesex Ave., Carteret, N. J.

A method of studying the rate of passivity of an anode has been developed using an oscilloscope to record decay phenomena. This method has been applied to 41 copper electrolytes, including those of commercial importance, and to four different types of copper anodes. The passivity of an anode is not a function of its conductivity. Anodes containing phosphorus passivate more slowly than other types in copper sulfate electrolytes. Anodes containing no oxygen passivate more slowly than other types in alkaline solutions.

Abstract No. 167

Anode Design for Mercury Cells

W. C. Gardiner and **W. J. Sakowski,** Olin Mathieson Chemical Corp., P.O. Box 480, Niagara Falls, N. Y.

This paper covers work done on mercury cell anode design in a 500-amp experimental horizontal mercury cell. The anodes were cut from 3-in. thick AGX graphite, some of the anodes being drilled with various sized holes, others slotted, and some with both holes and slots. Comparison also was made between certain configurations on the bottoms of the anodes. Conclusions were drawn as to the best anode design tested with respect to the economics of cell operation.

Abstract No. 168

Effects of Graphite Oil-Level and Density on Hooker Cell Operation

W. J. Baker, Hooker Chemical Corp., Niagara Falls, N. Y.

The relationship of oil-level and density of graphite to service life and cell voltage is indicated. These factors are then compared on an economic basis. Current efficiency, anolyte *p*H, caustic soda concentration, and sodium chlorate concentration relationships to anode life and to cell operation are discussed.

Abstract No. 169

The Solvay and Company Mercury Cell V-200

A. G. Basilevsky, North American Solvay, Inc., 50 Broadway, New York 4, N. Y.

A short description of the general operating principles of a mercury cell is made. The different inherent difficulties of the process are outlined and the description of the Solvay Cell V-200 is made showing how Solvay has overcome these difficulties to minimize investment per ton day of chlorine, its operating cost, and to improve the safety of operation and the quality of the products.

Abstract No. 170

Diamond Alkali Company's Rectangular-Diaphragm Cell at 34,000 Amp

R. H. Parsons, Diamond Alkali Co., Cleveland, Ohio

Competition in the chlor-caustic industry prompts ready acceptance of new technically advanced cell designs. Diamond offers its 30,000-amp rectangular-diaphragm cell now proven at 34,000 amp. This cell offers improved power efficiency, improved cell renewal techniques, low hydrogen content in cell gas, low chlorate contamination of cell liquor, and stability of operation under varying load conditions. A description of the cell and performance data at 34,000-amp load level are included.

Abstract No. 171

High-Pressure Electrolytic Hydrogen Oxygen Generator*

Robert Spitzer, M. H. Treadwell Co., Inc., 140 Cedar St., New York 6, N. Y.

A method of producing hydrogen and oxygen at 3000 psi in high-pressure electrolytic apparatus is explained. The apparatus was developed for the U. S. Navy for submarine service and is essentially a packaged electrolytic installation. Cells, special high-pressure devices applicable to electrolytic apparatus, and automatic control features are explained.

* Work sponsored by The Industrial Gas Technical Code of the Bureau of Ships, U. S. Navy.

THEORETICAL ELECTROCHEMISTRY

Abstract No. 172

Adsorption of Ions at the Metal-Solution Interface and Its Influence on Electrode Kinetics

A. N. Frumkin, Institute of Electrochemistry, Academy of Sciences of the U.S.S.R., Leninsky Prospekt 31, Moscow

The paper is a review of recent work on ionic adsorption. The topics discussed are: a direct method for the determination of adsorption potentials at the metal-solution interface; the specific adsorbability of some inorganic cations; phenomena observed on simultaneous adsorption of surface active anions and cations; the role of polycations formation in the catalysis of electroreduction processes by La^{3+} ions; the mechanism of the $Fe(CN)_6^{3-}$ ion electroreduction.

Abstract No. 173

Mechanism of Hydrogen Electrode Reaction

Juro Horiuti, Research Institute for Catalysis, Hokkaido University, Sapporo, Japan

Since 1936 the present author has maintained the dual theory of hydrogen electrode reaction, i.e., that it proceeds alternatively through the catalytic and the electrochemical mechanisms, in which the rate is governed respectively by the recombination of chemisorbed hydrogen atoms and by the neutralization of chemisorbed hydrogen molecule-ion, depending on the sorts of electrode and electrolyte, polarization, and other conditions. Theoretical and experimental evidences for the dual theory accumulated since then are reviewed.

Abstract No. 174

Determination of Electrochemical Reaction Mechanisms by the Electrochemical Reaction Order

K. Vetter, Fritz-Haber Institut der Max Planck Gesellschaft, Faradayweg, Berlin-Dahlem, Germany

Theoretical properties of the transfer reaction and transfer-overvoltage are given. The dependence of the transfer-overvoltage on the concentrations yields electrochemical reaction orders. This is demonstrated by several known electrode mechanisms with only one transfer reaction. Criterion for a mechanism with two transfer reactions and the determination of the two transfer coefficients and of the two exchange current

densities are explained. As examples, the quinhydron electrode and the recently cleared up Tl^{3+}/Tl^{+} redox-electrode are considered.

Abstract No. 175

A Contribution to the Study of the Electrode Behavior of Metallic Single Crystals

R. Piontelli, G. Poli, and **G. Serravalle,** Laboratorio di Chimica Fisica, Elettrochimica e Metallurgia, Politecnico di Milan, Italy

A suitable technique to study the electrode behavior of oriented surfaces of metallic single crystals is described. Typical results are given concerning variously oriented surfaces of several metals (Pb, Cd, Sn, Ag, Cu, Ni) in different conditions. The theoretical aspects involved by these results are discussed.

Abstract No. 176

Double Layer and Rate of Electrode Processes

L. Gierst, Universite Libre de Bruxelles, Avenue F-D. Roosevelt, 50, Brussels, Belgium

The influence of the structure of the electrochemical double layer on the morphology of the polarization curves is discussed, considering the characteristics of the interphase (ψ potentials, half-thickness κ, occurrence of specific adsorption), the properties of the depolarizing particles (charge, dimension), the type of reaction mechanism, the order of magnitude of the discharge rate, and the method employed. The apparent anomalies affecting the discharge of the $Cd(CN)_4^{=}$, Ni^{++}, $CrO_4^{=}$, Eu^{II} and Eu^{III}, IO_4^{-}, BrO_3^{-}, and Co^{III} ions are interpreted in the light of the proposed theories.

Abstract No. 177

Acousto-Electrochemical Effects in Electrode Systems*

Ernest Yeager, Dept. of Chemistry, Western Reserve University, Cleveland, Ohio

When sound waves impinge on an electrode, both directional and alternating changes may be produced in the electrode potential. The former usually occur with polarized electrodes and represent primarily the interaction of the sound waves with concentration gradients at the electrode surface. Alternating components may be produced by several mechanisms, the most interesting of which involve the dependence of the electrode kinetics and the double layer on pressure and temperature. The use of sinusoidal as well as pressure step function techniques for the study of electrode kinetics is considered in detail and preliminary experimental data are presented.

* Research partially supported by the Office of Naval Research under Contracts Nonr 2391(00) and Nonr 1439(04).

Abstract No. 178

The Electrodeposition and Dissolution of Metals

J. O'M. Bockris, John Harrison Lab. of Chemistry, University of Pennsylvania, Philadelphia 4, Pa.

The study of the kinetics of metal ion exchange with aqueous solutions and molten electrolytes is discussed from the point of view of general kinetics and those of transfer and surface diffusion. The considerations lead to the deduction of the path and rate-determining step of deposition and dissolution in a number of systems. An analysis of the electrode kinetics of metal deposition in molten electrolytes is given which gives rise to certain relations between the mechanism of deposition and the crystal form produced.

Abstract No. 179

Effect of Specific Adsorption of Anions on the Kinetics of Anodic Dissolution of Some Metals

J. Kolotyrkin, Karpov Institute of Physical Chemistry, Ulitza Obucha 10, Moscow, U.S.S.R.

(No abstract received)

Abstract No. 180

Search for Specific Adsorption of Cesium Ions in the Absence of Specifically Adsorbed Anions

D. C. Grahame,* **A. E. Higinbotham,** and **F. R. M. Deane,** Amherst College, Amherst, Mass.

Three lines of evidence are presented tending to show that the cesium ion is not specifically adsorbed on mercury in the absence of specifically adsorbed anions. The potential of the e.c. max. in solutions of cesium fluoride is found to be constant at a value of 0.475 $\pm$0.003 v relative to a normal calomel electrode. The behavior of the capacity of the double layer is normal in that it can be predicted almost quantitatively by a theory which assumes the absence of specific adsorption of both cations and anions and simple dependence of the capacity of the inner region on the surface charge density, q, and not on the concentration of the electrolyte. The slight dependence of the capacity of the inner region of the double layer on the identity of the associated cation found by Damaskin, Nikolaeva-Fedorovich, and Frumkin is confirmed but is explained in a manner which does not require their postulate of specific adsorption of cesium ions on positively charged mercury.

* Deceased. The paper will be presented by Dr. Roger Parsons.

Abstract No. 181

Kinetic Parameters of Very Rapid Metal Ion-Amalgam Electrode Reactions

J. E. B. Randles, Chemistry Dept., University of Birmingham, Birmingham 15, England

Measurement of the rate constants and transfer coefficients of the most rapid electrode reactions is difficult and apart from the ordinary a-c method, methods based on a current—or potential—step and on the partial rectification of a radio-frequency alternating current have been used. The last has resulted in some unexpectedly small and large (approaching 1) values of the transfer coefficient for ion-amalgam electrode reactions for lead, thallium, and cadmium. In the present paper the limit of applicability of the ordinary a-c method is discussed in comparison with the other methods. Also recent results obtained with the ordinary a-c method are presented, and the significance of the transfer coefficients is discussed.

Abstract No. 182

Faradaic Impedance in Anodic Formation of Halogens

J. Llopis, J. Fernandez-Biarge, and **M. Perez-Fernandez,** Instituto de Quimica Fisica Rocalolano, Serrano, 119, Madrid, Spain

The influence of the formation of trihalogenide X_3^{-} ions in equilibrium on the faradaic impedance is analyzed when an inert electrode acts in a system X_2/X^{-}. If the equilibrium is reached at an extremely high rate, the faradaic impedance may be represented by a transfer resistance in series with a Warburg impedance, which in these cases depends on the equilibrium constant as well as on the actual concentrations of each component. The possibility of finite rates of establishing the equilibrium is also studied. Finally, it is shown that the dependence of impedance on frequency cannot be accounted for without considering the adsorption of reactants at the electrode interface.

Abstract No. 183

A Theory of Electron Transfer Processes at Electrodes*

R. A. Marcus, Dept. of Chemistry, Polytechnic Institute of Brooklyn, 333 Jay St., Brooklyn 1, N. Y.

When the electrode and the electrochemically active ion in solution interact but weakly electronically, the activated complex for electron transfer has unusual properties. Its electronic wave function can be shown to have equal probability contributions from two charge distributions which interact differently with

the surrounding medium and, sometimes, with the coordination shell of the ion. Its atomic configuration lies at the intersection of two potential energy surfaces in many-dimensional nuclear configuration space. Attaining such configurations requires a large rearrangement of the atomic positions. Special methods for calculating the probability of this event have been given earlier by the author for ion-solvent interactions in a structureless medium. Corresponding calculations will be reported for changes which may occur in the coordination shell as well. The additional data needed for this theoretical calculation of the current-voltage curve are bond force constants and bond lengths in the two redox forms of the ion.

Depending on the extent of electronic interaction, the electron transfer can be shown to proceed adiabatically or nonadiabatically. Using the many-dimensional potential energy curves, the applicability of the Franck-Condon principle to the electron transfer can be assessed. Some conclusions based on the behavior of *one*-dimensional potential energy curves have been incorrect, because of the important part played by the rearrangement of the atomic configuration of the entire system in effecting an electron transfer.

* This research is supported by the Office of Naval Research.

Abstract No. 184

Effect of Quaternary Ammonium Ions on the Rate of the V^{3+}/V^{2+} Reaction at a Mercury Electrode

K. M. Joshi, Wolfgang Mehl, and **Roger Parsons,** Dept. of Physical & Inorganic Chemistry, The University, Bristol 8, England

Both alternating and direct current techniques are used to study the rate of the V^{3+}/V^{2+} reaction at mercury in the presence of varying concentrations of tetra alkyl ammonium ion and as a function of temperature. The large increase of apparent energy of activation is due to displacement of the organic ion from the surface at higher temperatures. True heats of activation are calculated with the aid of double layer studies and are discussed in the light of current theories of the effect of the double layer on electrode reaction rates. The transfer coefficient is virtually unaffected by the presence of the organic ion.

Abstract No. 185

Isotopic Effects in Electrode Reactions

B. E. Conway, Dept of Chemistry, University of Ottawa, Ottawa, Ont., Canada

The electrolytic separation factors for various mechanisms of hydrogen evolution are deduced theoretically, and it is shown that the simple discharge reaction, e.g., at Hg, Sn, Pb, leads to theoretical values of S equal to 3 while the atom-ion ("electrochemical") reaction leads to values of 6 or 7. Such a division of values is found experimentally for these groups of metals. Ratios of rates of H_2 and D_2 evolution from acid solutions in pure H_2O and D_2O, respectively, also follow theoretically and are diagnostic of reaction mechanism. Experimental results for the rates of cathodic H_2 and D_2 evolution reactions in H_2O and D_2O are reported and discussed in terms of reaction mechanisms.

Abstract No. 186

On the Theory of Convective Diffusion

B. Levich, Institute of Electrochemistry, Leninsky Prospekt 31, Moscow, U.S.S.R.

This paper is concerned with some results reached in the theory of mass transfer in moving solutions: (*a*) convective diffusion to the surface of a rotating disk electrode in the case of a slow electrode reaction; (*b*) convective diffusion to the electrodes of other shapes, in particular, to the electrode where only part of its surface is active (ring electrode, lacquered electrode); (*c*) convective diffusion in the case of a turbulent regime of the liquid motion; (*d*) convective diffusion near the boundary between two liquids or near liquid-gas boundary; the theory of the influence on convective diffusion on the phenomenon of polarographical maxima; the theory of the dissolution of bubbles and drops.

Abstract No. 187

Kinetics of Hydrogen Evolution and Dissolution at Activated Platinum Metals

Manfred Breiter, Physikalisch-chemisches und Elektrochemisches Institut der Technischen Hochschule München, Arcisstrasse 21, Munchen, Germany

Mass transfer processes are rate-determining at activated smooth electrodes of platinum, iridium, rhodium, and palladium in acid solutions. The formation of adsorbed hydrogen atoms by discharge of hydrogen ions on free sites and the ionization of adsorbed atoms are studied by impedance measurements at positive electrode potentials. The coverage with hydrogen atoms in dependence on the electrode potential (adsorption isotherm) is determined by anodic charging curves and by impedance measurements. The influence of coverage on the kinetics is discussed. The free energy of adsorption is found from the temperature dependence of the adsorption isotherm on platinum in 5*N* H_2SO_4.

Abstract No. 188

Use of Faradaic Rectification for the Study of Electrode Processes

G. C. Barker, Atomic Energy Research Establishment, Harwell, England

A new method for studying the kinetics of electrode processes is described which is particularly suitable for the study of very rapid processes. The method makes use of the nonlinearity of the faradaic impedance, measurements being made of the current required to keep the mean potential of an electrode constant when the electrode is polarized by an amplitude-modulated radio-frequency current.

Abstract No. 189

Electrode Kinetics and Electrostatic Interaction in the Double Layer

P. Rüetschi, Research Center, The Electric Storage Battery Co., Yardley, Pa.

The dependence of the surface free energy of an electrochemical interface on electrode potential (Lippmann equation) is applied to calculate the energy of adsorbed activated complexes and the reaction rates. The value of the transfer coefficient α is shown to be determined by electrostatic interaction in the double layer and to depend on the fraction of double layer charge due to the reacting species themselves. If the polarization is due largely to the accumulation of the reacting species themselves, α assumes in the limiting case the value ½.

Abstract No. 190

Surface Coverage during Hydrogen and Oxygen Evolution

P. Rüetschi, J. B. Ockerman, and **R. Amlie,** Research Center, The Electric Storage Battery Co., Yardley, Pa.

The relation between surface coverage and electrode potential during hydrogen and oxygen evolution was studied with various inert electrodes of very large surface area. Desorption of gas after interruption of current was followed with microvolumetric techniques, and overvoltage decay was measured simultaneously. The potential changed linearly with the amount of gas desorbed. The true surface area of the electrodes was determined with the BET method, and the capacity was obtained from charging curves. An average effective charge per adsorbed particle in the double layer was calculated from these data.

Abstract No. 191

The Oxygen-Evolution Reaction at Gold Anodes, II. Overpotential Measurements and Reaction Mechanism in Sulfuric Acid Solutions

Sidney Barnartt, Research Labs., Westinghouse Electric Corp., Pittsburgh, Pa.

The paucity of accurate overpotential measurements has left in doubt the mechanism of the oxygen-evolution reaction at most metal anodes. This report covers measurements on gold anodes in sulfuric acid solutions, with and without added potassium sulfate, over the pH range 0 to 2.7 at 25°C. A cell with uniform current distribution over a spherical anode was used to obtain overpotentials with an accuracy of ± 1 mv. Within current density limits imposed by the cell and the solution, Tafel's equation was obeyed to ± 1 mv. The observed variations of overpotential with current density, pH, and neutral salt additions are compared with the theoretical values for various proposed mechanisms.

Abstract No. 192

Surface-to-Volume Considerations in the Palladium-Hydrogen System

J. P. Hoare, Scientific Lab., Ford Motor Co., Dearborn, Mich.

The rate of hydrogen absorption by palladium electrodes of various sizes and shapes was followed in highly purified, hydrogen-stirred, acid solutions by measuring the electrical resistance and potential vs. a Pt/H_2 electrode in the same solution on open-circuit conditions. From the observed surface-to-volume effects a mechanism of hydrogen occlusion by palladium may be suggested which may be more compatible with the existing published information.

Abstract No. 193

Temperature Coefficient of Electrode Potentials: Isothermal and Thermal Coefficients; Standard Ionic Entropy of Electrochemical Transport of the Hydrogen Ion

A. J. deBethune, T. S. Licht and **N. Swendeman,** Chemistry Dept., Boston College, Chestnut Hill, Mass.

Isothermal temperature coefficients (i.e., referred to SHE at same temperature) are governed by reaction entropies of metal hydrogen cells. Thermal temperature coefficients (i.e., referred through salt bridges to same electrode at some fixed temperature) are governed by transport entropies of single electrode reactions. From Fales and Mudge's data, thermal coefficients of SHE obtained as +0.858 mv/°C (hot electrode + terminal). Standard electrochemical transport entropy of hydrogen ion is −4.18 e.u. Isothermal and thermal coefficients of other electrodes computed and compared with experiment.

Abstract No. 194

An Absolute Null Electrode from Double-Layer Capacity Measurements

R. B. Stein, Ecole Nationale Superieure d'Electrochemie et d'Electrometallurgie, Grenoble, France (Present address: 219 Grace Drive, South Pasadena, Calif.)

Measurements of the differential capacity of the double layer in fused NaCl-KCl eutectic show that specific adsorption is totally absent. This condition is shown to be favorable for the establishment of an absolute null electrode. Such an electrode was realized on a platinum surface in conjunction with the now-familiar Ag/AgCl reference electrode. In this manner the absolute potential of the silver chloride electrode was measured as a function of temperature.

Abstract No. 195

The Mechanism of Electrode Reactions, I. Discharge of Pb^{++} in Fused NaCl-KCl

R. B. Stein, Ecole Nationale Superieure d'Electrochimie et d'Electrometallurgie, Grenoble, France (Present address: 219 Grace Drive, South Pasadena, Calif.)

The kinetics of the discharge of lead ion in fused NaCl-Kcl eutectic were determined by the method of oscillographic polarography. With the aid of the theory of absolute reaction rates a discharge mechanism is proposed. The agreement between calculated and measured entropies supports the hypothetical mechanism.

Abstract No. 196

Molten Salt Thermocells

B. R. Sundheim, Dept. of Chemistry, New York University, New York 3, N. Y.

Thermocells may be formed of two identical electrodes connected by molten salts in which a temperature gradient is maintained. The expression for emf of such a thermocell (or molten salt thermocouple) takes a particularly simple form because of the absence of terms dealing with the salt. Experimental results on a series of systems where the electrodes are silver and the salt is silver nitrate, silver chloride, silver bromide, silver iodide, or a solution of silver nitrate in sodium are presented. From the thermopotentials the Peltier heats may be calculated. The theory of such solutions is described with particular reference to the terms involving the heats of transport of the salts and the transference numbers.

Abstract No. 197

The Effect of Electrolytes on the Streaming Currents of Bulk Metals

L. Rice and **N. Hackerman,** Dept. of Chemistry, University of Texas, Austin 12, Texas

The electrokinetic (ζ) potential of platinum, gold, and silver was determined as a function of concentration in dilute aqueous solutions of potassium nitrate, potassium sulfate, and potassium chromate from the direct measurement of the streaming currents. A theory is presented that explains the qualitative relationship of the zeta-potential to the solubility of the corresponding metal-ion compound.

Abstract No. 198

The Relation between the Kinetics of Self-Discharge of the Nickel-Nickel Oxide Electrode and Electrode Composition over a Range of Temperatures

B. E. Conway and **P. Bourgault,** Faculty of Pure and Applied Science, University of Ottawa, Ottawa 2, Ont., Canada

Studies on the kinetics of the self-discharge reaction at nickel-nickel oxide electrodes have been continued by examining the effect of elevated (60°C) and low (−25°C) temperatures on the rates of emf decay and open-circuit evolution of oxygen. The effect of temperature on the rate-determining mechanism(s) in self-discharge is discussed, and the observed kinetics are related to the electrode composition at various temperatures and electrode potentials. The roles of KOH and water activities in determining the quasi-reversible potential of the nickel oxide electrode in various solutions have been investigated.

Abstract No. 199

Cathode Polarization in the Electrodeposition of Metals and Alloys

T. L. Rama Char, Electrochemistry Lab., Dept. of Inorganic and Physical Chemistry, Indian Institute of Science, Bangalore-3 India

The significance of polarization during the cathodic process of metal ion discharge has been discussed for the electrodeposition of several metals and alloys from the pyrophosphate bath. The results have been examined with respect to the nature of the potential curves, structure of deposits, and throwing power of single metal plating solutions. The utility of potential data in alloy deposition has been discussed with reference to: feasibility of codeposition, plate composition and structure, and mutual influence of the metals.

Abstract No. 200

The Significance of the Flade Potential

M. J. Pryor, Metallurgical Labs., Olin Mathieson Chemical Corp., New Haven, Conn.

Previous explanations of the Flade Potential have been reviewed critically. A new explanation based

on a single phase passive film of γ-Fe_2O_3 having non-uniform defect concentration and type is advanced. The potential-determining reaction is considered to be that between excess oxygen in the outer layers and hydrogen ions and electrons. The inner 'n' type oxide is destroyed by reductive dissolution in acid media and by exchange of oxygen ions with hydroxyl ions in solutions having pH values higher than 3.0.

Abstract No. 201

Electrochemical Calorimetry, II. The Absolute Entropy of the Cupric Ion

J. M. Sherfey and **Abner Brenner**, Electrodeposition Section, National Bureau of Standards, Washington 25, D. C.

The absolute entropy of the copper ion has been measured in a "siamese twin" calorimeter. An electrolytic cell within the calorimeter—two copper electrodes in an acid copper sulfate solution—is divided by a diaphragm into anode and cathode compartments. The heat effects due to the entropy change of the two half-cell reactions are equal and opposite. From the magnitude of these heat effects the entropy change can be determined.

Abstract No. 202

The Anodic Behavior of Nickel

J. C. Banter, (Present address: Oak Ridge National Lab., A Division of Union Carbide Corp., Oak Ridge, Tenn.) **Ernest Yeager**, and **Frank Hovorka**, Dept. of Chemistry, Western Reserve University, Cleveland, Ohio

Anodic polarization measurements have been made using nickel electrodes in aqueous solutions of nickel chloride and nickel sulfate. A Tafel slope of 0.10 was obtained over the current density range 10^{-4} to 10^{-2} amp/cm^2 from 25° to 45°C and pH 1.5 to 2.5. The concentration dependence of the polarization in the range 0.125 to 0.50M nickel suggests that the rate-determining step for the dissolution process involves an adsorbed species. The experimentally determined activation energy of 10 kcal/mole is not inconsistent with this mechanism.

Abstract No. 203

Some Aspects of the Nonaqueous Chemistry of the Uranium Chlorides

R. E. Panzer (Present address: U. S. Naval Ordnance Laboratory, Corona, Calif.) and **John F. Suttle** (Present address: University of California, Radiation Lab. Berkeley, Calif.) Dept. of Chemistry, University of New Mexico, Albuquerque, N. Mex.

The preparation and properties of the compound, $UCl_5.PCl_5$, have been investigated. Chemical and physical (including crystallographic) properties are reported. The compound dissolved in phosphorus oxychloride apparently dissociates into the ions, (UCl_6^-) and (PCl_4^+). Electrolysis of this solution results in the formation of uranium hexachloride at the anode followed by a secondary reaction forming the complex solvated compound $2UCl_4.UCl_5.6POCl_3$. The cathode reaction involves the formation of phosphorus trichloride and phosphorus pentachloride. Equations for the electrode reactions and data for ionization of the parent compound are presented. Ektachrome transparencies of the various compounds are shown.

Abstract No. 204

Mass Transfer and Current Distribution under Free Convection Conditions

Kameo Asada, **Fumio Hine**, **Shiro Yoshizawa**, and **Shinzo Okada**, Dept. of Industrial Chemistry, Faculty of Engineering, Kyoto University, Kyoto, Japan

How current distributions over vertical electrodes occupying the opposite sides of the rectangular cross section of a cell are affected by the difference from point to point in the ease of mass transfer by free convection is discussed. The Laplace equation and the equation of mass transfer, determining the potential and concentration distributions, respectively, were solved simultaneously, and the results were found to explain most features of observed current distributions.

Abstract No. 205

Mass Transfer at the Streaming Mercury Electrode

Kameo Asada, **Fumio Hine**, **Shiro Yoshizawa**, and **Shinzo Okada**, Dept. of Industrial Chemistry, Faculty of Engineering, Kyoto University, Kyoto, Japan

Mass transfer at the streaming mercury electrode was studied theoretically. Momentum equations were solved simultaneously for the mercury stream and the boundary layer of solutions formed along it, on the assumption that both of the flows were laminar. Numerical calculation for some typical systems resulted in flow characteristics essentially identical with those observed experimentally. Limiting currents were measured for reduction of Tl^+, Pb^{++}, and Zn^{++} in solutions 0.1M in KCl and at 25°C, and found to be in good agreement with those predicted from theoretical expressions of the flows.

INDEX TO AUTHORS

(The number in the right hand column is the abstract number used in the Technical Program and in the Abstracts.)

	Abstract No.
Affleck, J. H.	97
Allen, W. T.	50
Allred, W. P.	84, 85
Amlie, R.	190
Anderson, D. E.	101
Andrew, K. F.	106, 107
Apple, E. F.	56, 57
Armstrong, J. W.	149
Arnold, K. M.	72
Asada, Kameo	204, 205
Astor, M. S.	93
Bachman, C. H.	50
Back, R. A.	17
Baker, W. J.	168
Bakish, R.	111
Bakker, C.	41
Banter, J. C.	202
Barker, G. C.	188
Barnartt, Sidney	191
Basilevsky, A. G.	169
Baumann, E.	12
Beach, A. L.	99
Beaver, W. W.	133
Beck, Richard	113
Behrens, H. C.	155
Berg, D.	16
Berkey, F. M.	163
Billups, R. R.	70
Birkle, A. J.	134
Birman, J. L.	61
Blocher, J. M., Jr.	143
Blum, S. E.	83
Bockris, J. O'M.	178
Bono, M.	25
Bourgault, P.	198
Bourke, R. C.	84
Bramley, Arthur	71
Breiter, Manfred	187
Brenner, Abner	201
Brinkmann, K.	6
Brown, Norman	128
Bryant, K. L., Jr.	118
Buck, T. M.	79
Butler, K. H.	44
Caldwell, C. W.	99
Callinan, T. D.	33
Campbell, I. E.	143
Chadsey, E. E., Jr.	108
Chamberlin, R. R.	68
Chandrasekhar, B. S.	120
Church, H. F.	2
Clarke, S. C.	1
Clark, W. R.	32
Cleiren, A. P. D. M.	55
Cline, C. F.	142
Coelho, R.	25
Coerdt, R. J.	67
Conway, B. E.	185, 198
Cortesi, A. A.	31
Dakin, T. W.	16
Danforth, W. E.	98
Danner, G. P.	160
D'Asaro, L. A.	88
Dauer, A. W.	159
Day, G. A.	164
Dean, R. S.	127
Deane, F. R. M.	180
deBethune, A. J.	193
Destriau, G.	51, 52
Dillon, D. M.	35
Dillon, J. F., Jr.	34
Duga, J. J.	132
Egerton, L.	35
Ehlers, N. J.	156
Eich, E. D.	3
Elliott, J. F.	110
Elsfelder, W.	30
Eubank, W. R.	141
Feick, George	3
Feild, A. L., Jr.	118, 146
Fernandez-Biarge, J.	182
Fincham, C. J. B.	108
Flinn, P. A.	120
Foster, P. A., Jr.	112
Freitag, Harlow	28
Frost, H. B.	103
Frumkin, A. N.	172
Fuhrman, N.	104
Gardiner, W. C.	167
Gardner, W. L.	70
Garton, C. G.	2
Gashurov, G.	59
Gee, R. C.	103
Gibbons, M. G.	100
Gierst, L.	176
Glaser, P. E.	115
Goldberg, Paul	48
Goldwater, D. L.	98
Grahame, D. C.	180
Grala, E. M.	131, 137
Graney, E. T.	99
Green, L., Jr.	124
Griffis, R. C.	109
Grinthal, R. D.	135, 140
Gruen, D. M.	161
Guard, R. W.	125
Guizonnier, R.	27
Gulbransen, E. A.	106, 107
Guldner, W. G.	99
Gullett, W. W.	27
Haberecht, R. R.	105
Hackerman, N.	197
Hampel, C. A.	156
Handelin, C. B.	162
Harper, J. G.	93
Harrison, D. E.	65
Haupin, W. E.	153
Hegyi, I. J.	54
Helliwell, G. C.	19
Hershinger, L. W.	82
Higham, J. B.	11
Higinbotham, A. E.	180
Hiltz, R. H., Jr.	145
Himes, R. C.	87
Hine, Fumio	204, 205
Hoare, J. P.	192
Hoffman, M. V.	65
Holden, R. B.	104
Homer, H. H.	46
Honda, Ryukicki	129
Horiuti, Juro	173
Hovorka, Frank	202
Hummel, F. A.	43
Hunt, B. E.	40
Jackson, W. H.	79
Jaffe, P. M.	63
Johnson, R. R.	102
Joshi, K. M.	184
Kao, K. C.	11
Kern, H. E.	99
Klein, C. A.	73
Koelmans, H.	62
Kolotyrkin, J.	179
Kopell, Lawrence	36
Kornilov, I.	136
Krasucki, Z.	2
Kremheller, Alfred	49, 59
Krubsack, W. L.	134
Ku, S. M.	81

	Abstract No.
Laitinen, H. A.	158
Lanzl, R. H.	89
Lasser, M. E.	82
LeBlanc, O. H., Jr.	22
Lehmann, W.	47
Lehovec, K.	91, 92
Lempicki, A.	60
Lenie, Camille	144
Levich, B.	186
Levine, A. K.	59
Levinger, B. W.	72
Lewis, T. J.	13, 14, 18
Licht, T. S.	193
Llopis, J.	182
Loebner, E. E.	54, 66
London, Charles	113
Lyman, R. C.	69
Lyons, V. J.	86
Macfadyen, K. A.	19
Mack, D. J.	134
Maduk, E. A.	153
Mantell, C. L.	166
Marcus, R. A.	183
Martin, G. L.	108
Martusevich, G. P.	166
Matare, H. F.	72
Mattler, J.	53
McAndrew, J. B.	131
McCawley, F. X.	127
McCullough, H. M.	146
McKeag, A. H.	40
McKim, F. S.	79
McLellan, G. W.	38
McQuillan, A. D.	148
Mefferd, W. L.	85
Mehl, Wolfgang	184
Mergner, G. C.	32
Miller, G. T.	152
Miller, J. F.	87
Miller, S. E.	84
Minden, H. T.	81
Mooney, R. W.	42, 64
Morant, M. J.	21
Motock, G. T.	157
Nichols, P. L., Jr.	74
Norante, N. J.	37
Ockerman, J. B.	190
Okada, S.	151, 204, 205
Olds, W. F.	3
Paine, R. M.	133
Palandri, G. L.	10
Panzer, R. E.	203
Parsons, R. H.	170
Parsons, Roger	184
Parthe, Erwin	139
Pashley, D. W.	130
Patterson, Andrew, Jr.	28
Peattie, C. G.	80
Pell, E. M.	78
Perez-Fernandez, M.	182
Pihl, C.	91, 92
Pingault, F.	51
Piontelli, R.	154, 175
Plymale, C. E.	24
Pohl, H. A.	23, 24, 29
Poli, G.	175
Potter, R. F.	138
Potter, R. M.	58
Prener, J. S.	39, 57
Presland, A. E. B.	130
Priaroggia, P. G.	10
Pruitt, L. E.	141
Pryor, M. J.	200
Raetzsch, C. W.	165
Rama Char, T. L.	199
Randles, J. E. B.	181
Reid, F. J.	83, 87
Resnick, L. D.	127
Rey, M. F.	160
Reynolds, E. H.	1
Rice, L.	197
Roe, D. K.	158
Ropp, R. C.	42
Rüetschi, P.	189, 190
Sah, C. T.	90
Sakowski, W. J.	167
Salomon, T.	5
Sarver, J. F.	43
Savage, W. R.	80
Savitskii, E. M.	123
Schieler, Leroy	74
Schwab, G.-M.	122
Schwar, J. P.	23
Sell, H. G.	119
Sello, H.	90
Serravalle, G.	175
Sharbaugh, A. H.	20
Sherfey, J. M.	201
Shulze, C. E.	117
Silvey, G. A.	86
Speiser, Rudolph	113
Spitzer, Robert	164, 171
Stahr, H. M.	4
Stehsel, M. L.	124
Stein, R. B.	194, 195
Stern, H. A.	96
Stonehouse, A. J.	133
Stout, V. L.	100
Straub, W. D.	73
Strigel, R.	7, 15
Suiter, John	150
Sundheim, B. R.	196
Suttle, J. F.	203
Swendeman, N.	193
Taoka, Tadami	129
Taylor, K. M.	144
Thomas, M. J. B.	45
Thorpe, M. L.	116
Thurmond, C. D.	75
Thurnauer, H.	141
Tischer, R. P.	158
Todd, F. C.	114
Torti, M. L.	147
Tremere, D.	90
Tropper, H.	9
Trumbore, F. A.	75
Tunison, D. E.	165
Turkalo, A. M.	125
Turnbull, J. E.	95
van Gool, W.	55
Verhagen, C. M. C.	62
Vetter, K.	174
Wagener, J. S.	94
Waller, C. E.	124
Wanmaker, W. L.	41
Wasilik, J. H.	138
Watanabe, N.	151
Watson, P. K.	20
Watson, R. E.	32
Weil, D. J.	56, 57
Westbrook, J. H.	121
White, J. S.	37
Whitman, C. I.	104
Wilder, T. C.	110
Willardson, R. K.	83, 85
Winkler, C. A.	17
Witt, H. T.	26
Wood, D. L.	126
Wrigley, C.	91, 92
Yasukochi, Ko	129
Yeager, Ernest	177, 202
Yoshizawa, Shiro	151, 204, 205
Zimmerman, M. D.	70

Precision-formed Sylvania ingots yield more single-crystal Germanium . . .

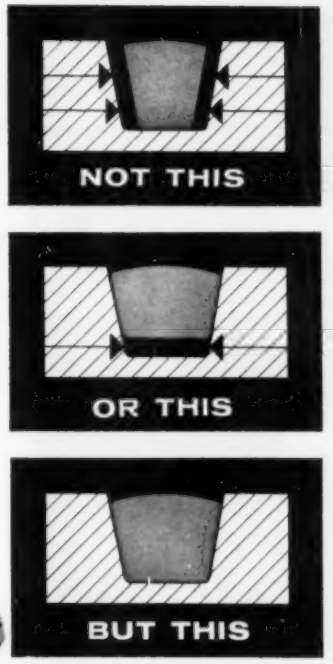

Sylvania ingots are made to fit your boat exactly for maximum yield of monocrystalline germanium in horizontal crystal growing. Poorly formed ingots result in uneven melting, increased shrinkage and greater polycrystalline formation

SEMICONDUCTOR device manufacturers can rely on a greater yield of monocrystalline germanium when they specify Sylvania ingots. The size and shape of Sylvania ingots are held to tolerances within 0.005 inch on base and radius dimensions, 0.1 inch on height, and ½ degree on taper. As a result a Sylvania ingot will fit your horizontal crystal growing boat precisely, and deter polycrystalline formation. Melting is even, surface drop is held to a minimum and shrinkage is reduced. You get a greater yield of doped single crystals and lower unit costs.

Sylvania germanium ingots are available in any one of seven standard cross sections or in designs made to your specifications. Whatever form you specify, you can count on a maximum yield from Sylvania germanium ingots. Contact your Sylvania representative for further information on precision-formed germanium or write the Chemical and Metallurgical Division directly.

SYLVANIA

SYLVANIA ELECTRIC PRODUCTS INC.
Chemical & Metallurgical Div.
Towanda, Penna.

TUNGSTEN • MOLYBDENUM • CHEMICALS • PHOSPHORS • SEMICONDUCTORS

Current Affairs

Philadelphia Meeting, May 3 to 7, 1959

E. G. Enck

Once again, The Electrochemical Society returns to its place of origin, Philadelphia, for its 115th Meeting from May 3 to 7, 1959.

For more than a year, the Convention Committees of the Philadelphia Section have been working on arrangements for the meeting. According to the latest report, the members of the various committees express satisfaction with the program and it is expected that both the social and technical schedules will prove gratifying to the large attendance that is anticipated.

The members of the Philadelphia Local Committee are: Ernest G. Enck, General Chairman; George W. Bodamer, Vice-Chairman; G. Franklin Temple, Finance; Edgar L. Eckfeldt, Hotel Arrangements; E. Charles Evers, Registration; John G. Miller, Entertainment; Harry C. Mandell, Jr., Publicity; Mrs. Ernest G. Enck, Chairman, Ladies' Program.

Convention headquarters will be in the new Sheraton Hotel, 1725 Pennsylvania Blvd. This hotel, designed primarily for large conventions, should provide the proper facilities and atmosphere for The Electrochemical Society Convention. Room reservations should be made directly with the hotel management, *as early as possible. Be sure* to mention your intention to attend The Electrochemical Society Convention.

Conveniently located to Philadelphia's shopping center and historic sites, the Sheraton is just a half hour away from International Airport and five minutes from the Pennsylvania Railroad's main station, 30th St., with connecting trains operating directly from the Concourse level of the hotel. The hotel's 1000-car garage is directly across the street and has a drive-in registration desk as well as an underground entrance to the hotel.

Old Timers Get-Together

The Philadelphia Section thinks it would be a good idea to use this meeting as an occasion for a large turnout of the Old Timers, especially for those who for some reason or another do not attend the national meetings as frequently as they did in the past. Past President Hiram S. Lukens of the Local Committee is spearheading this phase. It is planned to have special tables reserved for the Old Timers at the annual banquet on Tuesday, May 5. Come out and see your friends.

Entertainment

A program is being arranged which should give everyone an opportunity to renew old friendships and to make new ones. On Monday, all are cordially invited to attend a get-acquainted Mixer at 8:00 P.M. On Tuesday evening, because of the outstanding plans for the annual banquet, no special entertainment has been planned. On Wednesday, a most unique program has been planned. A famous river boat has been chartered for the exclusive use of the Society to provide an evening cruise on the Delaware River. During the cruise, a buffet supper will be served. Entertainment and surprises for all should make this an outstanding event of the meeting.

Ladies' Program

With a crowded schedule of technical sessions, it is important that the ladies attending the convention are not left to the mercy of shopping temptations while the men are advancing the frontiers of science. The Ladies' Committee, under the chairmanship of Mrs. Ernest G. Enck, has prepared a well-rounded program. A get-together coffee hour will start the day on Monday. In the afternoon, there will be a guided bus tour of historic Philadelphia, or an alternate visit to the University of Pennsylvania's Robert Tait McKenzie exhibit. On

Sheraton Hotel, Philadelphia, Pa.

Tuesday morning following the coffee hour, buses will leave for a luncheon to be held at the Dupont Country Club in Wilmington, Del. Following this, the ladies will visit the Henry Francis du Pont Winterthur Museum and gardens. It has been said that Winterthur represents the largest and richest assemblage of American decorative arts, especially furniture, ever brought together. On Wednesday following the usual coffee hour, buses will leave for a trip through one of the beautiful sections of suburban Philadelphia, stopping off for a visit to the Morris Arboretum. Following luncheon at the Philadelphia Cricket Club, it is planned to visit the widely known stained glass studio of Henry Lee Willets. The Philadelphia suburbs are at their best during May, and it is hoped that there will be a large attendance of ladies.

The weather at this time of the year is usually pleasant, with temperatures in the range 51°-72°F. Comfortable shoes are suggested for the enjoyment of the trips, and rain wear is also suggested "just in case"!

The Committee would be most appreciative if, when reservations are sent to the hotel, the ladies' attendance is indicated.

Complete Program

The complete program, including general information, technical sessions, and abstracts, appears on pp. 45C-76C of this issue.

Symposium on Electrode Processes

For the Philadelphia Meeting, the Theoretical Electrochemistry Division has planned a three-day Symposium on Electrode Processes, sponsored jointly by The Electrochemical Society and the Air Force Office of Scientific Research of the Air Research and Development Command. Among the speakers will be many distinguished visitors from abroad.

Presentation and Discussion

Approximately one-half of the period for each speaker will be devoted to presentation of material. The other half will cover discussion and short presentation of related unpublished material by the audience.

Extended Abstracts

Extended Abstracts of the symposium papers and the papers for the general session of the Theoretical Division will be available at $3.00 each about April 1, 1959 from: Dr. Ralph Roberts, 3308 Camalier Dr., Washington 15, D. C.

Publication

The Symposium papers will be published in a volume with the discussion. Remarks on the papers by those who do not plan to attend the meeting can be sent *before May 1, 1959* to the editor of the symposium volume: Professor Ernest Yeager, Dept. of Chemistry, Western Reserve University, Cleveland 6, Ohio.

Program

(For the complete program, including titles, see pp. 45C-76C of this issue.)

May 4

10:00 A.M.—Paul Delahay, Chairman of Symposium
10:05 A.M.—A.N. Frumkin, Institute of Electrochemistry, Academy of Sciences of the U.S.S.R., Leninsky Prospekt 31, Moscow
2:00 P.M.—Juro Horiuti, Research Institute for Catalysis, Hokkaido University, Sapporo, Japan
3:00 P.M.—K. Vetter, Fritz-Haber Institut der Max Planck Gesellschaft, Berlin-Dahlem, Germany
4:00 P.M.—R. Piontelli, G. Poli, and G. Serravalle, Laboratorio di Chimica Fisica, Elettrochimica e Metallurgia, Politecnico di Milano, Italy

May 5

9:00 A.M.—L. Gierst, Université Libre de Bruxelles, Brussels, Belgium
10:00 A.M.—Ernest Yeager, Dept. of Chemistry, Western Reserve University, Cleveland, Ohio
11:00 A.M.—J. O'M. Bockris, University of Pennsylvania, Philadelphia, Pa.
2:00 P.M.—J. Kolotyrkin, Karpov Institute for Physical Chemistry, Moscow
3:00 P.M.—D. C. Grahame (Deceased), A. E. Higinbotham, and F. R. M. Deane, Chemistry Dept., Amherst College, Amherst, Mass. (Paper to be presented by Dr. Roger Parsons of The University, Bristol, England)
3:30 P.M.—J. E. B. Randles, Chemistry Dept., University of Birmingham, England
4:15 P.M.—J. Llopis, J. Fernandez-Biarge, and M. Perez-Fernandez, Institute de Quimica Fisica Rocalolano, Serrano, Madrid, Spain

May 6

9:00 A.M.—R. A. Marcus, Dept. of Chemistry, Polytechnic Institute of Brooklyn, Brookyln, N. Y.
10:00 A.M.—K. M. Joshi, Wolfgang Mehl, and Roger Parsons, Dept. of Physical and Inorganic Chemistry, The University, Bristol, England
11:00 A.M.—B. E. Conway, Dept. of Chemistry, University of Ottawa, Ottawa, Canada
2:00 P.M.—B. Levich, Academy of Sciences of the U.S.S.R., Moscow
3:00 P.M.—Manfred Breiter, Physikalisch-chemisches und Elektrochemisches Institut der Technischen Hochschule München, München, Germany
3:45 P.M.—G. C. Barker, Atomic Energy Research Establishment, Harwell, England
4:30 P.M.—Paul Delahay, Chairman of Symposium.

December 1959 Discussion Section

A Discussion Section, covering papers published in the January-June 1959 JOURNALS, is scheduled for publication in the December 1959 issue. Any discussion which did not reach the Editor in time for inclusion in the June 1959 Discussion Section will be included in the December 1959 issue.

Those who plan to contribute remarks for this Discussion Section should submit their comments or questions in triplicate to the Managing Editor of the JOURNAL, 1860 Broadway, New York 23, N. Y. *not later than September 1, 1959*. All discussions will be forwarded to the author(s) for reply before being printed in the JOURNAL.

Symposium on Liquid Dielectrics

For the Philadelphia Meeting, the Electric Insulation Division has scheduled a symposium on Liquid Dielectrics—Gassing of Oils and Aging Studies, Factors Influencing Electrical Breakdown, and Conductivity Mechanisms—sponsored by the National Science Foundation, Office of Naval Research, and The Electrochemical Society. Among the speakers will be many distinguished visitors from abroad.

Program

(For complete program, including titles, see pp. 45C-76C of this issue.)

May 4

Gassing of Oils and Aging Studies

9:45 A.M.—H. Basseches, Chairman of Symposium

10:00 A.M.—E. H. Reynolds and S. C. Clarke, Research Organization, British Insulated Callender's Cables Ltd., London, England

10:30 A.M.—Z. Krasucki, H. F. Church, and C. G. Garton, British Electrical and Allied Industries Research Assn., Surrey, England

11:00 A.M.—George Feick and W. F. Olds, Arthur D. Little, Inc., Cambridge, Mass., and E. D. Eich, Anaconda Wire and Cable Co., Hastings-on-Hudson, N. Y.

11:30 A.M.—H. M. Stahr, General Electric Co., Hudson Falls, N. Y.

2:00 P.M.—T. Salomon, Institut Francais du Petrole, Paris, France

2:30 P.M.—K. Brinkman, Geschäftsführer der Kabelwerk Vohwinkel G.m.b.H., Wipperfürth, Rhld., Germany

3:00 P.M.—R. Strigel, Technische Universität Berlin, Berlin, Charlottenburg, Germany

May 5

Factors Influencing Electrical Breakdown

9:00 A.M.—H. Tropper, Queen Mary College, University of London, London, England

9:30 A.M.—P. Priaroggia and G. L. Palandri, Società Italiana Pirelli, Milan, Italy

10:00 A.M.—K. C. Kao (present add: English Electric Co., Ltd., Stafford, England) and J. B. Higham (present add: Pilkington Brothers, Ltd., St. Helens, Lanc., England), Electrical Engineering Dept., University of Birmingham, Birmingham, England

10:30 A.M.—E. Baumann, Technische Hochschule Fridericiana Karlsruhe, Karlsruhe, Germany

11:00 A.M.—T. J. Lewis, Queen Mary College, University of London, London, England

11:30 A.M.—T. J. Lewis

2:00 P.M.—R. Strigel, Technische Universität Berlin, Berlin-Charlottenburg, Germany

2:30 P.M.—T. W. Dakin and D. Berg, Westinghouse Electric Corp., East Pittsburgh, Pa.

3:00 P.M.—R. A. Back and C. A. Winkler, McGill University, Montreal, Canada

3:30 P.M.—T. J. Lewis, Queen Mary College, University of London

May 6

Conductivity Mechanisms

9:00 A.M.—K. A. Macfadyen and G. C. Helliwell, Dept. of Physics, The University, Edgbaston, Birmingham, England

9:30 A.M.—A. H. Sharbaugh and P. K. Watson, General Electric Co., Schenectady, N. Y.

10:00 A.M.—M. J. Morant, Queen Mary College, University of London, London, England

10:30 A.M.—O. H. LeBlanc, Jr., Research Lab., General Electric Co., Schenectady, N. Y.

11:00 A.M.—H. A. Pohl and J. P. Schwar, Plastics Lab., Princeton University, Princeton, N. J.

11:30 A.M.—H. A. Pohl and C. E. Plymale, Plastics Lab., Princeton University, Princeton, N. J.

2:00 P.M.—R. Coelho and M. Bono, Lab. for Insulation Research, Massachusetts Institute of Technology, Cambridge, Mass.

2:30 P.M.—H. T. Witt, University of Marburg, Marburg, Germany

3:00 P.M.—R. Guizonnier, University of Bordeaux, Bordeaux, France

3:30 P.M.—Andrew Patterson, Jr., and Harlow Freitag, Sterling Chemistry Lab., Yale University, New Haven, Conn.

4:00 P.M.—H. A. Pohl, Plastics Lab., Princeton University, Princeton, N. J.

Section News

Detroit Section

At a joint meeting of the Detroit Section of The Electrochemical Society and the Detroit Branch of the American Electroplaters' Society, an interested audience of 150 heard Dr. J. O'M. Bockris, from the University of Pennsylvania, talk on "The Mechanisms of Electrodeposition."

In a lucid and forthright presentation, Dr. Bockris discussed his research with "very clean" solutions and electrodes in an attempt to discover the manner in which the first layer of metal is deposited on an electrode. He presented convincing evidence indicating a difference in ion transport existing at high and at low current densities, and which involves surface diffusion of the ions over the electrode surface to reach lattice sites for crystal building.

Mr. Manual Ben, Past Chairman of the Section, is General Chairman for the Fall Meeting of The Electrochemical Society to be held in Detroit in October 1961.

S. E. Beacom, *Sec.-Treas.*

Washington-Baltimore Section

The first regular meeting of the Section was held on October 16, 1958 at the National Bureau of Standards. The meeting was held jointly with the local section of the American Electroplaters' Society. The speaker was Dr. Abner Brenner, of the National Bureau of Standards, who spoke on the topic "A Visit to Moscow." In May, Dr. Brenner attended a conference on Corrosion and the Protection of Metals which was held in Moscow under the auspices of the USSR Council of Scientific and Engineering Societies. He reported on the Conference and also on personal impressions of Moscow. About half of the lecture was devoted to showing colored slides.

The second regular meeting of the Washington-Baltimore Section was held on November 20, 1958 at the Brook Farm Restaurant. The main business of the meeting was the presentation of the first William Blum Award to Dr. William Blum. After opening remarks by the Chairman of the Section, Dr. Gwendolyn B. Wood, Dr. Edward Wichers spoke on "William Blum—The Man," and Dr. Abner Brenner on "William Blum—The Scientist." Following the presentation of the award, of $100.00 and a scroll, by Dr. Wood, Dr. Blum presented the first William Blum lecture, "The Language of Electrochemistry," in which he urged the adoption of standard conventions and nomenclature for the science of electrochemistry.

Jerome Kruger, *Secretary*

Electronics Division Enlarged Abstracts, Spring 1959

The Electronics Division again will print an "Enlarged Abstracts" booklet containing 1000-word abstracts of papers to be presented before the Electronics Division's symposia on Luminescence, Semiconductors, Thermionic Cathodes, and Electroluminescent Devices at the Philadelphia Meeting of The Electrochemical Society, May 3-7, 1959.

The booklets are expected to be ready for distribution sometime during the first two weeks of April.

The price will be *$3.50* per copy, with a discount of $1.00 per copy for orders accompanied by payment and requiring no invoicing. This is by action of the Executive Committee of the Electronics Division. *Note that orders requiring invoicing will be charged the full price even though payment accompanies order.*

Checks should be made payable to: Electronics Division, The Electrochemical Society, and should be sent to

Martin F. Quaely
c/o Westinghouse Electric Corp.
Lamp Div., Research Dept.
Bloomfield, N. J.

Extra copies, if any, will be on sale at the convention in Philadelphia.

☆ ☆ ☆

Theoretical Division Extended Abstracts, Spring 1959

The Theoretical Electrochemistry Division will print Extended Abstracts of the papers to be presented before the Symposium on Electrode Processes, sponsored jointly by The Electrochemical Society and the Air Force Office of Scientific Research of the Air Research and Development Command, and the papers to be presented at the General Session, at the Philadelphia Meeting of the Society, May 3-7, 1959.

The Extended Abstracts will be available at $3.00 each about April 1, 1959 from

Dr. Ralph Roberts
3308 Camalier Drive
Washington 15, D. C.

Division News

Electronics Division

The Nominating Committee (A. L. Smith, Chairman; L. W. Evans, A. E. Middleton) has selected the following nominees for officers of the electronics Division during the 1959-1961 term (two years):

Chairman—M. F. Quaely, Westinghouse Electric Corp., Bloomfield, N. J.

Vice-Chairman (Luminescence)—J. S. Prener, General Electric Research Lab., Schenectady, N. Y.

Vice-Chairman (Semiconductors)—P. H. Keck, Sylvania Electric Products Inc., Bayside, N. Y.

Vice-Chairman (General Electronics)—A. E. Martin, McGraw-Hill Book Co., New York, N. Y.

Secretary-Treasurer—A. E. Hardy, Radio Corp. of America, Lancaster, Pa.

Each nominee has given assurance of his willingness to serve if elected.

The Bylaws of the Division provide that additional nominations may be made by petition signed by five members of the Division. Such petitions must be in the hands of the Chairman of the Nominating Committee before the election, and the nominees must have given assurance of their willingness to serve if elected.

The election will be held at the business meeting of the Electronics Division during the Spring Meeting of the Society in Philadelphia, May 3-7, 1959.

M. F. Quaely, *Sec.-Treas.*

Electrothermics and Metallurgy Division

The Nominating Committee (B. W. Gonser, Chairman; I. E. Campbell, A. C. Haskell) reports that the following have been nominated as candidates for officers of the Electrothermics and Metallurgy Division, to be elected during the Spring Meeting of the Society in Philadelphia, May 3-7, 1959:

Chairman—G. M. Butler, Carborundum Co., Niagara Falls, N. Y.

Vice-Chairman—J. H. Westbrook, General Electric Co., Schenectady, N. Y.

Vice-Chairman—E. M. Sherwood, Battelle Memorial Institute, Columbus, Ohio.

Secretary-Treasurer—L. H. Juel, Great Lakes Carbon Corp., Niagara Falls, N. Y.

Members-at-Large—M. A. Steinberg, W. E. Kuhn, E. W. Johnson, L. M. Litz.

B. W. Gonser, *Chairman Nominating Committee*

New Members

In January 1959, the following were approved for membership in The Electrochemical Society by the Admissions Committee:

Active Members Sponsored by a Sustaining Member

J. G. Buck, Erie Resistor Corp., 644 W. 12 St., Erie 6, Pa. (Electronics)

H. M. Schillbach, Allen-Bradley Co., 136 W. Greenfield, Milwaukee 4, Wis. (Electronics)

Active Members

P. H. Arnold, Accumulatoren-Fabrik A. G., Stockener-Str. 351, Hannover-Stocken, Germany (Battery)

A. C. Beer, Battelle Memorial Institute, 505 King Ave., Columbus 1, Ohio (Electronics)

E. J. Bielecki, Kawecki Chemical Co.; Mail add: 310 E. 6 St., Boyerton, Pa. (Electrothermics & Metallurgy)

L. G. Bockstie, Jr., Philco Corp.; Mail add: 7818B Penrose Ave., Elkins Park 17, Pa. (Battery)

W. S. Bundy, Research Labs., National Lead Co., 105 York St., Brooklyn 1, N. Y. (Theoretical Electrochemistry)

E. J. Comeau, Jr., W. R. Grace, Dewey & Almy Chemical Div.; Mail add: Lovejoy Rd., Andover, Mass. (Battery)

G. B. Cooper, Jones & Laughlin Steel Corp., 900 Agnew Rd., Pittsburgh 30, Pa. (Electrodeposition)

G. L. Cornwell, Exolon Co., Thorold, Ont., Canada (Theoretical Electrochemistry)

G. A. Dalin, Yardney Labs.; Mail add: 1563 Van Ness Terrace, Union, N. J. (Battery)

E. D. Dilling, Titanium Metals Corp. of America; Mail add: 1811 Cochran St., Las Vegas, Nev. (Electrodeposition)

N. J. Egli, Allegheny Electronic Chemicals Co.; Mail add: 41 Orchard Place, Bradford, Pa. (Electronics)

O. L. Forchheimer, General Abrasive Co., Inc., Niagara Falls, N. Y. (Electrothermics & Metallurgy)

G. W. Fust, Thiokol Chemical Co.; Mail add: 410½ So. Plymouth Rd.,

By action of the Board of Directors of the Society, all prospective members must include first year's dues with their applications for membership.

Also, please note that, if sponsors sign the application form itself, processing can be expedited considerably.

Third Printing of "Vacuum Metallurgy" Now Available

The third printing of "Vacuum Metallurgy," edited by J. M. Blocher, Jr., of Battelle Memorial Institute, is now available from Society Headquarters, 1860 Broadway, New York 23, N. Y., at the price of $5.00, less a 20% discount to ECS members.

The 216-page book, in hard paper binding, contains papers presented at the Vacuum Metallurgy Symposium held in Boston, Mass., October 6 and 7, 1954.

Sponsored by the Electrothermics and Metallurgy Division of The Electrochemical Society, this symposium brought together, for the first time, those interested in the relation of vacuum to metallurgy.

In the keynote address, J. D. Nisbet, director of research of the Universal-Cyclops Steel Corp., outlines the rapid progress in this field, together with a consideration of what the future may hold. Eighteen papers follow on vacuum melting, vacuum heat treating, vacuum distillation of metals, and on new apparatus. A valuable review of the present status of theory and techniques for the determination of the vapor pressures of metals and alloys is included.

Huntsville, Ala. (Electrodeposition, Electro-Organic, Electrothermics & Metallurgy, Theoretical Electrochemistry)

Robert Fyfe, W. Canning & Co., Ltd., 137 Great Hampton St., Birmingham, England (Corrosion, Electrodeposition, Electro-Organic, Theoretical Electrochemistry)

E. A. Gootman, Handy & Harman; Mail add: Newton Ave., Norwalk, Conn. (Battery)

L. L. Gruss, Frankford Arsenal; Mail add: 7201 Revere St., Apt. E10, Philadelphia 49, Pa. (Electronics)

Hans Haug, P. R. Mallory & Co., Inc.; Mail add: 1730 No. Graham Ave., Indianapolis 18, Ind. (Corrosion, Electric Insulation, Electrodeposition, Electronics)

F. R. Hays, U. S. Radium Corp., Whippany, N J. (Electronics)

E. L. Henderson, University of Detroit, 4001 W. McNichols Rd., Detroit 21, Mich. (Theoretical Electrochemistry)

Edward Hines, Detroit Edison Co., 2000 Second Ave., Detroit 26, Mich. (Electric Insulation)

Richard Huber, Petrix-Union G.m.b.H.; Mail add: Marienstr. 20, (14a) Ellwangen/Jagst, W. Germany (Battery)

B. G. Koehl, Battelle Memorial Institute, 505 King Ave., Columbus 1, Ohio (Corrosion)

Herman Koretzky, I.B.M. Corp., c/o General Delivery, Yorktown Heights, N. Y. (Electrodeposition, Theoretical Electrochemistry)

Frank Lawson, School of Metallurgy, University of N.S.W., Kensington, N.S.W., Australia (Electrothermics & Metallurgy, Theoretical Electrochemistry)

J. D. Lawyer, Tinker Airforce Base; Mail add: RR 1, Box 14 K, Choctaw, Okla. (Electrodeposition, Theoretical Electrochemistry)

Sing Bay Li, Sperry Semiconductor Div.; Mail add: 12 Arbor Dr., South Norwalk, Conn. (Electronics)

Louis Meyerhoff, Research Lab., General Cable Corp., 236 W. First St., Bayonne, N. J. (Electric Insulation)

T. O. Mumper, Lindberg Engineering Co.; Mail add: Harts Lane, Conshohocken, Pa. (Electronics)

I. L. Newell, Henry Souther Engineering Co., 11 Laurel St., Hartford 6, Conn. (Electrodeposition)

J. A. Peterson, Hooker Chemical Corp.; Mail add: 812-87 St., Niagara Falls, N. Y. (Industrial Electrolytic)

E. R. Piatti, Lignes Telegraphiques et Telephoniques Lab., 223 Av. Pierre Brossolette, Montrouge (Seine), France (Corrosion, Electric Insulation, Electrodeposition, Electronics, Electrothermics & Metallurgy, Industrial Electrolytic, Theoretical Electrochemistry)

Egons Rasmanis, CBS-Hytron; Mail add: 6 Greenwood Rd., Burlington, Mass. (Electronics)

Harry Robbins, Hughes Aircraft Co.; Mail add: 2919 W. 139 Place, Gardena, Calif. (Electronics)

T. H. Venkata Setty, University of Mysore; Mail add: First Grade College, Tumkur, Mysore State, So. India (Electrodeposition, Theoretical Electrochemistry)

G. A. Silvey, Research Lab., I.B.M. Corp., Bldg. 701, Poughkeepsie, N. Y. (Electric Insulation, Electronics)

J. A. Sluss, Jr., Lansdale Tube Co., Div. of Philco Corp., Lansdale, Pa. (Electronics)

A. R. Smith, Jr., Cochran Foil Corp., P.O. Box 1654, Louisville, Ky. (Electric Insulation, Electrodeposition, Electrothermics & Metallurgy, Industrial Electrolytic)

R. J. Stamets, General Electric Co., Bldg. 8-4, Hudson Falls, N. Y. (Theoretical Electrochemistry)

J. S. Taylor Aluminum Co. of Canada Ltd., Beauharnois, P. Q., Canada (Industrial Electrolytic)

A. B. Tillman, Diamond Alkali Co., 300 Union Commerce Bldg., Cleveland, Ohio (Industrial Electrolytic)

R. T. Trebing, Lindberg Engineering Co.; Mail add: 2299 Scott Rd., Northbrook, Ill. (Electronics)

G. J. Trudeau, Aluminum Co. of Canada, c/o Alcan P.O. Box 127, Shawinigan, Que., Canada (Electrothermics & Metallurgy, Industrial Electrolytic, Theoretical Electrochemistry)

S. S. Wagle, Standard Batteries Ltd.; Mail add: Rm. 108, 4th floor, Old Hanuman Bldg., Kiln Ln, Proctor Rd., Bombay 7, India (Battery)

R. D. Wales, Lockheed Missile Systems Div.; Mail add: 2418 Thaddens Dr., Mountain View, Calif. (Battery, Theoretical Electrochemistry)

R. P. Yeck, Central Research Labs., American Smelting & Refining Co., So. Plainfield, N. J. (Electrodeposition)

Rèné Zwobada, Lignes Telegraphiques et Telephoniques, 223 Av. Pierre Brosselette, Montrouge (Seine), France (Electronics)

E. G. Tsumura, Hughes Aircraft Co.; Mail add: 14630 Budlong Ave., Apt. #B, Gardena, Calif. (Corrosion, Electrodeposition, Electronics, Electrothermics & Metallurgy)

Associate Members

O. P. Webb, Burgess Battery Co.; Mail add: 416 Sunset Ave., Rockford, Ill. (Battery, Electro-Organic)

Harry Rosenberg, Hughes Aircraft Co.; Mail add: 10234-10th Ave., Inglewood 4, Calif. (Electric Insulation, Electronics, Theoretical Electrochemistry)

Notice to Members

According to the Constitution of the Society, Article III, Section 9, "Any member delinquent in dues after April 1 of each year shall no longer receive the Society's publications . . . ." Such delinquents will not receive the May issue of the JOURNAL. A reminder notice was mailed to delinquents about the middle of February; a final notice will go out the middle of March.

Student Associate Members

B. L. Chamberland, University of Pennsylvania; Mail add: 3622 Chestnut St., Philadelphia 4, Pa. (Electronics)

R. P. Frosch, Union College 88, Schenectady, N. Y. (Theoretical Electrochemistry)

D. W. James, Rensselaer Polytechnic Institute; Mail add: 3-3 Edgehill Terrace, Troy, N. Y. (Theoretical Electrochemistry)

Michael Miller, Union College; Mail add: 1017 Glenwood Blvd., Schenectady 8, N. Y. (Theoretical Electrochemistry)

F. A. Muller, Union College; Mail add: 528 Summit Ave., Schenectady, N. Y. (Electronics, Theoretical Electrochemistry)

Reinstatement to Active Membership

J. W. Nash, Battelle Memorial Institute; Mail add: 5526 Riverside Dr., Dublin, Ohio (Corrosion, Electrothermics & Metallurgy, Industrial Electrolytic)

Transfers from Associate to Active Membership

S. L. Cooke, Jr., Research Instruments Corp., 18 So. 12 St., Richmond, Va. (Electronics, Electro-Organic)

W. S. Harris, U. S. Naval Ordnance Lab.; Mail add: P.O. Box 146, Norco, Calif. (Battery, Electro-Organic, Theoretical Electrochemistry)

R. E. Henriks, Hughes Products; Mail add: 29635 Enrose Ave., San Pedro, Calif. (Electronics)

H. E. Munns, Diamond Alkali Research Center, P.O. Box 348, Painesville, Ohio (Electrodeposition, Electrothermics & Metallurgy, Industrial Electrolytic)

R. A. Parker, National Bureau of Standards, Section 5.2, Washington 25, D. C. (Theoretical Electrochemistry)

Transfers from Student Associate to Active Membership

Sheldon Evans, Continental Can Co., C.R.&E., 7622 So. Racine Ave., Chicago 20, Ill. (Corrosion, Theoretical Electrochemistry)

A. M. Wilson, Dept. of Chemistry, Wayne State University, Detroit 2, Mich. (Theoretical Electrochemistry)

Transfer from Student Associate to Associate Membership

Herman Wissenberg, Electro Metallurgical Co.; Mail add: 65 Kies Court, Niagara Falls, N. Y. (Electrodeposition)

Deceased Members

J. H. Bower, Berkley Heights, N. J.
W. M. Fotheringham, Buffalo, N. Y.
F. P. Gilligan, Hartford, Conn.
Alastair McLeod, London, England
G. J. Shiple, Detroit, Mich.
E. A. Vuilleumier, Carlisle, Pa.
E. D. Wilson, Worcester, Mass.

News Items

Stress Corrosion Conference

On April 2 and 3, 1959, the Metallurgical Society of AIME will sponsor the National Conference on the Physical Metallurgy of Stress Corrosion Fracture, in cooperation with NACE, ASTM, and The Electrochemical Society. The conference will be held at the Mellon Institute, Pittsburgh, Pa., and inquiries concerning registration should be directed to: Professor William R. Bitler, Dept. of Metallurgical Engineering, Carnegie Institute of Technology, Pittsburgh 13, Pa.

In view of the anticipated wide interest in the conference and the limited capacity of the hall (about 450), those interested in attending are urged to pre-register. The proceedings of the conference will be published as a monograph with preprints available at no additional cost to pre-registrants. The complete program is presented here.

Session I (9:00 A.M.)
Introduction and Theoretical Aspects of Stress, Corrosion, and Fracture
Discussion Chairman, G. M. Pound

"Brief Remarks on Objectives of Conference" by T. N. Rhodin
"New Perspectives in the Stress Corrosion Problem" by H. H. Uhlig
"Characteristics of Stress Corrosion Cracking" by A. W. Dana
"Relationships of Microstructure to Fracture" by J. Gilman
"Elastic Stress and Chemical Potentials" by Ling Yang, G. T. Horne, and G. M. Pound
"Surface Structure and Chemical Interaction" by D. Turnbull and G. Ehrlich

Session II (2:30 P.M.)
Experimental Aspects of Stress, Corrosion, and Fracture
Discussion Chairman, H. H. Uhlig

"Propagation of Stress Corrosion Cracks" by C. Edeleanu
"Effect of Stress and Environment on the Microtopology of the Corrosion Product" by E. A. Gulbransen and T. Copon
"Role of the Corrosion Product" by N. A. Nielsen

Session III (9:00 A.M.)
Physical Metallurgical Aspects of Stress Corrosion

Part 1. Discussion Chairman, F. L. LaQue

"Stress Corrosion Cracking of Single Crystals of Stainless Steel" by H. Paxton
"Electrochemical Aspects of Stress Corrosion" by H. J. Engell
"Dependence of a Stress Corrosion Cracking Susceptibility on Age-Hardening in a Copper-Nickel-Silicon Alloy" by W. D. Robertson, E. G. Grenier, W. Davenport, and V. Nole
"Mechanisms of Stress Corrosion of Stainless Steels and Other Materials by High-Temperature Chloride Waters and by Hot Salts" by M. G. Fontana
"The Phenomena of Fissuration and Fracture in Steel in the Presence of Hydrogen" by P. G. Bastien

Session IV (2:30 P.M.)
Physical Metallurgical Aspects of Stress Corrosion
Discussion Chairman, E. J. Kreh

"Effect of Composition on Stress Corrosion Cracking of Some Alloys Containing Nickel" by H. R. Copson
"Crack Propagation in Ductile Crystals and Its Bearing of Stress Corrosion" by A. J. Forty
"Stress Corrosion Cracking in Low Carbon Steel" by H. L. Logan
"Summary and Comments on Conference" by L. R. Sharfstein.

New Sustaining Members

The following recently became Sustaining Members of The Electrochemical Society:
Allen-Bradley Co., Milwaukee, Wis.
Basic Inc., Maple Grove, Ohio
Hill Cross Co., Inc., New York, N. Y.
New York Air Brake Co., Vacuum Equipment Div., Camden, N. J.

Frontiers in Chemistry Lecture Series

The 18th annual Frontiers in Chemistry lectures, an activity of the Dept. of Chemistry of Western Reserve University, Cleveland, Ohio, began on February 13 and will continue through April 24. The 18th annual series covers two major topics: Part I. Modern Instrumental Methods, and Part II. Recent Advances in Organic Reactions.

The Lepel line of induction heating equipment represents the most advanced thought in the field of electronics as well as the most practical and efficient source of heat yet developed for numerous industrial applications.
If you are interested in induction heating you are invited to send samples of the work with specifications. Our engineers will process and return the completed job with full data and recommendations without any cost or obligations.

FLOATING ZONE FIXTURE FOR METAL REFINING AND CRYSTAL GROWING

A new floating zone fixture for the production of ultra-high purity metals and semi-conductor materials. Purification or crystal growing is achieved by traversing a narrow molten zone along the length of the process bar while it is being supported vertically in vacuum or inert gas. Designed primarily for production purposes, Model HCP also provides great flexibility for laboratory studies.

Features

- A smooth, positive mechanical drive system with continuously variable up, down and rotational speeds, all independently controlled.
- An arrangement to rapidly center the process bar within a straight walled quartz tube supported between gas-tight, water-cooled end plates. Placement of the quartz tube is rather simple and adapters can be used to accomodate larger diameter tubes for larger process bars.
- Continuous water cooling for the outside of the quartz tube during operation.
- Assembly and dis-assemby of this system including removal of the completed process bar is simple and rapid.

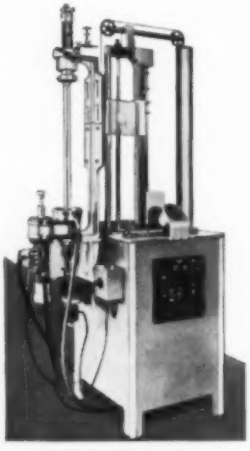

Model HCP

Electronic Tube Generators from 1 kw to 100 kw.
Spark Gap Converters from 2 kw to 30 kw.

WRITE FOR THE NEW LEPEL CATALOG . . . 36 illustrated pages packed with valuable information.

All Lepel equipment is certified to comply with the requirements of the Federal Communications Commission.

LEPEL HIGH FREQUENCY LABORATORIES, INC.
55th STREET and 37th AVENUE, WOODSIDE 77, NEW YORK CITY, N. Y.

The lectures are scheduled on consecutive Fridays, with the exception of March 27 and April 17. In addition to the Friday evening lectures, a special Saturday session will be held on April 18 on "Nuclear Magnetic and Electron Paramagnetic Resonance."

The complete program follows.

Part I

Feb. 13—"Nucleonics in Analytical Chemistry" by G. W. Leddicotte
Feb. 27—"Infrared Spectra of Chemisorbed Molecules" by R. P. Eischens
March 13—"Organic Polarography" by Stanley Wawzonek
April 3—"Recent Study of the Atomic Structure of Metal Surfaces by Field Emission Microscopy" by Erwin Mueller
April 18 (A.M.)—"Instrumentation and Chemical Applications of High Resolution Nuclear Magnetic Resonance" by J. N. Shoolery
April 18 (P.M.)—"Electron Spin Resonance of Free Radicals" by S. I. Weissman

Part II

Feb. 20—"Autoxidation" by F. R. Mayo
March 6—"Recent Advances in Organometallic Chemistry" by R. A. Benkeser
March 20—"The Problem of Stereochemical Control in Multistep Synthesis" by W. S. Johnson
April 10—"Methylenes as Intermediates in Organic Chemistry" by J. S. Hine
April 24—"Selective Reductions and Hydroboration" by H. C. Brown.

1959 Appalachian Underground Corrosion Short Course

The program for the 1959 Appalachian Underground Corrosion Short Course, which will be held at West Virginia University, June 2, 3, and 4, 1959, is being planned. The present agenda calls for 64 classes and field demonstrations. The school covers basic, intermediate, and advanced education on the following:

(*A*) Fundamentals of underground metallic corrosion and corrosion control practices as related to underground pipe and cable systems. This phase covers 32 one and one-half hour classes.

(*B*) Water—Internal and external corrosion of metallic water systems and corrosion control measures; 8 classes.

(*C*) Coatings—Corrosion control materials and material control practices; 8 classes.

(*D*) Special—Instrumentation, ma-

terials, and test procedures; 16 classes.

There are 4 class periods a day from which students attending can choose. It is planned to show movies during the evening in the Field House where the exhibits are set up.

A final program will be published at a later date.

Sylvania Announces Profitable Germanium Scrap Plan

Sylvania Electric Products Inc. is offering manufacturers of semiconductor devices a new cost-saving plan for converting germanium scrap.

As a leading supplier of semiconductor materials, Sylvania's volume processing methods make it possible to return high-purity germanium ingots or cut pieces with a minimum resistivity of 40 ohms cm, regardless of the percentage of germanium in the scrap.

Details of the new Sylvania plan can be obtained from Sylvania Electric Products Inc., Towanda, Pa.

Committee Named to Study Scientific Agencies of Commerce

Appointment by the National Academy of Sciences of a special committee of scientists and research administrators to study the scientific programs of the U. S. Dept. of Commerce, and to recommend new steps to gear them to the rapidly changing needs of science and industry, was announced recently by L. L. Strauss, Secretary of Commerce, and Dr. D. W. Bronk, president of the National Academy of Sciences-National Research Council. Dr. M. J. Kelly, board chairman of Bell Telephone Labs., will head the committee.

Other members of the committee are Professor H. R. Byers, Dept. of Meteorology, University of Chicago; Dr. H. A. Leedy, Armour Research Foundation, Illinois Institute of Technology, Chicago; Dr. C. G. Suits, vice-president and director of research, General Electric Co. Research Labs., Schenectady, N. Y.; Professor Abel Wolman, Johns Hopkins University, Baltimore; Dr. Augustus Kinzel, vice-president (research), Union Carbide Corp., New York City; Dr. Michael Ference, Jr., director of engineering staff, Ford Motor Co., Dearborn, Mich.; and F. W. Herring, deputy director for comprehensive planning, Port of New York Authority, New York City. J. C. Green, Director of Commerce's Office of Technical Services, has been named executive secretary.

Secretary Strauss and Dr. Bronk stated that the committee will study the requirements of science and industry for services of the type the Dept. of Commerce can provide, new or improved means of meeting these requirements, and assured methods of relating the Department's programs to the improving techniques afforded by scientific and technological progress.

Commerce agencies under study include the Bureau of Public Roads, Maritime Administration, Patent Office, Weather Bureau, Coast and Geodetic Survey, National Bureau of Standards, and Office of Technical Services.

The committee will spend several months reviewing the operations of these agencies. The committee plans to submit a report to the Secretary of Commerce about June 1.

Address of the committee is: Special Advisory Committee to Dept. of Commerce, National Academy of Sciences, 2101 Constitution Ave., N. W., Washington, D. C.

The National Academy of Sciences-National Research Council is a private organization of distinguished scientists dedicated to the furtherance of science and its application to the general welfare. Under its Congressional Act of Incorporation, it is called on to advise the Federal Government, on request, on all matters of scientific and technical interest.

Ferroelectric Polarization Reversal in Barium Titanate

Recent experiments on single-crystal barium titanate have demonstrated for the first time that complete ferroelectric polarization reversal can be accomplished under an applied electric field, with a single expanding domain which grows through extensive sidewise motion of the 180° domain walls. These experiments were described in a paper by R. C. Miller, of Bell Telephone Labs., which was presented to the Conference on the Physics of Dielectrics at Moscow on November 26, 1958. It was one of the first foreign papers presented to this meeting, and was read by P. W. Anderson, also of Bell Labs.

JOURNAL ELECTROCHEMICAL SOCIETY

Wanted to Buy.
Back sets, volumes, and issues of this JOURNAL and TRANSACTIONS.
Especially volumes 1, 3 and from volume 60 to date.
We pay good prices.
Buy also Technical and Scientific Periodicals.
E. O. ASHLEY, 27 E. 21 St., New York 10, N. Y.

ELECTROCHEMISTS
PHYSICAL CHEMISTS
B.S. — M.S. — PH. D.

POSITIONS OPEN IN BASIC RESEARCH AND DEVELOPMENT WORK ON NEW BATTERY TYPES. EXPERIENCE OF 3 TO 5 YEARS DESIRED ON OTHER THAN LEAD-ACID BATTERIES.

BATTERY CHEMISTS
OR ENGINEERS

POSITIONS OPEN FOR MEN EXPERIENCED IN NICKEL-CADMIUM AND/OR SILVER-ZINC BATTERY DEVELOPMENT.

All inquiries will be held confidential.
Address inquiries with résumé to

M. J. Cavanaugh, Director of Salaried Personnel
Delco-Remy Division, General Motors Corp.
Anderson, Indiana Dept. 135A

Very little work has been reported previously on sidewise motion of 180° domain-walls in ferroelectrics. These 180° domain-walls are the boundaries between two adjacent areas or domains of opposite polarization. Sidewise motion involves the movement of boundaries in a direction perpendicular to the dipole moment of the domain. In Dr. Miller's work, a single crystal of $BaTiO_3$ is mounted with liquid electrodes applied to either side, and is subjected to an external applied field. The electrodes used were silver or platinum rods 1.0 mm in diameter, with a small hole drilled in one end. An aqueous lithium chloride solution, saturated at room temperature, was placed in the hole as the electrolyte.

Partially switched crystals were studied by removing them from the apparatus and etching them for a short time in weak hydrofluoric acid. The positive dipole ends etch preferentially; examination with a microscope after etching allows one to observe the domains visually.

With the liquid electroded crystals, the number and size of the reversed domains in the partially switched crystals was of great interest. In numerous cases, a single reversed domain comparable in size to the total electrode area was observed. Many of the domains appeared to nucleate at obvious crystalline imperfections.

In a further refinement of the technique, Dr. Miller took advantage of this nucleation phenomenon by "manufacturing" a nucleation site. This site was a sandblasted dimple about 1/3 the crystal thickness deep, and with a diameter about 1/4 that of the electrode.

When a dimpled sample is placed in the liquid electrode holder, nucleation of reversed domains is most probable in the dimpled region because it is subjected to a high field compared to that of the surrounding area. Once a nucleation has occurred in the dimpled region, the domain grows out from the dimple through sidewise wall motion. The single domain is roughly square, as has been shown by successive etching of the partially switched crystal. In this way, complete reversal of polarization has been accomplished for the first time with a single expanding domain, starting from a predetermined point on the crystal.

There is some evidence to indicate that impurities have an effect on the velocity of the domain wall motion, but the evidence is meager. The experiments performed here indicate that the velocity is given by the equation

$$v = v_\infty e^{\beta/E}$$

for over three decades of velocity. The velocity for the field $E = \infty$ is v_∞, and is of the order of 10 cm/sec. The activation field varies from 2000 to 4000 v/cm.

It appears that, under these conditions, this polarization reversal is analogous to magnetization reversal in some ferromagnetic materials.

Union Carbide's Metals Division Changes Name

Union Carbide Corp. has announced a new name for its metals division. Electro Metallurgical Co. becomes Union Carbide Metals Co.

This change of name is another step in the program initiated by Union Carbide Corp. in 1957 designed to identify all of its divisions more closely with the parent corporation. In 1957, Union Carbide Corp. shortened its name from Union Carbide and Carbon Corp. and created the Union Carbide hexagon symbol.

As Electro Metallurgical Co., the firm was the pioneer producer of ferroalloys for use in the production of iron and steel, having been founded in 1906. Today, Union Carbide Metals Co. is the major producer of ferroalloys, metals, and other metallurgical products for the iron, steel, and nonferrous metal industries.

Literature from Industry

Dow Corning Silicone Products Guide. The 1959 Reference Guide to Dow Corning silicone products describes what silicones can best meet the needs of an unbelievable variety of problems ranging from adhesives to release agents, resins to rubbers, dielectrics to water repellents.

This 16-page, up-to-date reference guide is heavily illustrated and features an expanded indexing system to facilitate quick and easy location of the more than 150 Dow Corning silicone products now commercially available.

For copies write to Dow Corning Corp., Midland, Mich.

Button Cell Battery Brochure. Publication of a brochure on the smallest, most complete line of button cell batteries has been announced by Gulton Industries, Inc. The four-page, colored and illustrated bro-

Tektronix, Inc.

Portland, Oregon

A manufacturer of universal recognition in cathode ray oscilloscopes and allied instrumentation, Tektronix is continually seeking to advance the oscilloscope art. To this end we rely on internal design of fundamental components as well as complete instruments.

Creative physicists and engineers with experience in vacuum and cathode-ray tube design, semi-conductor research, and circuit design will be interested in a program of major expansion in our Engineering Division.

For further information please contact Mr. Robert Mitchell, Barbizon-Plaza Hotel, New York City, March 20, 21 and 23 through 27.

chure highlights the features, design potentials, and specifications of the VO-Series, nickel cadium, button cell battery line which includes types from 100 MAH to 1750 MAH capacities in more than 50 distinct sizes and voltages. The rechargeable, hermetically sealed cells are produced by the Alkaline Battery Div., Gulton Industries, Inc.

Copies of the brochures are available from Sales Manager, Alkaline Battery Div., Gulton Industries, Inc., Metuchen, N. J. Specify Bulletin No. VO-110, VO-Series, Button Cell Batteries.

Bulletin on Germanium. A technical information bulletin, which describes the physical characteristics and purity standards of germanium dioxide used in the manufacture of semiconductor devices, has been made available by Sylvania Electric Products Inc. The new booklet lists the minimum resistivity specifications of electronic-grade germanium measured with a 4-point probe at 25°C, and, in addition, includes data on the specifications and chemical characteristics of the finished product.

A major producer of silicon and germanium, Sylvania's Chemical and Metallurgical Div. is one of the few suppliers of both semiconductor materials.

Copies of the new bulletin may be obtained from Sylvania Electric Products Inc., Towanda, Pa.

Employment Situations

Please address replies to box shown, c/o The Electrochemical Society, Inc., 1860 Broadway, New York 23, N. Y.

Position Wanted

Physical Chemist, Ph.D. 1958, desires research position in electrochemistry and/or solid state. Strong instrumentation background; research experience; publications; honor societies. Will consider position in New York City or Metropolitan New Jersey area only. *Reply to Box 365.*

Positions Available

Electrochemist—Qualified chemist to investigate physics and chemistry of aluminum and tantalum capacitors. Direct or closely related experience required. Opportunity to participate in all phases of development. Send complete resumé to: Peter P. Grad, Technical Director, Aerovox Corp., New Bedford, Mass.

Science or Engineering Graduate, B.S. minimum to do electroplating research, modern laboratory, suburban Pittsburgh. Experience desirable but not necessary. *Reply to Box A-279.*

Engineers (Aeronautical, Electrical, Electronic, Industrial, General, Mechanical, and Power Plant), **Electronic Scientists, Metallurgists, Physicists, Technologists**—Vacancies exist for professional personnel in the above positions. Starting salaries range from $4490 per annum to $10,130 per annum. The Naval Air Material Center is currently engaged in an extensive program of aeronautical research, development, experimentation, and test operations for the advancement of Naval aviation. Experimental work also is being conducted in the guided missile field. Personnel are needed for work on projects involving modification, overhauling, and testing of aeronautical equipment, materials, accessories, power plants, launching and arresting devices, and for modification and structural testing of aircraft. Also, for work involving the basic design of catapults, launchers, arresting gear and their component parts; test and development work at shore stations and on board U. S. Navy ships; evaluation of new equipment and establishment of performance parameters, and applied research on the many problems relevant to this field.

Interested persons should file an Application for Federal Employment, Standard Form 57, with the Industrial Relations Dept., Naval Air Material Center, Naval Base, Philadelphia 12, Pa. Applications may be obtained from the above address or information as to where they are available may be obtained from any first or second class post office.

Advertiser's Index

Bell Telephone Laboratories, Inc.	44C
Enthone, Incorporated	Cover 4
General Motors Corp., Delco-Remy Division	85C
Grace Electronic Chemicals, Inc.	41C
Great Lakes Carbon Corp., Electrode Division	Cover 2
Hughes Aircraft Company	43C
Keithley Instruments, Inc.	40C
Lepel High Frequency Laboratories, Inc.	84C
Lockheed Missiles & Space Division	87C
Sylvania Electric Products Inc.	77C
Tektronix, Inc.	86C

ELECTRO-CHEMISTRY

EXPANDING THE FRONTIERS OF SPACE TECHNOLOGY

Solid state activities in electrochemistry play a highly important role at Lockheed in overcoming difficult problems in test, materials research, metallurgy and other related fields.

Special emphasis is directed to the development of high-energy batteries and fuel cells, and related fuel research in electrode reaction kinetics and materials synthesis by electrochemical methods and vacuum deposition. In the solution of complex electrochemical problems, Lockheed's scientists and engineers are instrumental in developing products that will serve both government and commercial use.

As weapons systems manager for such major, long-term projects as the Navy Polaris FBM; Discoverer Satellite; Army Kingfisher; Air Force Q-5 and X-7; and other important research and development programs, Lockheed is engaged in expanding the frontiers of technology in all areas.

The advanced nature of Lockheed's projects in electrochemistry provides an excellent opportunity for high level scientists and engineers to advance their professional status and offer an ideal environment for working conditions. You are invited to share in a company that has a history of continual progress and play an important role in the development of space technology. Write: Research and Development Staff, Dept. C-26, 962 W. El Camino Real, Sunnyvale, California.

"The organization that contributed most in the past year to the advancement of the art of missiles and astronautics." NATIONAL MISSILE INDUSTRY CONFERENCE AWARD.

Lockheed
MISSILES AND SPACE DIVISION

SUNNYVALE, PALO ALTO, VAN NUYS, SANTA CRUZ, SANTA MARIA, CALIFORNIA
CAPE CANAVERAL, FLORIDA
ALAMOGORDO, NEW MEXICO

The Electrochemical Society

Patron Members

Aluminum Co. of Canada, Ltd.,
Montreal, Que., Canada
International Nickel Co., Inc.,
New York, N. Y.
Olin Mathieson Chemical Corp.,
Niagara Falls, N. Y.
Industrial Chemicals Div., Research
and Development Dept.
Union Carbide Corp.
Divisions:
Union Carbide Metals,
New York, N. Y.
National Carbon Co., New York, N. Y.
Westinghouse Electric Corp., Pittsburgh, Pa.

Sustaining Members

Air Reduction Co., Inc.,
New York, N. Y.
Ajax Electro Metallurgical Corp.,
Philadelphia, Pa.
Allen-Bradley Co., Milwaukee, Wis.
Allied Chemical & Dye Corp.
General Chemical Div., Morristown, N. J.
Solvay Process Div., Syracuse, N. Y.
(3 memberships)
Allied Research Products, Inc.,
Detroit, Mich.
Alloy Steel Products Co., Inc., Linden, N. J.
Aluminum Co. of America,
New Kensington, Pa.
American Machine & Foundry Co.,
Raleigh, N. C.
American Metal Co., Ltd.,
New York, N. Y.
American Potash & Chemical Corp.,
Los Angeles, Calif. (2 memberships)
American Zinc Co. of Illinois,
East St. Louis, Ill.
American Zinc, Lead & Smelting Co.,
St. Louis, Mo.
American Zinc Oxide Co., Columbus, Ohio
M. Ames Chemical Works, Inc.,
Glens Falls, N. Y.
Auto City Plating Company Foundation,
Detroit, Mich.
Basic Inc., Maple Grove, Ohio
Bell Telephone Laboratories, Inc.,
New York, N. Y. (2 memberships)
Bethlehem Steel Co., Bethlehem, Pa.
(2 memberships)
Boeing Airplane Co., Seattle, Wash.
Burgess Battery Co., Freeport, Ill.
(4 memberships)
C & D Batteries, Inc., Conshohocken, Pa.
Canadian Industries Ltd., Montreal, Que.,
Canada
Carborundum Co., Niagara Falls, N. Y.
Catalyst Research Corp., Baltimore, Md.
Chrysler Corp., Detroit, Mich.
Ciba Pharmaceutical Products, Inc., Summit,
N. J.
Columbian Carbon Co., New York, N. Y.
Columbia-Southern Chemical Corp.,
Pittsburgh, Pa.
Consolidated Mining & Smelting Co. of
Canada, Ltd., Trail, B. C., Canada
(2 memberships)
Continental Can Co., Inc., Chicago, Ill.
Cooper Metallurgical Associates, Cleveland,
Ohio
Corning Glass Works, Corning, N. Y.
Crane Co., Chicago, Ill.
Diamond Alkali Co., Painesville, Ohio
(2 memberships)
Dow Chemical Co., Midland, Mich.
Wilbur B. Driver Co., Newark, N. J.
(2 memberships)
E. I. du Pont de Nemours & Co., Inc.,
Wilmington, Del.
Eagle-Picher Co., Chemical Div., Joplin, Mo.
Eastman Kodak Co., Rochester, N. Y.
Electric Auto-Lite Co., Toledo, Ohio
Electric Storage Battery Co.,
Philadelphia, Pa.
Englehard Industries, Inc., Newark, N. J.
(2 memberships)
The Eppley Laboratory, Inc., Newport, R. I.
(2 memberships)
Erie Resistor Corp., Erie, Pa.
Fairchild Semiconductor Corp., Palo Alto,
Calif.
Federal Telecommunication Laboratories,
Nutley, N. J.
Food Machinery & Chemical Corp.
Becco Chemical Div., Buffalo, N. Y.
Westvaco Chlor-Alkali Div., South
Charleston, W. Va.
Ford Motor Co., Dearborn, Mich.
General Electric Co., Schenectady, N. Y.
Chemistry & Chemical Engineering
Component, General Engineering
Laboratory
Chemistry Research Dept.

(Sustaining Members cont'd)

General Electric Co. (cont'd)
Metallurgy & Ceramics Research Dept.
General Motors Corp.
Brown-Lipe-Chapin Div., Syracuse, N. Y. (2 memberships)
Guide Lamp Div., Anderson, Ind.
Research Laboratories Div., Detroit, Mich.
General Transistor Corp., Jamaica, N. Y.
Gillette Safety Razor Co., Boston, Mass.
Gould-National Batteries, Inc., Depew, N. Y.
Grace Electronic Chemicals, Inc., Baltimore, Md.
Great Lakes Carbon Corp., New York, N. Y.
Hanson-Van Winkle-Munning Co., Matawan, N. J. (3 memberships)
Harshaw Chemical Co., Cleveland, Ohio (2 memberships)
Hercules Powder Co., Wilmington, Del.
Hill Cross Co., Inc., New York, N. Y.
Hoffman Electronics Corp., Evanston, Ill.
Hooker Chemical Corp., Niagara Falls, N. Y. (3 memberships)
Houdaille Industries, Inc., Detroit, Mich.
Hughes Aircraft Co., Culver City, Calif.
International Business Machines Corp., Poughkeepsie, N. Y.
International Minerals & Chemical Corp., Chicago, Ill.
Jones & Laughlin Steel Corp., Pittsburgh, Pa.
K. W. Battery Co., Skokie, Ill.
Kaiser Aluminum & Chemical Corp.
Chemical Research Dept., Permanente, Calif.
Div. of Metallurgical Research, Spokane, Wash.
Kennecott Copper Corp., New York, N. Y.
Keokuk Electro-Metals Co., Keokuk, Iowa
Libbey-Owens-Ford Glass Co., Toledo, Ohio
P. R. Mallory & Co., Indianapolis, Ind.
McGean Chemical Co., Cleveland, Ohio
Merck & Co., Inc., Rahway, N. J.
Metal & Thermit Corp., Detroit, Mich.
Metals and Controls Corp., Attleboro, Mass.
Minnesota Mining & Manufacturing Co., St. Paul, Minn.
Monsanto Chemical Co., St. Louis, Mo.
Motorola, Inc., Chicago, Ill.
National Cash Register Co., Dayton, Ohio
National Lead Co., New York, N. Y.
National Research Corp., Cambridge, Mass.
National Steel Corp., Weirton, W. Va.
New York Air Brake Co., Vacuum Equipment Div., Camden, N. J.
Northern Electric Co., Montreal, Que., Canada
Norton Co., Worcester, Mass.
Olin Mathieson Chemical Corp., Niagara Falls, N. Y.
High Energy Fuels Organization (2 memberships)
Pennsalt Chemicals Corp., Philadelphia, Pa.
Phelps Dodge Refining Corp., Maspeth, N. Y.
Philco Corp., Philadelphia, Pa.
Philips Laboratories, Inc., Irvington-on-Hudson, N. Y.
Pittsburgh Metallurgical Co., Inc., Niagara Falls, N. Y.
Poor & Co., Promat Div., Waukegan, Ill.
Potash Co. of America, Carlsbad, N. Mex.
Radio Corp. of America, Harrison, N. J.
Ray-O-Vac Co., Madison, Wis.
Raytheon Manufacturing Co., Waltham, Mass.
Reynolds Metals Co., Richmond, Va. (2 memberships)
Schering Foundation, Inc., Bloomfield, N. J.
Shawinigan Chemicals Ltd., Montreal, Que., Canada
Speer Carbon Co.
International Graphite & Electrode Div., St. Marys, Pa. (2 memberships)
Sprague Electric Co., North Adams, Mass.
Stackpole Carbon Co., St. Marys, Pa.
Stauffer Chemical Co., Henderson, Nev., and New York, N. Y. (2 memberships)
Sumner Chemical Co., Div. of Miles Laboratories, Inc., Elkhart, Ind.
Sylvania Electric Products Inc., Bayside, N. Y. (2 memberships)
Sarkes Tarzian, Inc., Bloomington, Ind.
Tennessee Products & Chemical Corp., Nashville, Tenn.
Texas Instruments, Inc., Dallas, Texas
Titanium Metals Corp. of America, Henderson, Nev.
Udylite Corp., Detroit, Mich. (4 memberships)
Universal-Cyclops Steel Corp., Bridgeville, Pa.
Upjohn Co., Kalamazoo, Mich.
Victor Chemical Works, Chicago, Ill.
Western Electric Co., Inc., Chicago, Ill.
Wyandotte Chemicals Corp., Wyandotte, Mich.
Yardney Electric Corp., New York, N. Y.

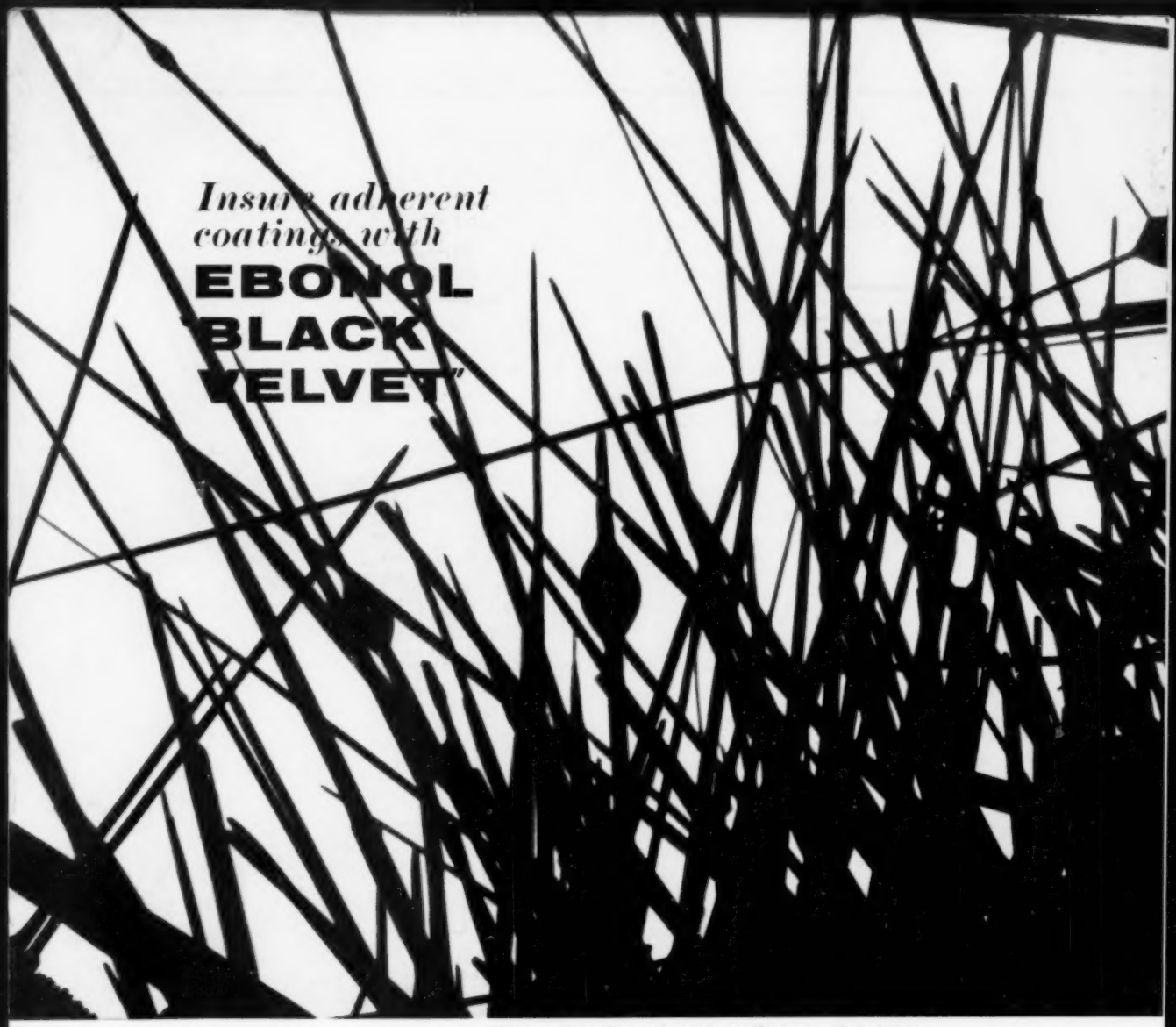

Photograph of the cupric oxide needles (magnified 6500x) produced by immersion of copper part in hot solution of Ebonol "C" Special.

Treating copper and brass surfaces with Ebonol "C" Special will insure high adhesion for almost every type of coating. This patented product of Enthonics Research forms thousands of jet black cupric oxide needles per square inch. Once these needles become imbedded in the coat or adhesive, and the coating sets, adhesion is tight and long-lasting. Lacquers, enamels and plastics are all bonded firmly to copper or brass surfaces when these surfaces have been pre-treated with Ebonol "C" Special.

Use Ebonol "C" coatings to achieve extremely low reflectivity on military equipment and optical parts. The coatings absorb oil, giving better lubrication of copper surfaces. They resist corrosion and produce an attractive finish with little dimensional change. Heat radiating and absorbing abilities of the surface are increased. Printed circuit manufacturers oxidize copper foil in Ebonol "C" Special before coating with adhesive and bonding to the plastic laminate. Result: double the bond strength.

Write for the complete story on Ebonol "C." We promise it will be immediately rewarding.
Enthone, Incorporated, 442 Elm Street, New Haven, Connecticut.

ASARCO

ENTHONE

A subsidiary of American Smelting and Refining Company